REPORT NO.
UCB/EERC-94/07
JUNE 1994

EARTHQUAKE ENGINEERING RESEARCH CENTER

ACCIDENTAL AND NATURAL TORSION IN EARTHQUAKE RESPONSE AND DESIGN OF BUILDINGS

by

JUAN C. DE LA LLERA
ANIL K. CHOPRA

A Report on Research Conducted Under
Grant No. BCS-8921932 from the
National Science Foundation

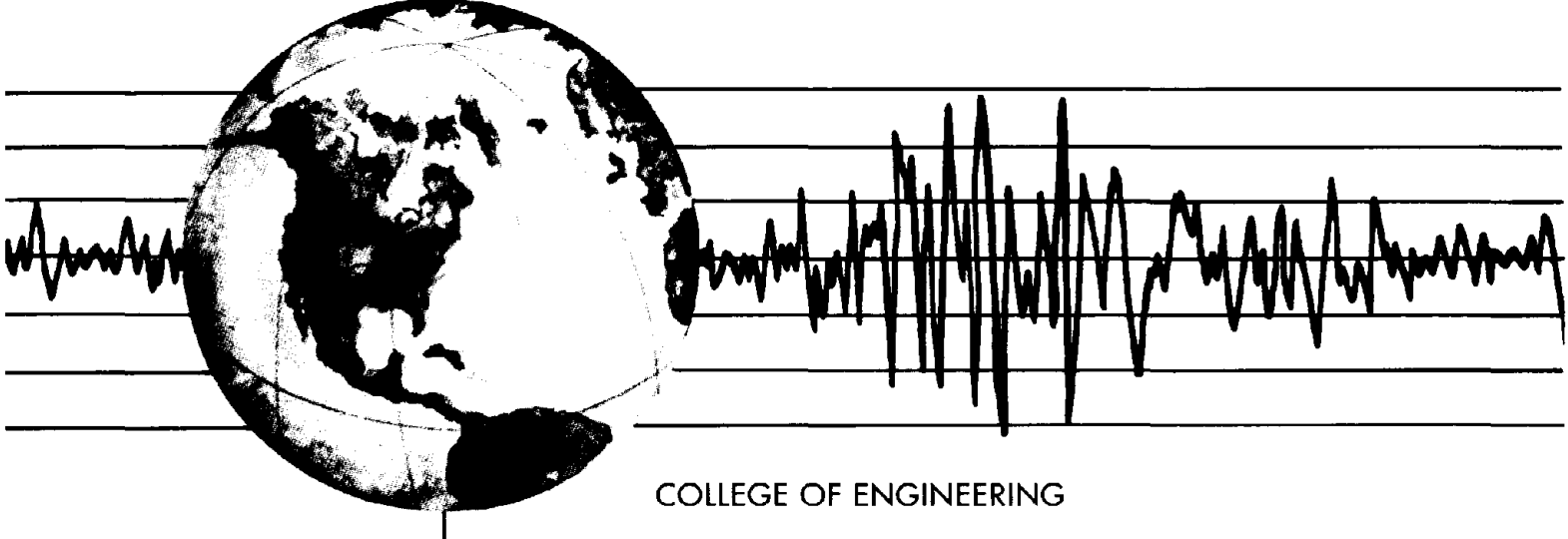

COLLEGE OF ENGINEERING

UNIVERSITY OF CALIFORNIA AT BERKELEY

For sale by the National Technical Information Service, U.S. Department of Commerce, Springfield, Virginia 22161

See back of report for up to date listing of EERC reports.

ACCIDENTAL AND NATURAL TORSION IN EARTHQUAKE RESPONSE AND DESIGN OF BUILDINGS

by

Juan C. De la LLera

and

Anil K. Chopra

A Report on Research Conducted Under
Grant No. BCS-8921932 from the National Science Foundation

Report No. UCB/EERC-94/07
Earthquake Engineering Research Center
University of California
Berkeley, California

June 1994

ABSTRACT

Because of the torsional vibrations of a building during an earthquake, the displacement demands on the different resisting planes of the building may increase relative to those of a similar system with no torsion. It is the overall objective of this work to develop procedures that would enable engineers to predict such increase in building response resulting from accidental and natural torsion.

This work on the effects of building torsion is divided into two parts. In part I, the increase in building response due to accidental torsion is evaluated with the objective of developing an improved procedure to account for these effects in building analysis. Such a procedure is based on: (1) the results of individual studies of the increase in response due to different sources of accidental torsion, such as stiffness uncertainty and rotational excitation at the base; (2) a critical evaluation of the use of accidental-torsion provisions in code-static and dynamic analyses of single and multistory systems; and (3) actual recorded earthquake motions in three nominally-symmetric buildings.

The increase in building response due to stiffness uncertainty is evaluated in Chapter 2. Discrepancies between the computed and actual values of the structural element stiffnesses imply that a building with nominally-symmetric plan is actually asymmetric to some unknown degree and will undergo torsional vibration when subjected to purely translational ground motion. Such accidental torsion leads to increase in structural element deformations which is shown to be essentially insensitive to the uncoupled lateral vibration period of the system but is affected strongly by the ratio of uncoupled lateral and torsional vibration periods. The structural deformations increase, in the mean, by at most 10 and 5 percent for R/C and steel buildings, respectively; and by much smaller amounts for a wide range of system parameters. The increase in structural deformations due to stiffness uncertainty is shown to be much smaller than implied by the accidental torsional provisions in the Uniform Building Code and most other building codes.

Considered in Chapter 3 is the accidental torsion in buildings resulting from rotational excitation (about a vertical axis) of the building foundation as a result of spatially non-uniform ground motions. Because of this accidental torsion, the displacements and deformations in the structural elements of the building are likely to increase. This increase in response is evaluated using actual base rotational excitations derived from translational components of motions recorded at the base of

thirty buildings during recent California earthquakes. Accidental torsion has the effect of increasing the building displacements, in the mean, by less than five percent for systems that are torsionally stiff or have lateral vibration periods longer than half a second. On the other hand, short-period (less than half a second) and torsionally-flexible systems may experience significant increases in response due to accidental torsion. Since the dependence between this increase in response and the system parameters is complex, two simplified methods are developed for conveniently estimating this effect of accidental torsion. They are the 'accidental eccentricity' and the 'response spectrum' method. The computed accidental eccentricities are much smaller than the typical code values, $0.05b$ or $0.1b$, except for buildings with very long plan dimensions ($b \geq 50$ m). Alternatively, by using the response spectrum method the increase in response can be estimated by computing the peak response to translational and rotational base motions independently and combining the peak values using the SRSS rule.

The differences between the increase in building response due to accidental eccentricity predicted by code-specified static and dynamic analyses are studied for symmetric and unsymmetric single and multistory buildings in Chapter 4. The increase in response computed from static analysis of the building is obtained by applying the equivalent static forces at distance e_a, equal to the story accidental eccentricity, from the center of mass at each floor. Alternatively, this increase in response is computed by dynamic analysis of the building with the center of mass of each floor shifted through a distance e_a from its nominal position. A parametric study is performed on single-story systems in order to evaluate the differences in response predicted by both analysis procedures. It is shown that these results are essentially the same as the ones obtained for a special class of multistory systems. Upper and lower bounds for the differences in response computed from static and dynamic analyses are obtained for multistory systems. These differences in response depend primarily on the ratio of uncoupled lateral and torsional vibration periods of the building. They are larger for small values of the frequency ratio and decrease to zero as the frequency ratio becomes large. Further, these discrepancies are in many cases of the same order as the code-intended increase in response due to accidental eccentricity. This implies that the code-specified static and dynamic analyses to account for accidental torsion should be modified to be mutually consistent.

Finally, a procedure is developed in Chapter 5 for including the effects of accidental torsion in seismic design of buildings. It has four steps. First, the ratio between the uncoupled lateral

and torsional vibration periods of the building is computed. This ratio and plan dimensions are then used to estimate the increase in displacements at the edge of the building resulting from identifiable sources of accidental torsion. Third, from these edge displacements the increase in displacements at the location of interior resisting planes are estimated. Finally, the design forces in structural members are computed by amplifying the forces ignoring accidental torsion by the increase in building displacements determined previously. This procedure has several advantages over the code-specified static and dynamic analysis procedures to include accidental torsion, such as: (1) the elimination of cumbersome static or three-dimensional dynamic analyses to account for accidental torsion effects in building design, and (2) the inclusion of the effects of all sources of accidental torsion, as opposed to current seismic codes, which consider only those effects that can be represented by a constant accidental eccentricity. Two building examples are presented to illustrate these advantages as well as the computational steps required to implement the new procedure.

In part II of this work, the nonlinear torsional response of single and multistory asymmetric buildings is considered with the objective of developing a simple **conceptual framework** in order to understand the earthquake performance of different asymmetric structural configurations, and to develop a **simplified method** for nonlinear analysis of asymmetric buildings.

Studied in Chapter 2 (part II) is the inelastic seismic behavior of asymmetric-plan buildings using the histories of base-shear and torque. The first step in understanding this behavior is to construct the base-shear and torque (BST) surface for the building, which represents all combinations of shear and torque that applied statically lead to collapse of the structure. Several factors controlling the shape of this surface, such as strength eccentricity and bidirectional ground motion, are identified. Also, their effects on the building response are studied considering several structural configurations. The results obtained show that the BST surface, in conjunction with the base shear and torque histories, provides a useful conceptual framework for understanding the behavior of asymmetric systems. Furthermore, using these surfaces, relevant aspects of the behavior and design of such buildings become apparent even before dynamic analysis of the structure.

This conceptual framework is extended and used in Chapter 3 to study the inelastic seismic behavior and design of asymmetric multistory buildings emphasizing, primarily, the use of story shear and torque histories. Six different structural characteristics and their effect on the torsional

response of buildings are analyzed: strength of orthogonal resisting planes, stiffness asymmetry, strength asymmetry, planwise distribution of strength, number of resisting planes, and intensity of the ground motion component in the orthogonal direction. As a result of these analyses several techniques and conceptual guidelines are developed to correct the planwise unbalance in deformation demands typical of asymmetric structures. The three most important are: (1) the increase in torsional capacity of the system by introducing resisting planes in the orthogonal direction, (2) the variation of stiffness and strength eccentricity to concentrate yielding in selected resisting planes, and (3) the reduction of torsional capacity by lumping strength close to the center of mass. Using these guidelines the undesirable earthquake response of a very asymmetry building is effectively corrected by changing slightly the strength of a few key resisting planes. It is demonstrated that the use of the story shear and response histories in conjunction with the corresponding story yield surfaces is a powerful tool for conceptual understanding of the earthquake behavior of asymmetric structures.

Finally, a new simplified model for analysis and design of multistory buildings is developed in Chapter 4. The model is based on a single super-element per building story capable of representing the elastic and inelastic properties of the story. This is done by matching the stiffness matrices and ultimate yield surface of the story with that of the element; this surface relates story shear and story torque. For practical convenience, these surfaces are parameterized in terms of seven important physical parameters controlling the seismic response of asymmetric structures. Several numerical studies showed that the accuracy of the super-element model is satisfactory for most design purposes; the errors in peak responses are expected to be less than twenty percent for most practical structures. Among the important advantages of this simplified model is that the time required in formulating analyzing, and interpreting the structural model and its response is at least an order of magnitude smaller than for any conventional 3-D inelastic model. This enables the engineer to try different structural configurations and, thus, produce designs that have the desired seismic behavior and are cost-effective. Furthermore, it is shown through a multistory building example that the super-element model is a powerful tool for conceptual design of a building. In spite of its simplicity, the model uses an accurate representation of the story-shear and torque surfaces, which enables it to capture the fundamental features controlling the inelastic behavior of the building.

Acknowledgments

This investigation was supported by the National Science Foundation under Grant BCS-8921932. The authors are grateful for this support.

The authors are also grateful of Professors W.J. Hall, S. Mahin, B. Parlett, E. Rosenblueth, and W.K. Tso, for reviewing and suggesting improvements on different chapters of this manuscript.

TABLE OF CONTENTS

Blank Page

Part I

Accidental Torsion in Buildings

Blank Page

1. INTRODUCTION

Building codes require that the effects of torsion be considered by applying the equivalent static forces at a distance e_d from the CS (center of stiffness), resulting in story torques in addition to shears and overturning moments. The design eccentricity e_d specified in most codes is of the form

$$e_d = \alpha e_s + \beta b \quad \text{or} \quad \mathrm{e_d = \delta e_s - \beta b} \tag{1}$$

where e_s is the static stiffness eccentricity—the distance between the CM (center of mass) and CS; b is the plan dimension of the building perpendicular to the direction of ground motion; and α, δ, and β are specified coefficients. For each structural element, the e_d value leading to the larger design force is to be used. The first terms, αe_s and δe_s, are intended to account for the coupled lateral torsional response of the building arising from lack of symmetry in plan. The second term, $\pm\beta b$, known as accidental eccentricity, is introduced to account for eccentricities due to discrepancies between the mass, stiffness, and strength distributions used in analysis and true distributions at the time of an earthquake; torsional vibrations induced by rotational excitation at the base; and other sources of torsion not considered explicitly in the analysis.

The coefficients α, δ, and β vary among building codes. For instance, $\alpha = \delta = 1$ and $\beta = 0.05$ in the Uniform Building Code [1]; $\alpha = 1.5$, $\delta = 1$, and $\beta = 0.1$ in the Mexico Federal District Code [2]; and $\alpha = 1.5$, $\delta = 0.5$, and $\beta = 0.1$ in the National Building Code of Canada [3].

It is the objective of this part of the dissertation to study the effects of accidental torsion in buildings and its corresponding code provisions. This is done in three phases. First, the increase in building response due to different sources of accidental torsion, such as stiffness uncertainty and rotational excitation at the base, is studied. Second, the use of accidental-torsion provisions in code-static and dynamic analyses of single and multistory systems is evaluated. Third, a new procedure for incorporating the effects of accidental torsion in building design is developed.

Accidental torsion in a building may be conceptually understood as the result of unforeseen variability (or uncertainty) in the structural properties of the building and its input. Part of this variability leads to changes in the lateral response of the structure, another part leads to changes in its torsional response. It is the latter effect the one attributed hereafter to accidental torsion.

This definition of accidental torsion is amenable of a simple mathematical characterization. Let us assume, for the sake of the discussion, that we are interested in studying the change in building displacements u as a result of accidental torsion. This change in building response may be

represented by expanding u in a Taylor series about the displacements $\bar{u}$, which would be predicted analytically using the nominal values of the structural properties and input for the building, i.e.

$$u(\boldsymbol{p}, \boldsymbol{u}_g(t)) = \underbrace{\bar{u}(\bar{\boldsymbol{p}}, \bar{\boldsymbol{u}}_g(t))}_{\text{nominal response}} + \sum_i \frac{\partial u}{\partial p_i}(p_i - \bar{p}_i) + \Delta \boldsymbol{u}_g + \text{h.o.t.} \tag{2}$$

where $\boldsymbol{p} = \{p_1,\ p_2, \ldots, p_{N_p}\}$ is the vector of system parameters; $\boldsymbol{u}_g(t) = \{u_{gx}\ u_{gy}\ u_{g\theta}\}$ is the vector containing the x, y, and rotational components of base motion; $\frac{\partial u}{\partial p_i}$ represents the sensitivity of the building displacements to changes in parameter p_i; $\Delta \boldsymbol{u}_g$ the change in building response due to changes in the input; the over-bar represents nominal values; and 'h.o.t' stands for higher order terms.

Equation (2) shows that if the system parameters and ground motion coincide with their nominal values and history, respectively, the displacement u becomes, as it should, the nominal displacement. In practice, however, neither the nominal values of the system parameters nor the assumed ground motion histories will coincide with the actual values at the time of an earthquake. Therefore, discrepancies between the nominal and actual building displacements will always exist. It is apparent that these discrepancies result from two distinct sources (Eq. (2)). One is the uncertainty in the value of the random properties $\boldsymbol{p}$ of the system; the other is the uncertainty in the random ground motion process $\boldsymbol{u}_g$, specifically, the rotational excitation at the base of the building.

The study of uncertainty in the building parameters, specifically for the case of stiffness uncertainty, is the topic of Chapter 2. The procedure described therein is applicable to most other elastic sources of accidental torsion as well, such as uncertainty in the location of the CM or stiffness and mass uncertainty in stories other than the one considered in the analysis. On the other hand, the change in building response due to base rotational excitation is studied in Chapter 3 using recorded motions obtained in thirty buildings during recent California earthquakes.

In Chapter 4, the use of accidental eccentricity βb in code-static and dynamic analyses of buildings is evaluated. The main objectives of the chapter are: (1) to investigate the increase in building response that is implicit in the use of a constant accidental eccentricity βb, and (2) to understand any discrepancies between the increases in response due to accidental torsion predicted by code-specified static and dynamic analyses. Besides, two other interesting issues regarding the use and interpretation of code-accidental torsion provisions are identified and discussed: discrepancies between measures of accidental torsion based on global response quantities instead of element deformations and internal forces, and the heightwise variation of accidental eccentricity.

Finally, a new procedure is developed in Chapter 5 for including the effects of accidental torsion in seismic design of buildings. This procedure integrates the results of Chapters 2,3, and 4 and other related research [4,5] in order to define new design envelopes for the increase in building edge-displacements resulting from the most important sources of accidental torsion. The new procedure has several advantages over the code-specified static and dynamic analysis procedures to include accidental torsion, such as: (1) the elimination of cumbersome static or three-dimensional dynamic analyses to account for accidental torsion effects in building design, and (2) the inclusion of the effects of all sources of accidental torsion, as opposed to current seismic codes, which consider only those effects that can be represented by a constant accidental eccentricity.

Each of the chapters presented is a self-contained unit and it could be read, in principle, in any sequence. It is advisable, however, to read Chapter 5 last because it borrows material from the previous three chapters.

References

1. *Uniform building code.* (1988). Int. Conf. of Build. Off., Whittier, Calif.

2. *Earthquake resistant regulations, a world list.* (1988). International Association for Earthquake Engineering, Tokyo, Japan.

3. *National building code of Canada.* (1985). Associate Committee on the National Building Code, National Research Council of Canada, Ottawa, Ontario.

4. De la LLera, J.C. and Chopra, A.K.'Evaluation of code accidental torsion provisions from building records', Journal of Structural Engineering, ASCE, Vol. 120, No. 2, Feb. 1994, pp. 597-616.

5. De la LLera, J.C. and Chopra, A.K.'Accidental torsion in buildings', Proceedings of the 5th U.S. National Conference on Earthquake Engineering, July, 1994. To be published.

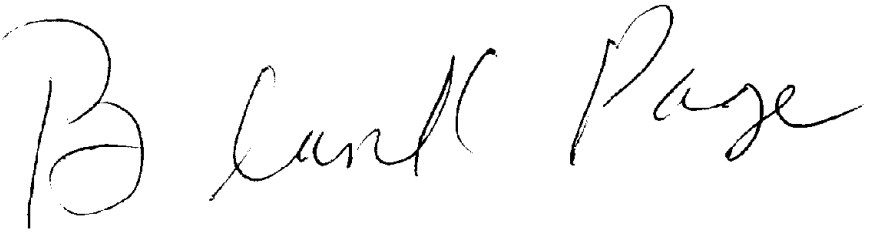

2. ACCIDENTAL TORSION IN BUILDINGS DUE TO STIFFNESS UNCERTAINTY

2.1 Introduction

This chapter is concerned with accidental torsion due to uncertainty in the stiffnesses of structural elements. Several factors contribute to this stiffness uncertainty, including: uncertainty in material properties and element dimensions, variability in fabrication methods and quality control, loading history of the element, and because analytical procedures are inexact predictors of the actual stiffnesses. Consequently, the nominal values of element stiffnesses used in building analysis and design are different from the actual values, leading to discrepancies in the plan-wise distribution of stiffness. This has the implication that a building with nominally-symmetric plan is actually asymmetric to some unknown degree and will undergo torsional vibration when subjected to purely translational ground motion.

This research of accidental torsion due to stiffness uncertainty emphasizes nominally-symmetric systems because it is shown that such systems are affected more than asymmetric systems. Using available and inferred experimental data, the uncertainty in the stiffness properties of the system is defined and characterized. Thereafter, the response of nominally symmetric-plan systems is studied using (1) an approximate analytical model for the probability distribution of the system response, and (2) Monte Carlo simulations based on sampling the probability distributions of structural element stiffnesses. Finally, design implications of the increase in building response due to stiffness uncertainty are discussed.

2.2 Systems and design spectrum considered

The systems considered are idealized single-story buildings consisting of a rigid roof diaphragm, where all the system mass is lumped; lateral resistance is provided by vertically-rigid structural elements located along resisting planes in the x and y-directions. These y-planes are numbered 1-6 and x-planes as 1-3 in Fig. 1. Several structural elements, such as shear walls or columns, may be located in one resisting plane. As shown in the building plan (Fig. 1), these planes are symmetrically located about the x and y axes passing through the center of mass (CM). The system consists of N resisting planes providing lateral resistance in the y-direction, and M resisting planes acting in the x-direction.

The dynamic response of the system to earthquake ground acceleration in the y-direction, $a_{gy}(t)$, is described by two degrees of freedom: the translational displacement u_y of the CM along the y-direction, and the rotation u_θ of the rigid diaphragm. The equations of motion of the system can be written:

$$\begin{bmatrix} m & 0 \\ 0 & m \end{bmatrix} \begin{Bmatrix} \ddot{u}_y \\ r\ddot{u}_\theta \end{Bmatrix} + \begin{bmatrix} \bar{K}_y & 0 \\ 0 & \bar{K}_\theta/r^2 \end{bmatrix} \begin{Bmatrix} u_y \\ ru_\theta \end{Bmatrix} = \begin{Bmatrix} -m \\ 0 \end{Bmatrix} a_{gy}(t) \tag{1}$$

where r is the radius of gyration of the system plan about a vertical axis passing through the CM and m is the lumped mass at the roof diaphragm; $\bar{K}_y = \sum_{i=1}^{N} \bar{k}_{yi}$ and $\bar{K}_\theta = \sum_{i=1}^{N} \bar{k}_{yi}x_i^2 + \sum_{i=1}^{M} \bar{k}_{xi}y_i^2$, are the nominal values for the lateral and torsional stiffness of the building, respectively; $\bar{k}_{xi}$ and $\bar{k}_{yi}$ are nominal values of the combined lateral stiffnesses of all structural elements along the i^{th} resisting plane in the x or y directions, respectively. Pairs of resisting planes located symmetrically about the y-axis are assumed to have the same nominal stiffness. Thus, the system is symmetrical about the y-axis with uncoupled equations of motion (Eq.(1)). Later when we consider uncertainty in the element stiffness, $\bar{k}_{xi}$ and $\bar{k}_{yi}$ will represent the mean values of the lateral stiffness along the i^{th} resisting plane. Throughout this work, the over-bar stands for mean (or nominal) values.

The lateral resisting planes in the direction of ground motion as well as the transverse direction contribute to the torsional stiffness $\bar{K}_\theta$. The fraction contributed by the transverse elements is $\alpha = \sum_{i=1}^{M} \bar{k}_{xi}y_i^2/\bar{K}_\theta$. A value of $\alpha = 0$ implies that no torsional stiffness is provided by the transverse elements; a value of $\alpha = 1$ implies that transverse elements provide all the torsional stiffness.

The equations of motion of the system have to be restated in order to recognize the uncertainty in the stiffness of resisting elements acting in the y-direction; stiffnesses of the transverse elements are fixed at their nominal values $\bar{k}_{xi}$. Thus, even with the stiffness uncertainty considered, the system remains symmetric about the x-axis, and the equations of motion are:

$$\begin{bmatrix} m & 0 \\ 0 & m \end{bmatrix} \begin{Bmatrix} \ddot{u}_y \\ r\ddot{u}_\theta \end{Bmatrix} + \begin{bmatrix} K_y & K_{y\theta}/r \\ K_{y\theta}/r & K_\theta/r^2 \end{bmatrix} \begin{Bmatrix} u_y \\ ru_\theta \end{Bmatrix} = \begin{Bmatrix} -m \\ 0 \end{Bmatrix} a_{gy}(t) \tag{2}$$

where $K_y = \sum_{i=1}^{N} k_{yi}$ and $K_\theta = \alpha\bar{K}_\theta + \sum_{i=1}^{N} k_{yi}x_i^2$ are the true values of the lateral and torsional stiffnesses of the building, respectively; $K_{y\theta} = \sum_{i=1}^{N} k_{yi}x_i$. These are the equations of motion for a nominally symmetric system which is actually asymmetric because of the uncertain stiffnesses of elements. Thus, K_y, K_θ and $K_{y\theta}$ are uncertain parameters. In contrast, most previous work has been concerned with the dynamics of asymmetric-plan systems with deterministic properties.

Dividing Eq. (1) by m leads to

$$\begin{Bmatrix} \ddot{u}_y \\ r\ddot{u}_\theta \end{Bmatrix} + (2\pi/\bar{T}_y)^2 \begin{bmatrix} 1 & 0 \\ 0 & \bar{\Omega}^2 \end{bmatrix} \begin{Bmatrix} u_y \\ ru_\theta \end{Bmatrix} = \begin{Bmatrix} -1 \\ 0 \end{Bmatrix} a_{gy} \tag{3}$$

where $\bar{T}_y = 2\pi\sqrt{m/\bar{K}_y}$ is the uncoupled lateral vibration period of the nominally-symmetric system, and $\Omega = \sqrt{\bar{K}_\theta/(\bar{K}_y r^2)}$, is the ratio between the uncoupled lateral and torsional periods of the nominally-symmetric system. Similarly, Eq. (2) can be rewritten as

$$\begin{Bmatrix} \ddot{u}_y \\ r\ddot{u}_\theta \end{Bmatrix} + (2\pi/\bar{T}_y)^2 \begin{bmatrix} \hat{K}_y & \hat{e} \\ \hat{e} & \hat{K}_\theta\bar{\Omega}^2 \end{bmatrix} \begin{Bmatrix} u_y \\ ru_\theta \end{Bmatrix} = \begin{Bmatrix} -1 \\ 0 \end{Bmatrix} a_{gy} \tag{4}$$

where $\hat{K}_y = K_y/\bar{K}_y$, and $\hat{K}_\theta = K_\theta/\bar{K}_\theta$ are the ratios between the true and nominal values of the translational and torsional stiffnesses of the system, respectively; $\hat{e} = K_{y\theta}/(\bar{K}_y r)$ is the normalized static eccentricity of the system. The three parameters, $\hat{K}_y$, $\hat{K}_\theta$, and $\hat{e}$, that arise in the transition between the deterministic symmetric system (Eq. (3)) and the system with uncertain element stiffnesses (Eq. (4)) are random. A comparison of Eq. (3) and (4) indicates that the uncertainty in element stiffness has two effects. Firstly, the lateral and torsional stiffnesses, and hence the uncoupled vibration periods, are modified as indicated by the differences between the actual values of the parameters $\hat{K}_y$ and $\hat{K}_\theta$ and their nominal values of unity. Secondly, the plan-wise distribution of element stiffnesses is no longer symmetric about the y-axis, resulting in coupling between the lateral and torsional motions of the system. This torsional coupling is one of several sources of accidental torsion in nominally symmetric-plan systems.

All the systems considered are analyzed for the smooth response spectrum shown in Fig. 2. This spectrum is developed by well established techniques [1] for a ground motion with peak acceleration, velocity, and displacement of $0.5g$, 24 in/sec, and 18 in, respectively. Amplification factors of 2.71, 2.3, and 2.01 are chosen for the acceleration, velocity, and displacement sensitive regions of the spectrum (Fig. 2). These amplification factors are appropriate for five percent damping and 84.1 percentile response.

2.3 Analysis procedure

The maximum earthquake response of the structural systems described earlier and governed by Eqs. (3) or (4) is estimated by the Response Spectrum Analysis (RSA) method. This procedure is summarized as a sequence of computational steps: (1) define the structural properties of the system

$\bar{T}_y, \bar{\Omega}, \hat{K}_y, , \hat{K}_\theta$, and $\hat{e}$; (2) estimate the modal damping ratios ξ_n—chosen here as 5% in both modes of vibration; (3) compute the two natural frequencies and modes of vibration of the system; (4) compute the maximum response separately for each individual vibration mode; (5) estimate the maximum response by combining the modal maxima using the CQC rule.

The response quantities of interest in this investigation are the lateral displacements $u_{\pm r}$ at distance $\pm r$ from the CM, the larger absolute value $(u_r)_o$ of these two lateral displacements, and the corresponding displacement response quantity $(u_{b/2})_o$ for the edges of the building plan. These displacements are normalized with respect to the maximum lateral displacement, u_o, of the nominally-symmetric system governed by Eq. (3): $\hat{u}_{\pm r} = u_{\pm r}/u_o$, $(\hat{u}_r)_o = (u_r)_o/u_o$, $(\hat{u}_{b/2})_o = (u_{b/2})_o/u_o$. The normalized response $(\hat{u}_r)_o$ is independent of the plan aspect ratio b/a (Fig. 1) but $(\hat{u}_{b/2})_o$ is influenced by this aspect ratio for which two limiting cases are considered: $b/a = 1$, i.e. a square plan, and $b/a = \infty$ to represent buildings with very long plan dimension transverse to the direction of ground motion. Defined in this manner, normalized displacements that are larger than unity, imply an increase in lateral displacement arising from accidental torsion due to uncertain element stiffnesses.

Direct Monte Carlo simulation is one of the approaches used herein to study the influence of stiffness uncertainty on the response of nominally-symmetric buildings. The stiffness k_i of the i^{th} resisting element is defined by sampling from its probability density function (PDF), assumed to be Gaussian with mean equal to its nominal value $\bar{k}_i$, and a coefficient of variation (ratio between the mean and standard deviation) equal to 0.14 and 0.08 for R/C and steel structures, respectively. With the stiffness of each element defined in this manner, the earthquake response of the resulting system is determined by the RSA procedure described earlier. This stiffness sampling and analysis procedure is repeated two-thousand times to enable a statistical analysis of the system response.

The resulting PDF of the response $(u_r)_o$ of a R/C nominally-symmetric system with eight resisting elements in the direction of ground motion, $\bar{T}_y = 1.5$ sec. and $\bar{\Omega} = 1.25$, is shown in Fig. 3. The PDF was obtained by appropriate normalization of the histogram of 2000 values. Figure 3 shows that the response $(\hat{u}_r)_o$ is always greater than one; implying that stiffness uncertainty has the effect of increasing the displacement $(u_r)_o$ relative to that of the nominally-symmetric system. Note that there is essentially zero probability of this increase in response exceeding 20 percent. Note also that the mean of $(\hat{u}_r)_o$ corresponds to a probability of exceedance slightly smaller than 0.4 (and not 0.5) because the PDF is not symmetric with respect to its mean.

2.4 Uncertainty in system parameters

The actual lateral stiffness of a frame, shear wall or column differs in general from its nominal value due to uncertainty in the material properties, element dimensions, fabrication methods, quality control, loading history of the element, and the theoretical models used for predicting the element stiffness. Background information that enables formulating a model for the probability distributions of the stiffness of concrete and steel resisting elements is presented next.

The statistical properties of the lateral stiffness of reinforced concrete (R/C) resisting elements are inferred from available statistical descriptions of element deformations. In particular, the PDF of the ratio between the actual and theoretically predicted deformations of beams is approximately normal with its mean value approximately equal to one, and its coefficient of variation equal to 0.14 [2]. The same PDF, mean, and coefficient of variation approximately model the ratio of actual to nominal values of the element stiffness, which is the reciprocal of the deformation ratio (in the case of specified forces). We conservatively assume that: (1) the coefficient of variation of the lateral stiffness of a resisting plane with several resisting elements is the same as that of an individual resisting element, and (2) the coefficient of variation for the stiffness ratio of beam elements predicts the coefficient of variation of the stiffness ratio of other laterally resisting R/C structural elements such as columns, shear walls, or frames. The latter assumption seems reasonable because the lateral stiffnesses of columns or walls should be less uncertain because such structural elements crack less than beams under gravitational loads. Furthermore, the lateral resisting elements will all crack (although they may not yield) under moderate ground motion, and the computed stiffness of the cracked section should be a less uncertain predictor of the actual stiffness.

Uncertainty in the stiffness of steel structural elements is due mainly to uncertainty in the properties of steel and the cross-sectional geometry of the elements. Statistical information on both sources of uncertainty is available [3,4]. The stiffness of a steel structural element is assumed to be proportional to the product $E_s I_s$, where E_s is the Young's modulus of the material and I_s is the moment of inertia of the element cross section. The ratio between the actual and theoretical values of E_s was found to be normally distributed with mean equal to one and coefficient of variation equal to 0.06; the ratio between the actual and theoretical values of I_s was also found to be normally distributed with mean equal to one and coefficient of variation 0.05. Based on the statistics of the actual to theoretical ratios of E_s and I_s, it is possible to show, analytically or by direct simulation on $E_s I_s$, that the true to theoretical stiffness ratio for a steel element is approximately normally

distributed with mean equal to one and coefficient of variation equal to 0.08. These are the values used in this investigation.

Among the sources of uncertainty, in-batch variability (variability of a set of elements manufactured identically) in R/C resisting elements contributes about 70 percent of the total stiffness uncertainty. In the case of steel elements, the statistics presented for E_s and I_s correspond to mean in-batch variability for different steel mills in the U.S. It seems reasonable to assume that the statistical correlation between stiffnesses of different elements is small. Lack of good statistical information precludes confirmation of this statement. For this investigation it is conservative to assume uncorrelated element stiffnesses, because as we will see later, statistical correlation among element stiffnesses reduces the torsional response of the system.

The elements of the stiffness matrix of a system with stiffness uncertainty (Eq. (4)): $\hat{K}_y$, $\hat{K}_\theta$, and $\hat{e}$ are all linear functions of the individual element stiffnesses, k_i, that are assumed to be normally distributed. Therefore, these elements of the stiffness matrix are also normally distributed. Consider, for instance, the system shown in Fig. 1, and assume statistical independence among the lateral stiffnesses of the N resisting planes of the structure. Each resisting plane has the same coefficient of variation V_k. The mean, standard deviation, and correlation coefficients for $\hat{K}_y, \hat{K}_\theta$, and $\hat{e}$ are for this case:

$$\mu_{\hat{K}_y} = 1, \qquad \mu_{\hat{K}_\theta} = 1, \qquad \text{and} \quad \mu_{\hat{e}} = 0 \tag{5}$$

$$\sigma_{\hat{K}_y} = \frac{V_k}{\sqrt{N}}, \quad \sigma_{\hat{K}_\theta} = \sqrt{\frac{\sum_{i=1}^{N} x_i^4}{\sum_{i=1}^{N} x_i^2}}\,(1-\alpha)\,V_k, \quad \text{and} \quad \sigma_{\hat{e}} = \sqrt{\frac{1-\alpha}{\mathrm{N}}}\bar{\Omega}\mathrm{V_k} \tag{6}$$

$$\rho_{\hat{K}_y\hat{e}} = 0, \qquad \rho_{\hat{K}_\theta\hat{e}} = 0, \qquad \text{and} \quad \rho_{\hat{\mathrm{K}}_\mathrm{y}\hat{\mathrm{K}}_\theta} = \frac{\sum_{\mathrm{i}=1}^{\mathrm{N}} \mathrm{x}_\mathrm{i}^2}{\sqrt{\mathrm{N}}\sqrt{\sum_{\mathrm{i}=1}^{\mathrm{N}} \mathrm{x}_\mathrm{i}^4}} \tag{7}$$

where $\mu_{(\cdot)}$, $\sigma_{(\cdot)}$ and $\rho_{(\cdot)}$ stand for mean, standard deviation and correlation coefficient, respectively.

Figure 4 shows the standard deviation of the normalized static eccentricity $\sigma_{\hat{e}}$ (Eq. (6)) as a function of the lateral to torsional period ratio $\bar{\Omega}$ and the number N of resisting planes in the y-direction. The standard deviation $\sigma_{\hat{e}}$ decreases as $1/\sqrt{N}$ with increasing number of elements; it also decreases linearly with decreasing $\bar{\Omega}$. The latter observation can be justified by recognizing that small values of $\bar{\Omega}$ imply that the torsional vibration period of the nominally symmetric system is long relative to its lateral vibration period, a situation that is typical of buildings with lateral resisting elements close to the center of the building plan. For such systems, uncertainty in the element stiffnesses leads to smaller $\sigma_{\hat{e}}$ which tends to induce smaller static eccentricities. The former observation can be explained by noting that a larger value of N implies a more uniform distribution

of the structural elements in the building plan, and elements closer to the center of the plan will contribute less to static eccentricity. Consequently, static eccentricity will tend to be smaller for systems with larger N. Consistent with the smaller standard deviation for the stiffness of steel elements compared to R/C elements, the standard deviation of the normalized static eccentricity is also smaller in the former case.

The PDF of $\hat{e}$ is shown in Fig. 5 for selected values of the system parameters: $\bar{\Omega} = 1$, $\alpha = 0.5$, and $N = 2, 4, 8, 12$. The PDF's are narrower for steel buildings compared to R/C structures and for systems with larger N, consistent with the standard deviation trends (Fig. 4). Figure 5 also shows the probability of exceedance associated with specific values of normalized static eccentricity $\hat{e}$. For example, in the case of a R/C building with $N = 8$, i.e., eight resisting planes, there is a 17 percent probability that the normalized static eccentricity exceeds 0.05. For a steel building, this probability of exceedance is reduced to less than two percent.

If the stiffnesses of different resisting elements are statistically correlated, the standard deviation $\hat{e}$ of the normalized static eccentricity is always reduced relative to the above mentioned values based on uncorrelated element stiffnesses. If the correlation coefficient between the stiffnesses of two resisting planes is ρ, it can be shown that:

$$\sigma_{\hat{e}} = \sqrt{\frac{(1-\alpha)(1-\rho)}{N}}\,\bar{\Omega}\,V_k \tag{8}$$

Thus, the standard deviation of $\hat{e}$ for a system with particular $\bar{\Omega}$ and N, varies between the value shown in Fig. 4 for $\rho = 0$, and zero for $\rho = 1$. The latter case ($\rho = 1$) implies perfectly correlated element stiffnesses and hence all element stiffnesses increase or decrease relative to their nominal values by the same factor. Thus, a nominally-symmetric system remains symmetrical in spite of stiffness uncertainty, i.e. $\hat{e} = 0$. Completely uncorrelated element stiffnesses ($\rho = 0$) produce the largest standard deviations in $\hat{e}$ and hence increase the probability of a larger normalized eccentricity $\hat{e}$. Because some correlation will always exist among the stiffnesses of resisting elements in a building, the assumption of uncorrelated stiffnesses in this work will overestimate building torsion due to stiffness uncertainty.

The relative contributions of the uncertainty in the values of $\hat{K}_y$, $\hat{K}_\theta$, and $\hat{e}$ on the response of nominally-symmetric buildings is evaluated for the system analyzed previously whose results are shown in Fig. 3. The mean values of the normalized displacement $(\hat{u}_r)_o$ are presented in Fig. 6 as a function of $\bar{T}_y$ for three values of $\bar{\Omega}$. The increase in $(\hat{u}_r)_o$ over one indicates the increased response due to element stiffness uncertainty. The solid lines, represent results for systems governed

by Eq. (4), i.e. considering the actual sampled values of all three terms of the stiffness matrix: $\hat{K}_y$, $\hat{K}_\theta$, and $\hat{e}$; the dashed lines represent systems governed by Eq. (4) with $\hat{K}_y = 1$ and $\hat{K}_\theta = 1$, i.e. considering only the eccentricity arising from the uncertainty in element stiffnesses. It is apparent that the eccentricity term, $\hat{e}$, is the primary contributor to the increase in displacement response. For this reason and because $\hat{e}$ is the only factor arising from uncertainty in the element stiffnesses that produces torsional response of the system, the stiffness uncertainty of the system is modeled in the rest of this study only by the parameter $\hat{e}$. The other uncertain terms of the stiffness matrix, $\hat{K}_y$ and $\hat{K}_\theta$, are assumed fixed at one, i.e. the lateral and torsional stiffnesses of the system are taken as their nominal values.

2.5 Sensitivity analysis of nominally symmetric-plan systems

For a specified earthquake response or design spectrum, the earthquake response of a system with uncertain element stiffness depends on three parameters: $\bar{T}_y$, $\bar{\Omega}$, and $\hat{e}$. In order to understand how the response of a system with fixed $\bar{T}_y$ and $\bar{\Omega}$ depends on $\hat{e}$ which is uncertain, consider the normalized displacement of the system at distance r to the right of its CM. The Taylor expansion of $\hat{u}_r$, about $\hat{e} = 0$ is:

$$\hat{u}_r = 1 + \hat{e} \left. \frac{\partial \hat{u}_r}{\partial \hat{e}} \right|_{\hat{e}=0} \tag{9}$$

Equation (9), with all terms of $O(\hat{e}^2)$ and higher order dropped, represents the linearization of the system response in the neighborhood of $\hat{u}_r$ for $\hat{e} = 0$. The linear approximation given by Eq. (9) without the higher order terms is compared with the actual value of $\hat{u}_r$ in Figure 7. For normalized eccentricity $\hat{e}$ smaller than 0.05, the linearized solution provides a good estimate of the system response; however, the errors tend to be larger for systems with larger $\hat{e}$ and $\bar{\Omega}$ values somewhat less or larger than one. Because the probability of $\hat{e}$ exceeding 0.05 is small (Fig. 5), the linear approximation of Eq. (9) should provide a good estimate of $\hat{u}_r$.

The partial derivative, $|\partial \hat{u}_r / \partial \hat{e}|$, appearing in Eq. (9) is presented as a function of $\bar{T}_y$ and $\bar{\Omega}$ in Fig. 8a. For the selected earthquake design spectrum (Fig. 2), it is seen to be essentially independent of $\bar{T}_y$. Therefore, Eq. (9) indicates that the response $\hat{u}_r$ will be also insensitive to changes in $\bar{T}_y$. A cross-section of Fig. 8a at $T_y = 1.5$ sec. is presented in Fig. 8b, which shows that $|\partial \hat{u}_r / \partial \hat{e}|$ is largest near $\bar{\Omega} = 0.9$ and 1.1. For $\bar{\Omega}$ smaller than 0.9 and greater than 1.1 the derivative decreases steadily; between $\bar{\Omega} = 0.9$ and 1.1 it varies rapidly and changes sign just below

$\bar{\Omega} = 1$. This implies that the lateral earthquake response of nominally-symmetric systems with equal uncoupled lateral and torsional vibration periods would be increased very little because of uncertainty in the element stiffnesses. In fact, it can be analytically proven (Appendix A) that the response $\hat{u}_r$ of systems with $\bar{\Omega} = 1$ and $\hat{e} \ll 1$ does not depend on $\hat{e}$. Such is the case because the two natural periods and modes of vibration of the nominally-symmetric system with $\bar{\Omega} = 1$ are independent of $\hat{e}$. Consequently, the system response $\hat{u}_r$ does not depend on $\hat{e}$. However, systems with $\bar{\Omega}$ near 0.9 and 1.1 are expected to be most sensitive to the uncertainty in element stiffnesses.

Using the linear approximation of the system response given by Eq. (9), the PDF $f_{(\hat{u}_r)_o}$ of the normalized displacement $(\hat{u}_r)_o$ is obtained as follows. From Eq. (9) and using the fact that $|\partial \hat{u}_r/\partial \hat{e}|$ and $|\partial \hat{u}_{-r}/\partial \hat{e}|$ are equal in a symmetric system (Fig. 8b), $(\hat{u}_r)_o$ can be expressed as

$$(\hat{u}_r)_o = 1 + \ |\hat{e}||\partial \hat{u}_r/\partial \hat{e}| \tag{10}$$

Equation (10) shows that $(\hat{u}_r)_o$, as mentioned earlier, will always be greater than one. The probability of $(\hat{u}_r)_o$ being less than a response level β_u is

$$P((\hat{u}_r)_o \leq \beta_u) = P(\frac{|\hat{e}|}{\sigma_{\hat{e}}} \leq \frac{\beta_u - 1}{\sigma_{\hat{e}}|\partial \hat{u}_r/\partial \hat{e}|}) = 2\ \Phi(\frac{\beta_u - 1}{\sigma_{\hat{e}}|\partial \hat{u}_r/\partial \hat{e}|}) \ - 1 \tag{11}$$

where $\Phi(\cdot)$ represents the well known CDF of the standard normal distribution. Equation (11) represents the CDF of $(\hat{u}_r)_o$ and it was computed using the fact that $\hat{u}_r$ is normally distributed because it is a linear function of $\hat{e}$ (Eq. (9)). Differentiating Eq. (11) with respect to β_u we obtain

$$f_{(\hat{u}_r)_o} = \sqrt{\frac{2}{\pi}} \frac{1}{\sigma_{\hat{e}}\ |\partial \hat{u}_r/\partial \hat{e}|}\ \ exp\{-\frac{1}{2}(\frac{\beta_u - 1}{\sigma_{\hat{e}}|\partial \hat{u}_r/\partial \hat{e}|})^2\},\ \ \beta_u \geq 1 \tag{12}$$

The PDF given by Eq. (12) is a one-sided normal distribution scaled by a factor of two and with the origin shifted to one. The mean and standard deviation of $(\hat{u}_r)_o$, computed from Eq. (12) are

$$\mu_{(\hat{u}_r)_o} = 1 + \frac{\sqrt{2}}{\sqrt{\pi}} \sigma_{\hat{e}}\ |\partial \hat{u}_r/\partial \hat{e}| \tag{13}$$

and

$$\sigma_{(\hat{u}_r)_o} = \sqrt{1 + \frac{2}{\pi}}\ \sigma_{\hat{e}}\ |\partial \hat{u}_r/\partial \hat{e}| \tag{14}$$

These equations show that the mean and standard deviation of $(\hat{u}_r)_o$ depend not only on the magnitude of the element stiffness uncertainty, characterized by $\sigma_{\hat{e}}$, but also on the magnitude of $|\partial \hat{u}_r/\partial \hat{e}|$ which is a measure of how sensitive the system response is to eccentricity. Thus, larger values of $\sigma_{\hat{e}}$ and $|\partial \hat{u}_r/\partial \hat{e}|$ imply larger mean and standard deviation for the PDF of $(\hat{u}_r)_o$, and hence greater increase in the lateral response due to "accidental" torsion.

Figure 9 presents the PDF of Eq. (12) for a R/C system with $\bar{T}_y = 1.5$ sec., $\bar{\Omega} = 1.25$, and $N = 8$, which was computed using the values of $\sigma_{\hat{e}}$ and $|\partial \hat{u}_r / \partial \hat{e}|$ obtained from Figs. 4 and 8b, respectively. Also shown is the result of Fig. 3 which was obtained by the Monte Carlo simulation procedure. The agreement observed between the analytical and simulated PDF's is particularly good in this case because Eq. (9) is accurate for $\bar{\Omega} = 1.25$ (Fig. 7).

The values of the normalized displacements $(\hat{u}_r)_o$, corresponding to probabilities of exceedance $p = 0.5, 0.3, 0.15,$, and 0.05 are shown in Fig. 10 for systems with $\bar{T}_y = 1.5$ sec. and $N = 8$. These results, obtained by solving for β_u in Eq. (11) for the selected levels of p, show that the increase in $(\hat{u}_r)_o$ due to accidental torsion is relatively small, specially in steel buildings; e.g. for a exceedance probability 0.15 this increase is less than 15% and 10% for R/C and steel buildings, respectively.

2.6 Increased response due to stiffness uncertainty

Presented in this section are results of Monte Carlo simulations performed to study the increase in system deformations as a consequence of the accidental torsion induced by uncertainty in stiffnesses of resisting elements. As mentioned earlier, 2000 simulations were carried out for each nominally symmetric system with particular values of parameters $\bar{T}_y$ and $\bar{\Omega}$.

Figure 11 presents the normalized response $(\hat{u}_r)_o$ for various exceedance probabilities p, obtained by Monte Carlo simulation and from the linearized analytical result of Eq. (9); the latter were presented earlier in Fig. 10. It is apparent that the analytical results are a good approximation to the simulation results, especially for values of $\bar{\Omega}$ outside the interval $0.9 \leq \bar{\Omega} \leq 1.1$. As mentioned earlier, the linearization of response with respect to $\hat{e}$ (Eq. 9) is less accurate in this interval of $\bar{\Omega}$, where the sensitivity of the response varies rapidly with $\bar{\Omega}$ (Fig. 8b). The analytical results tend to overestimate the increased response of the system due to accidental torsion.

The mean value of $(\hat{u}_r)_o$ obtained by Monte Carlo simulation is shown in Figs. 12 and 13 for a wide range of system parameters $\bar{T}_y$ and $\bar{\Omega}$. Results are presented for R/C and steel systems with 2, 4, 8, and 12 resisting planes. These figures show that for the earthquake design spectrum considered, the mean values of $(\hat{u}_r)_o$ are insensitive to the uncoupled lateral vibration period $\bar{T}_y$ of the nominally-symmetric system; an exception to this observation are systems in the acceleration sensitive region of the design spectrum with values of $\bar{\Omega}$ near 1.1. This observation is consistent with the fact that the partial derivative of the response with respect to $\hat{e}$ was also insensitive to $\bar{T}_y$ (Fig. 8a). As expected, the increase in response due to accidental torsion induced by uncertainty

in element stiffnesses is much smaller for steel buildings compared to R/C buildings (Figs. 12 and 13). This is a direct consequence of the smaller coefficient of variation in the stiffnesses of steel resisting elements. The increase in response due to accidental torsion is less for systems with larger number of resisting elements. This can be noted by studying Figs. 12 and 13, but is clearly observed in Fig. 14 where each curve corresponds to a cross section of the surfaces of Figs. 12 and 13 at $\bar{T}_y = 1.5$ sec. As mentioned earlier, when N increases, more elements are distributed over the building plan which decreases the chances of generating large eccentricities due to uncertainty in element stiffnesses (Fig. 5).

The mean values of $(\hat{u}_{b/2})_o$, the larger of the displacements at the two edges of the system plan are shown in Figs. 15 and 16 for R/C and steel buildings, respectively. Results are presented for systems with uncoupled lateral period $\bar{T}_y = 1.5$ sec. , two different plan aspect ratios ($b/a = 1$, and $b/a = \infty$), and $N = 2, 4, 8$, and 12. These results demonstrate that systems with their transverse plan dimension perpendicular much longer than the dimension along the direction of ground motion ($b/a = \infty$) are affected more by accidental torsion due to stiffness uncertainty than buildings with square plans ($b/a = 1$). For example, the largest (over all $\bar{\Omega}$ considered) increase in the response of a R/C building with $\bar{T}_y = 1.5$ sec. and $N = 8$, is about eight percent if the building has a square plan $b/a = 1$ and fourteen percent for buildings with long plan dimension in the transverse direction. In general, the increase in response of steel buildings due to accidental torsion is about 60% of the increase in response for R/C buildings with the same properties.

Figures 17 and 18 show the values of $(\hat{u}_{b/2})_o$ for different probabilities of exceedance $p = 0.5, 0.3, 0.15$, and 0.05. Results are presented for systems with uncoupled lateral vibration period $\bar{T}_y = 1.5$ sec. , two different plan aspect ratios ($b/a = 1$, and $b/a = \infty$), and $N = 8$. The mean values of $(\hat{u}_{b/2})_o$ obtained previously (Figs. 15 and 16) are presented again as a reference, and are seen to correspond to probabilities of exceedance of 0.4 or less. Therefore, it seems reasonable to use the mean values of $(\hat{u}_{b/2})_o$ to consider the effects of stiffness uncertainty for design purposes. These figures show also that even for rather small probabilities of exceedance such as 0.15, the largest (over all $\bar{\Omega}$ considered) increase in deformation is about 15% and 9% for R/C and steel buildings, respectively.

2.7 Sensitivity analysis of asymmetric-plan buildings

So far, the effects of stiffness uncertainty have been considered only for nominally-symmetric buildings. If the plan-wise distribution of stiffness—based on nominal values—is asymmetric, the equations of motion of the system are:

$$\begin{bmatrix} m & 0 \\ 0 & m \end{bmatrix} \begin{Bmatrix} \ddot{u}_y \\ r\ddot{u}_\theta \end{Bmatrix} + \begin{bmatrix} \bar{K}_y & \bar{K}_y \hat{e}_s \\ \bar{K}_y \hat{e}_s & \bar{K}_\theta / r^2 \end{bmatrix} \begin{Bmatrix} u_y \\ r u_\theta \end{Bmatrix} = \begin{Bmatrix} -m \\ 0 \end{Bmatrix} a_{gy}(t) \tag{15}$$

Comparison with Eq. (1) indicates that, because of plan-asymmetry the stiffness matrix includes an off-diagonal coupling term involving $\hat{e}_s = e_s/r$, where e_s is the nominal static eccentricity of the building:

$$e_s = \frac{\sum_{i=1}^{N} \bar{k}_{yi} x_i}{\sum_{i=1}^{N} \bar{k}_{yi}} \tag{16}$$

where $\bar{k}_{yi}$ are the nominal values of the combined lateral stiffnesses of all structural elements along the i^{th} resisting plane. If the stiffnesses of the structural elements of the asymmetric-plan system are uncertain, the equations of motion are still given by Eq. (4), but the mean value of $\hat{e}$ is now $\hat{e}_s$, in contrast to zero for the nominally-symmetric case.

Consider again the normalized lateral displacement $\hat{u}_r$ of the system at distance r to the right of its CM. However, let $\hat{u}_r$ be normalized this time with respect to the displacement $\bar{u}_r$ at the same location of the asymmetric system with nominal values of stiffness; this system is governed by Eq. (15). Also let $\hat{e}$ be the actual normalized static eccentricity of the system with uncertain element stiffnesses. Expanding $\hat{u}_r$ in a Taylor series about the system response corresponding to $\hat{e} = \hat{e}_s$ and ignoring terms with order higher than linear leads to:

$$\hat{u}_r = 1 + (\hat{e} - \hat{e}_s) \left. \frac{\partial \hat{u}_r}{\partial \hat{e}} \right|_{\hat{e} = \hat{e}_s} \tag{17}$$

Equation (17) represents linearization of the system response in the neighborhood of $\hat{e} = \hat{e}_s$. The PDF of $\hat{u}_r$ is normal because Eq. (17) is a linear function of the normal variable $(\hat{e} - \hat{e}_s)$. In particular, the response $\hat{u}_r$ has unit mean and standard deviation equal to $\sigma_{\hat{e}} \, |\partial \hat{u}_r / \partial \hat{e}|$, where $\sigma_{\hat{e}}$ is the same as in the nominally-symmetric plan case (Fig. 4). This implies that differences between the normalized responses $\hat{u}_r$ of symmetric and asymmetric systems are only due to differences in $|\partial \hat{u}_r / \partial \hat{e}|$ in these two cases.

As mentioned earlier, $|\partial \hat{u}_r / \partial \hat{e}|$ is a measure of how sensitive the system response is to eccentricity. This measure is determined analytically from the exact solution of Eq. (15) for systems

with lateral vibration period $\bar{T}_y = 1.5$ sec. and is plotted against $\bar{\Omega}$ in Fig. 19 for several values of the normalized nominal static eccentricity $\hat{e}_s$. The results for nominally symmetric buildings, i.e. $\hat{e}_s = 0$, are obviously the same as in Fig. 8. It is seen that, for most values of $\bar{\Omega}$, $|\partial \hat{u}_r / \partial \hat{e}|$ is larger for nominally symmetric-plan systems compared to asymmetric-plan systems. This observation implies that the normalized response $\hat{u}_r$ will tend to be larger, ,i.e., the increase in response $(u_r)_o$ due to uncertainty in element stiffnesses would be larger, for nominally symmetric systems.

Figure 20 shows the PDF of $(\hat{u}_r)_o$, obtained by Monte Carlo simulation on a R/C system with $\bar{T}_y = 1.5$ sec., $\bar{\Omega} = 1.25$, $N = 8$, and several values of static eccentricity. Increase in the nominal eccentricity $\hat{e}_s$ has two effects: the PDF moves to the left, and it gets narrower in most cases, i.e. the mean value of the normalized response $(\hat{u}_r)_o$ decreases and the standard deviation of $(\hat{u}_r)_o$ also decreases. The probabilities of $(\hat{u}_r)_o$ exceeding specified response values, computed from the PDF's of Fig. 20a, are presented in Fig. 20b. It is apparent that, for a fixed probability of exceedance, the largest increase in response due to stiffness uncertainty would occur in nominally symmetric systems ($\hat{e}_s = 0$). Alternatively, the probability of the normalized response $(\hat{u}_r)_o$ exceeding a level β_u is largest for nominally symmetric system.

2.8 Implications for design

We now determine the eccentricity e_d relative to the center of mass at which the equivalent static lateral force or base shear, V, for a nominally symmetric building should be applied to account for the accidental torsion arising from uncertainty in element stiffnesses. The resulting displacement at the edge of the building plan should equal the dynamic response $(u_{b/2})_o$ determined earlier. Thus,

$$(u_{b/2})_o = \frac{V}{\bar{K}_y} + \frac{V e_d}{\bar{K}_\theta} \frac{b}{2} \tag{18}$$

Noting that the earthquake induced base shear V and deformation u_o of the nominally -symmetric system are related through $V = \bar{K}_y u_o$, and that $\bar{\Omega} = \sqrt{\bar{K}_\theta / \bar{K}_y r^2}$ is the ratio of the uncoupled lateral and torsional vibration periods of the nominally-symmetric system, Eq. (18) can be rewritten as

$$\frac{e_d}{b} = [(\hat{u}_{b/2})_o - 1] \, \bar{\Omega} \, 2(\frac{r}{b})^2 \tag{19}$$

where, as defined earlier, $(\hat{u}_{b/2})_o = (u_{b/2})_o / u_o$ and the ratio r/b depends on the plan aspect ratio a/b.

Equation (19) relates the design eccentricity e_d to the displacement $(u_{b/2})_o$ at the edge of the building plan. The mean values of $(u_{b/2})_o$ were presented in Figs. 15 and 16 for concrete and steel

systems, respectively, for two extreme values of the plan aspect ratio: $b/a = 1$ and $b/a = \infty$. With $(u_{b/2})_o$ known from Figs. 15 and 16, the normalized design eccentricity e_d/b is determined using Eq. (19) and presented as function of $\bar{\Omega}$ for systems with N resisting planes in the direction of the ground motion; N has been varied as 2, 4, 8 and 12 (Fig. 21). It is seen that the design eccentricity increases with $\bar{\Omega}$ up to $\bar{\Omega} \simeq 0.9$, has a minimum value just below $\bar{\Omega} = 1$, increases up to $\bar{\Omega} \simeq 1.2$, and then remains essentially constant for $\bar{\Omega} \geq 1.2$. The design eccentricity e_d for systems with eight resisting elements [1] is less than 4% and 2% of the plan dimension for R/C and steel systems, respectively.

The Uniform Building Code specifies an accidental eccentricity of $0.05b$ independent of the period ratio $\bar{\Omega}$. The corresponding value of $(u_{b/2})_o$ is determined from Eq. (19) and presented in Fig. 22 for the two extreme values of the plan aspect ratio: $b/a = 1$, and $b/a = \infty$. For comparison, the value of $(u_{b/2})_o$ considering accidental torsion due to stiffness uncertainty, presented earlier in Fig. 15, is repeated in Fig. 22. These are smaller than the code values over a wide range of period ratios. The code values are especially large for torsionally-flexible systems with smaller $\bar{\Omega}$, and are significantly larger in the practical range of $\bar{\Omega} = 0.8$ to 1.25.

2.9 Conclusions

Accidental torsion occurs in elastic response of buildings due to uncertainty in the stiffness distribution, uncertainty in the mass distribution, foundation rotation, and other sources of torsion not considered explicitly in analysis. This investigation of accidental torsion in buildings due to one of these factors, uncertainty in structural element stiffnesses, has led to the following conclusions:

1. Uncertainty in stiffnesses of structural elements implies that the true values of lateral and torsional stiffnesses can not be predicted exactly, and that a nominally-symmetric system is really asymmetric to some unknown degree. The plan asymmetry introduces coupling between the lateral and torsional motions of the structure. This torsional coupling is the primary contributor to the increase in deformations of structural elements arising from stiffness uncertainty.

2. The increase in structural element deformations due to stiffness uncertainty is the largest under the assumption that stiffnesses of different resisting elements are statistically uncor-

[1] A sample of 50 buildings showed that the mean number of resisting frames in real structures was above seven, therefore, systems with $N = 8$ are considered in this study to represent real structures.

related. The results presented under this assumption overestimate building torsion due to stiffness uncertainty because some correlation will always exist among the actual element stiffnesses in a building.

3. The increase in response due to the accidental torsion caused by stiffness uncertainty is relatively insensitive to the uncoupled vibration period of the system $\bar{T}_y$. However, this increase is very sensitive to the value of the lateral to torsional period ratio $\bar{\Omega}$; it has local maxima at $\bar{\Omega} \simeq 0.9$ and $\bar{\Omega} \simeq 1.1$; decreases steadily for $\bar{\Omega}$ values less than 0.9 and greater than 1.1; and changes rapidly from its maxima at $\bar{\Omega} = 0.9$ and 1.1, to a minimum at $\bar{\Omega} \simeq 1$. Therefore, the increase in response of systems with $\bar{\Omega} \simeq 1$ due to stiffness uncertainty in small. This is a consequence of the fact that the response of such systems is insensitive to the introduction of stiffness eccentricity.

4. The increase in structural element deformations arising from accidental torsion due to stiffness uncertainty decreases with increasing number of laterally resisting planes. For buildings with eight resisting planes, a number representative of many practical structures, the mean values of structural element deformations increase by less than 10 and 5 percent, respectively, for R/C and steel buildings with square plans. These are the largest increases for systems with $\bar{\Omega} \simeq 0.9$ or 1.1; for other values of $\bar{\Omega}$ the increases are much smaller.

5. A sensitivity analysis of the building response with respect to the uncertainty in the element stiffnesses shows that the response of nominally symmetric-plan systems increases by a greater amount relative to asymmetric-plan systems.

6. The design accidental eccentricity e_d that accounts for the increase in the edge displacements due to accidental torsion, increases from zero at $\bar{\Omega} = 0$ to a maximum at $\bar{\Omega} \simeq 0.9$, decreases to a minimum at $\Omega \simeq 1$, increases to a maximum at $\Omega \simeq 1.2$, and then remains approximately constant for $\bar{\Omega} \geq 1.2$. In contrast, the accidental eccentricity of $0.05b$, or $0.01b$ specified in most building codes does not account for the dependence on $\bar{\Omega}$.

7. The mean value of the increase in structural deformations due to stiffness uncertainty is much smaller than implied by the accidental eccentricity of $0.05b$ or $0.01b$ specified in most building codes.

2.10 References

1. Newmark, N.M. and Hall, W.J. *Vibration of Structures Induced by Ground Motion.* Shock and Vibration Handbook, McGraw Hill Inc., New York, 2nd edition, 1976.

2. Ramsey, R., Mirza, S. and MacGregor, J.'Monte Carlo study of short time deflections of reinforced concrete beams', ACI Journal 76(8), 897-918, August 1979.

3. Ellingwood, B., Galambos, T., MacGregor, J. and Cornell, C.,'Development of a probability based load criterion for American National Standard A58, building code requirements for minimum design loads in buildings and other structures', Special Publication No. 577, National Bureau of Standards, Washington, D.C., June 1980.

4. Melchers, R.E. *Structural Reliability: Analysis and Prediction.* Ellis Horwood, Chichester, W. Sussex, England, 1987.

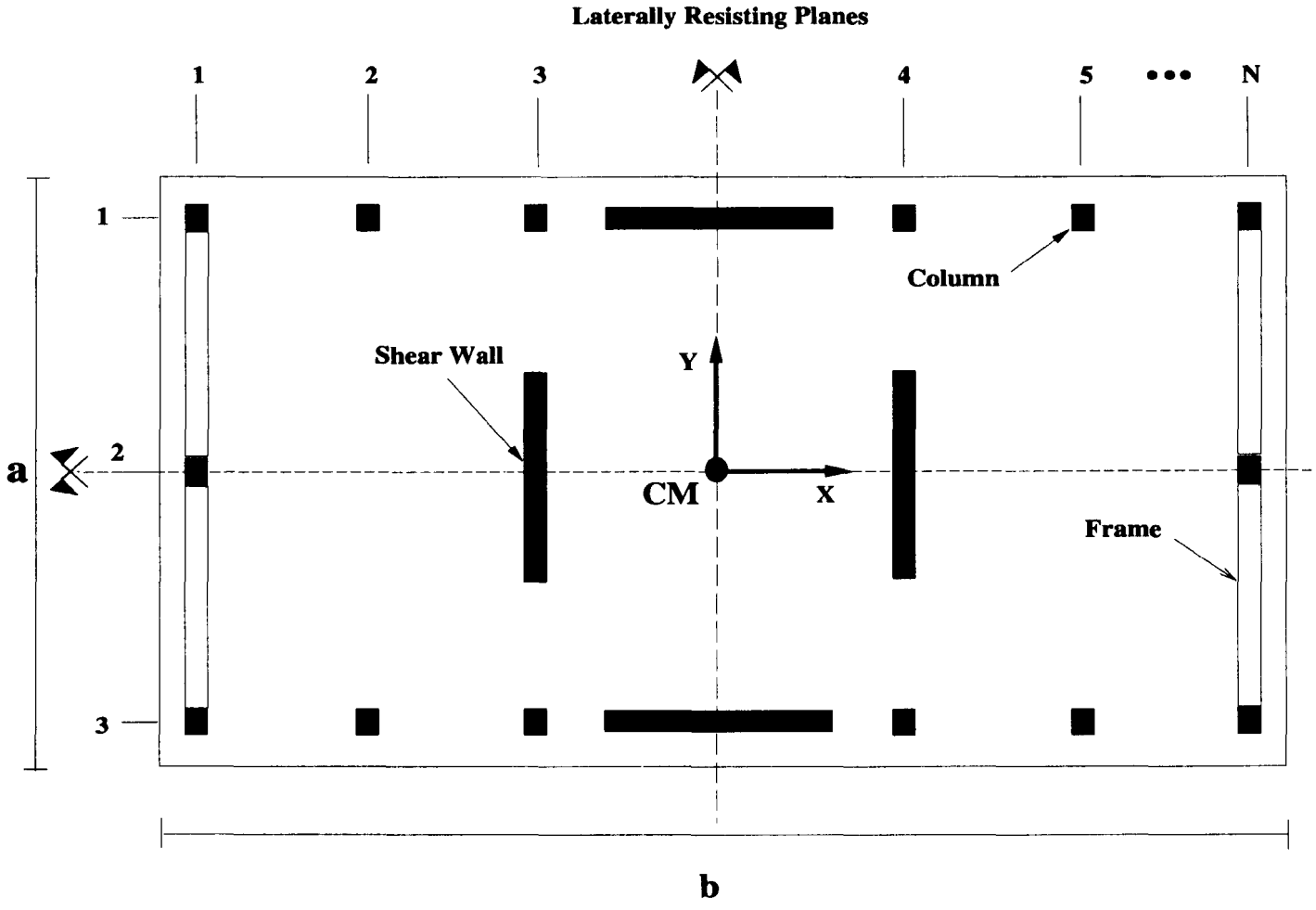

Figure 1 Plan of nominally–symmetric single–story system considered

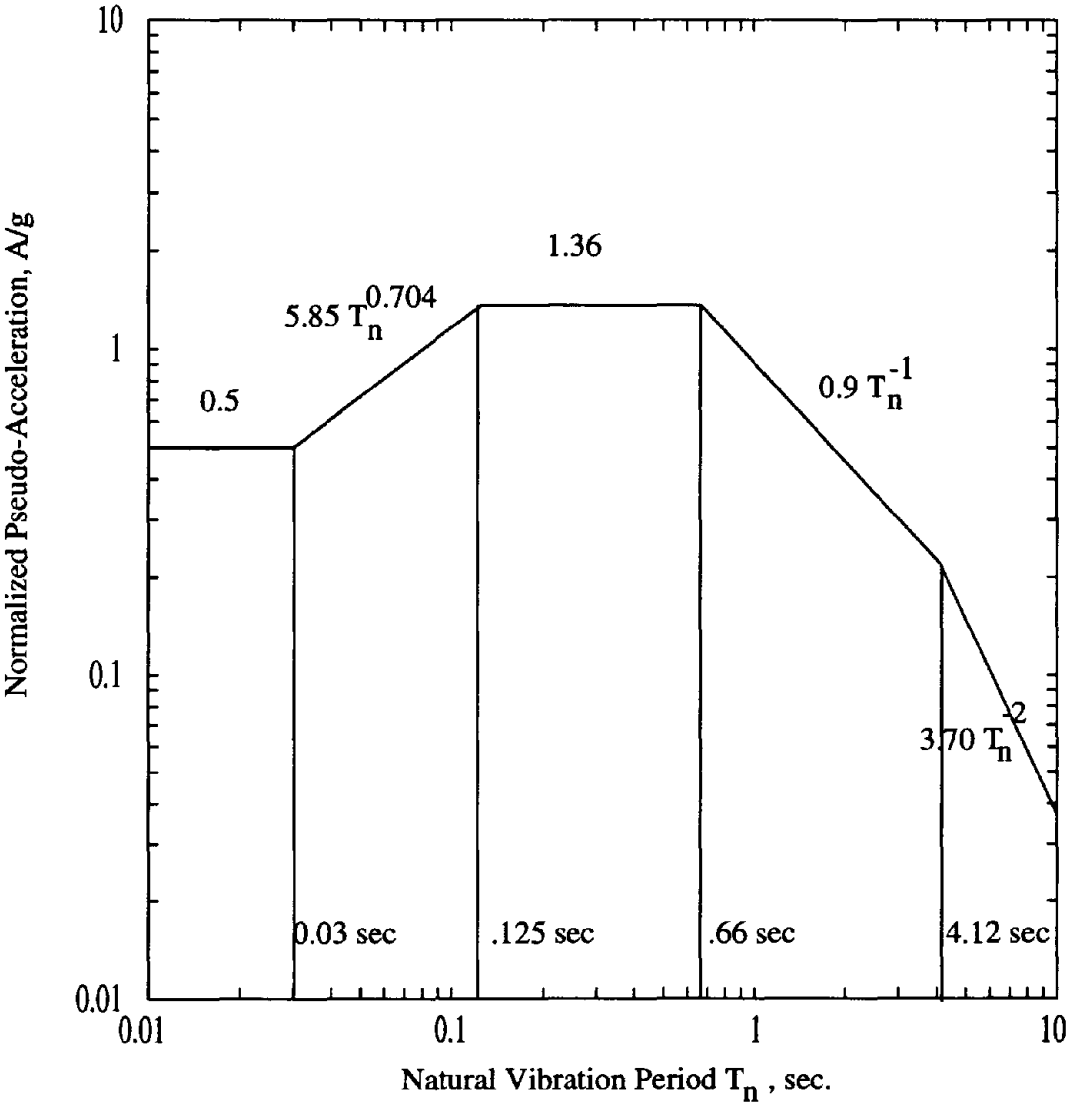

Figure 2 Design Spectrum

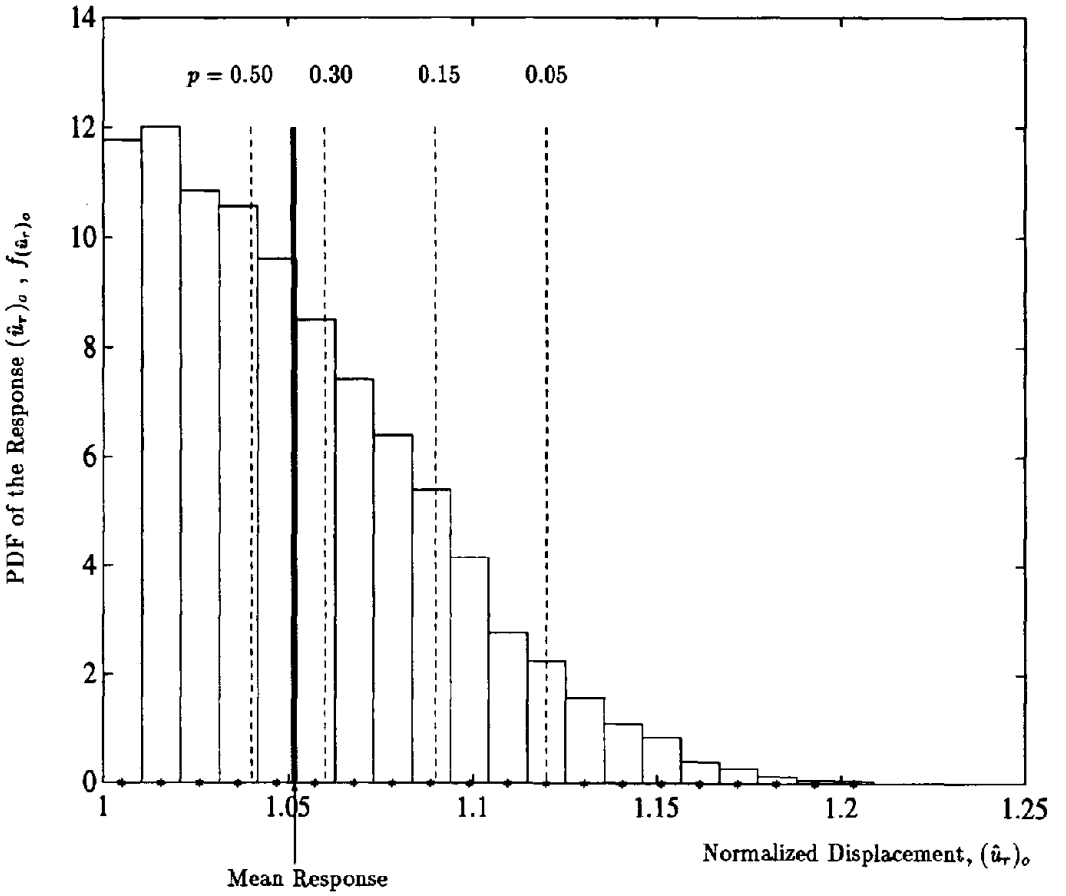

Figure 3 PDF of the response $(\hat{u}_r)_o$ of a R/C single story system with $\bar{T}_y = 1.5$ sec., $\bar{\Omega} = 1.25$, and $N = 8$

a) Concrete Structures

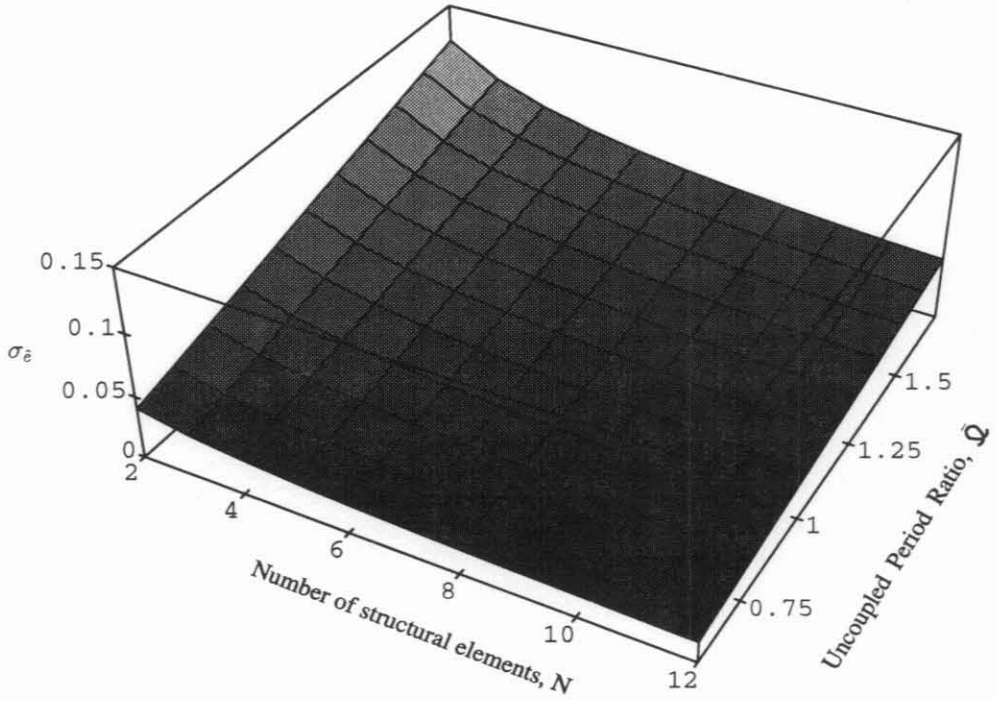

b) Steel Structures

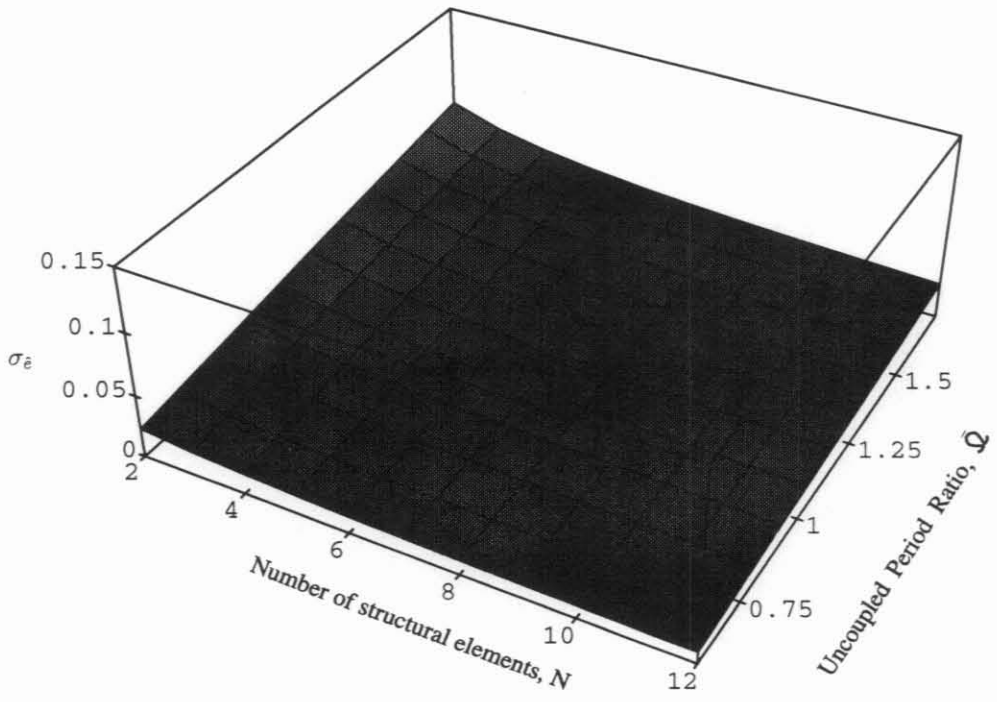

Figure 4 Variation of $\sigma_{\hat{e}}$, the standard deviation of the normalized static eccentricity, with system parameters N and $\bar{\Omega}$

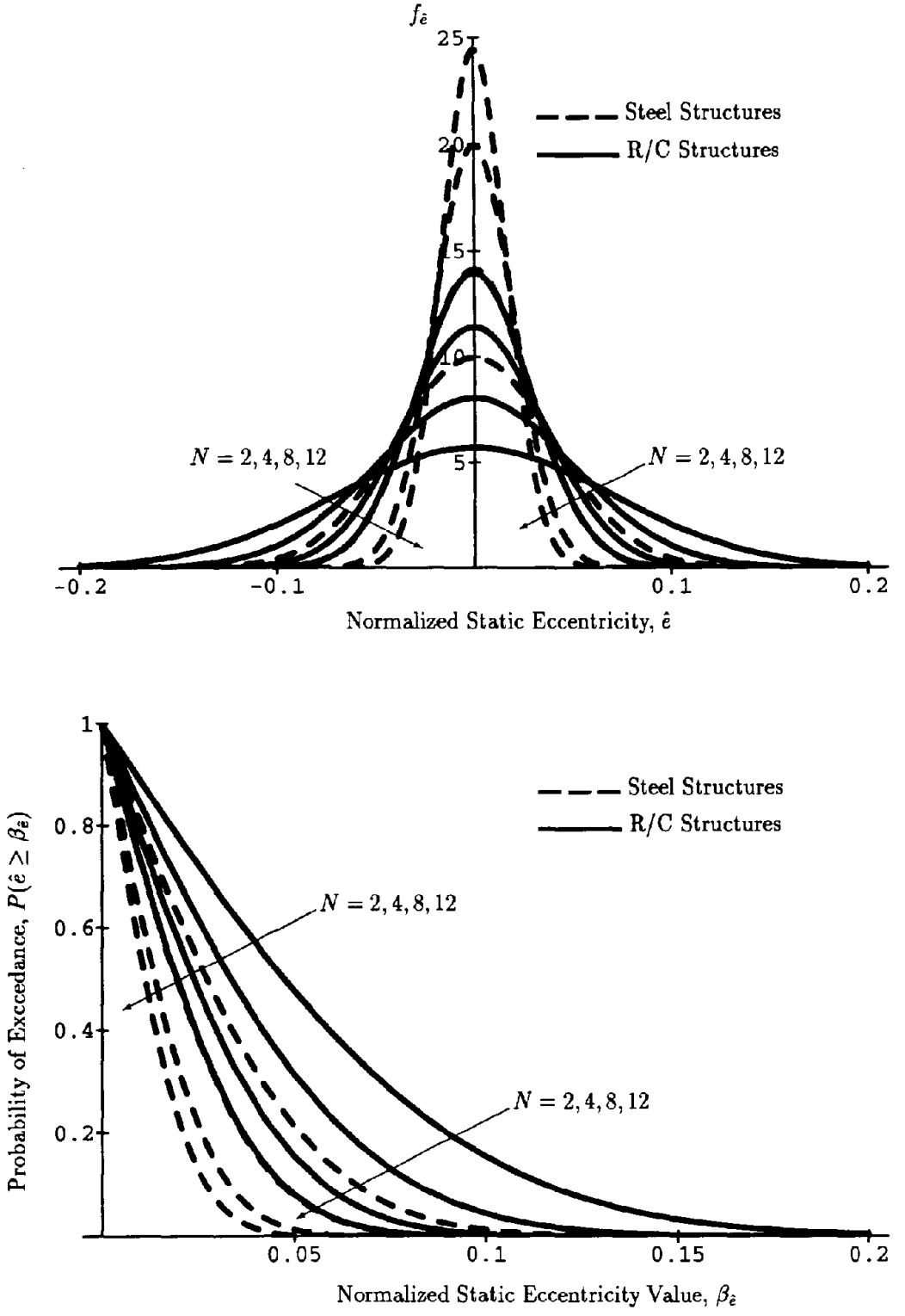

Figure 5 PDF and probabilities of exceedance of the normalized static eccentricity $\hat{e}$ for systems with N resisting elements; $N = 2, 4, 8$ or 12

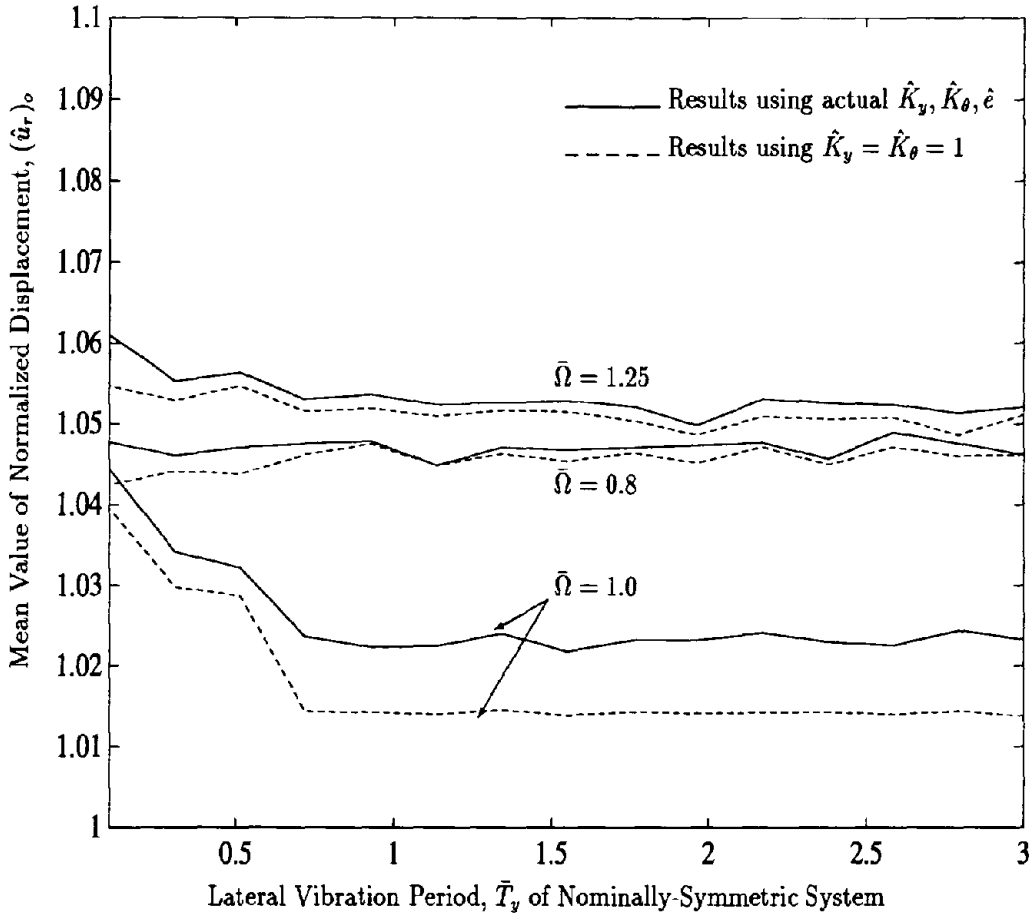

Figure 6 Comparison between the mean values of $(\hat{u}_r)_o$ computed by considering (1) all uncertain terms in the stiffness matrix: $\hat{K}_y$, $\hat{K}_\theta$, and $\hat{e}$, and (2) only the eccentricity $\hat{e}$ ($\hat{K}_y = \hat{K}_\theta = 1$)

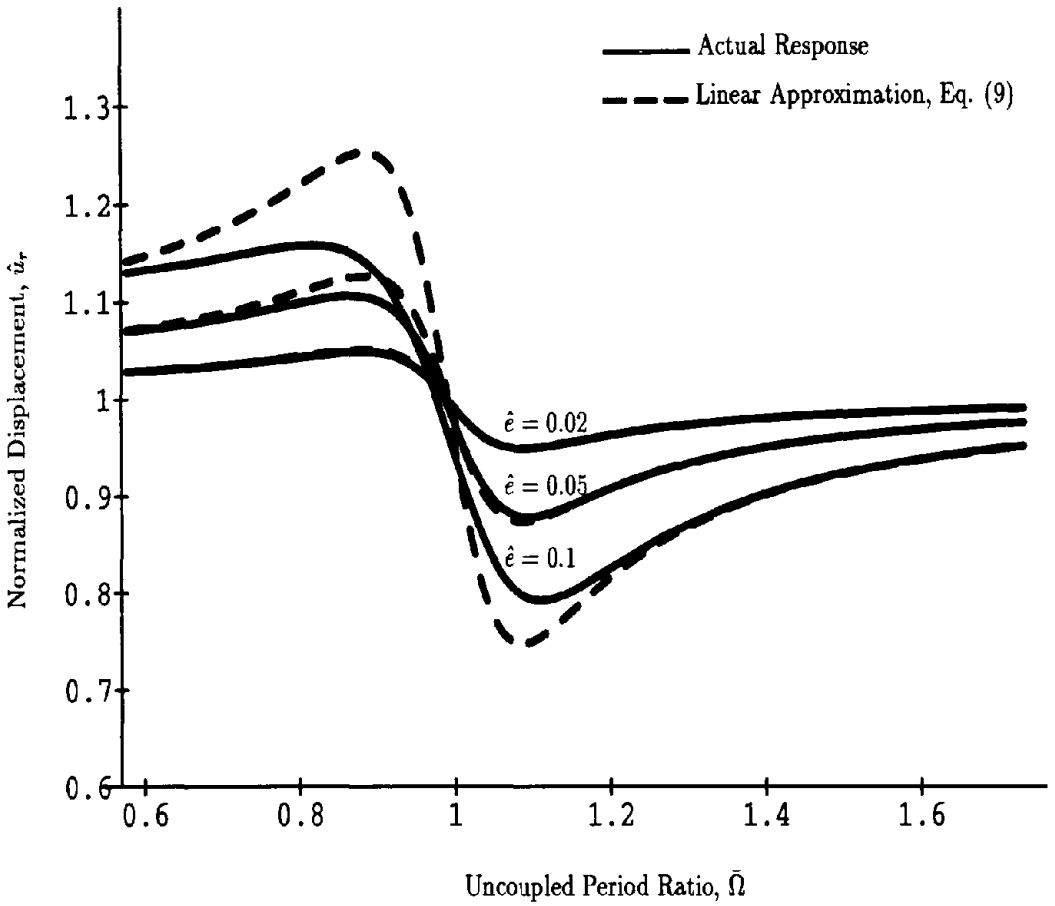

Figure 7 Evaluation of the accuracy of the linearization of the response around $\hat{u}_r$ for $\hat{e} = 0$ as a function of $\bar{\Omega}$ for three values of normalized static eccentricity $\hat{e}$ $\hat{e} = 0.02, 0.05$, and 0.1

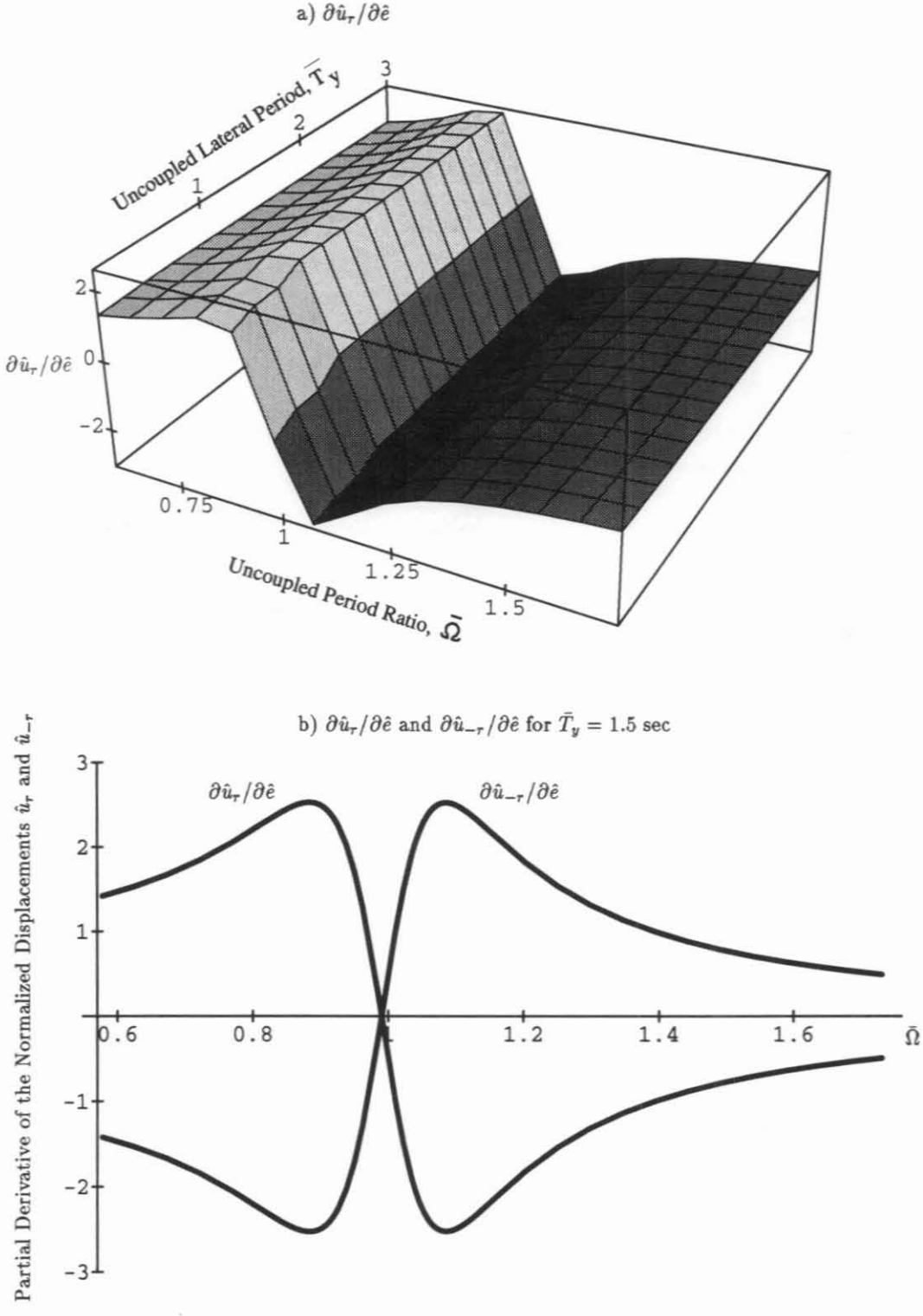

Figure 8 Variation of partial derivatives $\partial\hat{u}_r/\partial\hat{e}$ and $\partial\hat{u}_{-r}/\partial\hat{e}$ with $\bar{T}_y$ and $\bar{\Omega}$

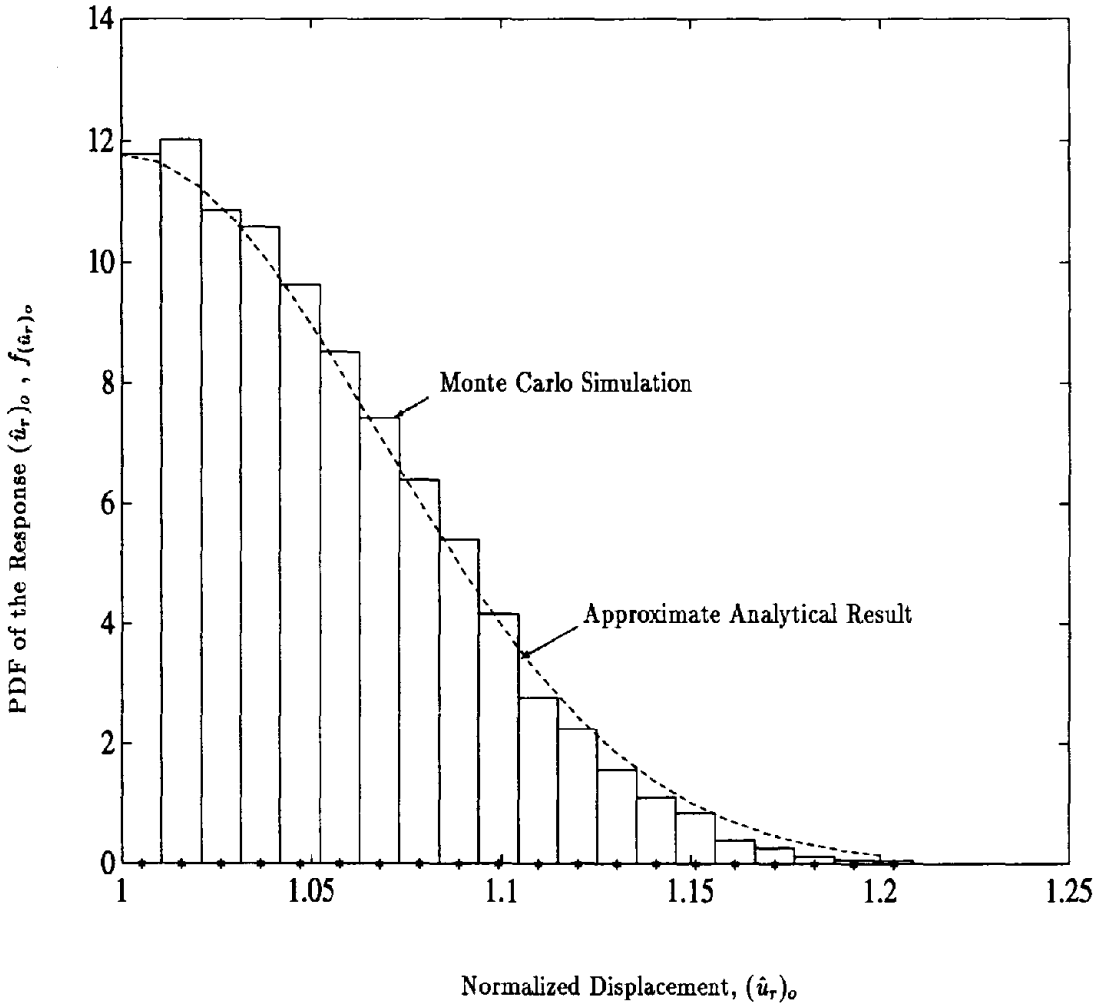

Figure 9 Probability density functions for $(\hat{u}_r)_o$ determined by (1) approximate analytical procedure and (2) Monte Carlo simulation

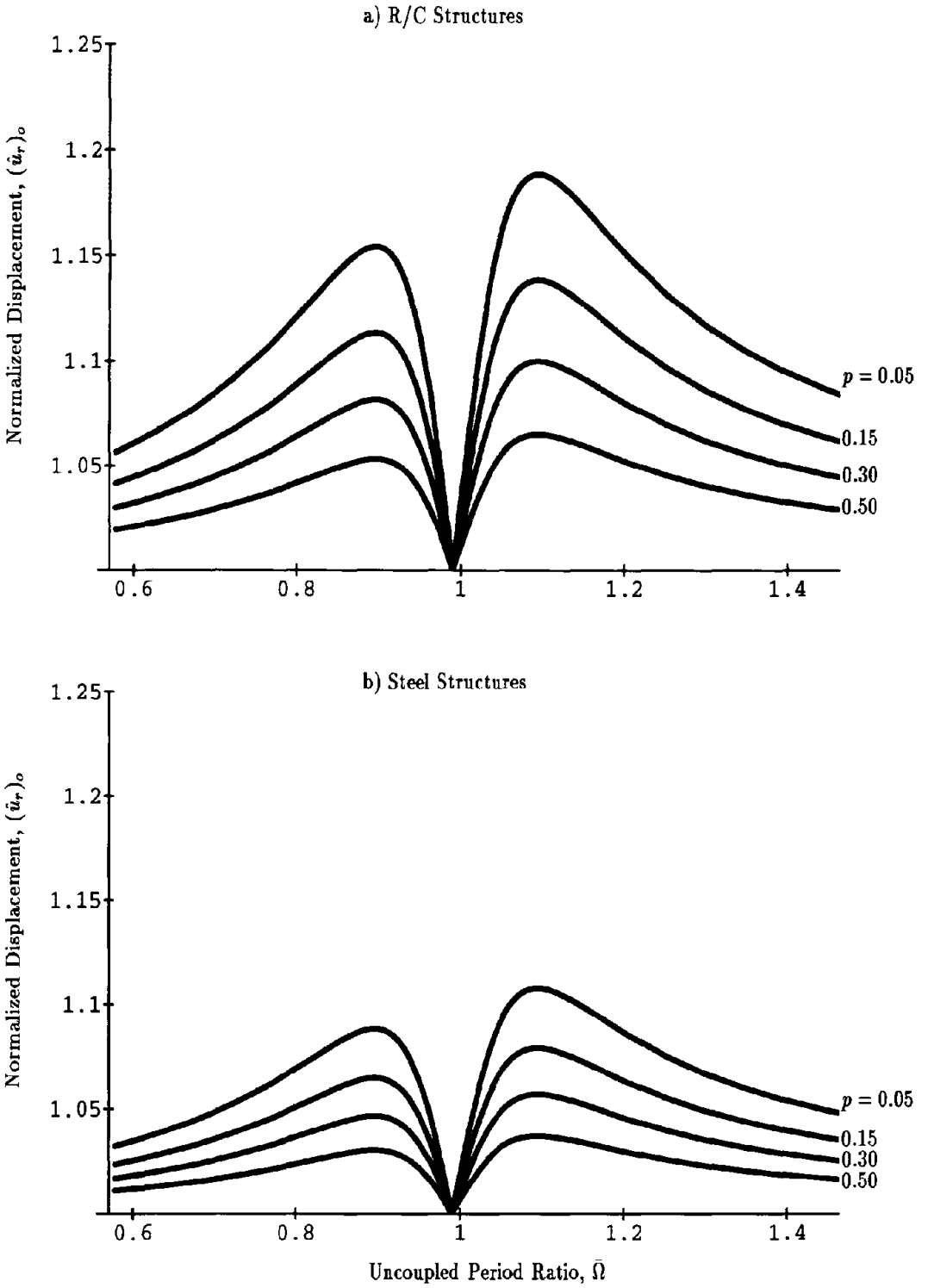

Figure 10 Normalized displacement $(u_r)_o$ corresponding to probability of exceedance $p = 0.5, 0.3, 0.15$ and 0.05 in R/C and steel structures using the approximate analytical solution

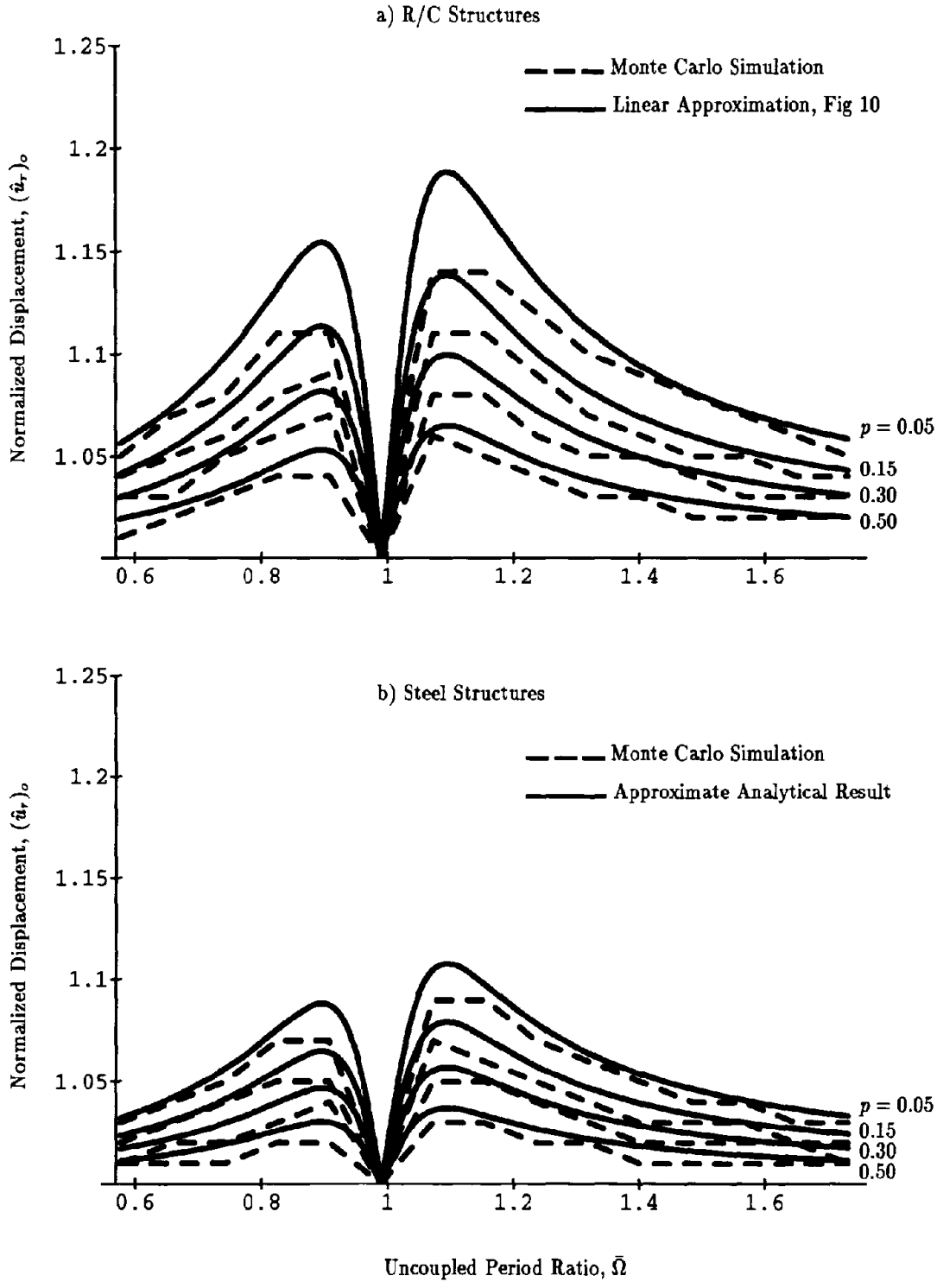

Figure 11 Comparison of the normalized displacement $(u_r)_o$ obtained by Monte Carlo simulation with the analytical results for different levels of probability of exceedance

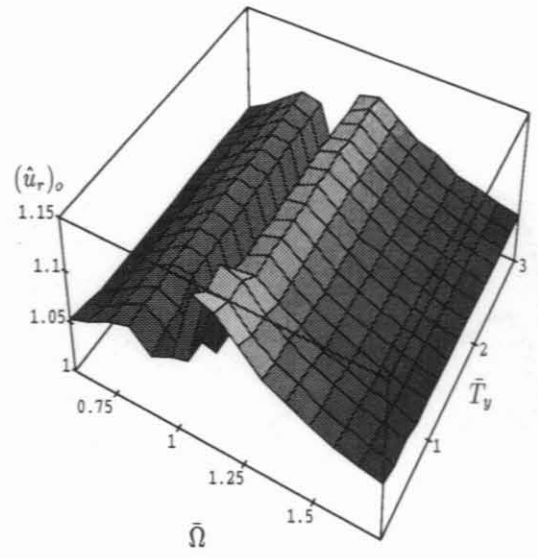

a) Number of resisting elements, $N = 2$

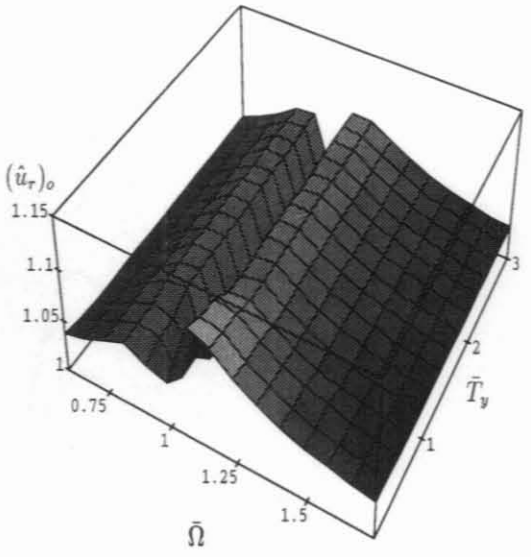

b) Number of resisting elements, $N = 4$

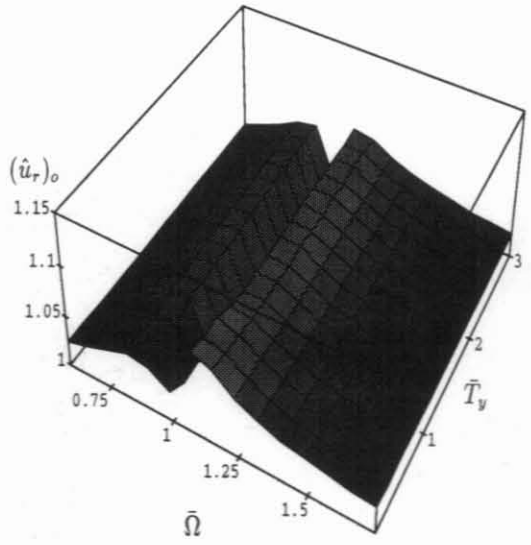

c) Number of resisting elements, $N = 8$

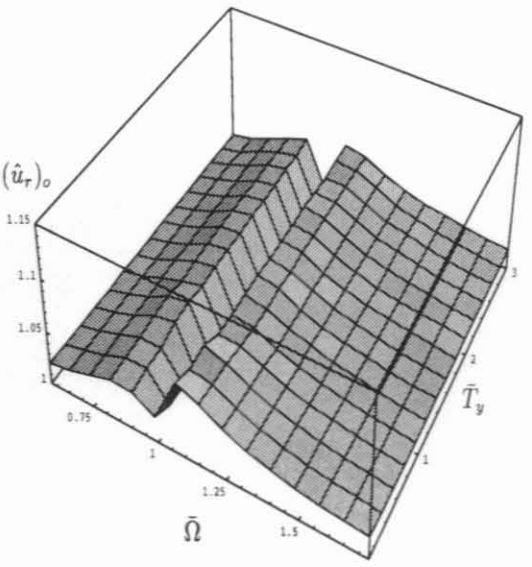

d) Number of resisting elements, $N = 12$

Figure 12 Mean values of the normalized response $(\hat{u}_r)_o$ of R/C structures obtained by Monte Carlo simulation for a wide range of parameters $\bar{T}_y$ and $\bar{\Omega}$ and systems with 2,4,6 or 8 resisting elements

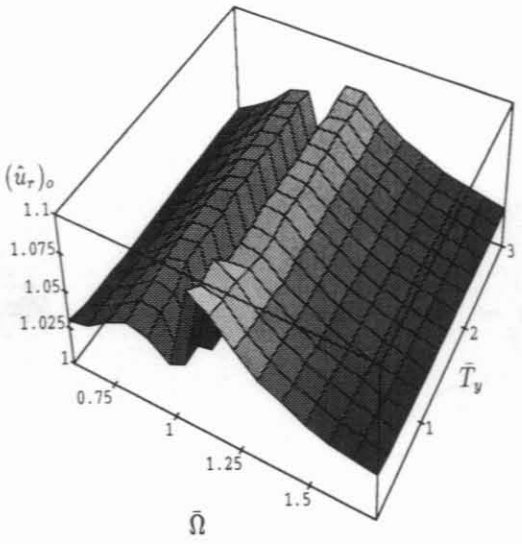

a) Number of resisting elements, $N = 2$

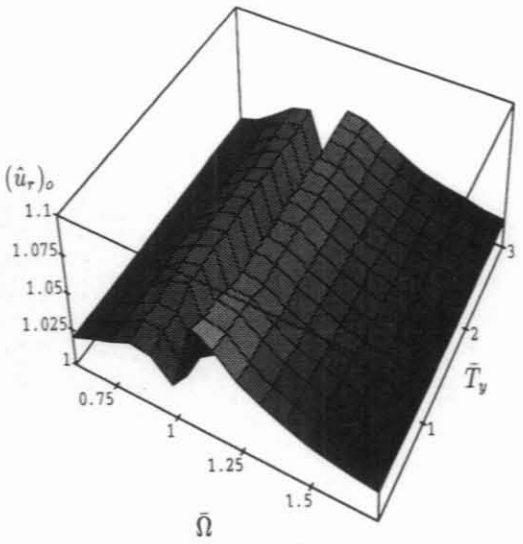

b) Number of resisting elements, $N = 4$

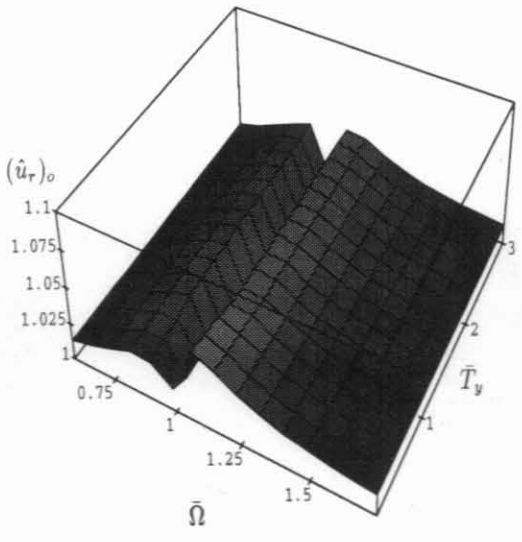

c) Number of resisting elements, $N = 8$

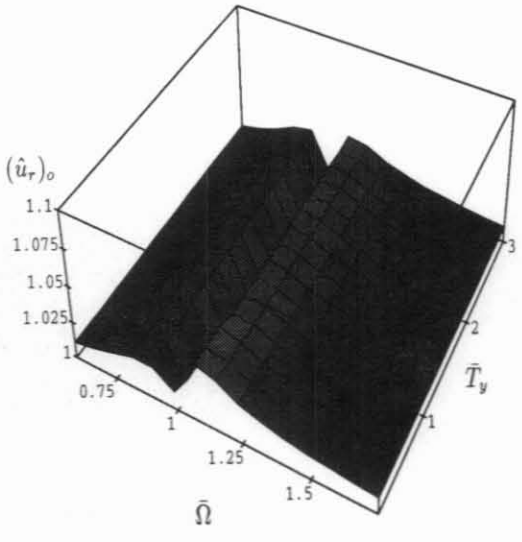

d) Number of resisting elements, $N = 12$

Figure 13 Mean values of the normalized response $(\hat{u}_r)_o$ of steel structures obtained by Monte Carlo simulation for a wide range of parameters $\bar{T}_y$ and $\bar{\Omega}$ and systems with 2,4,6 or 8 resisting elements

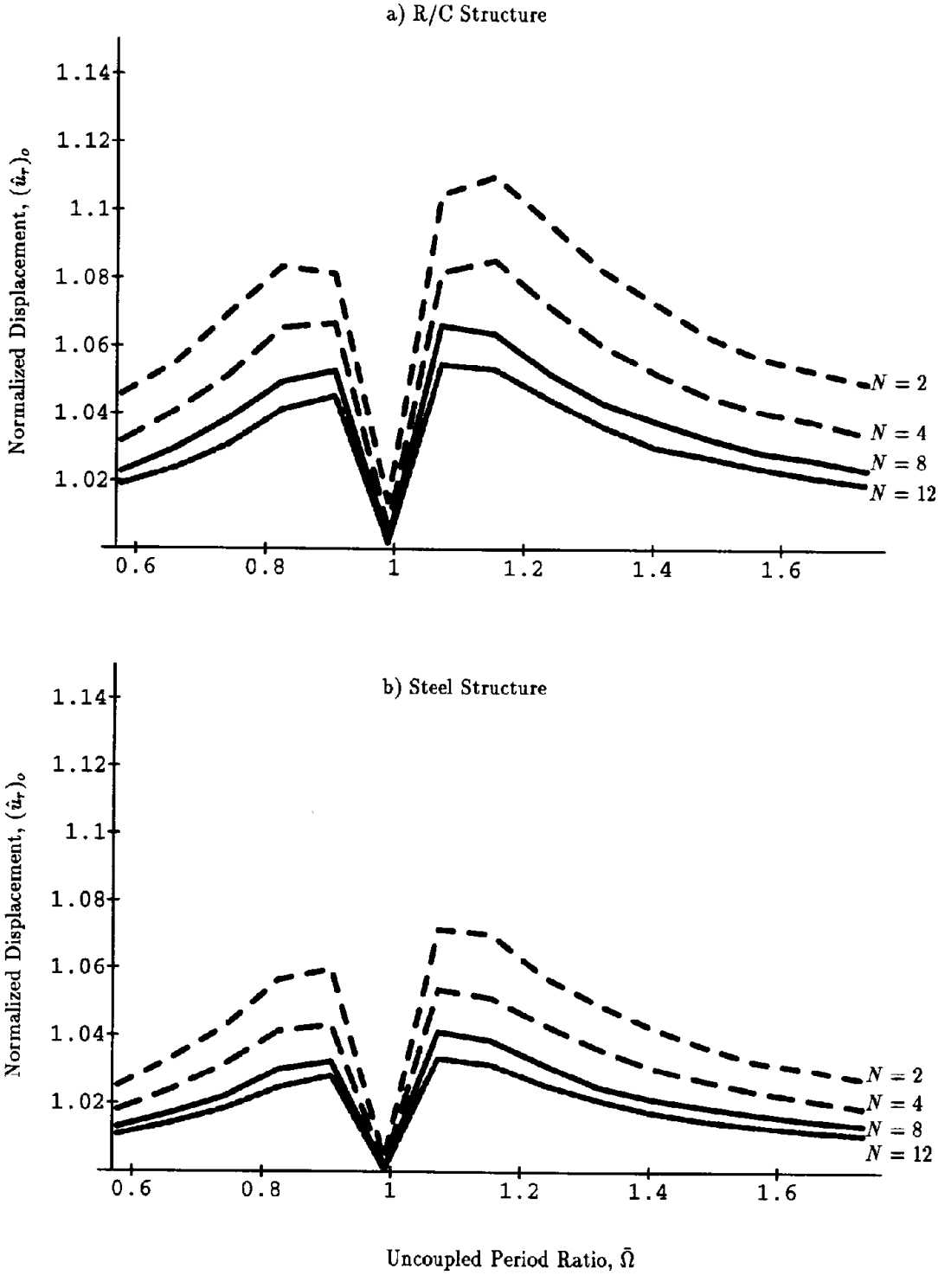

Figure 14 Mean values of the normalized response $(\hat{u}_r)_o$ obtained by Monte Carlo simulation for systems with $\bar{T}_y = 1.5$ sec and 2, 4, 8 or 12 resisting elements

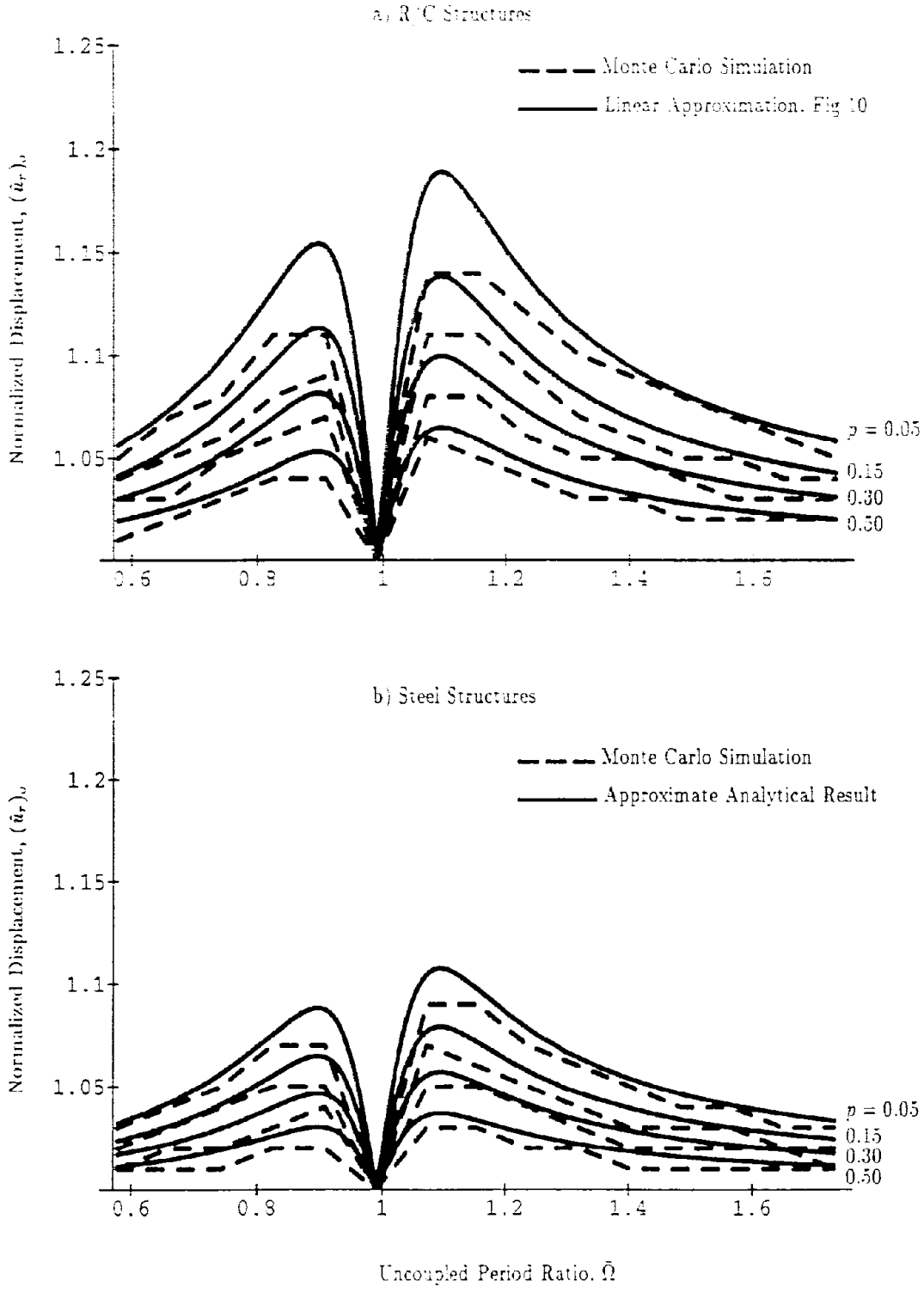

Figure 11 Comparison of the normalized displacement $(u_r)_o$ obtained by Monte Carlo simulation with the analytical results for different levels of probability of exceedance

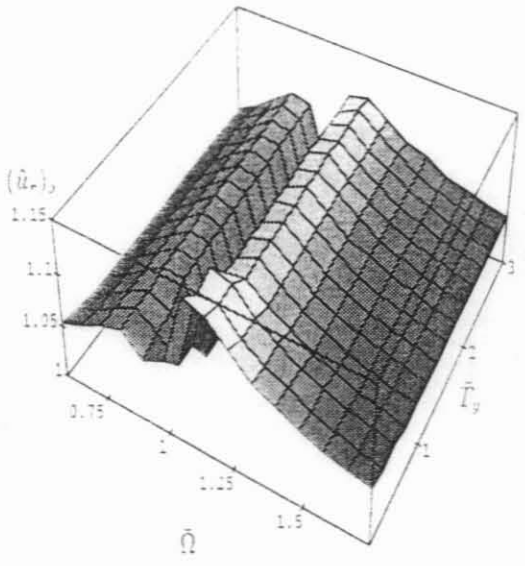

a) Number of resisting elements, $N = 2$

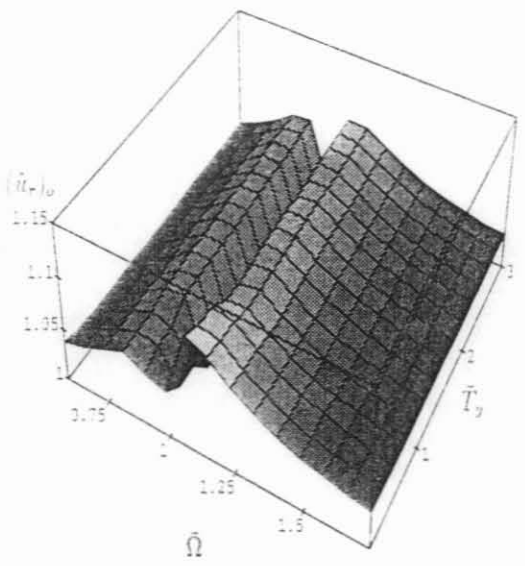

b) Number of resisting elements, $N = 4$

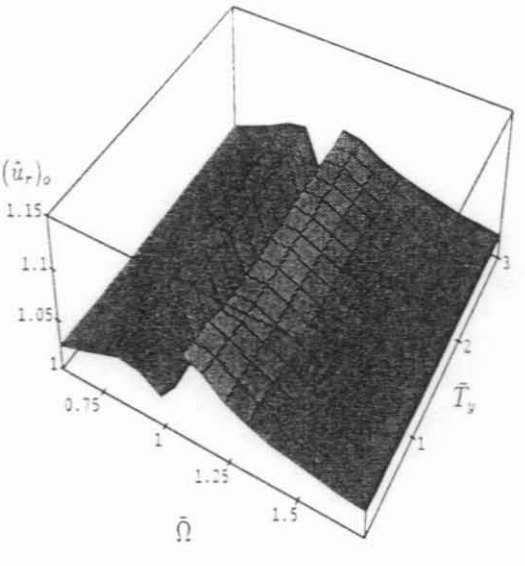

c) Number of resisting elements, $N = 8$

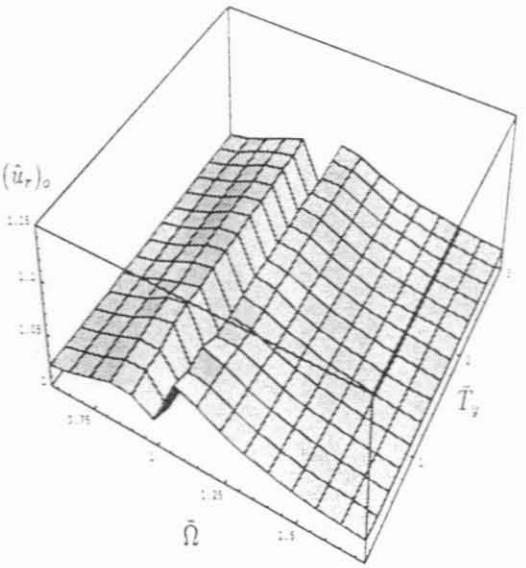

d) Number of resisting elements, $N = 12$

Figure 12 Mean values of the normalized response $(\hat{u}_r)_o$ of R/C structures obtained by Monte Carlo simulation for a wide range of parameters $\bar{T}_y$ and $\bar{\Omega}$ and systems with 2,4,6 or 8 resisting elements

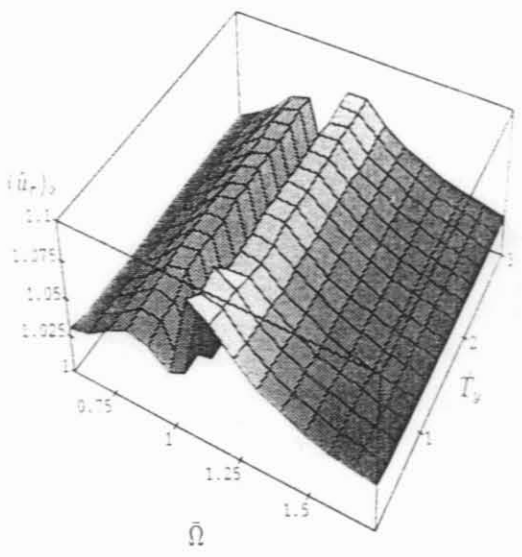

a) Number of resisting elements, $N = 2$

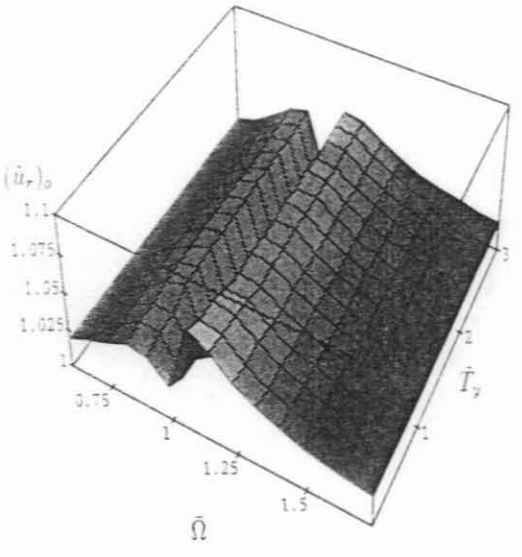

b) Number of resisting elements, $N = 4$

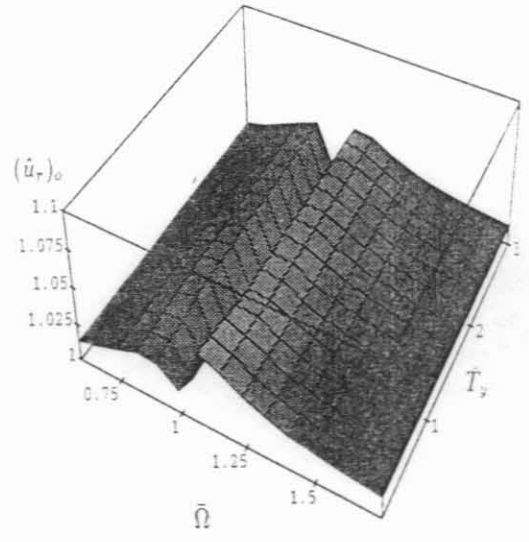

c) Number of resisting elements, $N = 8$

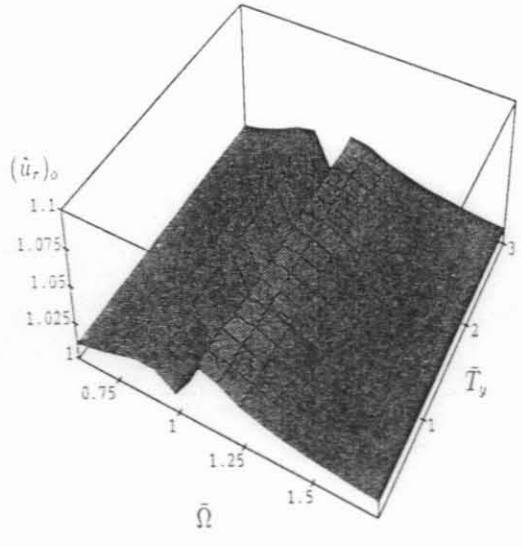

d) Number of resisting elements, $N = 12$

Figure 13 Mean values of the normalized response $(\hat{u}_r)_o$ of steel structures obtained by Monte Carlo simulation for a wide range of parameters $\bar{T}_y$ and $\bar{\Omega}$ and systems with 2,4,6 or 8 resisting elements

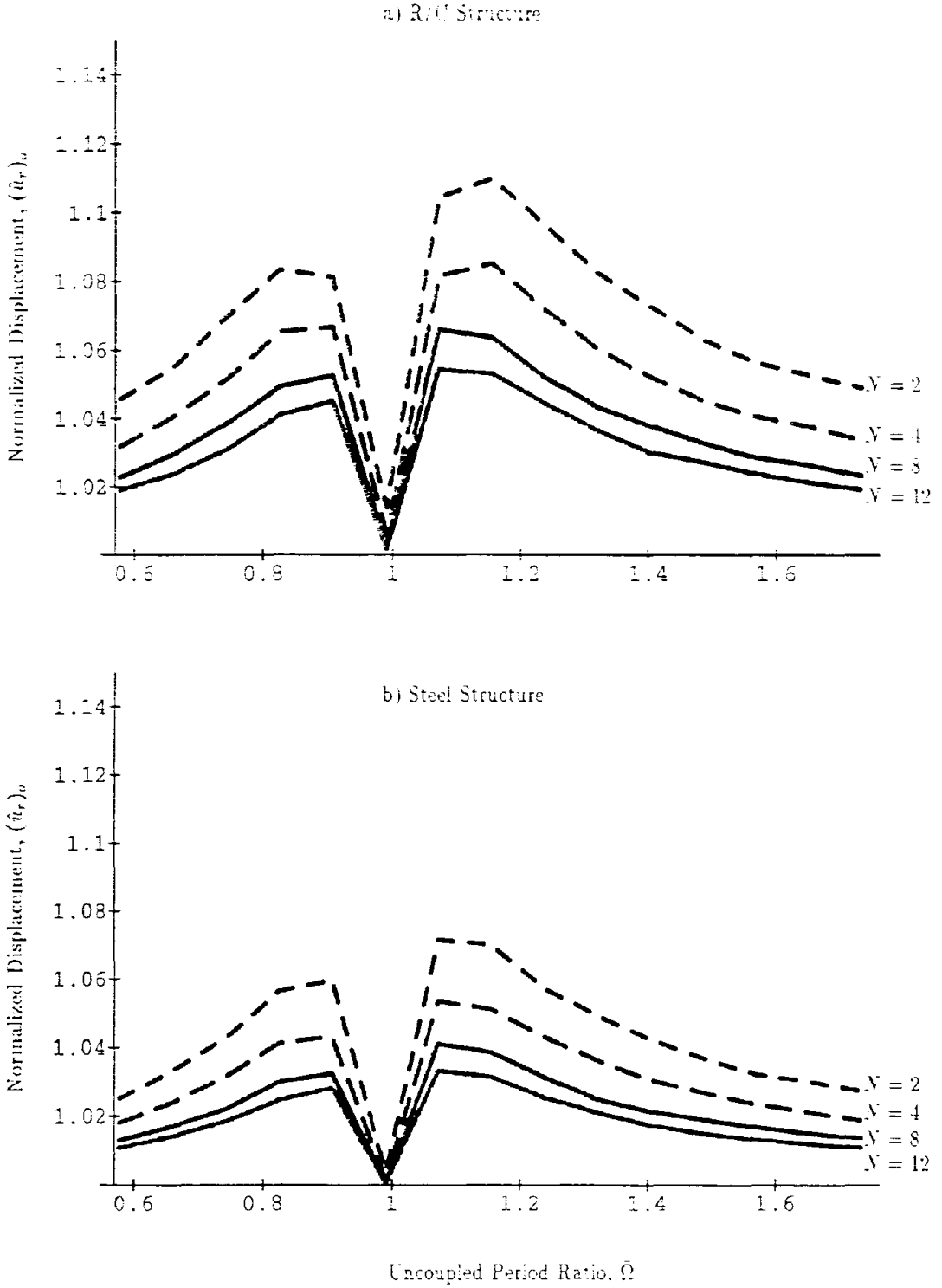

Figure 14 Mean values of the normalized response $(\hat{a}_r)_o$ obtained by Monte Carlo simulation for systems with $\bar{T}_y = 1.5$ sec and 2, 4, 8 or 12 resisting elements

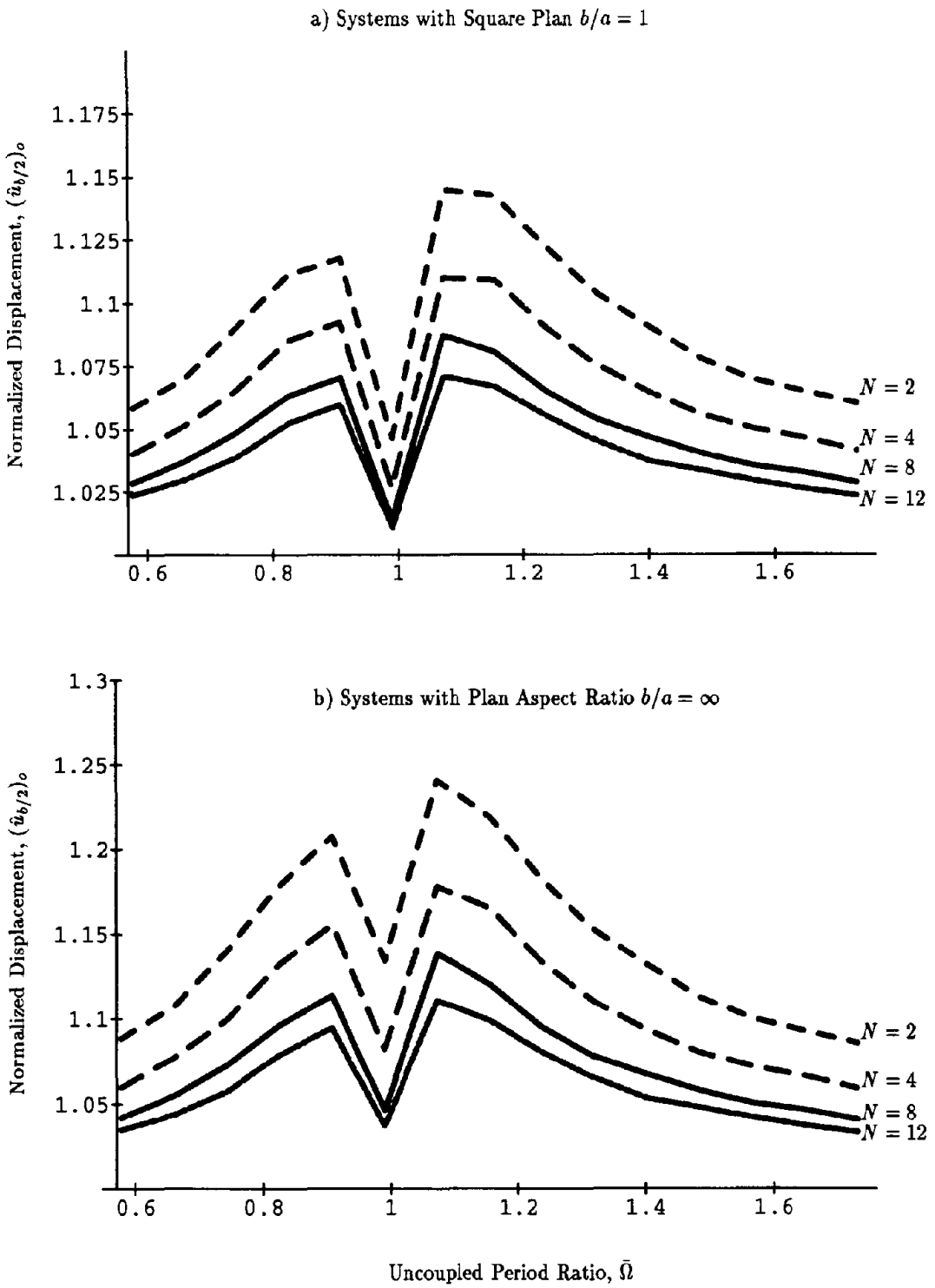

Figure 15 Mean values of the normalized edge displacement $(\hat{u}_{b/2})_o$ of R/C structures with $\bar{T}_y = 1.5$ sec., two different plan aspect ratios b/a, and variable N

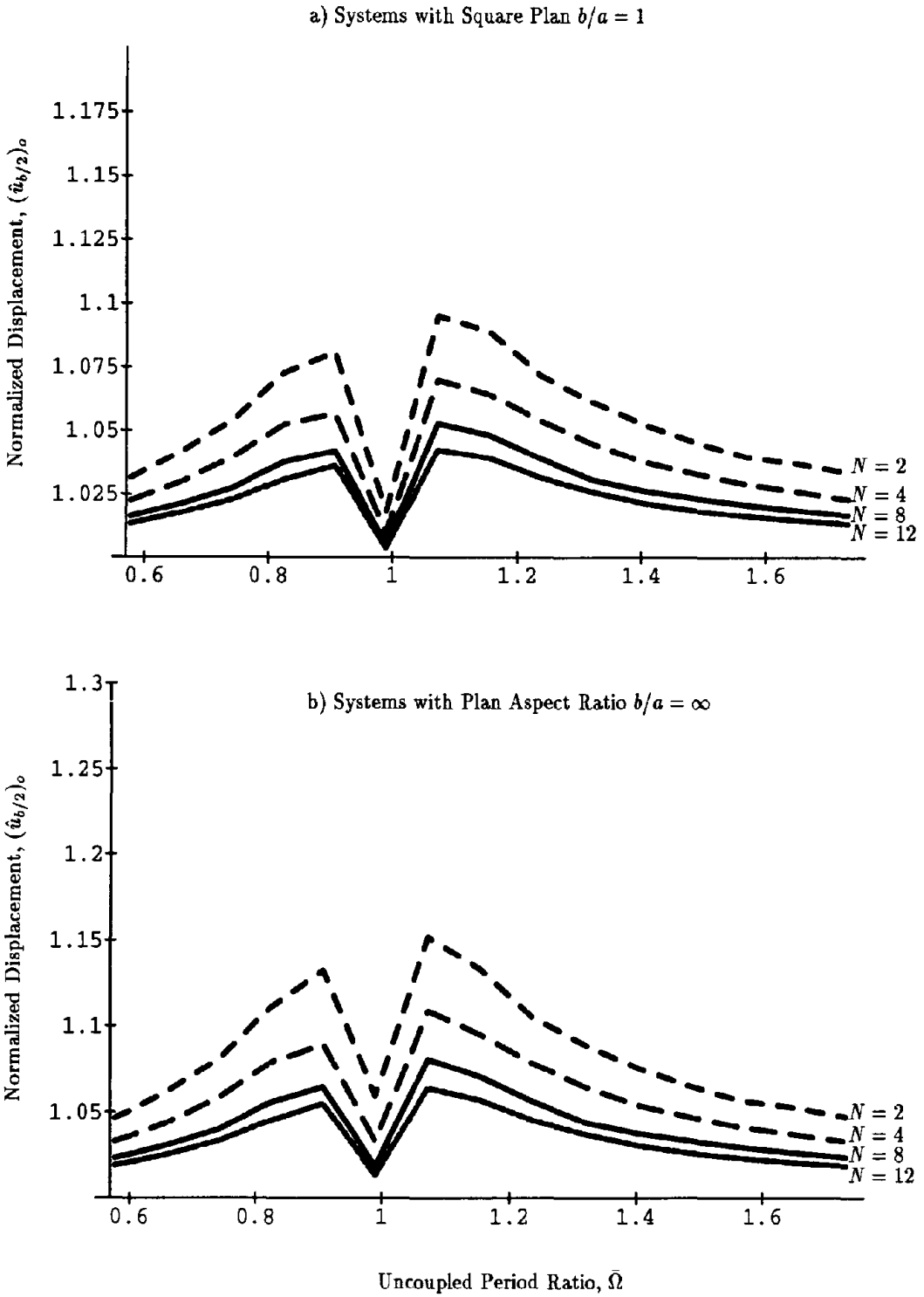

Figure 16 Mean values of the normalized edge displacement $(\hat{u}_{b/2})_o$ of steel structures with $\bar{T}_y = 1.5$ sec., two different plan aspect ratios b/a, and variable N

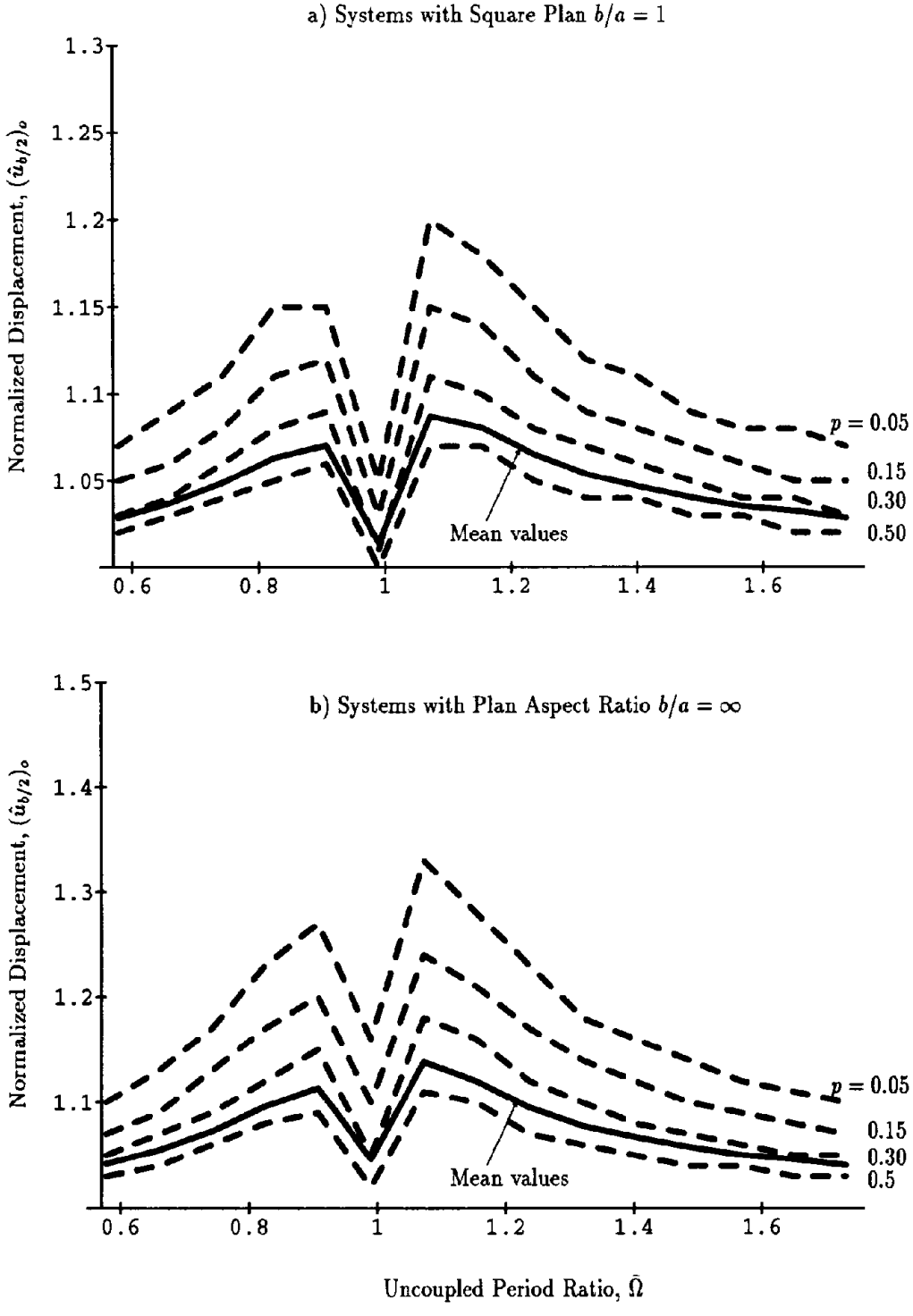

Figure 17 Normalized edge displacements $(\hat{u}_{b/2})_o$ corresponding to different levels of probability of exceedance p. Results are presented for R/C structures with $\bar{T}_y = 1.5$ sec., $N = 8$, and two different plan aspect ratios b/a

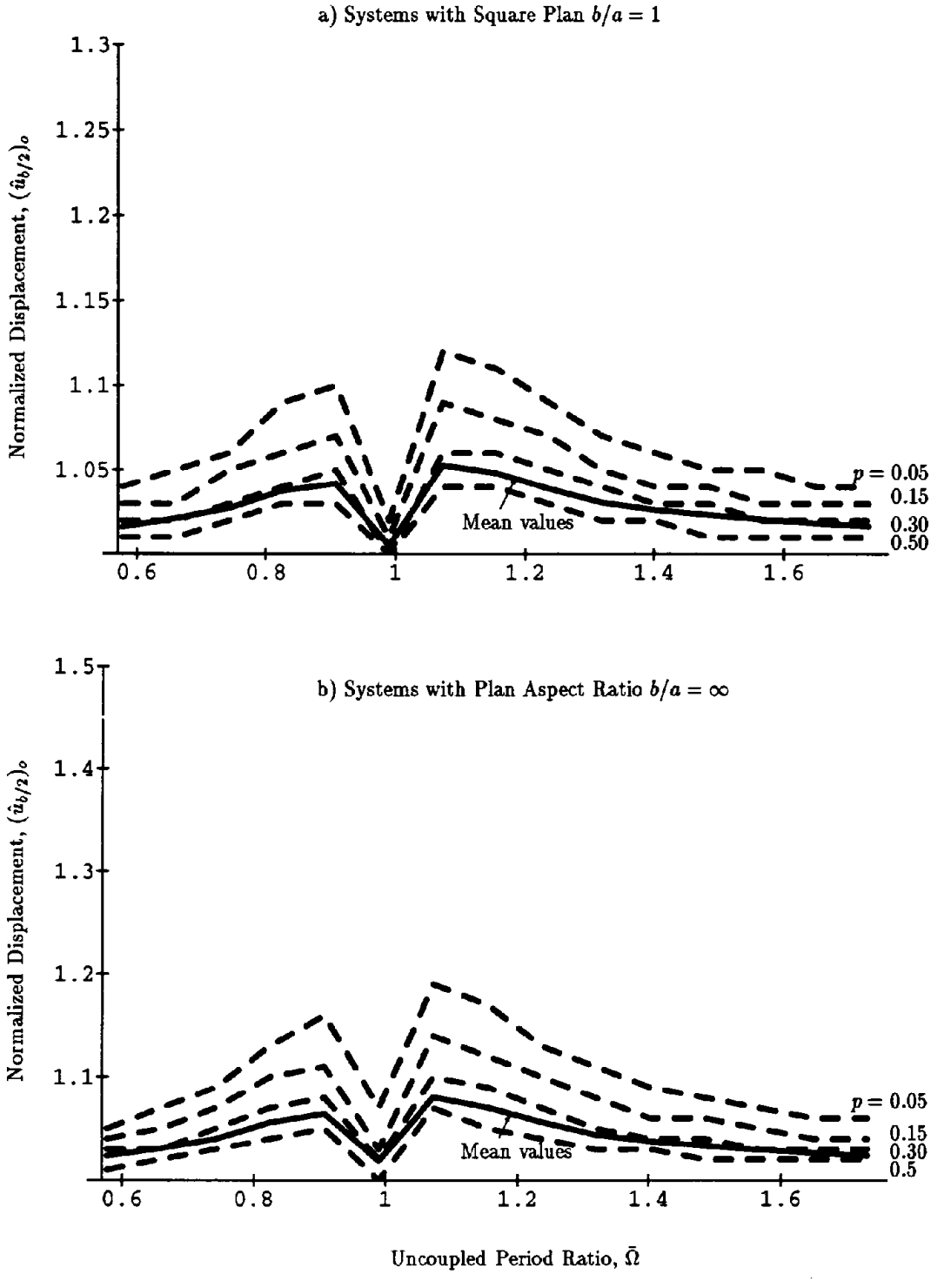

Figure 18 Normalized edge displacements $(\hat{u}_{b/2})_o$ corresponding to different levels of probability of exceedance p. Results are presented for steel structures with $\bar{T}_y = 1.5$ sec., $N = 8$, and two different plan aspect ratios b/a

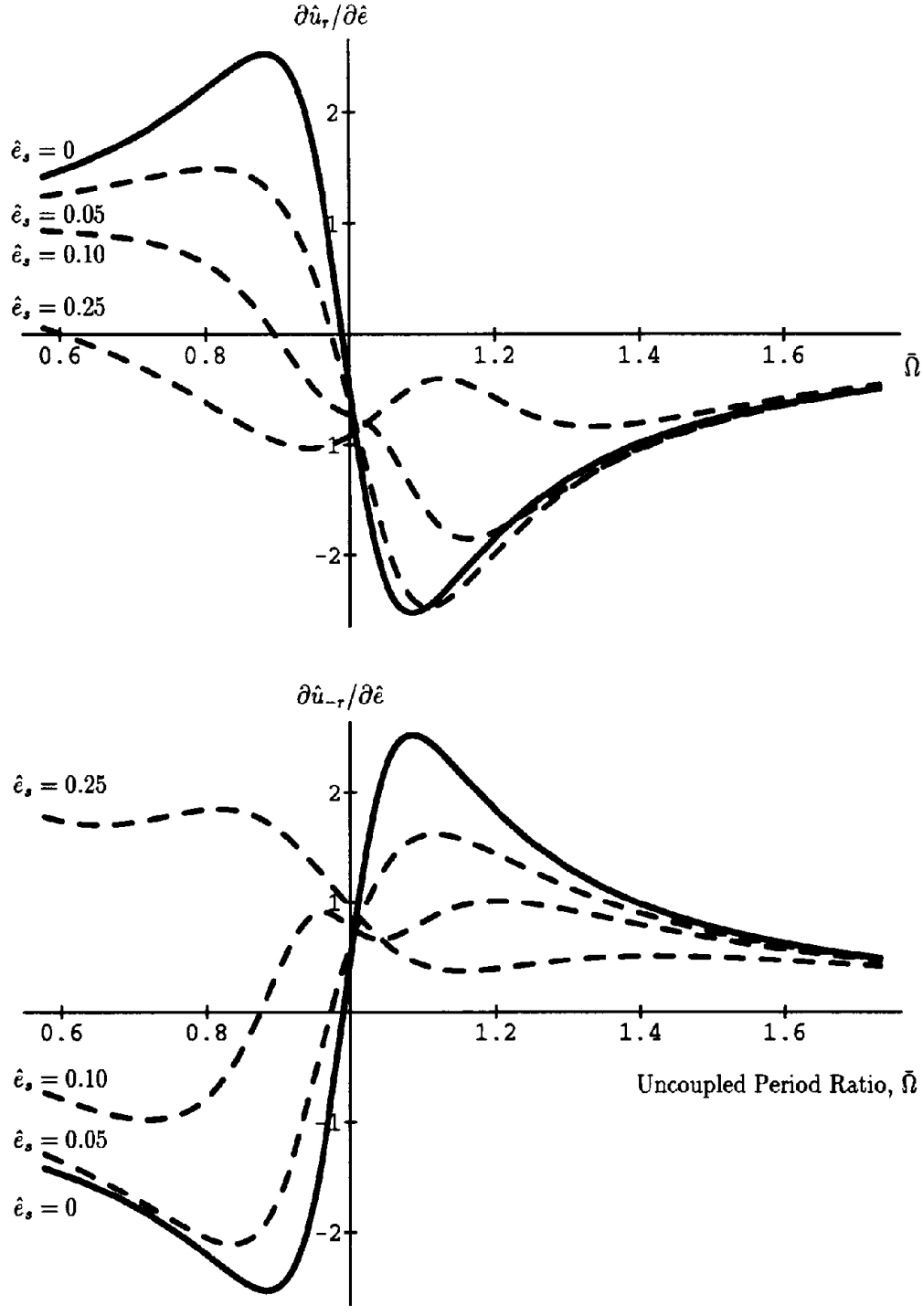

Figure 19 Partial derivatives $\partial\hat{u}_r/\partial\hat{e}$ and $\partial\hat{u}_{-r}/\partial\hat{e}$ as a function of $\bar{\Omega}$ for different normalized nominal eccentricities $\hat{e}_s$

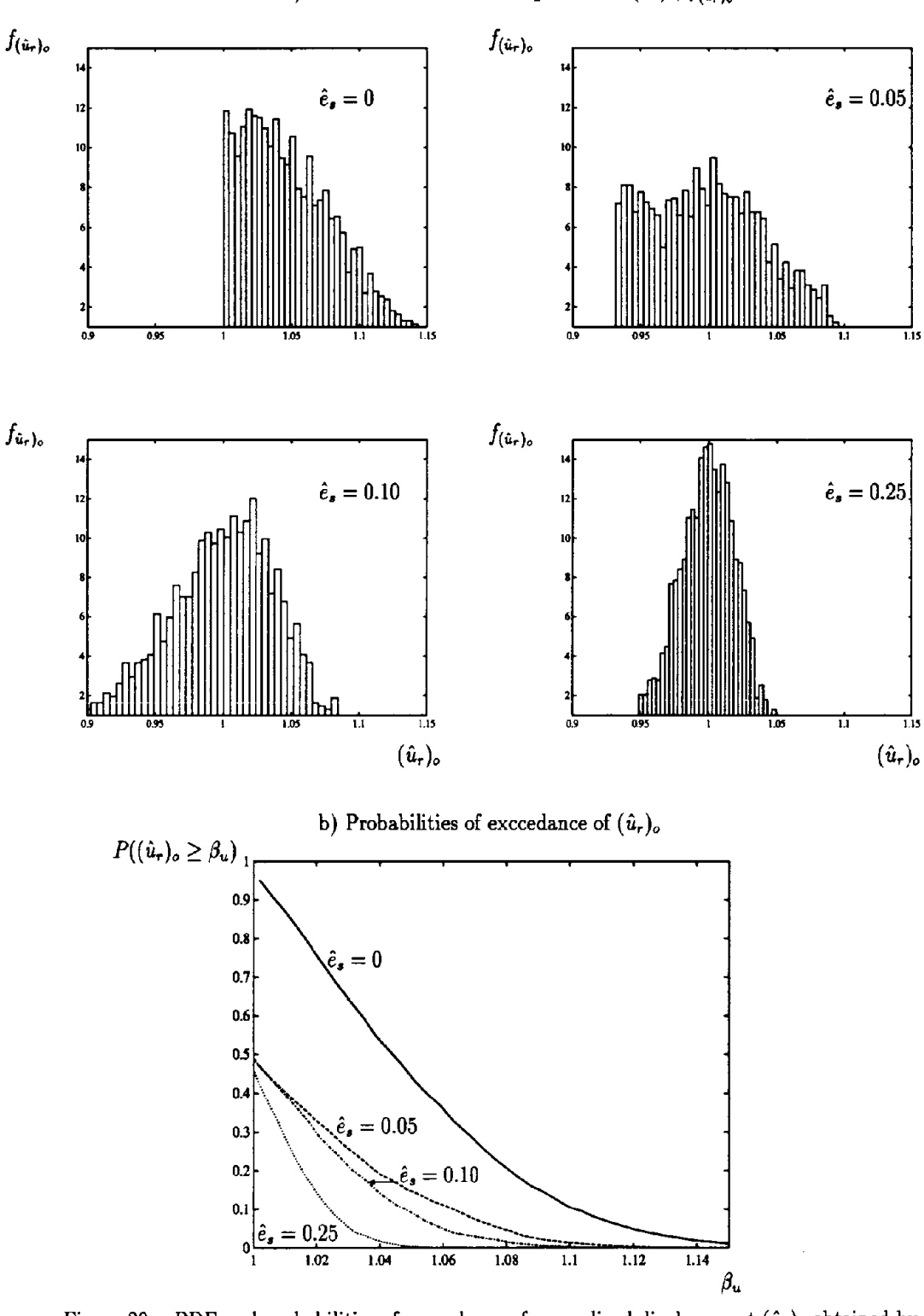

Figure 20 PDF and probabilities of exceedance of normalized displacement $(\hat{u}_r)_o$ obtained by Monte Carlo simulation for several values of normalized static eccentricity $\hat{e}_s$ and R/C structures with $\bar{T}_y = 1.5$ sec., $\bar{\Omega} = 1.25$, and $N = 8$

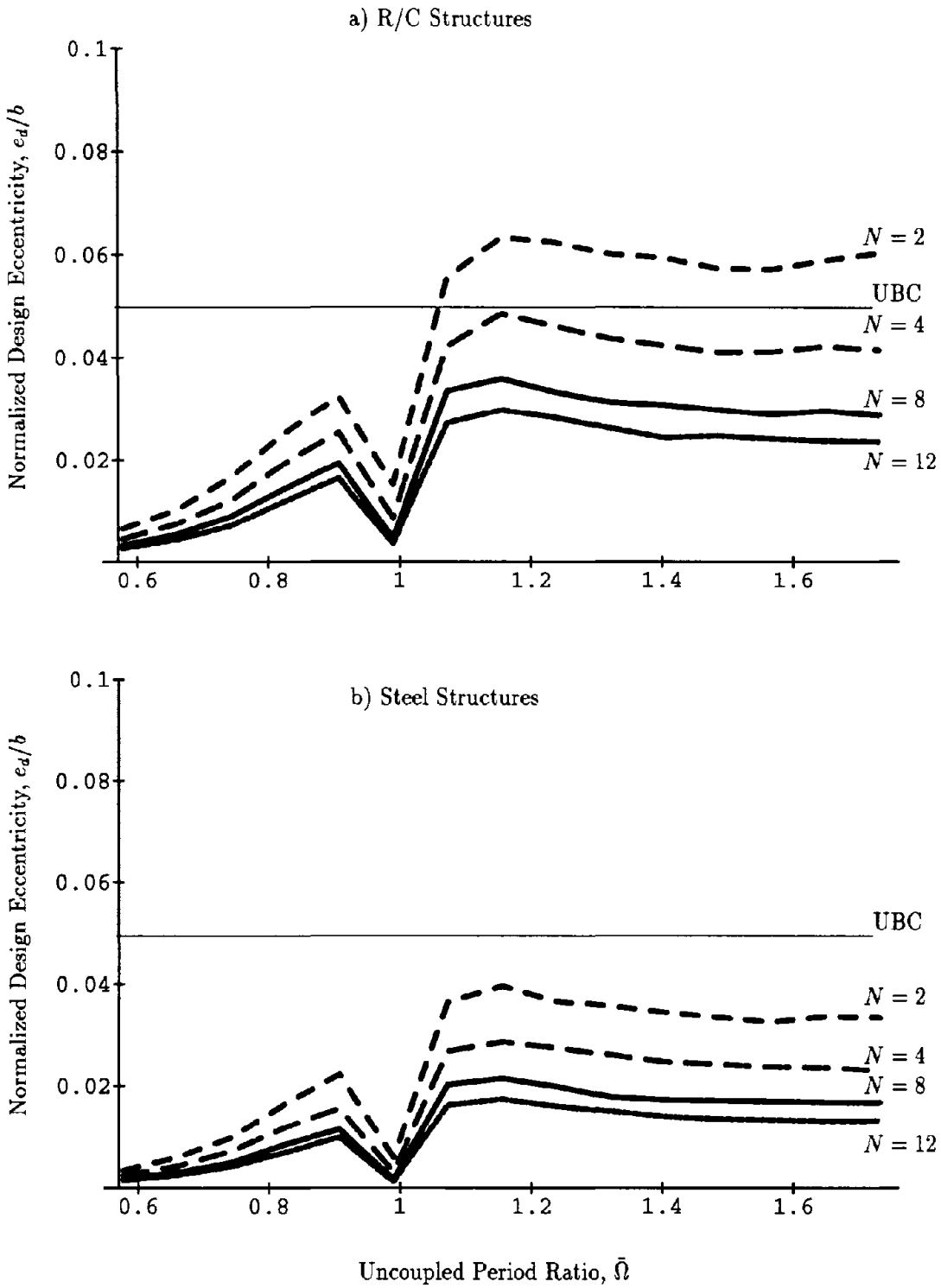

Figure 21 Normalized design eccentricity e_d/b for R/C and steel structures presented as a function of uncoupled period ratio $\bar{\Omega}$, for systems with 2, 4,8, and 12 resisting elements

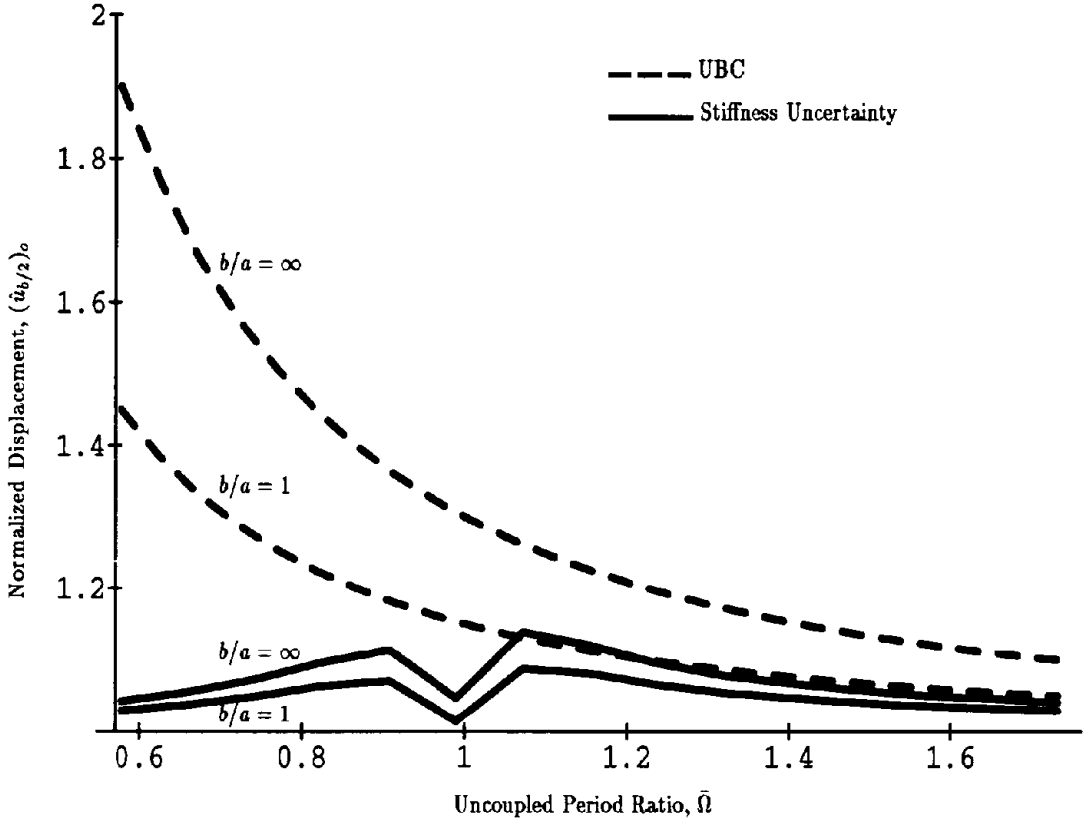

Figure 22 Amplification of edge displacements associated with (1) accidental eccentricity provisions in the UBC code, and (2) uncertainty in stiffnesses of resisting elements as a function of the uncoupled period ratio $\bar{\Omega}$ for R/C structures with $\bar{T}_y = 1.5$ sec., and eight structural elements

APPENDIX A : Response of systems with $\bar{\Omega} = 1$ and small static eccentricity

This appendix explains why the response of a system with $\bar{\Omega} = 1$ and small static eccentricity $\hat{e}$ is not importantly affected by changes in the static eccentricity of the system (Fig. 8b).

Consider the equations of motion of a torsionally-coupled single story system:

$$\begin{Bmatrix} \ddot{u}_y \\ r\ddot{u}_\theta \end{Bmatrix} + \bar{\omega}_y^2 \begin{bmatrix} 1 & \hat{e} \\ \hat{e} & \bar{\Omega}^2 + \hat{e}^2 \end{bmatrix} \begin{Bmatrix} u_y \\ ru_\theta \end{Bmatrix} = \begin{Bmatrix} -1 \\ 0 \end{Bmatrix} a_{gy}(t) \tag{20}$$

where $\bar{\omega}_y = 2\pi/\bar{T}_y$ represents the uncoupled lateral vibration frequency of the system; $\bar{\Omega}$ the lateral to torsional period ratio–the latter is computed with the torsional stiffness of the system referred to the center of stiffness of the building plan; and r is the radius of gyration of the building plan.

Solving the characteristic equation of the system described by Eq. (1), it can be shown that the natural vibration frequencies of the system are

$$\hat{\omega}_i \equiv \frac{\omega_i}{\bar{\omega}_y} = \left[\frac{1 + \hat{e}^2 + \bar{\Omega}^2}{2} \pm \sqrt{(\frac{1 + \hat{e}^2 - \bar{\Omega}^2}{2})^2 + \hat{e}^2\, \bar{\Omega}^2} \right]^{\frac{1}{2}} \quad i = y, \theta \tag{21}$$

Assuming in Eq. (2) $\bar{\Omega} = 1$ and $\hat{e}$ small, the two natural vibration frequencies of the system are

$$\hat{\omega}_y = \sqrt{1 + \hat{e} + O(\hat{e}^2)} \simeq \sqrt{1 + \hat{e}} \tag{22}$$

$$\hat{\omega}_\theta = \sqrt{1 - \hat{e} + O(\hat{e}^2)} \simeq \sqrt{1 - \hat{e}} \tag{23}$$

If $\hat{e} \ll 1$ is clear that the natural vibration frequencies of the system are equal to their uncoupled frequencies.

The vibration mode shapes corresponding to the natural vibration frequencies of Eq. (2) can be written as

$$\phi_i = \begin{Bmatrix} \phi_{yi} \\ \phi_{\theta i} \end{Bmatrix} = \frac{1}{\sqrt{\hat{e}^2 + (1 - \bar{\omega}_i)^2}} \begin{Bmatrix} -\hat{e} \\ (1 - \bar{\omega}_i)^2 \end{Bmatrix} \quad i = y, \theta \tag{24}$$

Therefore assuming again that $\Omega = 1$ and $\hat{e}$ small, it can be shown that the modes of the system are

$$\Phi = [\phi_y\ \phi_\theta] = \frac{1}{\sqrt{2}} \begin{bmatrix} 1 & -1 \\ 1 & 1 \end{bmatrix} \tag{25}$$

i.e. the vibration modes are independent of the normalized eccentricity $\hat{e}$. This independence of $\hat{e}$ in the vibration modes, that applies for $\hat{e}$ small, implies that any system response only depends on $\hat{e}$ through the system frequencies $\hat{\omega}_i$ (Eqs. (3) and (4)). Using the fact that $\hat{e}$ is small compared

to one, the system frequencies ω_i do not change importantly by the presence of $\hat{e}$, thus the system response for systems with $\bar{\Omega} = 1$ is relatively insensitive to small changes in the normalized static eccentricity $\hat{e}$. In the particular case of a flat design spectrum, the response of systems with $\bar{\Omega} = 1$ and small $\hat{e}$ is independent of $\hat{e}$. However, since the design spectrum (Fig. 2) considered varies with the system frequency, the value of $\bar{\Omega}$ for which systems are independent of $\hat{e}$ is shifted slightly from one.

3. ACCIDENTAL TORSION IN BUILDINGS DUE TO BASE ROTATIONAL EXCITATION

3.1 Introduction

This chapter is concerned with accidental torsion in buildings resulting from base rotational excitation, which is defined as the rotational motion (about a vertical axis) experienced by the building foundation as a result of spatially non-uniform motions. This spatial variability of the ground motion underneath the foundation has been traditionally attributed to two effects: (1) *wave passage*, because of which different points of the ground surface are excited by the same motion but with a phase lag, and (2) *ground motion incoherence*, a term used to recognize that different points of the ground experience motions with different amplitudes and phase characteristics because of incoming waves from different locations of an extended earthquake source, wave reflections and refractions around the building foundation, or changes produced in the waves when traveling from the source to the structure through paths of different physical properties.

The effects of base rotational excitations on the response of buildings have been extensively studied in the past. They were first studied in a classic paper by Newmark [1], wherein he presented a deterministic procedure for estimating the increase in displacements in symmetric-plan buildings caused by rotational motions of the base due to wave passage effect. Later, Veletsos and co-workers [2] extended Newmark's work to include the effect of shearing distortion of flexible foundation systems. Since then, many authors have studied the problem of building foundations subjected to spatially varying ground motion [e.g. 3,4,5]. Recently, Veletsos and co-workers [6] have studied the increase in displacements resulting from wave passage and ground motion incoherence in symmetric-plan buildings supported on rigid circular foundations. All these studies, however, have been based on assumed models for spatial variability of the ground motions that have not been yet verified against recorded motions at the base of buildings.

Thus, rotational excitations derived from earthquake motions recorded at the base of buildings provide an excellent opportunity to evaluate the resulting increase in building response. Fortunately, multiple channels of translational motions at building foundations have been recorded during recent California earthquakes. Enough channels of translational motions were recorded at the base of over thirty buildings to enable computation of base rotational excitations. In this investigation, thirty of these rotational accelerations are generated and used to compute the resulting increase in building response.

Consequently, the objectives of this chapter are to: (1) compute the increase in building response resulting from 'actual' rotational motions of the building base, (2) develop simplified analysis procedures to account for this increase in building response, and (3) evaluate results presented in Newmark's classic paper, in light of the available ground motion data.

3.2 Base translational and rotational motions

The translational motions recorded by the accelerometers at the foundation level of a building correspond to averages of the motions of the ground underlying the foundation. Such is the case because in most buildings, the foundation system is considerably stiff and, therefore, cannot undergo arbitrary motions at different points. If the foundation is rigid its motion during an earthquake can be described by six degrees of freedom, in the gross sense: horizontal (x and y) and vertical (z) translations, rocking about x and y axes, and torsion about the vertical axis. It is this torsional motion of the foundation, the one denoted here as base rotational excitation, that is of concern in this investigation.

Considered in this investigation are buildings with stiff foundation systems and that are instrumented with at least two parallel accelerometers at their base, so that the rotational excitation can be computed from the translational motions. Typical foundation systems for the buildings considered included: (1) spread column footings interconnected by grade beams and a slab on grade (usually 6 in. thick or less), (2) combinations of spread column footings and continuous wall footings interconnected by grade beams and a slab on grade, and (3) mat foundations. For such foundation systems it is reasonable to neglect their in-plane bending and shearing deformations and compute the rotational acceleration of the building base as $a_{g\theta}(t) = (a_{g1}(t) - a_{g2}(t))/d$, where $a_{g1}(t)$ and $a_{g2}(t)$ are the translational accelerations (both x or both y components) recorded at location 1 and 2 at the base, and d is the distance between the two locations. If $a_{g1}(t)$ and $a_{g2}(t)$ are in units of in/sec^2 and d is in inches, $a_{g\theta}(t)$ is in radians/sec^2. Similarly, the average translational acceleration of the base is defined as $a_g(t) = (a_{g1}(t) + a_{g2}(t))/2$.

Building records obtained during the Whittier (1987), Loma Prieta (1989), Upland (1990), and Sierra Madre (1992) earthquakes that are used in this study are listed in Table 1. Also presented for each building are the peak values of the translational and rotational motions of the building base computed as indicated above. The peak values of translational acceleration and velocity are denoted by $(a_{gy})_o$ and $(v_{gy})_o$; and for rotational acceleration and velocity by $r(a_{g\theta})_o$ and $r(v_{g\theta})_o$.

Rotational accelerations and velocities scaled by $r = 20.4$m are also presented in order to compare them with translational accelerations and velocities. We note that most of the scaled peak rotational accelerations vary between 0.01g and 0.1g in contrast to the range 0.05g to 0.35g for the peak values of translational accelerations.

Figure 1 shows the $a_g(t)$ and $ra_{g\theta}$ acceleration histories, computed as described above, for ten of the buildings in Table 1. The rotational accelerations contain higher frequencies than the corresponding translational accelerations because the former are computed as the difference between similar translational motions at two locations on the base. The ratio between the peak values of the scaled rotational and translational base accelerations varies considerably from record to record; the mean value of this ratio for the thirty records is about twenty percent.

A more meaningful way to compare base rotational and base translational accelerations is to obtain the response spectra for each pair of records, and then compute the mean translational and torsional response spectra over all pairs of records. The response spectrum for translational acceleration $a_g(t)$ is a well known concept in earthquake engineering. The response spectrum for rotational acceleration $a_{g\theta}(t)$ is defined similarly as the peak value of torsional response of a SDF torsional oscillator subjected to $a_{g\theta}(t)$ plotted against its torsional vibration period T_θ. Such spectra were computed for each of the thirty pairs of base motions of Fig. 1. The mean pseudo-velocity response spectra for base translational and rotational accelerations are presented in Fig. 2 (this figure also includes four other curves which will be discussed later). As before, the ordinates of the torsional spectra have been scaled by $r = 20.4$m, the radius of gyration of the hypothetical building plan, so that the translational and torsional response spectra can be directly compared. Both pseudo-velocity response spectra have been normalized by the mean peak ground velocity for the base translations considered , i.e., $\bar{V}_{gy} = 16$ cm/sec. This figure shows that the spectral ordinates for rotational excitation are an order of magnitude smaller than for translational excitation. Also, because of the higher frequencies noted previously in the former (Fig. 1), the peak values for the torsional response spectra occur at shorter periods compared to the translational response spectra. This observation suggests that rotational excitation is expected to cause a larger increase in the response of short period systems compared to long period systems.

3.3 Systems considered and analysis procedure

The systems analyzed are idealized single-story buildings consisting of a rigid roof diaphragm, where all the system mass is lumped; lateral resistance is provided by vertically-rigid structural elements located along resisting planes in the x and y-directions. As shown in the building plan (Fig. 3), the ith resisting plane in the x-direction has stiffness k_{xi} and is located at distance y_i from the CM (center of mass) of the building; analogously, the stiffness and location of plane i in the y-direction are defined by k_{yi} and x_i, respectively. These resisting planes may have different stiffnesses in the y-direction and may be unsymmetrically located about the y axis, creating an eccentricity e between the CM and the CR (center of rigidity) of the building. On the other hand, the system considered is symmetric about the x axis. The number of resisting planes in the x and y directions is N_x and N_y, respectively.

The dynamic response of the system to base acceleration in the y-direction, $a_{gy}(t)$, and base rotational acceleration, $a_{g\theta}(t)$, is described by two degrees of freedom: the translational displacement u_y of the CM along the y-direction, and the displacement ru_θ of the rigid diaphragm at distance r to the right of the CM due only to the rotation u_θ of the rigid diaphragm. The equations of motion of the system can be written

$$\begin{bmatrix} m & 0 \\ 0 & m \end{bmatrix} \begin{Bmatrix} \ddot{u}_y \\ r\ddot{u}_\theta \end{Bmatrix} + \begin{bmatrix} K_y & K_y e/r \\ K_y e/r & K_\theta/r^2 \end{bmatrix} \begin{Bmatrix} u_y \\ ru_\theta \end{Bmatrix} = -m \begin{bmatrix} 1 & 0 \\ 0 & 1 \end{bmatrix} \begin{Bmatrix} a_{gy}(t) \\ ra_{g\theta}(t) \end{Bmatrix} \quad (1)$$

where r, as mentioned before, is the radius of gyration of the system plan about a vertical axis passing through the CM and m is the lumped mass at the roof diaphragm; $K_y = \sum_{i=1}^{N_y} k_{yi}$ is the lateral stiffness of the system, $K_\theta = \sum_{i=1}^{N_y} k_{yi}x_i^2 + \sum_{i=1}^{N_x} k_{xi}y_i^2$, is the torsional stiffness of the building with respect to the CM; and $e = \sum_{i=1}^{N_y} k_{yi}x_i / \sum_{i=1}^{N_y} k_{yi}$ is the static eccentricity of the building.

Dividing Eq. (1) by m, the equations of motion can be conveniently written as follows:

$$\begin{Bmatrix} \ddot{u}_y \\ r\ddot{u}_\theta \end{Bmatrix} + \omega_y^2 \begin{bmatrix} 1 & e/r \\ e/r & \Omega^2 + (e/r)^2 \end{bmatrix} \begin{Bmatrix} u_y \\ ru_\theta \end{Bmatrix} = - \begin{bmatrix} 1 & 0 \\ 0 & 1 \end{bmatrix} \begin{Bmatrix} a_{gy}(t) \\ ra_{g\theta}(t) \end{Bmatrix} \quad (2)$$

where $\omega_y = \sqrt{K_y/m}$ is the uncoupled lateral frequency of the building; $\Omega = \omega_\theta/\omega_y$ is the ratio between the uncoupled torsional and lateral frequencies; $\omega_\theta = \sqrt{K_{\theta R}/(mr^2)}$ is the uncoupled torsional frequency of the building; and $K_{\theta R} = K_\theta - K_y e^2$ is the torsional stiffness of the building with respect to the CR. Thus, the single-story system considered is characterized by four parameters: $\omega_y, \Omega, e/r$, and r.

The equations of motion for the special case of a symmetric-plan building are obtained by letting $e/r = 0$ in Eq. (2). Consequently, the off-diagonal term of the stiffness matrix becomes zero and, hence, the lateral and torsional motions in such a structure become uncoupled, i.e., the lateral motions of the CM, u_y, and rotational motions of the building diaphragm, u_θ, result independently from the translational and rotational excitations, respectively. This fact implies that the response of the symmetric-plan system can be computed from two independent single degree of freedom systems: a SDF translational oscillator with natural frequency ω_y and a SDF torsional oscillator with natural vibration frequency $\omega_\theta = \Omega\,\omega_y$.

Equation (2) is solved to determine the response of systems for two excitation cases: (1) $a_{gy}(t)$ and $a_{g\theta}(t)$ acting simultaneously, and (2) $a_{gy}(t)$ only. The ratio between building responses computed for these two excitation cases, which is denoted here as normalized building response, provides a measure of the modification in response due to the rotational excitation. Normalized response larger than unity implies that accidental torsion resulting from rotational excitation has the effect of increasing the building response above that due to translational excitation alone.

The response quantities of interest are the peak values over time of the lateral displacements at distance $\pm r$ from the CM. These are denoted as $(u^*_{+r})_o$ [or $(u^*_{-r})_o$] and $(u_{+r})_o$ [or $(u_{-r})_o$] when computed for the previously mentioned excitation cases (1) and (2), respectively. The normalized displacement $(\hat{u}_{+r})_o = (u^*_{+r})_o/(u_{+r})_o$ [or $(\hat{u}_{-r})_o = (u^*_{-r})_o/(u_{-r})_o$] is computed for each system defined by parameters $\omega_y, \Omega, e/r$, and r, and for each of the thirty base motions considered (Table 1). From this set of thirty pieces of data, their mean value and mean value plus one standard deviation are computed.

The normalized response $(\hat{u}_{+r})_o$ [or $(\hat{u}_{-r})_o$] depends on the plan dimension b orthogonal to the direction of horizontal ground motion (Fig. 3), and the plan aspect ratio a/b for which two limiting cases are considered: $a/b = 1$, i.e., square plan, and $a/b = 0$, i.e., the limiting case of a unidimensional plan. Such is the case because the rotational excitation of the system $ra_{g\theta}$ is proportional to r, which, in turn, is a function of b and a/b.

Although normalized displacements for both locations at distances $+r$ and $-r$ from the CM were computed for each system, only the results for $(\hat{u}_{-r})_o$ on the flexible side of the building (Fig. 3) are presented since the response trends are similar in both cases. The results for $(\hat{u}_{+r})_o$ on the stiff side of the building, are included in Appendix A.

Next, the increase in building displacements due to rotational excitation over the response due to translational excitation alone is first studied for symmetric-plan systems ($e/r = 0$) because of

their simplicity and practical importance, followed by unsymmetric-plan systems. Moreover, as will be shown later, the increase in displacements resulting from rotational excitation tends to be larger in symmetric-plan systems than for unsymmetric systems.

3.4 Increase in response of symmetric buildings

Presented in this section are results for the increase in displacements of symmetric-plan buildings resulting from accidental torsion induced by rotational excitation. Results are presented for buildings with uncoupled vibration period $T_y = 2\pi/\omega_y$ varying between 0.05 and 3 sec; torsional to lateral frequency ratio Ω varying between $1/\sqrt{3}$ and $\sqrt{3}$; three different plan dimensions $b = 25, 50,$ and 100 m; and plan aspect ratios $a/b = 0$ and 1.

Figure 4 presents the mean (heavier lines) and mean plus one standard deviation (lighter lines) values of the normalized displacement $(\hat{u}_{-r})_o$ of systems with three different values of the frequency ratio $\Omega = 2/3, 1.0,$ and $3/2$; plan aspect ratio $a/b = 1$, and plan dimension b=50 m. The normalized displacement $(\hat{u}_{-r})_o$ tends to increase as T_y becomes shorter and Ω decreases; it reaches a maximum value of 1.4 when $T_y \simeq 0.1$ sec and $\Omega = 2/3$, which implies that displacements would increase, in the mean, by at most 40% due to rotational excitation. However, the values of $(\hat{u}_{-r})_o$ reduce quickly as T_y and Ω increase. Indeed, for symmetric systems with vibration periods T_y longer than about half a second or frequency ratio Ω equal to or greater than one, the mean increase in displacements is always less than 5%. The mean plus one standard deviation values also decrease with increasing T_y and Ω. Furthermore, the standard deviation for the response $(u_{-r})_o$ is approximately 0.2 for short period systems and decreases to 0.05 for systems with vibration periods T_y over half second. Note also that these standard deviations are in most cases larger than the mean values of increase in displacements due to the rotational excitation.

Similarly, values for the normalized response $(\hat{u}_{-r})_o$ are shown in Fig. 5 for a wide range of Ω values, fixed values of $T_y = 0.5, 1,$ and 2 sec, $a/b = 1$ and $b = 50$ m. The increase in building displacements resulting from rotational excitation is insensitive to changes in the frequency ratio Ω unless the building is very stiff (T_y is very small), and the mean increase is less than 5% for the range of system parameters considered.

These trends observed for $(\hat{u}_{-r})_o$ can be qualitatively explained, using the translational and torsional response spectra already presented in Fig. 2, as follows. Consider first, the scaled torsional response spectra, $(ru_\theta)_o$, shown for three different values of Ω: 2/3, 1, and 3/2. Because $T_y = \Omega\, T_\theta$,

the torsional response spectrum for systems with $\Omega \neq 1$ can be interpreted as translation of the response spectrum for $\Omega = 1$ along the period scale by $(\Omega - 1)T_y$; thus, the shifts are $T_y/3$ and $T_y/2$ for $\Omega = 2/3$ and $3/2$, respectively. Now, intuitively, the larger the ratio between the ordinates of the rotational and translational response spectra, i.e., the closer the two spectral ordinates, the higher the expected increase in building displacements due to rotational excitation. Therefore, Fig. 2 indicates that the two spectra are closer for smaller values of Ω, which implies that rotational excitation will especially affect such systems. This is especially clear for stiff systems (small T_y); however, as T_y increases these two spectra separate from each other, implying that the response to rotational excitation will decrease with increasing T_y (Fig. 3). Furthermore, for systems with vibration periods over about half a second, changes in Ω do not significantly affect the ratio between the ordinates of the two spectra; therefore, in these systems the increase in displacements due to rotational excitation tends to be insensitive to changes in Ω (Fig. 5).

Figure 6 shows the mean and mean plus one standard deviation values of $(\hat{u}_{-r})_o$ as a function of T_y (upper figure) and Ω (lower figure) for the two extreme values of plan aspect ratio, a/b. The increase in building displacement induced by rotational excitation is larger in systems with square plans $(a/b = 1)$ than in systems with very narrow plans $(a/b = 0)$. Such is the case because, for a given plan dimension b and fixed plan aspect ratio, the corresponding radius of gyration r is larger for a building with square plan $(a/b = 1)$ than for a building with narrow plan $(a/b = 0)$. Therefore, the building displacement ru_θ due to rotation of the building plan will increase with increasing r (or a). Thus, buildings with square plans $(a/b = 1)$ provide in most cases an upper bound for the increase in displacements resulting from rotational excitation. Consequently, the results to follow are restricted to square-plan buildings.

Structural displacements resulting from rotational excitation will increase with the plan dimension b. This is apparent in Figs. 7 and 8, where the mean and mean plus one standard deviation of the response $(u_{-r})_o$ are presented for three different plan dimensions $b = 25, 50$, and 100 m, and a wide range on values of the uncoupled period T_y and frequency ratio Ω, respectively. The results for the new cases $b = 25$ m and 100 m show similar trends as did the results for $b = 50$ m presented in Figs. 4 and 5. In particular, for all plan dimensions considered the increase in response due to rotational excitation tends to be larger for small values of T_y and Ω, and decreases rapidly with increasing values of these two parameters (Fig. 7). Moreover, this increase in building displacement seems insensitive to changes in the frequency ratio Ω when the translational vibration period of the building is longer than about half a second (Fig. 8). Note also that the increase in

building displacement is not proportional to the plan dimension b. For instance, when $b = 50$ m and $\Omega = 2/3$ (Fig. 7), the largest increase (over all T_y) in displacement resulting from rotational excitation is approximately 40%; however, when $b = 100$ m this increase is larger than 100%.

The observed trends of the building response $(\hat{u}_{-r})_o$ (Figs. 7 and 8) can be qualitatively explained using, again, the translational and torsional response spectra presented in Fig. 2. Consider first the scaled torsional response spectra $(ru_\theta)_o$ shown for three different $b = 25, 50$, and 100 m. Because $r = b/\sqrt{6}$ for a plan aspect ratio $a/b = 1$, an increase in the building plan dimension from b to b' (with radius of gyration changes from $r = b/\sqrt{6}$ to $r' = b'/\sqrt{6}$) is represented by translation of the torsional response spectrum along the response scale by $(b'/b-1)\, r\, \omega_\theta\, (u_\theta)_o = (r'/r-1)\, r\, \omega_\theta\, (u_\theta)_o$. Consequently, when $b = 100$ m and $\Omega = 2/3$ the response spectrum for ru_θ is slightly above the u_y response spectrum, which suggests that, in this case, the increase in building displacements due to rotational excitation should be larger as previously noted in Fig. 7. Moreover, when the translational vibration period T_y of the building is longer than about one second, the ratio between the pseudo-velocity spectral ordinates for rotational and translational excitations (Fig. 2) is essentially independent of the frequency ratio Ω; this observation explains the trends observed from Fig. 8.

3.5 Increase in response of unsymmetric buildings

In this section, results are presented for unsymmetric-plan buildings, analogous to those presented in the preceding section for symmetric structures. The translation and rotation of such systems are coupled because of the static eccentricity e (Eq. (2)). This implies that the building will simultaneously undergo translation and torsion when subjected to either of the two base motions, $a_{gy}(t)$ or $a_{g\theta}(t)$. Results for the increase in building displacements due to rotational excitation in these systems are presented next for buildings with plan aspect ratio $a/b = 1$ and plan dimension $b = 50$ m, which is large enough to cover most buildings.

Mean and mean plus one standard deviation values of the normalized response $(\hat{u}_{-r})_o$ are shown in Fig. 9 for a wide range of uncoupled vibration periods T_y, three different values of the normalized static eccentricity $e/r = 0$, 0.25, and 0.5, and frequency ratio $\Omega = 2/3$, 1, and 3/2. The results corresponding to the symmetric case ($e/r = 0$), presented in Fig. 4, are reproduced here. For a constant value of e/r the mean increase in displacements due to rotational excitation reaches a maximum for small values of T_y and Ω, and reduces rapidly with increasing values of these parameters. For instance, the maximum increases in building displacement are 40, 19, and

11 percent for buildings with $e/r = 0, 0.25$, and 0.5, respectively and $\Omega = 2/3$. However, this mean increase in displacements is below 5 percent for a wide range of values of T_y and Ω. In most cases, the increase in displacements resulting from rotational excitation is larger for symmetric buildings, compared to unsymmetric structures. This observation is especially evident for systems with short T_y and small Ω, where the increase in building displacements due to rotational excitation is the largest. It also carries over to the increase in displacements at distance r to the right of the CM (Appendix A) if Ω and T_y are small, but not otherwise.

Figure 10 shows the mean and mean plus one standard deviation values of $(\hat{u}_{-r})_o$ as a function of the frequency ratio Ω, for three values of the normalized static eccentricity $e/r = 0, 0.25$, and 0.5, and three values of the uncoupled vibration period $T_y = 0.5, 1$, and 2 sec. The mean increase in building displacements due to rotational excitation decreases with increasing T_y and Ω, and it is generally less than 5% for all buildings which are torsionally stiff ($\Omega > 1$), regardless of the value of static eccentricity e/r. Again, the mean values of $(\hat{u}_{-r})_o$ are remarkably insensitive to changes in the value of Ω for the range of T_y considered; this observation also applies to the mean plus one standard deviation results. The latter show that the standard deviation is about 0.13 for small values of T_y and Ω, but less than 0.05 otherwise.

3.6 Simplified analysis methods

For design applications, it would be useful to have simplified procedures for conveniently estimating the increase in building displacements due to rotational excitation. In this section two such methods are developed. The first is based on the concept of design accidental eccentricity, e_a, which is calibrated in such a way that when used together with the equivalent static lateral forces the increase in building displacement is identical to that computed from response history analysis (Figs. 7-10). The second method is based on an extension of standard response spectrum analysis to consider the simultaneous effects of translational and rotational components of base motion. The two methods are intended for static or dynamic analyses of the structure, respectively, but not both.

3.6.1 Design accidental eccentricity

We now determine the eccentricity e_a relative to the CM at which the equivalent static lateral force or base shear, V, should be applied to a one story system in order to account for the accidental

torsion of the system arising from rotational excitation. The accidental eccentricity e_a is first derived for an unsymmetric plan building and later specialized for the symmetric case.

For the derivation presented next, V is chosen as the static force applied at the CM that produces a displacement at $x = -r$ equal to $(u_{-r})_o$, the peak dynamic displacement due only to the translational component of ground motion (Fig. 11a), i.e.

$$(u_{-r})_o = \frac{V}{K_y} + \frac{V\,e}{K_\theta}(e + r) \tag{3}$$

Now the same static force V is applied eccentrically relative to the CM at distance e_a, yet to be determined. This accidental eccentricity is determined to satisfy the requirement that the the displacement at $x = -r$ is the same as $(u^*_{-r})_o$, the peak dynamic displacement due to the simultaneous action of translational and rotational components of ground motion (Fig. 11b), i.e.

$$(u^*_{-r})_o = \frac{V}{K_y} + \frac{V(e_a + e)}{K_\theta}(e + r) \tag{4}$$

Dividing Eq. (4) by (3), and solving for e_a we obtain

$$\frac{e_a}{b} = [(\hat{u}_{-r})_o - 1]\,(\frac{\Omega^2}{1+e/r} + e/r)\,(\frac{r}{b}) \tag{5}$$

Now, if the building is symmetric, i.e., $e/r = 0$, Eq. (5) reduces to

$$\frac{e_a}{b} = [(\hat{u}_{-r})_o - 1]\,\Omega^2\,(\frac{r}{b}) \tag{6}$$

Note that V does not appear in the equations for e_a/b. This accidental eccentricity can therefore be used in conjunction with any reasonable value of V including the code value. Equations (5) and (6) relate the accidental eccentricity e_a to the normalized displacement $(\hat{u}_{-r})_o$ at distance r to the left of the CM. Normalized displacements at other locations, such as the left edge of the building plan, could be used in determining e_a. The resulting accidental eccentricities e_a are, however, quite insensitive to the location selected; however, the value e_a obtained from the location $x = r$ can be slightly larger than that computed using the location $x = -r$ (Appendix A).

Substituting for the values of $(\hat{u}_{-r})_o$ from Figs. 7-10 in Eqs. (5) and (6) leads to the e_a/b values presented in Fig. 12 for a wide range of uncoupled vibration periods T_y, frequency ratios $\Omega = 2/3, 1$, and $3/2$, and normalized static eccentricities $e/r = 0, 0.25$, and 0.5. The computed accidental eccentricities show similar trends as did the values of $(\hat{u}_{-r})_o$ because e_a/b is proportional to $(\hat{u}_{-r})_o - 1$, the increase in displacement due to rotational excitation (Eqs. (5) and (6)). Consequently, the accidental eccentricity e_a/b tends to be larger for systems with short uncoupled vibration periods T_y

and smaller Ω, which implies increasingly torsionally flexible systems; e_a/b reaches a maximum of 7% for systems with $\Omega = 2/3$ and $T_y \simeq 0.1$ sec, and is less than 2% for a wide range of combinations of T_y and Ω. In some cases, the design eccentricity e_a/b is negative, indicating that the structural response is reduced because of rotational acceleration.

Additional results of e_a/b for a wide range of Ω values, three values of uncoupled vibration period $T_y = 0.5, 1$, and 2 sec., and normalized static eccentricity $e/r = 0, 0.25$, and 0.5 are shown in Fig. 13. The accidental eccentricity, e_a/b, is insensitive to changes in Ω, in the same way as $(\hat{u}_{-r})_o$ in Figs. 8 and 10, and is smaller than 2% for all values of Ω; for most cases it is less than 1%, and eventually becomes negative for some combinations of the building parameters.

The Uniform Building Code specifies an accidental eccentricity of $0.05b$ independent of the translational vibration period T_y and frequency ratio Ω. The computed values of e_a presented here are much smaller than the code values except for systems with long plan dimension, say $b \geq 50$ m, short vibration periods T_y, say $T_y < 0.5$ sec, and small torsional stiffness ($\Omega < 1$). For such systems the computed accidental eccentricities are similar to, or slightly larger, than the UBC.

One advantage of using accidental eccentricity to account for the increase in building displacements due to rotational acceleration is that the concept is appealing and easy to use in conjunction with equivalent static analysis of the building. Although developed here with reference to a one-story system, the concept is extendible to a special class of buildings that satisfy the following properties [7]: (1) the CM of all floors lie on a vertical line, (2) the resisting planes are arranged such that their principal axes form an orthogonal grid in plan and are connected at each floor by a rigid diaphragm, and (3) the lateral stiffness matrices of all resisting planes along one direction are proportional to each other.

Unfortunately, the computed values of e_a/b vary considerably depending upon the values of the system parameters T_y, Ω, e/r and b. It is impractical to account for such variations of e_a/b in the context of code design of buildings. On the other hand, a constant value selected to cover all system parameters has the drawback that it would provide overly conservative results for many situations. More importantly, the value of the accidental eccentricity used says very little about the actual increase in response expected in the structural elements, since the latter depends importantly on the values of the frequency ratio Ω and normalized static eccentricity e/r for the building.

3.6.2 Response spectrum method

An alternative simplified analysis procedure to include the increase in response resulting from rotational acceleration, especially suited for dynamic analysis of a structure, is the response spectrum method. This well known method is widely used to estimate the peak structural response due to a single component of base motion. Here, we are dealing with translational and rotational accelerations acting simultaneously and the peak responses to the two individual excitations need to be appropriately combined. This problem is not very different, however, from the one of computing the peak response of a building subjected to two horizontal components of ground motion for which a combination rule is available [8].

When applying the response spectrum method to estimate the structural response to multiple components of base motion, three pieces of information are required: (1) the mean response spectrum for each of the base motion components—for the problem at hand these response spectra are available in Fig. 2; (2) a rule for combining the peak responses of the structure due to each ground motion component, separately (Appendix B); and (3) the correlation coefficients between different modal responses and ground motions (Appendix B).

Using the mean pseudo-velocity response spectra of u_y and ru_θ (Fig. 2), the maximum response of the one-story building is estimated as follows: (1) define the system parameters T_y, Ω, e/r, and r; (2) define the modal damping ratios for each of natural vibration mode—these modes are uncoupled if the system has a symmetrical plan; (3) compute the natural vibration frequencies and modes of the system, (4) compute the peak response $(r_y)_o$ of the structure due to translational (y) component of base motion by combining the peak modal responses obtained using the mean response spectrum in Fig. 2; (5) compute, analogous to step (4), the peak response $(r_\theta)_o$ of the structure due to the rotational component of base motion characterized by the mean response spectrum of Fig. 2; and (6) combine the peak responses $(r_y)_o$ and $(r_\theta)_o$ appropriately.

Because the natural vibration frequencies in coupled lateral motions of buildings are often closely spaced, the modal correlation terms should be included in the modal combination procedures needed in steps (4) and (5). This can be accomplished by the CQC rule.

Similarly, in step (6) a cross response term should be included in combining the peak responses to the individual components of base motion (Appendix B). However, the mean cross correlation between the translational and rotational excitations is small (Appendix B) and the building response can be estimated by combining its peak response to each base motion independently using the square

root of the sum of the squares (SRSS) rule:

$$r_o \simeq \sqrt{(r_y)_o^2 + (r_\theta)_o^2} \tag{7}$$

Note that Eq. (7) is not restricted to a single story system; it is equally applicable to compute the peak response of a multistory building due to the simultaneous action of translational and rotational excitations. However, the computation of peak responses $(r_y)_o$ and $(r_\theta)_o$ to individual components of base motion should be modified to recognize the $2N$ natural modes of a one-way unsymmetric N-story building in contrast to the two modes of a one-story building. Further, Eq. (7) can still be used for general unsymmetric plan systems provided the peak responses $(r_y)_o$ and $(r_\theta)_o$ are computed based on the $3N$ vibration modes of the building.

Figure 14 compares the normalized building displacement $(\hat{u}_{-r})_o$ estimated using Eq. (7) and its mean values determined from response history analysis (Figs. 7-10). In most cases, Eq. (7) provides reasonably good estimates of the exact response including the effects of rotational acceleration for any combination of the system parameters; thus, avoiding the excessive conservatism inherent in a constant accidental eccentricity.

Fig. 14 also presents the values of the normalized response $(\hat{u}_{-r})_o$ computed using the thirty percent rule, i.e., $(r_y)_o + 0.3(r_\theta)_o$, present in the UBC and other building codes to combine the effects of two components of base motion. This is done even though there is no statistical justification to use this rule in the case of translational and rotational excitations. These results show that the thirty percent rule always overestimates the 'exact' mean value of $(\hat{u}_{-r})_o$. Both the SRSS and thirty percent rules require similar computational work; therefore, the SRSS rule, given its statistical justification and more accurate results, is preferable.

The additional computational effort required to include in Eq. (7) the response to rotational acceleration is minimal since identical vibration modes and frequencies are used to compute the structural response to both excitations. However, most commercially available structural analysis programs are not able to handle the case of response spectrum analysis of buildings with multiple excitations; this can be achieved, however, with slight modifications of the computational codes.

3.7 Comparison with Newmark's approach for symmetrical buildings

A deterministic procedure for estimating the increase in building response resulting from rotational excitation in symmetric-plan buildings was presented in 1969 by Newmark [1]. In this section we examine and compare the results presented in his classic paper with the ones presented here

using the available ground motion data for rotational excitation. Let us first summarize briefly Newmark's approach.

Newmark assumed that the rotation of the building foundation $u_{g\theta}$ is equal to the rotation experienced by an infinitesimal element of the ground surface due to a wave with components $u_{gx}(y - ct)$ and $u_{gy}(x - ct)$ traveling at speed c along the building foundation, i.e.,

$$u_{g\theta} = 1/2(\frac{\partial u_{gx}}{\partial y} - \frac{\partial u_{gy}}{\partial x}) \simeq \frac{\partial u_{gy}}{\partial x} \tag{8}$$

He showed that, for this motion, the peak values of the rotational excitation $(u_{g\theta})_o$, angular velocity $(\dot{u}_{g\theta})_o$, and angular acceleration $(\ddot{u}_{g\theta})_o$ satisfy

$$(u_{g\theta})_o = (\dot{u}_{gy})_o/c \ , \ (\dot{u}_{g\theta})_o = (\ddot{u}_{gy})_o/c \ , \text{ and } \ (\ddot{u}_{g\theta})_o = (\dot{\ddot{u}}_{gy})_o/c \tag{9}$$

Newmark considered translational ground motion with a peak ground displacement $(u_{gy})_o$, velocity $(\dot{u}_{gy})_o$, and acceleration $(\ddot{u}_{gy})_o$ of 25.4 cm, 38.1 cm/sec, and 304.8 cm/sec^2, respectively. He also estimated the peak value of $(\dot{\ddot{u}}_{gy})_o$, the time derivative of the ground acceleration, as 12700 cm/sec^3—this was needed for computing the peak rotational acceleration of the base (Eq. (9)). Using these parameters for translational ground motion in Eq. (9), he estimated $(u_{g\theta})_o$, $(\dot{u}_{g\theta})_o$ and $(\ddot{u}_{g\theta})_o$. Using appropriate elastic response amplification factors he then constructed the elastic response spectrum for the translational and rotational component of base motion as shown in Fig. 15. The response spectrum for rotational excitation is presented for two values of the transit time τ, the time required for the wave to travel across the building plan dimension b; $\tau = b/c = 0.05$ and 0.1. Note that the torsional response spectrum has been scaled by $b/2 = 15.25$ m (50 ft). Both, translational and torsional response spectra, have been normalized with respect to the peak ground velocity (=38.1 cm/sec) of the translational ground motion.

Newmark then developed a result for accidental eccentricity which can be expressed as:

$$e_a/b = 2(\frac{r}{b})^2 \frac{(b/2)\,(u_\theta)_o}{(u_y)_o}\,\Omega^2 \ = \ \frac{r\,(u_\theta)_o}{(u_y)_o}\,\Omega^2\,\frac{r}{b} \tag{10}$$

where $(u_y)_o$ is the ordinate of the translational response spectrum for the lateral vibration period T_y of the system, and $(u_\theta)_o$ is the ordinate of the torsional response spectrum for the torsional vibration period $T_\theta = T_y/\Omega$ of the system.

Newmark's results can be compared with ours in three stages: (1) the response spectra for the rotational and translational excitations, (2) the ratio between torsional response and lateral response, and (3) the normalized accidental eccentricity e_a/b.

Figure 15 shows the mean response spectra for translational and rotational excitations computed from the recorded base motions (Table 1) superimposed over Newmark's spectra presented above. For proper comparison the mean response spectrum for 'recorded' rotational excitations has been scaled by the ratio $(b/2)/r = (30.5/2)/50 = 0.305$, to account for the change in building plan dimensions between Figs. 2 ($b = 50$m) and Newmark's work ($b = 30.5$m). The shapes of the two translational spectra are similar; however, the magnitudes of the two spectra are different since the peak ground velocity used to normalize each response spectrum was different. This difference in magnitude between the two spectra is not important since we are concerned with the relative increase in structural displacements due to rotational excitation. However, Newmark's spectra for rotational excitation are between two and seven times larger than the one computed from the recorded motions, depending on the value chosen for the transit time τ. Despite this difference, Newmark identified the higher frequency content in the torsional response spectra; this effect was observed in Figs. 1 and 2.

Next we compare the ratio between the responses $(u_\theta)_o$ and $(u_y)_o$ of a symmetric system to rotational and translational base motions, respectively. Fig. 16 shows the quantity $(b/2)\,(u_\theta)_o/(u_y)_o$ computed from the values of $(u_\theta)_o$ and $(u_y)_o$ given by the response spectra for rotational and translational components of base motion (Fig. 15). The results obtained using Newmark's response spectra are shown for two transit times, together with the mean values obtained from the response spectra from earthquake records. The trends of this displacement ratio are similar in both cases; the ratio decreases with increasing T_y up to 3 sec, approximately, and then remains essentially constant for longer periods. However, Newmark's results are three to seven times larger than those from recorded motions.

We now identify an important difference between Newmark's approach and this work in calibrating the design eccentricity to represent the torsional response of buildings to rotational excitation. The difference lies in the measure used to define this response. In our work (Eq. (6)) this measure is $(\hat{u}_{-\tau})_o - 1 = ((u^*_{-\tau})_o - (u_y)_o)/(u_y)_o$, which is the increase in peak response due to the simultaneous action of the two base motion components over the maximum response $(u_y)_o$ due to translational excitation alone; this increase was computed exactly from response history analyses. In contrast, Newmark's measure $(b/2)\,(u_\theta)_o/(u_y)_o$ is the peak torsional response $(b/2)\,(u_\theta)_o$ to the rotational excitation alone normalized relative to the peak translational response $(u_y)_o$ to the translational excitation alone. This measure would be identical to ours if the responses $(b/2)\,u_\theta(t)$ and $u_y(t)$ attained their peak values at the same time instant and the two were additive. Thus Newmark's

measure is equivalent to the assumption that the maximum response of a system subjected to the two excitations simultaneously can be computed by the absolute sum of the response to the two excitations individually. It is because of this excessively conservative assumption that the accidental eccentricities computed by Newmark's approach (Eq. (10)) will be very conservative.

This expectation is confirmed by Fig. 17 where we compare our results with those from Newmark's approach. The latter were computed from Eq. (10) and the values for $(u_y)_o$ and $(u_\theta)_o$ from Newmark's spectra presented in Fig. 16. Our results were obtained from Eq. (6) and the values of $(\hat{u}_{-r})_o$ presented in Fig. 7. Newmark's results are for buildings with plan dimension $b = 30.5$m whereas ours are for $b = 25$ m. However, this discrepancy is of little consequence because our results are about the same even for $b = 50$ m (Fig. 12). It is seen that Newmark's approach leads to much larger values of accidental eccentricity over a wide range of system parameters, especially for short period systems or torsionally flexible systems. Note that the results from Newmark's approach are presented for $\tau = 0.05$ sec; the larger value of $\tau = 0.1$ gives even larger values of e_a/b, especially for smaller values of Ω. Two factors explain the large difference in the accidental eccentricity obtained by the two approaches. First, the torsional response spectrum considered by Newmark is three to seven times larger than the one obtained from recorded motions whereas the two normalized translational response spectra are similar (Fig. 16). Second, Newmark's approach to compute accidental eccentricity assumes that the peak values of the torsional and lateral responses of a symmetric-plan building occur simultaneously, which leads to very conservative values of accidental eccentricity.

3.8 Conclusions

This investigation of accidental torsion in buildings induced by base rotational motions has led to the following conclusions:

1. The time-history of rotational excitation, computed from the difference between translational motions recorded at two different points of the building foundation, shows higher frequency content compared to the base translation. Response spectra for earthquake motions recorded at thirty building sites showed that the ordinates of the mean response spectrum for rotational excitation are an order of magnitude smaller than for base translation.

2. The increase in displacements of symmetric buildings resulting from accidental torsion due to rotational excitation is larger for systems with small vibration periods (less than about half a second) and small ratios of the torsional to translational frequencies ($\Omega < 1$). However, this

increase in displacements is less than five percent for long period systems (longer than half a second) or systems that are torsionally stiff ($\Omega > 1$).

3. The increase in building displacements resulting from accidental torsion is insensitive to changes in the frequency ratio Ω unless the building is very stiff ($T_y < 0.5$ sec).

4. Buildings with longer plan dimension perpendicular to the direction of ground motion undergo greater accidental torsion due to rotational excitation, with the building displacement increasing by over a hundred percent for building plans of about one hundred meters.

5. The accidental torsion effects, when significant, are larger for symmetric-plan buildings compared to unsymmetric-plan systems.

6. The accidental eccentricity e_a that accounts for the increase in building displacements due to rotational excitation is larger for systems with short uncoupled vibration period T_y and small Ω. In fact, e_a/b reaches a maximum of 7% for systems with $T_y \simeq 0.1$ sec, decreases quickly with increasing T_y, and is less than 2% for systems with $T_y > 0.5sec$, regardless of the value of the frequency ratio. The computed values of accidental eccentricity are much smaller than the code values of $0.05b$ to $0.1b$ except for systems with long plan dimension, say $b \geq 50$ m.

7. These accidental eccentricities are shown to be between seven to twenty times smaller than the values computed using Newmark's approach. Two factors explain the large difference in the accidental eccentricities obtained by the two approaches. First, the torsional response spectrum developed by Newmark is three to seven times larger than the mean torsional response spectrum computed from earthquake records. Second, Newmark's approach to compute accidental eccentricity assumes that the peak values of the torsional and lateral responses of a symmetric-plan building occur simultaneously, which leads to very conservative values of accidental eccentricity.

8. Alternatively, the building response due to the rotational and translational excitations, acting simultaneously, can be estimated by computing the peak response to each base motion independently and combining the peak values using the SRSS rule.

3.9 References

1. Newmark, N.M.'Torsion in symmetrical buildings', Proc. Fourth World Conf. Earthq. Engrg., Santiago, Chile, pp. A3, 19-32, 1969.

2. Veletsos, A.S., Erdik, M. and Kuo, P.,'Response of structures to propagating ground motions', Report No. 22, Structural Research at Rice, Rice University, Houston, Texas, 1975.

3. Luco, J.E.'Torsional response of structures to obliquely incident seismic SH waves', Earthquake eng. struct. dyn. 4, 207-219 (1976).

4. Iguchi, M.,'Earthquake response of embedded cylindrical foundations to SH and SV waves', Proc. Eighth World Conf. Earthq. Engrg., San Francisco, California, pp. 1081-1088, 1984.

5. Luco, J.E. and Mita, A.'Response of a circular foundation to spatially random ground motion', J. eng. mech. div. ASCE 113, 1-15 (1987).

6. Veletsos, A.S., Prasad, M. and Tang, Y.'Design approaches for soil-structure interaction', Technical Report NCEER-88-0031, Rice University, Houston, Texas, 1988.

7. Hejal, R. and Chopra, A.K.'Earthquake response of torsionally-coupled buildings', Report No. 87-20, Earthquake Engineering Research Center, University of California, Berkeley, CA., 1987.

8. Smeby, W. and Der Kiureghian, A.,'Modal combination rules for multicomponent earthquake excitation', Earthquake eng. struct. dyn. 13, 1-12 (1985).

Table 1: General description of base rotational and translational excitations considered in the analyses

Earthquake	CSMIP Station No.	Channels	Separation d (cm)	$(a_{gy})_o/g$	$(v_{gy})_o$ (cm/sec)	$r(a_{g\theta})_o/g$	$r(v_{g\theta})_o$ (cm/sec)
Whittier	24511	6,7	2528	0.0457	2.1542	0.0112	0.2852
'	24468	1,14	4999	0.2703	20.0361	0.0750	3.2365
'	24463	8,9	11022	0.1236	12.6256	0.0204	0.6929
'	24236	1,9	3036	0.1183	9.4175	0.0241	0.9520
'	24370	8,9	3658	0.1609	9.7200	0.0219	0.8320
'	14323	13,16	5392	0.0729	8.6828	0.0098	0.5787
'	24322	11,12	2579	0.2572	8.1114	0.0724	1.5408
'	24386	1,13	4517	0.1403	7.8060	0.0610	2.3796
'	24514	8,9	9162	0.0494	2.9378	0.0080	0.3856
Loma Prieta	47459	9,10	2155	0.2625	25.4094	0.0972	3.8294
'	47391	8,9	8931	0.2397	39.5641	0.0206	1.6992
'	58235	10,11	4307	0.3547	35.8806	0.0365	2.3421
'	57356	11,12	6447	0.1045	25.7662	0.0132	0.8204
'	57355	11,12	5709	0.0980	24.7113	0.0154	1.3805
'	57357	20,21	3520	0.0823	19.6421	0.0166	1.0755
'	58261	4,5	6035	0.1549	23.5018	0.0287	2.5227
'	58479	6,7	5294	0.0682	13.7574	0.0089	0.3773
'	58480	8,9	2838	0.1315	14.4559	0.0434	2.1969
'	58532	4,6	4267	0.1032	13.6951	0.0235	1.9298
'	57502	9,10	5060	0.0905	9.7765	0.0144	0.7843
'	58462	7,9	6553	0.1105	10.5106	0.0116	0.7752
'	58483	11,16	4493	0.1715	27.4607	0.0220	1.6891
'	58224	6,7	4798	0.2440	32.1426	0.0430	2.0103
'	58503	8,9	7833	0.1046	15.8061	0.0117	0.9731
'	58348	10,11	3871	0.1175	19.2894	0.0218	2.5883
'	57562	3,4	7315	0.1705	14.8729	0.0268	0.9382
Sierra Madre	24370	8,9	3658	0.1022	7.9699	0.0105	0.4754
'	24541	13,14	4075	0.1245	7.4976	0.0403	1.1465
'	24385	1,13	6227	0.1064	8.5029	0.0351	1.9246
Upland	24511	6,7	2528	0.1033	8.2472	0.0345	0.8269

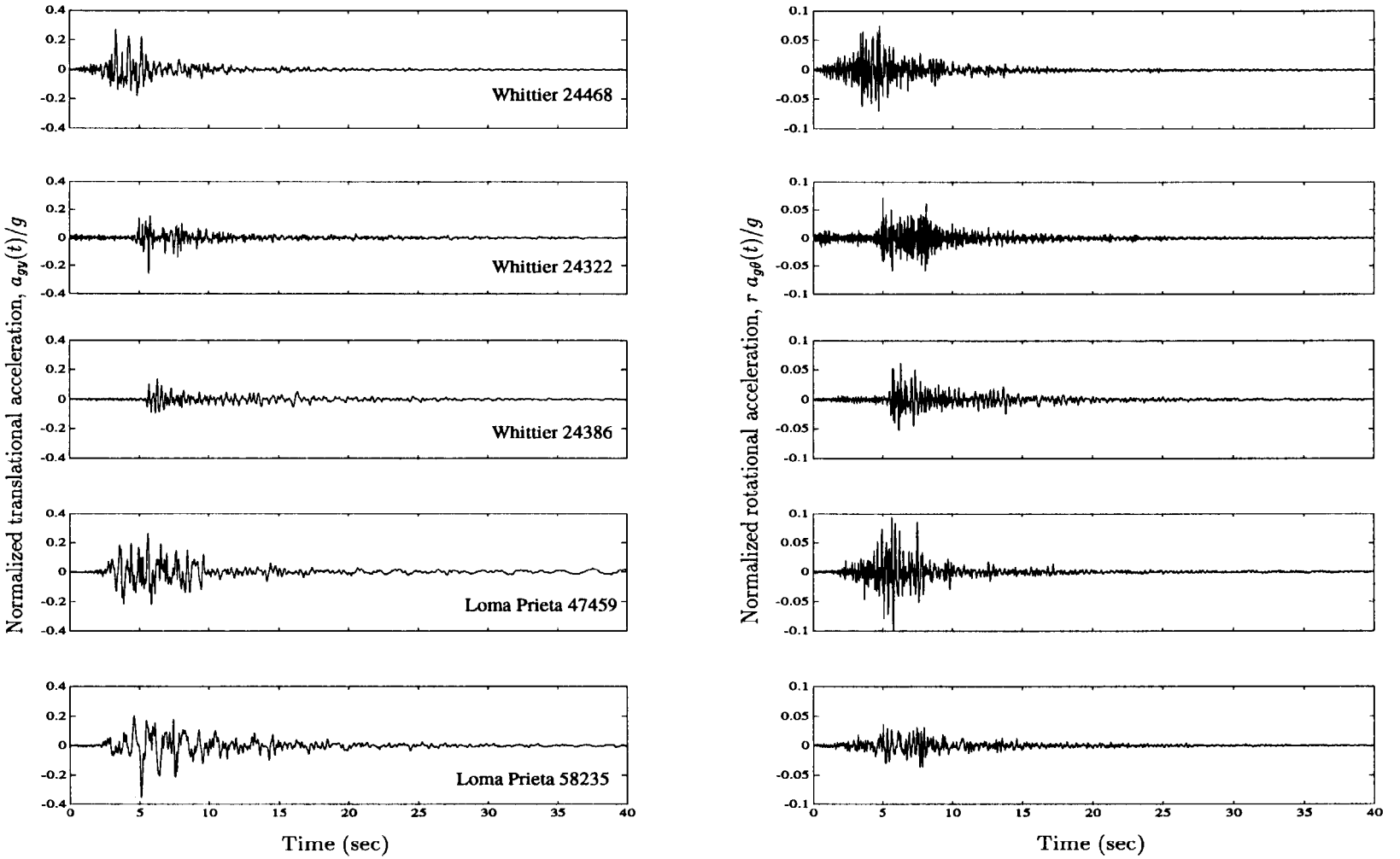

Figure 1: Typical base translation and rotation acceleration histories

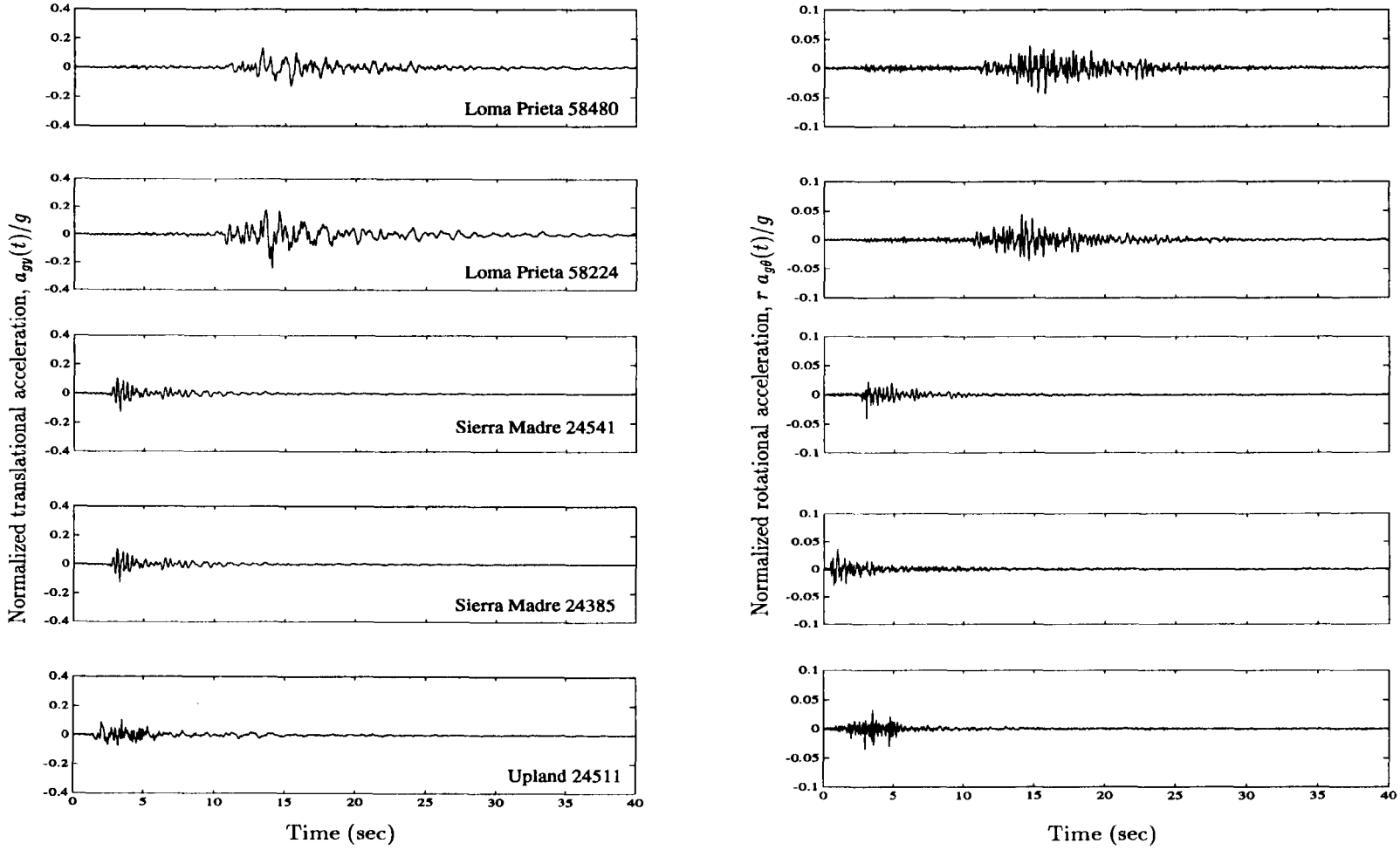

Figure 1 (cont.): Typical base translation and rotation acceleration histories

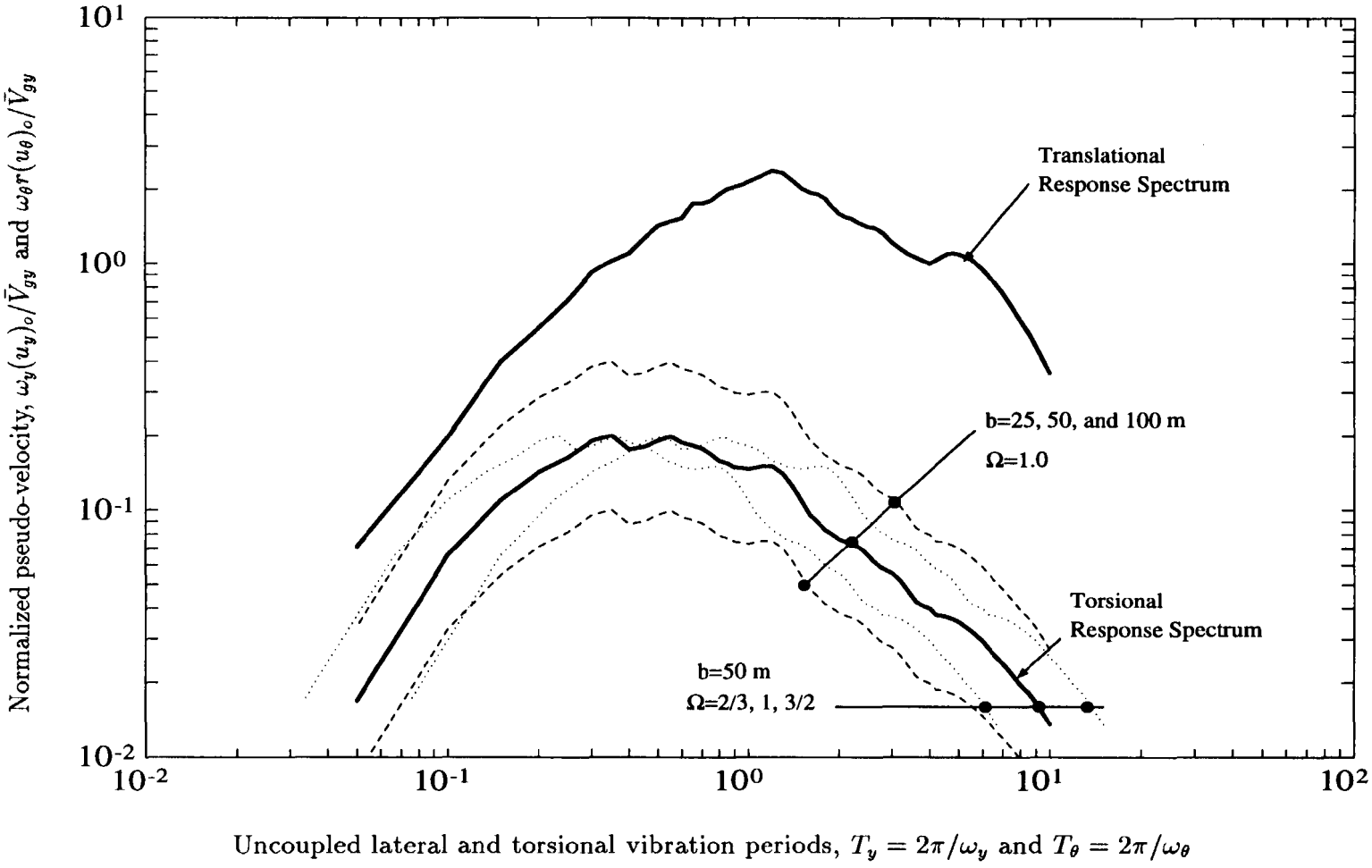

Figure 2: Mean pseudo-velocity response spectrum for base translation and rotation

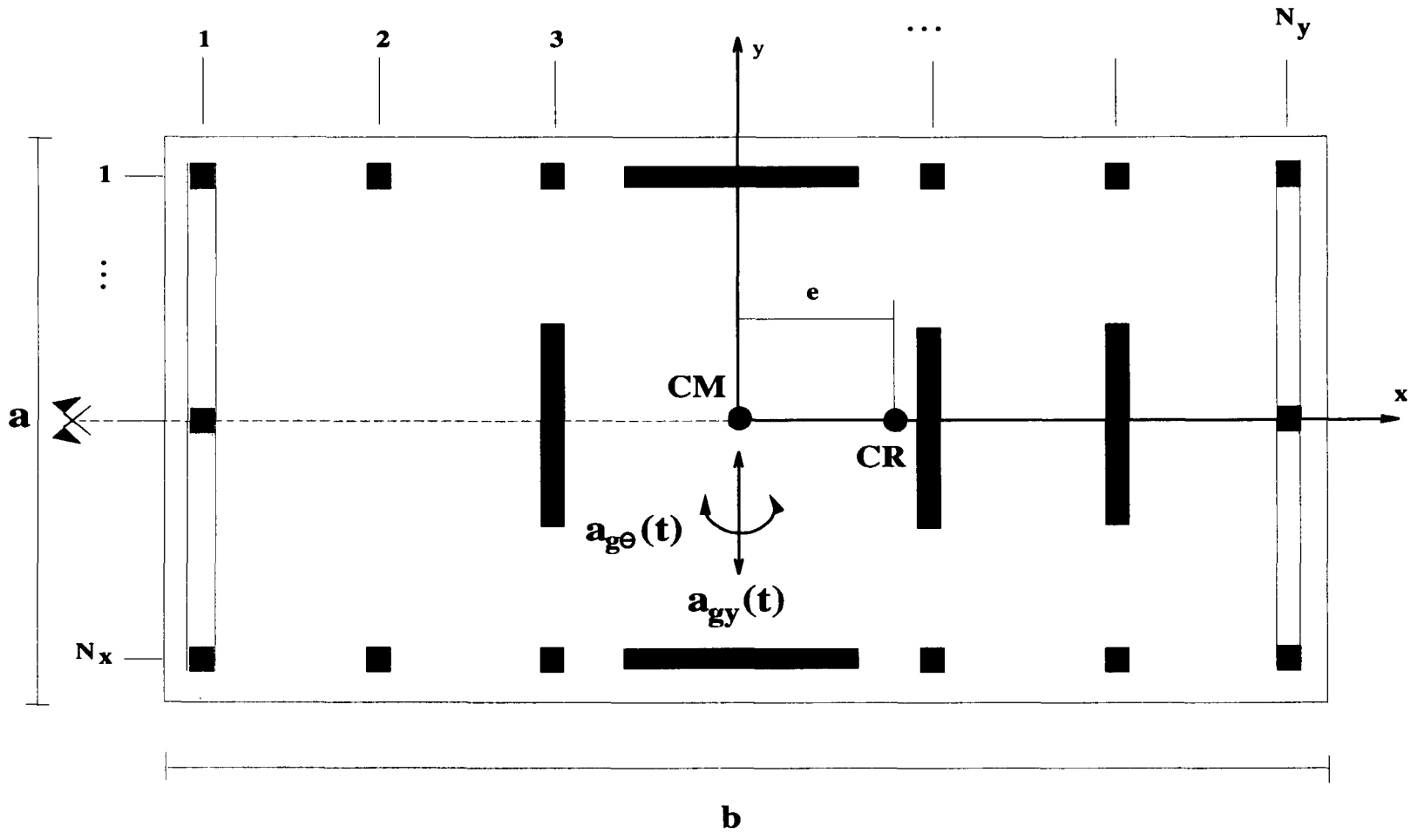

Figure 3: Plan of single–story system considered

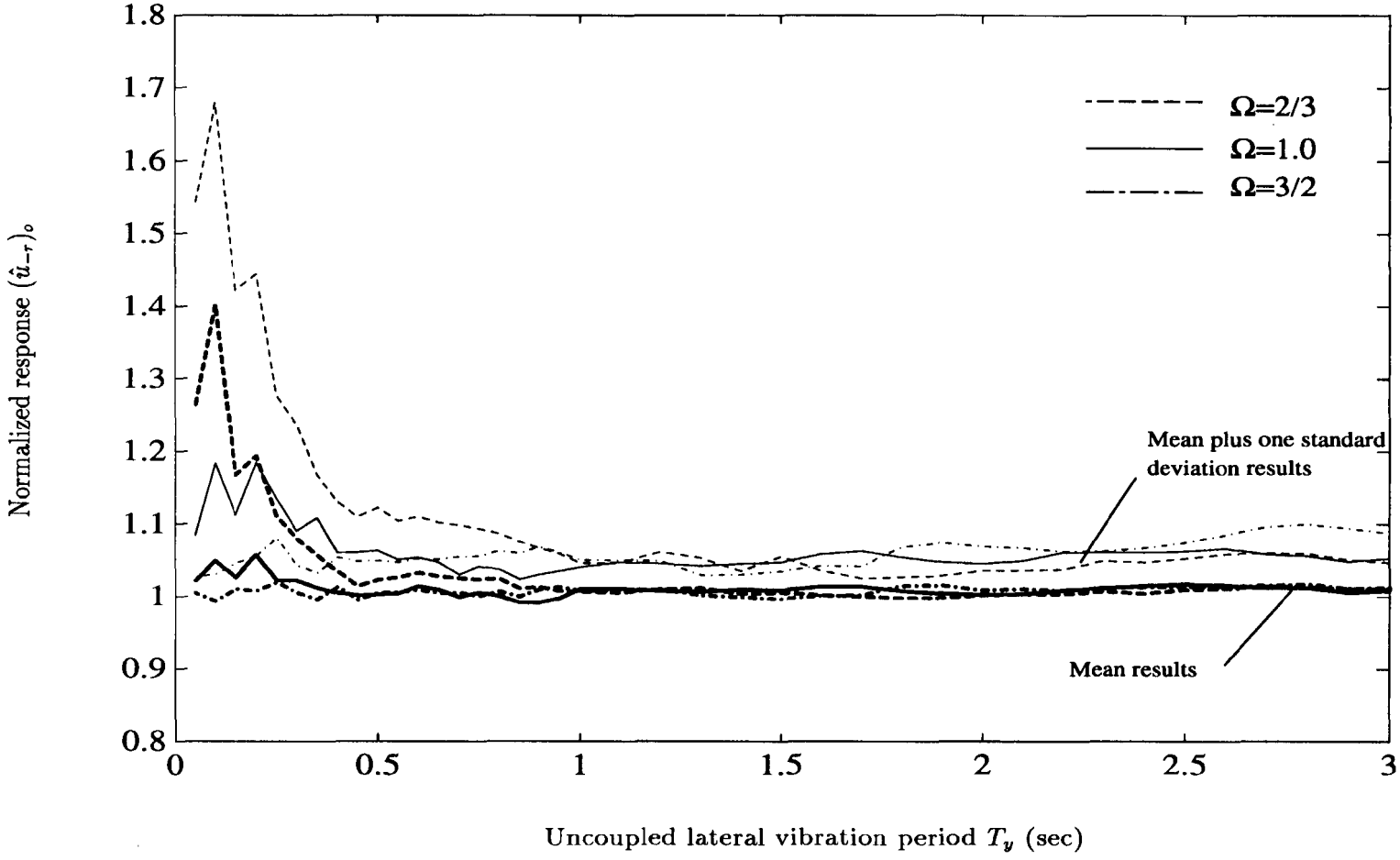

Figure 4: Mean and mean plus one standard deviation of the normalized response $(\hat{u}_{-r})_o$ as a function of T_y, for systems with $\Omega = 2/3, 1$, and $3/2$; $a/b = 1$, and $b = 50$m.

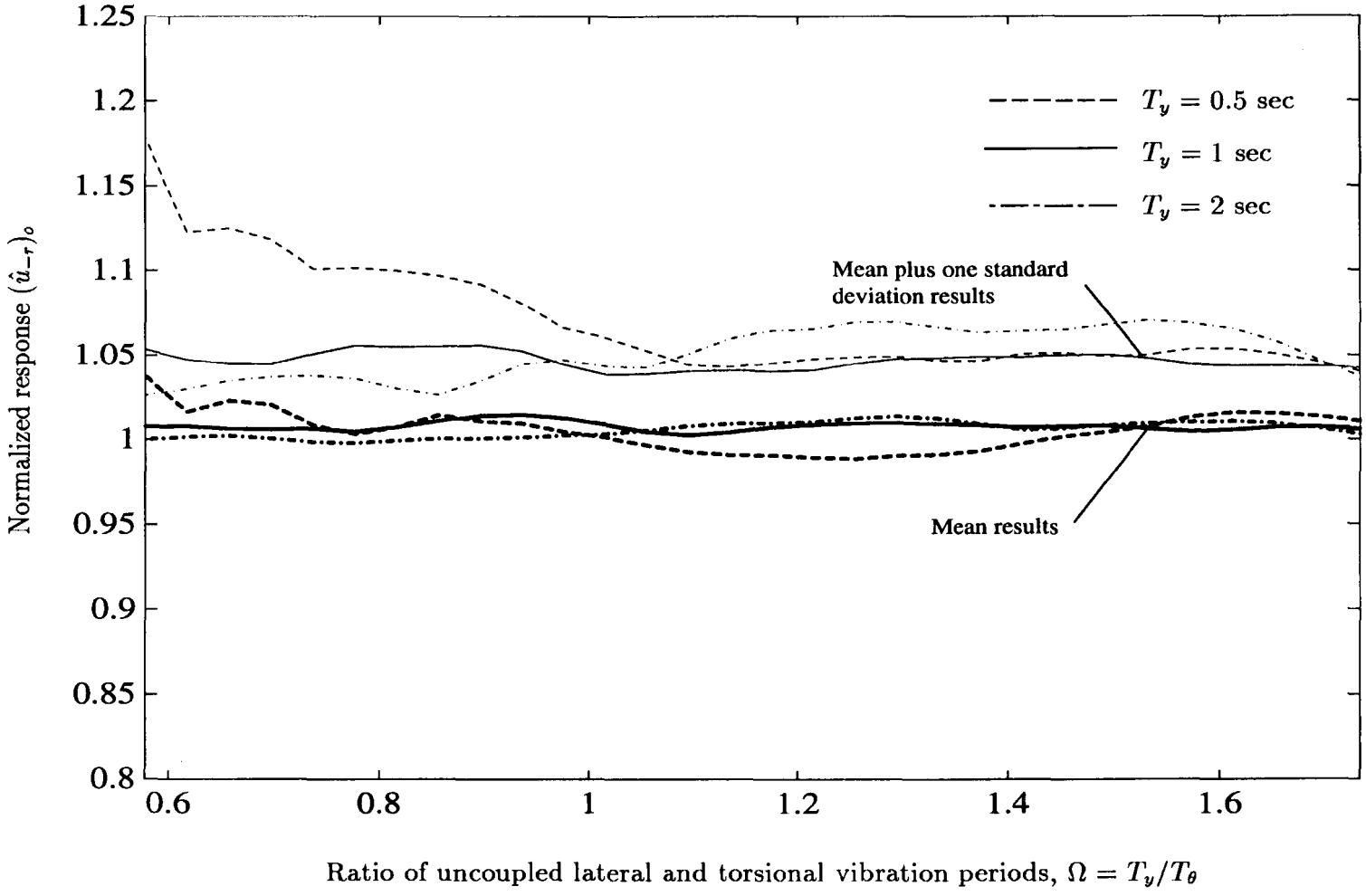

Figure 5: Mean and mean plus one standard deviation of the normalized response $(\hat{u}_{-r})_o$ as a function of Ω, for systems with $T_y = 0.5, 1$ and 2 sec, $a/b = 1$, and $b = 50$m.

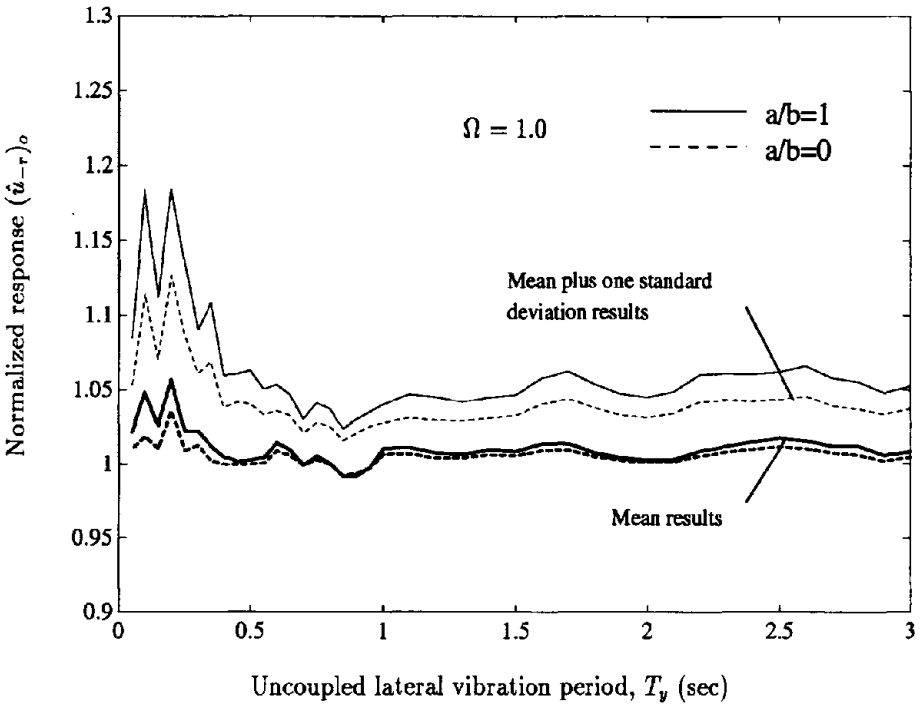

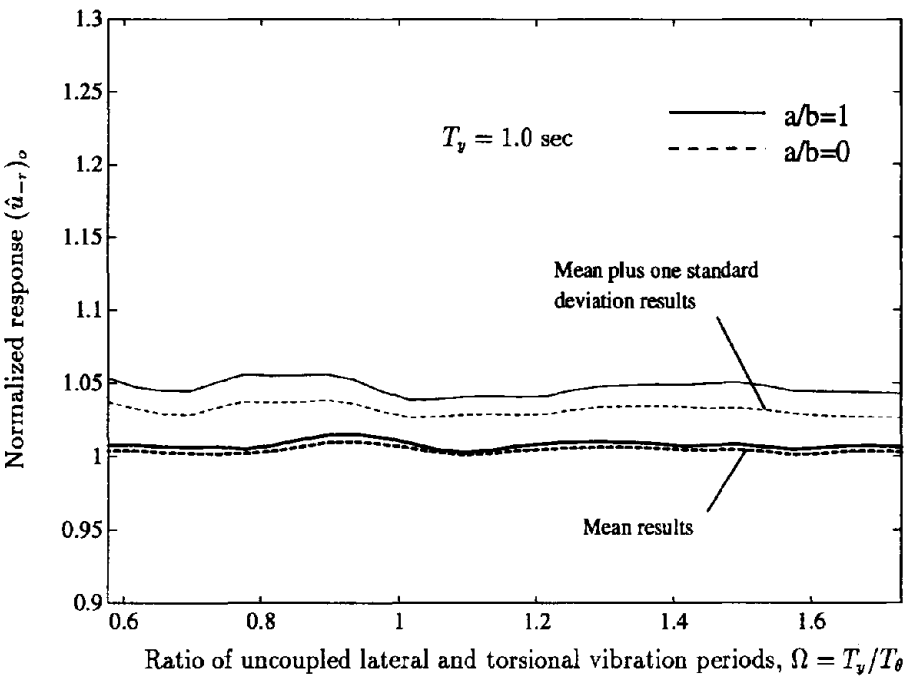

Figure 6: Normalized building response $(\hat{u}_{-r})_o$ for two values of the building plan aspect ratio, $a/b = 1$ and 0

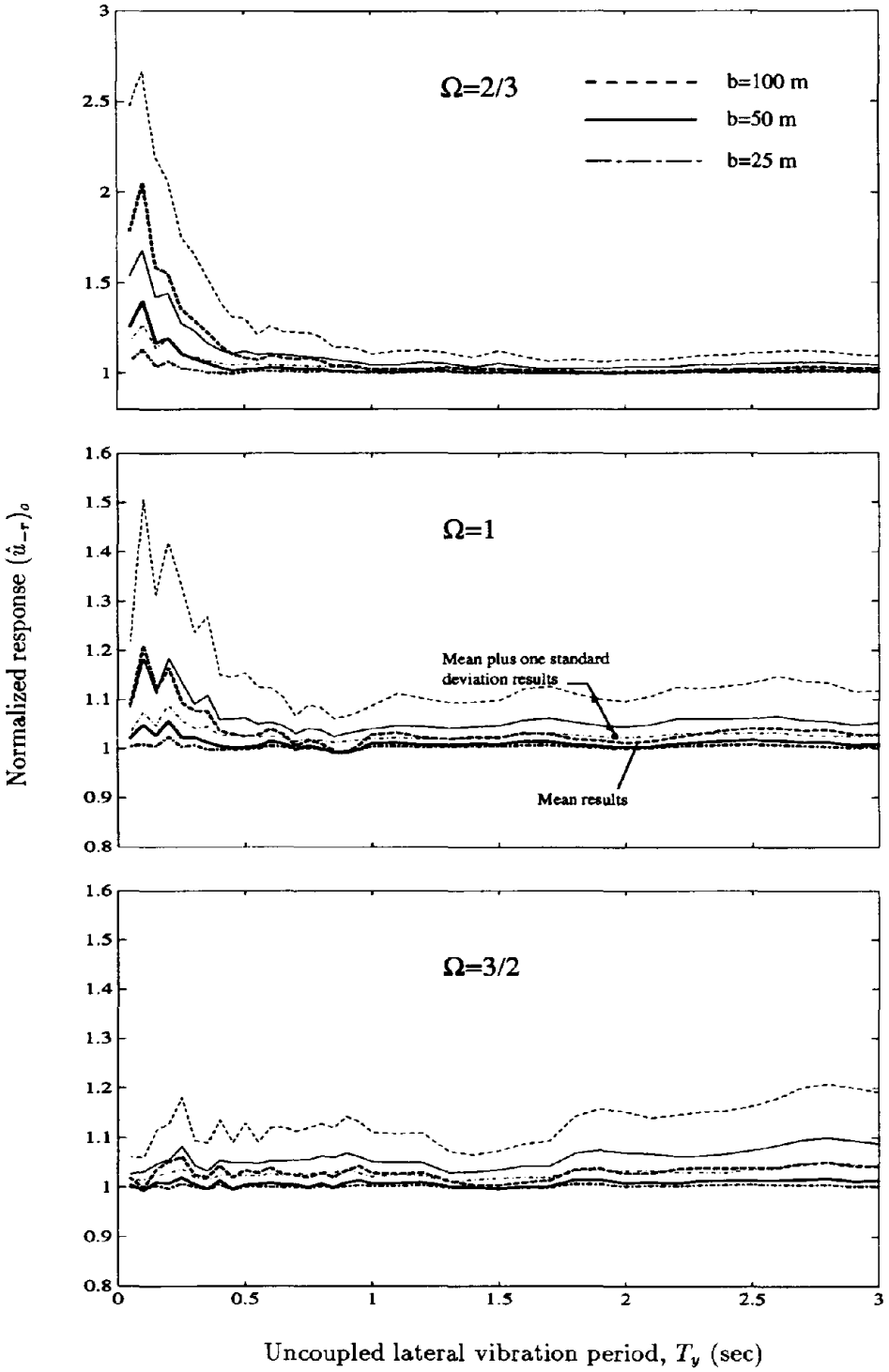

Figure 7: Normalized response $(\hat{u}_{-r})_o$ as a function of T_y for $\Omega = 2/3, 1$ and $3/2$; $b = 25, 50$, and 100 m; and $a/b = 1$

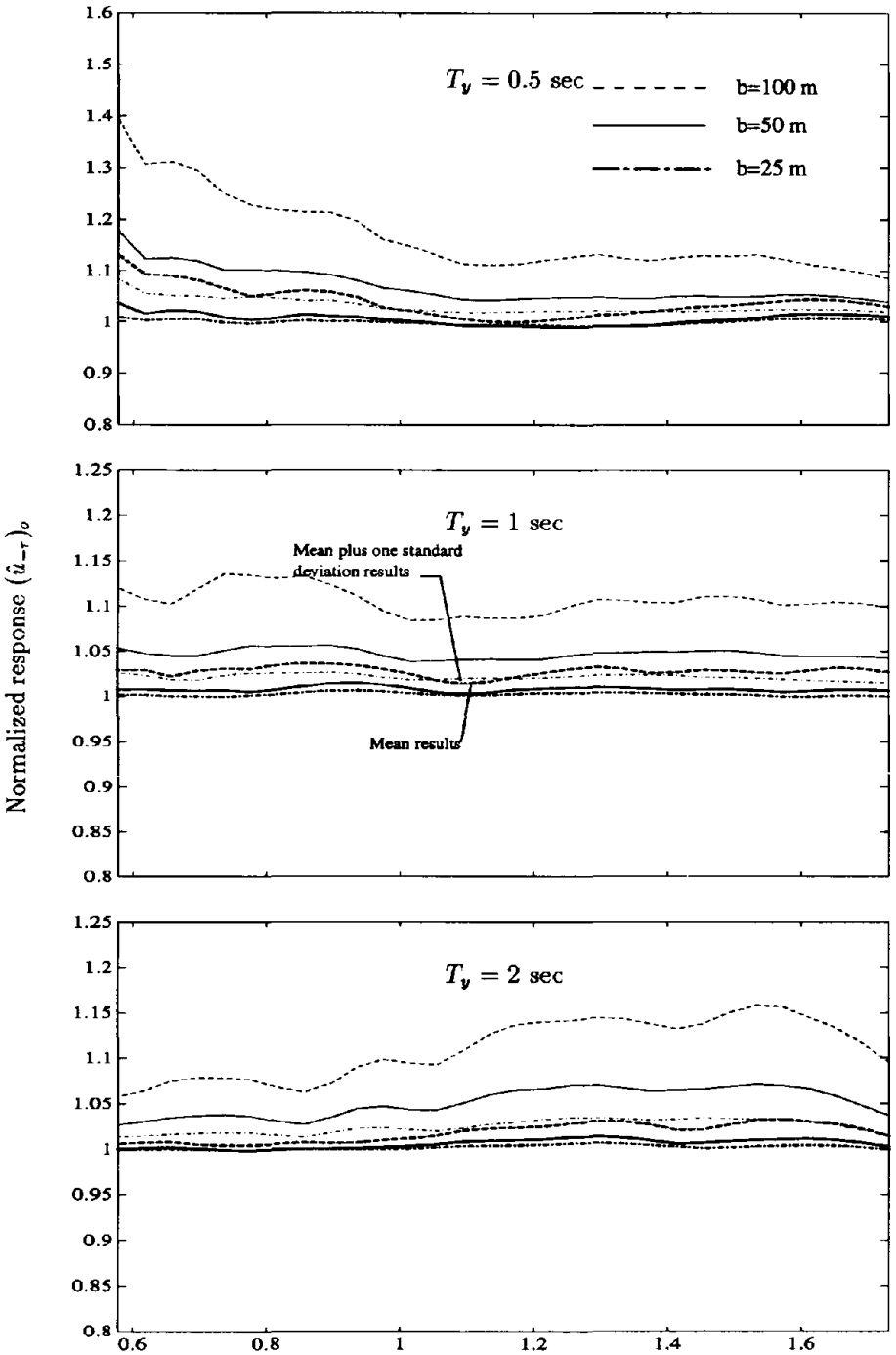

Figure 8: Normalized response $(\hat{u}_{-r})_o$ as a function of Ω for $T_y = 0.5, 1$ and 2 sec; $b = 25, 50$, and 100 m; and $a/b = 1$

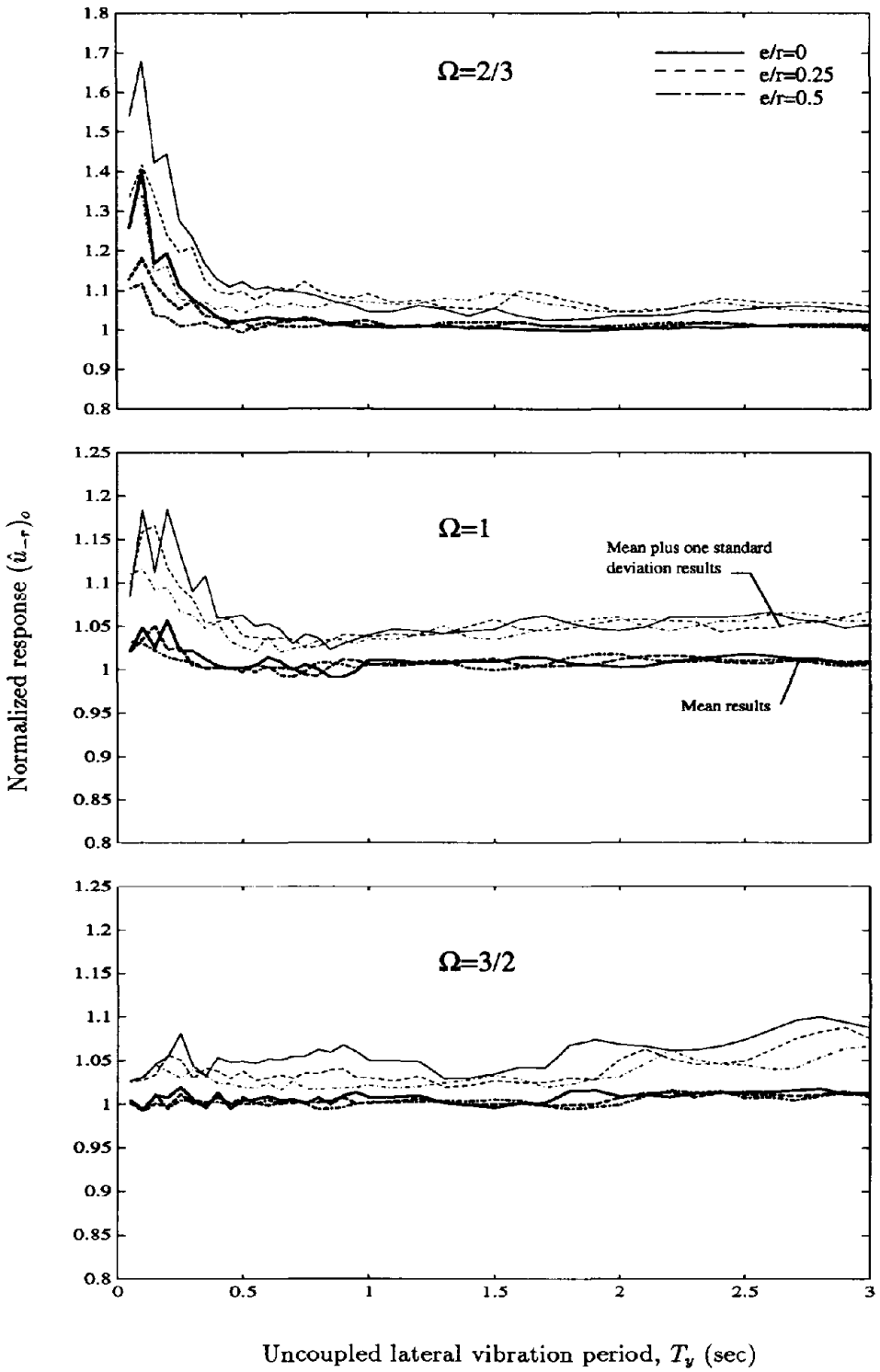

Figure 9: Normalized response $(\hat{u}_{-r})_o$ as a function of T_y for $\Omega = 2/3, 1$ and $3/2$; $e/r = 0, 0.25$, and 0.5; $b = 50$ m; and $a/b = 1$

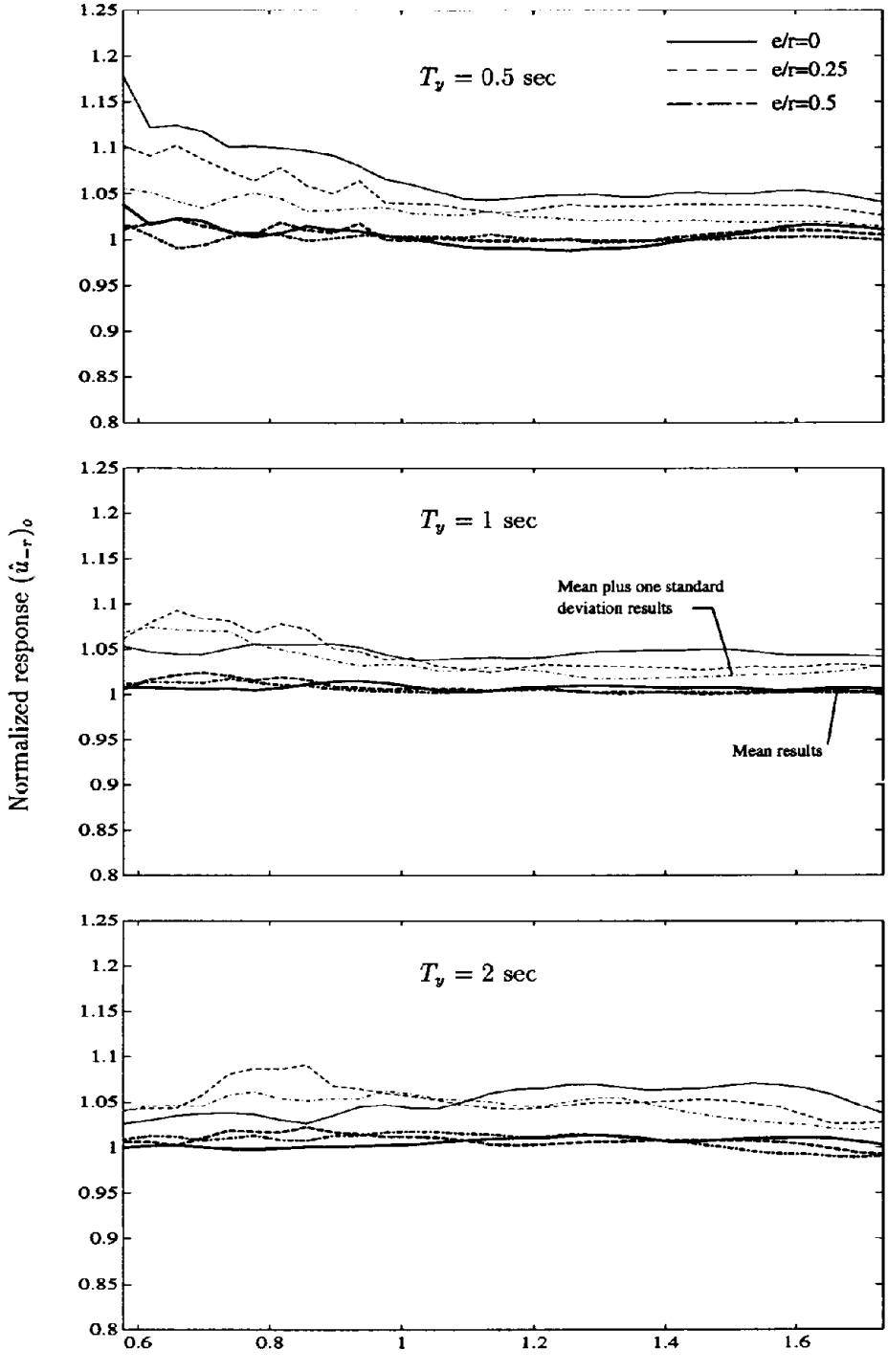

Figure 10: Normalized response $(\hat{u}_{-r})_o$ as a function of Ω for $T_y = 0.5, 1$ and 2 sec; $e/r = 0, 0.25$, and 0.5; $b = 50$ m; and $a/b = 1$

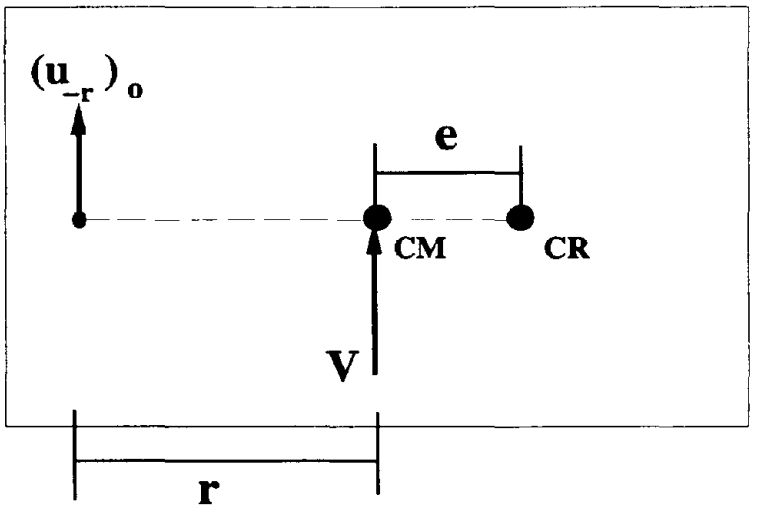

a) Equivalent static force associated with translational base motion

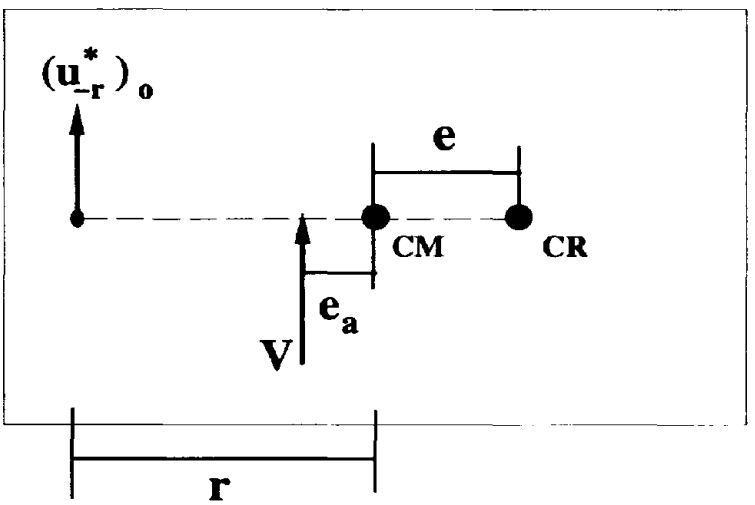

b) Accidental eccentricity e_a to represent response to base rotation

Figure 11: Calibration of accidental eccentricity

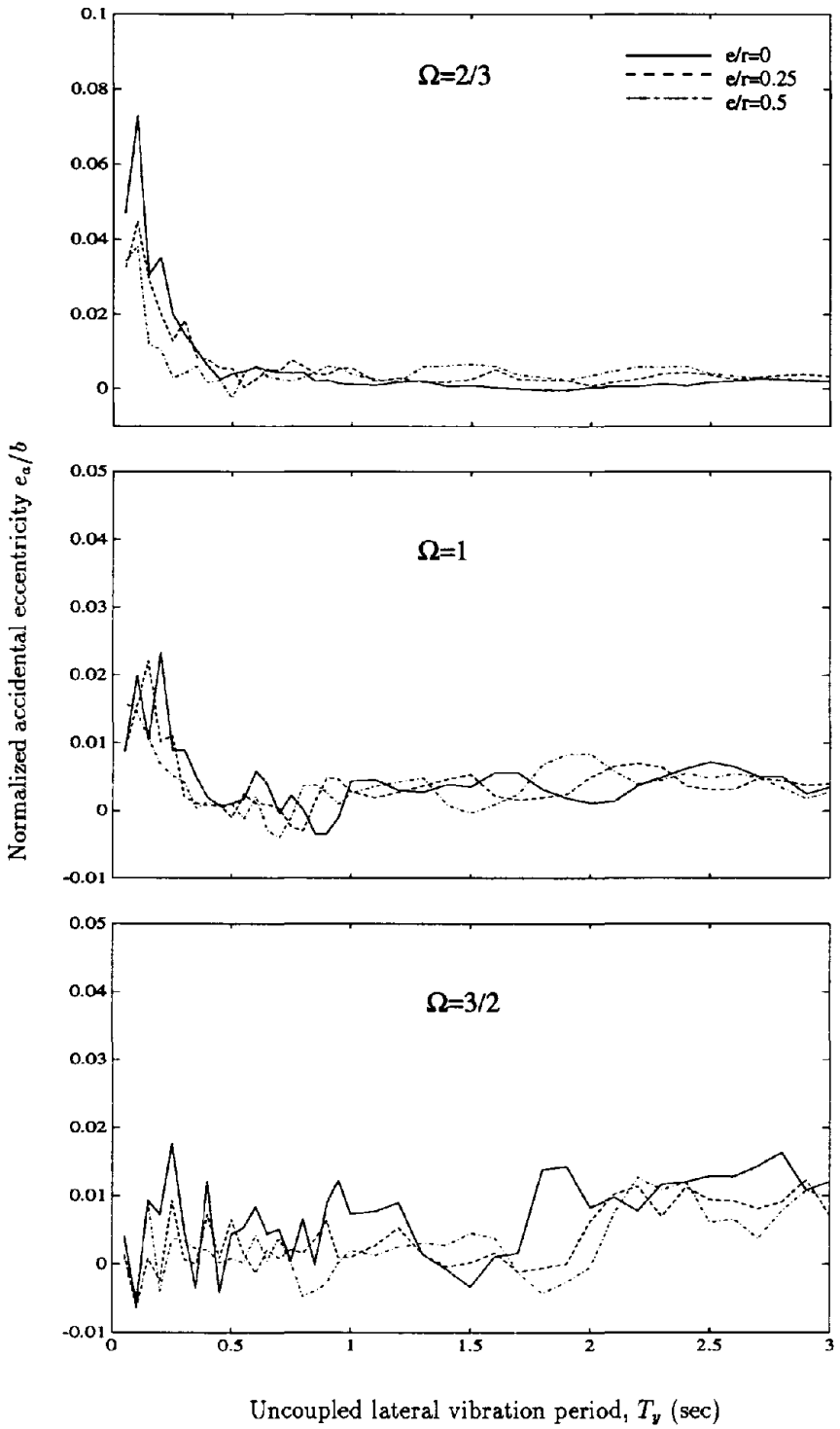

Figure 12: Normalized accidental eccentricity e_a/b as a function of T_y for $\Omega = 2/3, 1$ and $3/2$; $e/r = 0, 0.25$, and 0.5; $b = 50$ m; and $a/b = 1$

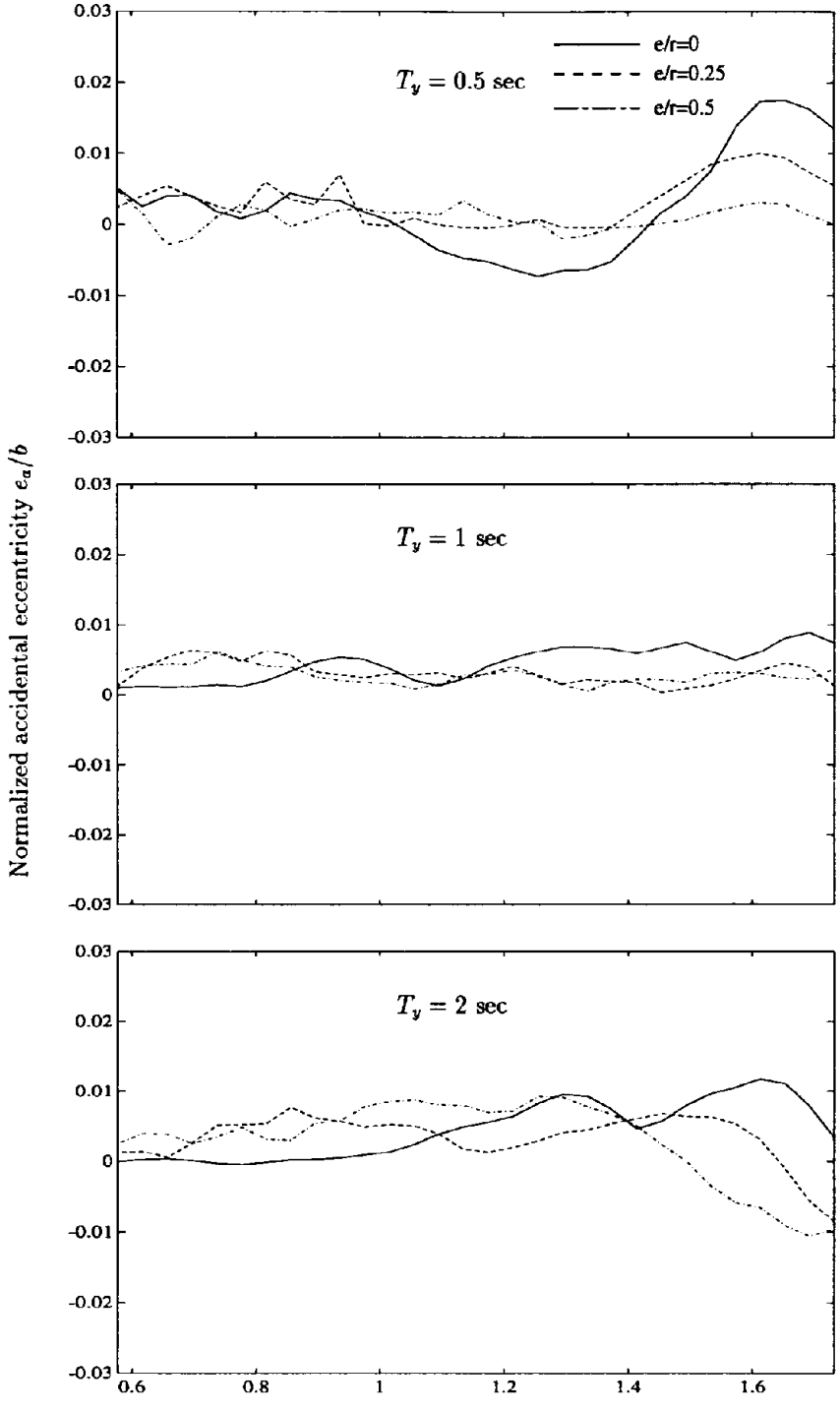

Figure 13: Normalized accidental eccentricity e_a/b as a function of Ω for $T_y = 0.5, 1$ and 2 sec; $e/r = 0, 0.25$, and 0.5; $b = 50$ m; and $a/b = 1$

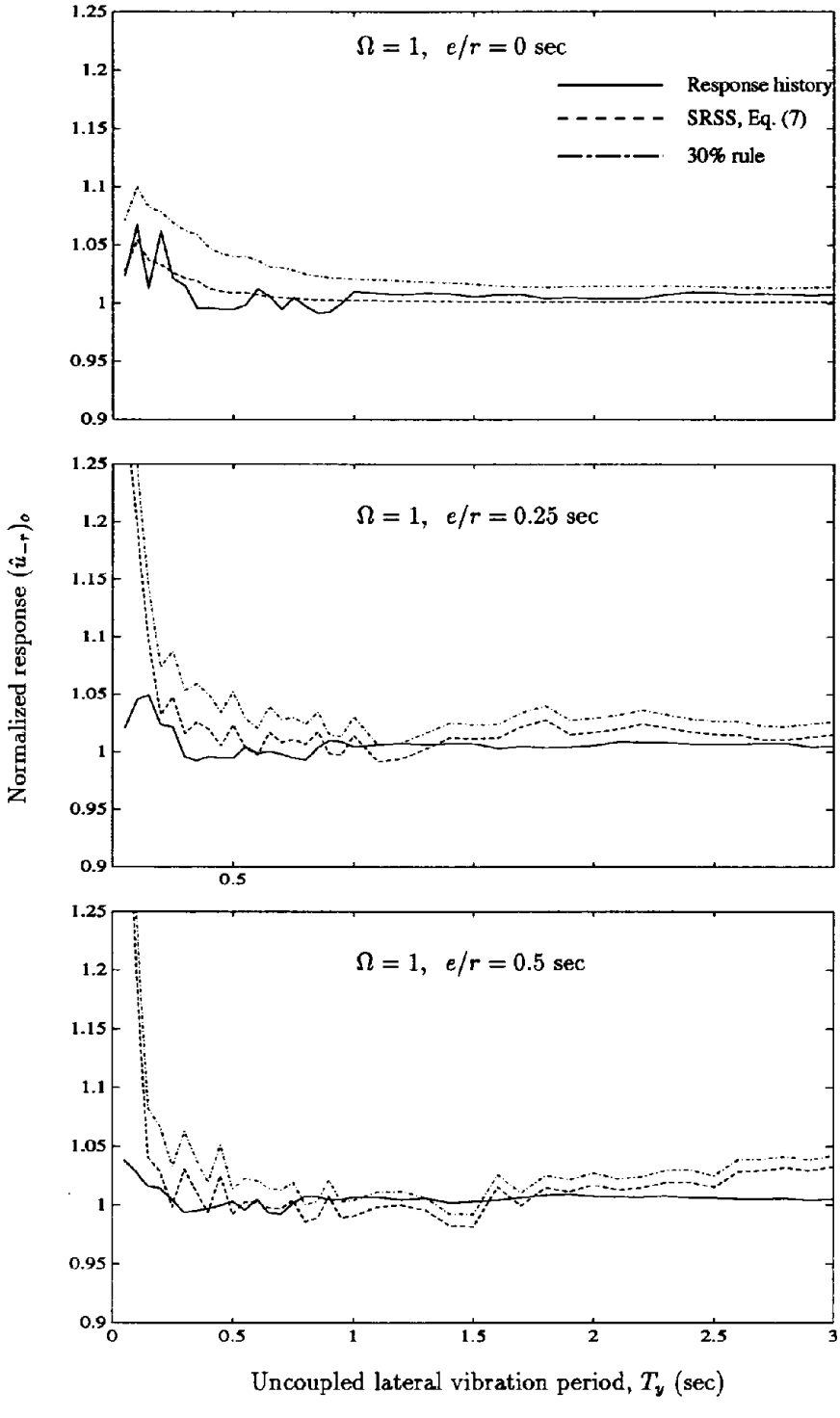

Figure 14: Comparison between the normalized response $(\hat{u}_{-r})_o$ estimated using response history analysis, the SRSS rule (Eq. (7)), and the 30% rule

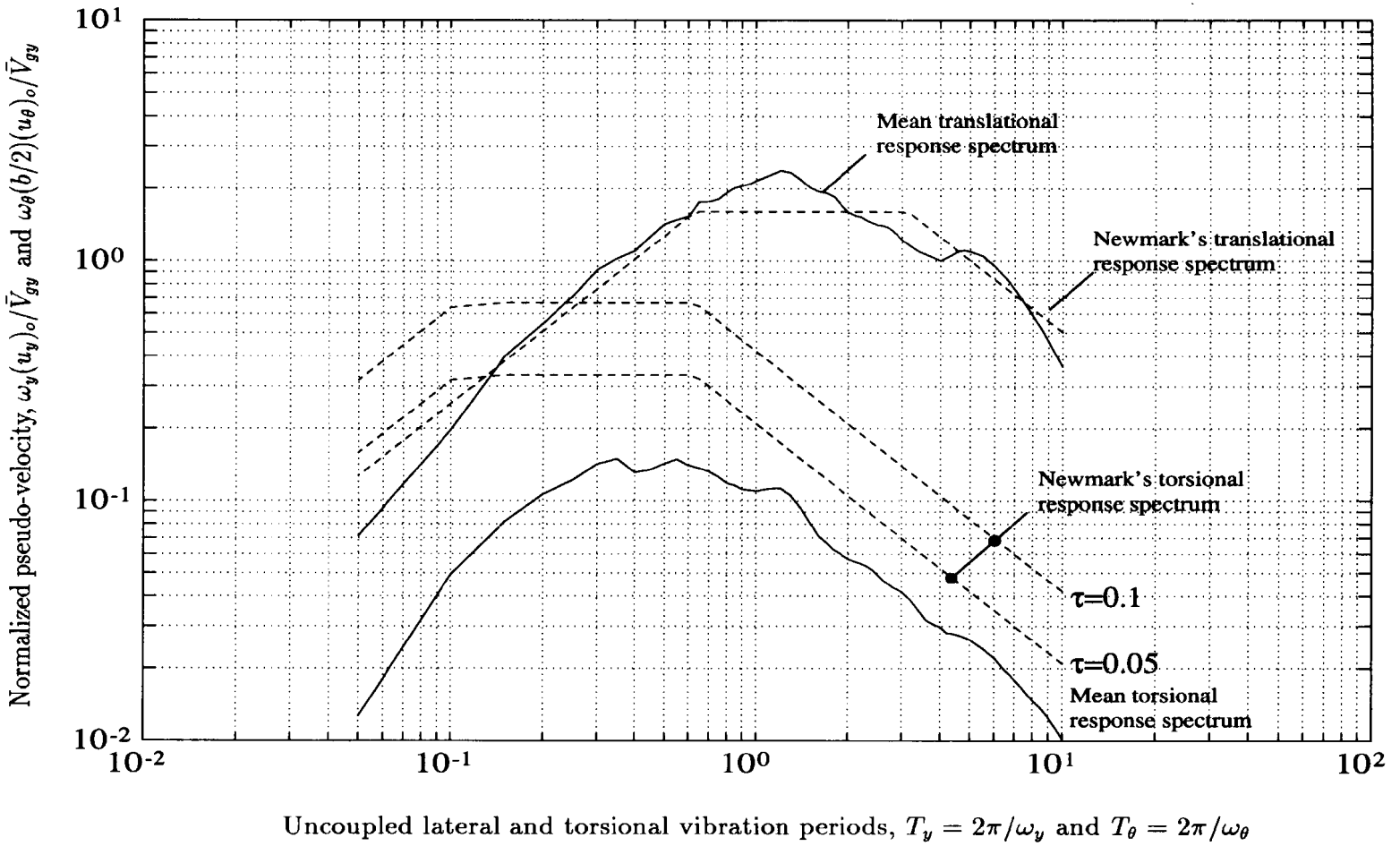

Figure 15: Comparison between Newmark's translational and torsional response spectra and mean response spectra computed from recorded motions

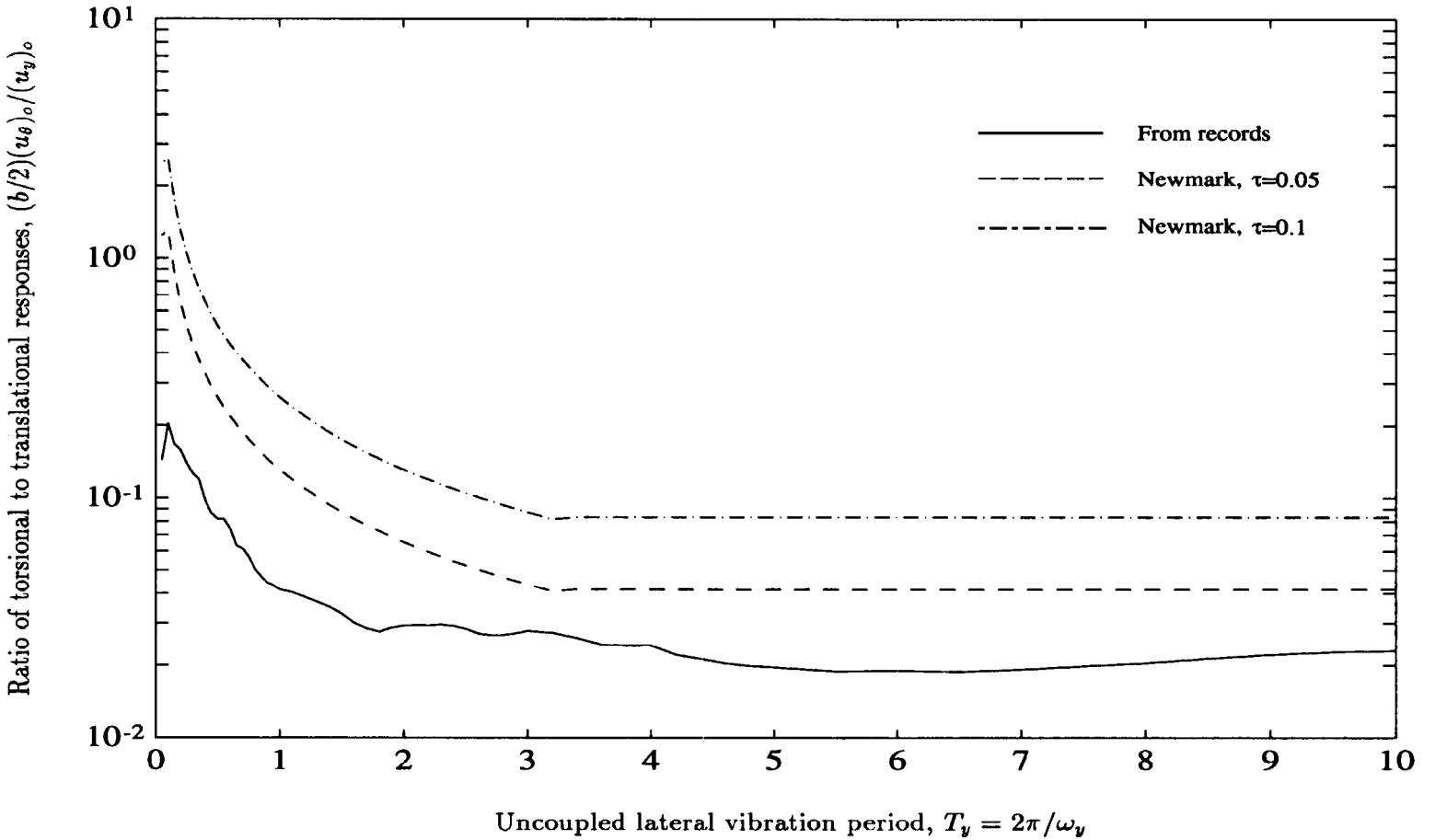

Figure 16: Ratio of torsional and translational responses computed by Newmark's method and using mean values of responses to earthquake records ($\Omega = 1$)

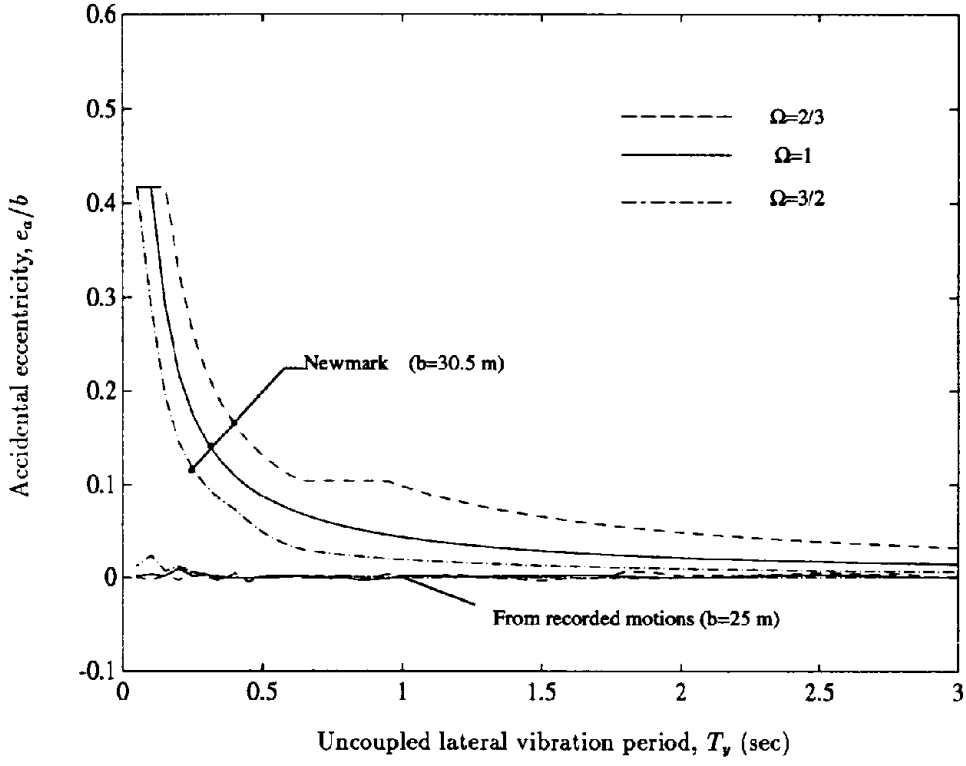

Figure 17: Comparison between Newmark's accidental eccentricity e_a/b and the one computed from recorded motions

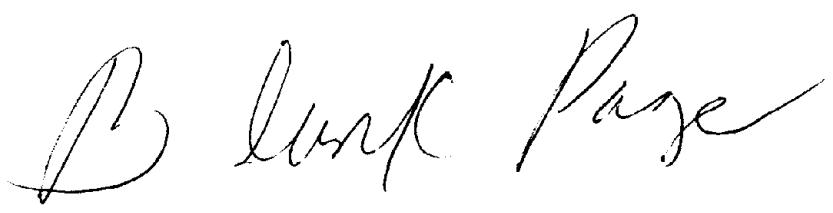

APPENDIX A: Increase in response at the stiff edge of buildings

This appendix contains results of the increase in building displacements, due to accidental torsion, at distance $+r$ to the right of the CM (stiff side). Results are presented for the normalized response $(\hat{u}_{+r})_o$ and calibrated accidental eccentricity e_a/b.

Mean and mean plus one standard deviation values of the normalized response $(\hat{u}_{+r})_o$ are shown in Fig. A.1 for a wide range of uncoupled vibration periods T_y, three different values of static eccentricity e/r= 0, 0.25, and 0.5, and frequency ratio Ω= 2/3, 1, and 3/2. The increase in displacements at the stiff side of the building, $(u_{+r})_o$, shows similar trends as the increase in displacements at the flexible side (Fig. 9), i.e., $(\hat{u}_{+r})_o$ decreases with increasing values of the uncoupled vibration period T_y or increasing values of Ω. However, $(\hat{u}_{+r})_o$ is not always larger for symmetric systems than for unsymmetric ones, as it was in the case of $(\hat{u}_{-r})_o$. Larger responses for symmetric systems occur only for small values of the frequency ratio Ω, and the tendency is reversed as Ω increases. In general, values of the normalized response $(\hat{u}_{+r})_o$ are smaller than 5% unless T_y is very short (less than half a second) and Ω is small ($\Omega < 1$), in which case the increase in displacements due to rotational excitation may reach up to 30%. Furthermore, comparison between Figs. A.1 and 9 shows that the increase in response due to accidental torsion is slightly larger at the stiff side of the building when the frequency ratio Ω is larger than one; this observation is evident for large values of e/r.

Figure A.2 shows the normalized response $(\hat{u}_{+r})_o$ for a wide range of frequency ratios Ω, e/r = 0, 0.25, and 0.5, and T_y = 0.5, 1, and 2 sec. Consistent with the results at the flexible side of the building (Fig. 10), the response $(\hat{u}_{+r})_o$ shows little dependence with the value of Ω for the range of uncoupled vibration periods considered.

Using the normalized responses presented in Figs. A.1 and A.2, we now compute accidental eccentricities calibrated for the increase in response due to accidental torsion at the stiff side of the building. Equation (5) is re-written for points at the right of the CR as follows:

$$\frac{e_a}{b} = [(\hat{u}_r)_o - 1]\,(\frac{\Omega^2}{1 - e/r} - e/r)\,(\frac{r}{b}) \qquad (11)$$

All terms in this equation were previously defined in Eq. (5). Comparison between Eqs. (11) and (5) shows that if the static eccentricity e/r and the frequency ratio Ω are large, the factor $(\Omega^2/(1 - e/r)) - e/r$ (Equation (11)) is considerably larger than the factor $(\Omega^2/(1 + e/r)) + e/r$ in Eq. (5). This implies that accidental eccentricities computed from Eq. (11) can be larger than those computed from Eq. (5) even if the normalized response $(\hat{u}_{+r})_o$ is smaller than $(\hat{u}_{-r})_o$.

Values of e_a/b thus derived are shown in Figs. A.3 and A.4 for a wide range of uncoupled vibration periods T_y and frequency ratios Ω, respectively. Comparing the values of accidental eccentricity presented in Figs. A.3 and 12 for the stiff and flexible side, respectively, it is apparent that in torsionally flexible systems (uppermost figure) the values of e_a/b at the flexible side of the building (Fig. 12) are larger than for the stiff side; the opposite occurs when Ω is large. In either case, however, the accidental eccentricity shows similar trends, i.e., it decreases with increasing T_y or increasing Ω. Similar observations are obtained when comparing the accidental eccentricity as a function of the frequency ratio Ω (Figs. A.4 and 13).

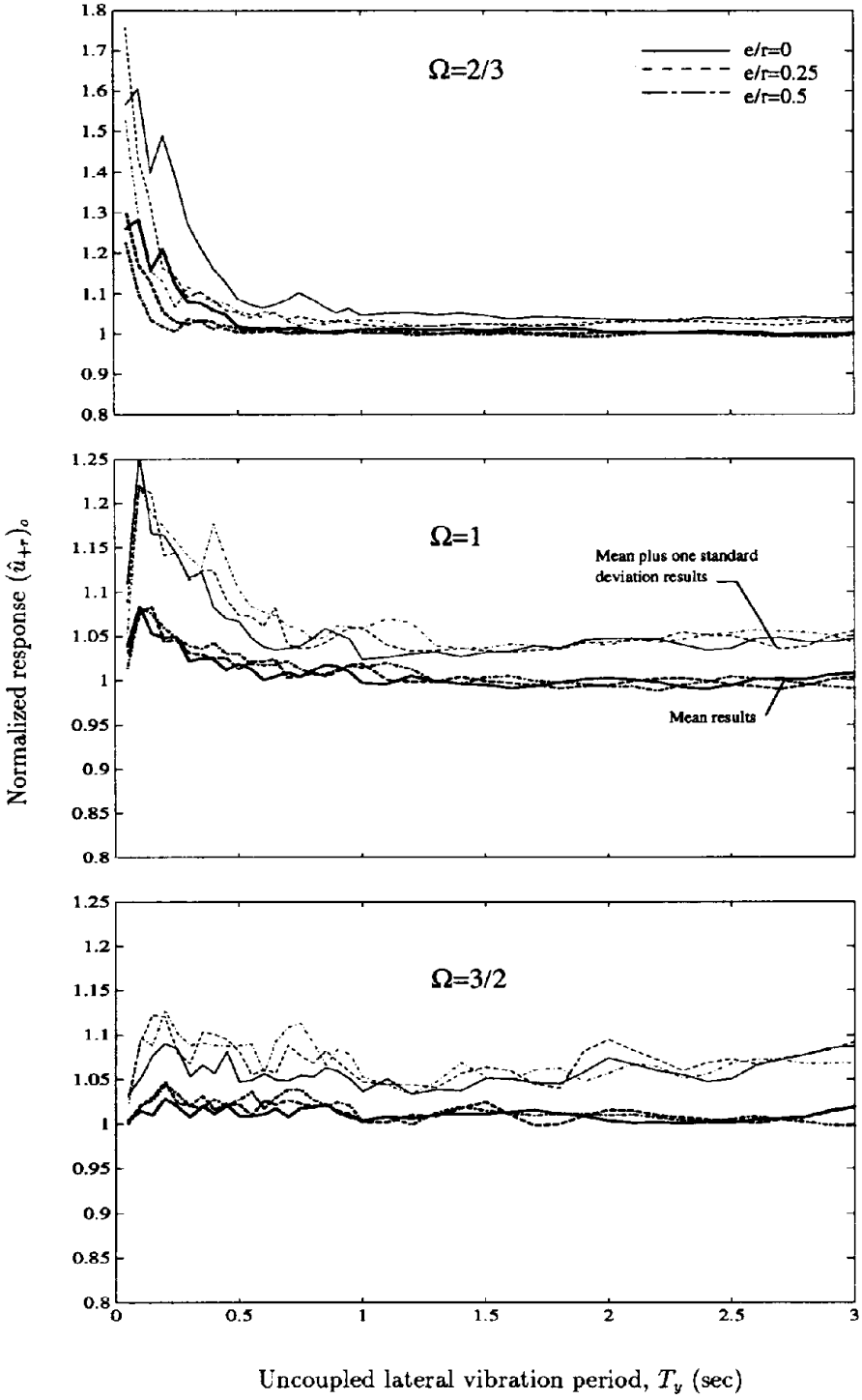

Figure A.1: Normalized response $(\hat{u}_{+r})_o$ as a function of T_y for $\Omega = 2/3, 1$ and $3/2$; $e/r = 0, 0.25$, and 0.5; $b = 50$ m; and $a/b = 1$

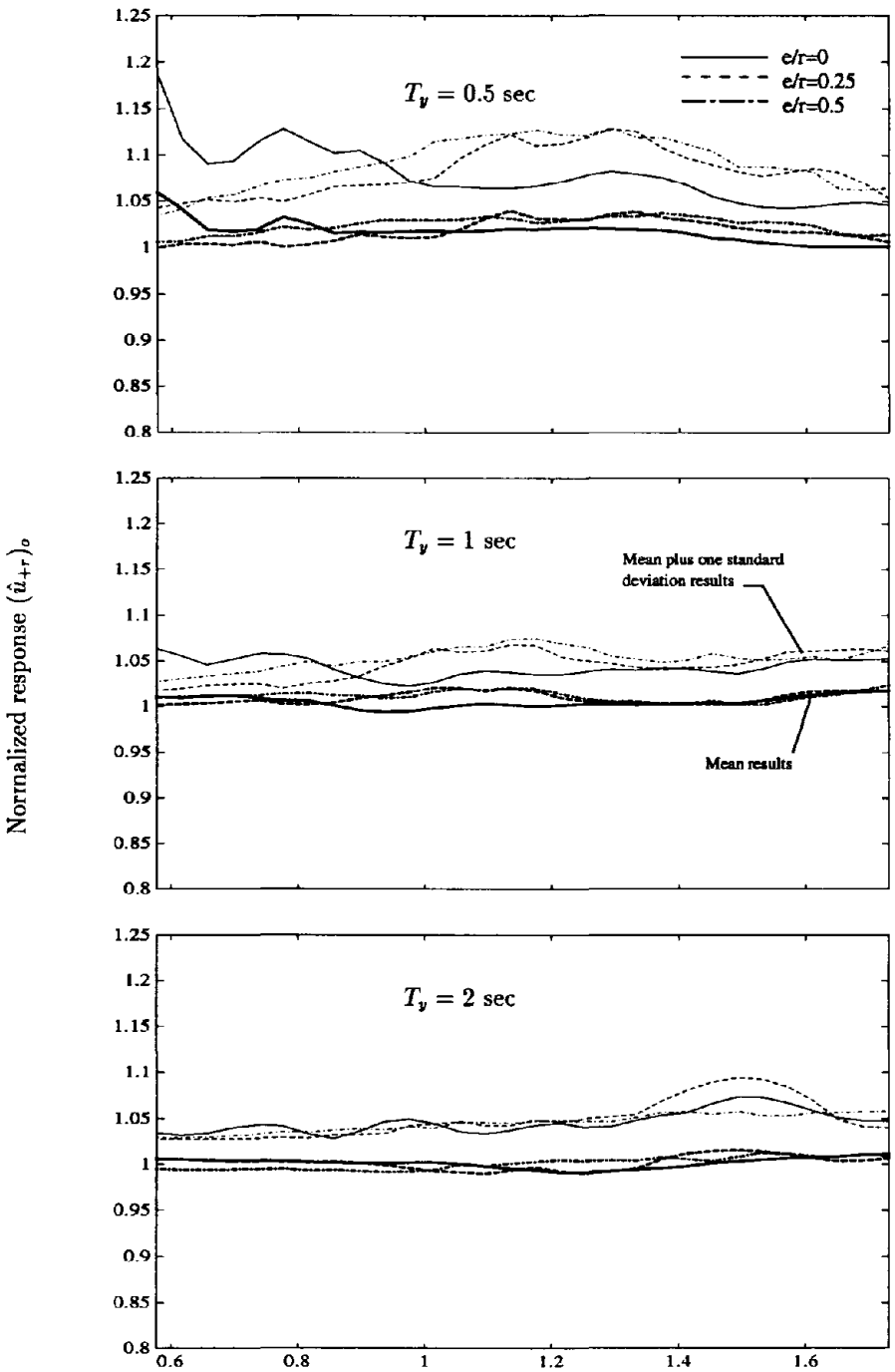

Figure A.2: Normalized response $(\hat{u}_{+r})_o$ as a function of Ω for $T_y = 0.5, 1$ and 2 sec; $e/r = 0, 0.25$, and 0.5; $b = 50$ m; and $a/b = 1$

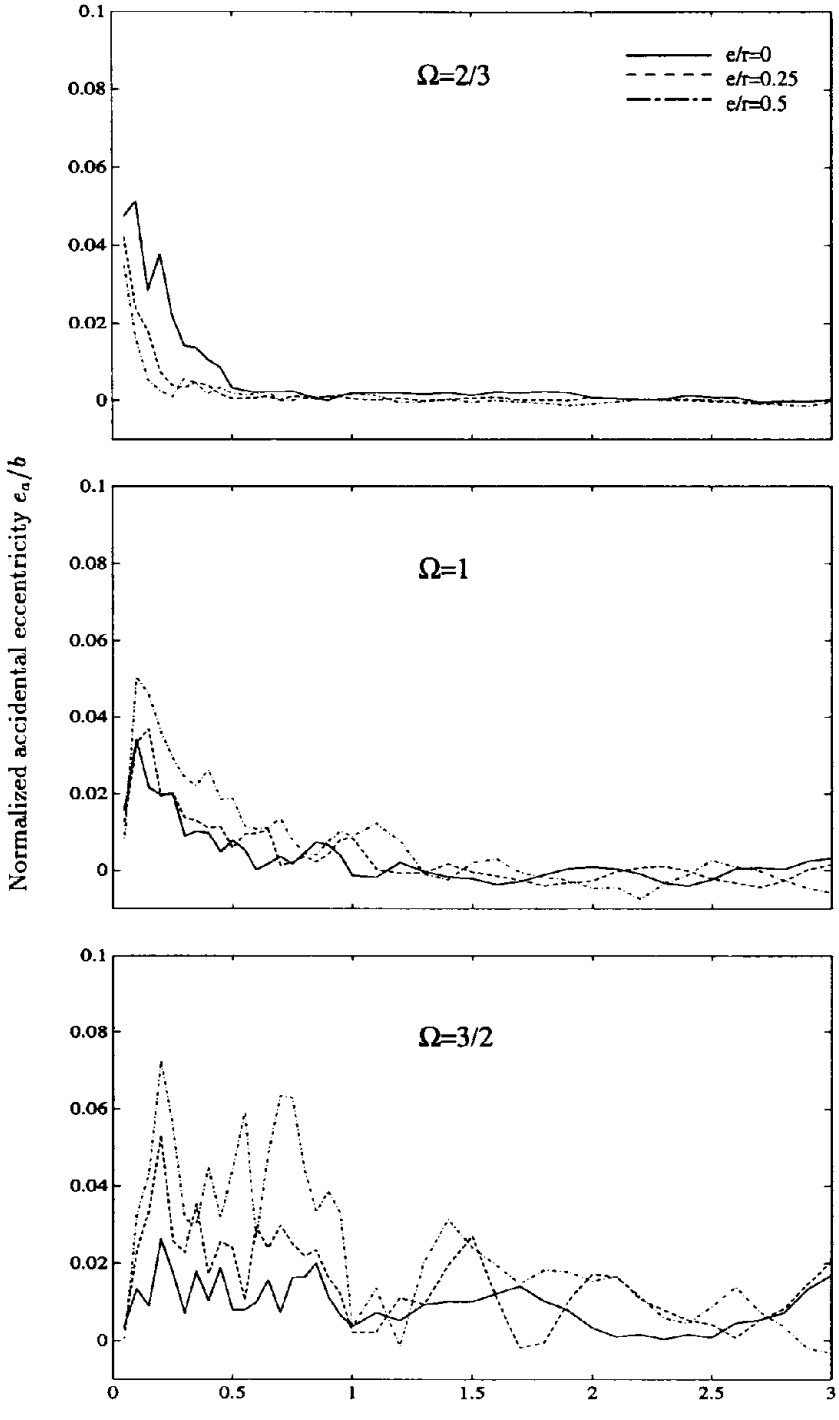

Figure A.3: Normalized accidental eccentricity e_a/b as a function of T_y for $\Omega = 2/3, 1$ and $3/2$; $e/r = 0, 0.25$, and 0.5; $b = 50$ m; and $a/b = 1$

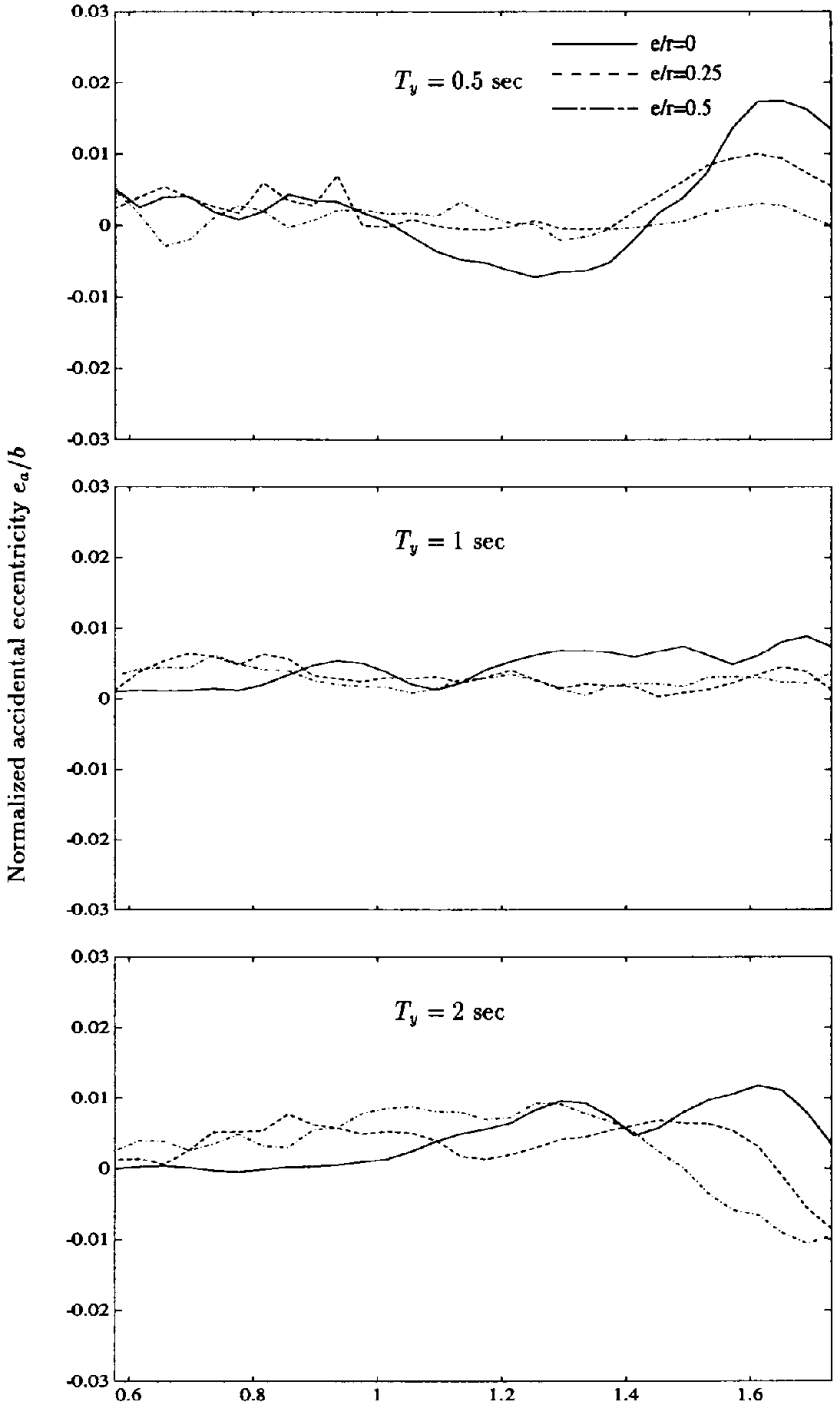

Figure A.4: Normalized accidental eccentricity e_a/b as a function of Ω for $T_y = 0.5, 1$ and 2 sec; $e/r = 0, 0.25$, and 0.5; $b = 50$ m; and $a/b = 1$

APPENDIX B: Modal superposition rule to account for base rotation

The use of the response spectrum method for computing the expected value of the mean peak response of a system subjected to multiple base motions requires three pieces of information: (1) the response spectra for each base motion present, (2) a combination rule for estimating the peak response from the peak modal responses of the structure resulting from each base motion, and (3) the correlation coefficient between different modal responses and different base motions. This appendix reviews aspects of the implementation of steps (2) and (3) above that have been studied earlier by Der Kiureghian [1].

In his work, Der Kiureghian shows that the expected value of any peak response, r_o, of the system can be computed using the following approximate combination rule for the peak modal responses r_{ui}, where u and i denote the excitation and vibration mode, respectively:

$$r_o = E[\max|r(t)|] = \sqrt{\sum_{u=1}^{2}\sum_{v=1}^{2}\sum_{i=1}^{N}\sum_{j=1}^{N} r_{ui}r_{vj}\rho_{q_{ui}q_{vj}}} \tag{12}$$

where the outer two summations are over the base motions and the inner two over the vibration modes; q_{ui} and q_{vj} are the unit mass modal responses for modes i and j and base motions u and v, respectively; $\rho_{q_{ui}q_{vj}}$ is the correlation coefficient between the unit mass modal responses q_i and q_j for the base motions u and v, respectively; and N is the number of vibration modes.

Equation 12 can be re-written in simpler terms as follows:

$$r_o = \sqrt{(r_y)_o^2 + (r_\theta)_o^2 + (r_{y\theta})_o} \tag{13}$$

where $(r_y)_o^2 = \sum_{i=1}^{N}\sum_{j=1}^{N} r_{1i}r_{1j}\rho_{q_iq_j}$ and $(r_\theta)_o^2 = \sum_{i=1}^{N}\sum_{j=1}^{N} r_{2i}r_{2j}\rho_{q_iq_j}$ are the peak responses of the building computed independently for the translational and rotational excitations, respectively; and $(r_{y\theta})_o = \sum_{u\neq v}^{2}\sum_{v\neq u}^{2}\sum_{i=1}^{N}\sum_{j=1}^{N} r_{ui}r_{vj}\rho_{q_{ui}q_{vj}}$ is a cross excitation-response term.

In using Eq. (B.2), the correlation coefficient $\rho_{q_{ui}q_{vj}}$ needs to be specified. Geometrically, this correlation coefficient is equal to the area underneath the cross PSD (Power Spectral Density function) between the two modal responses q_{ui} and q_{vj} normalized by the product of the standard deviations of these responses [1], i.e.

$$\rho_{q_{ui}q_{vj}} = \frac{1}{\sigma_{q_{ui}}\sigma_{q_{vj}}}\int_{-\infty}^{\infty} H_i(i\omega)H_j(-i\omega)G_{\ddot{u}\ddot{v}}\,\mathrm{d}\omega \tag{14}$$

where $H_i(i\omega)$ and $H_j(-i\omega)$ are the frequency response functions for modes i and j, and $G_{\ddot{u}\ddot{v}}$ is the cross PSD between base accelerations $\ddot{u}$ and $\ddot{v}$.

A difficult problem when using Eq. (14) is to specify an appropriate cross PSD $G_{\ddot{u}\ddot{v}}$ for the two base motions. If these base motions u and v are assumed to be correlated white noises, with correlation coefficient $\rho_{\ddot{u}\ddot{v}}$ independent of frequency, the resulting correlation coefficient $\rho_{q_{ui}q_{vj}}$ is (using [2]):

$$\rho_{q_{ui}q_{vj}} = \frac{8\sqrt{\xi_i\xi_j}(\xi_i + \beta_{ij}\xi_j)\beta_{ij}^{3/2}}{(1-\beta_{ij}^2)^2 + 4\xi_i\xi_j\beta_{ij}(1+\beta_{ij}^2)^2 + 4(\xi_i^2+\xi_j^2)\beta_{ij}^2}\ \rho_{\ddot{u}\ddot{v}} \tag{15}$$

where $\beta_{ij} = \omega_i/\omega_j, \omega_j > \omega_i$ is the ratio between the vibration frequencies in modes i and j.

Equation (15) shows that the correlation coefficient $\rho_{q_{ui}q_{vj}}$ is proportional, by a factor $\rho_{\ddot{u}\ddot{v}}$, to the well known modal correlation coefficient ρ_{ij} used in the CQC method [2] (Fig. B.1). This fact simplifies considerably the numerical implementation of the combination rule described by Eq. (13) since the only extra piece of information required is the correlation between base motions $\rho_{\ddot{u}\ddot{v}}$. Figure B.1 shows values of $\rho_{\ddot{u}\ddot{v}}$ computed from the thirty base motions used in this investigation (Table 1). Their magnitude is in most cases less than 0.3, and their mean is approximately zero.

A more 'realistic' approximation for the correlation coefficient can be computed assuming that the random process, for which the base motions presented are realizations, is ergodic. If this assumption holds, we can estimate numerically from each record the cross PSD $G_{\ddot{u}\ddot{v}}$ using for instance Welch's method [3] for spectral estimation, and proceed numerically with the integration of Eq. (14). Figure B.2 shows examples of $\rho_{q_{ui}q_{uj}}$, computed from eight base translations and rotations obtained from records of the Loma Prieta earthquake, as a function of the frequency ratio β_{ij}. As shown in the figure, this correlation coefficients are quite different in magnitude to the ones obtained by the assumption of whiteness in the random process. Indeed, the maximum values for the correlation coefficient obtained from the records can be a hundred percent larger than the ones shown in Fig. B.1. Both keep still certain common features such as a peak for values of $\beta_{ij} \simeq 1$ and a steady decrease for values of β_{ij} departing from one. Moreover, the correlation coefficients computed from the base motions vary from record to record since the process is in fact non-stationary and thus non-ergodic. However, in a mean sense, the effect of statistical correlation between translational and rotational excitations on the building response is expected to be small since the sign changes in $\rho_{q_{ui}q_{vj}}$ from record to record.

Consequently, for most practical cases, the effect of correlation between the base motions could be neglected. In that case, Eq. (13) reduces to

$$r_o = E[\max|r(t)|] = \sqrt{\sum_{u=1}^{M}\sum_{i=1}^{N}\sum_{j=1}^{N} r_{ui}\, r_{uj}\, \rho_{q_{ui}q_{uj}}} \;=\; \sqrt{(r_y)_o^2 + (r_\theta)_o^2} \tag{16}$$

i.e., the SRSS rule for combining the peak responses due to each base motion independently.

References

1. A. Der Kiureghian and A. Neuenhofer,'A response spectrum method for multiple-support seismic excitations', Report No. EERC 91-08, Earthquake Engineering Research Center, University of California, Berkeley, CA., 1991.

2. A. Der Kiureghian,'A response spectrum method for random vibration analysis of MDF systems', Earthquake eng. struct. dyn 9, 419-435 (1981).

3. A. V. Oppenheim and R. W. Schafer, *Digital Signal Processing*, Prentice-Hall, 1975.

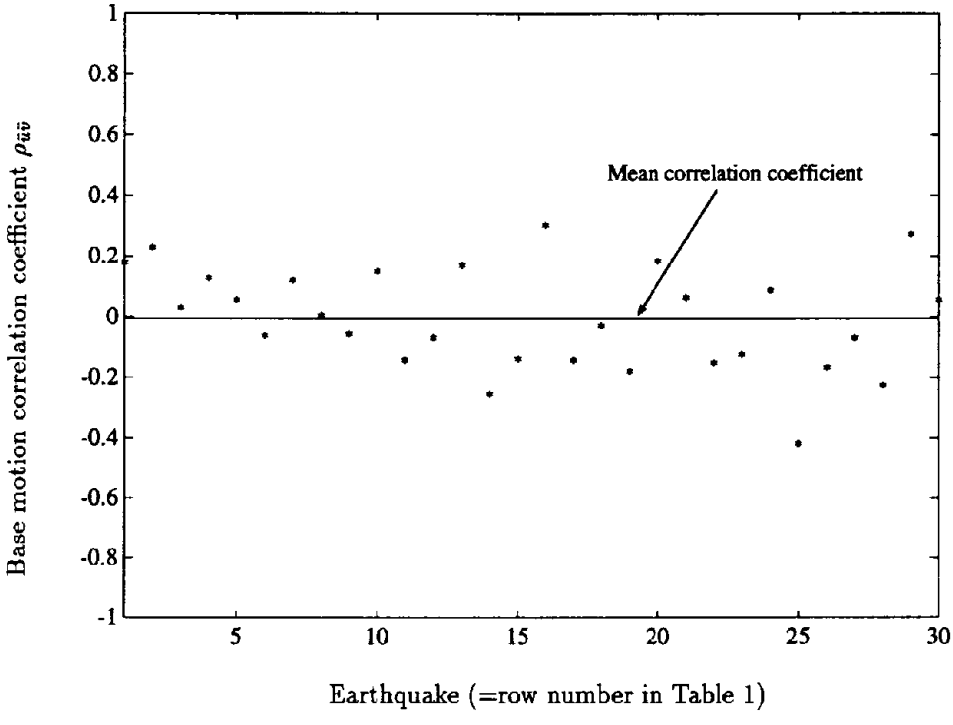

a) Correlation coefficient between base rotation and translation

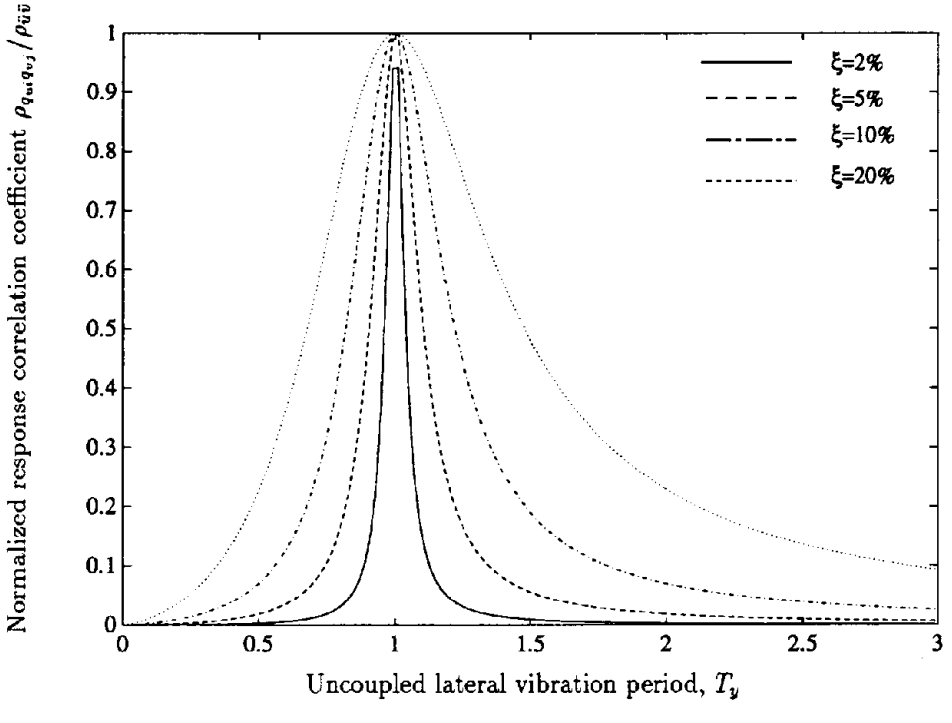

b) Normalized correlation coefficient between base motions and modal responses

Figure B.1: Correlation coefficient between different base motions and modal responses

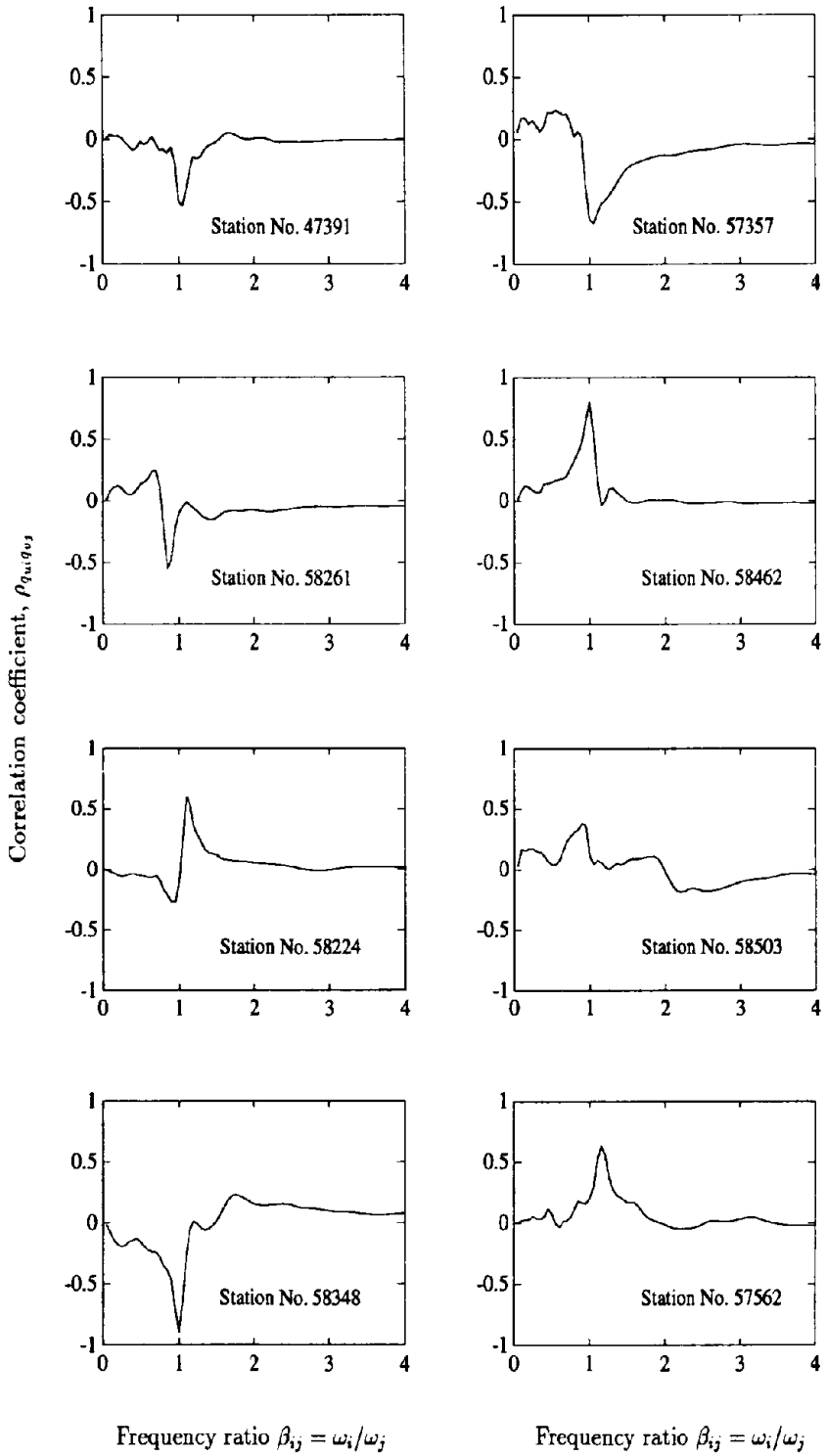

Figure B.2: Correlation coefficients $\rho_{q_{ui}q_{uj}}$ computed from Equation (B.3) and ergodicity assumption

Blank Page

4. USING ACCIDENTAL ECCENTRICITY IN CODE-SPECIFIED STATIC AND DYNAMIC ANALYSES OF BUILDINGS

4.1 Introduction

As mentioned in Chapter 1, building codes require for static analysis of a building that the effects of torsion be considered by applying the equivalent lateral forces at a distance e_d from the CS (center of stiffness). For most codes this design eccentricity e_d has the form:

$$e_d = \alpha e_s + \beta b \quad \text{or} \quad \mathrm{e_d} = \delta \mathrm{e_s} - \beta \mathrm{b} \tag{1}$$

where e_s is the static stiffness eccentricity and βb the accidental eccentricity. For each structural element the value $\pm\beta b$ leading to the larger design force is to be used.

The use of accidental eccentricity in dynamic analysis of buildings varies among building codes. For instance, the UBC specifies that accidental torsion effects may be included in dynamic analysis by shifting the CM of each floor a distance equal to the accidental eccentricity $\pm\beta b$ from its nominal position, and that for each element the accidental eccentricity $\pm\beta b$ leading to the larger design force is to be used. This procedure has not only become an accepted practice in the profession in the US but also in several other seismic countries. Now, the increase in building response due to accidental eccentricity computed using code-specified dynamic analysis of the system is in general different from the increase in response obtained using static analysis with equivalent static forces shifted a distance $\pm\beta b$ from the CM on each floor.

Consequently, the objectives of this chapter are to: (1) evaluate the differences in building response resulting from the use of the code specified accidental eccentricity βb in dynamic or static analysis of the building, and (2) identify, in light of these results, possible inconsistencies between the two alternative code analysis procedures for incorporating the effects of accidental torsion.

This investigation considers the effects of accidental eccentricity βb in three different types of systems: single-story buildings, a special class (defined later) of multistory buildings, and general multistory buildings. Each of these systems is studied in the sequence stated in different sections of this paper. Besides, two other interesting issues regarding the use and interpretation of code accidental-torsion provisions are identified and discussed: (1) discrepancies between measures of accidental torsion based on global response quantities (base shear and torque) instead of element deformations and internal forces, and (2) the heightwise variation of accidental eccentricity. Finally, implications of these results in terms of the current code accidental-torsion provisions are presented.

4.2 Response quantities

In this investigation the response quantities of interest are the: (1) responses of the building r_s^* and r_s, computed from static analysis of the system with code lateral forces and considering accidental eccentricity or without considering it, respectively; (2) peak values over time of the dynamic response of the building, r_d^* and r_d, computed by shifting the CM a distance $e_a = \pm\beta b$—selecting for each element the e_a value leading to the larger response— or without shifting it, respectively; (3) ratio between static responses, $\hat{r}_s = r_s^*/r_s$, and dynamic responses, $\hat{r}_d = r_d^*/r_d$, denoted hereafter as **normalized static and dynamic responses** , respectively; and (4) ratio between the normalized dynamic and static responses, Γ, denoted hereafter as the **dynamic response factor.**

The normalized static and dynamic responses $\hat{r}_s$ and $\hat{r}_d$ will exceed one because most codes do not permit reduction in response below its value excluding accidental eccentricity. Values of the dynamic response factor Γ above one imply that the increase in building response due to accidental eccentricity predicted by dynamic analysis is larger than that from static analysis.

4.3 Single-story systems

The systems analyzed are single-story buildings consisting of a rigid diaphragm, where all the story mass is lumped; lateral resistance is provided by vertically-rigid structural elements located along resisting planes in the x and y-directions (Fig. 1). As shown in the building plan (Fig. 1), the i^{th} resisting plane in the x-direction has stiffness k_{xi} and is located at distance y_i from the CM (center of mass) of the building; analogously, the stiffness and location of the i^{th} resisting plane in the y-direction are defined by k_{yi} and x_i, respectively. The resisting planes in the y-direction may have different stiffnesses and may be unsymmetrically located about the y-axis, creating an eccentricity e_s between the CM and the CS of the building. On the other hand, the system considered is symmetric about the x-axis. The building plan may be divided into flexible and stiff sides, as shown in Fig. 1, where the stiff and flexible edges are also identified.

The static and dynamic responses of the system are described by two degrees of freedom: the translational displacement u_y of the CM along the y-direction, and the rotation u_θ of the rigid diaphragm about a vertical axis through the CM. Any other response quantity is computed as a linear combination of these two degrees of freedom, i.e., $r = \boldsymbol{d}^T\boldsymbol{u}$, where $\boldsymbol{u} = [u_y \quad u_\theta]^T$. For instance, the edge displacements at the stiff and flexible edges of the system are computed using $\boldsymbol{d}^T = [1 \quad \pm b/2]$ in the static case and $\boldsymbol{d}^T = [1 \quad \pm (b/2 \mp e_a)]$ in the dynamic case. The plus and

minus sign in front of $b/2$ are used for computing the displacements at the stiff and flexible edges of the building, respectively; the $\mp e_a$ term is introduced to account for the shift in the position of the center of mass in the dynamic case.

The static response of the building to an equivalent lateral force V in the y-direction applied at distance e_d from the CS is obtained explicitly by solving the system of equations

$$\begin{bmatrix} K_y & K_y e_s \\ K_y e_s & K_\theta \end{bmatrix} \begin{Bmatrix} u_y \\ u_\theta \end{Bmatrix} = \begin{Bmatrix} V \\ V(e_s - e_d) \end{Bmatrix} \tag{2}$$

where $K_y = \sum_{i=1} k_{yi}$ is the lateral stiffness of the system, $K_\theta = \sum_i k_{yi} x_i^2 + \sum_i k_{xi} y_i^2$ is the torsional stiffness of the system with respect to the CM, $e_s = \sum_i k_{yi} x_i / \sum_i k_{yi}$ is the static eccentricity between the CM and CS, and e_d is the design eccentricity presented in Eq. (1). Using this equation, the static responses r_s^* and r_s are computed from the displacement and rotation u_y and u_θ of the system with and without accidental eccentricity, i.e., for e_d as in Eq. (1) and $e_d = \alpha e_s$ [or $e_d = \delta e_s$], respectively. Hence the normalized static response of the system, $\hat{r}_s$, is computed as the ratio between r_s^* and r_s. The system parameters controlling these static responses are the lateral stiffness K_y, the torsional stiffness K_θ, and the static eccentricity e_s.

The dynamic response of the system to base acceleration in the y-direction, $a_{gy}(t)$, is described by the following equations of motion:

$$\begin{Bmatrix} \ddot{u}_y \\ r\ddot{u}_\theta \end{Bmatrix} + \omega_y^2 \begin{bmatrix} 1 & e/r \\ e/r & \Omega^2 + (e/r)^2 \end{bmatrix} \begin{Bmatrix} u_y \\ r u_\theta \end{Bmatrix} = - \begin{Bmatrix} 1 \\ 0 \end{Bmatrix} a_{gy}(t) \tag{3}$$

where r is the radius of gyration of the system plan about a vertical axis passing through the CM; $\Omega = \omega_\theta / \omega_y$ is the ratio between the uncoupled torsional frequency $\omega_\theta = \sqrt{K_{\theta R}/(mr^2)}$ and lateral frequency $\omega_y = \sqrt{K_y/m}$ of the building; $K_{\theta R} = K_\theta - K_y e^2$ is the torsional stiffness of the system with respect to the CS; and $e = e_s + e_a$. Using this equation, the dynamic responses of the system r_d^* and r_d are computed from the system displacement and rotation u_y and u_θ of the system with and without accidental eccentricity, i.e., for $e = e_s \pm \beta b$ and $e = e_s$, respectively. Hence, the normalized dynamic response, $\hat{r}_d$, is computed from the ratio between r_d^* and r_d. Finally, the dynamic response factor Γ is computed from the ratio between the normalized dynamic response $\hat{r}_d$ and the normalized static response $\hat{r}_s$. Three parameters control significantly this dynamic response factor: the uncoupled lateral frequency of the system ω_y, the ratio between uncoupled torsional and lateral frequencies Ω, and the static eccentricity e_s.

The effect of accidental eccentricity e_a is to modify the external forces in static analysis but the stiffness matrix in dynamic analysis. As a result, the vibration frequencies and mode shapes of the system change when accidental eccentricity is introduced, implying that a new dynamic analysis of the system is required to compute the system response for each different value of accidental eccentricity e_a. Thus, dynamic analyses are required for two systems, one with $e_a = +\beta b$ and the other with $e_a = -\beta b$.

For dynamic analysis of the system the ground motion is characterized by the smooth response spectrum described in Chapter 2 (Fig. 2). This spectrum is developed by well established techniques [1] for a ground motion with peak acceleration, velocity, and displacement of $0.5g$, 24 in/sec, and 18 in, respectively. Amplification factors of 2.71, 2.3, and 2.01 are chosen for the acceleration, velocity, and displacement sensitive region of the spectrum. These amplification factors, are appropriate for 5% damping and 84.1% percentile response.

The peak value of the earthquake response of the structural systems described earlier and governed by Eq.(3) is estimated by the RSA (Response Spectrum Analysis) method using the CQC modal combination rule. Five percent modal damping is assumed throughout this study.

Two different sets of response quantities are considered in comparing the effects of accidental eccentricity predicted by dynamic and static analysis of the building. These are (1) the peak lateral displacements at the stiff and flexible edges of the building plan in the y-direction, $u_{\pm b/2}$, respectively, and (2) the peak values of base shear and base torque.

4.3.1 Lateral displacements

Presented in this section are results for the normalized static and dynamic displacements at the stiff and flexible edges of the building plan $(\hat{u}_{\pm b/2})_s$ and $(\hat{u}_{\pm b/2})_d$, respectively, and the dynamic response factor $\Gamma_{\pm b/2}$. Such results are presented first for systems with symmetric-plan and later for unsymmetric-plan systems.

Figure 2 presents the normalized displacements $(\hat{u}_{-b/2})_s$ and $(\hat{u}_{-b/2})_d$, and the dynamic response factor $\Gamma_{-b/2}$ for a wide range of frequency ratios Ω in symmetric systems with uncoupled lateral vibration period $T_y = 1$ sec, and plan aspect ratio $a/b = 1$ (Fig. 1). The normalized static displacements are computed using the UBC values $\alpha = \delta = 1$ in Eq. (2), and results presented for two values of accidental eccentricity $e_a/b = \pm 0.05$ and 0.01. Both cases show similar trends in response. First, the normalized static displacement $(\hat{u}_{-b/2})_s$ decreases monotonically as Ω increases

implying, as expected, that the increase in response due to accidental eccentricity is smaller in torsionally stiff systems (Ω large). Second, the normalized dynamic displacement $(\hat{u}_{\pm b/2})_d$ remains relatively constant for $\Omega < 0.8$, decreases to a minimum at Ω close to one, increases again to a peak at Ω between 1.1 and 1.2, and decreases steadily with larger values of the frequency ratio. And third, the dynamic response factor $\Gamma_{-b/2}$, which is computed as the ratio between the values of $(\hat{u}_{\pm b/2})_d$ and $(\hat{u}_{\pm b/2})_s$ presented above, shows that the increase in response predicted by dynamic analysis is larger than that from static analysis for values of $\Omega > 0.75$ (except for Ω in the neighborhood of 1) if $\beta = 0.05$ and for $\Omega > 1.1$ if $\beta = 0.1$. On the other hand, this increase in response is smaller than that predicted by static analysis for $\Omega < 0.75$ if $\beta = 0.05$ and for $\Omega < 1.1$ if $\beta = 0.1$. Note that since the buildings considered in this figure are symmetric, these results for the flexible edge of the building also apply to the stiff edge of the building.

The dynamic response factor $\Gamma_{-b/2}$ is presented in Fig. 3 as a function of the frequency ratio Ω, for buildings with uncoupled vibration period $T_y = 1$ sec, and three values of building plan aspect ratio $a/b = 0, 1/2$, and 1. The normalized static responses are computed using again the UBC values $\alpha = \delta = 1$ and $\beta = 0.05$ in Eq. (2); these values are used in all subsequent figures unless stated otherwise. The values of $\Gamma_{-b/2}$ deviate more from unity in buildings with smaller plan aspect ratio a/b; i.e., the differences between the increase in response due to accidental eccentricity predicted by dynamic and static analysis are least for squared-plan systems ($a/b = 1$). These systems are selected in all subsequent analyses because of this property, which implies that the differences in the increase of building response predicted by code-specified dynamic and static analysis will be in general larger than the values presented in this investigation.

Values of the dynamic response factor $\Gamma_{-b/2}$ are shown in Fig. 4 for a wide range of Ω values, and four different values of the uncoupled vibration period $T_y = 0.1, 0.5, 1$, and 5 sec. These periods were chosen to cover different spectral regions (Chapter 2: Fig. 2). The dynamic response factor shows similar trends for all values of T_y; as T_y increases, the differences between the responses predicted by dynamic and static analysis are reduced if Ω is, roughly, larger than one and smaller than 0.8. This situation is reversed when Ω is in the range $0.8 \leq \Omega \leq 1$. Since the trends of the dynamic response factor are rather insensitive to the value of the uncoupled period, we chose systems with uncoupled period $T_y = 1$ sec for all further analyses.

Figure 5 shows the values of the normalized static and dynamic displacements $(\hat{u}_{\pm b/2})_s$ and $(\hat{u}_{\pm b/2})_d$ for a wide range of Ω values, five values of static eccentricity $e_s/b = 0$, 0.05 , 0.1 , 0.15 , and 0.25, and accidental eccentricity $e_a/b = \pm 0.05$. As seen in the figure, the static responses $(\hat{u}_{\pm b/2})_s$

are quite insensitive to the value of static eccentricity if the frequency ratio Ω is, say, larger than one. However, for $\Omega < 1$ the responses at the stiff side of the building, $(\hat{u}_{+b/2})_s$, increase considerably with decreasing Ω and increasing static eccentricity. Indeed, the static response $(\hat{u}_{+b/2})_s$ approaches infinity as $\Omega \longrightarrow (b/r)\ \sqrt{e/b\,(1/2 - e/b)}$, because for these systems the static displacement at the stiff edge of the building, $(u_{+b/2})_s$, is zero. In contrast, $(\hat{u}_{-b/2})_s$ always decreases with increasing values of static eccentricity. On the other hand, the normalized dynamic response $(\hat{u}_{\pm b/2})_d$ present trends with the frequency ratio that are different from those of the static case, except for large Ω. In particular, the dynamic response of systems with small Ω is increased to a lesser degree than predicted by static analysis. Moreover, the increase in response due to accidental eccentricity is generally largest for symmetric systems compared to unsymmetric systems (with $e_s/b < 0.25$) implying that symmetric systems are in general the most sensitive to the introduction of accidental eccentricity. This observation is consistent with results obtained in Chapter 2.

Figures 6 and 7 show values of the dynamic response factor $\Gamma_{\pm b/2}$ for a wide range of Ω values, five different values of static eccentricity $e_s/b = 0, 0.05, 0.10, 0.15$ and 0.25, and two values of accidental eccentricity $e_a/b = \pm 0.05$ and 0.1, respectively. The values of $\Gamma_{\pm b/2}$ for symmetric systems ($e = 0$), originally presented in Fig. 2, are repeated in these figures. In contrast to the symmetric case, Fig. 6 shows that the values of $\Gamma_{+b/2}$ and $\Gamma_{-b/2}$ for the stiff and flexible edges of the building, respectively, differ considerably when the system is unsymmetric. Indeed, the dynamic response factor $\Gamma_{+b/2}$ for the stiff side of unsymmetric-plan buildings deviates considerably from one if $\Omega < 0.8$. This is because the normalized static displacement at the stiff edge of the system increases quickly for $\Omega < 0.8$; however, the normalized dynamic response at this edge is relatively constant for this range of frequency ratio. On the other hand, the dynamic response factor at the flexible side, $\Gamma_{-b/2}$, deviates less from one than $\Gamma_{+b/2}$ as expected from the results presented earlier in Fig. 5. The largest deviations of $\Gamma_{-b/2}$ from unity occur usually for symmetric systems. In general, the values of $\Gamma_{-b/2}$ are smaller than one if the system is unsymmetric, implying that for these systems the increase in response predicted by dynamic analysis is smaller than that from static analysis.

All these observations carry over to systems with accidental eccentricity $e_a/b = \pm 0.1$ (Fig. 7); however, as the accidental eccentricity increases, the dynamic response factor tends to deviate more from one. Exceptions to this rule are symmetric systems with Ω larger than one.

So far, the dynamic response factor $\Gamma_{\pm b/2}$ has been obtained for normalized static responses computed using the UBC values $\alpha = \delta = 1$ and in Eq. (2). Comparative results for the dynamic

response factor $\Gamma_{\pm b/2}$ corresponding to parameters $\alpha = 1.5$, $\delta = 0.5$ and $\beta = 0.1$ as in the NBCC, and $\alpha = 1.5$, $\delta = 1.0$, and $\beta = 0.1$ as in the Mexico Federal District code, are presented in Fig. 8 for a wide range of frequency ratios and two values of static eccentricity $e_s/b = 0.05$ and 0.25. The dynamic response factor in all three cases shows similar trends; the largest differences between dynamic and static analysis occur at the stiff edge of the building and for the UBC and Mexican values of α, δ and β. The improvement shown by the NBCC results is due to the parameter $\delta = 0.5$, which implies smaller normalized static responses of the system when Ω is small. Thus, with no important loss of generality the UBC values $\alpha = \delta = 1$ and $\beta = 0.05$ are chosen in subsequent static analyses.

4.3.2 Equivalent static accidental eccentricity

It is desired to reinterpret the dynamic response results presented earlier in terms of an equivalent static accidental eccentricity e_D. This is the distance from the CM at which a static lateral force or base shear V should be applied to produce the same displacement $(u^*_{\pm b/2})_d$ as computed from code dynamic analysis of the system with accidental eccentricity. A comparison of this equivalent static eccentricity with $e_a = \beta b$ provides a measure of how the increase in edge displacements due to accidental eccentricity predicted by code dynamic analysis compares with that determined from code static analysis.

In order to determine the equivalent static eccentricity, V is chosen as the static force that applied at distance αe_s from the CS produces a displacement of the flexible edge equal to $(u_{-b/2})_d$, the peak dynamic displacement when the system has no accidental eccentricity ($\beta = 0$), i.e.,

$$(u_{-b/2})_d = \frac{V}{K_y} + \frac{V\ \alpha e_s\ (b/2 + e_s)}{K_\theta} \tag{4}$$

Now the same static force V is applied eccentrically relative to the CS at distance $\alpha e_s + e_D$, where e_D is yet to be determined. This accidental eccentricity is determined to satisfy the requirement that the displacement of the flexible edge is the same as $(u^*_{-b/2})_d$, the peak dynamic displacement of the system with accidental eccentricity $\pm\beta b$, i.e.,

$$(u^*_{-b/2})_d = \frac{V}{K_y} + \frac{V\ (\alpha e_s + e_D)\ (b/2 + e_s)}{K_\theta} \tag{5}$$

Dividing Eq. (5) by (4) and solving for e_D we obtain

$$\frac{e_D}{\beta b} = [(\hat{u}_{-b/2})_d - 1]\ \left(\frac{\Omega^2}{(1/2 + e_s/b)(b/r)^2} + \alpha\ e/b\right)\ (\frac{1}{\beta b}) \tag{6}$$

Similarly, the accidental eccentricity e_D^+ calibrated for the peak displacements at distance $x = +b/2$ from the CM (stiff edge) can be obtained from

$$\frac{e_D^+}{\beta b} = [(\hat{u}_{+b/2})_d - 1] \left(\frac{\Omega^2}{(1/2 - e_s/b)(b/r)^2} - \delta \, e/b \right) \left(\frac{1}{\beta b} \right) \tag{7}$$

Note that V does not appear in Eqs. (6) or (7) for computing $e_D^{\pm}/(\beta b)$. This accidental eccentricity can therefore be used in conjunction with any reasonable value of V including the code value. Both equations relate the accidental eccentricity $e_D^{\pm}$ to the normalized displacement $(\hat{u}_{\pm b/2})_d$ at the stiff and flexible edges of the building plan, respectively. Normalized displacements at other locations of the building plan could be used in determining e_D. The resulting accidental eccentricities e_D are, however, quite insensitive to the location selected.

Substituting for the values of $(\hat{u}_{\pm b/2})_d$ presented in Fig. 5 into Eqs. (6) and (7), we obtain the values of $e_D/(\beta b)$ presented in Fig. 9 as a function of the frequency ratio Ω, for three values of static eccentricity, $e_s/b = 0, 0.05$, and 0.25. Values of $e_D/(\beta b)$ larger than one imply that the increase in building response due to accidental eccentricity predicted by code dynamic analysis is larger than that from code static analysis. The computed $e_d/(\beta b)$ values corresponding to both edges of the building plan are usually quite different, except for symmetric systems in which case they coincide. These values of accidental eccentricity clearly depend on the frequency ratio of the system; they vary between zero and up to three times the code accidental eccentricity $0.05b$. The general trends of these results are in agreement with those presented earlier for the dynamic response factor $\Gamma_{\pm b/2}$ in Fig. 6.

It is useful to compare the results just presented for the equivalent static accidental eccentricity with those from a traditional approach [2] in which this eccentricity is calibrated to give the torque computed from dynamic analysis. In the context of accidental eccentricity, the traditional approach may be interpreted as follows. First, consider the peak base shear and torque determined from dynamic analysis of two single-story systems: (1) a building with no accidental eccentricity, and (2) a building with its CM shifted through $\pm\beta b$. Thus, the difference in the peak values of base shear and torque V_o and T_o for system (1) and V_o^* and T_o^* for system (2) are clearly due to the accidental eccentricity $\pm\beta b$. Second, define the equivalent static eccentricity $e_o = T_o/V_o$ for system (1) and $e_o^* = T_o^*/V_o^*$ for system (2). This conventional definition of equivalent static eccentricity can be physically interpreted as the distance from the CS at which the peak base shear V_o [or V_o^*] has to be applied statically to produce the peak base torque T_o [or T_o^*]. Note that this definition assumes implicitly that the peak base shear and torque occur at the same instant of time.

According to the procedure described above, the difference between e_o^* and e_o, represents the part of the eccentricity e_o^* that can be associated with the accidental eccentricity βb. Mathematically,

$$e_o^* = e_o \ + (e_o^* \ - e_o) = e_o + e_T \tag{8}$$

where $e_T = e_o^* - e_o$. The two terms e_o and e_T are directly comparable to αe_s [or δe_s] and βb in Eq. (1), respectively. Comparison between e_o and αe_s has been the subject of previous research [3,4,5]. In this investigation of accidental eccentricity we compare e_T with βb, to determine how the increase in torque due to accidental eccentricity predicted by code dynamic analysis compares with that determined by code static analysis.

The values of $e_T/(\beta b)$ are superimposed on the data for $e_D/(\beta b)$ in Fig. 9, for a wide range of frequency ratios Ω, four different values of the static eccentricity in the system, $e_s = 0, 0.05, 0.10$, and 0.25, and accidental eccentricity $e_a/b = 0.05$. Clearly, the two procedures for defining the equivalent static eccentricity lead to very different results. For symmetric systems or unsymmetric systems with static eccentricity $e_s < 0.1$, the traditional approach shows amplifications of the accidental eccentricity $0.05b$ that are considerably larger than those computed from the building displacements. For instance, the traditional approach shows that the most critical systems in terms of amplification of the response due to accidental eccentricity would be those with similar uncoupled torsional and lateral frequencies, $\Omega \simeq 1$, and small static eccentricity; however, if we look to the accidental eccentricity $e_D/(\beta b)$ calibrated from the response quantities of interest, in this case the edge displacements, these systems are no longer critical. In fact, systems with $\Omega \simeq 1$ are particularly insensitive to the effects of accidental torsion as has been noted earlier in Chapter 2 and is confirmed in Fig. 9. The misconception that systems with similar uncoupled lateral and torsional vibration periods present the largest increase in response due to torsion is in part due to the erroneous results derived from the traditional approach based on peak values of base shear and torque assumed to occur simultaneously.

Consequently, when using equivalent static accidental eccentricity to indirectly account for the effects of accidental torsion in code dynamic analysis of buildings, this eccentricity should be based on the response quantity of interest, usually the element deformations or internal forces, and not on a global response such as the base torque.

4.4 Special class of multistory buildings

The systems analyzed in this section are multistory buildings satisfying the following properties [3]:

1. The centers of mass of all floors lie on a vertical line.

2. The resisting elements (frames, columns, shear walls or shear-wall cores) are arranged such that their principal axes form an orthogonal grid in plan and are connected at each floor level by a rigid diaphragm.

3. The lateral stiffness matrices of all resisting elements along one direction are proportional to each other; i.e., the lateral stiffness matrix of the ith resisting element in the x-direction $\boldsymbol{k}_{xi} = C_{xi}\ \boldsymbol{k}_x$, where C_{xi} is a proportionality constant and $\boldsymbol{k}_x$ is a characteristic stiffness matrix for the resisting elements. Similarly, the stiffness matrix of the ith resisting element in the y-direction satisfies $\boldsymbol{k}_{yi} = C_{yi}\ \boldsymbol{k}_y$.

4. The building is symmetric in the X-direction.

For buildings having properties 2 and 3 listed above, it can be shown [3] that the centers of stiffness of all stories lie on the same vertical line. Thus, for this special class of buildings, the static eccentricity for each floor, which is defined as the distance between the CM of the floor and its CS, is the same.

The dynamic response of the system to base acceleration in the y-direction, $a_{gy}(t)$, is described as before by two degrees of freedom per floor: the translational displacement u_{yj} of the CM along the y-direction, and the rotation $u_{\theta j}$ of the j^{th} floor rigid diaphragm about a vertical axis through the CM. The equations of motion of the system can be written [3]

$$\begin{bmatrix} \boldsymbol{m} & 0 \\ 0 & \boldsymbol{m} \end{bmatrix} \begin{Bmatrix} \ddot{\boldsymbol{u}}_y \\ r\ddot{\boldsymbol{u}}_\theta \end{Bmatrix} + \begin{bmatrix} \boldsymbol{K}_y & \boldsymbol{K}_y(\frac{e}{r}) \\ \boldsymbol{K}_y(\frac{e}{r}) & [(\frac{e}{r})^2 + \frac{C_{\theta R}}{r^2 C_y}]\boldsymbol{K}_y \end{bmatrix} \begin{Bmatrix} \boldsymbol{u}_y \\ r\boldsymbol{u}_\theta \end{Bmatrix} = -\begin{Bmatrix} \boldsymbol{m}\,\mathbf{1} \\ \mathbf{0} \end{Bmatrix} a_{gy}(t) \qquad (9)$$

where $\boldsymbol{u}_y$ and $\boldsymbol{u}_\theta$ are the Nx1 vectors of u_{yj} and $u_{\theta j}$, respectively; $\boldsymbol{m}$ is a diagonal matrix of dimension N, the number of stories, with diagonal entries equal to m_j, the mass at the jth floor, $j = 1, \ldots, N$; $\boldsymbol{K}_y = \sum_i \boldsymbol{k}_{yi}$ is the sum of lateral stiffnesses of all resisting planes in the y-direction; $e/r = \sum_i C_{yi}x_i / \sum_i C_{yi}$ is the normalized static eccentricity of the building at each story; $C_y = \sum_i C_{yi}$ is the sum of all proportionality constants C_{yi} for the frames in the y-direction; $C_{\theta R} = \sum_i (C_{yi}x_i^2 + C_{xi}y_i^2) - C_y e^2$ is a parameter directly related to the torsional stiffness of the system

with respect to the CS; and $\mathbf{1}$ and $\mathbf{0}$ are vectors of dimension N with all elements equal to one or zero, respectively.

It can be shown that the dynamic response of a torsionally-coupled system belonging to the special class can be related to the responses of two systems: a corresponding torsionally uncoupled multistory system, governed by Eq. (9) with $e/r = 0$; and an associated torsionally-coupled, single-story system (Eq. (3)) with the following properties: (1) the static eccentricity ratio e/r for the torsionally-coupled single-story system is the same as for all the floors of the torsionally-coupled multistory system, and (2) the ratio $K_{\theta R}/(r^2 K_y)$ of the associated torsionally coupled one-story system equals the ratio $C_{\theta R}/(r^2 C_y)$ of the torsionally-coupled multistory system, implying that the ratio Ω of uncoupled frequencies is identical in the two systems.

The $2N$ natural frequencies and mode shapes of a system belonging to the special class described are given by [3] (Appendix A)

$$\omega_{nj} = \bar{\omega}_n \omega_{yj} \tag{10}$$

and,

$$\boldsymbol{\phi}_{nj} = \begin{Bmatrix} \alpha_{yn} \boldsymbol{\psi}_j \\ \alpha_{\theta n} \boldsymbol{\psi}_j \end{Bmatrix} \tag{11}$$

for $n = 1, 2$ and $j = 1, \ldots, N$, where ω_{yj} and $\boldsymbol{\psi}_j$ are the lateral vibration frequencies and modes of the torsionally-uncoupled, N-story system; and $\bar{\omega}_n$ and $\boldsymbol{\alpha}_n = \{\alpha_{yn} \;\; \alpha_{\theta n}\}^T$ are the normalized vibration frequencies and modes shapes of the torsionally-coupled single-story system.

The systems considered are analyzed for the smooth response spectrum already described (Chapter 2: Figure 2), and the peak earthquake response estimated by the RSA method using the CQC modal combination rule.

Next, we will show that because of the special properties of the class of multistory systems considered, the normalized values $\hat{r}_d$ and $\hat{r}_s$ of the dynamic and static normalized responses of the building, respectively, are essentially the same as the ones corresponding to the single-story systems studied in the previous section. Consequently, the dynamic response factor $\Gamma = \hat{r}_d/\hat{r}_s$ is essentially the same for single-story and the special class of multistory systems, and all observations derived previously for single-story systems are also applicable to this special class of multistory systems. A proof of this statement is developed first by comparing the normalized dynamic response $\hat{r}_d$ of single-story and multistory buildings, followed by the static case.

Consider first the dynamic response of the special class of systems described above. It can be demonstrated [3] (Appendix A) that the peak value of any response quantity, r_{nj}, of a torsionally-

coupled multistory building in its njth mode of vibration is given by:

$$r_{nj} = \bar{r}_{nj} r_j \tag{12}$$

for $n = 1,2;\ \ j = 1,\ldots,N$, where r_j is the value of the same response quantity in the corresponding torsionally-uncoupled multistory system in its jth lateral mode of vibration; and $\bar{r}_{nj}$ is the normalized response of the torsionally-coupled single-story system with uncoupled lateral vibration frequency ω_y equal to ω_{yj}. The bar over r_{nj} indicates that the response of the torsionally-coupled single-story system is normalized by the response corresponding to a torsionally-uncoupled single-story system, a system with coincident CM and CS, but all other properties coincident to the torsionally-coupled single-story system [3].

We can now use Eq. (12) to determine any response of a multistory system. In particular, consider two analysis cases: (1) a system with eccentricity $e = e_s$ and no accidental eccentricity, and (2) a system with $e = e_s \pm \beta b$, i.e., with accidental eccentricity $\pm\beta b$. Let the response of the system computed from the first analysis case be represented by Eq. (12). Then, using the symbol '$*$' to identify as before building responses computed considering accidental eccentricity $\pm\beta b$, the system response corresponding to the second case (system with accidental eccentricity) can be expressed as

$$r^*_{nj} = \bar{r}^*_{nj}\ \ r_j \tag{13}$$

Note that $\bar{r}_{nj}$ is modified to $\bar{r}^*_{nj}$ because of accidental eccentricity whereas the response r_j of the torsionally-uncoupled $N-$story system in the jth mode, r_j, is unaffected. Thus, dividing Eq.(13) by (12) gives the normalized response in the nj^{th} vibration mode

$$\hat{r}_{nj} = \bar{r}^*_{nj} / \bar{r}_{nj} \tag{14}$$

Therefore, the normalized response $\hat{r}_{nj}$ in the nj^{th} mode is identical to the one that would be computed using Eq. (3) for a single-story torsionally-coupled system in its n^{th} vibration mode $(n = 1,2)$.

This equivalence between the modal responses $\hat{r}_{nj}$ of single and multistory torsionally-coupled systems does not necessarily imply that the total normalized responses of the two systems are the same because response contributions of $2N$ modes are to be combined in the multistory case, in contrast to only two modes in the case of single-story systems. However, as shown in Ref. [3], if the earthquake pseudo-acceleration design spectrum is flat or hyperbolic, the combined responses

using the CQC superposition rule also satisfy an equation that is analogous to Eq. (12):

$$r_d = \bar{r}\ r_o \tag{15}$$

where r_o is the value of the same response quantity in the corresponding torsionally-uncoupled multistory system, and $\bar{r}$ is the normalized response of the corresponding torsionally-coupled single-story system. Consequently, for these particular spectra the normalized dynamic responses $\hat{r}_d$ turn out to be identical for single and multistory systems. Small differences between the responses for these two systems may arise if the multistory system has vibration modes, higher than the first $(n = 1)$ modal pair $(j = 1, 2)$, contributing significantly to the response and lying on different regions of the pseudo-acceleration design spectrum.

This completes the proof of why the response $\hat{r}_d$ computed from dynamic analysis of single and multistory systems belonging to the special class are essentially the same. We now turn to the question of the static response of these two systems with and without accidental eccentricity.

Consider the response of the special class of multistory systems subjected to arbitrary equivalent static lateral forces $\boldsymbol{f}$ applied at the CM of each floor in accordance with UBC. Any building response, r_s, can be expressed as (Appendix A)

$$r_s = \bar{r}\ r_o \tag{16}$$

where r_o represents the static response of the corresponding torsionally-uncoupled multistory system, and $\bar{r}$ is the response of the associated torsionally-coupled single-story system divided by the response of the corresponding torsionally-uncoupled single-story system, a system with coincident CM and CS, but all other properties coincident to the torsionally-coupled single-story system.

Consider the following static analysis cases: (1) a building with equivalent static forces $\boldsymbol{f}$ applied at the CM of the building, and (2) the building with the same equivalent static forces applied at distance $e = e_s \pm \beta b$ from the CS of the structure. Let the building response for the first analysis case with no accidental eccentricity be defined by Eq. (16). Now, when accidental eccentricity $\pm\beta b$ is considered in the analysis (analysis case (2)), only the static response of the torsionally-coupled single story system, $\bar{r}$, is modified, since the response r_o, by definition, is unaffected by eccentricity. Therefore, dividing the static responses of the building for analysis cases (2) and (1), the normalized static response of the building $\hat{r}_s$ can be expressed again as

$$\hat{r}_s = \bar{r}^*/\bar{r} \tag{17}$$

i.e., the ratio of responses in the corresponding torsionally coupled single-story system with and without accidental eccentricity. Note that in the static case $\hat{r}_s$ for the special class of multistory systems and the single-story system are exactly the same. This concludes our proof.

Although Eq. (17) was derived for an equivalent static analysis procedure in accordance with UBC, i.e., $\alpha = \delta = 1$, this equation holds for arbitrary values of the parameters α, δ and β (Appendix A).

Therefore, based on Eqs. (14) and (17) for $\hat{r}_d$ and $\hat{r}_s$, we conclude that the dynamic response factor $\Gamma = \hat{r}_d/\hat{r}_s$ for single-story systems is expected to be very similar to that for multistory systems.

Figure 10 shows, for instance, the dynamic response factor $\Gamma_{\pm b/2}$ associated with the edge displacements of five story shear-type buildings with fundamental uncoupled vibration period of 1 sec., for a wide range of frequency ratios Ω, accidental eccentricity $e_a/b = 0.05$, and four values of static eccentricity $e/b = 0, 0.05, 0.10$, and 0.15. Furthermore, the results for the dynamic response factor on single-story systems already presented in Fig. 6 are included in this figure for the sake of comparison. The dynamic response factors for single and multistory systems belonging to the special class are identical, for all practical purposes. Based on these results and the proof stated earlier we conclude that all observations and conclusions presented before for single-story buildings are also valid for the special class of multistory systems considered.

An important corollary of this result is that since the normalized dynamic and static responses presented in Eqs. (14) and (16) depend only on the properties of the corresponding torsionally coupled single story system, their values are identical in all stories of the building. For instance, the dynamic response factor $\Gamma_{\pm b/2}$ presented in Fig. 10 is valid for the edge displacements at every floor. Moreover, this dynamic response factor not only applies to the edge displacements at different floors but to any response of the building that is a linear function of these edge displacements, such as the story drifts at $x = \pm b/2$, or the bending moments and shears of the structural elements of a resisting plane at the edge of the building.

4.5 General multistory buildings

The systems considered in this section are idealized multistory buildings that do not belong to the special class studied previously, and consist of rigid floor diaphragms, where the floor masses are lumped; lateral resistance is provided by resisting planes in the x and y-directions. The i^{th} resisting

plane in the x-direction has a lateral stiffness matrix $\boldsymbol{k}_{xi}$ and is located at distance y_{ij} from the CM at floor j; analogously, the stiffness matrix and location at floor j of plane i in the y-direction are defined by $\boldsymbol{k}_{yi}$ and x_{ij}. The resisting planes may have arbitrary stiffness matrices in the y-direction and may be unsymmetrically located about the y-axis, creating variable eccentricities between the CM and CS[2] at different floors. On the other hand, the systems are considered symmetric about the x-axis.

The dynamic response of the system to base acceleration in the y-direction, $a_{gy}(t)$, is described as before by the vector $\boldsymbol{u}_y$ of displacements u_{yj} of the j^{th} floor CM along the y-direction, and the vector $\boldsymbol{u}_y$ of rotations $u_{\theta j}$ of the j^{th} floor rigid diaphragm about a vertical axis through the CM. The equations of motion of the system can be written

$$\begin{bmatrix} \boldsymbol{m} & 0 \\ 0 & \boldsymbol{m} \end{bmatrix} \begin{Bmatrix} \ddot{\boldsymbol{u}}_y \\ r\ddot{\boldsymbol{u}}_\theta \end{Bmatrix} + \begin{bmatrix} \boldsymbol{K}_y & \frac{1}{r}\boldsymbol{K}_{y\theta} \\ \frac{1}{r}\boldsymbol{K}_{y\theta} & \frac{1}{r^2}\boldsymbol{K}_\theta \end{bmatrix} \begin{Bmatrix} \boldsymbol{u}_y \\ r\boldsymbol{u}_\theta \end{Bmatrix} = -\begin{Bmatrix} \boldsymbol{m}\,\mathbf{1} \\ \mathbf{0} \end{Bmatrix} a_{gy}(t) \qquad (18)$$

where $\boldsymbol{m}$ and $\boldsymbol{K}_y$ are the translational mass and lateral stiffness matrix of the system as defined earlier for Eq. (7); $\boldsymbol{K}_{y\theta} = \sum_i \boldsymbol{k}_{yi}\boldsymbol{X}_i$ is the lateral-torsional coupling matrix and $\boldsymbol{X}_i$ is a diagonal matrix with diagonal terms x_{ij}; and $\boldsymbol{K}_\theta = \sum_i(\boldsymbol{X}_i\boldsymbol{k}_{yi}\boldsymbol{X}_i + \boldsymbol{Y}_i\boldsymbol{k}_{xi}\boldsymbol{Y}_i)$ is the torsional stiffness matrix of the system with respect to the CM and $\boldsymbol{Y}_i$ is a diagonal matrix with diagonal terms y_{ij}.

The systems considered are analyzed for the smooth response spectrum already described (Chapter2: Fig. 2), and their peak earthquake response estimated by the RSA method using the CQC modal combination rule.

Since the number of parameters required to define multistory buildings rapidly becomes unmanageable as the number of stories increases, results presented next aim only to provide practical engineering bounds for the differences between the increase in building response due to accidental eccentricity predicted by dynamic analysis versus that predicted from static analysis.

Consider two five-story shear-type buildings with static eccentricities—computed as the distance between the CM and the CS for each story as a single-story system—from bottom to top $\boldsymbol{e}_s/b = \{0.10\ \ 0.10\ \ 0.05\ \ 0.05\ \ 0.05\}^T$ and $\boldsymbol{e}_s/b = \{0.25\ \ 0.25\ \ 0.125\ \ 0.125\ \ 0.125\}^T$, accidental eccentricity $e_a/b = 0.05$, identical masses and stiffnesses in all stories, and fundamental vibration period of 1 sec. This example is motivated by the fact that lower stories of many actual buildings are unsymmetric to a greater degree than the upper stories. Note that these systems do not belong to the special

[2]It is well known that the location of the CS at each floor is dependent on the way we define these points; however, for the sake of the discussion here, discrepancies between different definitions are not relevant

class of buildings defined in the previous section since their centers of stiffness do not lie on the same vertical line.

Figure 11 shows the dynamic response factor $\Gamma_{+b/2}$ computed for the two five-story buildings described above. Results are presented as a function of the parameter Ω, which is assumed equal for all stories and defined as $\Omega_j = \sqrt{K_{\theta Rj}/(K_y r^2)}, \quad j = 1, \ldots, N$, where $K_{\theta Rj}$ is the torsional stiffness of the j^{th} story with respect to its CS, K_y is a reference lateral stiffness, and r is the radius of gyration of story j, assumed constant for all stories. This parameter is indeed the ratio between the uncoupled torsional and lateral frequencies of the two systems considered; this observation is always true for shear-type buildings with uniform heightwise distribution of story lateral and torsional stiffnesses. We compare the values of $\Gamma_{+b/2}$ thus computed with the ones that would be obtained for two multistory systems belonging to the special class, in which the floor eccentricities are assumed uniform in height and equal to the largest or smallest values of the floor eccentricities in the five-story building. These two cases are identified in Fig. 11 by the values of static eccentricity used. It is interesting to note, that in spite of the rather abrupt change in planwise distribution of stiffness between the second and third stories in each of the example buildings, the variation with Ω of the dynamic response factor $\Gamma_{\pm b/2}$ for the actual building is quite similar to that for the two special class multistory systems. Moreover, the $\Gamma_{\pm b/2}$ for these two systems seems to bound the $\Gamma_{\pm b/2}$ of the actual building. This suggests that the values of $\Gamma_{\pm b/2}$ in general multistory systems are not expected to be very different from those predicted by the special class of multistory systems.

In order to provide useful bounds for the normalized dynamic and static responses and the dynamic response factor for general multistory buildings, we consider two cases: (A) buildings belonging to the special class of multistory systems considered previously but in which the accidental eccentricity e_a may vary between stories; and (B) buildings with variable static and accidental eccentricities at each story. In both cases, the static eccentricity of the building at each story is allowed to vary between $\pm 0.25b$, and the accidental eccentricity e_a between $\pm 0.05b$.

4.5.1 Case A

The problem considered is to determine the maximum value of normalized dynamic displacement $(\hat{u}_{\pm b/2})_d$ and of the dynamic response factor $\Gamma_{\pm b/2}$ over all possible multistory buildings belonging to the special class and for which the accidental eccentricity may vary from story to story in the range $\pm 0.05b$. This is of interest because, we do not know a priori which combination of accidental

eccentricities e_a/b at various stories leads to the largest dynamic response of the building. In practice, buildings are frequently analyzed by shifting the CM of all floors the same amount e_a in the same direction; however, it is not obvious how conservative or not this procedure is.

We choose the normalized dynamic response $(\hat{u}_{\pm b/2})_d$ at the top floor of the building as the response quantity of interest. This response depends on the values of accidental eccentricity e_{aj}, $j = 1, \ldots, N$ at different stories for which we are interested in: finding the combination that produces the maximum dynamic response and quantifying by how much this response differs from the one computed by shifting in all floors the centers of mass the same accidental eccentricity e_a in the same direction.

In mathematical terms the problem is stated as

$$\begin{aligned} &\max \ (\hat{u}_{\pm b/2})_d \ \text{ subjected to :} \\ &-0.05 \leq e_{aj}/b \leq 0.05, \quad j = 1, ..., 5 \end{aligned} \tag{19}$$

This problem, which is a nonlinear constrained optimization problem, was solved using the sequential programming method implemented in the optimization toolbox available in MATLAB [6].

Figure 12 shows schematically the values of story accidental eccentricity $(e_a/b)_i$ that produce the maximum value of normalized dynamic responses $(\hat{u}_{\pm b/2})_d$ for different ranges of the frequency ratio Ω, and two values of the static eccentricity $e_s/b = 0$ and 0.10. These and all subsequent results are for five-story shear-type buildings with fundamental uncoupled lateral vibration period of 1 sec. The maximum normalized dynamic response of the system is always achieved for maximum values $\pm 0.05b$ of the accidental eccentricity. However, the vertical distribution of accidental eccentricity, as shown in the figure, does not in general coincide with the conventional analysis procedure of shifting all the masses e_a toward the same side of the CM. Despite this fact, the differences in response that can be attributed to this discrepancy are small and usually occur for small values of Ω as presented next.

Figure 13 presents the corresponding peak values of the response $(\hat{u}_{\pm b/2})_d$ as a function of Ω for the combination of e_{aj} that produces the largest response, and five values of static eccentricity $e_s = 0, 0.05, 0.1, 0.15$ and 0.25. By comparing this figure with the corresponding results for single-story and multistory systems belonging to the special class (Fig. 5), it is apparent that the maximum normalized dynamic responses are about 10% larger than those computed by shifting all the centers of mass a distance e_a toward the same side of the CM for systems with $\Omega < 1$; the largest difference

between these two figures occurs for the normalized displacement at the flexible edge of the building , $(\hat{u}_{-b/2})_d$.

Although the maximum value of the dynamic response factor, $\Gamma_{\pm b/2} = (\hat{u}_{\pm b/2})_d/(\hat{u}_{\pm b/2})_s$, could be found similarly to the maximum value of $(\hat{u}_{\pm b/2})_d$, we must impose the constraint that static analysis in practice is always performed by applying the equivalent lateral forces shifted $e_a = \pm\beta b$ to the same side of the CM in all floors. Indeed, it is with respect to this static analysis that we want to study the differences against dynamic response. This condition implies, however, that $(\hat{u}_{\pm b/2})_s$ is constant and will not depend on the values of accidental eccentricity e_{aj}/b at each story that maximize the normalized dynamic response. Consequently, the values of story accidental eccentricity e_{aj}/b that maximize $(\hat{u}_{\pm b/2})_d$ are the same as those that maximize $\Gamma_{\pm b/2}$. Then, $\Gamma_{\pm b/2}$ can be computed by simply taking the ratio between the normalized dynamic response presented in Fig. 13 and the corresponding static response for an accidental eccentricity of $0.05b$. Recall that since these systems belong to the special class, their static response is identical to the response computed from the corresponding torsionally-coupled single story system (Fig. 5).

The maximum values of $\Gamma_{\pm b/2}$ thus computed are presented in Fig. 14 as a function of Ω values, for five values of static eccentricity $e/b = 0, 0.05, 0.10, 0.15$ and 0.25. Comparing these results against those corresponding to the special class multistory systems or single-story systems presented in Fig. 6 we see that the peak values of the dynamic response factor $\Gamma_{\pm b/2}$ are only slightly larger than the ones computed using a constant accidental eccentricity of $0.05b$ in all stories. The maximum differences between dynamic and static analysis occur again at the stiff edge of the building ($x = +b/2$) and for small values of Ω.

4.5.2 Case B

We now consider a broader problem: what is the maximum dynamic response factor, $\Gamma_{\pm b/2}$, over all multistory systems systems in which the static and accidental eccentricities vary within the ranges $-0.25 \leq e/b \leq 0.25$ and $-0.05 \leq e_a/b \leq 0.05$, respectively. These ranges cover most of the actual unsymmetric multistory buildings.

The problem considered can be stated in mathematical terms as

$$\begin{aligned} \max \text{ [or min]} \quad & \Gamma_{\pm b/2} = (\hat{u}_{\pm b/2})_d/(\hat{u}_{\pm b/2})_s \quad \text{subjected to:} \\ & -0.25 \leq (e/b)_i \leq 0.25 \\ & -0.05 \leq (e_a/b)_i \leq 0.05, \quad i = 1, ..., 5 \end{aligned} \tag{20}$$

The maximum and minimum values of the dynamic response factor are of interest since both provide bounds for the differences between dynamic and static responses.

During the optimization, the normalized static responses $(\hat{u}_{\pm b/2})_s$ are always computed by shifting the equivalent lateral forces a distance $\pm 0.05b$ to the right and left of the CM, respectively. Because the static eccentricity changes at each story during the optimization process, the stiffness matrix of the system, and thus the normalized dynamic and static responses, change during the optimization. Therefore, in contrast to case A, maximizing the dynamic response factor $\Gamma_{\pm b/2}$ in case B is different than maximizing the normalized dynamic response of the system $(\hat{u}_{\pm b/2})_d$.

Given the problem as stated, we only need to consider the displacements at one edge of the building plan. Identical observations and conclusions would be obtained for the normalized displacements at the other edge because of the symmetry in the ranges of variability for the static and accidental eccentricities in each story.

Figure 15 shows schematically the combined values of story static and accidental eccentricities that lead to the maximum and minimum dynamic response factor $\Gamma_{-b/2}$ for four values of the frequency ratio $\Omega = 0.8, 1, 1.2$ and 1.5. Interestingly, the maximum values of $\Gamma_{-b/2}$ do not occur for the maximum possible story eccentricities, $e_s + e_a = \pm 0.3b$. Note also that the vertical distributions of static eccentricities producing the maximum and minimum values of $\Gamma_{\pm b/2}$, for a constant frequency ratio Ω, are not very different; it is apparent that a small horizontal translation of the vertical distribution of static eccentricities leading to the maximum $\Gamma_{\pm b/2}$ gives, roughly, the vertical distribution of static eccentricities leading to the minimum of $\Gamma_{\pm b/2}$. Further, these vertical distributions of accidental eccentricity do not seem impractical, implying that these bounds are likely to be achieved by real buildings.

The maximum values of the dynamic response factor and the corresponding static and dynamic responses, $(\hat{u}_{-b/2})_s$ and $(\hat{u}_{-b/2})_d$, are presented in Fig. 16. It is apparent that the dynamic response factor is increased, as it should, in comparison to the one obtained before for the special class of multistory systems (Fig. 6) for almost all frequency ratios. The maximum values of $\Gamma_{-b/2}$ range between 1.2 and 1.3 for systems with frequency ratio within the range 0.6 to 1.2, and they reduce to less than 1.1 for systems with $\Omega > 1.5$. On the other hand, the minimum values of $\Gamma_{\pm b/2}$ are usually less than 0.6 if $\Omega < 1$ and slowly approach one as the frequency ratio is increased. These results imply that the difference between the increase in response due to accidental eccentricity predicted by dynamic and static analysis may be as large as 40% if the frequency ratio is $0.8 \leq \Omega \leq 1.25$, but it is reduced to less than 10% if $\Omega > 1.6$.

In some cases, the bounds of the dynamic response factor presented in Fig. 16 may be hard to achieve in practice because they imply abrupt changes in the static eccentricities from one story to the next. Frequently in buildings, the values of static eccentricity at different stories may vary but within certain narrower bounds—for instance, due to gradual set-backs in the upper stories of the building, or asymmetries in the basement and first few stories. Consequently, a more realistic scenario would be to take the same system and optimal problem as before (Eq. (20)) but considering the static eccentricity at each story to be constrained to vary within narrower limits. Five cases are considered: (1) $-0.05 \leq (e/b)_i \leq 0.05$, (2) $0 \leq (e/b)_i \leq 0.1$, (3) $0.05 \leq (e/b)_i \leq 0.15$, (4) $0.1 \leq (e/b)_i \leq 0.20$, and (5) $0.15 \leq (e/b)_i \leq 0.25$.

The peak values of the normalized response ratio $\Gamma_{\pm b/2}$ corresponding to these five cases are shown in Figs. 17 and 18. As shown by these figures, these results are similar to those obtained before for single-story and the special class of multistory systems (Fig. 6). The values of $\Gamma_{\pm b/2}$ are increased primarily for frequency ratios $\Omega < 1$. They range between 0.6 and 1.3 for frequency ratios $0.8 \leq \Omega \leq 1.25$ and are reduced to less than 1.1 if $\Omega > 1.6$.

Because of the similarity between the bounds of response presented above and the results corresponding to the special class of multistory systems obtained earlier, it seems unnecessary to perform further parametric studies in order to evaluate the differences between the increase in response due to accidental eccentricity predicted by dynamic and static analysis.

4.6 Code Implications

According to the results presented above, we see that if two engineers chose to analyze the same building, one using the dynamic analysis procedure in the code and the other the equivalent static force method in the code, they might find that the resulting increase in building response due to accidental eccentricity is, say, 25% in the dynamic case, but 50% in the static case, situation that would occur if Ω is less than, say, 0.7 (Figs. 6, 17, and 18). Thus, the static analysis would predict an increase in response due to accidental eccentricity twice of that predicted from dynamic analysis of the same building.

On the other hand, the actual increase in building response due to accidental eccentricity is in many cases similar or even smaller than the difference in response predicted by dynamic and static analysis. Consider for instance a building with frequency ratio $\Omega = 1.1$, defined as the ratio between fundamental uncoupled torsional and lateral vibration frequencies, uncoupled vibration

period $T_y = 1$ sec, and static eccentricity $e_s = 0.1b$ at each story. The increase in response due to accidental eccentricity at the flexible edge of the building, computed from static analysis, is approximately 12% (Fig. 5); however, this increase is less than 5% if computed from dynamic analysis. In contrast, the increases in response predicted by static and dynamic analysis at the stiff edge of the building are 12 and 30%, respectively. No matter which method of analysis is considered more accurate, the differences between the predicted values for the increase in building response (7% and 18% respectively) are of the same order of magnitude as the actual increase in response due to accidental eccentricity. This implies that the code-specified static and dynamic analyses to account for accidental torsion should be modified to be mutually consistent.

4.7 Conclusions

This investigation of the differences in the increase of building response due to accidental eccentricity predicted by code-specified dynamic and static analyses has led to the following conclusions:

1. The increase in building response due to accidental eccentricity depends primarily on the value of the frequency ratio Ω of the system. For instance, if the equivalent static force method in the code is used, the predicted increase in building response is larger for systems with small frequency ratio Ω and decreases monotonically, asymptotically approaching zero, as Ω increases. The increase in response is largest for unsymmetric systems and for the elements located at the stiff side of the building plan. Further, the increase in response of buildings with $\Omega < 1$ due to accidental eccentricity calculated by dynamic analysis tends to be smaller than that predicted by static analysis; the opposite occurs for systems having a frequency ratio $\Omega > 1$ and small static eccentricities.

2. The increase in response due to accidental eccentricity and predicted by dynamic analysis is generally larger for symmetric systems compared to unsymmetric systems, implying that symmetric systems are usually the most sensitive to the introduction of accidental eccentricity.

3. The difference between values for the increase in displacements at the flexible edge of single-story systems computed by dynamic and static analyses is at most 15% and it is largest for symmetric systems. The corresponding difference in response at the stiff edge of the system is over 50% for systems with frequency ratio $\Omega < 0.7$ and static eccentricity $e_s > 0.15$, and reduces to less than 10% for symmetric and unsymmetric systems with $\Omega > 1.5$.

4. Alternatively, the values of the equivalent accidental eccentricity, calibrated from the building edge displacements, vary between zero and up to three times the UBC accidental eccentricity $0.05b$ depending on the value of the frequency ratio Ω. More importantly, the use of equivalent static accidental eccentricity calibrated from peak values of base shear and torque leads to incorrect results because of the implicit assumption that the peak values of base shear and torque occur at the same instant of time.

5. Systems with similar uncoupled lateral and torsional vibration periods, $\Omega \simeq 1$, are particularly insensitive to the introduction of accidental eccentricity.

6. The increase in response due to accidental eccentricity predicted by dynamic or static analyses of the special class of multistory systems is essentially the same as that for single-story systems.

7. The increase in building response resulting from accidental eccentricity varying among different stories is slightly (generally $< 10\%$) larger than the increase over the building response computed by using the same accidental eccentricity βb in all stories; this discrepancy occurs primarily for systems with frequency ratio $\Omega < 1$.

8. The maximum difference between the increase in response due to accidental eccentricity predicted by dynamic and static analysis, over all torsionally-coupled multi story systems considered, is as large as 40% for systems with frequency ratio in the range $0.8 < \Omega < 1.15$ and is reduced to less than 20% for systems with $\Omega > 1.6$.

9. The discrepancies between the increase in response due to accidental eccentricity predicted by dynamic and static analysis is in many cases of the same order of magnitude as the response increase itself. This implies that the code-specified static and dynamic analyses to account for accidental torsion should be modified to be mutually consistent.

4.8 References

1. Newmark, N.M. and Hall, W.J. *Vibration of Structures Induced by Ground Motion*, Shock and Vibration Handbook, McGraw Hill Inc., New York, 2nd edition, 1976.

2. Newmark, N.M. and Rosenblueth, E. *Fundamentals of Earthquake Engineering*, Prentice Hall, Inc., Englewood Cliffs, N.J., 1971.

3. Hejal, R. and Chopra, A.K.'Earthquake response of torsionally-coupled buildings', Report No. EERC 87-20, Earthquake Engineering Research Center, University of California, Berkeley, CA., 1987.

4. Rosenblueth, E. and Elorduy, J.'Response of linear systems to certain transient disturbances', Proceedings of the Fourth World Conference on Earthquake Engineering, Vol.1, Santiago, Chile, pp. A1-185 to A1-196, 1969.

5. Chandler, A.M. and Hutchinson, G.L.'Evaluation of code torsional provisions by a time history approach', Earthquake eng. struct. dyn. 15, 491-516, 1987.

6. MATLAB, 1993, The MathWorks, Inc., Natick, Massachusetts.

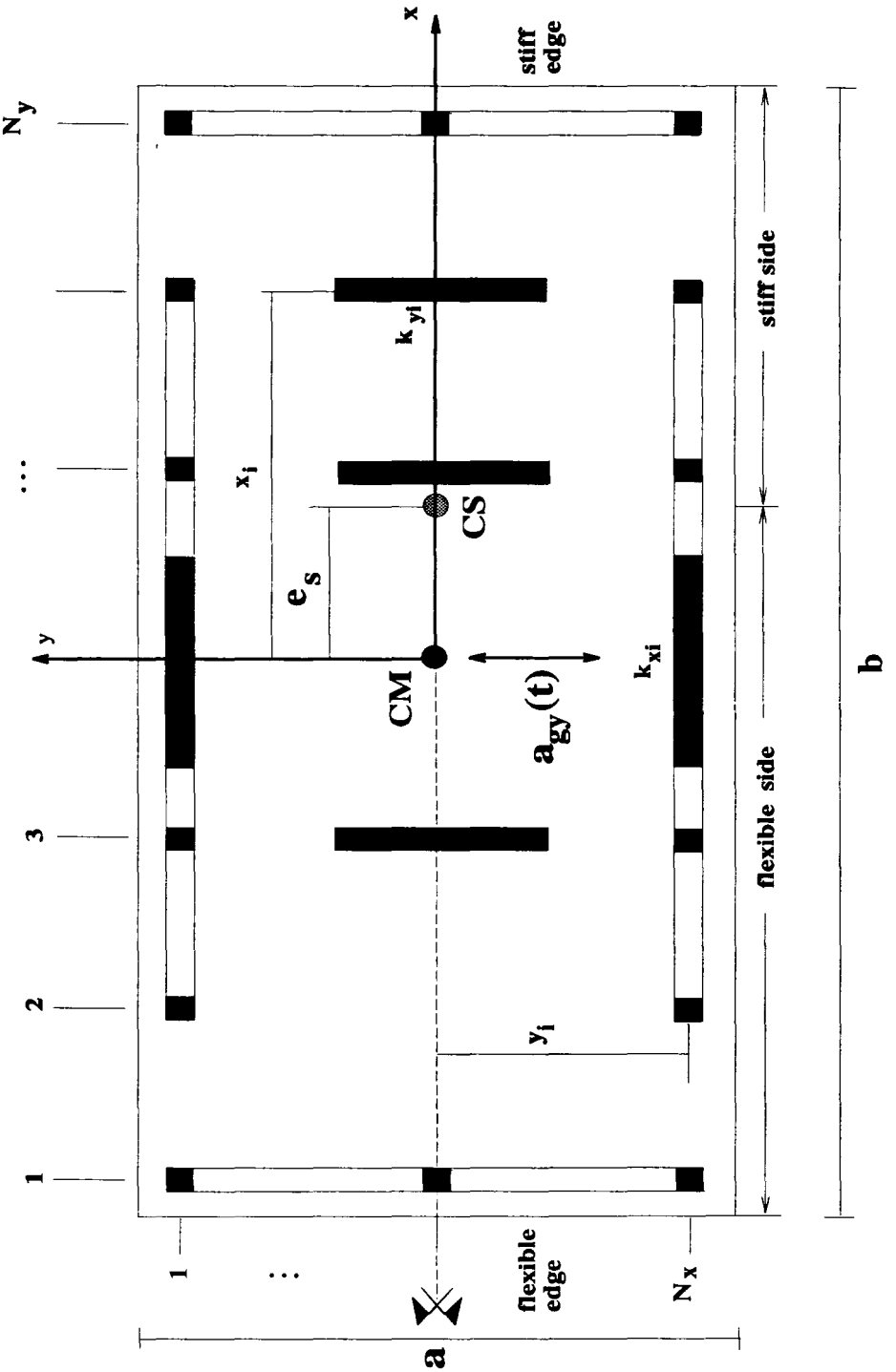

Figure 1: Typical building plan of the systems considered

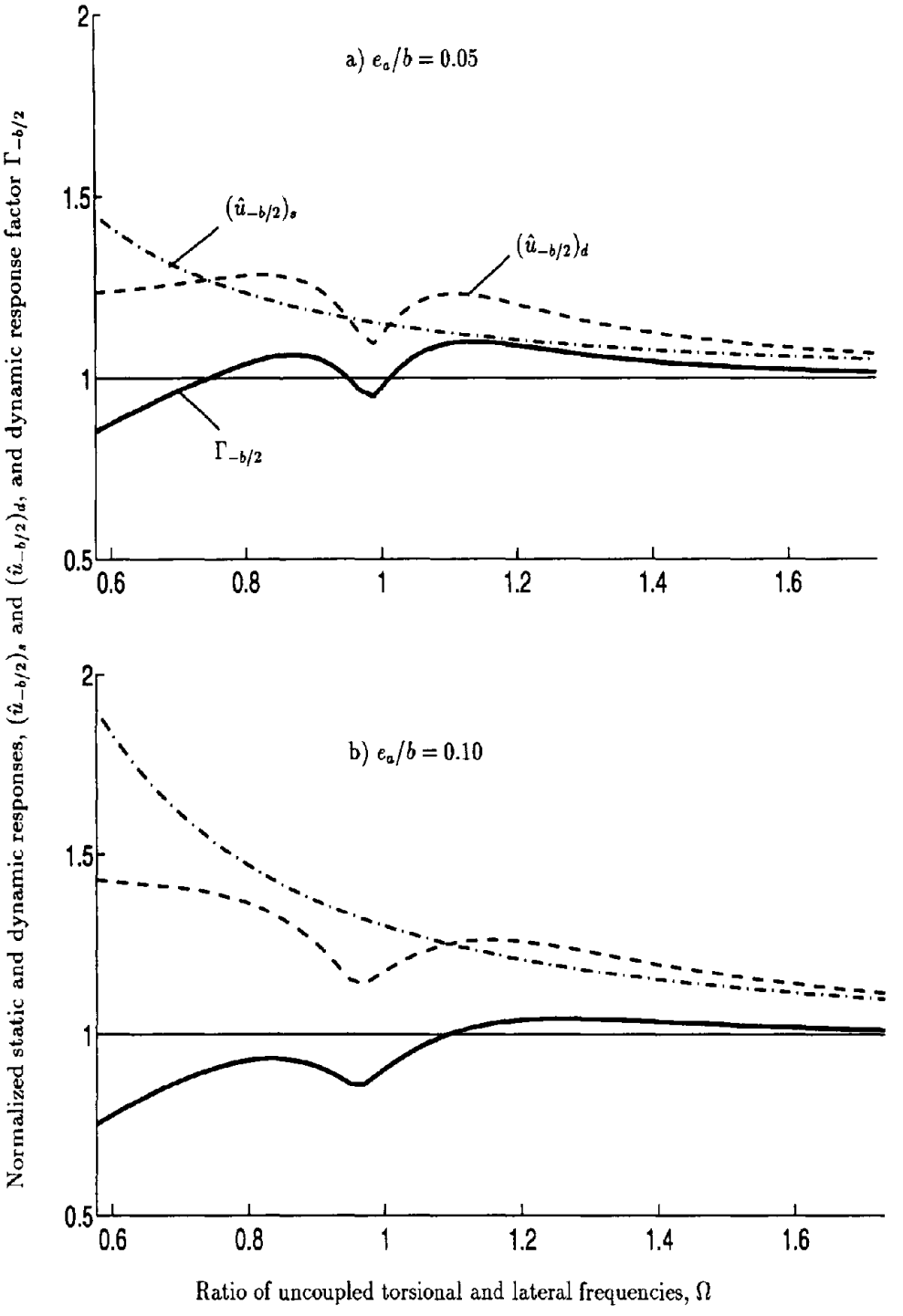

Figure 2: Normalized static and dynamic responses, $(\hat{u}_{-b/2})_s$ and $(\hat{u}_{-b/2})_d$, and dynamic response factor $\Gamma_{-b/2}$ as a function of Ω for symmetric systems with $e_a/b = 0.05$ and 0.1, $T_y = 1$ sec, and $a/b = 1$

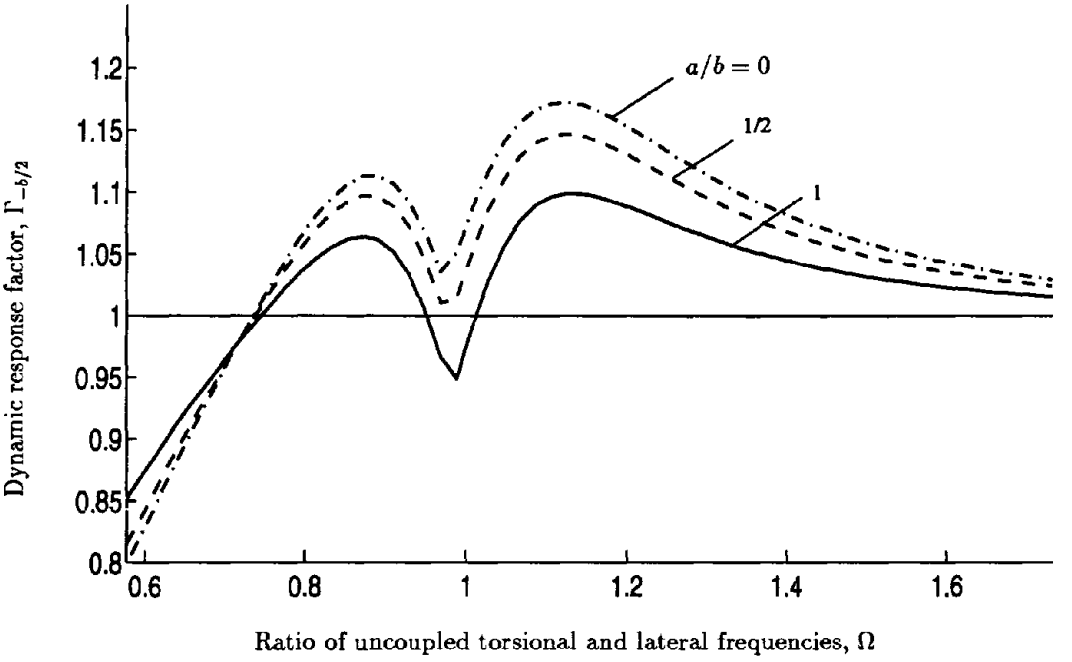

Figure 3: Dynamic response factor $\Gamma_{-b/2}$ for symmetric systems as a function of Ω, three values of the building plan aspect ratio $a/b = 0, 1/2$, and 1, accidental eccentricity $e_a/b = 0.05$, and $T_y = 1$ sec

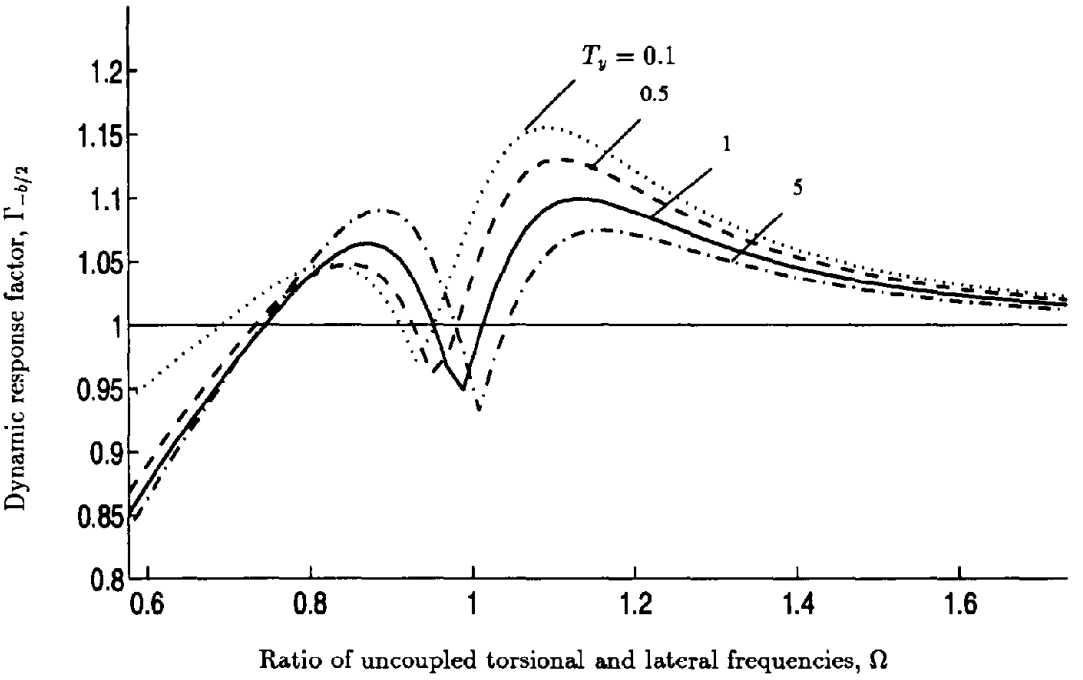

Figure 4: Dynamic response factor $\Gamma_{-b/2}$ for symmetric systems as a function of Ω, four different values of the uncoupled vibration period $T_y = 0.1, 0.5, 1$ and 5 sec, accidental eccentricity $e_a/b = 0.05$, and $a/b = 1$

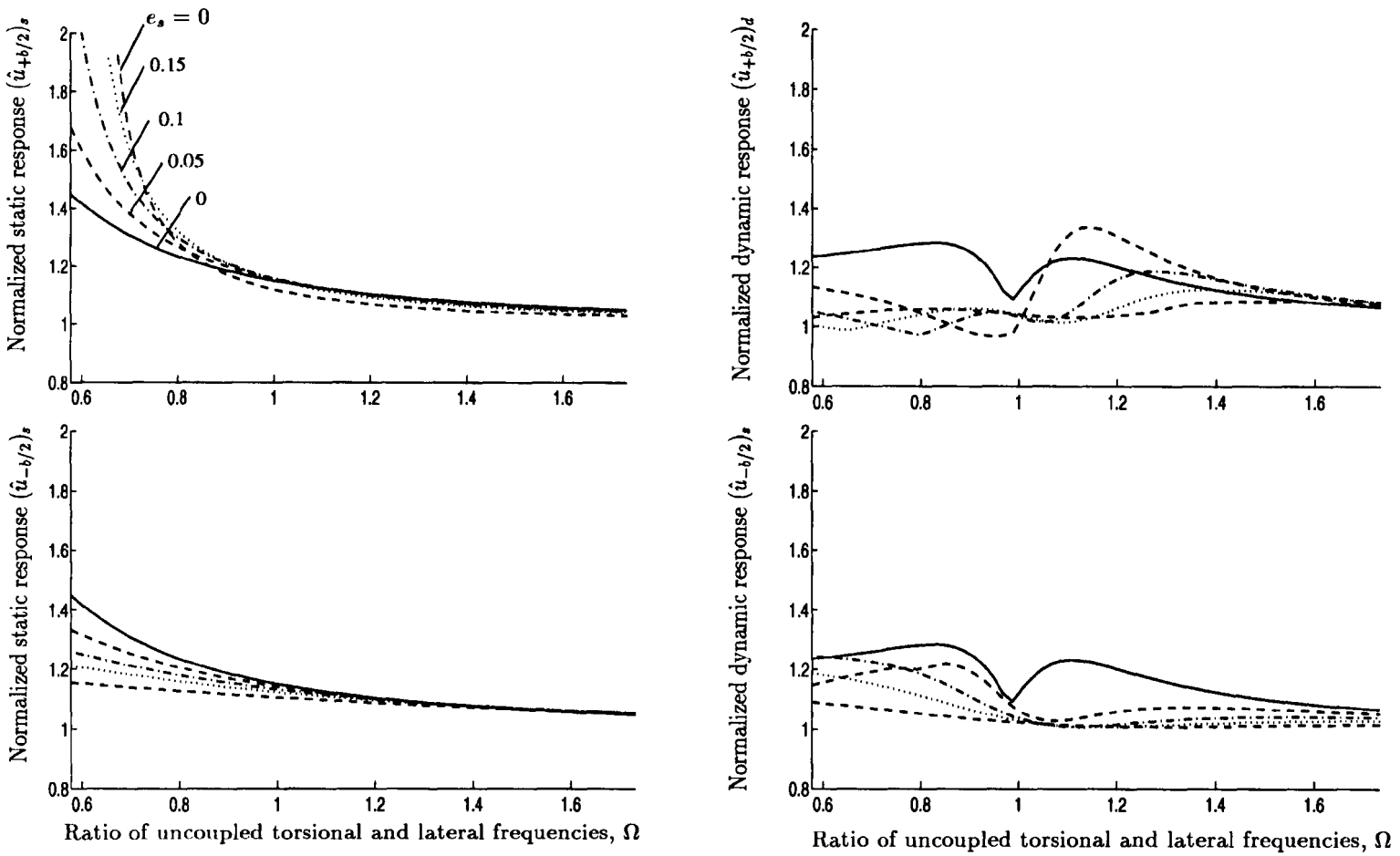

Figure 5: Normalized static and dynamic responses, $(\hat{u}_{\pm b/2})_s$ and $(\hat{u}_{\pm b/2})_d$ as a function of Ω, five values of static eccentricity $e_s/b = 0, 0.05, 0.1, 0.15$ and 0.25, accidental eccentricity $e_a/b = 0.05$, $T_y = 1$ sec, and $a/b = 1$

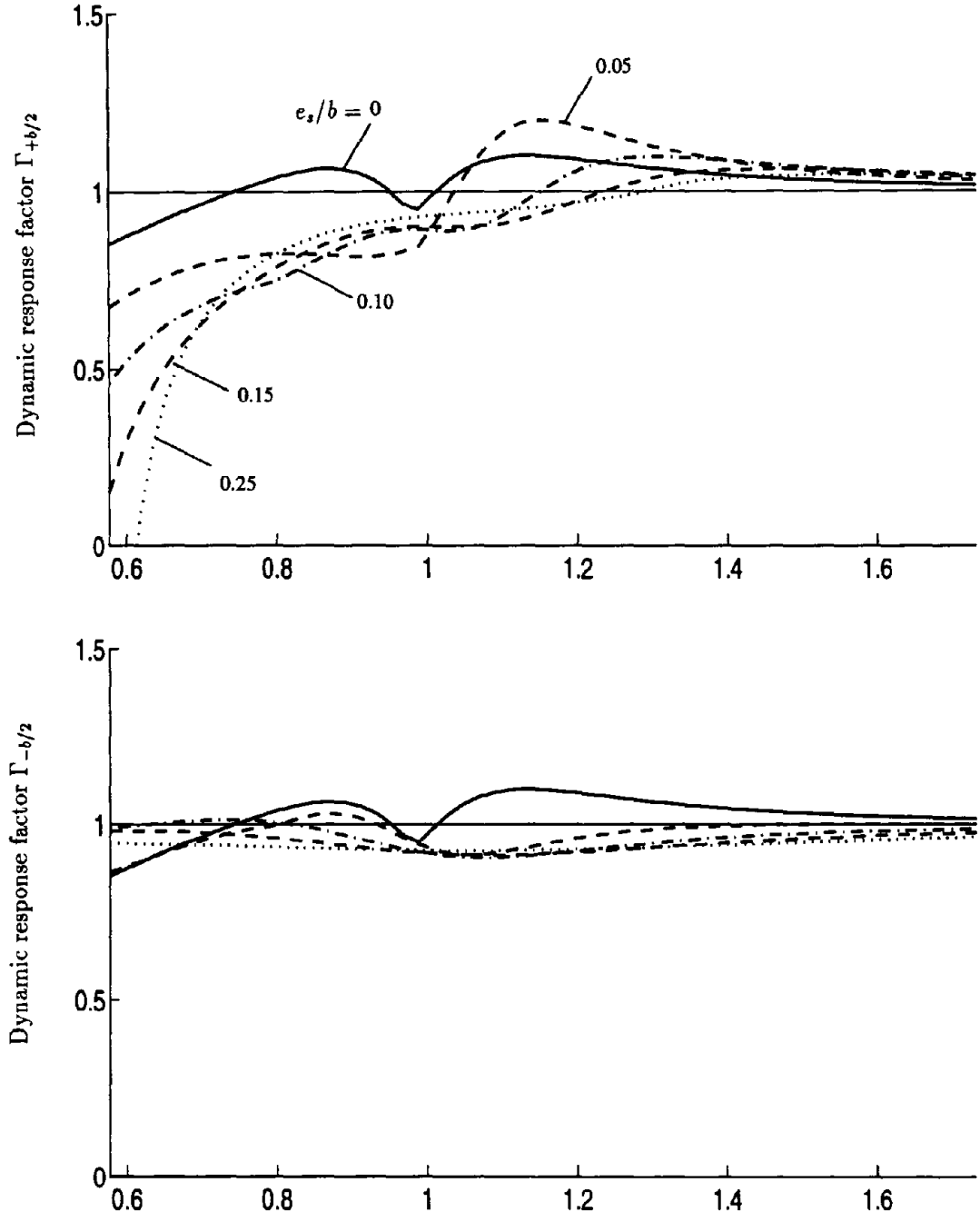

Figure 6: Dynamic response factor $\Gamma_{\pm b/2}$ as a function of Ω, five different values of static eccentricity $e_s/b = 0, 0.05, 0.1, 0.15$ and 0.25, $e_a/b = 0.05$, $T_y = 1$ sec, and $a/b = 1$

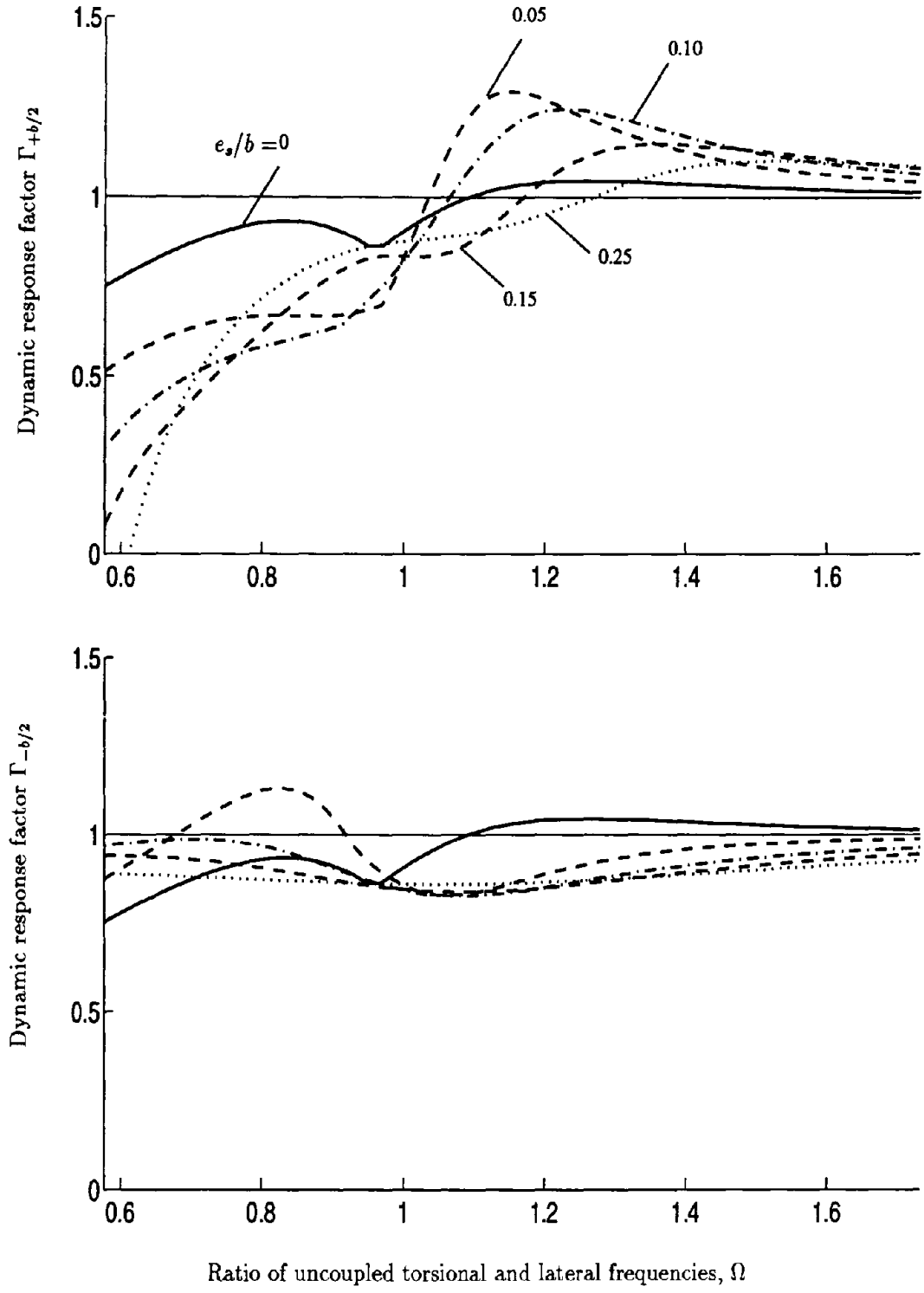

Figure 7: Dynamic response factor $\Gamma_{\pm b/2}$ as a function of Ω, five different values of static eccentricity $e_s/b = 0, 0.05, 0.1, 0.15$ and 0.25, $e_a/b = 0.10$, $T_y = 1$ sec, and $a/b = 1$

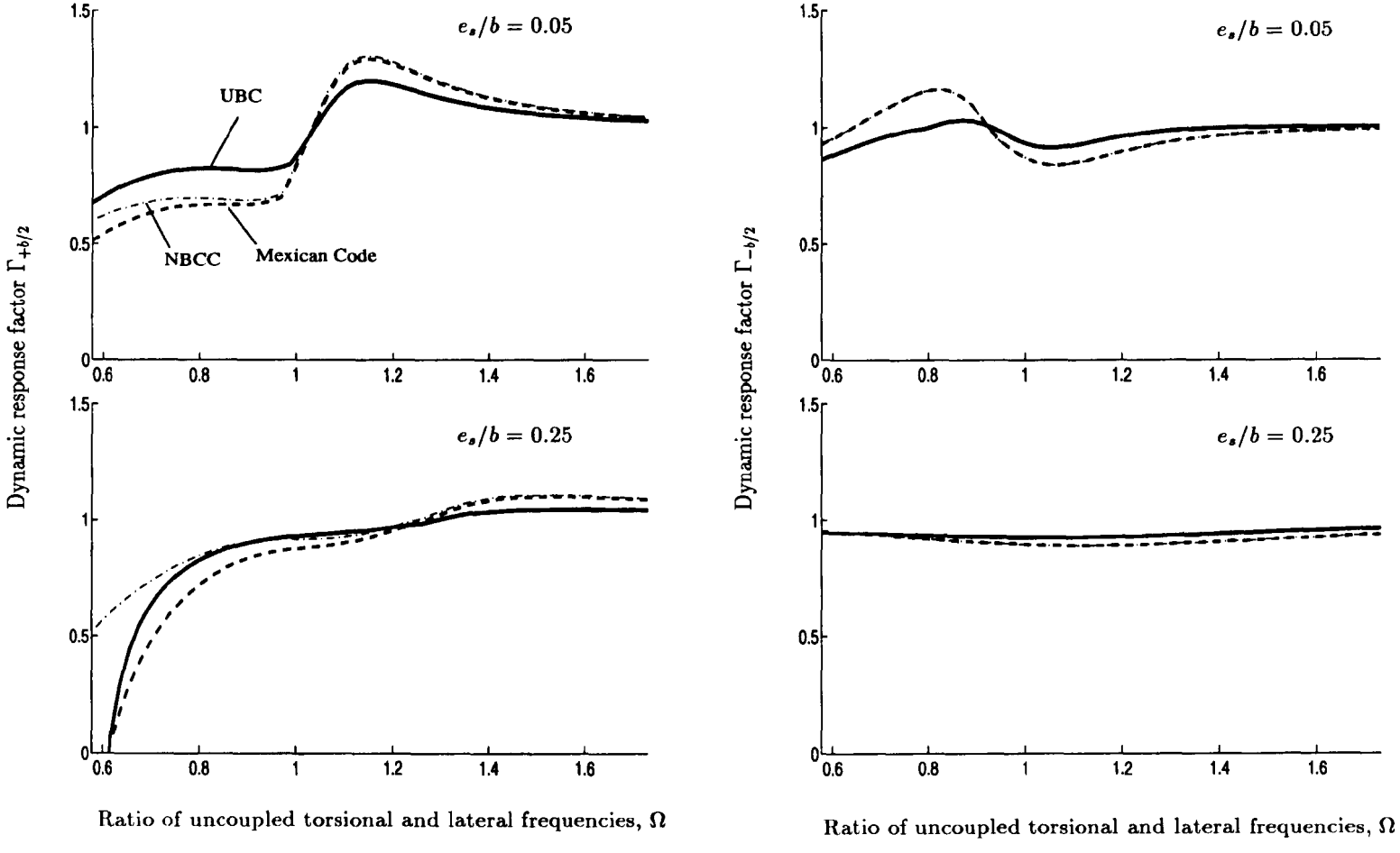

Figure 8: Dynamic response factor $\Gamma_{\pm b/2}$ as a function of Ω and corresponding to the UBC, NBCC, and Mexican codes, for systems with $e_s/b = 0.05$ and 0.25, $T_y = 1$ sec, and $a/b = 1$

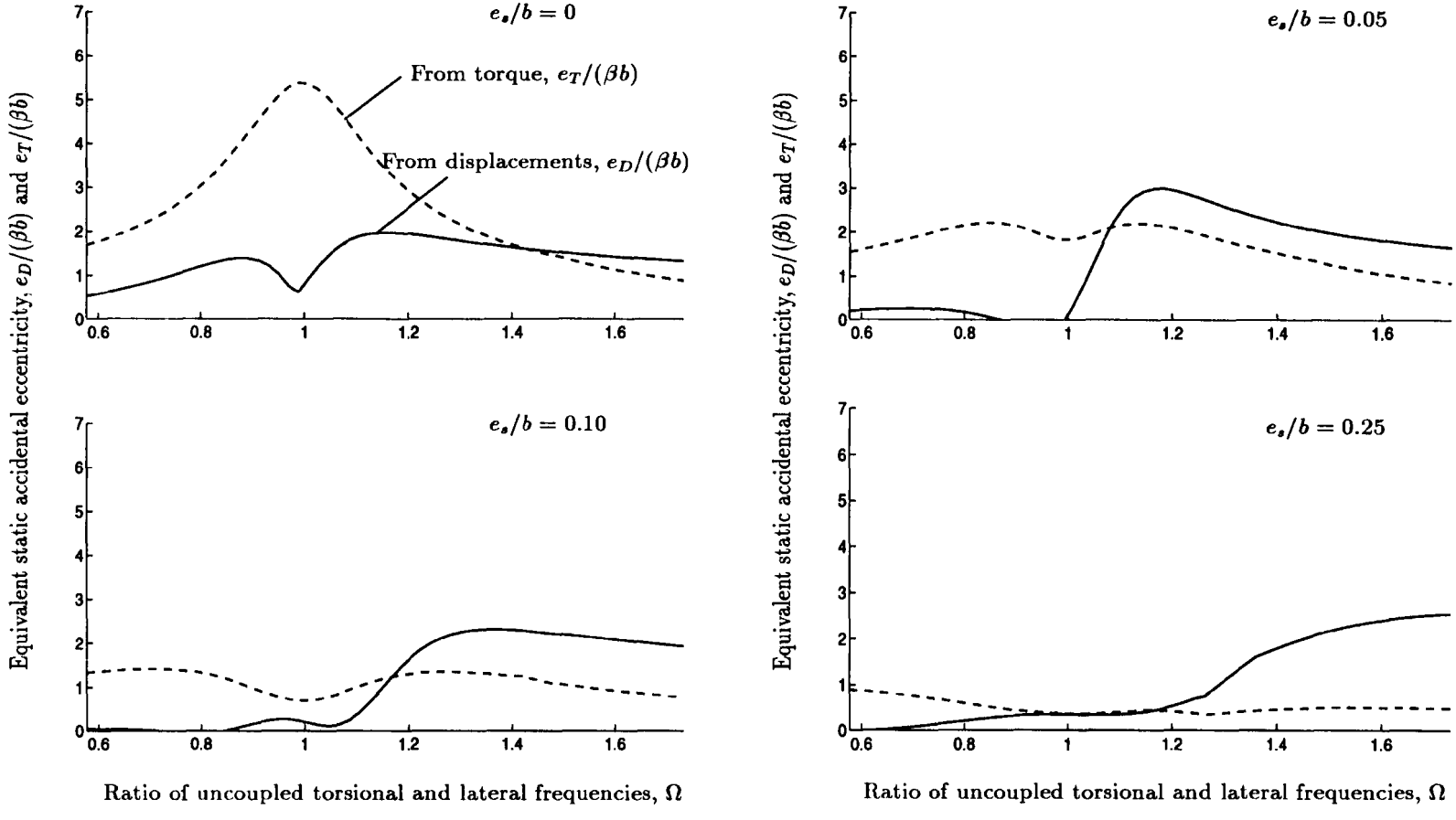

a) Stiff edge

Figure 9 : Equivalent static accidental eccentricities, $e_D/(\beta b)$ and $e_T/(\beta b)$, as a function of Ω, four values of static eccentricity $e_s/b = 0, 0.05, 0.10$, and 0.25, $T_y = 1$ sec, and $a/b = 1$

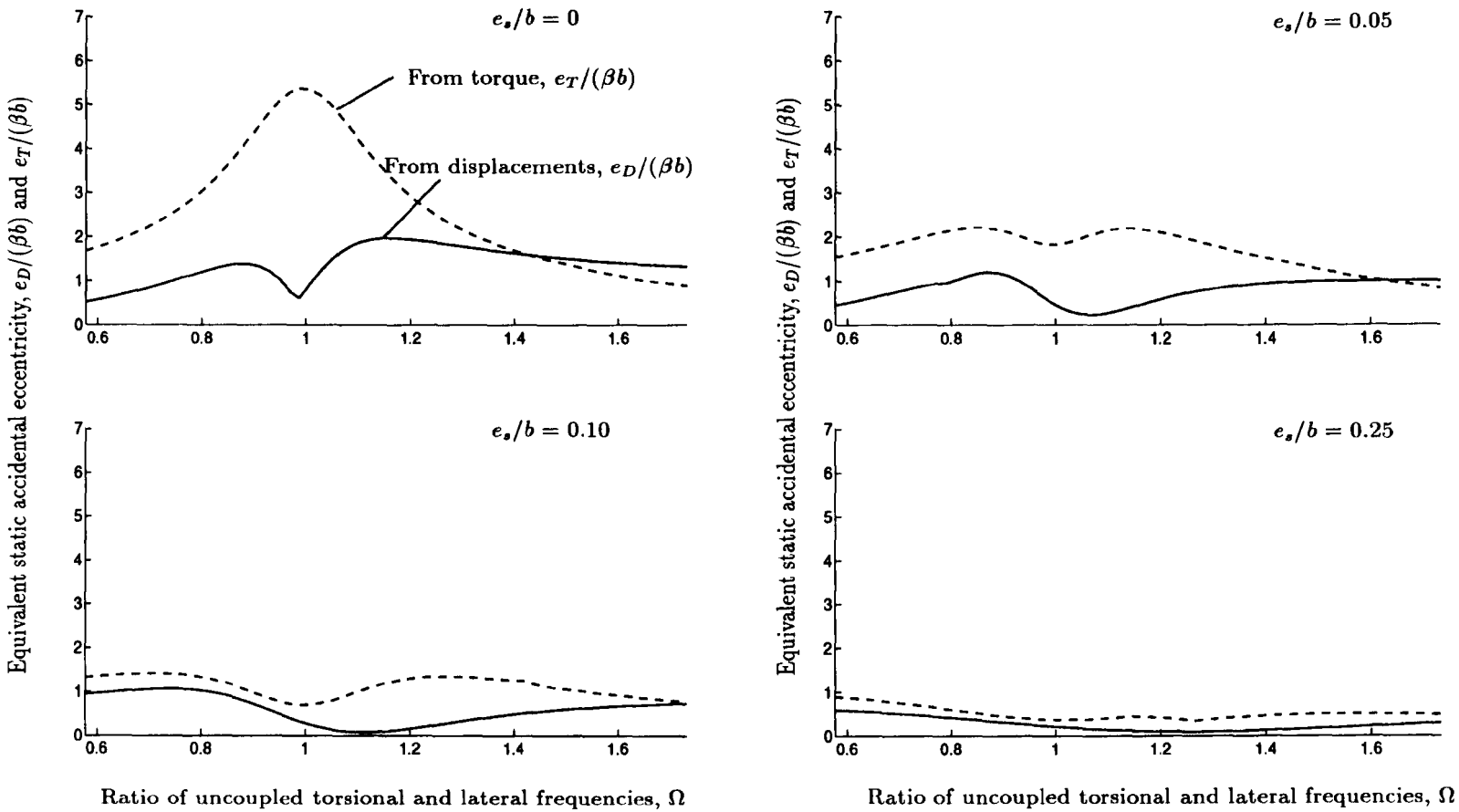

b) Flexible edge

Figure 9 (cont.): Equivalent static accidental eccentricities, $e_D/(\beta b)$ and $e_T/(\beta b)$, as a function of Ω, four values of static eccentricity $e_s/b = 0, 0.05, 0.10$, and 0.25, $T_y = 1$ sec, and $a/b = 1$

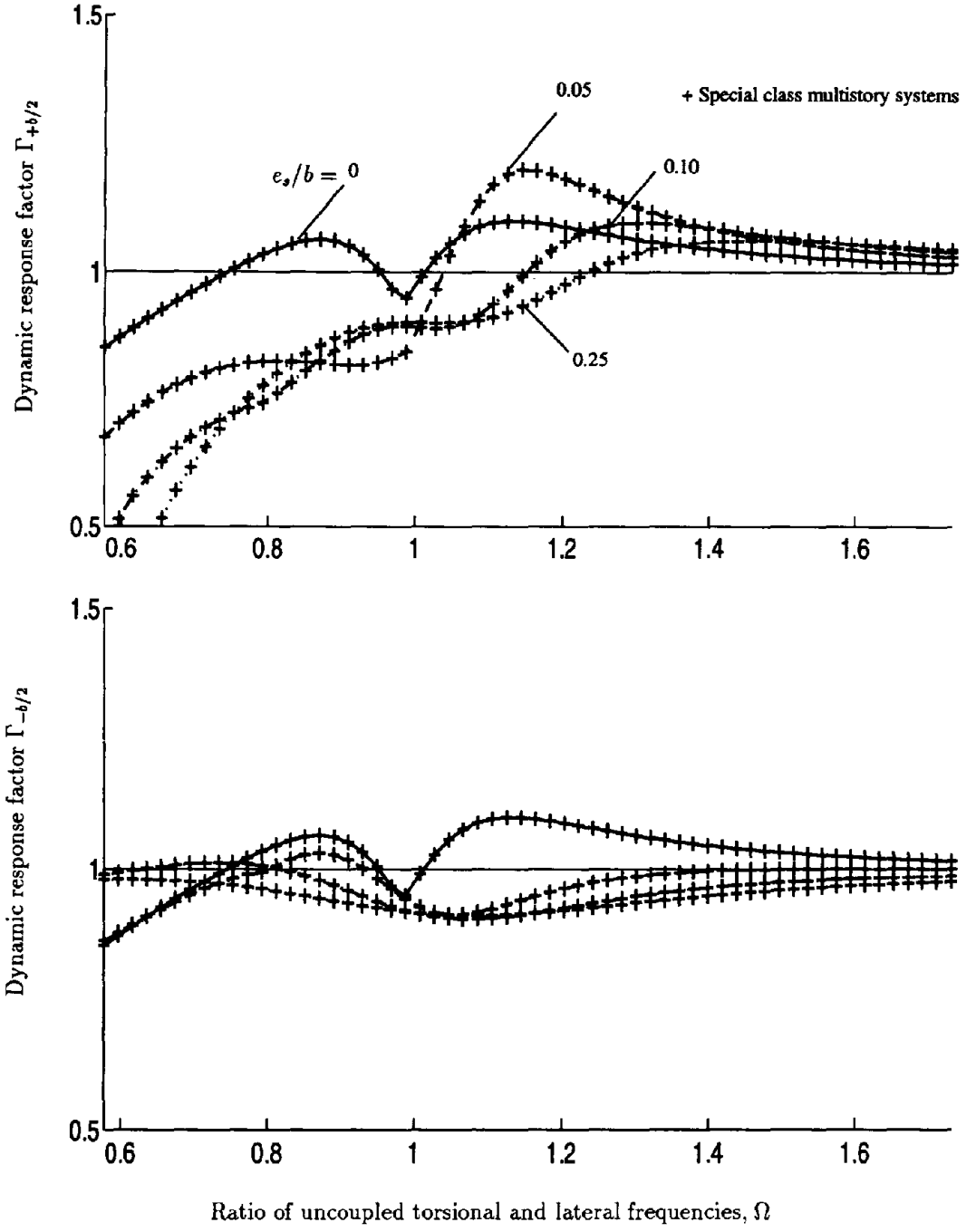

Figure 10: Dynamic response factor $\Gamma_{\pm b/2}$ as a function of Ω for single and the special class of multistory buildings considered, four values of static eccentricity $e_s/b = 0, 0.05, 0.1$, and 0.25, $e_a/b = 0.05$, $T_y = 1$ sec, and $a/b = 1$

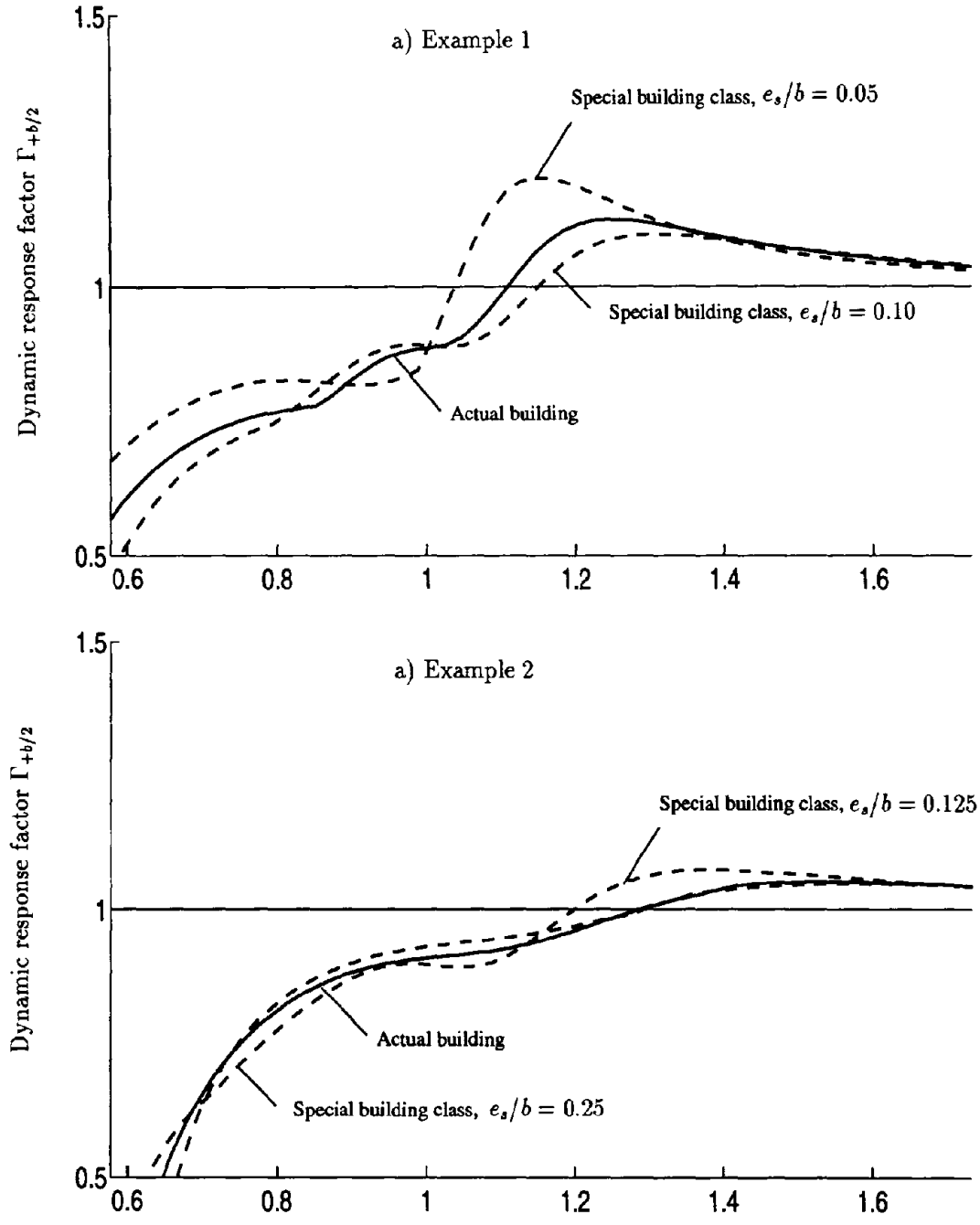

Figure 11: Comparison between the dynamic response factor $\Gamma_{+b/2}$ corresponding to five-story buildings with non-uniform story static eccentricities and the same response obtained for the special class multistory systems as a function of Ω, $e_s/b = 0.05$, $T_y = 1$ sec, and $a/b = 1$

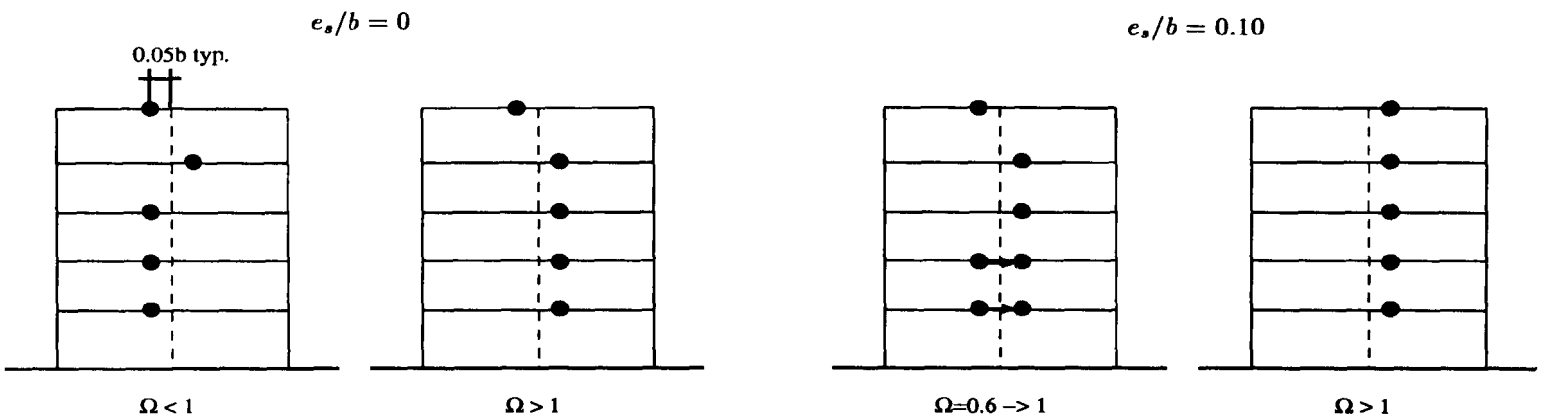

a) Stiff edge

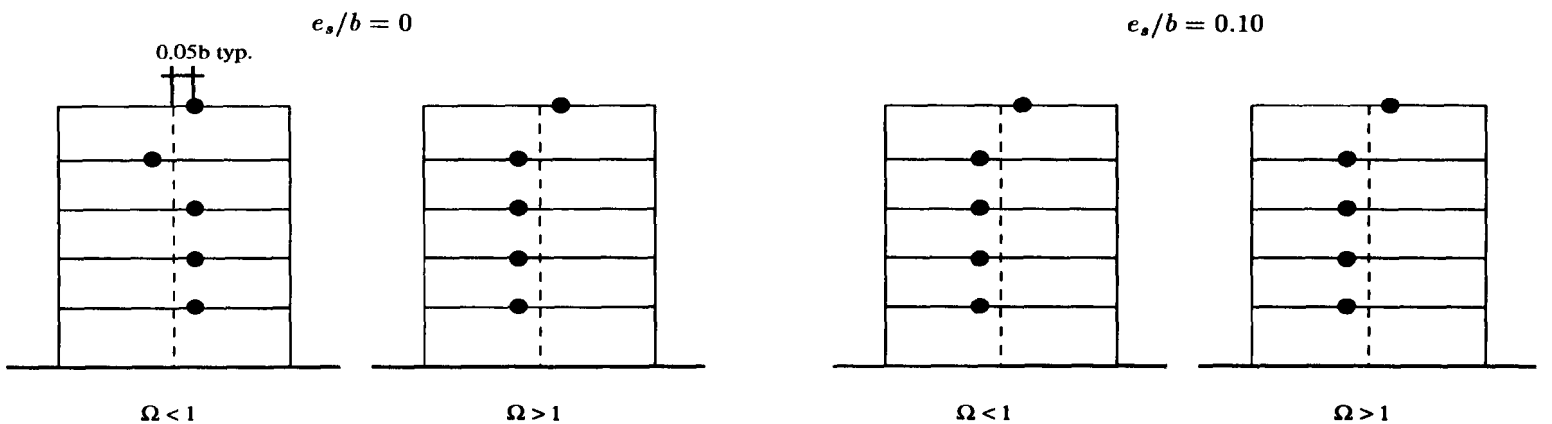

b) Flexible edge

Figure 12: Combination of story accidental eccentricities e_{aj}/b leading to the maximum normalized dynamic response $(\hat{u}_{\pm b/2})_d$, for systems with static eccentricity $e_s/b = 0$ and 0.1, $T_y = 1$ sec, and $a/b = 1$

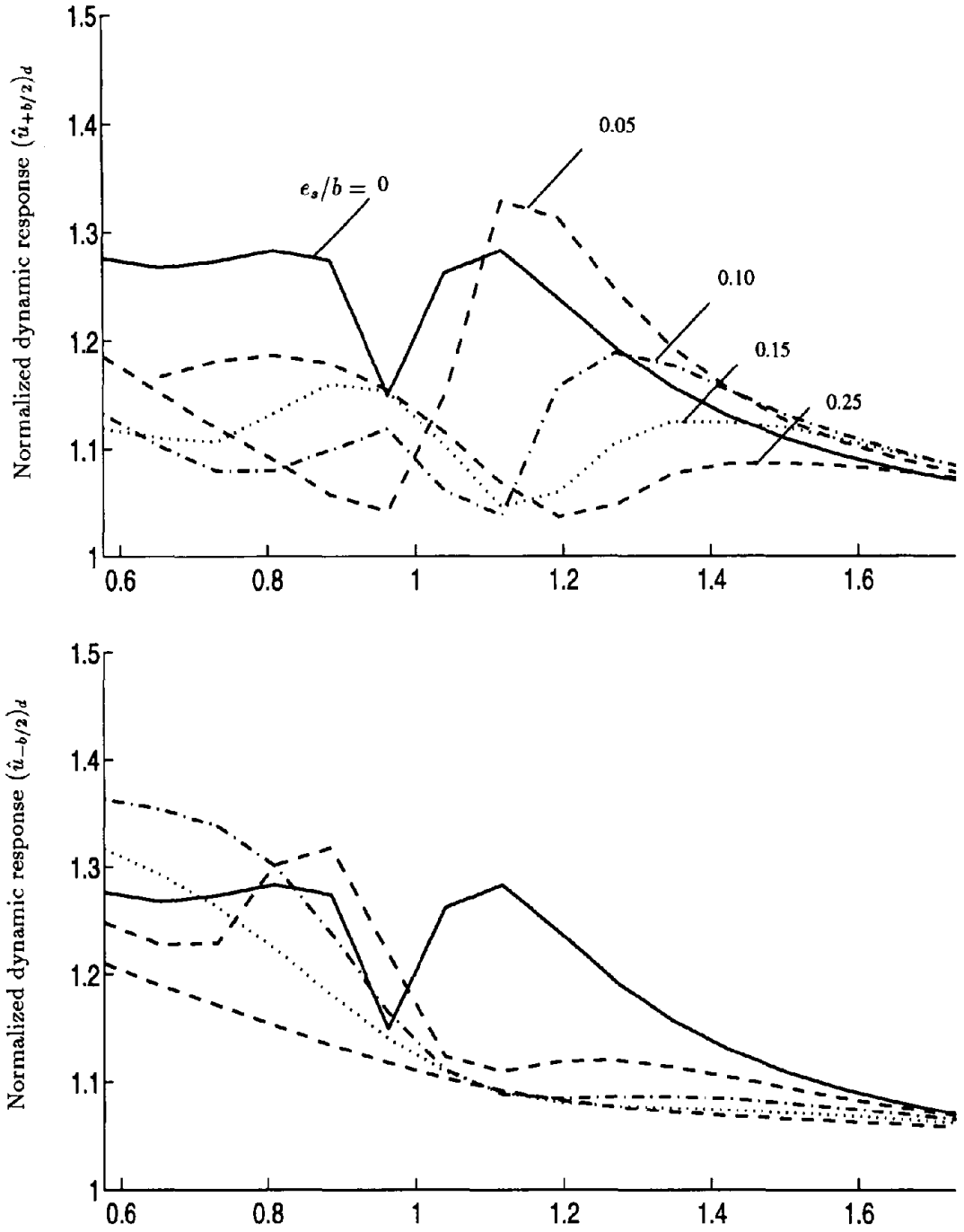

Figure 13: Maximum values of the normalized dynamic response $(\hat{u}_{\pm b/2})_d$ as a function of Ω, five values of static eccentricity $e_s/b = 0, 0.05, 0.1, 0.15$ and 0.25, $0.05 \leq e_{aj}/b \leq 0.05$, $T_y = 1$ sec, and $a/b = 1$

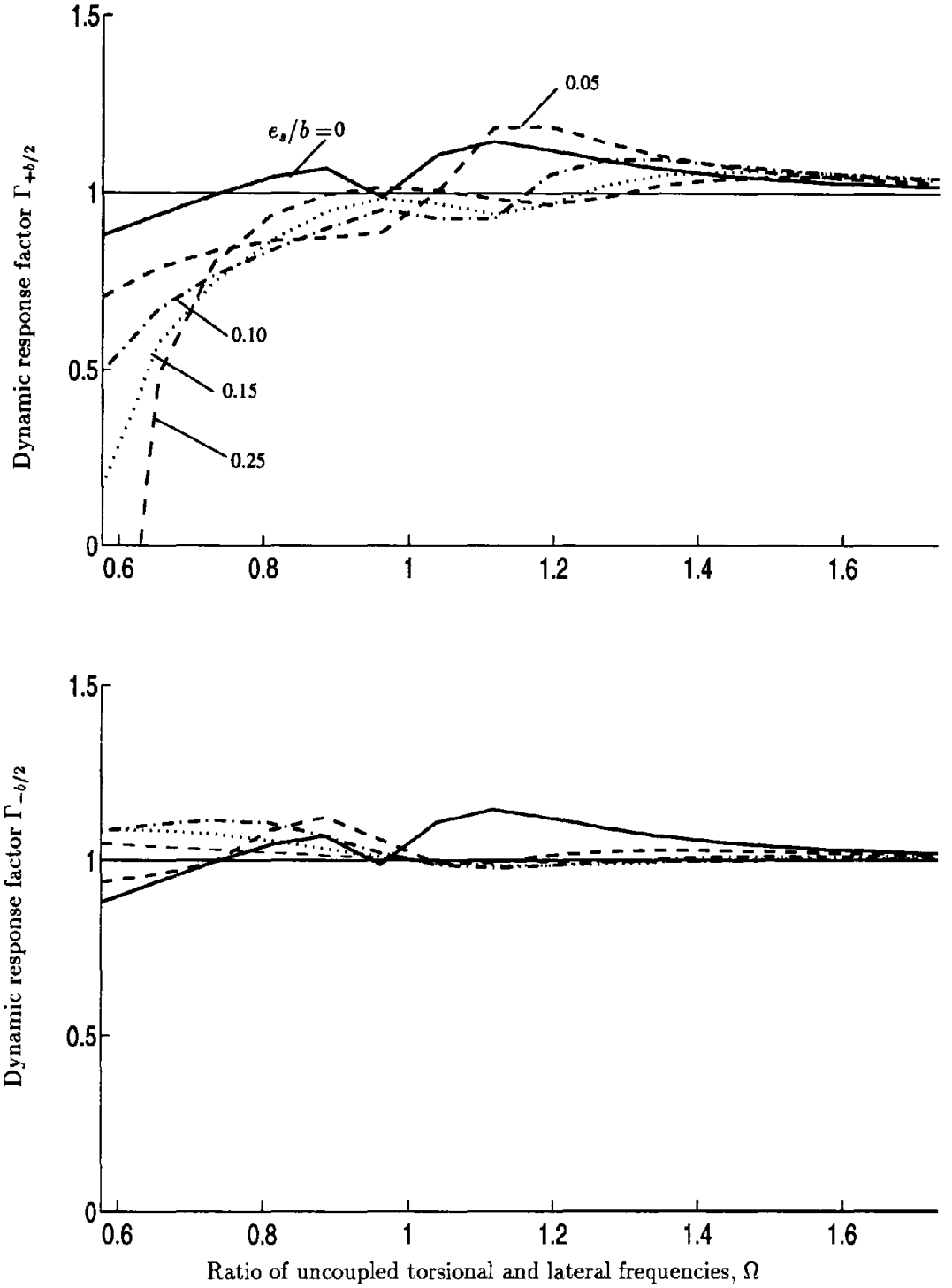

Figure 14: Maximum values of the dynamic response factor $\Gamma_{\pm b/2}$ as a function of Ω, five values of static eccentricity $e_s/b = 0, 0.05, 0.1, 0.15$ and 0.25, $0.05 \leq e_{aj}/b \leq 0.05$, $T_y = 1$ sec, and $a/b = 1$

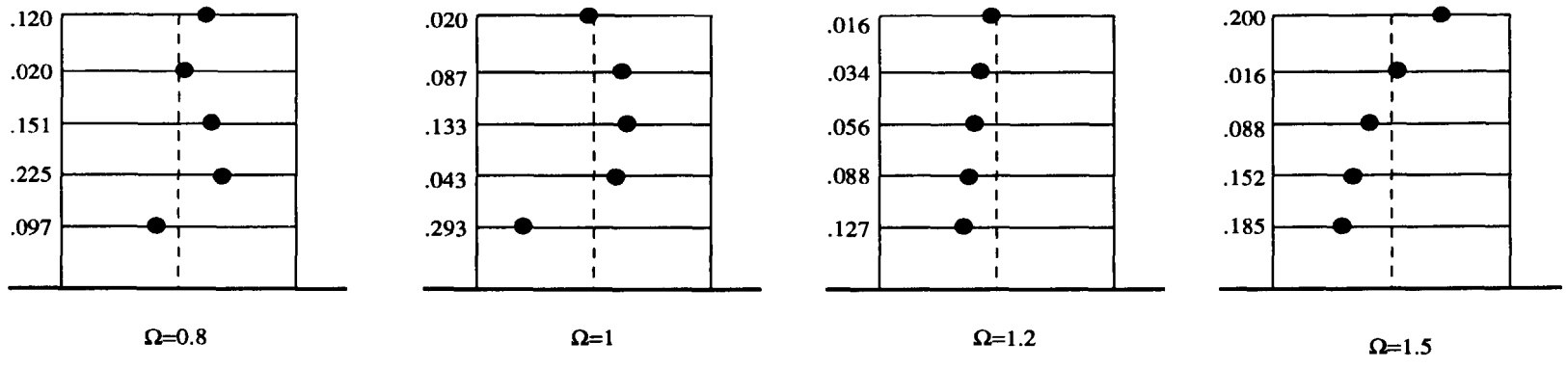

Figure 15: Combination of story eccentricities leading to the maximum dynamic response factor $\Gamma_{-b/2}$, for systems with story static eccentricities $-0.25 \leq e_{sj}/b \leq 0.25$ and accidental eccentricities $0.05 \leq e_{aj}/b \leq 0.05$, $T_y = 1$ sec, and $a/b = 1$

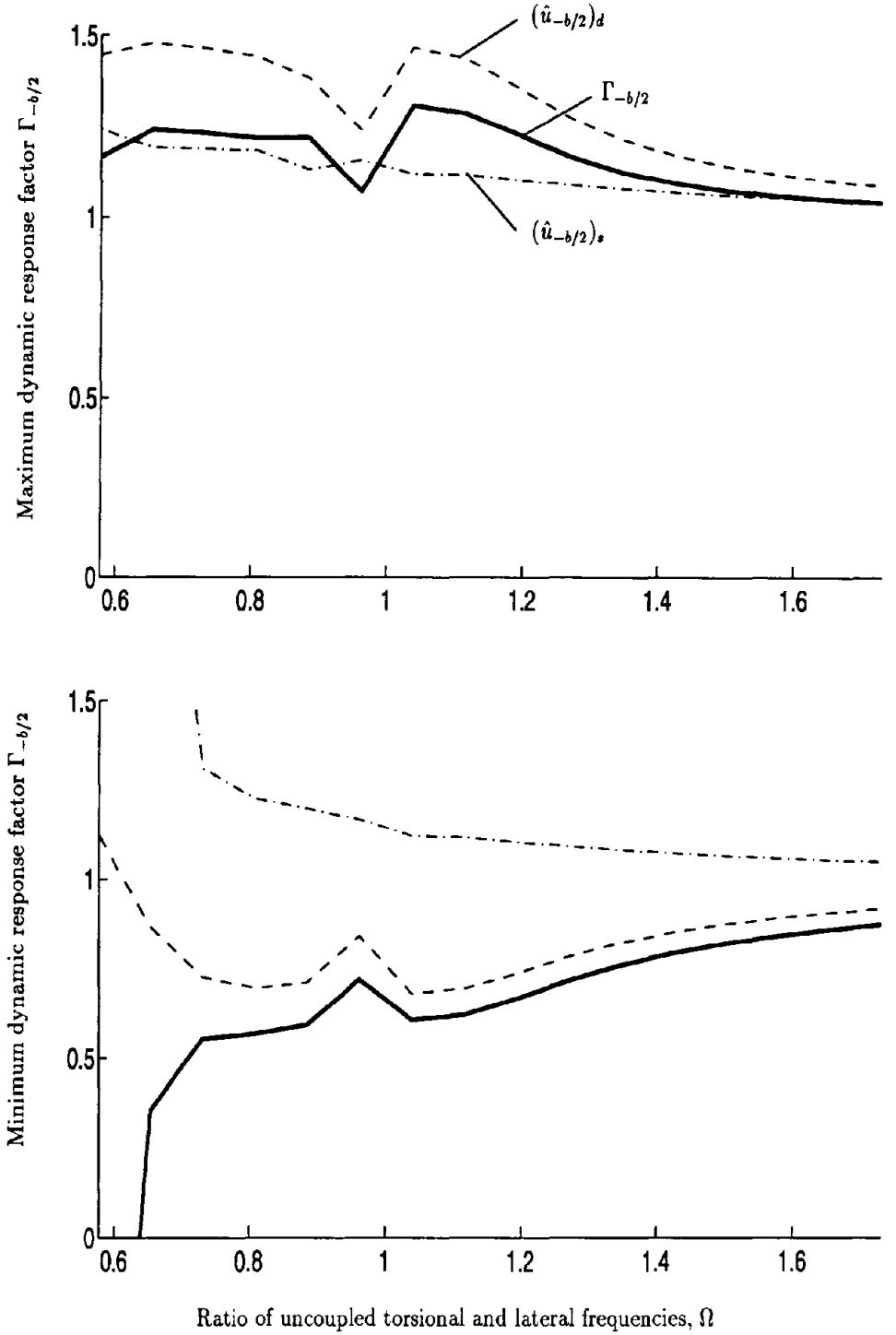

Figure 16: Maximum values of the dynamic response factor $\Gamma_{\pm b/2}$ and normalized responses $(\hat{u}_{-b/2})_s$ and $(\hat{u}_{-b/2})_d$ as a function of Ω, for systems with story static eccentricities $-0.25 \leq e_{sj}/b \leq 0.25$ and accidental eccentricities $-0.05 \leq e_{aj}/b \leq 0.05$, $T_y = 1$ sec, and $a/b = 1$

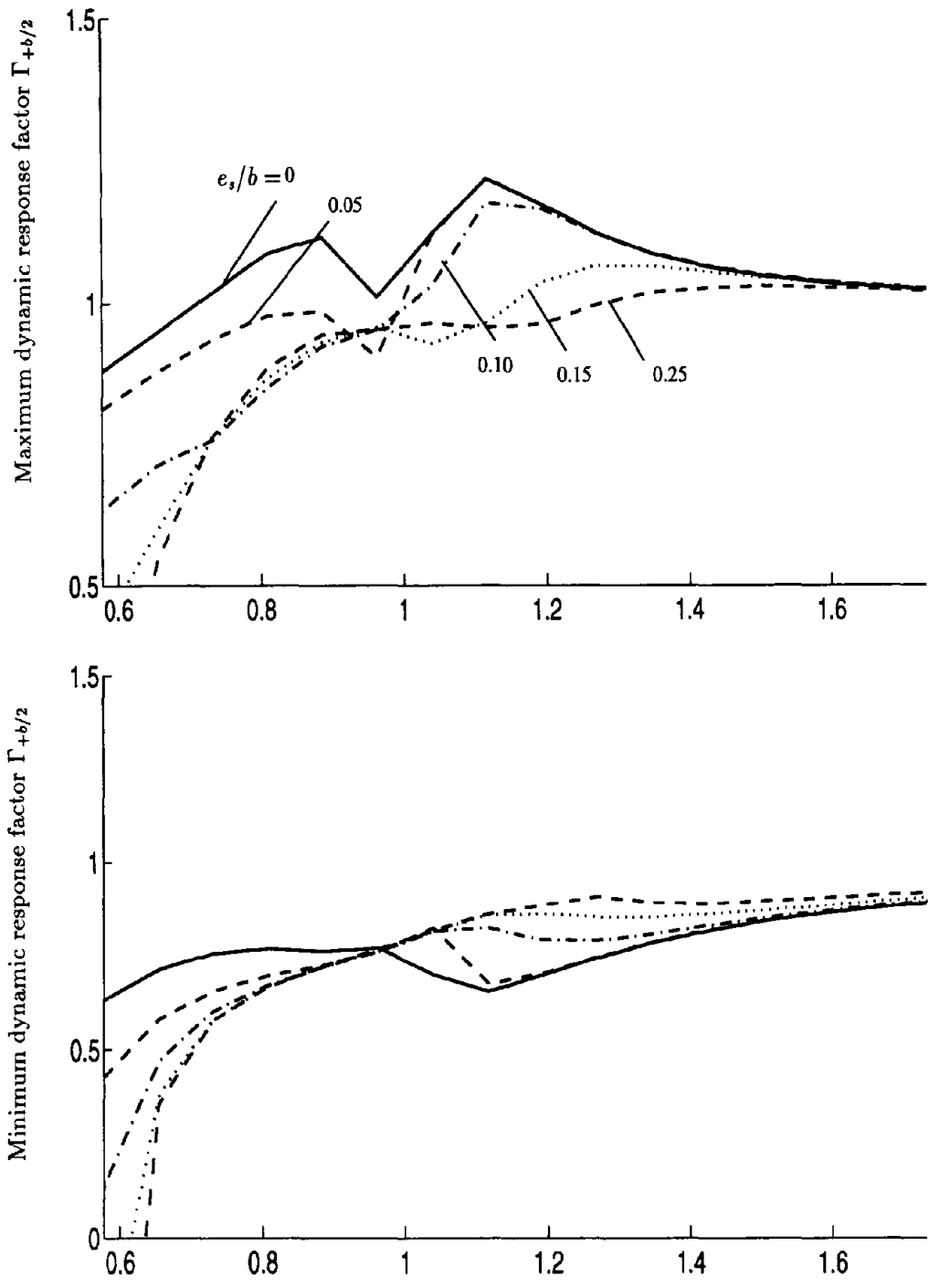

Figure 17: Maximum and minimum values of the dynamic response factor $\Gamma_{+b/2}$ as a function of Ω for systems with narrower bounds in the story static eccentricities, $T_y = 1$ sec, and $a/b = 1$

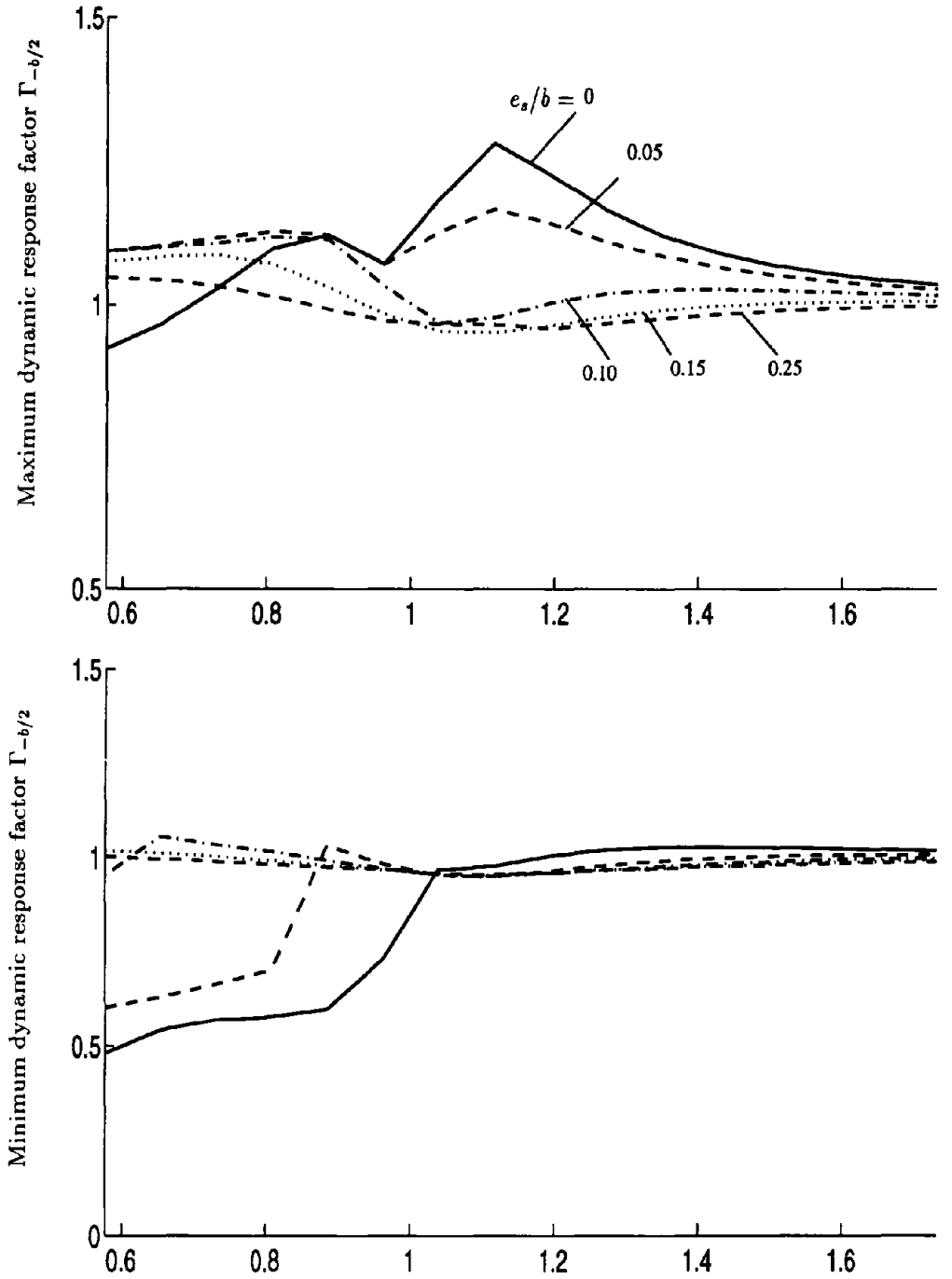

Figure 18: Maximum and minimum values of the dynamic response factor $\Gamma_{-b/2}$ as a function of Ω for systems with narrower bounds in the story static eccentricities, $T_y = 1$ sec, and $a/b = 1$

APPENDIX A: Static and dynamic response of torsionally-coupled multistory buildings belonging to the special class

This appendix describes important properties of the static and dynamic response of asymmetric buildings belonging to the special class.

Static Response

The static response of torsionally-coupled multistory buildings belonging to the special class described earlier is studied next.

Consider the static response of a N-story system subjected to equivalent static forces $\boldsymbol{f}^T = [\boldsymbol{f}_y^T \;\; \boldsymbol{f}_\theta^T]$, i.e.

$$\begin{bmatrix} \boldsymbol{K}_y & \boldsymbol{K}_y(e/r) \\ \boldsymbol{K}_y(e/r) & [(e/r)^2 + C_{\theta R}/(r^2 C_y)]\boldsymbol{K}_y \end{bmatrix} \begin{Bmatrix} \boldsymbol{u}_y \\ r\boldsymbol{u}_\theta \end{Bmatrix} = \begin{Bmatrix} \boldsymbol{f}_y \\ \boldsymbol{f}_\theta \end{Bmatrix} \tag{21}$$

where all sub-matrices and parameters were defined earlier for Eq. (9). For the case of static analysis considering accidental eccentricity, the static force $\boldsymbol{f}_\theta$ can be written

$$\boldsymbol{f}_\theta = -[(\alpha - 1)e_s/r + \beta b/r] \;\; \boldsymbol{f}_y \quad \text{or} \quad \boldsymbol{f}_\theta = [(1 - \delta)\mathrm{e_s/r} + \beta \mathrm{b/r}] \;\; \boldsymbol{f}_\mathrm{y} \tag{22}$$

where α, δ and β were defined earlier for Eq. (1). The first equation is used in general for the elements at the flexible side of the building and the second for the elements at the stiff side. In both cases, the static force $\boldsymbol{f}_\theta$ is proportional to $\boldsymbol{f}_y$, say, $\lambda_f^* \boldsymbol{f}_y$ and $\lambda_s^* \boldsymbol{f}_y$, respectively, where $\lambda_f^* = -[(\alpha - 1)e_s/r + \beta b/r]$ and $\lambda_s^* = [(1 - \delta)e_s/r + \beta b/r]$. For analysis of the building without accidental eccentricity, the static force $\boldsymbol{f}_\theta$ is written as $\lambda_{f,s}\boldsymbol{f}_y$ —$\lambda_{f,s}$ is short notation for λ_f or λ_s, where $\lambda_f = (1 - \alpha)e_s/r$ and $\lambda_s = (1 - \delta)e_s/r$.

In principle, to compute the static displacements $[\boldsymbol{u}_y \;\; \boldsymbol{u}_\theta]$ we need to solve the $2N^{th}$-order system of linear equations given by Eq. (21). However, for the special class of systems considered one can easily show, using simple block manipulation of matrices, that the inverse of the stiffness matrix is given by

$$\boldsymbol{K}^{-1} = 1/\Omega^2 \begin{bmatrix} [\Omega^2 + (e/r)^2]\boldsymbol{K}_y^{-1} & -e/r\boldsymbol{K}_y^{-1} \\ -e/r\boldsymbol{K}_y^{-1} & \boldsymbol{K}_y^{-1} \end{bmatrix} \tag{23}$$

where $\Omega = \sqrt{C_{\theta R}/(r^2 C_y)}$ is the frequency ratio of the system. Equation (23) is by itself a quite useful result, since it allows direct calculation of the static response of any multistory system belonging to the special class.

Consider the following static analysis cases: (1) a building with equivalent static forces $\boldsymbol{f}^T = [\boldsymbol{f}_y^T \;\; \lambda_{f,s}\boldsymbol{f}_y^T]$ and no accidental eccentricity, and (2) the same building considering accidental eccentricity, i.e., $\boldsymbol{f}^T = [\boldsymbol{f}_y^T \;\; \lambda_{f,s}^*\boldsymbol{f}_y^T]$.

The static displacements corresponding to the first analysis case, computed by the product of $\boldsymbol{K}_y^{-1}$ and $\boldsymbol{f}$ are given by

$$\begin{bmatrix} \boldsymbol{u}_y \\ r\boldsymbol{u}_\theta \end{bmatrix} = \begin{bmatrix} \frac{\Omega^2+(e/r)^2-e/r\lambda_{f,s}}{\Omega^2} \;\; \boldsymbol{K}_y^{-1}\boldsymbol{f}_y \\ \frac{-e/r+\lambda_{f,s}}{\Omega^2} \;\; \boldsymbol{K}_y^{-1}\boldsymbol{f}_y \end{bmatrix} \tag{24}$$

Similarly, the static displacement corresponding to the second analysis case are

$$\begin{bmatrix} \boldsymbol{u}_y^* \\ r\boldsymbol{u}_\theta^* \end{bmatrix} = \begin{bmatrix} \frac{\Omega^2+(e/r)^2-e/r\lambda_{f,s}^*}{\Omega^2} \;\; \boldsymbol{K}_y^{-1}\boldsymbol{f}_y \\ \frac{-e/r+\lambda_{f,s}^*}{\Omega^2} \;\; \boldsymbol{K}_y^{-1}\boldsymbol{f}_y \end{bmatrix} \tag{25}$$

Once the static displacements $\boldsymbol{u}_y$ and $\boldsymbol{u}_\theta$ are known, any other static response of the system, say r_s, can be computed in the building as a linear combination of these two displacements, i.e.

$$r_s = \boldsymbol{l}^T\boldsymbol{u} = [\boldsymbol{l}_y \;\; \boldsymbol{l}_\theta] \begin{bmatrix} \boldsymbol{K}_y^{-1}\boldsymbol{f}_y & 0 \\ 0 & \boldsymbol{K}_y^{-1}\boldsymbol{f}_y \end{bmatrix} \begin{bmatrix} \frac{\Omega^2+(e/r)^2-e/r\lambda_{f,s}^*}{\Omega^2} \\ \frac{-e/r+\lambda_{f,s}^*}{\Omega^2} \end{bmatrix} \tag{26}$$

where $\boldsymbol{l} = [\boldsymbol{l}_y \;\; \boldsymbol{l}_\theta]$ is a vector containing the coefficients of the linear combination. Note that the static response r_s can be generally interpreted as the product of two responses

$$r_s = \bar{r}\, r_o \tag{27}$$

where r_o represents the static response of the torsionally-uncoupled multistory system for equivalent static forces $\boldsymbol{f}_y$, and $\bar{r}$ is the response of the torsionally-coupled single-story system normalized by the response of a torsionally-uncoupled single-story system, a system with coincident CM and CS, but all other properties identical to the coupled single-story system.

As an example to verify Eq. (27), consider for instance the edge displacement at the roof of an N-story building. The vectors $\boldsymbol{l}_y$ and $\boldsymbol{l}_\theta$ are for this case $[0 \ldots 0 \; 1]$ and $[0 \ldots 0 \; b/(2r)]$, respectively. Replacing these vectors in Eq. (26) we obtain the edge displacement at the roof

$$\underbrace{(u_{b/2})_s}_{r_s} = \underbrace{1\frac{\Omega^2+(e/r)^2-e/r\lambda_{f,s}^*}{\Omega^2} + b/(2r)\,\frac{-e/r+\lambda_{f,s}^*}{\Omega^2}}_{\bar{r}} \underbrace{\boldsymbol{l}_y\boldsymbol{K}_y^{-1}\boldsymbol{f}_y}_{r_o} \tag{28}$$

The first term in the right hand side is the edge displacement of the torsionally-coupled single-story system, normalized with respect to the lateral displacement $1/K_y$ of a single-story symmetric

system. The second term is the lateral displacement of the torsionally-uncoupled multistory system at the CM, which is identical to the edge displacement in this case. It is apparent that Eq. (28) preserves the structure of the more general Eq. (27).

Although shown above for the particular case of the roof edge displacement, Eq. (27) holds for any response quantity in the building, provided the responses in the single-story torsionally-coupled and multistory uncoupled system are interpreted carefully.

Dynamic Response

The dynamic response of multistory systems belonging to the special class presented earlier is studied next.

The undamped equations of motion of the system (Eq. (9)) can be written

$$\begin{bmatrix} \boldsymbol{m} & 0 \\ 0 & \boldsymbol{m} \end{bmatrix} \begin{Bmatrix} \ddot{\boldsymbol{u}}_y \\ r\ddot{\boldsymbol{u}}_\theta \end{Bmatrix} + \begin{bmatrix} \boldsymbol{I} & (\frac{e}{r})\boldsymbol{I} \\ (\frac{e}{r})\boldsymbol{I}_y & [\Omega^2 + (\frac{e}{r})^2]\boldsymbol{I} \end{bmatrix} \begin{bmatrix} \boldsymbol{K}_y & 0 \\ 0 & \boldsymbol{K}_y \end{bmatrix} \begin{Bmatrix} \boldsymbol{u}_y \\ r\boldsymbol{u}_\theta \end{Bmatrix} = - \begin{Bmatrix} \boldsymbol{m}\,\mathbf{1} \\ \mathbf{o} \end{Bmatrix} a_{gy} \quad (29)$$

where all matrices and parameters were defined earlier for Eq. (9). Consider first the coordinate transformation

$$\begin{bmatrix} \boldsymbol{u}_y \\ r\boldsymbol{u}_\theta \end{bmatrix} = \begin{bmatrix} \boldsymbol{\Psi} & \mathbf{o} \\ \mathbf{o} & \boldsymbol{\Psi} \end{bmatrix} \begin{bmatrix} \boldsymbol{\zeta}_y \\ \boldsymbol{\zeta}_\theta \end{bmatrix} \quad (30)$$

such that $\boldsymbol{\Psi}$ diagonalizes the pair $(\boldsymbol{m}, \boldsymbol{K}_y)$. Introducing this transformation in Eq. (29) and pre-multiplying this equation, first, by the transpose of the transformation matrix, and then by the inverse of the resulting diagonal mass matrix in the new coordinates leads to

$$\begin{bmatrix} \boldsymbol{I} & \mathbf{o} \\ \mathbf{o} & \boldsymbol{I} \end{bmatrix} \ddot{\boldsymbol{\zeta}} + \begin{bmatrix} \boldsymbol{\Lambda} & (e/r)\boldsymbol{\Lambda} \\ (e/r)\boldsymbol{\Lambda} & [\Omega^2 + (e/r)^2]\boldsymbol{\Lambda} \end{bmatrix} \boldsymbol{\zeta} = \begin{bmatrix} -\boldsymbol{\Psi}^T \boldsymbol{m}\mathbf{1}./diag(\boldsymbol{\Psi}^T \boldsymbol{m} \boldsymbol{\Psi}) \\ \mathbf{o} \end{bmatrix} a_{gy}(t) \quad (31)$$

where $\boldsymbol{\Lambda}$ is a diagonal matrix with non-zero entries equal to ω_{yj}^2, $j = 1, \ldots, N$, the square of the vibration frequencies of the torsionally-uncoupled N-story system; and the symbol './' implies term-wise division of two vectors.

An easier interpretation of Eq. (31) can be achieved by introducing a new change in coordinates, this time represented by a permutation matrix $\boldsymbol{P}$, which reorders the degrees of freedom of the system such that the lateral displacement u_y and rotation of the floor plan u_θ at floor j are sequential; as opposed to the initial ordering in which the lateral displacements u_y for all floors come first and then their floor rotations. Such a permutation matrix is constructed as the product of N simple permutation matrices $\boldsymbol{P}_{ij}$ that interchange rows and columns i and j. Therefore,

introducing the coordinate transformation

$$\boldsymbol{\zeta} = \boldsymbol{P}\ \boldsymbol{\eta} \tag{32}$$

into Eq. (31) and pre-multiplying by $\boldsymbol{P}^T$ leads to a set of N two-by-two blocks of equations of motions that are uncoupled from each other of the form

$$\ddot{\eta}_n + \omega_{yj}^2 \begin{bmatrix} 1 & e/r \\ e/r & \Omega^2 + (e/r)^2 \end{bmatrix} \eta_n = \begin{bmatrix} -\psi_j^T m \mathbf{1} / \psi_j^T m \psi_j \\ 0 \end{bmatrix} a_{gy}(t) \tag{33}$$

for $n = 1, 2$ and $j = 1, \ldots, N$, where the eigenvector ψ_j represents the j^{th} column of the matrix Ψ. Note that Eq. (33) is identical to Eq. (3), i.e., the governing equation of motion of a torsionally-coupled single-story system with uncoupled lateral vibration frequency ω_{yj}, frequency ratio Ω, and static eccentricity e. This system is the so-called corresponding torsionally-coupled single story system.

Clearly, since the complete system of equations is block diagonal its set of eigenvalues and eigenvectors is computed from the union of the two eigenvalues and eigenvectors for each independent block. The eigenvalues of the two-by-two block presented in Eq. (33) can be written as

$$\omega_{nj} = \bar{\omega}_n \omega_{yj} \tag{34}$$

for $n = 1, 2$ and $j = 1, \ldots, N$, where ω_{yj} are the vibration frequencies of the torsionally-uncoupled N-story system; and $\bar{\omega}_n$ are the normalized vibration frequencies of the torsionally-coupled single-story system. Further, the nj^{th} eigenvector in η-coordinates, $\boldsymbol{\chi}_{nj}$, is

$$\boldsymbol{\chi}_{nj}^T = [0\ \ldots\ \alpha_{yn}\ \alpha_{\theta n}\ 0 \ldots 0] \tag{35}$$

where $\boldsymbol{\alpha}_n^T = [\alpha_{yn} \quad \alpha_{\theta n}]$, $n = 1, 2$ are the vibration modes of the torsionally-coupled single-story system. Transforming this eigenvector in η-coordinates back to original u_y and u_θ physical coordinates, using the inverse transformations that led to equation (33), one can show that the nj^{th} eigenvector $\boldsymbol{\phi}_{nj}$ in original coordinates is

$$\boldsymbol{\phi}_{nj}^T = [\alpha_{yn} \boldsymbol{\psi}_j^T \ \ \alpha_{\theta n} \boldsymbol{\psi}_j^T] \tag{36}$$

Similarly, the dynamic response of the system described by Eq. (33) can be obtained by first solving this equation in η-coordinates and then returning to physical coordinates. The peak value of the response η in mode $n = 1, 2$ is

$$\eta_n = \alpha_{yn} \Gamma_j S_{anj} / \omega_{nj}^2 \tag{37}$$

where $\Gamma_j = \boldsymbol{\psi}_j^T \boldsymbol{m}\mathbf{1}/\boldsymbol{\psi}_j^T \boldsymbol{m}\boldsymbol{\psi}_j$; and S_{anj} is the pseudo-acceleration of the system corresponding to its nj^{th} vibration mode. Transforming back to original coordinates leads to the building displacements for the nj^{th} vibration mode

$$\boldsymbol{u}_{nj} = \begin{bmatrix} \boldsymbol{\psi}_j \alpha_{yn}^2 \Gamma_j S_{anj}/\omega_{nj}^2 \\ \boldsymbol{\psi}_j \alpha_{yn} \alpha_{\theta n} \Gamma_j S a_{nj}/\omega_{nj}^2 \end{bmatrix} \tag{38}$$

Eq. (38) can be alternatively written in the form

$$\boldsymbol{u}_{nj} = \begin{bmatrix} \overbrace{\alpha_{yn}^2 \frac{S_{anj}}{\bar{\omega}_n^2 S_{aj}}}^{\bar{u}_{ynj}} & \overbrace{\boldsymbol{\psi}_j \Gamma_j S_{aj}/\omega_{yj}^2}^{\boldsymbol{u}_{yj}} \\ \underbrace{\alpha_{yn}\alpha_{\theta n} \frac{S_{anj}}{\bar{\omega}_n^2 S_{aj}}}_{\bar{u}_{\theta nj}} & \underbrace{\boldsymbol{\psi}_j \Gamma_j S_{aj}/\omega_{yj}^2}_{\boldsymbol{u}_{yj}} \end{bmatrix} \tag{39}$$

which shows that the dynamic response of the system in its nj^{th} mode can be expressed as the product of the same response quantity in the j^{th} lateral mode of vibration of the torsionally-uncoupled N-story system and the corresponding normalized response of the torsionally-coupled single-story system. In general this observation can be stated as

$$r_{nj} = \bar{r}_{nj} r_j \tag{40}$$

where r_j is the value of the same response quantity in the corresponding torsionally-uncoupled multistory system in its j^{th} lateral mode of vibration, and $\bar{r}_{nj}$ is the normalized response of the torsionally-coupled single-story system.

Although Eq. (40) holds strictly only for each vibration mode, it is not hard to show [3] that if the earthquake pseudo-acceleration design spectrum is flat or hyperbolic, the combined modal responses using the CQC superposition rule satisfy an equation analogous to this equation.

5. ESTIMATION OF ACCIDENTAL TORSION EFFECTS FOR SEISMIC DESIGN OF BUILDINGS

5.1 Introduction

The results presented in Chapter 4 demonstrate that the increase in design member forces resulting from code dynamic analysis, i.e., by shifting the CM of each floor a distance $e_a = \pm\beta b$ from its nominal position, differ in general from the results obtained using equivalent static forces shifted a distance e_a from the CM on each floor. In many cases, these discrepancies are of the same order as the code-intended increase in design forces due to accidental eccentricity. This implies that the code-specified static and dynamic analysis to account for accidental torsion should be modified to be mutually consistent.

Further, the increase in design forces due to accidental torsion predicted by the static or dynamic analysis procedures mentioned above, almost surely, will never coincide with the 'true' increase in member forces due to all the active sources of accidental torsion in a building during an earthquake. Indeed, until recently, very little was known about the response level that was implicit in the accidental torsion provisions of different seismic codes.

Because of this lack of knowledge Chapters 2 and 3, together with a recent study [1], have focused on trying to estimate the increase in building response due to several sources of accidental torsion: rotational motions of the building foundation, uncertainty in the stiffness of structural elements, uncertainty in the location of the CM, and uncertainty in stiffness and mass distributions of stories other than the one analyzed. So far, the effect of all these sources has been evaluated for elastic behavior of buildings. The results generated in these chapters enable us: (1) to asses the level of response that is implicit in the accidental torsion provisions of different seismic codes, and (2) to formulate modifications to the current code-provisions based on the recently available research results. Such modifications are presented in this chapter as a new procedure for incorporating the effects of accidental torsion in building analysis.

5.2 New analysis procedure for accidental torsion

This section describes the steps required for implementing a new analysis procedure for accidental torsion. Later sections will develop in detail each of the analysis steps summarized next:

1. Determine the ratio Ω between the fundamental frequencies of uncoupled torsional and lateral motions of the building.

2. Obtain the increase in displacements at the edge of the building resulting from all sources of accidental torsion; this increase is a function of Ω and the ratio b/r between the plan dimension orthogonal to the direction of ground motion and the radius of gyration of the building plan.

3. Compute, the increase in displacements due to accidental torsion at the locations of all interior resisting planes; each resisting plane may include frames, walls, and other structural elements.

4. Compute the forces in the structural members of each resisting plane by amplifying the forces corresponding to the system with no accidental torsion by the factors determined in steps 2 and 3.

5.3 Ratio of uncoupled vibration frequencies of a building, Ω

Among the system parameters that influence the torsional response of a building, perhaps the most significant is the ratio between its fundamental frequencies of uncoupled torsional and lateral vibration. A practical way of computing this frequency ratio is presented in this section.

The uncoupled frequency ratio Ω is defined herein as the ratio between ω_θ and ω_y (or ω_x), the fundamental torsional and lateral frequencies of a hypothetical symmetric-plan building defined by lateral and torsional stiffness matrices $\boldsymbol{K}_y$ (or $\boldsymbol{K}_x$) and $\boldsymbol{K}_\theta$, equal to those of the actual building. Although ω_θ and ω_y can be computed by using standard solution procedures for eigenvalue problems, they can be estimated to sufficient accuracy by Rayleigh's method.

Before using Rayleigh's method we need to guess a shape for the first lateral and torsional vibration modes. One alternative to estimate these two modes is to compute the static displacements corresponding to the following two systems, respectively: (1) symmetric-plan system with lateral stiffness matrix $\boldsymbol{K}_y$ (or $\boldsymbol{K}_x$ and any reasonable heightwise distribution of equivalent static forces F_i , $i = 1, \ldots, N$, such as the one specified by seismic codes, and (2) a symmetric-plan system with torsional stiffness matrix $\boldsymbol{K}_\theta$ subjected to any reasonable heightwise distribution of story torques T_i , $i = 1, \ldots, N$, such as $F_i e$, $i = 1, \ldots, N$, where e is an arbitrary eccentricity value (for instance, $e = \beta b$), and F_i are the forces used in obtaining the lateral vibration mode. If the resulting lateral displacements of the first system are denoted as δ_i , $i = 1, \ldots, N$ and the rotations in the second

system as θ_i , $i = 1, \ldots, N$, the uncoupled lateral and torsional frequencies of the system are:

$$\omega_y \simeq \sqrt{\frac{\sum_i F_i \delta_i}{\sum_i m_i \delta_i^2}} \qquad \omega_\theta \simeq \sqrt{\frac{\sum_i T_i \theta_i}{\sum_i I_{pi} \theta_i^2}} \tag{1}$$

The expression for ω_y is identical to the expression given in the UBC and other seismic codes, and a simple generalization gives the equation for ω_θ. Once ω_y and ω_θ are computed, the uncoupled frequency ratio $\Omega = \omega_\theta / \omega_y$ can be estimated. Numerical studies have shown that the resulting value of Ω is more accurate than ω_y and ω_θ individually, because the errors present in the computation of these frequencies tend to cancel when their ratio is determined. Note that for the computation of Ω one requires only the mass of each floor and the lateral stiffness of each resisting plane.

A large value of Ω for a building implies that the building is torsionally stiff with resisting elements near the perimeter of the building plan. On the other hand, a small value of Ω indicates a torsionally flexible building with a stiff central core but flexible perimeter. It has become customary to draw the line between flexible and stiff torsional systems at $\Omega = 1$. For most buildings Ω ranges between 0.8 and 1.5.

5.4 Increase in building response due to accidental torsion

The most important step in the new analysis procedure is to estimate the increase in building response that results from all sources of accidental torsion. In what follows, we define the normalized displacement of the building plan at distance x from the CM as the ratio $\hat{u}_x = u_x^* / u_x$ between the displacement u_x^* of the system considering the effect of all sources of accidental torsion and the displacement u_x of the system neglecting accidental torsion. Thus, a value of $\hat{u}_{b/2}$ larger than one implies an increase of $\hat{u}_{b/2} - 1$ in the building edge ($x = b/2$) displacement due to accidental torsion.

5.4.1 Analysis procedure

The increase in building displacements due to individual sources of accidental torsion, such as stiffness and mass uncertainty, base rotational excitation and other less important sources is a function of the system parameters $\boldsymbol{p}$, which are random variables describing the stiffness and mass matrices of the system, and a random base rotational excitation $a_{g\theta}(t)$. It can be shown [1] that a first order approximation for the mean and standard deviation of the normalized displacement is given by

$$\mu_{\hat{u}_{b/2}} = 1 + \mu_{\hat{u}_{g\theta}} \tag{2}$$

and

$$\sigma_{\hat{u}_{b/2}} = \sqrt{\sum_{i=1}^{Np} (\frac{\partial \hat{u}_{b/2}}{\partial p_i})^2 \, \sigma_{p_i}^2 \; + \; \sigma_{\hat{u}_{g\theta}}^2} \tag{3}$$

where $\mu_{(\cdot)}$ and $\sigma_{(\cdot)}$ denote the mean and standard deviation of $(\cdot)$; $\mu_{\hat{u}_{g\theta}}$ and $\sigma_{\hat{u}_{g\theta}}$ are the mean and standard deviation of $\hat{u}_{b/2}$ resulting from base rotational excitation; N_p is the number of system parameters; σ_{p_i} is the standard deviation of the parameter p_i; and $\frac{\partial \hat{u}_{b/2}}{\partial p_i}$ is the sensitivity of $\hat{u}_{b/2}$ with respect to parameter p_i. Equations (2) and (3) could also be extended to consider other response quantities by substituting the desired normalized response for $\hat{u}_{b/2}$.

5.4.2 Summary of results

This section summarizes briefly the most relevant results and ideas obtained in Chapters 2 and 3, as well as some of the results presented in [1]. These studies considered the increase in building response due to the following sources of accidental torsion: (1) rotational motions of the building foundation, (2) uncertainty in the stiffness of structural elements in both principal directions of analysis, (3) uncertainty in the location of the CM, and (4) uncertainty in stiffness and mass distributions in stories of a building other than the one analyzed. Where it applies, mean-plus-one standard deviation values for the normalized edge displacements $\hat{u}_{b/2}$ are discussed. The observations presented are, however, not tied to these results and apply to other levels of response as well.

1. The largest increase in building displacements results from uncertainty in the location of the CM orthogonal to the direction of ground motion (Fig. 1a). Somewhat smaller are the effects of uncertainty in the stiffness of structural elements in the direction of ground motion (Fig. 1b). It can be shown, that these two sources combined account for over 70% of the total increase in response due to accidental torsion [1].

2. Stiffness uncertainty and uncertainty in the location of the CM can be modeled as a perturbation of the static eccentricity of the system. This observation combined with the previous one are important because they partially justify the dynamic analysis procedure for accidental torsion specified in most seismic codes, in which accidental torsion of the system due to all sources is modeled exclusively as a shift of the CM of the building from its nominal position.

3. The increase in edge displacements due to base rotational motion has been derived from 'true' base rotations of thirty buildings during recent California earthquakes [3]. This increase is

generally less than 8% for systems with uncoupled lateral vibration period T_y over, say, 1/2 sec and a wide range of Ω (Fig. 1c); it may reach values as large as 40% for short period systems ($T_y < 1/2$ sec) that are torsionally flexible ($\Omega < 2/3$).

4. The increase in edge displacement resulting from uncertainty in the stiffness of structural elements in the direction orthogonal to the direction of ground motion and in the location of the CM along the direction of ground motion are in general less than 5% (Fig. 1d) [1]. Indeed, this increase is zero for nominally-symmetric systems and increases with increasing stiffness eccentricity in the system.

5. The increase in edge displacements due to uncertainty in the stiffness and mass distributions in stories other than the one analyzed (Fig. 1e) is between one-third to one-half of the increase due to the uncertainty is these properties in the story considered (Fig. 1b) [1].

6. Most sources of accidental torsion increase the response of nominally symmetric systems more than they do for unsymmetric systems (Chapter 2). This observation applies to buildings that are unsymmetric in one or both directions [1].

7. The increase in edge displacements due to stiffness and mass uncertainty is essentially insensitive to changes in the value of the uncoupled lateral vibration period T_y of the building (Chapter 2). For this reason only a single uncoupled vibration period $T_y = 1$ sec will be considered here.

8. Buildings with the plan dimension perpendicular to the direction of ground motion much larger than the other dimension (large b/r) show the largest increase in response due to accidental torsion (see Fig. 7a later).

9. The increase in response of single story systems due to accidental torsion is also the exact result for a special class of multistory systems defined elsewhere [2,3,4] and later in this paper. A corollary of this observation is that the normalized response at a specified location in the building plan is identical for all stories. In fact, this observation also carries over approximately to general multistory buildings. Moreover, it implies, as shown later, that the same normalized response $\hat{u}_{b/2}$ also applies to other global or local response quantities of a resisting plane located at the building edge, such as story drifts, base shear, or forces in the structural elements.

Shown in Fig. 2 are the mean and mean-plus-one standard deviation of $\hat{u}_{b/2}$ resulting from all sources of accidental torsion considered. These results have been computed using Eqs. (3) and (4), the sensitivities $\partial\hat{u}_{b/2}/\partial p_i$ of the edge displacement with respect to each of the system parameters, and the mean and standard deviation of $\hat{u}_{b/2}$ due to each of the sources of accidental torsion. Buildings with uncoupled vibration period of $T_y = 1$ sec, square plans ($b/r = \sqrt{6}$), and constant modal damping ratio of 5% were selected to generate these results. The mean value of the increase in response, $\hat{u}_{b/2} - 1$, which results from building torsion due to base rotational excitation, is usually less than 3%. Furthermore, this mean increase in response seems quite insensitive to the uncoupled frequency ratio of the system Ω. The mean-plus-one standard deviation value of the response increase reaches a peak value of 45% for systems with $\Omega \simeq 0.85$ or $\Omega \simeq 1.1$; it decreases steadily for values of Ω larger and smaller than these two values; and it varies rapidly between its peaks at $\Omega \simeq 0.85$ and 1.1 to a minimum at $\Omega \simeq 1$. As shown in the figure this increase in response is larger for nominally symmetric systems ($e_s/b = 0$) than for unsymmetric systems.

5.4.3 Code increase in response

Let us consider the increase in edge displacements of a single-story system subjected to an equivalent lateral force V in the y-direction and shifted a distance e_a from the CM. The static displacement u_x^* at distance x from the CM produced by the static force V applied at distance $e_a = \beta b$ from the CM is

$$u_x^* = \frac{V}{K_y} - V\frac{(e_s - e_a)(x - e_s)}{K_{\theta s}} \tag{4}$$

where K_y is the lateral stiffness of the system in the y-direction; $K_{\theta s}$ is the torsional stiffness of the system about the CS; and $e_a = \pm\beta b$ is the accidental eccentricity. The corresponding displacement u_x when V is applied at the CM is obtained by letting $e_a = 0$ in Eq. (4) , i.e.

$$u_x = \frac{V}{Ky} - V\frac{e_s(x - e_s)}{K_{\theta s}} \tag{5}$$

The ratio $\hat{u}_x = u_x^*/u_x$ of static displacements is a measure of the increase in response due to accidental eccentricity e_a. After simple algebraic manipulations $\hat{u}_x$ is shown to be

$$\hat{u}_x = \frac{\Omega_s^2 - (b/r)^2(e_s/b - e_a/b)(x/b - e_s/b)}{\Omega_s^2 - e_s/b(b/r)^2(x/b - e_s/b)} \tag{6}$$

where $r = I_p/m$ is the radius of gyration of the building plan; and $\Omega_s^2 = \Omega^2 - (e_s/r)^2$. Equation (7) for $x = \pm b/2$ is plotted in Fig. 3a as a function of Ω for buildings with square plan, i.e., $b/r = \sqrt{6}$.

For both edges, $\hat{u}_{\pm b/2}$ decreases as Ω increases, as it should, since these systems are stiffer in torsion and, thus, less affected by accidental eccentricity.

The normalized displacements at the stiff and flexible edges of the above-described system computed by code-dynamic analysis of the building with the CM shifted $e_a = \pm\beta b$ are presented in Fig. 3b—these results were already presented in Chapter 4 (Fig. 5). It is apparent that the trends of $\hat{u}_x$ predicted by code-static and code-dynamic analysis of the building differ considerably, especially for torsionally flexible buildings, $\Omega < 1$ (Chapter 4). In contrast to code-static analysis, the normalized displacement, and hence the response increase due to accidental torsion predicted by code-dynamic analysis is usually larger for symmetric plan systems; the normalized displacement reaches 1.28 at $\Omega \simeq 0.85$, decreases to a minimum at $\Omega \simeq 1$, increases again to a peak at $\Omega \simeq 1.1$, and decreases steadily with increasing Ω.

Direct comparison between Figs. 2 and 3 shows that the normalized edge displacements determined from code-dynamic analysis have similar trends to those of the 'true' normalized response due to all sources of accidental torsion. However, the code-static analysis procedure for accidental torsion is not consistent with the 'true' increase in response due to accidental torsion and, therefore, it should be modified.

5.4.4 Design considerations

We now compare the normalized edge displacements $\hat{u}_{b/2}$ determined by considering several sources of accidental torsion with the values predicted by the code accidental-torsion provisions. Also, we present results of the 'recorded' increase in response of three nominally symmetric buildings due to accidental torsion computed from recorded earthquake motions in these buildings. Nominally symmetric buildings were chosen because they provide an upper bound for the increase in response due to accidental torsion (Fig. 2).

Compared in Fig. 4 is $\hat{u}_{b/2}$ predicted by code-dynamic analysis (Fig. 3b) with the 'true' value computed from Eqs. (3) and (4) and presented earlier in Fig. 2. The code-increase in edge displacements is much larger than the mean value of the 'true' increase; however, it is about one-half of the mean-plus-one standard deviation of the 'true' value. This implies that the probability of exceeding the code value is somewhere between 15% (mean-plus-one standard deviation) and 50 % (mean result). Indeed, under mild assumptions one can show that the increase in the system response is reasonably modeled by a Gaussian distribution with mean and standard deviation as

shown in Fig. 4. Based on this model it is possible to conclude that the code $\hat{u}_{b/2}$ corresponds to exceedance probabilities of about 30%. This implies that the chances of exceeding the increase in response predicted by the code-specified dynamic analysis using the accidental eccentricity $e_a = \pm 0.05b$ are, roughly, one in three cases.

Naturally, a question arises: what is the appropriate design level for accidental torsion, exceedance probability of 50%, 30%, 15%, or other? The answer to this question goes well beyond the scope of this work, in fact it goes directly to the roots of the earthquake design philosophy. The design level for accidental torsion should be consistent with the exceedance probability for lateral response implied in seismic codes. However, that response level is not defined explicitly in current building codes.

In order to assist code-writing professionals in choosing an appropriate response level, we present the 'recorded' accidental torsion effects determined from building motions recorded during earthquakes. While such data are scarce, they have been obtained for three nominally-symmetric buildings subjected to the Whittier (1987), Loma Prieta (1989), and Upland (1990) earthquakes [5]. The 'recorded' values of the normalized edge displacement computed from recorded motions in buildings A, B and C are equal to 1.03, 1.11 and 1.39, respectively, and they are plotted in Fig. 5 at the corresponding Ω values= 1.52, 1.42 and 1, respectively; together with those computed from code-dynamic analysis using $e_a = \pm 0.05b$, $b/r \simeq 3.12, 2.67$ and 3.22, and $T_y = 0.7, 0.3$, and 0.7 sec., the b/r and T_y values of Buildings A, B, and C, respectively. Clearly, the 'recorded' increase in $\hat{u}_{b/2}$ obtained for Buildings A and B is smaller than the increase in response predicted by the code. On the other hand, the 'recorded' increase in response of Building C is seen to be larger than the code prediction. Because Building A is torsionally stiffer than the other two buildings, it is not surprising that the effects of accidental torsion are smaller in this building. As the frequency ratio Ω decreases the effects of accidental torsion increase, as they should. Note that although the 'recorded' increase in edge displacements in Building C is larger than the one predicted by code-dynamic analysis of the building, a slight change in the value of Ω will bring this building close to the code results. This observation suggests that for design purposes we should ignore the dip in the curves at $\Omega \simeq 1$, where the system response is very sensitive to the value of Ω.

As mentioned earlier, one important drawback in the current code provisions is that the specified static and dynamic analysis procedures predict considerably different increase in design forces due to accidental torsion. This discrepancy can be avoided by defining a unique design envelope for the

increase in edge displacements due to accidental torsion. The design envelope proposed is:

$$\hat{u}_{b/2} = \begin{cases} A & 0 \leq \Omega \leq 1 \\ A - \frac{A-1}{\Omega_c - 1}(\Omega - 1) & 1 < \Omega \leq \Omega_c \\ 0 & \Omega > \Omega_c \end{cases} \tag{7}$$

Thus, the design value is constant at A from $\Omega = 0$ to 1 and decreases linearly to zero as Ω increases from 1 to Ω_c. Based on our research experience we have selected $\Omega_c = 1.8$ because for larger values of Ω, the increase in response due to accidental torsion is negligible for design purposes.

The value of A is defined as a function of b/r for convenience in design applications. Numerical values for the maximum value of $\hat{u}_{b/2}$ over all Ω, for a fixed b/r and exceedance probability, are plotted as a function of b/r in Fig. 6a. The range for b/r selected in this figure $0 \leq b/r \leq \sqrt{12}$ covers most buildings in practice, from narrow plans to very elongated plans perpendicular to the direction of ground motion. These data, obtained from results of code-specified dynamic analysis, such as those presented in Fig. 6b, are for nominally-symmetric systems. It is apparent that the variation of A with b/r is quadratic, and can be approximated by

$$A = 1 + 0.0475(b/r)^2 \tag{8}$$

The values of A computed from this equation correspond to probability of exceedance of about 30%, implicit, as mentioned earlier, in the Uniform Building Code. For more conservative designs associated with smaller exceedance probability, the coefficient 0.0475 should be increased in Eq. (8).

Shown in Fig. 6b is a comparison between $\hat{u}_{b/2}$ from Eq. (7) and the prediction from code-specified dynamic analysis for systems with $T_y = 1$ sec and $b/r \simeq 3.5, 3$ and 2.5. Equations (7) and (8) have been intentionally calibrated to produce values that are conservative especially for the range $0.9 \leq \Omega \leq 1.1$. There are three reasons for this. First, the estimation of the uncoupled frequency ratio of the system is obviously subject to error; therefore, taking advantage of the dip in the response curves near $\Omega = 1$ is not appropriate for design. Second, as will be shown in the next section, this conservatism proves to be useful in preventing resisting planes in the interior of the building plan to be under-designed by the procedure developed. And third, the empirical evidence presented by Building C (Fig. 5) shows that the 'recorded' increase in response for a system with $\Omega \simeq 1$ can certainly be larger than predicted by code-specified dynamic analysis for accidental torsion.

5.5 Increase in displacements for interior resisting planes

We now turn to the problem of how to determine the accidental torsion effects on the displacements along a resisting plane located at distance x from the CM once the displacement increase at the edge of the building plan is known. This problem has been studied earlier in the context of natural torsion of buildings [6].

One possibility is to use Eq. (6) to express the normalized displacement $\hat{u}_x$ of a resisting plane at distance x from the CM in terms of the normalized displacement $\hat{u}_{b/2}$ at the edge

$$\hat{u}_x = 1 + (\hat{u}_{b/2} - 1)\frac{\frac{\Omega_s^2}{(\pm 1/2 - e_s/b)(b/r)^2} - \frac{e_s}{b}}{\frac{\Omega_s^2}{(x/b - e_s/b)(b/r)^2} - \frac{e_s}{b}} \tag{9}$$

The $\pm 1/2$ term in the numerator implies that both combinations must be tried and the larger value of $\hat{u}_x$ selected. Note that for the particular case of symmetric systems, i.e., $e_s/b = 0$, or any system with Ω_s sufficiently large, Eq. (9) indicates a linear variation of displacements along the building plan. Further, it was shown in Chapter 4 that Eq. (9) is also exact for a special class of multistory systems, but an approximation for the case of general multistory systems.

The normalized displacement $\hat{u}_x$ computed from Eq. (9) is a function of the static eccentricity of the system e_s/b. This eccentricity can be easily computed in single-story and multistory systems belonging to the special class mentioned above. However, a unique definition of e_s for other multistory systems is not possible. Fortunately it is not needed either, as shown by the results of Fig. 7 where the increase in displacements computed from dynamic analysis is compared against the result obtained from Eq. (9) considering first and then neglecting the contribution of the static eccentricity term in this equation. These results have been obtained for single-story systems with uncoupled vibration period $T_y = 1$ sec, static eccentricity $e_s/b = 0, 0.2$ and 0.4, $b/r = \sqrt{6}$, and frequency ratios $\Omega = 0.8, 1.25$ and 1.5. It is apparent from the figure that knowing the static eccentricity of the system does not lead to better estimates for the increase in displacements of resisting planes within the building plan, and sufficiently accurate estimates also result from assuming $e_s/b = 0$. Furthermore, Eq. (9) predicts satisfactorily the increase in displacements in systems with Ω, say, larger than 1.25 or less than 0.8; however, it can overestimate or underestimate by different degrees the increase in response of resisting planes close to the CM of the system when $0.8 \leq \Omega \leq 1.25$. As mentioned earlier, this is one of the reasons for the conservatism over this range of Ω introduced into the design envelope of Eq. (7).

Therefore, an approximate expression for the normalized displacement $\hat{u}_x$ may be formulated

by imposing $e_s/b = 0$ in Eq. (9), leading to

$$\hat{u}(x) = 1 + (\hat{u}_{b/2} - 1) \left|\frac{x}{b/2}\right| \tag{10}$$

which states that the increase in response due to accidental torsion varies linearly within the building plan with no increase at the CM and $\hat{u}_{b/2}$ at the building edges.

5.6 Increase in member forces

So far, we have visualized the effects of accidental torsion as an increase in the lateral displacements of each resisting plane in the building. In this section we show how the corresponding increase in design forces for structural elements can be determined.

Consider the effects of accidental torsion in three different types of buildings: (1) single-story; (2) general multistory systems; and (3) multistory belonging to a special class with the following properties: (a) the centers of mass of all floors lie on a vertical line, (b) the resisting planes are arranged such that their principal axes form an orthogonal grid in plan and are connected at each floor by a rigid diaphragm, (c) the lateral stiffness matrices of each resisting plane are proportional to each other.

It was demonstrated in Chapter 4 that the normalized edge displacements $\hat{u}_{b/2}$ considering accidental torsion are essentially the same for a single-story system and a multistory system belonging to the special class if both have the same frequency ratio Ω, uncoupled lateral vibration period T_y, and static eccentricity e_s. An important corollary of this result is that the amplification factor $\hat{u}_x$ obtained for a given resisting plane applies to all stories of a multistory building belonging to the special class and hence to the forces in all structural elements in the same resisting plane. This result is not true for general multistory systems. However, numerical experimentation with different buildings has shown that it is a good approximation in most practical situations (Chapter 4).

Consequently, the effects of accidental torsion may be considered in building analysis by amplifying the member forces of a resisting plane, computed for the building with no accidental torsion, by the factors given in Eqs. (8), (9) and (11).

5.7 Examples

In this section, we compute the response considering accidental torsion in two hypothetical five-story steel buildings, the first belonging to the special class but not the second, subjected to

ground motion in the y-direction. This response is computed using the simplified analysis procedure described in the preceding sections; also presented are the results of the dynamic analysis procedure specified in the UBC.

The plans and elevations of moment-resisting frames in the two buildings are presented in Fig. 8. Two different moment-resisting steel frames are used for lateral resistance. These frames are arranged symmetrically about both principal directions in Building E1 but unsymmetrically about the y-axis in Building E2; it is expected that Building E2 will have significant coupling lateral and torsional motions. Building E1 has a rectangular plan with dimensions a = 22.8 m (75 ft) and b = 45.6 m (150 ft) and story heights equal to 5.48 m (18 ft) and 4.1 m (13.5 ft) for the first and other stories, respectively. The lateral and rotational (about the CM) masses of each floor are presented in Table 1. On the other hand, Building E2 has an L-shaped plan with identical wing dimensions b = 45.6 m (150 ft) and story heights and masses identical to Building E1 (Table 1).

We first estimate the increase in response due to accidental torsion in Building E1 by implementing the previously defined sequence of steps:

1. **Uncoupled frequency ratio Ω** . The fundamental frequency ω_y of y-lateral vibration of the system is computed by Eq. (1a) with δ_i equal to the displacements due to the heightwise variation of UBC lateral forces (column 4 of Table 1): ω_y = 7.5382 rad/sec or T_y = 0.83 sec. This value compares very well against the exact ω_y = 7.5311 rad/sec. Similarly, by using Eq. (1b) and the building rotations due to the code-prescribed heightwise variation of accidental torques = $0.05bF_i$ leads to ω_θ = 8.7043 rad/sec or T_θ = 0.72 sec, which compares well against the exact ω_θ = 8.6961 rad/sec. Thus, the approximate uncoupled frequency ratio of the system is:

$$\Omega = \omega_\theta/\omega_y = 1.1547 \tag{11}$$

   One can easily check that this value of Ω is essentially exact (up to four digits).

2. **Increase in displacements at the building edge.** The design envelope (Eq. (7)) is defined corresponding to a given probability of exceedance, selected for these examples as about 1/3. Thus Eq. (8) applies and noting that the building plan aspect ratio is $a/b = 1/2$, which implies that $b/r = \sqrt{12/(1+(a/b)^2)} \simeq 3.1$, we obtain

$$A = 1 + 0.0475(3.1)^2 = 1.46 \tag{12}$$

   Using this value of A we compute the increase in edge displacements for Building E1 from

Eq. (7):

$$\hat{u}_{b/2} = 1.46 + \frac{1 - 1.46}{1.8 - 1}(\underbrace{1.1547}_{\Omega} - 1) = 1.37 \tag{13}$$

This value of $\hat{u}_{b/2}$ implies that for this structure the displacements of the resisting planes at the edge of the building should be increased by 37% to account for accidental torsion.

3. **Increase in response of interior resisting planes** . For frames 2 and 3, Eq. (10) gives

$$\hat{u}_{x=-b/6} = \hat{u}_{x=b/6} = 1 + (1.37 - 1)(b/6)/(b/2) = 1.12 \tag{14}$$

4. **Increase in element forces** . Since Building E1 belongs to the special class, the shear and bending moments in the structural elements of the exterior frames (1 and 4) and interior frames (2 and 3) are amplified by 1.37 and 1.12, respectively, in order to account for accidental torsion.

In contrast, the code-specified dynamic analysis of this building predicts edge displacement increase of 35% (Table 2). The 37% increase in member forces computed by the new procedure (Eq. (13)) is similar to the 35% increase computed from dynamic analysis. This is not surprising since we have chosen a numerical value of A that was calibrated to an exceedance probability of about 1/3, similar to that implicit in the code. It is important to note that for computing the 37% increase in member forces, no additional structural analysis–static or dynamic–of the building was required, whereas two dynamic analyses are necessary to implement the code procedure. Although for this building both procedures lead to similar results, such is not the case always as shown by the next example.

Proceeding similarly with Building E2 we estimate an uncoupled frequency ratio $\Omega = 1.3160$, which again coincides almost exactly with the true uncoupled frequency ratio $\Omega = 1.3163$. Note that this structure does not belong to the special class since frames A and B do not have proportional stiffness matrices. It can be shown that b/r for this building is equal to 2.72 implying that $A = 1.35$ from Eq. (8). From Eq. (7) we obtain that $\hat{u}_{b/2} = 1.35 - (1.35 - 1)/(1.8 - 1)\ (1.316 - 1) = 1.21$, i.e., 21% increase in edge displacements due to accidental torsion. As mentioned before, $\hat{u}_{b/2}$ is computed by a procedure based on the results of nominally-symmetric structures and it should be an upper bound for the true increase in displacements in the building. Substituting $\hat{u}_{b/2}$ in Eq. (10), the increase in displacements for frame 2 (Fig. 8) turns out to be 4%. In summary, for building E2, our estimated increase in member forces due to accidental torsion is 21% for frames 1 and 3 and 4% for frame 2.

Code-specified dynamic analysis of this building predicts an increase in right- and left-edge displacements of 13% and 2%, respectively; the associated increase for frame 2 is 9%. In spite of the two three-dimensional dynamic analyses required to compute these code values, they have several deficiencies relative to the values resulting from the new approach. To mention some, the code values: (1) do not recognize that for Building E2 and others alike the 'true' increase in edge displacements should be similar for the stiff and flexible edges (Fig. 3); (2) only consider those sources of accidental torsion that can be represented by a constant value of accidental eccentricity (i.e. independent of Ω), thus, failing to include accidental torsion due to other sources such as base rotational excitation and stiffness uncertainty that cannot be modeled by a constant accidental eccentricity; and (3) do not reflect the fact that since unsymmetric buildings have usually poorer seismic performance than symmetric buildings, it would be desirable to design the former for at least the same increase in response (or a smaller exceedance probability) than their symmetric counterparts.

5.8 Summary and conclusions

A new procedure for including the effects of accidental torsion in seismic design of buildings has been developed. This procedure has four important advantages over the current code-specified static and dynamic analysis procedures for accidental torsion. Firstly, it avoids the additional structural analyses needed to account for the effects of accidental torsion. Thus, it avoids the typical two additional static analyses of the building in each lateral direction with equivalent static forces shifted $\pm\beta b$ from the CM, or two three-dimensional dynamic analyses of the building with the CM shifted $\pm\beta b$. Secondly, it includes the effects of all sources of accidental torsion whereas seismic codes include only those that can be represented by a constant accidental eccentricity. Thirdly, it gives a unique value for the increase in a design force due to accidental torsion in the building, whereas current building codes give very different results depending on whether the analysis is static or dynamic (Chapter 4). Fourthly, the procedure states explicitly what is the expected increase in design forces due to accidental torsion. This is in contrast to the current use of accidental eccentricity, which implies an indirect increase in member forces that may be large or small depending on the system parameters, mainly on the uncoupled frequency ratio Ω of the building. And finally, the increase in design forces specified by the new procedure has a well established probability of exceedance.

Using the new procedure is simple. First, we need to determine the frequency ratio Ω of the building; then, obtain the increase in edge displacements in the building from the proposed design envelope (Eq. (7)), and use this increase to compute the increase in displacements for all interior resisting planes (Eq. (10)). Finally, the member forces in each resisting plane are determined by amplifying the forces computed without accidental torsion by the factors obtained from Eqs. (8) and (11).

It is the authors' opinion that the computational simplicity inherent in this procedure is consistent with the current state of knowledge about the 'true' effects of accidental torsion in buildings. The use of three-dimensional dynamic analyses specified in building codes to account for accidental torsion seems unjustified since no additional accuracy is gained, in fact, the accuracy is less than that of the new procedure. Furthermore, the code static analysis procedure leads in many cases to erroneous results, which are sometimes conservative (e.g., torsionally flexible systems) but other times unconservative (e.g., torsionally stiff systems).

Although conceptually appealing, the accidental torsion provisions in building codes are for some structures a refinement that has small influence on the sizing and detailing of structural members, especially when considered in the context of other larger approximations inherent in structural design. In particular, if the mean increase in response due to accidental torsion is used as a design basis, these effects are small (Fig. 2). On the other hand, if the design is more conservative, say based on mean-plus-one standard deviation (Fig. 2), the accidental torsion effects can be significant; they may still be neglected, however, for torsionally stiff systems with values of Ω, say larger than 1.8.

5.9 References

1. De la LLera, J.C., and Chopra A.K. (1994). "Accidental torsion in buildings." *Proc. of the 6th US National Conf. in Earthquake Engrg.*, July, 1994. To appear.

2. Vasquez, J., and Riddell, R. (1984)."Existence of centers of resistance and torsional uncoupling of earthquake response of buildings". *Proc. of the 8th World. Conf. in Earthquake Engrg.*, Prentice Hall, Inc., Englewood Cliffs, New Jersey, IV, 187-194.

3. Tso, W.K. and Cheung, W.T. (1986). " Decoupling of equations of equilibrium in lateral load analysis of multistory buildings." *Computers and Structures*, 23 (5), 679-684.

4. Hejal, R. and Chopra, A.K. (1989). "Response spectrum analysis of class of torsionally-coupled buildings." *J. Engrg. Mechanics*, ASCE, 115(8).

5. De la LLera, J.C., and Chopra A.K. (1994). "Evaluation of code accidental-torsion provisions from building records." *J. Struc. Div.*, ASCE, 120(2).

6. Dempsey, K.M., and Tso, W.K. (1982). "An alternative path to seismic torsional provisions." *Soil Dynamics and Earthquake Engrg.*, 1 (1).

Table 1: Building masses and code equivalent lateral forces

Story	m_i (N $-$ s^2/cm)	Ip_i (kN $-$ s^2 $-$ cm)	F_i (kN)
5	1.58	3436.793	0.2669 V
4	2.63	5727.988	0.2677 V
3	2.63	5727.988	0.2059 V
2	2.63	5727.988	0.1442 V
1	3.68	8019.184	0.1153 V

Table 2: Increase in building response due accidental torsion

Analysis type	Frame No.			
	1	2	3	4
	Building E1			
code-dynamic	1.35	1.03	1.03	1.35
new approach	1.37	1.12	1.12	1.37
	Building E2			
code-dynamic	1.02	1.09	1.13	
new approach	1.21	1.04	1.21	

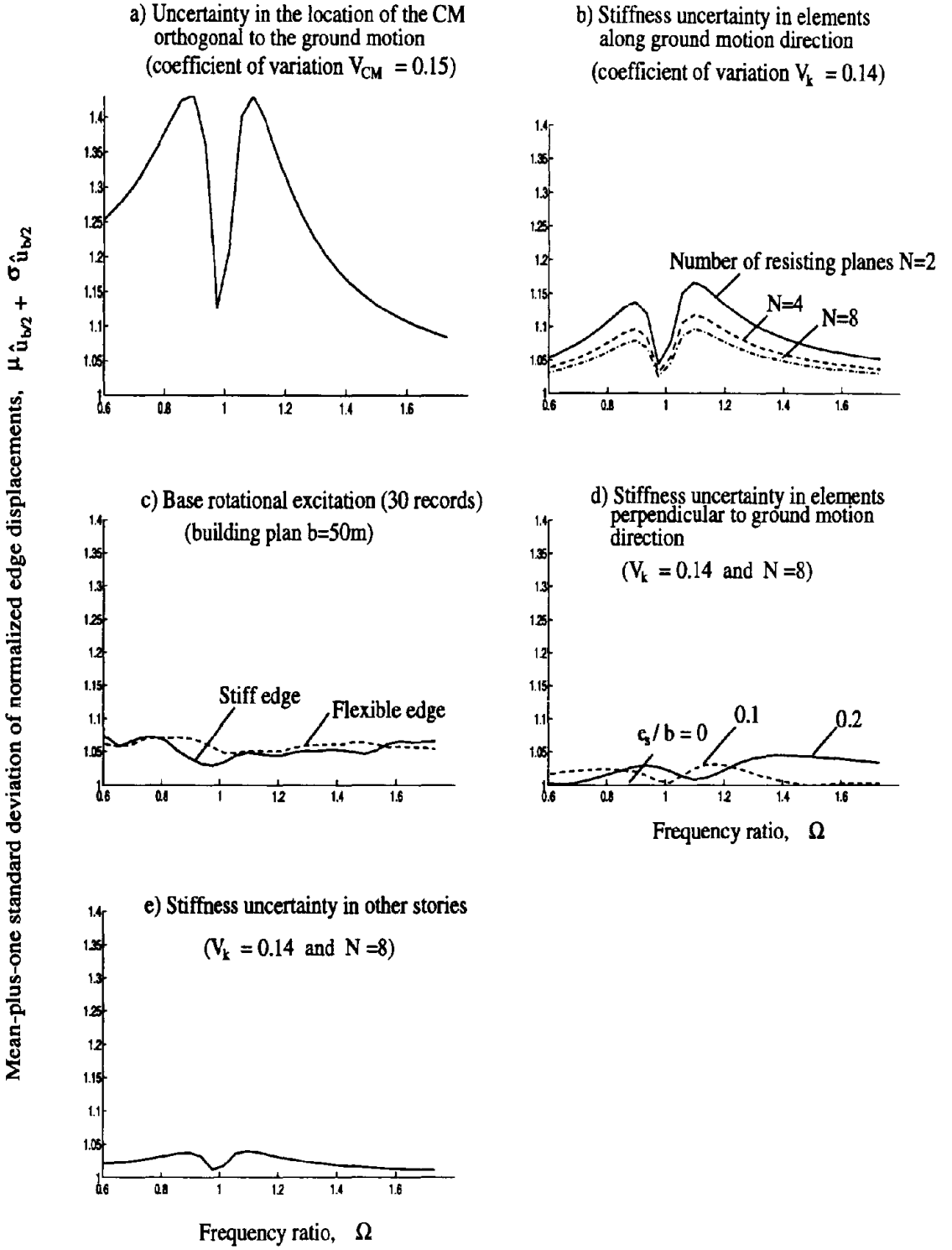

Figure 1: Mean-plus-one standard deviation $\mu_{\hat{u}_{b/2}} + \sigma_{\hat{u}_{b/2}}$ of the normalized edge displacement $\hat{u}_{b/2}$ due to different sources of accidental torsion in buildings with $T_y = 1$ sec and square plan $b/r = \sqrt{6}$

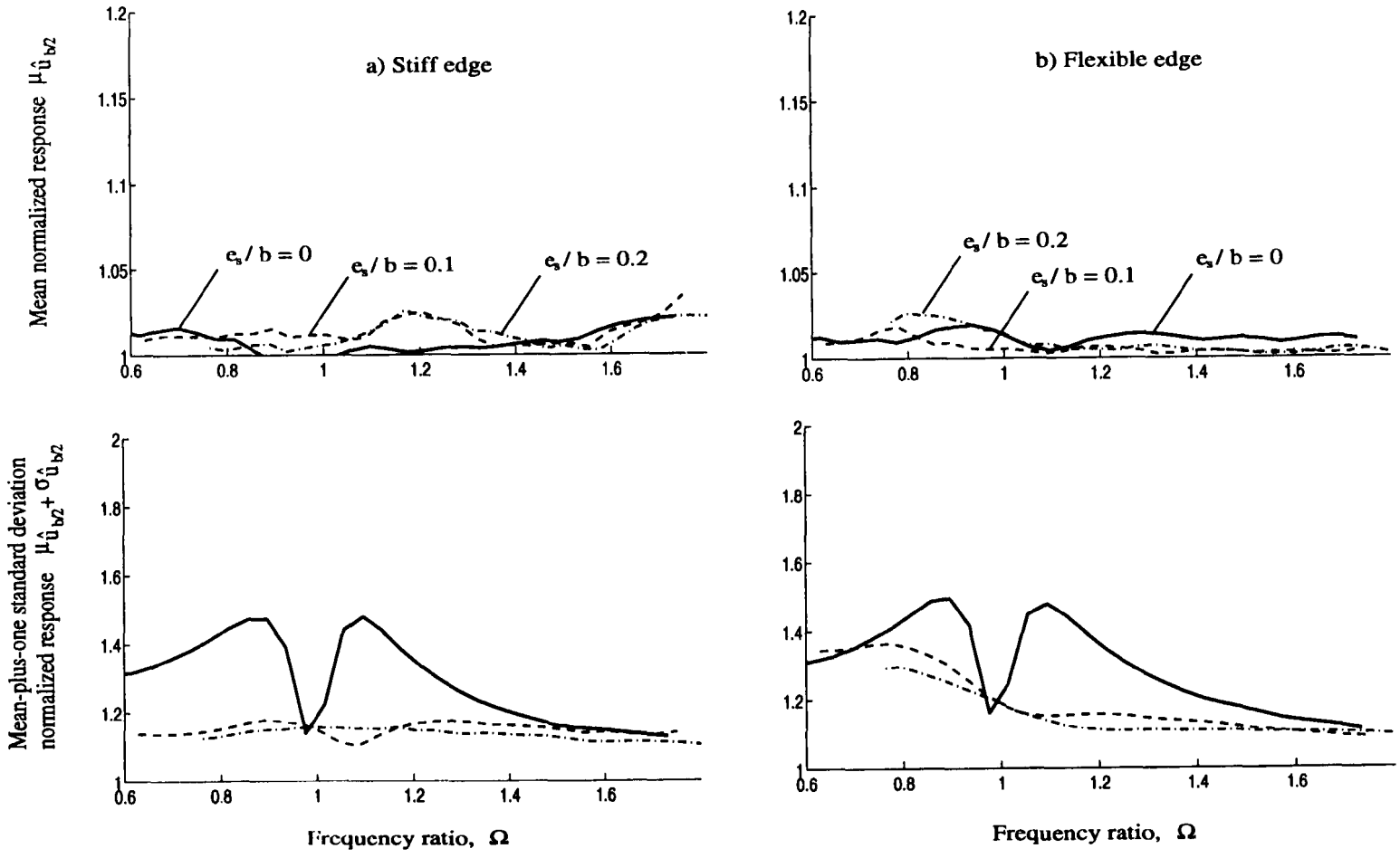

Figure 2: Mean and mean-plus-one standard deviation of the normalized edge displacement $\hat{u}_{b/2}$ as a function of Ω in systems with $T_y = 1$ sec and square plan $b/r = \sqrt{6}$

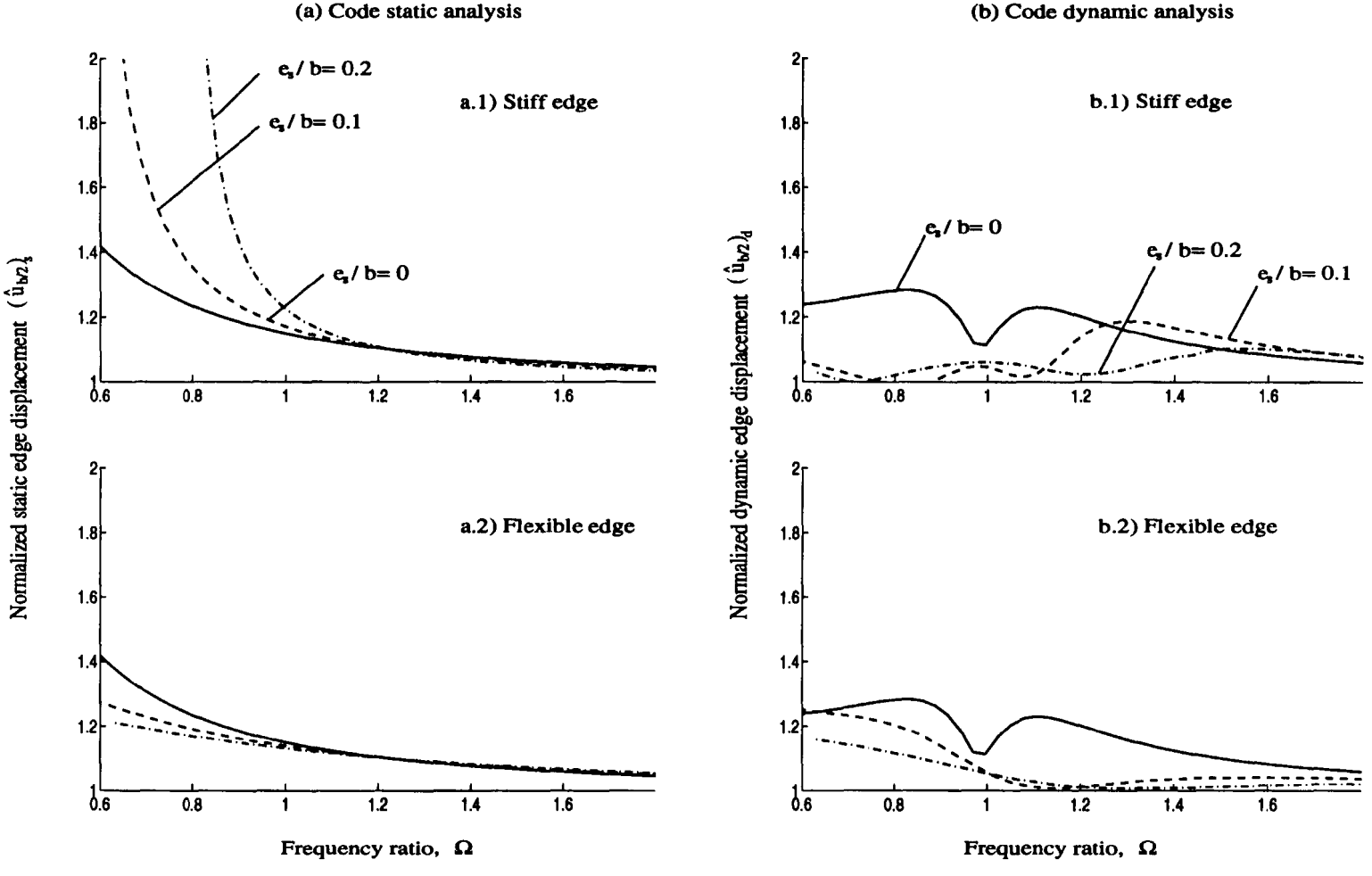

Figure 3: Normalized edge displacement $\hat{u}_{b/2}$ computed from code-static and dynamic analyses for accidental torsion in systems with $T_y = 1$ sec, square plan $b/r = \sqrt{6}$, and static eccentricity $e_s/b = 0, 0.1$, and 0.2

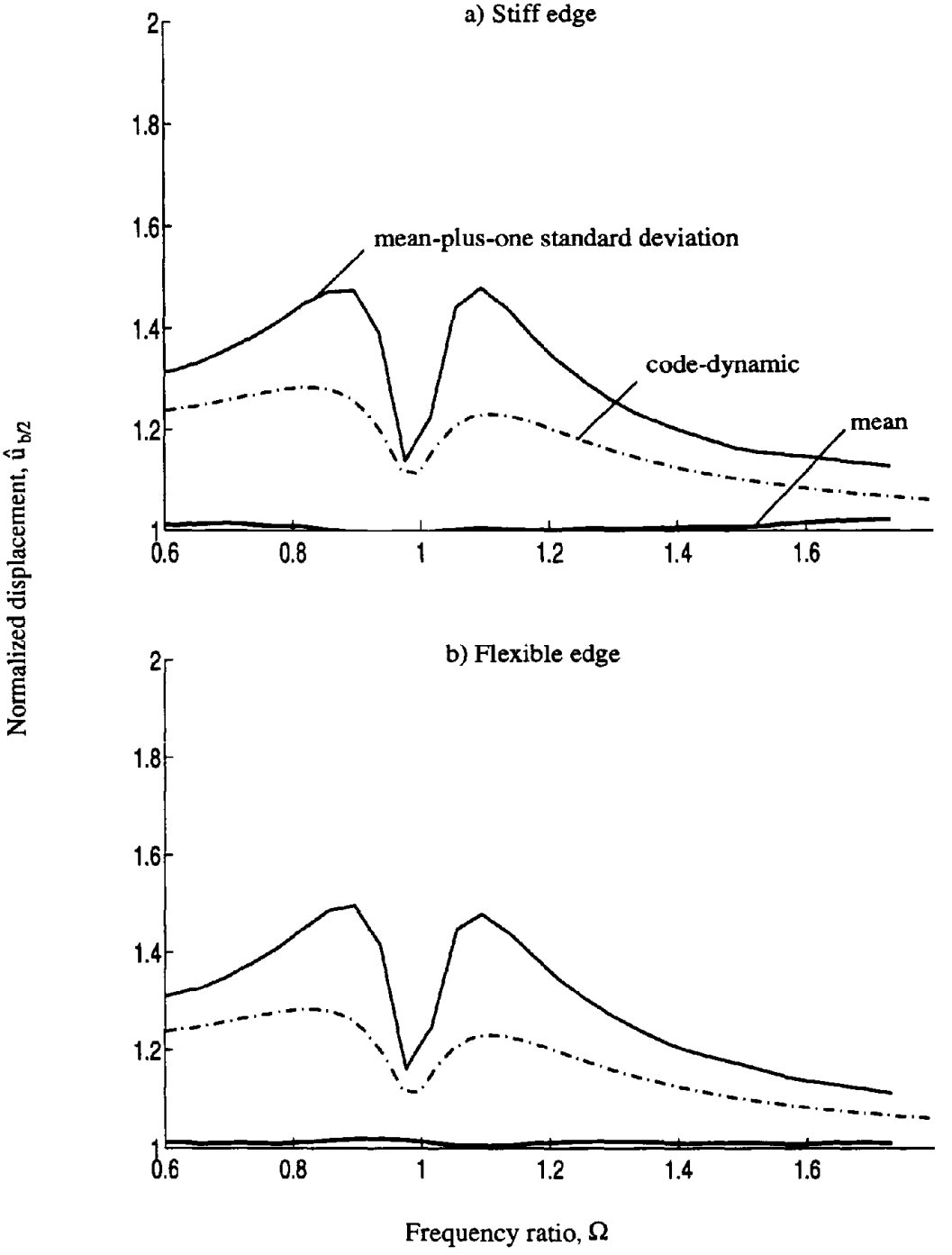

Figure 4: Comparison between the normalized edge displacement $\hat{u}_{b/2}$ in nominally symmetric systems computed from code-dynamic analysis and from statistical analysis of different sources of accidental torsion; systems with $T_y = 1$ sec and square plan $b/r = \sqrt{6}$

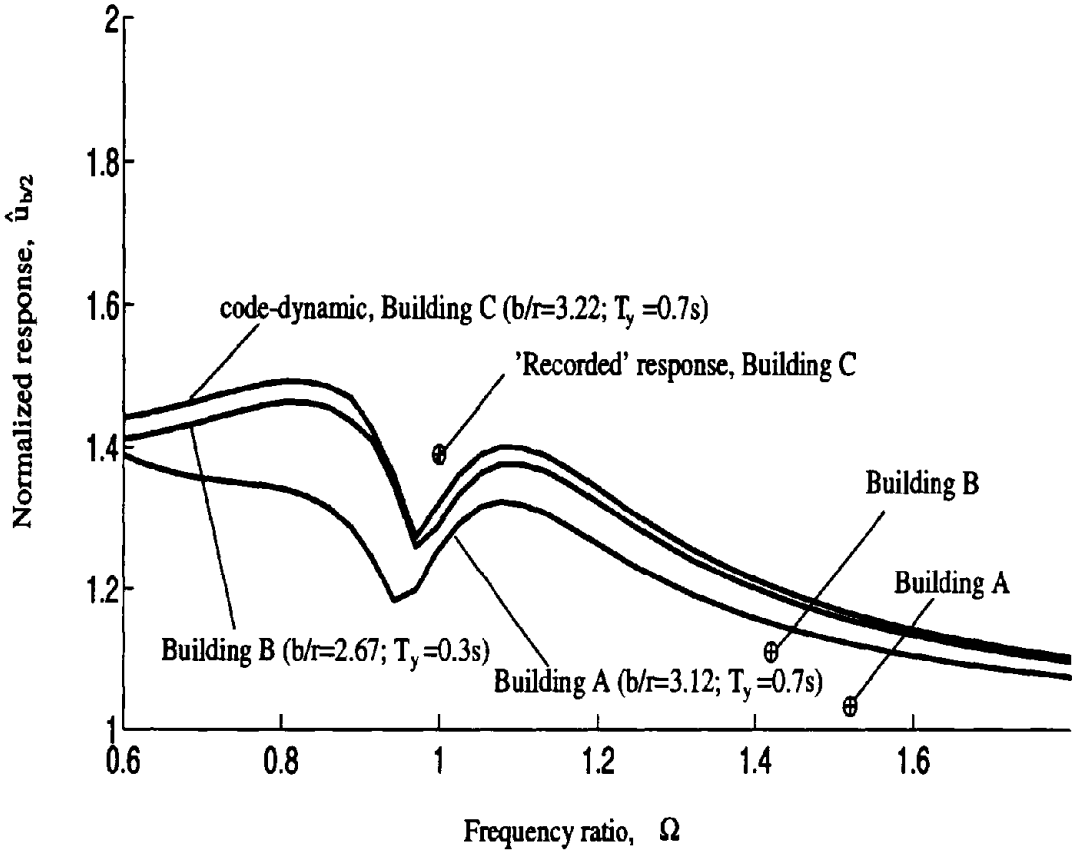

Figure 5: Comparison between the 'recorded' normalized edge displacement $\hat{u}_{b/2}$ obtained from records in three nominally-symmetric buildings and the normalized displacements computed from code-dynamic analysis with $e_a = \pm 0.05b$; $b/r = 3.12, 2.67$ and 3.22; and $T_y = 0.7, 0.3$, and 0.7 sec, respectively

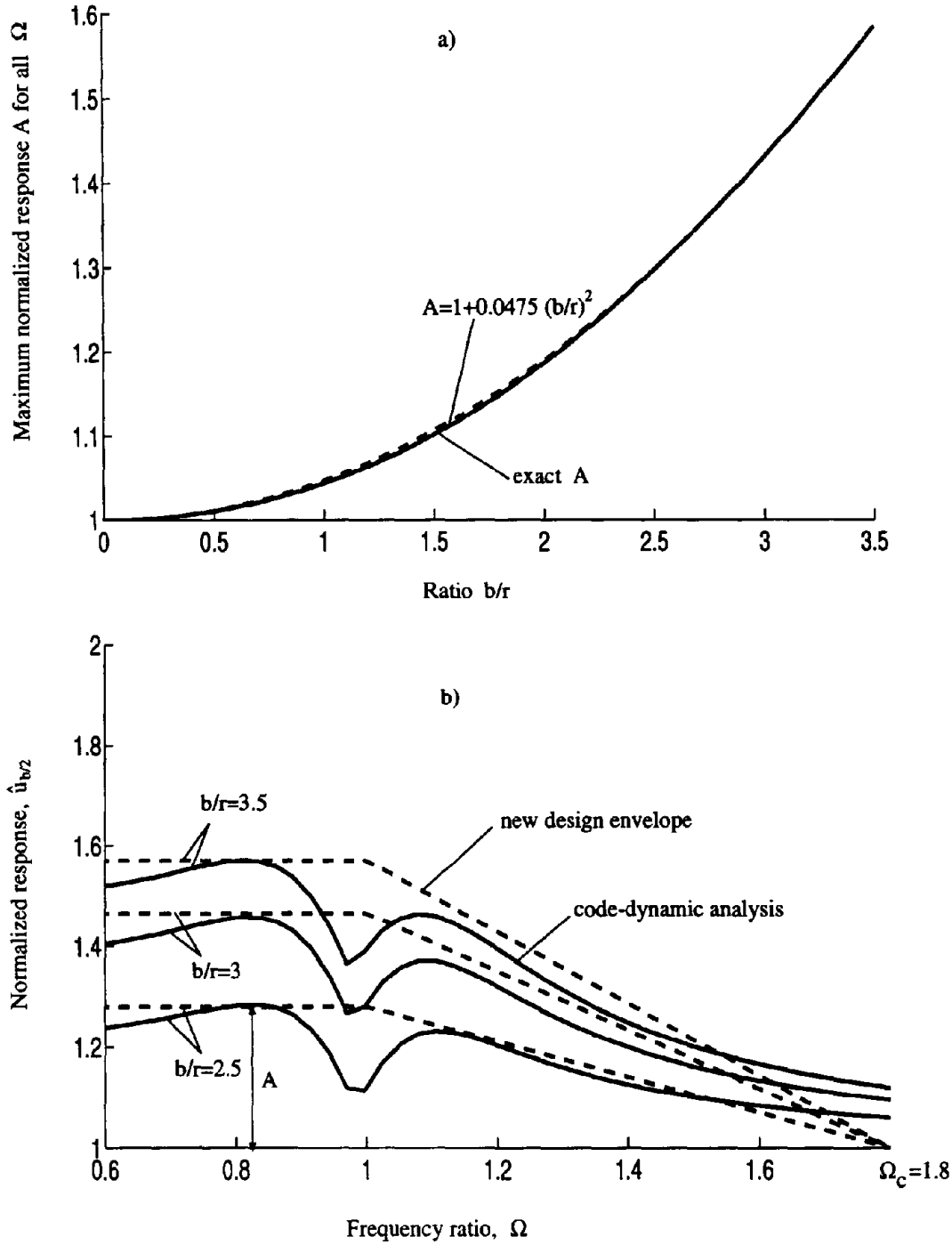

Figure 6: Design envelopes for the normalized edge displacement $\hat{u}_{b/2}$: (a) variation of the maximum normalized response A as a function of the ratio b/r; and (b) design envelopes for three values of $b/r = 2.5, 3$ and 3.5 in systems with $T_y = 1$ sec

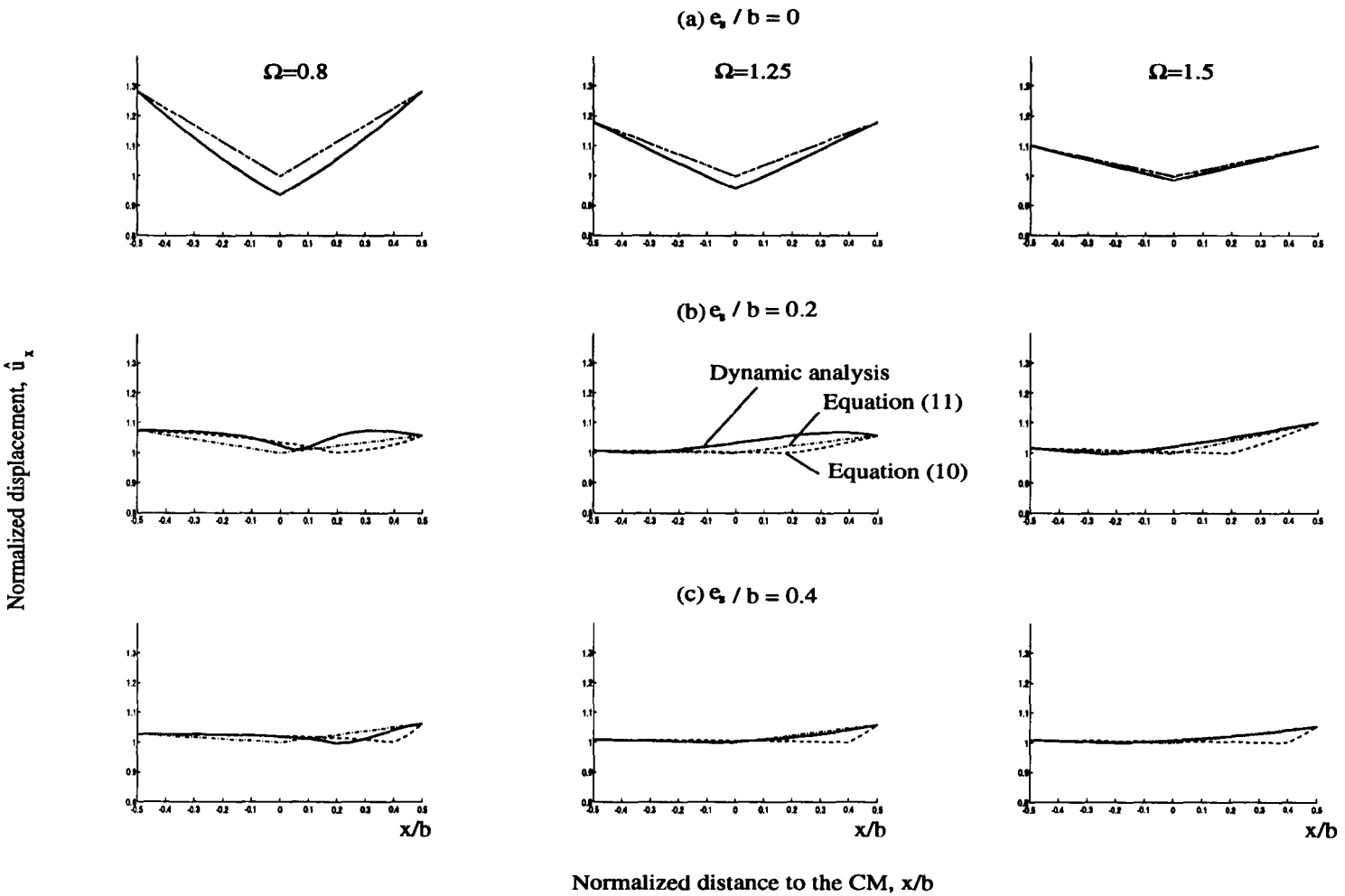

Figure 7: Planwise variation of normalized displacements $\hat{u}_x$ computed from dynamic analysis with the CM shifted $e_a = \pm 0.05b$ from its nominal position, and from Eqs. (10) and (11) in systems with $T_y = 1$ sec and square plan $b/r = \sqrt{6}$

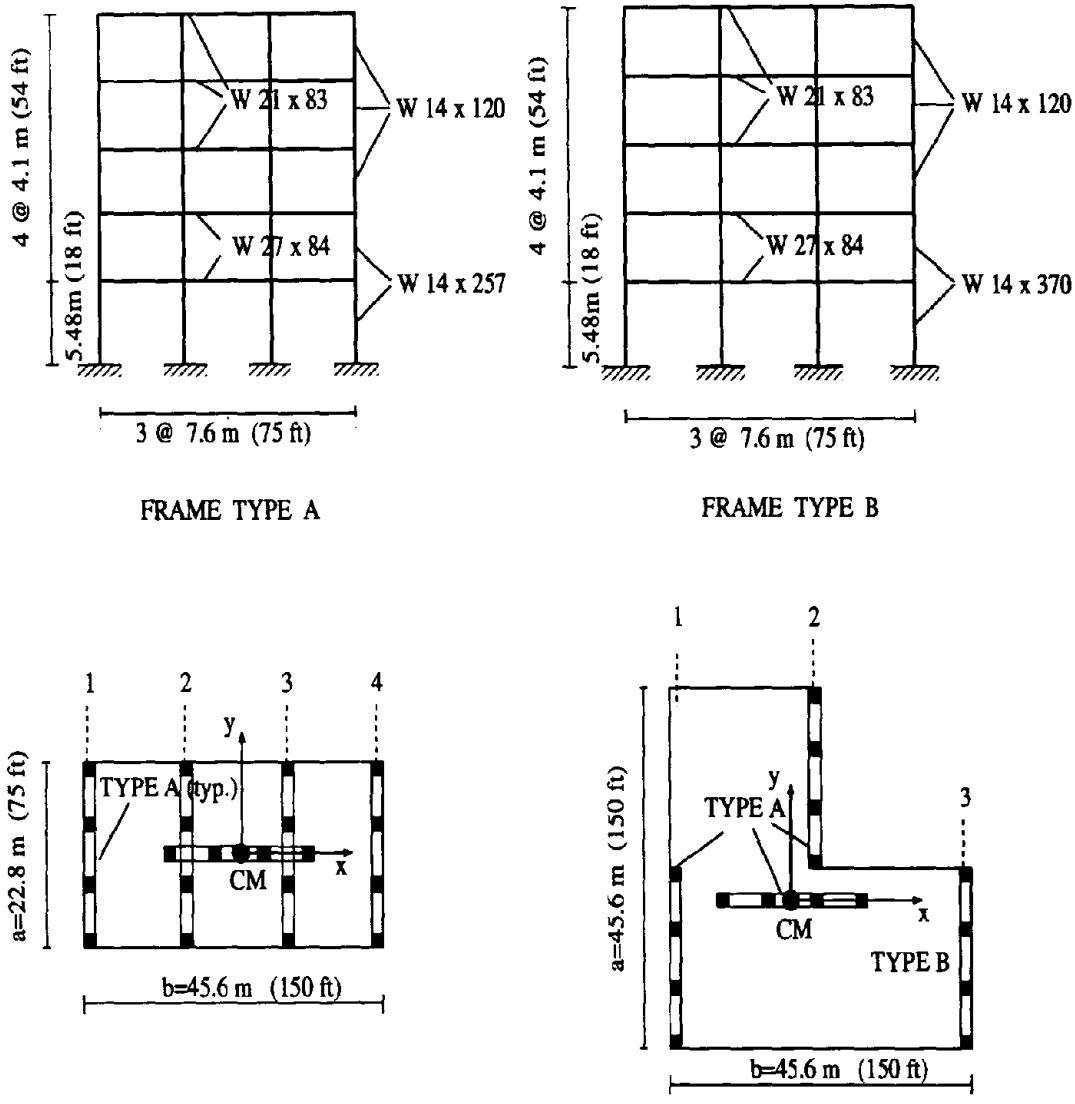

Figure 8: Building plans and frame elevations for the two examples considered.

Part II

Natural Torsion in Buildings

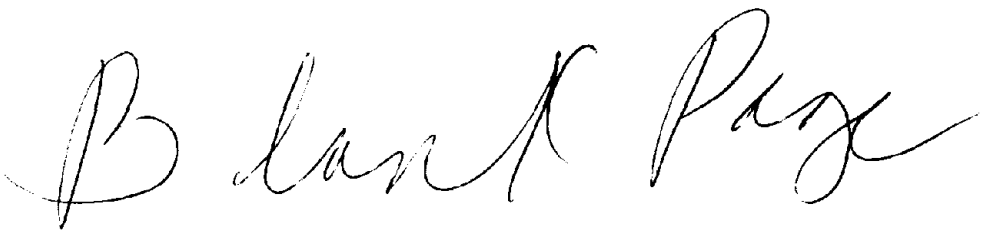

1. INTRODUCTION

The coupling existing between lateral and torsional motions in a building with plan asymmetry, denoted here as natural torsion, inevitably leads to non-uniform displacement demands on the lateral resisting planes of the system. Such displacement demands are of principal interest in the sizing and detailing of structural elements for earthquake resistance.

Consequently, many studies have focused in trying to understand the change in building displacements that arise from building asymmetry. Researchers studied first the elastic response of these buildings [e.g., 1,2,3] and evaluated, based on their results, most of the torsional provisions in seismic codes [e.g., 4,5,6,7]. More recently, research efforts have focused mainly on studying the inelastic response of asymmetric single-story buildings. The ultimate goal of all this research has been to generate globally accepted design guidelines for asymmetric structures that could be transfered into new seismic code provisions.

Most of the available results concerning the inelastic behavior of asymmetric buildings comes from the interpretation of exhaustive parametric studies of the earthquake response of simplified models of asymmetric single-story structures [e.g., 8, 9,10]. Although these results are an important step in trying to understand the behavior of asymmetric systems, they have two important drawbacks. First, because of the inherent complexity of the problem, it is very difficult to extract from them general trends that apply to structures other than those analyzed and to propose new design guidelines. Second, their extension to the practical case of multistory buildings is not obvious. Naturally, most researchers have been discouraged to look into the multistory case in light of the already complex response of single-story asymmetric structures.

In practice, engineers have two options to account realistically for the effects of lateral-torsional coupling in building design; or they look at the results of the numerous investigations on the subject and based on that extrapolate to the building to be designed, or they perform an inelastic dynamic analysis of the three-dimensional structure using a special purpose computer program [11]. The latter option, however, has also certain drawbacks. Firstly, such analyses are frequently costly, not only regarding computational effort, but mainly in the definition of the model and interpretation and checking of the results generated. This difficulty usually discourages engineers to try alternative structural configurations that would lead to new models and, thus, to repeat the structural modeling and interpretation of response results. As a result of this, for most buildings the final structural configuration usually correspond to the first computational model of the structure, which does

not correspond usually to the most seismically efficient and cost-effective configuration. Finally, and very important, since we know that the behavior of a building will depend on the frequency content and intensity of the ground motion, which are unknown, the final design of the structure should be based on responses representative of many excitations, and not the response to a single ground motion. Indeed, a good design should aim to induce certain desirable behavior of the system regardless of the ground motion characteristics.

Thus, we see on one hand that the results from earlier investigations are hard to synthesize into simpler design guidelines, and on the other hand, complex analytical models are not practical for trying out alternative designs. Consequently, the global objectives of this part of the dissertation are to: (1) develop a simple **conceptual framework** enabling scientists and engineers to understand the relative performance of different asymmetric structural configurations, prior to any sophisticated nonlinear dynamic analysis; and (2) develop a **simplified method** for nonlinear analysis of asymmetric buildings, which combines the available knowledge of the seismic performance of these structures with some of the analytical tools for more refined inelastic analyses.

These objectives are considered in three related investigations described in the next three chapters. Developed in Chapter 2 is a conceptual framework for understanding the seismic performance of asymmetric-plan single-story systems. The most fundamental idea used is to study the effects of plan asymmetry by considering the base shear and torque response histories of different structural configurations. These histories are represented in the force space spanned by the base shears V_x and V_y in the x and y-directions, respectively, and base torque T. At each instant of the response the base shears and torque define one point in this space. These combinations of base shear and torque happened to be bounded in this space by a surface denoted, for single-story systems, as the BST (base shear and torque) ultimate surface. The BST surface is defined by the set of base shear and torque combinations corresponding to the different collapse mechanisms that can be developed in the system. Because important information about the inelastic properties of the system is contained in this surface, its understanding is essential for the purpose of this study. The idea of the BST surface is not new; indeed, it goes back to the early work of Kan and Chopra (1979) [12] and it has been considered later by other researchers [13].

Studied in Chapter 3 is the extension of this conceptual framework to the case of the inelastic behavior of asymmetric multistory buildings. The emphasis in this chapter is put in using such framework to answer, without the need of very complex parametric studies, practical issues concerning the design and retrofit of asymmetric structures. The following questions are the thrust

of the chapter. What can be said about the torsional behavior of an asymmetric structure before performing inelastic dynamic analysis?. How can we adjust the planwise distribution of stiffness and strength in the system in order to achieve a good performance?. How can we localize or spread the damage among resisting planes?. What resisting planes should be stiffened or strengthened?. What is the effect of the orthogonal component of ground motion regarding the design of resisting planes in the direction of the first component of ground motion?. How is the system going to collapse?. The ability to answer such questions will go a long way toward improving the current understanding of the inelastic seismic response of asymmetric buildings. It is the objective of this chapter to provide generally applicable design guidelines that enable us to answer the above-stated questions.

Finally, developed in Chapter 4 is a simplified method for the analysis and design of asymmetric-plan structures. Such method is based on the conceptual framework developed in Chapters 2 and 3 and some of the analytical tools of more refined inelastic analyses. The new simplified analysis method considers one structural super-element (SE) per building story, which is capable of representing the elastic and inelastic properties of the story. The idea of a SE model is not new; it was first considered by Kan and Chopra [12], but the model was overly simplified and ignored some fundamental aspects regarding the true inelastic behavior of the system. In contrast, the SE model presented herein is, in general, in close agreement with the actual inelastic properties of the story.

The three chapters presented are self-contained units and could be read, in principle, in any sequence. However, since Chapter 2 contains the development of basic concepts such as the BST surface and properties that are extensively used in the other chapters, it is recommended to read this chapter first.

References

1. Erdik, M.O., 'Torsional effects in dynamically excited structures', Ph.D. Thesis, Rice University, Houston, Texas, May 1975.

2. Kan, C.L. and Chopra, A.K., 'Effects of torsional coupling on earthquake forces in buildings', Journal of Structural Division ASCE 103, 805-820 (1977).

3. Hejal, R. and Chopra, A.K., 'Earthquake response of torsionally-coupled frame buildings', Journal of Structural Division ASCE 115, 834-851 (1989).

4. Tso, W.K. and Meng, V., 'Torsional provisions in building codes', Canadian Journal of Civil Engineering 9, 38-46 (1982).

5. Chandler, A.M. and Hutchinson, G.L., 'Evaluation of code torsional provisions by a time history approach', Earthquake Engineering and Structural Dynamics 15, 491-516 (1987).

6. Humar, J.L. and Awad, A.M., 'Design for seismic torsional forces', Canadian Journal of Civil Engineering 11, 150-163 (1984).

7. Rutenberg, A. and Pekau, O.A., 'Earthquake response of asymmetric buildings: a parametric study', Proceedings of the 4th Canadian Conference on Earthquake Engineering, Vancouver, 271-281, June 1983.

8. Tso, W.K. and Sadek, A.W., 'Inelastic seismic response of simple eccentric structures', Earthquake Engineering and Structural Dynamics 19, 255-269 (1985).

9. Tso, W.K. and Hongshan, Y., 'Additional seismic inelastic deformation caused by structural asymmetry', Earthquake Engineering and Structural Dynamics, 19, 243-258 (1990).

10. R. K. Goel and A. K. Chopra, 'Inelastic seismic response of one-story, asymmetric plan systems', Report No. EERC 90/14, University of California, Berkeley, CA., Oct. 1990.

11. Guendelman-Israel, R. and Powell, G.H.'DRAIN-TABS: A computer program for inelastic earthquake response of three-dimensional buildings', Report No. EERC 77-08, University of California, Berkeley, CA, 1977.

12. Kan, C.L. and Chopra A.K., 'Torsional coupling and earthquake response of simple elastic and inelastic systems', Journal of Structural Division ASCE 107, 1569-1588 (1981).

13. Palazzo, B. and Fraternali, F., 'Seismic ductility demand in buildings irregular in plan: A new single story nonlinear model', Proceedings of the 9th World Conference on Earthquake Engineering, Tokyo-Kyoto, Japan, Vol. V, V-43 to V-48, Aug. 1988.

2. UNDERSTANDING THE INELASTIC SEISMIC BEHAVIOR OF ASYMMETRIC PLAN BUILDINGS

2.1 Introduction

The objectives of this investigation are to: (1) study conceptually the effects of building asymmetry in different structural configurations rather than by extensive numerical experimentation; (2) develop a conceptual framework that will enable design engineers to evaluate the torsional behavior of different structural configurations; and (3) obtain general guidelines for improving the seismic design of asymmetric structures.

This investigation is organized in six sections covering the objectives mentioned. First, the systems considered are described in section 2.2 together with the procedure used for integrating the equations of motion of the system. Section 2.3 explains the construction and properties of the BST ultimate surface and is conceptually the most fundamental section in this study. Then we re-consider in section 2.4 the behavior of asymmetric plan buildings subjected to unidirectional ground motion in light of the BST surface; several fundamental conclusions about the behavior and design of asymmetric-plan buildings are obtained. Similarly, section 2.5 deals with the response of asymmetric structures subjected to bidirectional ground motion. Finally, section 2.6 contains the conclusions of this investigation.

2.2 Systems considered and analysis procedure

The systems analyzed are single story buildings consisting of a rigid diaphragm, where all the story mass is lumped; lateral resistance is provided by elasto-plastic vertically-rigid structural elements located along resisting planes in the x- and y-directions (Fig. 1). As shown in the building plan, the i^{th} resisting plane in the x-direction has stiffness k_{xi}, lateral strength f_{xi}, and is located at distance y_i from the CM (center of mass) of the building; analogously, the stiffness, strength, and location of the j^{th} resisting plane in the y-direction are defined by k_{yj}, f_{yj}, and x_j, respectively. The resisting planes in the y-direction may have different stiffnesses and strengths, and may be unsymmetrically located about the y-axis, creating an eccentricity e_x between the CM and the CS (center of stiffness) of the building plan. On the other hand, the system considered is symmetric about the x-axis.

The dynamic response of the system is described by three degrees of freedom: the translational

displacements u_x and u_y of the CM relative to the ground along the x and y-directions, respectively, and the rotation u_θ of the rigid diaphragm about a vertical axis through the CM. The dynamic response of the system to base acceleration $a_{gx}(t)$ and $a_{gy}(t)$ in the x and y-directions, respectively, is described by the following equations of motion:

$$\boldsymbol{M\ddot{u} + C\dot{u} + R(\delta, \dot{\delta}) = -Mra_g} \tag{1}$$

where $\boldsymbol{u} = \{u_x\ u_y\ u_\theta\}^T$; $\ddot{\boldsymbol{u}}$ and $\dot{\boldsymbol{u}}$ are the accelerations and velocities of the diaphragm; $\boldsymbol{\delta}$ and $\dot{\boldsymbol{\delta}}$ are the vectors containing the deformations and deformation rates of the different resisting elements, which are computed from the displacements $\boldsymbol{u}$ and velocities $\dot{\boldsymbol{u}}$ as $\boldsymbol{\delta} = \boldsymbol{L}\ \boldsymbol{u}$ and $\boldsymbol{\delta} = \boldsymbol{L\dot{u}}$, where $\boldsymbol{L}$ is the displacement-deformation transformation matrix; $\boldsymbol{M}$ and $\boldsymbol{C}$ are the mass and damping matrices; $\boldsymbol{R(\delta, \dot{\delta})}$ is the vector of restoring forces in the system; $\boldsymbol{r}$ is a $3x2$ matrix with its two columns $\boldsymbol{r}_x = \{1\ 0\ 0\}^T$ and $\boldsymbol{r}_y = \{0\ 1\ 0\}^T$, i.e., the influence vector for excitations $a_{gx}(t)$ and $a_{gy}(t)$, respectively; and $\boldsymbol{a}_g(t) = \{a_{gx}(t)\ \ a_{gy}(t)\}^T$. In this investigation the ground accelerations selected are the two horizontal components of the El Centro earthquake (1940).

The equations of motion presented above (Eq. 1) are integrated numerically using the partitioned predictor-corrector scheme developed in Ref. [1]. In this approach the restoring force vector $\boldsymbol{R(\delta, \dot{\delta})}$ is transferred to the right hand side of Eq.1 and treated as an extra loading term, which is first assumed constant during the integration step and later corrected. The algorithm has shown essentially the same accuracy and stability properties as any Newmark integration method [2]; however, it is particularly efficient when part of the system is known to remain elastic during the complete response history.

The response quantities of interest in this study are: (1) the combinations of V_x, V_y, and T, the base shears in the x- and y-directions and base torque; (2) the displacement histories at the building edges and at the CM; and (3) the element force-displacement histories.

2.3 Understanding base-shear and torque ultimate surfaces

As mentioned earlier, the fundamental idea of this investigation is to study the effects of building asymmetry by considering the base shear and torque response histories. Consequently, we start by discussing the construction and properties of the BST surface bounding these response histories.

2.3.1 Definition of the BST ultimate surface

The BST surface for a structure in the space spanned by V_x, V_y, and torque T defines all combinations of base shears and torque that applied statically lead to the collapse of the system.

In order to facilitate the understanding of the behavior of asymmetric systems, we will assume next, as in conventional plastic analysis, that the elasto-plastic deformations of the building in the transition between its elastic and perfectly plastic states (mechanism) are small compared to the plastic deformations occuring along the different building mechanisms (plastic state). This is equivalent to assume that the building has an elasto perfectly plastic force-deformation relation; hence, we can distinguish clearly between elastic and plastic deformations. Note, however, that this assumption is used hereafter in our conceptual discussion of the problem but not for the computation of building responses.

Consequently, the BST surface divides the force space into two sharp regions: the interior, containing combinations of base-shear and torque representing elastic behavior of the structure, and the exterior, containing statically inadmissible base shear and torque combinations. This surface is the boundary between these two regions and is where all the inelastic action of the system takes place; in the same way as the inelastic behavior of a single degree of freedom system takes place along the yielding plateau of the elasto-plastic force-deformation relation.

2.3.2 Construction of a BST ultimate surface

Let us start by computing the BST surface of the symmetric single-story system shown in Fig. 2a. The system selected has five resisting planes all with identical stiffness k and lateral strength f and is subjected to a static base shear V_y and torque T. Certain points of the BST surface are immediately obvious, such as the maximum lateral capacity of the system being $V_{yo} = 3f$ or the maximum torsional capacity $T_o = f\ (a + b)$; others, however, require a bit more analysis.

The BST surface (Fig. 2b) can be obtained from physical considerations using an extension of the well known pivot diagrams familiar in R/C design. Although this method is not as formal as the event-to-event strategy presented in Appendix A, it is worth pursuing because it provides important physical insight into the kinematics of the system at incipient collapse. Besides, if the structure has few resisting planes, it could be well used to construct the BST surface by hand.

Consider for example the pivot diagram shown in Fig. 3d. This diagram should be read as follows. The lengths of the solid vertical and horizontal bars, located where resisting planes exist,

are assumed to be proportional to the yield deformations $u_y = f/k$ of the planes (all identical in this example). Further, the kinematics of different collapse mechanisms in the system are represented by the solid and dashed lines, which are denoted here-after by a pair of numbers (e.g., 1-1' and 2-2' in Fig. 3d). For example, mechanism 1-1' (Fig. 3d) implies that resisting planes 1,2, and 3 are yielding while 4 and 5 have no force; similarly, mechanism 2-2' (Fig. 3d) implies that planes 1,2, and 3 are yielding in the same direction while 4 and 5 in opposite directions.

Let us determine using pivot diagrams the first quadrant of the BST surface presented in Fig. 2b—the other three quadrants can be determined in this case by symmetry arguments:

1. **Point P1** . This point corresponds to a purely translational mechanism of the plan (Fig. 3a), and implies that all resisting planes in the y-direction must yield. The collapse condition is presented in the pivot diagram shown in Fig. 3b. At collapse, the system has translated from 0-0' (undeformed configuration) to 1-1' (Fig. 3b) producing simultaneous yielding of all resisting planes in the y-direction. Therefore, equilibrium in the system dictates that $V_y = 3f$ and $T = 0$.

2. **Branch P1-B.** Along this branch the system starts to develop mechanisms involving rotation of the plan (Fig. 3c); these mechanisms are such that the plan rotation increases linearly leaving always the deformation of resisting plane 1 equal to u_y. The collapse mechanisms associated with this branch are generated by the rotation of line 1-1', about resisting plane 1, to the new line 2-2' in the pivot diagram of Fig. 3d . This implies also that the orthogonal planes 4 and 5 (Fig. 3c) start developing forces which produce a couple with respect to the CM, thus, leading to an increase in the base torque T resisted by the structure. From equilibrium of the system at mechanism 2-2' (point B), we easily see that the base shear V_y is still $3f$ (Fig. 3d) and the base torque T is fa.

3. **Branch B-C.** As shown in Fig. 3e, all the mechanisms associated with this branch have the same plan rotation already attained at configuration 2-2' (point B) and smaller deformations of the resisting planes in the y-direction. An alternative characterization of this branch (with direct implications for design later) is that it corresponds to mechanisms such that resisting plane 1 is always in the elastic range. This can be checked in the pivot diagram of Fig. 3f where line 2-2' translates down to line 3-3', keeping the deformations of resisting plane 1 always less than or equal to u_y. Because of this translation, the forces in resisting plane 1 are reduced, which in turn reduces the base shear V_y and increases the base torque T resisted by

the system. Equilibrium of the system at 3-3' (point C) gives $V_y = f$ and $T = f(a+b)$ (Fig. 3f). Such is the case because at this point, planes 1 and 3 are yielding in opposite direction canceling out their contributions to the base shear but not to the base torque.

4. **Branch C-P2.** This last branch is a sequel of the previous mechanisms of branch B-C (Fig. 3g); the plan rotation is still fixed at the maximum value attained at point B (Fig. 3d) and the lateral deformation in the y-direction keeps decreasing. Alternatively, these mechanisms are characterized by keeping resisting plane 2 in the elastic range. This is shown in Fig. 3h where the deformations of this plane remain bounded between u_y and zero during the translation from line 3-3' to line 4-4'. Besides, since the force in plane 2 is reduced during this translation, the base shear V_y is also decreased. Indeed, at 4-4' (point P2), equilibrium of the system in the y-direction shows that $V_y = 0$ (Fig. 3h) and $T = f(a+b)$. Hence, the mechanism developed at this point is purely torsional.

Thus, the first quadrant of the BST surface corresponding to $V_x = 0$ can be computed using simple plastic analysis concepts. The other three quadrants of the surface are all identical in this case because the strength in resisting planes is symmetric under load reversals and these planes are symmetrically arranged about the x and y axes.

2.3.3 Properties of the BST surface

As shown in the example above, the BST surface can be constructed knowing a finite number of points (four in the example of Fig. 2b). These and other properties are extremely useful in understanding the meaning and shape of the BST surface. Stated next are those relevant for this investigation. For the moment, we will concentrate on the case $V_x = 0$, i.e., when the base shear is zero in the direction orthogonal to the ground motion. Proofs for all these properties may be found in Appendix B.

1. The BST surface is convex and it is composed of linear branches.

2. The slope of a tangent to the BST surface tell the position of the element in the building plan that remains elastic during the mechanism (or branch) considered. Besides, this slope also defines the center of plastic rotation of the building.

3. The BST ultimate surface has as many branches with finite slope as the number of resisting planes in the structure. Starting in a counter-clockwise sense from the branch of constant

base shear in the first quadrant, the first branch is associated with mechanisms that leave the leftmost resisting plane in the elastic range, the second branch the second farthest plane to the left, and so forth until we reach the rightmost resisting plane.

4. The BST surface is point-symmetric with respect to the origin if the element yield displacements are the same under load reversals.

5. The BST surface of the system contracts along the torque axis as the base shear in the x-direction V_x increases from zero to its maximum value V_{xo}.

2.3.4 Parameters that control the shape of the BST surface

Because the inelastic behavior of a building is developed along the BST surface, its shape essentially controls this behavior; in the same way as the yielding force controls the seismic behavior of a single degree of freedom system. Therefore, even without dynamic analysis, it is possible to compare the expected performances of different structural configurations based on their BST surfaces. This is one of the advantages of the BST surface approach relative to traditional analysis methods where comparisons among systems can only be done after computing their responses.

Therefore, we must concentrate first on studying the factors that control the shape of the BST surface: (1) the strength of resisting planes in the x and y-directions, (2) strength of resisting planes in the orthogonal (x-) direction, (3) asymmetry in stiffness, (4) asymmetry in strength, (5) planwise distribution of strength, and (6) number of resisting planes. As we will show later, all these factors have important physical meaning in the context of the design of asymmetric structures. For this purpose, consider the reference single-story system shown in Fig. 4a, which has plan aspect ratio $a/b = 1/2$ and five resisting planes, three in the y-direction (1 through 3), and two in the x-direction (4 and 5), all with identical stiffnesses k and strength f.

(a) **Strength of resisting planes**

Consider doubling the strength of each resisting plane. The resulting BST surface of the new system is shown in Fig. 4b together with the one of the reference system. It is apparent that the surface has expanded by a factor of two in all directions. This is not surprising since each branch of the BST surface is a linear function of the base shear and torque, which, in turn, are linear functions of the strength of the resisting planes. Therefore, an increase (or decrease) in the strength of the resisting planes produces an isotropic dilation (or contraction) of the surface proportional to the increase (or decrease) in strength.

(b) **Strength of resisting planes in the orthogonal direction**

Assume now that only the strength of the orthogonal planes 4 and 5 is doubled. The resulting BST surface is shown in Fig. 4c together with the one corresponding to the reference case. Comparison between the two surfaces shows that the increase in strength of planes 4 and 5 produces a stretching of the surface along the base torque axis in the positive and negative directions. This stretching corresponds to an increase in torque of fa. Note also that as a result of this increase in strength, the length of the constant base-shear branches of the BST surface is also increased (Fig. 4c). Justification for this effect becomes apparent when looking at the pivot diagrams shown in Figs. 3d, 3f, and 3h. There, resisting planes 4 and 5 are contributing fully to resist the base torque in the building. Consequently, an increase in strength of these planes leads to a proportional increase in the resisted base torque for all regions of the surface (Fig. 4c).

The lengthening of the constant base-shear branches of the BST surface has important consequences in terms of the dynamic behavior of the system. Suppose that we superimpose on top of the BST surface (Fig. 4c) the base shear and torque response histories of the system when subjected to an earthquake. Clearly, the response must be constrained to be inside the BST surface if the behavior of the structure is elastic or on the surface itself if it is inelastic. Thus, since the constant base-shear branches of the system have lengthened, it is very likely that the inelastic behavior of the system is going to be developed on them. Now, since these branches correspond to mechanisms in which all resisting planes in the y-direction yield, we expect relatively uniform displacement demands for all resisting planes. As a rule then, systems with larger (smaller) constant base-shear branches will tend to impose more (less) uniform displacement demands on the resisting planes. This idea will be explored further in the next section.

(c) **Asymmetry in stiffness**

It is well known that stiffness asymmetry, characterized by stiffness eccentricity, is an important parameter controlling the elastic response of asymmetric systems. As we will see later, it controls partially how the base shear and torque combinations move inside the BST surface. Then, it determines in what branches of the surface the inelastic behavior is likely to take place. However, the shape of the BST surface is independent of the stiffness asymmetry in the system, which controls only the distribution of forces among resisting planes in the elastic range. At collapse, the yield strength of the resisting planes, their locations, and the equilibrium conditions are the ones determining the ultimate base shear and torque resisted by the structure.

(d) **Asymmetry in strength**

Consider the system shown in Fig. 4d having asymmetry in strength. Relative to the reference case (Fig. 4a), resisting plane 1 has doubled its stiffness and strength, and planes 2 and 3 have reduced theirs to half of the initial value. As a result, the system (Fig. 4d) has important strength eccentricity $e_p/b = fa/2(1/2-2)/(3\,fa) = -0.25$. It is apparent that the most important effect of strength asymmetry is to skew and stretch the BST surface toward the second and fourth quadrants.

The surface changes for two reasons. First, recalling property 2 of the BST surfaces, there is a branch of the surface with slope equal to the position of resisting plane 1. This is the longest branch in Fig. 4d having a slope $dT/dV_y = -(fb/2)(3.5+5)/(4f) = -b/2$, the x-coordinate of plane 1. Besides, since this plane has (large) strength $2f$, the range of maximum and minimum base torques in the BST surface is very large, and the surface becomes skewed.

The skewness and stretching of the BST surface observed is expected to have important consequences on the inelastic seismic behavior of these systems. Intuitively, any of these systems excited well into the inelastic range will present inelastic behavior along the long branches (Fig. 4d), implying that the strongest resisting plane in the plan will remain essentially elastic while the other planes will yield significantly. Thus, the lateral capacity of the system provided mainly by the large strength of the strongest element will never be developed; the system will perform inefficiently showing a premature torsional mechanism that keeps the strongest element elastic. Several examples of this behavior have been observed during previous earthquakes [3].

(e) **Planwise distribution of strength**

Another factor that affects the shape of the BST ultimate surface is the distribution of strength along the building plan. Such effect is studied considering the system shown in Fig. 4e, which has increased strength in resisting plane 2 passing through the CM, as in a building with a strong central core of R/C walls. It is apparent that increasing the strength of resisting plane 2 relative to other planes has two effects: (1) it reduces the torsional capacity of the system, and (2) it produces a stretching of the constant base-torque branches of the BST surface associated with purely torsional mechanisms.

The first effect is obvious since a reduction in the strength of resisting planes 1 and 3 implies a reduction in the torsional capacity of the system. The second effect may be understood when looking at the pivot diagram shown in Fig. 4h. We recall from this figure that the purely torsional mechanisms corresponding to these branches are such that resisting plane 2 (Fig. 4e) goes from yielding in one direction to yielding in the other. Consequently, the length of the constant base-

torque branch is twice the strength of this plane and, hence, an increase in strength of this plane will imply an equal increase in the length of these branches.

The reduction in the torsional capacity of systems with very strong cores seems to suggest that these systems may undergo significant inelastic torsional deformations. However, such large rotations are not likely in a structure with a strong central core because the system will tend to be relatively symmetric in strength; they might come, however, from an exceptionally strong base rotation of the building foundation. Several examples to understand the behavior of such systems will be considered in the next section.

(f) **Number of resisting planes**

In order to study the change produced on the BST surface resulting from a larger number of resisting planes, we consider the building shown in Fig. 4f having five resisting planes in the y-direction and two in the x-direction. The planes are symmetrically located with respect to the CM and have the distribution of stiffness and strength shown in the figure.

Consistent with property 3 of the BST surface, the number of branches with finite slope for the system considered is now five, making the BST surface look rounder than the surface corresponding to the reference system. The two new branches of smaller slope correspond to building mechanisms that leave resisting planes 2 and 4 elastic.

Comparing the BST surfaces for the systems of Figs. 4f and 4a, both having the same shear and torque capacities, we observe that both surfaces differ only in the region corresponding to high values of base torque. This implies that the seismic response of buildings with three or more resisting planes should be for most practical cases very similar, unless unusually large values of base torque are developed. Further discussion of this observation is presented in the next section.

2.4 Response to unidirectional ground motion

In the previous section we analyzed the effects of different building characteristics on the shape of the BST surface, and predicted the consequences that changes in this surface might have in terms of the seismic response of a system. In light of these observations, we now study the earthquake response of asymmetric-plan systems. For this purpose we will examine the influence of five of the structural characteristics considered in the previous section on the response of single-story buildings having uncoupled lateral vibration period $T_y = 0.5$ sec in the y-direction, plan aspect ratio $a/b = .5$ ($b = 60$ ft), and subjected to the N-S component of the El Centro ground motion in the y-direction.

From now on, the stiffnesses and strengths of resisting planes will be given in terms of the reference values $k = 409$ kips/ft and $f = 10$ kips, respectively. The response results will be presented in a special format (see for example Fig. 5). Each row, a) through c), contains the response results of the building whose plan configuration is shown in the first column. Shown in the second column are the base shear and torque histories that have been superimposed on the BST surface. In the third column the displacements of the resisting planes at the edges and CM are presented. Finally, the force-displacement relation for these planes are shown in the fourth column.

2.4.1 Strength of resisting planes in the orthogonal direction

To study the effect of varying the strength of the resisting planes orthogonal to the direction of ground motion, consider the five structural configurations (a.1) through (e.1) presented in Fig. 5. These structural configurations are such that their lateral capacity in the y-direction is the same and equal to $0.12W$, where W is the weight of the structure, but their capacities in the x-direction vary from zero to a maximum of $0.08W$. All systems selected have equal normalized stiffness eccentricity $e_s/b = 0.125$ and strength eccentricity $e_p/b = 0.125$. Note that because of the increase in torsional stiffness introduced by the resisting planes in the orthogonal direction, the elastic responses of these systems are not necessarily identical. However, as shown by the similar elastic base shear and torque response histories shown in Figs. (a.2) through (c.2), the changes in elastic response among these systems are very small, implying that the differences observed next in their responses result mainly from their different inelastic properties.

Considering first the response in terms of the base shear and torque plot, we note the following interesting points. Firstly, as explained earlier (Fig. 4c), a change in the strength of the orthogonal resisting planes produces two effects in the shape of the BST ultimate surface: the torsional capacity T_o of the system and the length of the constant base-shear branches of the BST surface (Fig. 2) increase as these planes get stronger. The change in T_o does not seem to be crucial for these structures since very few base shear and torque combinations reach the condition of a purely torsional mechanism (constant base-torque branches in Figs. (a.2) through (e.2)); indeed, such mechanism occurs only at few instants in case (a.2), where no orthogonal resisting planes are present. On the other hand, the lengthening of the constant base-shear branches, representing an increase in the number of mechanisms that involve yielding of all y-direction planes, is very important since most of the nonlinear behavior will be developed along them.

Secondly, Fig. (a.2) shows that most of the nonlinear behavior experienced by the system with no orthogonal planes occurs along the two parallel branches of the BST surface with positive slope. According to the second property of these surfaces, this implies that resisting plane 3, the strongest element in the y-direction, remains essentially elastic at many instants during the response. Because this plane also works as the instantaneous center of plastic rotation during these instants, it is expected that resisting plane 1, the farthest plane from 3, will experience a significant increase in displacements relative to plane 3 due to the plan rotation. A corollary of this observation indicates that systems with no orthogonal resisting planes will attain their peak displacements associated to large rotations of the plan, as has been noted by earlier research [4].

Thirdly, as the strength of the orthogonal resisting planes increases (Fig. (a.1) to (e.1)), a larger proportion of the inelastic behavior migrates from the branches of the BST surface with positive slope (Fig. (a.2)) to the constant base-shear branches (Fig. (e.2)). This implies that systems with strong orthogonal resisting planes will see in many of their inelastic excursions mechanisms involving yielding of all resisting planes in the y-direction. Thus, more uniform displacement demands are expected for the resisting planes in these systems; equivalently, systems with strong orthogonal planes will undergo smaller rotations of the plan as has been noted earlier [5].

Finally, the above observation has important implications for the design of asymmetric plan structures. Let us consider, for instance, a typical retrofit scenario for an asymmetric structure like the one shown in Fig. (b.1). Let us assume that the damage after an earthquake has been classified as severe, moderate, and minor in resisting planes 1,2, and 3, respectively; also, the damage in the x-direction planes is classified as moderate. A good retrofit solution for this case, although not the only one, would be first to recover the initial strength of all y-direction resisting planes, but more importantly, to increase the strength of the orthogonal planes 4 and 5 beyond their original capacity to induce more uniform displacement demands on the y-direction planes (Fig. (e.2)).

The second and third observations above can be verified by considering the histories of displacements in the resisting planes (Figs. (a.3) through (e.3)). For building case a, the displacements of y-direction planes 1 to 3 are substantially different (Fig. (a.3)). In fact, the presence of large plan rotations about plane 3 is obvious from the large differences between displacement of planes 1 and 3. For future reference, the ratio between the peak displacements of these two planes is about 3.5. Note also that plane 3 yields mainly for negative displacements (Fig. (a.4)) while the opposite occurs for plane 1.

The displacement histories of building cases b through e (Figs. (b.3) through (e.3)) show how

the responses of the three y-direction planes become closer as a result of the increase in the strength of the orthogonal planes and consequent decrease in the plan rotations. For building case e (Fig. (e.3)), for instance, the ratio between the peak displacements between planes 1 and 3 has reduced to about 1.8, i.e., 50% with respect to case a (Fig. (a.3)), and more importantly, the resisting planes now yield in both directions (Fig. (e.4)). Further increase in the strength of the orthogonal planes would lead to more uniform displacement demands on the resisting planes.

2.4.2 Stiffness asymmetry

Let us consider the effect of stiffness asymmetry in the inelastic response of asymmetric structures by studying the response of the five structural configurations presented in Fig. 6 ((a.1) through (e.1)). The lateral capacities in the x and y-directions for all the systems are identical and equal to $0.08W$ and $0.12W$, respectively. Their normalized strength eccentricity $e_p/b = 0.125$ is also identical but the normalized stiffness eccentricity $e_s/b = 0, 0.05, 0.125, 0.25$ and 0.4 for building cases a (Fig. (a.1)) through e (Fig. (e.1)), respectively. As mentioned earlier (section 3.4 (c)), the BST surface of a building is independent of the stiffness eccentricity.

In spite of the stiffness symmetry of building case a (Fig. (a.1)), torsional motions are present in the system since the strength of resisting planes is not symmetrically arranged about the CM. Nevertheless, a large number of base shear and torque combinations still lie close to the zero torque axis and most of the inelastic behavior takes place along the constant base-shear branches of the BST surface, implying yielding of all resisting planes in the y-direction (Fig. (a.2)).

As the stiffness eccentricity corresponding to building cases b through e (Figs. (b.2) through (e.2)) increases, larger values of base torque are developed in these systems. If the stiffness eccentricity is large, as in building case e (Fig. (e.2)), the base shear and torque combinations tend to lie on the second and fourth quadrants of the BST surface. Such is the case because we have assumed positive stiffness eccentricity (CS at the right of the CM) in the buildings, implying that positive base shears should frequently accompany clockwise (negative) base torques and vice-versa.

More important, as the stiffness eccentricity increases among systems more base shear and torque combinations move to the branches of the BST surface with positive slope, as can be checked by comparing building cases a (Fig. (a.2)) and c (Fig. (c.2)). This implies, as it should, that systems with large stiffness eccentricity will experience inelastic behavior in mechanisms that leave the stiffest resisting plane in the plan, plane 3, essentially elastic, while producing plan rotations

about this plane. Consequently, the displacements of resisting plane 1, the farthest plane from plane 3, will be increased substantially because of the plan rotation. Note, however, that to obtain a significant shift of the base shear and torque combinations from the mainly translational mechanisms (constant base-shear branches) toward mechanisms leaving the stiffest plane essentially elastic (positive slope branches), rather large values of the stiffness eccentricity, say $e_s/b \geq 0.25$, are required.

These observations can all be verified when looking at the displacement histories (Fig. (a.3) through (e.3)) and force-displacement histories (Figs. (a.4) through (e.4)). The displacements of resisting planes in cases a, b, and c do not present substantial differences as expected from their similar base shear and torque histories. On the other hand, as stiffness eccentricity increases, say over $0.25b$ (Fig. (e.1)), an important increase in displacements (Fig. (e.3)) is observed for plane 1 as a result of the large plastic rotations of the building about the stiffer plane 3.

Thus, stiffness eccentricity is responsible for changing the pattern of the base shear and torque response history inside the BST surface. So, unless this change in pattern induces changes in the region of the BST surface where the inelastic behavior takes place, stiffness eccentricity will not affect the response as importantly as it does in the elastic case.

2.4.3 Strength asymmetry

The effects of strength asymmetry are studied considering the five structural configurations shown in Fig. 7 (cases (a.1) through (e.1)). These systems are such that they all have the same normalized stiffness eccentricity $e_s/b = 0.125$ and variable normalized strength eccentricities $e_p/b = 0, 0.0625, 0.125, 0.375$, and 0.342, respectively. Also, their lateral capacities are $0.08W$ and $0.12W$ in the x and y-directions, respectively, and all have the same torsional capacity $T_o = 0.13W(b/2)$ kips-ft. The elastic response of systems a through e will be identical, and the differences in behavior shown next can be attributed only to the change in shape of the BST surface because of strength asymmetry.

Strength asymmetry has an important effect on the shape of the BST ultimate surface as it was noted earlier (Fig. 4d) and is shown again in Fig. 7 (cases (a.2) through (e.2)). Initially, the BST surface in building case a (Fig. (a.2)) is symmetric about both axes. This symmetry is lost gradually as the strength asymmetry in buildings a through e increases, making the surfaces to narrow and lean toward the first and third quadrants (Fig. (e.2)). Such is the case because

resisting plane 3, is the strongest plane in the plan and it is farther from the CM.

The base shear and torque history corresponding to building case a (Fig. (a.2)) shows that the inelastic behavior of the system is developed along the constant base-shear branches of the BST surface, implying that different resisting planes will undergo similar displacement demands as a result of the predominantly translational displacements. For future reference, the ratio between the peak displacements between planes 1 and 3 is in this case about 1.25 (Fig. (a.3)).

As the strength asymmetry increases, more base shear and torque combinations start to migrate from the constant base-shear branches (Fig. (a.2)) of the BST surface toward the branches with positive slope (Fig. (e.2)), which are associated with torsional mechanisms leaving the strongest resisting plane (plane 3) essentially elastic during the earthquake. This fact results from the leaning of the surface and consequent shift of the constant base-shear branches to a higher region of the torque axis (Fig. (e.2)). Its consequence in terms of the seismic response of these structures is dramatic; large plastic rotations will tend to be produced about the strongest plane (plane 3), leading to huge displacement demands on the planes farther from it (Fig. (e.3)).

The above observations are also apparent when we analyze the displacement and force-displacement histories for each resisting plane (Figs. (a.3) through (e.3)). The displacement in plane 3, the strongest plane in the plan, is substantially reduced from case a to case e, although its stiffness is kept constant; contrarily, the displacement in plane 1, the weakest element in the plan, increases substantially between these cases. Indeed, the ratio between peak lateral displacements of planes 1 and 3 has changed from 1.25 in building case a (Fig. (a.3)) to 6 in case e (Fig. (e.3)). More important, building case e, which represents large asymmetry in strength, demonstrates that the strength of the strongest plane 3 is barely used since the inelastic behavior of the system is such that a torsional mechanism, about this plane, is activated most of the time.

Strength asymmetry is then an important parameter controlling the behavior of asymmetric structures; its importance comes from the way it controls the shape of the BST surface. Reducing the strength eccentricity in a system usually leads to more uniform displacement demands in all resisting planes, even if the system has significant stiffness eccentricity as shown by building case a (Figs. (a.2), (a.3), and (a.4)). Increasing the strength eccentricity of a system implies to develop torsional mechanisms that leave the strongest resisting plane essentially elastic during the response; thus, forcing other resisting planes farther from this plane to deform considerably.

2.4.4 Planwise distribution of strength

In order to study the changes in building response due to changes in the planwise distribution of strength, we consider the five building cases shown in Fig. 8 (cases (a.1) through (e.1)). All these buildings have the same stiffness eccentricity $e_s/b = 0.125$ but are symmetric in strength. The systems also have identical lateral capacities $0.08W$ and $0.12W$ in the x and y directions, respectively; their torsional capacities, however, vary from $T_o = 0.02W(b/2)$ kip-ft in case a to $0.1W(b/2)$ kip-ft in case e. This variation in strength is such that building case a (Fig. (a.1)) corresponds to a system with a very strong central core and weak resisting planes along the two edges in the y-direction, and building case e (Fig. (e.1)) is just the opposite, i.e., a system with very strong planes along the edges and a weak central core. Note that the elastic responses of all these systems are identical.

The BST surfaces corresponding to each of the five buildings are shown in Fig. 8 (cases (a.2) through (e.2)). Shifting the strength of resisting planes from a central core (Fig. (a.2)) to the edges (Fig. (e.2)) has two effects: (1) it increases the torsional capacity T_o of the system, and (2) it shortens the constant base-torque branches of the BST surface associated with predominantly torsional mechanisms.

The base shear and torque histories indicate that in spite of the small torsional capacity of building case a, no combination of base shear and torque is able to reach a purely torsional mechanism (constant base-torque branches of the BST surface in Fig. (a.2)). Such is the case because the system is unable to develop large base torques as a result of the small strength of resisting planes 1 and 3 and ends up responding primarily in translation as indicated by the essentially identical displacement histories of planes 1,2, and 3 (Fig. (a.3)). As the strength of the resisting planes at the edges increase, larger torques are developed in the systems together with an increase in the torsional capacity T_o. These larger torques make the system undergo yielding along the inclined branches of the BST surface (Fig. (e.2)), implying mechanisms with a significant torsional component. As a result, substantially different displacement demands occur in planes 1 and 3 (Fig. (e.3)).

Basically, the observation above is saying that a weak torsional structure is naturally isolated against the elastic torsional behavior imposed by stiffness asymmetry at the expense of larger deformations in the edge resisting planes. These results do not necessarily imply that building case a is always a better solution than building case e. Indeed, for service conditions of the structure

where accidental torsion coming from base rotational motion could be present, undesirably large displacements at the edges could be produced as a result of the torsional flexibility of the structure [6].

2.4.5 Number of resisting planes

So far we have considered buildings with three resisting planes along the direction of ground motion. Let us consider now the effect of having more resisting planes by studying the response of the three buildings shown in Fig. 9 (cases (a.1) through (c.1)). Buildings A,B, and C have 3,5, and 7 resisting planes in the y-direction, respectively, and they all have identical lateral capacities $0.08W$ and $0.12W$ in the x and y-directions, respectively. Their torsional capacities T_o vary, however, from $0.16W(b/2)$ kip-ft in case a to $0.1W(b/2)$ kip-ft in case c. All systems also have identical normalized stiffness and strength eccentricities $e_s/b = e_p/b = 0.125$. Note that the elastic response of these systems are not necessarily identical because their torsional stiffnesses decrease as the number of resisting planes increase. It can be shown, however, that the differences in the elastic response among the systems are small.

As mentioned before, increasing the number of resisting planes produces a rounding effect on the BST surface, especially for regions of large torque (Figs. (a.2) through (c.2)). However, since the inelastic behavior in these systems does not take place in this region of the BST surface, we expect similar responses in all configurations. This expectation is verified by looking at the displacement histories of the resisting planes (Fig. (a.3) through (c.3)), which show very little change among configurations. This observation has also been noted in different terms by earlier researchers [e.g.,5].

In conclusion, for analysis and design purposes, most multiple resisting plane structures could be reasonably approximated by a three plane model, if the latter matches certain minimum conditions of the actual structure, such as its elastic properties, lateral and torsional capacity, and location of resisting planes dictating the main slope of the BST surface. In other words, the three-plane model used to analyze the structure only needs to provide a close representation of the region of the BST where the inelastic behavior is localized. For instance, for the five-plane building shown in Fig. (c.1), according to the BST behavior presented in Fig. (c.2), the three-plane model used for the system could be the one presented in Fig. (a.1).

2.5 Response to bidirectional ground motion

In the previous sections we have considered the response of asymmetric buildings subjected to a single component of ground motion. However, most buildings in reality are subjected to bidirectional ground motion. Thus, it is the objective of this section to study, conceptually, the response of asymmetric buildings when both ground motion components act simultaneously.

Let us start considering the three-dimensional BST surface and the factors that control its shape. These factors were already described in section 3.4; the only difference here is that the normalized base shear in the x-direction $\hat{V}_x = V_x/V_{xo}$ is now assumed to vary between -1 and 1 instead of being fixed at 0 as it was in Fig. 4. Shown in Fig. 10 is the three-dimensional BST surface for several buildings; the cross-section of these surfaces at $V_x = 0$ was already presented in Fig. 4. The effect of the base shear in the x-direction is, as expected, to reduce the torsional capacity of the system proportional to $\hat{V}_x$; the proportionality constant being the torsional capacity provided by the resisting planes in the orthogonal direction (e.g., $2f(a/2)$ in this case). Except for this reduction in torsional capacity, the results presented in Figs. 10 and 4 show no difference; therefore, the observations stated before about the BST surface using $V_x = 0$ still carry over for other values of the base shear V_x.

In order to understand the behavior better, consider the seismic response of the buildings shown in Fig. 11 (case (a.1)) subjected to the N-S component of El Centro in the y-direction and five versions of its E-W component in the x-direction scaled by factors $\alpha = 0, 1$, and 3. The building considered has lateral capacities equal to $0.12W$ in both principal directions and torsional capacity equal to $0.15W(b/2)$. Besides, it has stiffness eccentricity $e_s/b = 0.125$ and strength eccentricity $e_p/b = 0.0625$.

If there is no ground motion in the x-direction ($\alpha = 0$), the base shear and torque histories of the system must stay inside, or on, the BST ultimate surface corresponding to $V_x = 0$ (Fig. (a.2)). Note that the inelastic behavior of the system is developed mainly on the constant base-shear branches of the BST surface corresponding to predominantly translational mechanisms (Fig. (a.3)), and that the ratio between the peak displacements at planes 1 and 3 is about 1.8.

As the intensity of the ground motion in the x-direction increases, the base shear and torque histories start moving out of the $V_x = 0$ plane of the BST surface, describing trajectories in the three-dimensional space spanned by V_x, V_y, and T (Figs. (b.2) through (e.2)). Furthermore, yielding occurs in resisting planes 4 and 5, reducing the proportion of base torque resisted by these planes.

In order to see this, we have included in Figs. (a.3) through (e.3) the BST surface corresponding to the two base shear values $V_x = 0$ and $V_x = V_{xo}$. As a result of the increase in ground motion intensity (α increase), the inelastic behavior of the system migrates from the constant base-shear branches of the surface at $V_x = 0$ (Fig. (a.3)) to the inclined branches of the surface at $V_x = V_{xo}$ (Fig. (e.3)). This effect is also clearly observed when looking at the spreading of the base shear and torque combinations from the $V_x = 0$ plane (Fig. (a.2)) toward the $V_x = V_{xo}$ plane (Fig. (e.2)) of the surface.

An important practical consequence of the above observation is that buildings having substantial yielding in the orthogonal resisting planes are almost always expected to develop torsional mechanisms in their inelastic response. These mechanisms will tend to reduce the displacement demands on the strongest resisting plane (plane 3, Fig. (a.1)) while increasing the displacements in the planes farther from it (plane 1). For example, the ratio of peak displacements of planes 1 and 3 increases from 1.8 in case a (Fig. (a.4)) to 2.8 in case e (Fig. (e.4)).

At this point it is pertinent to comment about the controversial issue of whether the orthogonal resisting planes should or should not be considered in the analytical model used to analyze an asymmetric structure [7]. According to these results (Fig. 11), in the academic case of no ground motion in the orthogonal direction, a model which considers the full strength of orthogonal resisting planes could be used. On the other extreme, if the ground motion component in the orthogonal direction produces many extended intervals of yielding in the resisting planes along this direction, an analytical model which disregards the orthogonal resisting planes would be appropriate. The BST surface is associated with base shear $V_x = 0$ for the first model and with $V_x = V_o$ for the second model. Neither of the two models is correct, because the actual forces travel, as shown in Figs. (a.2) through (e.2), continuously along different regions of the BST surface. Care should then be exercised in interpreting available results of asymmetric structures since this effect alone may induce significant discrepancies in displacement demands predicted by both simplified models.

2.6 Conclusions

This study of the seismic behavior of asymmetric buildings has led to the following conclusions:

1. Base shear and torque response histories, especially in conjunction with the BST surface, are a useful conceptual tool for understanding the behavior of different asymmetric buildings. The BST surface contains essentially all the information necessary to describe the inelastic

properties of a system. Moreover, its shape is directly related to the yielding mechanisms of the structure and, thus, controls the relative displacement demands among resisting planes.

2. The factors that determine the shape of the BST surface and, hence, influence importantly the inelastic behavior of an asymmetric plan building are the: (1) lateral and torsional capacities of the system, (2) strength of the resisting planes in the orthogonal direction, (3) strength eccentricity, (4) planwise distribution of strength, and (5) intensity of the ground motion in the orthogonal direction.

3. Resisting planes in the orthogonal direction control the length of the constant base-shear branches of the BST surface corresponding to predominantly translational mechanisms that involve yielding of all resisting planes in the direction of ground motion. Consequently, an increase in the lateral strength of the orthogonal planes leads to more uniform (less plan rotation) displacement demands of the resisting planes along the direction of ground motion.

4. Stiffness eccentricity does not affect the shape of the BST surface; however, it controls importantly where on this surface the system develops its inelastic behavior. An increase in the stiffness eccentricity of the system is reflected by a tendency of the base and torque combinations to lie in certain quadrants of the surface. Accordingly, the inelastic behavior of the system always tends to develop in these quadrants.

5. Strength eccentricity controls the width and skewness of the BST surface. As a result, the response of strength asymmetric systems is always biased to develop mechanisms that leave the strongest resisting plane in the plan essentially elastic while increasing importantly the deformations of planes farther from the elastic plane.

6. Changes in the planwise distribution of strength produces changes in the torsional capacity of the system and in the length of the constant base-torque branch of the BST surface corresponding to predominantly torsional mechanisms of the structure. It has been observed that a reduction in the torsional capacity of stiffness asymmetric systems may produce, at the expense of larger displacements, more uniform displacement demands among resisting planes.

7. An increase in the number of resisting planes in the structure leads to rounder BST surfaces. Analysis of several building configurations has shown that the change in building response

due to this rounding effect is in most cases small. Further, it has been noted that as long as the region of the BST surface where the inelastic behavior takes place remains invariant, the effect of structural characteristics controlling other regions of the surface can be neglected.

8. The existence of an orthogonal component of ground motion implies a reduction in the torsional capacity of the building as a result of the lateral motion in that direction. Because of this reduction, the inelastic behavior in these systems usually involves predominantly torsional mechanisms that concentrate the inelasticity in the resisting planes farther from the strongest plane, which usually remains essentially elastic. However, if the orthogonal component of ground motion is not intense, the resisting planes in that direction may be assumed to contribute to resist the base torque and could be included in the building model. On the other hand, for intense ground motion, frequent yielding of these planes is expected and, for all practical purposes, they should not be included in the model. In reality, the actual behavior of the system is actually bounded by these two cases.

2.7 References

1. Inaudi J.A. and De la Llera J.C., 'Dynamic analysis of nonlinear structures using state-space formulation and partitioned integration schemes', Report No. EERC 92/18, University of California, Berkeley, CA., Nov. 1992.

2. Newmark, N.M., 'A method of computation for structural dynamics', Proceedings ASCE 85(EM3), 67-94 (1959).

3. Rosenblueth, E. and Meli, R.,'The 1985 earthquake: causes and effects in Mexico City', Concrete International ACI, pp. 23-34, May 1986.

4. Tso, W.K. and Sadek, A.W., 'Inelastic seismic response of simple eccentric structures', Journal of Earthquake Engineering and Structural Dynamics 19, 255-269 (1985).

5. R. K. Goel and A. K. Chopra, 'Inelastic seismic response of one-story, asymmetric plan systems', Report No. EERC 90/14, University of California, Berkeley, CA., Oct. 1990.

6. De la Llera, J.C., and Chopra, A.K., 'Accidental torsion in buildings due to base rotation', Earthquake Engineering and Structural Dynamics. To be published.

7. Correnza, J.C. and Hutchinson G.L., 'Effect of transverse load-resisting elements on inelastic earthquake response of eccentric-plan buildings', Earthquake Engineering and Structural Dynamics 23, 75-89 (1994).

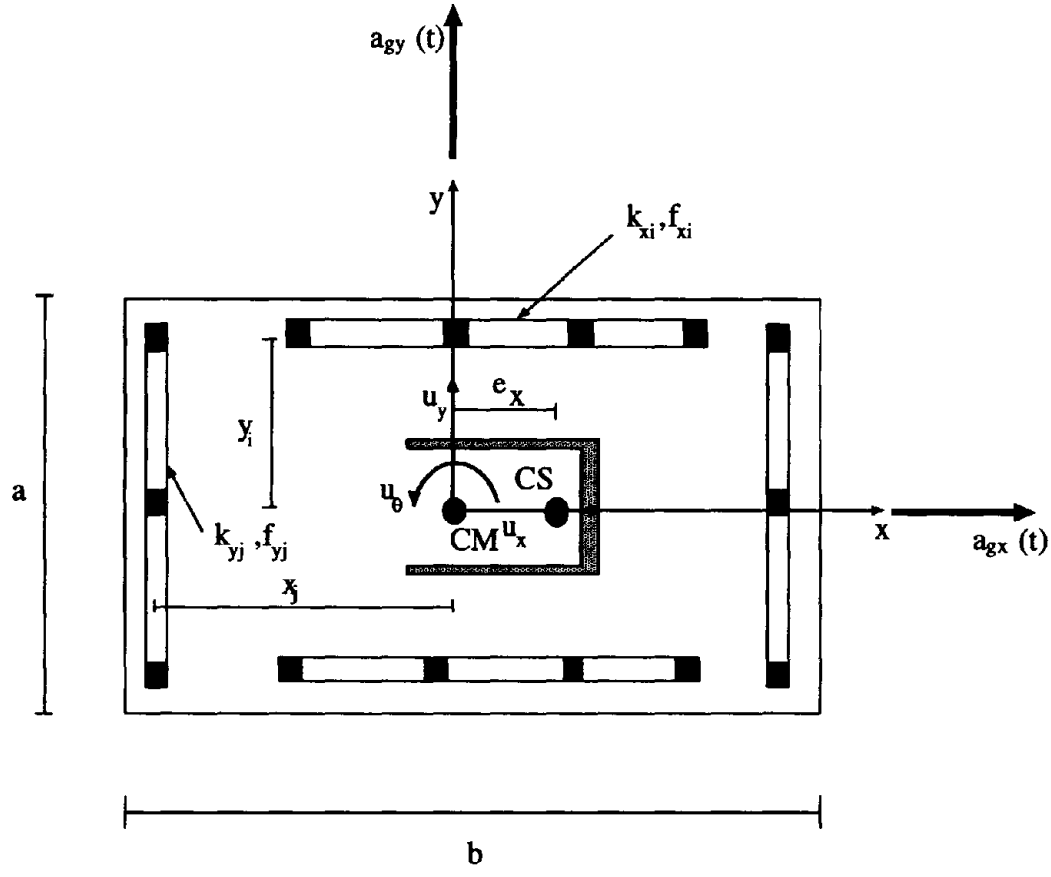

Figure 1 Typical plan of buildings considered

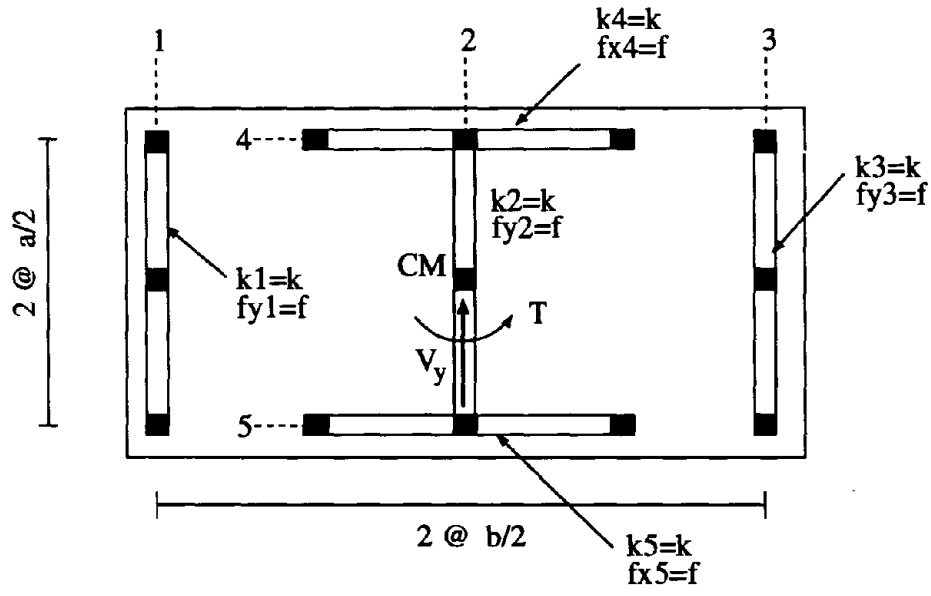

a)

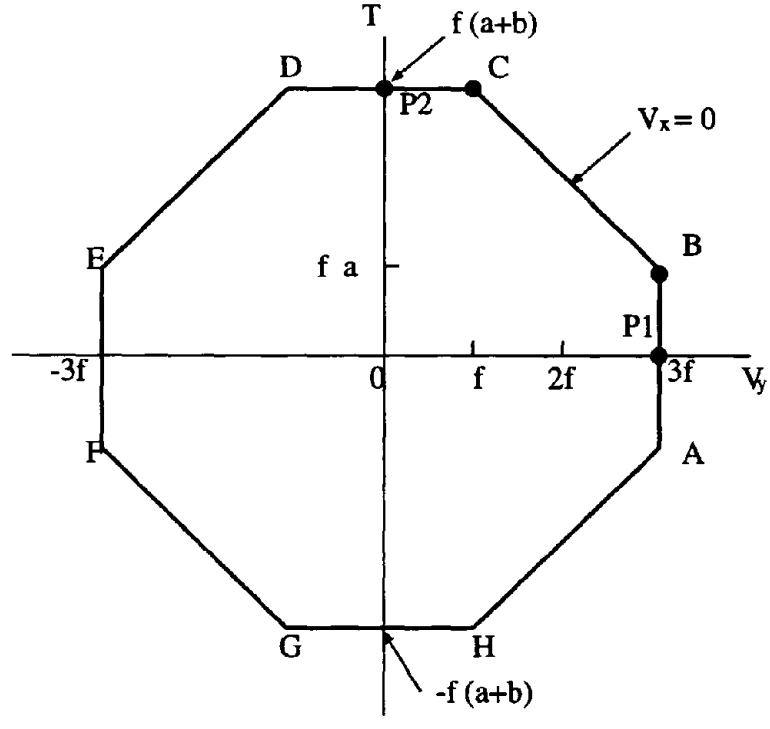

b)

Figure 2 Example for the construction of a BST ultimate surface

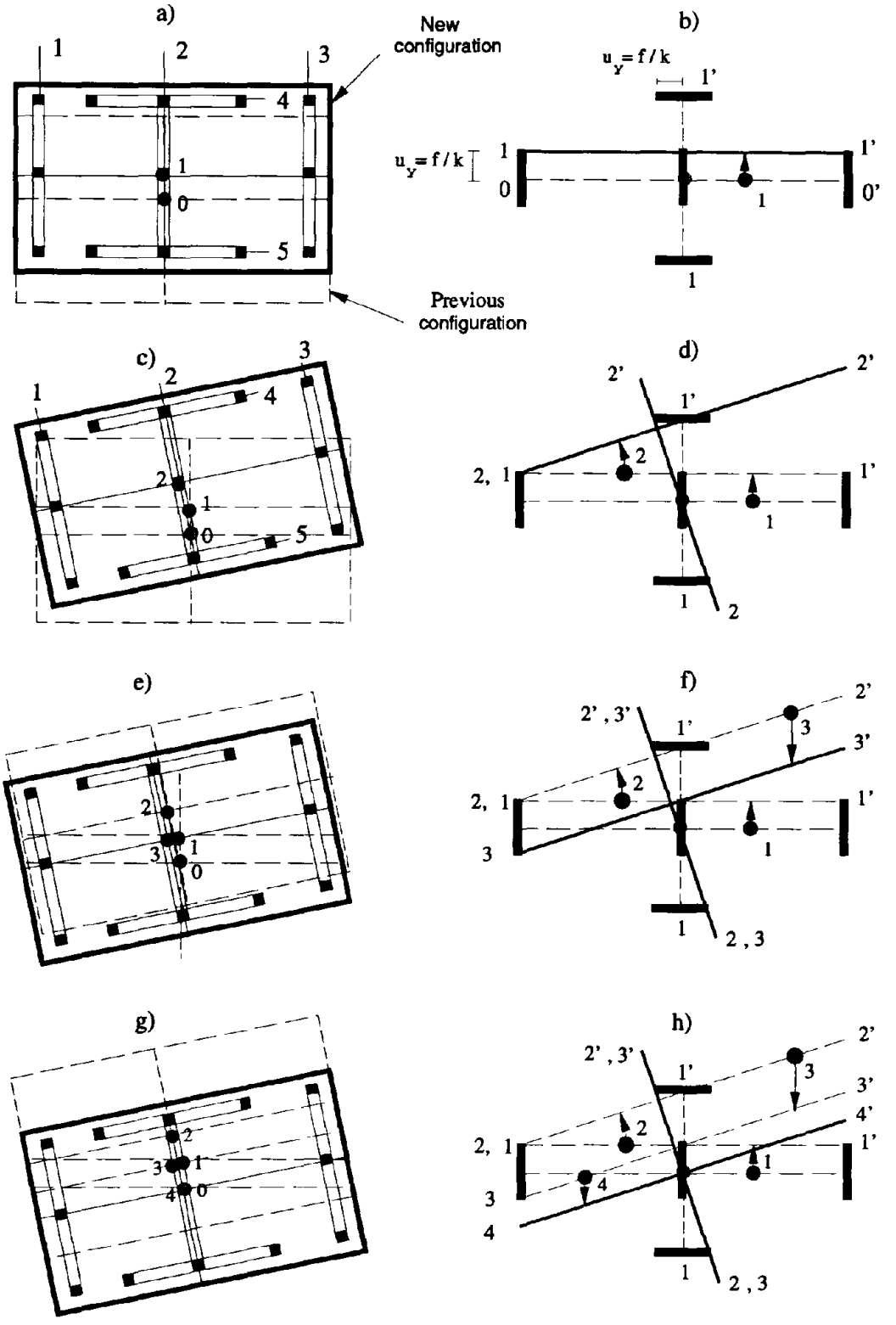

Figure 3 Construction of the BST surface in the first quadrant

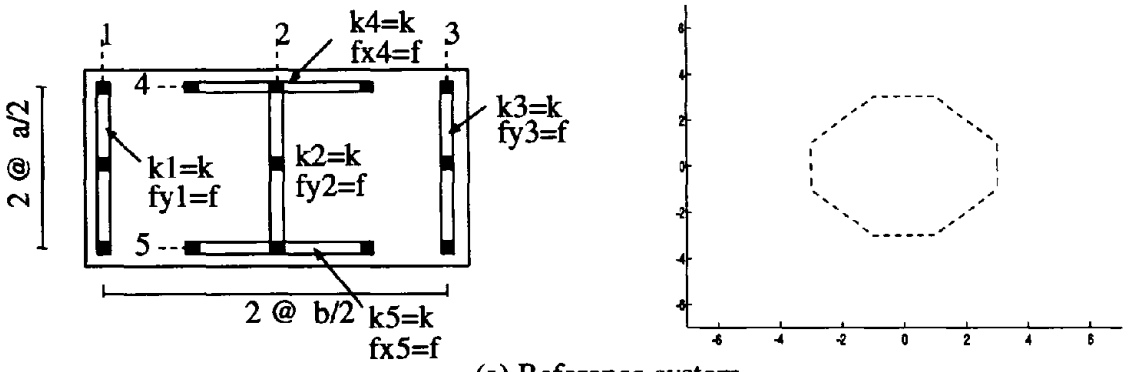

(a) Reference system

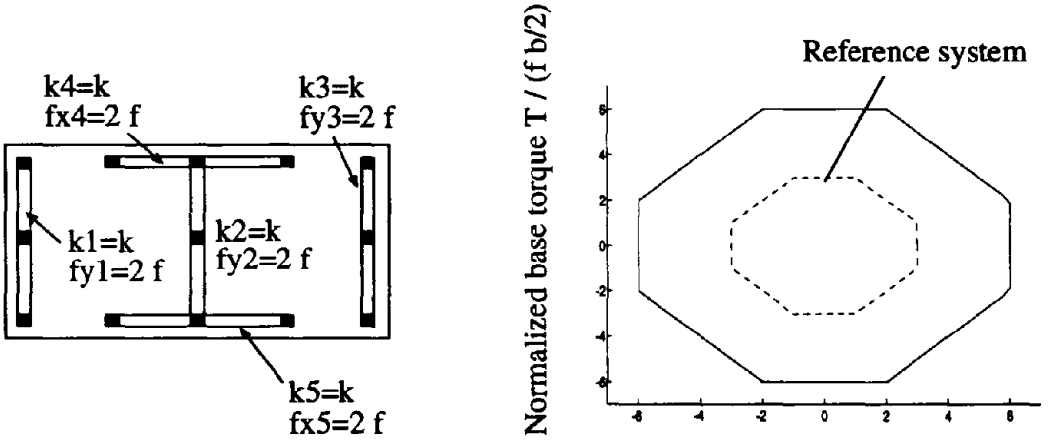

(b) Global increase in strength

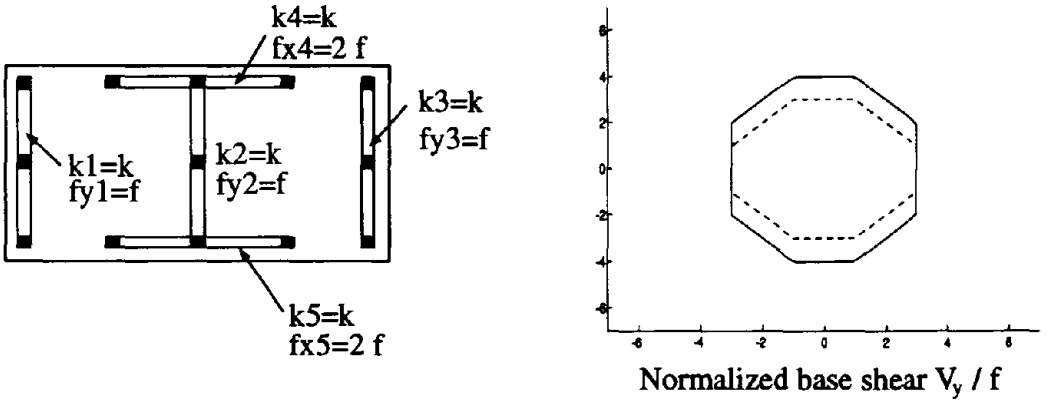

(c) Increase in strength of orthogonal resisting planes

Figure 4 Effect of different parameters on the shape of the BST surface

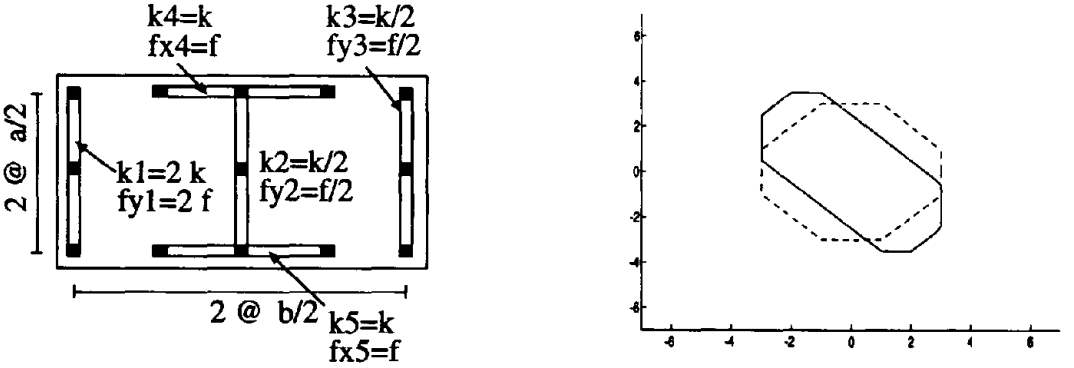

(d) Strength asymmetry

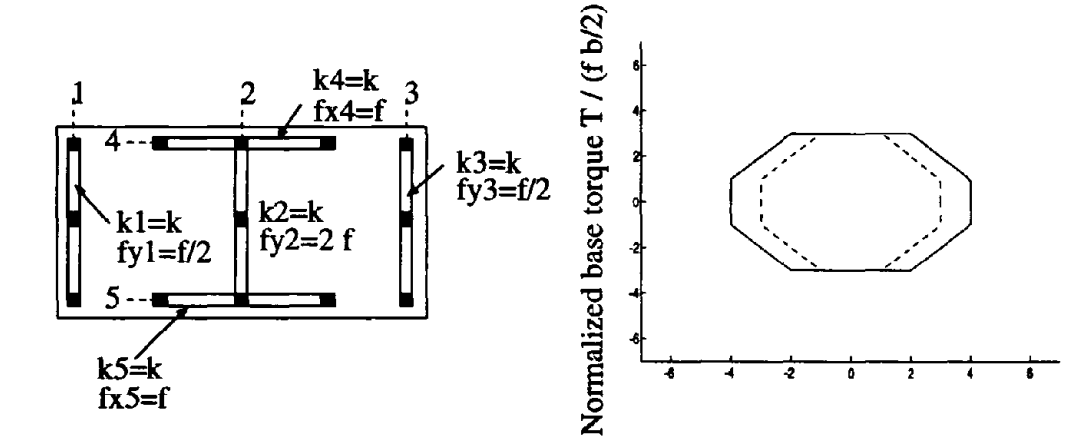

(e) Planwise distribution of strength

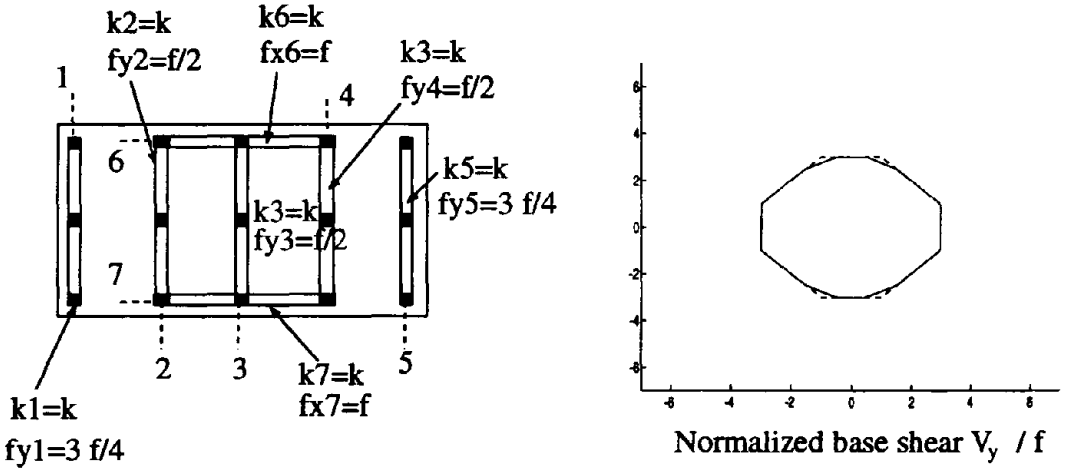

(f) Number of resisting planes

Figure 4 (cont.)

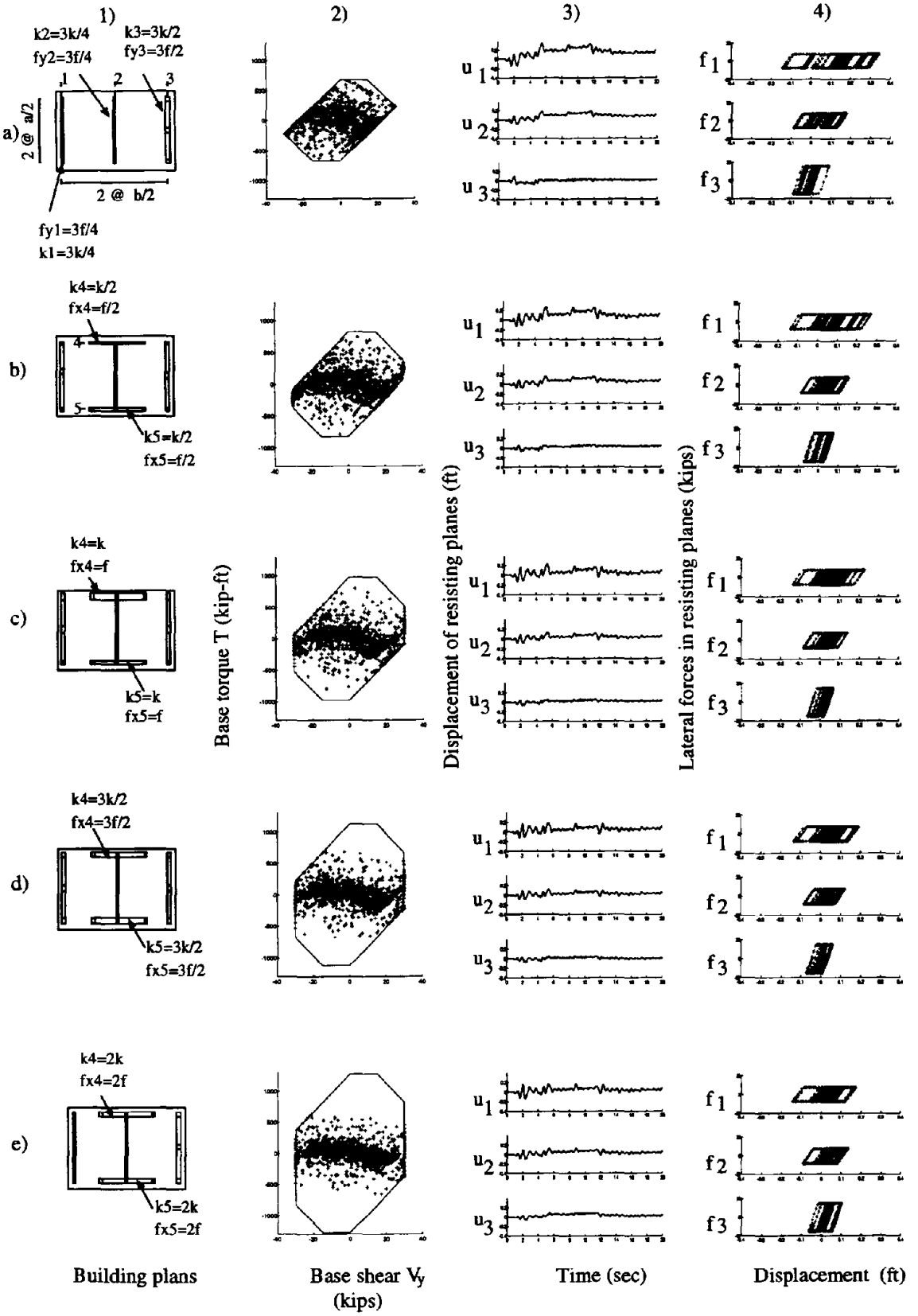

Figure 5 Effect of orthogonal resisting planes on the seismic response of asymmetric buidings

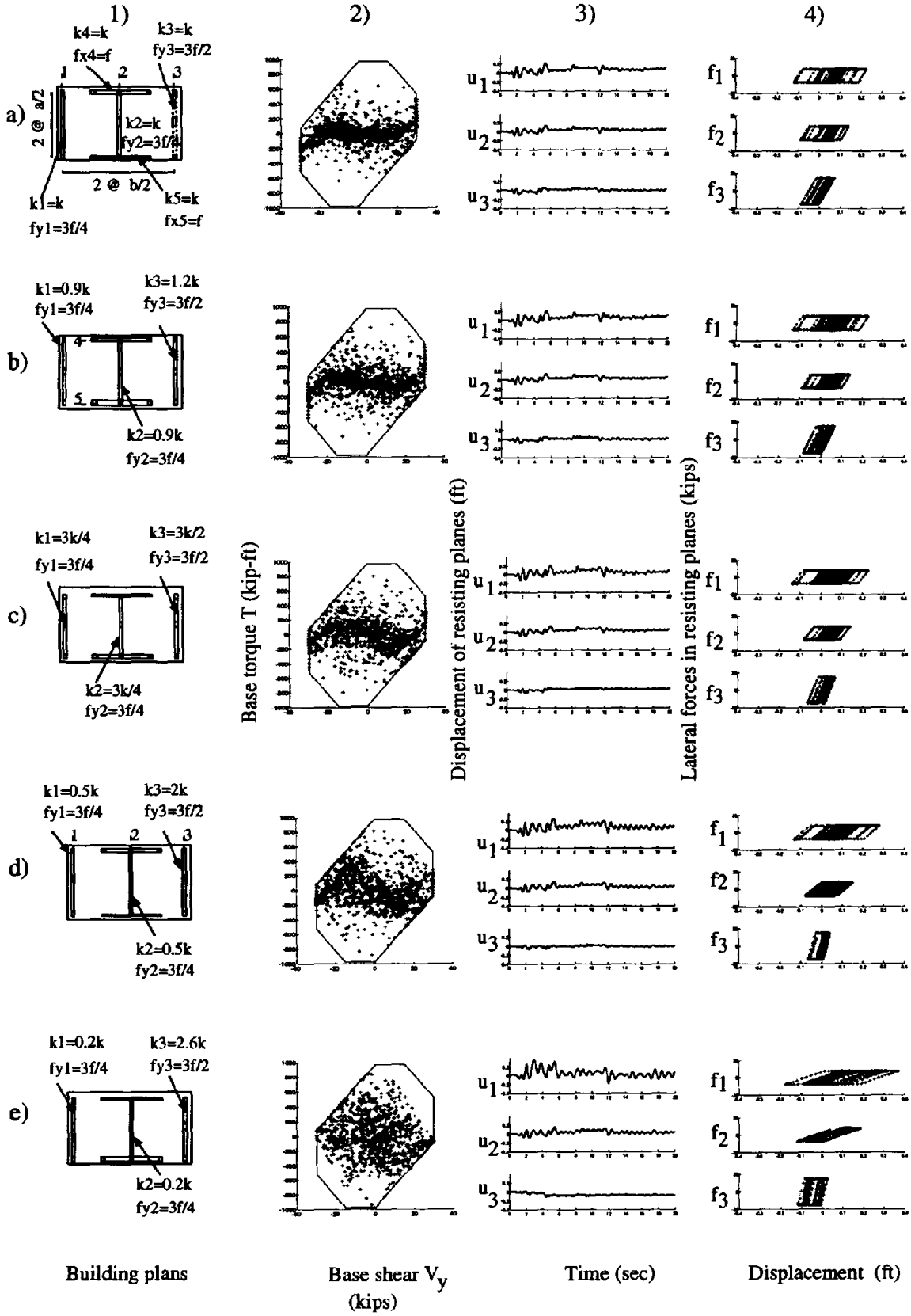

Figure 6 Effect of stiffness eccentricity on the seismic response of asymmetric buildings

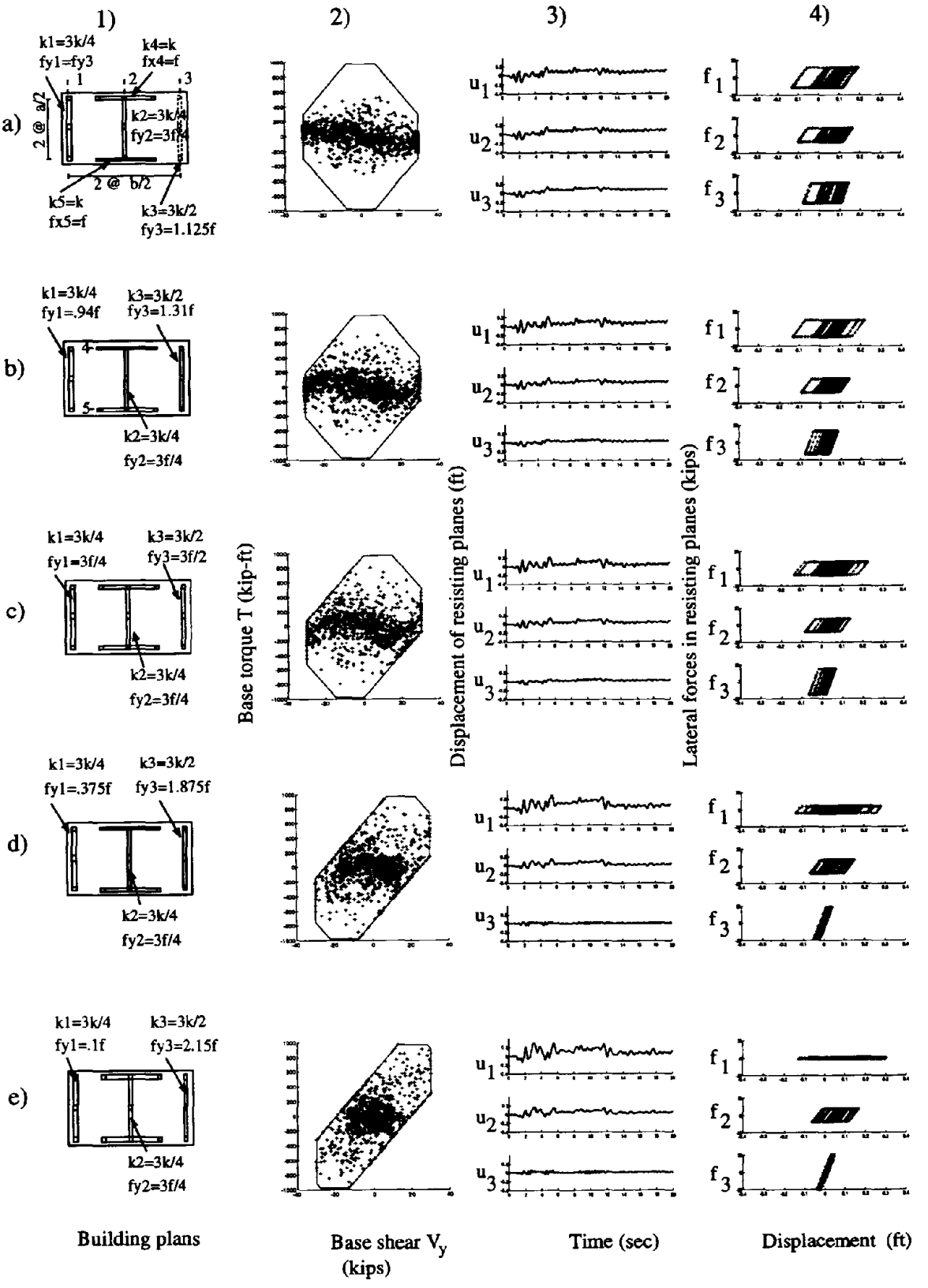

Figure 7 Effect of strength eccentricity on the seismic response of asymmetric buildings

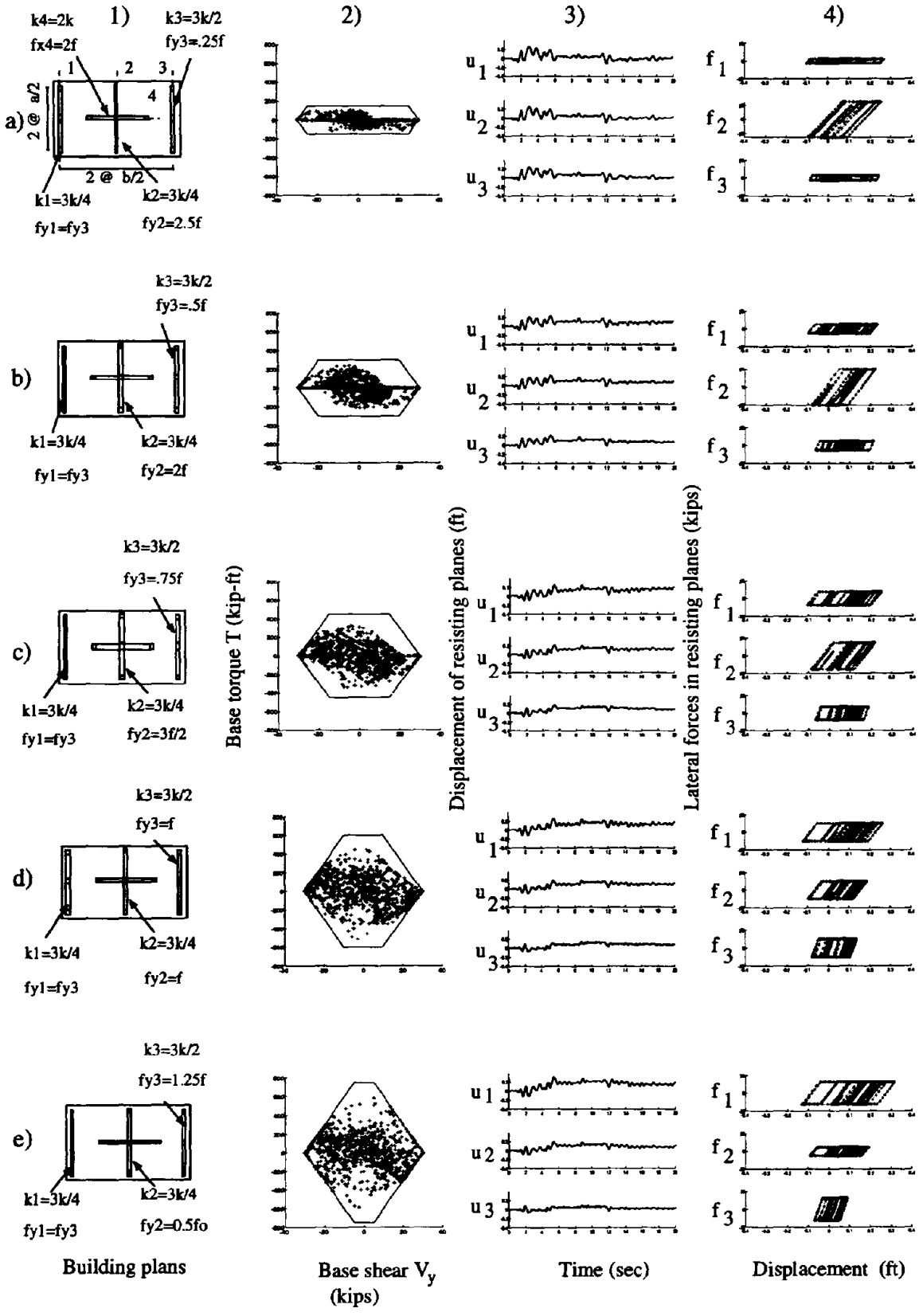

Figure 8 Effect of the planwise distribution of strength on the seismic response of asymmetric buildings

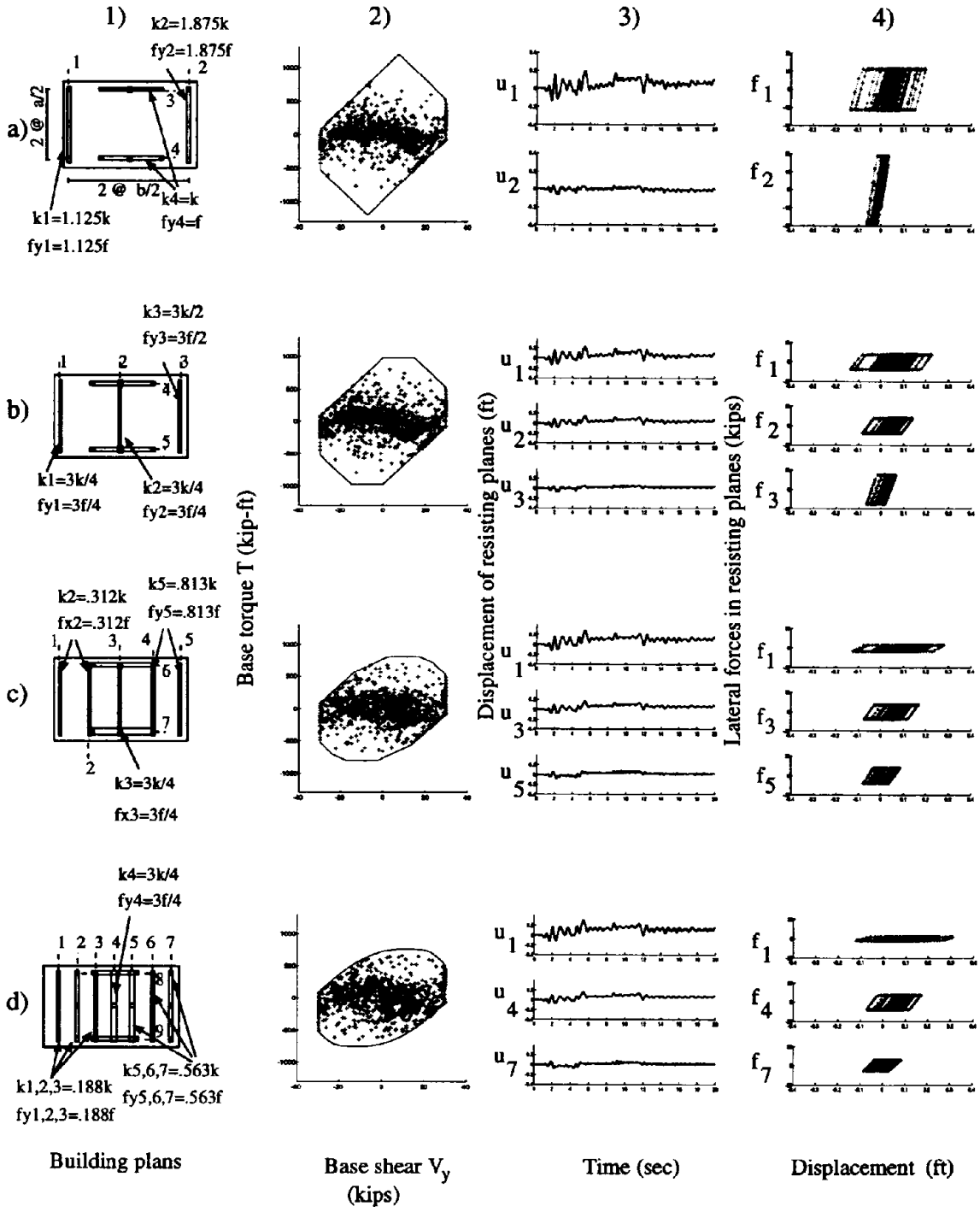

Figure 9 Effect of number of resisting planes on the seismic response of asymmetric buildings

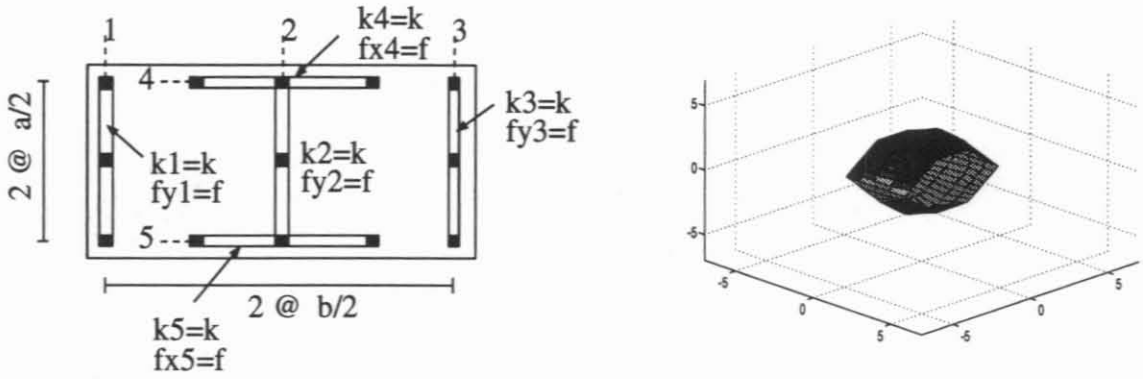

(a) Reference system

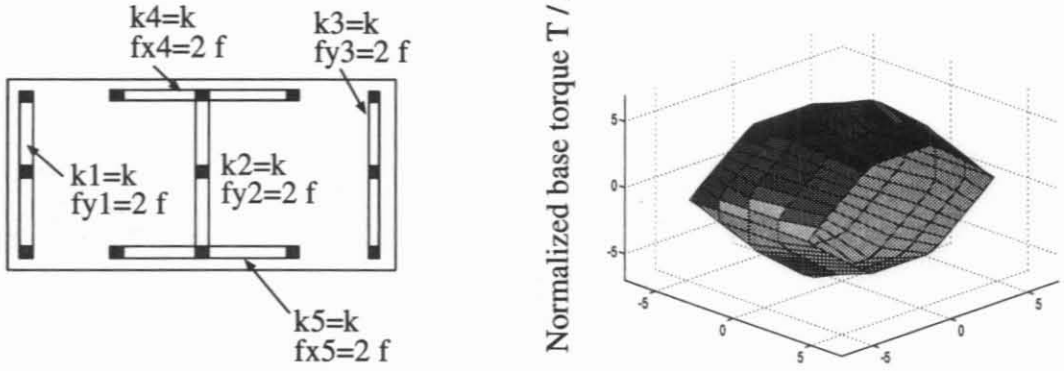

(b) Global increase in strength

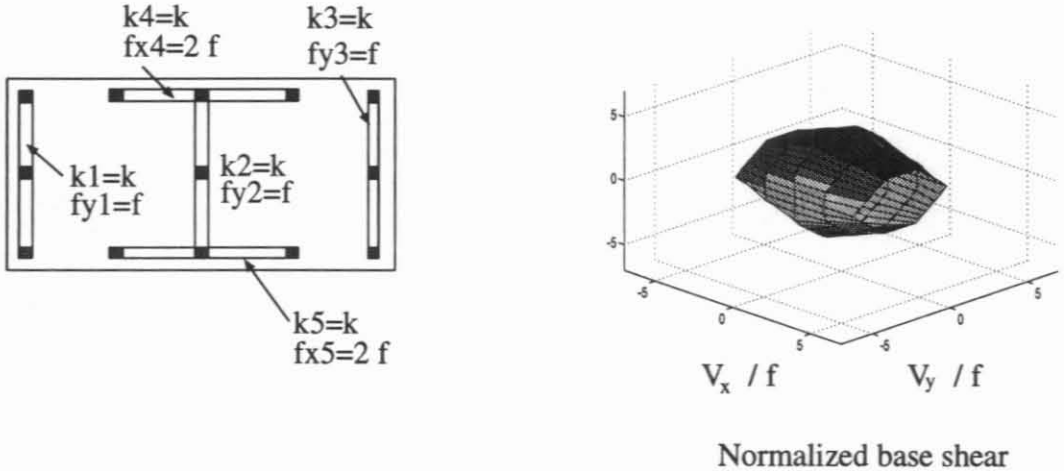

(c) Increase in strength of orthogonal resisting planes

Figure 10 Effect of different parameters on the shape of the three-dimensional BST surface

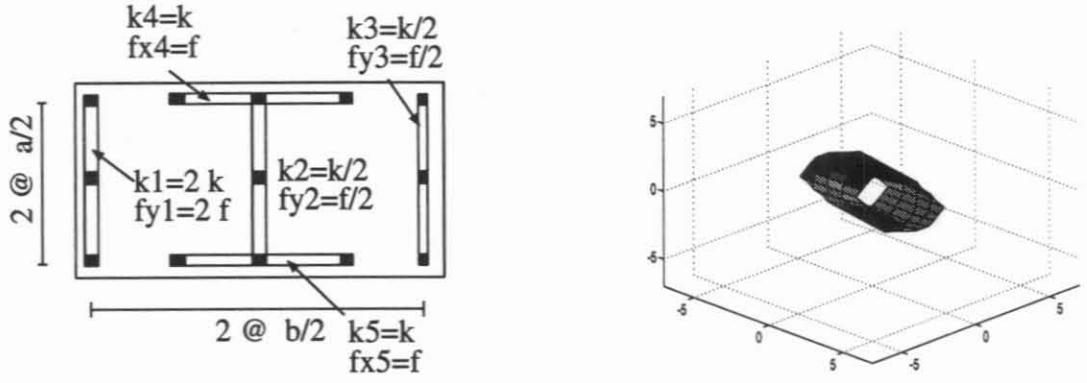

(d) Strength asymmetry

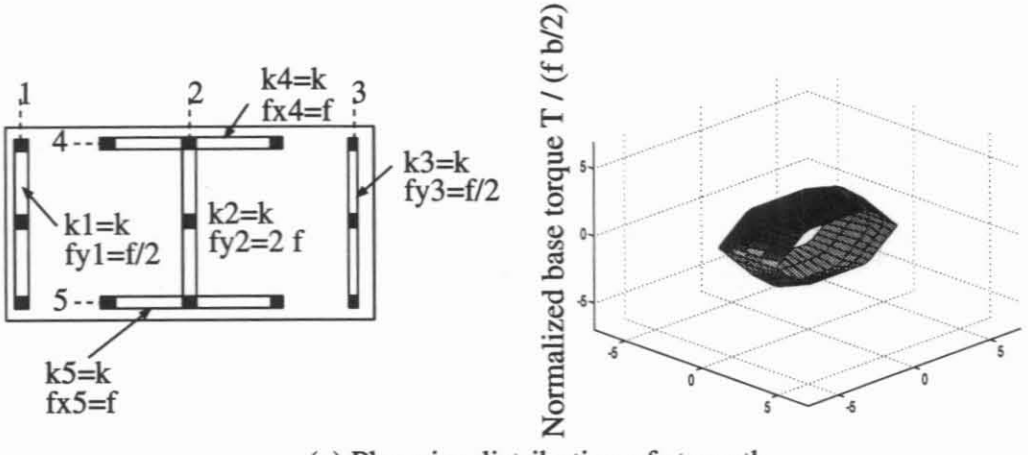

(e) Planwise distribution of strength

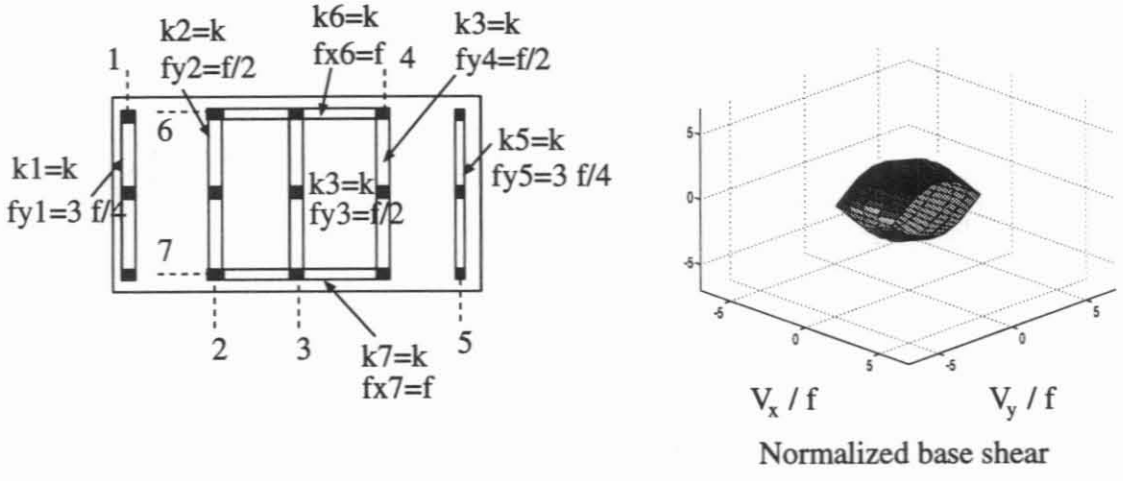

(f) Number of resisting planes

Figure 10 (cont.)

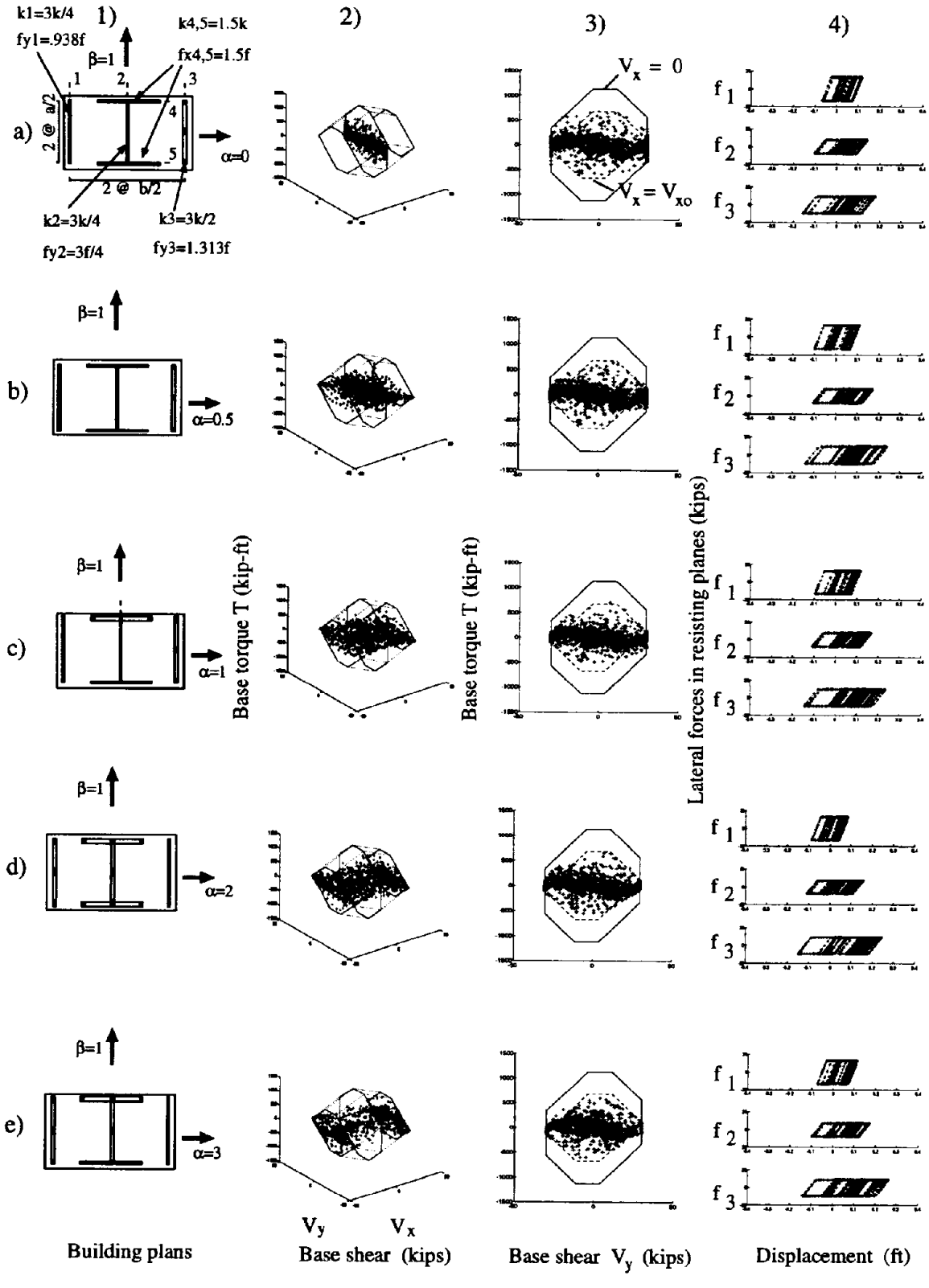

Figure 11 Effect on the seismic response of asymmetric buildings due to the ground motion component in the orthogonal direction

APPENDIX A: Computation of BST ultimate surfaces

This appendix presents the algorithm used to compute the BST surface for the buildings considered in this investigation. In principle, each point on the BST surface is computed by a nonlinear static analysis of the structure following, for instance, the algorithm shown schematically in Fig. A.1. Let us suppose that we first need to compute a section of the BST surface corresponding to a base shear $V_x = V^*$ in the x-direction. For doing so we may use the the following procedure:

1. Apply loads V_y and T at the ratio $\hat{m} = (T/T_o)/(V_y/V_{yo})$ and with magnitudes sufficiently large as to produce collapse in the structure (Fig. A.1). Note that for efficiency in the numerical computation of the surface it is convenient to normalize the force space with respect to the maximum base shears V_{xo} and V_{yo} in the x and y-directions, respectively, and maximum base torque T_o, such that the new coordinates V_x/V_{xo}, V_y/V_{yo}, and T/T_o all vary between -1 and 1.

2. Use as an iteration variable the normalized base shear in the x-direction, say, $V_x/V_o = \alpha^{(o)}$. Thus, a point on the surface is found when two conditions are met: (1) $\hat{m} = (T/T_o)/(V_y/V_{yo})$ and (2) $V_x = V^*$.

3. For the given $\hat{m} = (T/T_o)/(V_y/V_{yo})$ and $V_x/V_o = \alpha^{(o)}$ compute the base shear V_y and torque T that lead to collapse of the structure. This is done using for instance an event-to-event strategy. This combination of V_y and T defines one point on a BST surface (not necessarily the one sought) as shown in Fig. A.1.

4. Compute the corresponding restoring force V_x associated to the ultimate condition obtained in Step 3. If the condition $V_x = V^*$ is satisfied, the point belongs to the section of the BST surface sought; if not, a new value for the next iteration $V_x/V_o = \alpha^{(1)}$ is assumed and the procedure is repeated from step 3 until convergence is achieved (Fig. A.1).

5. Vary the value of $\hat{m}$ to compute another points on the surface at $V_x = V^*$.

6. Finally, repeat the process above for another section of the BST surface by assuming a different base shear V_x.

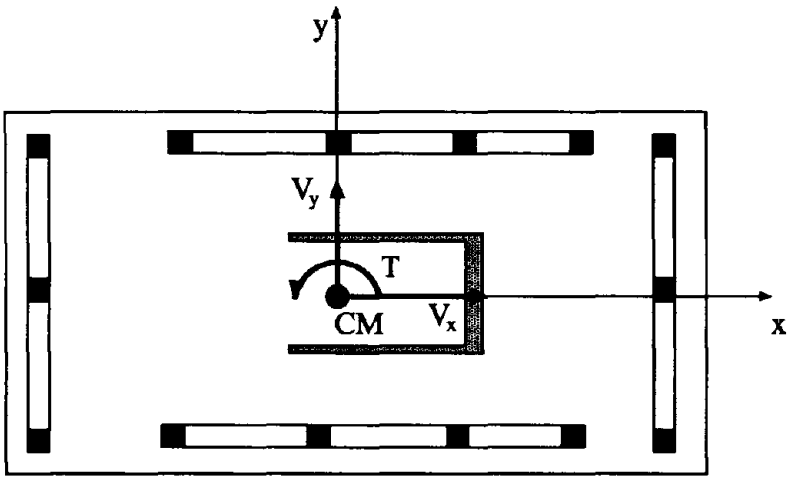

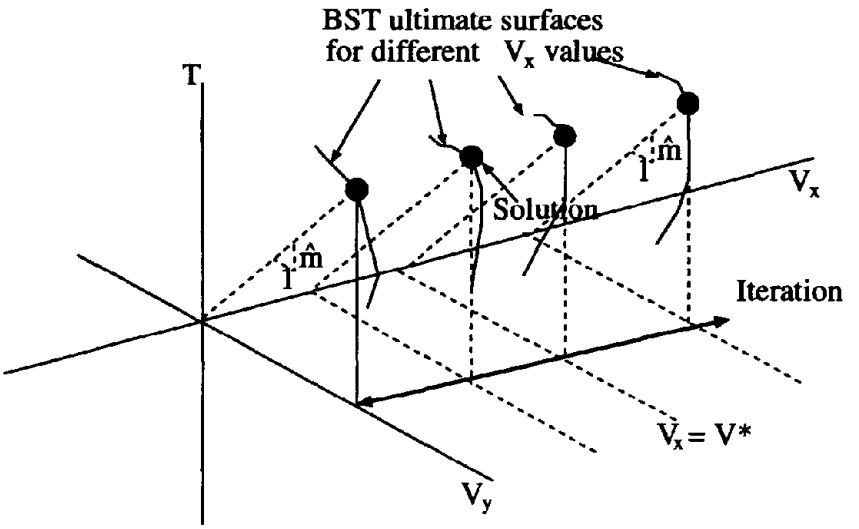

Figure A.1 Computation of the BST ultimate surface

APPENDIX B: Properties of the BST surface

This appendix contains proofs for the properties of the BST surface already described in section 2.3.3 of this chapter. The proofs are very simple; they provide, however, significant insight into the plastic behavior of asymmetric systems.

1. **The BST surface is convex** . A general proof for this statement can be found elsewhere [17] and it is based on the maximum dissipation postulate. For the particular case of a BST ultimate surface the proof goes as follows. Let us denote $\boldsymbol{Q} = \{V_x\ V_y\ T\}^T$ the vector containing the base shears and torque on the system, and $\boldsymbol{u} = \{u_x\ u_y\ u_\theta\}$ the vector of degrees of freedom. Also, the BST ultimate surface is denoted as $\Phi(\boldsymbol{Q}) = 0$. The principle of maximum plastic dissipation [17] states that

$$(\boldsymbol{Q} - \boldsymbol{Q}^*) \cdot \dot{\boldsymbol{u}} \geq 0 \tag{2}$$

where $\boldsymbol{Q}^*$ is an arbitrary point in the force space such that $\Phi(\boldsymbol{Q}^*) \leq 0$ and $\dot{\boldsymbol{u}}^p$ is the plastic deformation rate. A graphical representation of this principle is shown in Fig. B.1a. It is apparent from the figure that the only possibility to satisfy Eq. 1 is having the BST ultimate surface lying to the inward side of the tangent at point P. This implies that $\boldsymbol{Q}^*$ cannot lie outside the tangent to the surface at P and, hence, the BST ultimate surface must be convex.

2. **The BST surface is composed of linear branches** . A proof of this statement goes as follows. As shown earlier in Fig. 3, most collapse mechanisms in a system happen when one resisting plane is in the elastic range while the others yield. Let us denote the plane that remains elastic as k. At collapse, equilibrium of the system dictates

$$V_y = \underbrace{\sum_{i=1, i\neq k}^{N-1} f_{yi} + f_{yk}}_{V_c} \qquad T = \underbrace{\sum_{i=1, i\neq k}^{N-1} f_{yi} x_i + \sum_{j=1}^{M-1} f_{xi} y_i + f_{yk} x_k}_{T_c} \tag{3}$$

where f_{yi} is the capacity of the i^{th} element; f_{yk} is the elastic force in the k^{th} element; and V_c and T_c are the ultimate base shear and torque corresponding to a mechanism with zero force in the k^{th} element.

Solving for f_{yk} in the first equation of Eq. (2) and substituting in the second, we obtain a condition for the combinations of base shear and torque required to produce these mechanisms (Fig. B.1b)

$$T = T_c + x_k(V_y - V_c) \tag{4}$$

Therefore, Eq. (3) says that the BST surface is composed of linear segments and the property is proved. Note, however, that Eq. (3) cannot be used for mechanisms in which all resisting planes yield in one direction as in the case of a purely lateral mechanism (Fig. 3a). This case will be considered next.

3. **The slope of any of the branches of the BST surface tells the position of the element in the building plan that remains elastic during the mechanism considered** . Further, this slope also defines the **center of plastic rotation** of the building. The first statement is obvious from Eq. (3), which shows that the slope of the ultimate surface dT/dV_y must equal x_k, i.e., the position in plan of the element that remains elastic during the mechanism (Fig. B.1c). Therefore, each straight branch in the BST surface with finite slope implies that one and only one element in the plan remains elastic.

   The second statement can be proven using Drucker's postulate (Drucker, 1950). For perfectly plastic materials, the postulate implies that

$$d\boldsymbol{Q} \cdot d\boldsymbol{u}^p = 0 \tag{5}$$

   Therefore, Drucker's postulate can be rewritten in our case as

$$dV_y du_y^p + dT du_\theta^p = 0 \tag{6}$$

   For any mechanism involving rotation of the building plan, the plastic lateral deformation increment at the CM may be expressed as $du_y^p = -e \; du_\theta^p$ (Fig. B.1d). Thus, substitution in Eq. (5) leads to

$$\frac{dT}{dV_y} = e \tag{7}$$

   i.e, the slope of the BST ultimate surface is equal to the distance e between the CM and the center of plastic rotation. Moreover, this distance is then equal to the position x_k of the element that remains elastic during the mechanism considered.

   Clearly, if all resisting planes reach their capacity in a purely lateral mechanism, the center of plastic rotation of the plan will be at infinity as represented by point P1 in Fig. 2b. Furthermore, according to the mechanisms shown in Fig. 3b, the constant base shear branch P1-B of the BST surface (Fig. 2b) is such that $dV_y = 0$ and $dT \neq 0$, implying, based on Eq. (6), that there is no elastic element in the building plan. Therefore, the meaning of the constant base shear branches in the BST surface is that they correspond to mechanisms in which all resisting planes have yielding.

4. **The BST surface has B different branches with finite slope** , where B is the number of elements in the system. Further, the B branches are arranged according to decreasing distance from the plane to the CM. The first property is obvious from Eq. (3) since we expect to have one distinct branch for every mechanisms in which a resisting plane remains elastic. More interesting, convexity of the surface implies that the first branch after the constant base shear branch of the surface (Fig. B.1e) must be the branch corresponding to the mechanisms keeping the planes farther from the CM elastic, the second branch the one keeping the second farther planes elastic, and so forth, approaching to the resisting planes closer to the CM.

5. **If the element yield displacements are the same in both directions, the ultimate surface is point-symmetric with respect to the origin** . To prove this just observe that a reversal of sign in both V_y and T will produce identical results if the lateral capacities of the elements are symmetric. This symmetry occurs naturally in most structural elements designed to resist seismic loads.

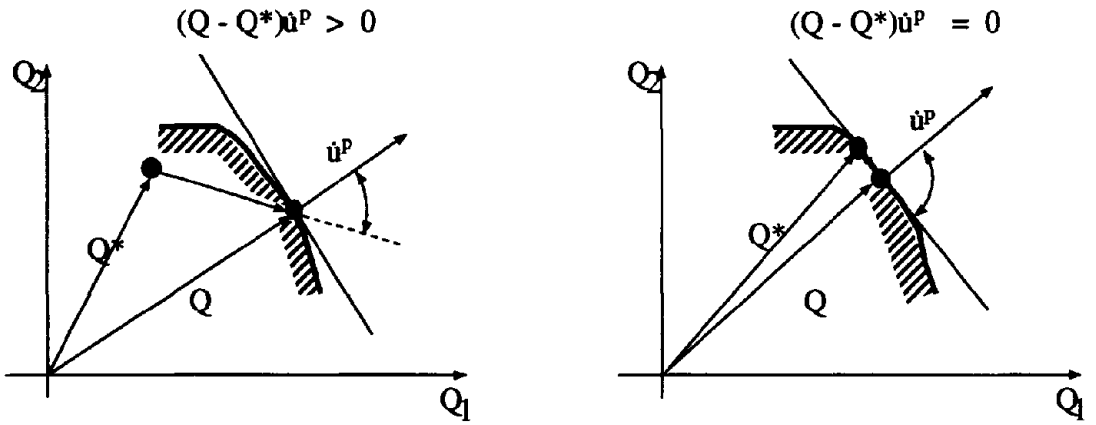

a) Convexity

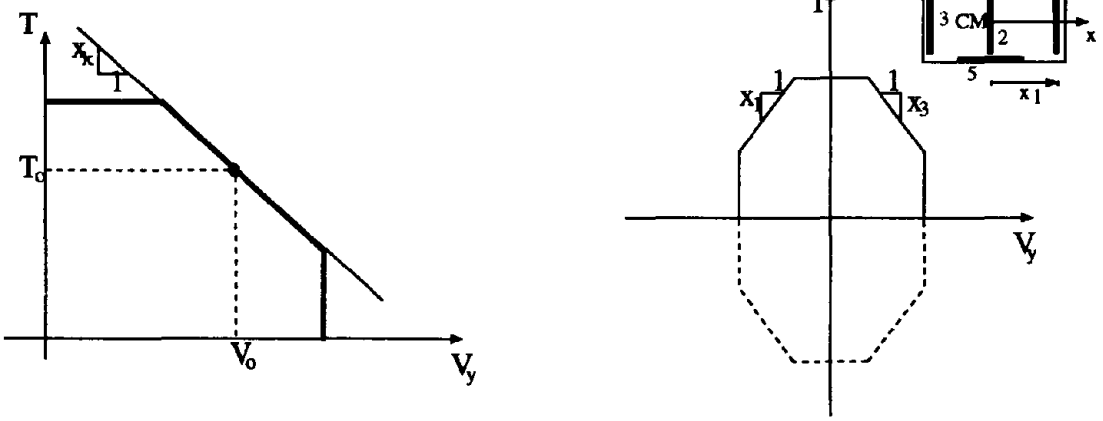

b) Straight branches

c) Slope of branches

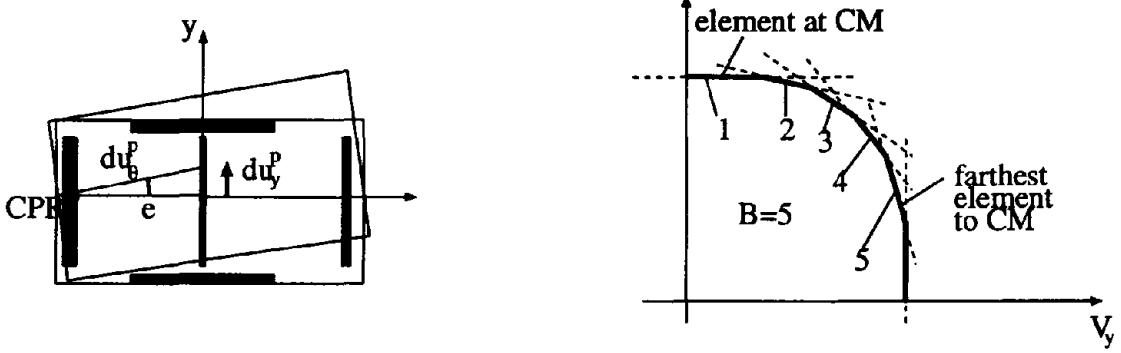

d) Center of plastic rotation (CPR)

e) Number of segments

Figure B.1 Properties of the base shear and torque ultimate surface

3. INELASTIC BEHAVIOR AND DESIGN OF ASYMMETRIC MULTISTORY BUILDINGS

3.1 Introduction

As mentioned in Chapter 1, the objectives of this investigation are to: (1) extend the conceptual framework developed in Chapter 2 to understand the inelastic seismic behavior of multistory systems, and (2) provide generally applicable design guidelines for asymmetric buildings that enable us to answer practical questions about the earthquake design and retrofit of asymmetric buildings.

This chapter is organized as follows. After describing the systems and analysis procedure used, several key aspects of the inelastic seismic behavior of asymmetric buildings are identified by studying the effect on the torsional response of six building characteristics: strength of orthogonal resisting planes, stiffness asymmetry, strength asymmetry, planwise distribution of strength, number of resisting planes, and intensity of the ground motion component in the orthogonal direction. The resulting understanding of the response is then used to propose several design guidelines for asymmetric buildings, which are considered later in evaluating two retrofit solutions for a practical building.

3.2 Systems considered and analysis procedure

The systems analyzed are multistory buildings consisting of floor diaphragms that are rigid flexurally and axially, where all the story masses are lumped; lateral resistance is provided by resisting planes in the x- and y-directions (Fig. 1) composed of elasto-plastic resisting elements. As shown in the building plan, the i^{th} resisting plane in the x-direction has lateral stiffness matrix $\boldsymbol{k}_x^{(i)}$ and is located at distance $x^{(i,j)}$ from the CM (center of mass) of the j^{th} floor, $j = 1, \ldots, n$; analogously, the stiffness matrix and location of the i^{th} resisting plane of story j in the y-direction are defined by $\boldsymbol{k}_y^{(i)}$ and $x^{(i,j)}$, respectively. The resisting planes in the y-direction may have different stiffness matrices and lateral capacities, and may be unsymmetrically located about the y-axis, creating eccentricities between the CM and CS (center of stiffness) in each story. On the other hand, the systems considered are symmetric in stiffness and strength about the x-axis. The structural model although simple, is deemed adequate for the computation and study of global building responses, such as floor displacements and story shears and torque [1].

The dynamic response of the system is described by the vector $\boldsymbol{u}_x$ of displacements $u_x^{(j)}$ and

the vector $\boldsymbol{u}_y$ of displacements $u_y^{(j)}$ of the j^{th} floor CM along the x and y-directions, respectively, and the rotation vector $\boldsymbol{u}_\theta$ of rotations $u_\theta^{(j)}$ of the j^{th} rigid floor diaphragm about a vertical axis through the CM (Fig. 1). Using these degrees of freedom, the dynamic response of the system to base acceleration $a_{gx}(t)$ and $a_{gy}(t)$ in the x- and y-direction , respectively, is described by the following equations of motion:

$$\boldsymbol{M}\ddot{\boldsymbol{u}} + \boldsymbol{C}\dot{\boldsymbol{u}} + \boldsymbol{R}(\boldsymbol{\delta},\dot{\boldsymbol{\delta}}) = -\boldsymbol{M}\boldsymbol{r}\boldsymbol{a}_g \tag{1}$$

where $\boldsymbol{u} = \{\boldsymbol{u}_x \boldsymbol{u}_y \boldsymbol{u}_\theta\}^T$; $\boldsymbol{M}$ is the mass matrix given by $\boldsymbol{M} = \text{diag}[\boldsymbol{m}\ \ \boldsymbol{m}\ \ \boldsymbol{I_p}]$, where $\boldsymbol{m}$ and $\boldsymbol{I_p}$ are diagonal matrices containing the masses and polar moments of inertia for each building story; $\boldsymbol{C}$ is the linear viscous damping matrix; $\boldsymbol{R}(\boldsymbol{\delta},\dot{\boldsymbol{\delta}})$ is the vector of restoring forces in the system; $\boldsymbol{r}$ is a $3n$ x 2 matrix made up of the influence vectors $\boldsymbol{r}_x = \{1\ \ 0\ \ 0\}^T$ and $\boldsymbol{r}_y = \{0\ \ 1\ \ 0\}^T$ for excitations $a_{gx}(t)$ and $a_{gy}(t)$, respectively; and $\boldsymbol{a}_g(t) = \{a_{gx}(t)\ \ \ a_{gy}(t)\}^T$. In this investigation the ground accelerations selected are the E-W and N-S components of the 1940 El Centro ground motion applied in the x and y directions, respectively. The equations of motion (Eq. 1) are integrated numerically using the partitioned predictor-corrector scheme developed in Ref. [2] and already used in Chapter 2.

The response quantities of interest in this study are: (1) the combinations of $V_x^{(j)}$, $V_y^{(j)}$, and $T^{(j)}$, the story shears in the x- and y-directions and story torque; (2) the displacement histories at the building edges and at the CM; and (3) the force-displacement histories in structural elements. For notational convenience, the principal direction of analysis always coincides with the y-direction (Fig. 1); because of that, the x-direction will be denoted hereafter as the orthogonal direction.

3.3 Response of inelastic systems

The purpose of this section is to investigate, in light of the results derived earlier for single-story systems (Chapter 2), the effect of the following six characteristics controlling the behavior of multistory asymmetric structures: (1) strength of resisting planes in the orthogonal direction, (2) stiffness asymmetry, (3) strength asymmetry, (4) planwise distribution of strength, (5) number of resisting planes, and (6) bidirectional ground motion.

These characteristics are studied using five-story buildings with uncoupled lateral vibration periods $T_x = T_y = 0.7$ sec. in the x- and y-directions, plan aspect ratio $a/b = 1/2$ where $b = 120$ ft (Fig.1), and subjected to twice the N-S component of the El Centro ground motion in the y-direction. This amplification of the ground motion, which is not unrealistic in light of the recent

earthquake data [3], was intended to drive the systems well into the inelastic range. The vertical distribution of story strengths in the building is as follows: V for the first two stories, $3/4V$ for the third and fourth stories, and $V/2$ for the fifth story. The story stiffnesses vary over the building height like the story strengths: K in the first two stories, $3/4K$ in the third and fourth stories, and K/2 in the 5th story. This heightwise distribution of strength is consistent with the code distribution of lateral forces but also accounts for the fact that properties of structural elements are not usually varied in every story. Hereafter, the stiffnesses and strengths of structural elements will be given in terms of the reference values $K = 42000$ kips/ft and $V = 840$ kips, respectively, corresponding to a realistic five-story structure.

The response results will be presented in a special format (see for example Fig. 2). Rows (1), (2), and (3) contain the response results for the first, third, and fifth stories of buildings with plan configurations shown in columns (a), (b), and (c); identical stiffnesses and capacities in resisting planes are only shown once.

It is important to note that in some cases changes in the building characteristics mentioned will not only imply changes in the inelastic response of the building but also in the elastic response. This distinguishes our study from traditional parametric studies where the goal is to keep identical elastic responses at the expense of adjustments to the structural system. In this study, the changes introduced to building characteristics are straight forward and motivated by practical actions that the engineer may take to modify a building plan. As an example, consider a hypothetical situation in which more resisting planes are introduced in the direction orthogonal to the ground motion considered. Because of these planes, not only the torsional capacity of the building will increase but also its torsional stiffness and, hence, both the elastic and inelastic responses will change.

3.3.1 Strength of resisting planes in the orthogonal direction

To study the effect of varying the strength of the resisting planes orthogonal to the direction of ground motion, consider the three structural plans (a) through (c) presented in Fig. 2. The lateral capacity V_y of these three structures in the y-direction is the same and equal to $0.15W$, where W is the weight of the structure, but their base shear capacities V_x in the x-direction vary from zero to a maximum of $0.3W$. Each system has equal normalized stiffness eccentricity $e_s/b = 0.125$ and strength eccentricity $e_p/b = 0.125$ in all stories; these values have been chosen arbitrarily as the reference values about which changes will be considered in this study. Note that the torsional

stiffness contributed by the resisting planes in the orthogonal direction differs among the three systems; however, as shown next, the differences in response among these systems can be explained mainly based on their different inelastic properties.

Let us consider first the story shear and torque response histories for the system, which have been superimposed on the SST surface shown by the polygon in solid lines (Fig. 2). It is apparent that the SST surfaces for the third and fifth stories are scaled versions, by factors 3/4 and 1/2, respectively, of the first story SST surface due to the smaller lateral capacities in these stories. Further, the increase in the capacity of the orthogonal resisting planes leads to an increase in the length of the constant base shear branch and to an increase in the torsional capacity of the system (Fig.2: 1a, 1b, 1c) (Chapter 2). The lengthening of the constant base-shear branch implies an increase in the number of story mechanisms that involve yielding of all y-direction planes. It is observed that the system with no orthogonal resisting planes (Fig.2: 1a, 2a, and 3a) undergoes most of its inelastic behavior along the branches of the SST surface with positive slope. This implies that at many time instants the system develops torsional mechanisms about the strongest resisting plane (plane 3) in the plan (Chapter 2). Consequently, most of the inelastic behavior of the system is expected to occur in plane 1, the farthest from plane 3, due to the plan rotation. A corollary of this observation indicates that peak displacements of systems with no orthogonal resisting planes are associated with large rotations of the plan, as has been noted earlier in the context of single-story systems [4].

As the strength of the orthogonal resisting planes increases, a larger proportion of the inelastic behavior of the system shifts from the branches of the BST surface with positive slope (Fig.2: 1a, 2a, 3a) to the constant base-shear branches (Fig.2: 1c, 2c, 3c). This implies that systems with strong orthogonal resisting planes will see in many of their inelastic excursions predominantly translational mechanisms involving yielding of all resisting planes in the y-direction. Thus, more uniform displacement demands are expected for the resisting planes in these systems; equivalently, systems with strong orthogonal planes will undergo smaller inelastic rotations of the plan as has been noted earlier in the context of single story systems [5].

Consistent with these observations are obtained the displacement histories at different plan locations (Fig. 3) and force-displacement histories for the three resisting planes (Fig. 4). For building (a), the peak floor displacements at the flexible edge (plane 1) of the building are over twice those at the stiff edge (plane 3) (Fig. 3: 1a, 2a, 3a) due to the large rotations of the plan about plane 3. The displacement histories of building (b) and (c) (Fig. 3: 1b-3b and 1c-3c) show

that the increase in the strength of the orthogonal planes leads to more uniform displacement demands among the y-direction planes. Thus, the ratio between the peak displacements at the flexible and stiff edges has reduced from over 2 in building (a) (Fig. 3: 1a, 2a) to about 1 and 1.4 in the first and second stories in building (c) (Fig. 3: 1c, 2c). These results are even clearer in the force-displacement histories for the resisting planes. Comparing, for instance, parts 1a through 1c of Fig. 4, we see that by increasing the strength of the orthogonal planes it is possible to make the peak deformation demands in the resisting planes quite similar in spite of the stiffness and strength asymmetry in the system; results for other stories are similar (Fig. 4: 2a-2c and 3a-3c). Note also that together with making these demands more uniform, the peak deformations in the resisting planes of building (c) are reduced relative to building (a) because are being used more efficiently.

3.3.2 Stiffness asymmetry

The effect of stiffness asymmetry in the inelastic response of asymmetric structures is studied considering the response of the three buildings with plans presented in Fig. 5 (a) through (c). The lateral base shear capacities in the x and y-directions for all the systems are $0.15W$. Their normalized strength eccentricity $e_p/b = 0.125$ is also identical but the normalized stiffness eccentricity is $e_s/b = 0, 0.125$, and 0.4 for buildings (a), (b) , and (c), respectively.

In single story systems, stiffness eccentricity has shown to influence the story shear and torque response histories inside the SST surface (Chapter 2). This influence is also apparent from the shear and torque histories for multistory systems presented in Fig. 5. As the stiffness eccentricity increases, larger values of base torque are developed in the system (e.g., Fig. 5: 2a, 2b, and 2c). If the stiffness eccentricity is large, as in building (c), the story shear and torque combinations produce a plot that is skewed toward the second and fourth quadrants of the SST surface (e.g., Fig. 5: 3c)—because we have assumed positive stiffness eccentricity (CS to the right of the CM), implying that positive story shears would frequently accompany clockwise (negative) base torques and vice-versa. As a result, yielding in building (a), which takes place along the constant shear branches of the SST surface (Fig. 5: 1a, 2a, 3a), tends to move to the positive slope branches for building (c) (Fig. 5: 1c, 2c, 3c). This implies, as it should, that these systems with large stiffness eccentricity will experience inelastic behavior in mechanisms associated with important rotation of the building plan about the stiffest, and usually strongest, resisting plane.

Consistent with these observations are the displacement histories of the building edges and CM

(Fig. 6) and the force-displacement histories of the resisting planes (Fig. 7). It is apparent that as the stiffness eccentricity increases from buildings (a) to (c), the displacements at the flexible and stiff edges of the building become increasingly different due to the larger plan rotations (Fig. 6: 3a, 3b, 3c). Also note that the amplitude of the displacements increases significantly as a result of plan asymmetry, justifying the concern for the seismic behavior of these systems. Additional verification of the described behavior is seen in the force-displacement histories of the resisting planes (Fig. 7). Comparing, for example, the force-deformation relations of resisting planes 1, 2, and 3 (Fig. 7: 2a, 2b, and 2c) it is evident that the increase in stiffness eccentricity produces increasingly different deformation demands among the resisting planes; being larger for the planes farther from the stiffest plane 3. As suggested by these results, collapse of building (c) will likely occur in a torsional mechanism about plane 3. Also note that the deformation demands on the resisting planes of building (b), in spite of the stiffness eccentricity in this building, are as uniform as for building (a), which is symmetric in stiffness.

3.3.3 Strength asymmetry

The effects of strength asymmetry are studied considering the three structural plans shown in Fig. 8. These systems are such that they all have the same normalized stiffness eccentricity $e_s/b = 0.125$, but variable normalized strength eccentricities—$e_p/b = 0, 0.125$, and 0.342, respectively. Also, their lateral base shear capacities are $0.15W$ in the x and y-directions, respectively, and the three systems have the same base torsional capacity $T_o = 0.1875W(b/2)$ kips-ft. The elastic responses of the three buildings to the given ground motion are identical, and differences in their inelastic responses can be attributed principally to changes in the shape of the SST surface because of strength asymmetry.

Strength asymmetry has an important effect on the shape of the SST ultimate surface as shown by the results presented in Fig. 8. The SST surfaces for the strength symmetric building (a) (Fig. 8: 1a, 2a, 3a) are symmetric about the shear and torque axes. This symmetry is lost gradually with increasing strength eccentricity in buildings (b) and (c), making the surfaces to narrow and lean toward the first and third quadrants (Fig. 8: 1c, 2c, 3c) (Chapter 2).

The story shear and torque histories corresponding to building (a) (Fig.8: 1a, 2a, 3a) show that the inelastic behavior of this strength symmetric system is developed along the constant base-shear branches of the SST surfaces. However, the shear and torque combinations tend to lie off the center of these branches, implying that the system will undergo, besides its predominantly

lateral yielding, some inelastic rotations as a result of its stiffness eccentricity. As the strength eccentricity increases, more base shear and torque combinations shift from the constant base-shear branches (Fig.8: 2a) of the SST surface toward the branches with positive slope (Fig.8: 2c); the latter being associated with torsional mechanisms leaving the strongest resisting plane (plane 3) essentially elastic during the earthquake (Chapter 2). The practical consequences of this shift are important; large plastic rotations will tend to be produced about the strongest plane (plane 3), leading to large displacement demands on the planes farther from it.

It is important to note that in some cases an increase in the strength asymmetry of a system may be beneficial or at least innocuous. A good example of this situation are buildings (a) and (b). We observe in building (b) that the change in the shape of the SST surface has not produced yielding along its inclined branches; therefore, the displacement and deformation demands for these buildings will be similar. In more general terms, unless the change in strength eccentricity is accompanied by a change in the region of the SST surface where the inelastic behavior takes place, the changes in response among different configurations will not be substantial.

The above observations are confirmed when we analyze the displacement histories at different floors (Fig. 9). The differences between the displacements at the flexible edge (plane 1) and stiff edge (plane 3) of buildings (a) and (b) are similar, and they become larger for building (c) (Fig. 9:1c, 2c, 3c); the ratio between the peak displacements at the flexible and stiff edges at the roof of the building is about 1 and 2.5 for buildings (a) and (c), respectively. Thus building (c) has significant rotations about plane 3, which lead to an excessive increase in the displacements at the flexible edge of the building.

Further confirmation of the above results is provided by the force-displacement relations of the elements (Fig. 10). It is apparent that the peak deformations in planes 1,2, and 3 are all similar for buildings (a) and (b) (Fig. 10: a and b); however, they become very different as the strength asymmetry increases (Fig. 10: 1c, 2c, 3c). More important, building (c), which represents large asymmetry in strength, demonstrates that the strength of the strongest plane 3 is of little help since the inelastic behavior of the system is such that a torsional mechanism, about this plane, is activated most of the time (Fig. 10: 1c, 2c, and 3c).

3.3.4 Planwise distribution of strength

In order to study the changes in building response due to other changes in the planwise distribution of strength, we consider the three building plans shown in Fig. 11. All these buildings have the same stiffness eccentricity $e_s/b = 0.125$ but are symmetric in strength. The three systems also have identical lateral capacities, $0.15W$, in the x and y directions; their torsional capacities, however, vary from $T_o = 0.025W(b/2)$ kip-ft in building (a) to $0.125W(b/2)$ kip-ft in building (c). This variation in strength is such that building (a) corresponds to a system with a very strong central core and weak resisting planes along the two edges in the y-direction, and building (c) is just the opposite, i.e., a system with very strong planes along the edges and a weak central core. Note that the elastic responses of all these systems are identical.

Shown in Fig. 11 are the SST surfaces for the three buildings considered. The surfaces for building (a) (Fig. 11: 1a, 2a, 3a) are very flat as a result of the small torsional capacity of the system. On the other hand, the larger torsional capacity of buildings (b) and (c) (Fig. 11) stretches the surface along the torque axis and a reduces the length of the constant torque branches (Chapter 2).

In spite of the small torsional capacity of building (a), the story torques due to the selected excitation (Fig. 11: 1a, 2a, 3a) remain below the capacity except at few time instants in the fifth story (Fig. 11: 3a). The system is unable to develop large story torques as a result of the small strength of resisting planes 1 and 3 and ends up responding primarily in translation as indicated by the essentially identical displacement histories of planes 1,2, and 3 (Fig.12 : 1a, 2a, 3a). In other words, the torsional weakness of this system impedes the development of large rotations of the plan despite the stiffness asymmetry in the system. As the strength of the resisting planes at the edges increase, larger torques are developed and the buildings undergo yielding along the inclined branches of the SST surface (Fig. 11: (b) and (c)). These mechanisms are predominantly torsional (especially c) and lead, as expected, to unequal displacement demands at the stiff and flexible edges of the building (Fig. 12: 2c, 3c). It is also apparent that the uniformity in displacement demands in building (a) is accompanied by an increase in the amplitude of the oscillations and their period (Fig. 12: 3a). This may impose rather large ductility demands on resisting planes at the edges of the building as shown by the results presented in Fig. 13 (Fig. 13: 1a, 2a, 3a). Nevertheless, the torsional behavior of an unsymmetric structure is essentially eliminated by reducing the torsional capacity of the system.

3.3.5 Number of resisting planes

So far we have considered buildings with three resisting planes along the direction of ground motion. Let us consider now the effect of having more resisting planes by studying the response of the three buildings shown in Fig. 14. Buildings (a), (b) and (c) have 3,5, and 7 resisting planes in the y-direction, respectively, and they all have the same stiffness eccentricity $e_s/b = 0.125$. Their lateral base shear capacities are the same and equal to $0.15W$ in the x and y-directions, but their base torsional capacities vary from $0.1875W(b/2)$ kip-ft in building (a) to $0.1125W(b/2)$ kip-ft in building (c). The systems also have identical strength eccentricities $e_p/b = 0.125$. Note that the elastic responses of these systems are not necessarily identical because their torsional stiffnesses decrease as the number of resisting planes increase. It will be shown next, however, that differences in elastic and inelastic responses among these systems are small.

Increasing the number of resisting planes of a building produces a rounding effect on the SST surfaces, especially for regions of large torque (compare Fig. 14: a, b, and c). However, since the inelastic behavior of buildings, usually, does not take place in this region of the surfaces, we should expect similar responses in all configurations. Consider, for example, the base shear and torque response histories on the first floor of buildings (a), (b) and (c). The inelastic behavior in all these systems is developed along the constant shear branches of the SST surface. Consequently, the displacements and deformation demands on the resisting planes of these systems should be similar. This expectation is verified by comparing the displacement histories (Fig. 15: 1a-1c, 2a-2c, 3a-3c) for these buildings and the element deformation demands (Fig. 16: 1a-1c, 2a-2c, 3a-3c). Slight differences in the values of these responses exist; however, the response behavior is conceptually identical for the three plans. Other researchers have made this observation but on a different basis [e.g., 5].

The results presented above are important in two respects. First, they justify the use of three-plane models in studying the response of asymmetric plan systems; an assumption that has been used by most previous researchers. Second, they suggest that, for simplified analysis and design purposes, most multiple resisting plane structures could be reasonably approximated by a three plane model, if the latter matches the relevant elastic and inelastic properties of the actual building. Such a model will developed in the next chapter.

3.3.6 Bidirectional ground motion

In the previous sections we have considered the response of asymmetric buildings subjected to a single component of ground motion. However, most buildings in practice are subjected to two horizontal components of ground motion. It is the objective of this section to study the response of asymmetric buildings when both ground motion components act simultaneously.

Consider the seismic response of the buildings shown in Fig. 17 subjected to twice the N-S component of the El Centro ground motion in the y-direction and three versions of its E-W component in the x-direction scaled by factors $\alpha = 0, 1$, and 3. The building considered has lateral capacities equal to $0.15W$ in both principal directions, torsional capacity equal to $0.1875W(b/2)$, and identical stiffness and strength eccentricity, $e_s/b = e_p/b = 0.125$.

The response of this system subjected only to ground motion in the y-direction ($\alpha = 0$) has been already considered in Figs. 2b, 5b, 8b, and 14a; in this case, the orthogonal planes 4 and 5 contribute entirely to resist the story torque generated by the asymmetry of the system about the y-axis. However, as the intensity of the orthogonal component of ground motion increases, story shears in the x-direction increase and planes 4 and 5 yield, thus limiting their capacity to resist the story torque. In the limit, when these planes yield in the same direction at most time instants during the response, their contribution to resist the story torque will be very small, and the system will respond in the y-direction as if no orthogonal planes existed. In order to verify this concept, we have included in Fig. 17 two SST surfaces, one corresponding to no yielding in the orthogonal planes (solid line), $\hat{V}_x = 0$, and the other, $\hat{V}_x = 1$, to complete yielding in these planes (dashed line) (Chapter 2). It is clear that as the intensity of the orthogonal component increases from $\alpha = 0$ to $\alpha = 3$ (Fig. 17: 1a-1c, 2a-2c, and 3a-3c), as predicted, more story shear and torque combinations move inside the SST surface corresponding to $\hat{V}_x = 1$ (dashed lines).

A more subtle but relevant point is to study where the yielding takes place on each of the SST surfaces. For example, yielding in building (a) (Fig. 17: 1a, 2a, and 3a) occurs along the constant shear branches, implying that the resisting planes in this system should experience relatively uniform deformation demands. This may be clearly seen in the force-displacement relations shown in Fig. 19 (1a, 2a, and 3a), where no substantial differences exist among the demands on the three planes of the building. On the other hand, when the intensity of the orthogonal component increases, more yielding occurs at the positive slope branches of the SST surface (see Fig. 17: 1c, 2c). This implies that the system responds at time many instants, as if it had no orthogonal resisting

planes and, hence, it develops predominantly torsional mechanisms in most of its inelastic excursions. As a result, the deformation demands among the resisting planes will tend to be uneven, i.e., smaller for the strongest resisting plane and larger for the one farther from it. Comparison of the results in columns (a), (b) and (c) of Figs. 19 confirms these observations. Similar trends are displayed, although not as clearly, by the building displacements shown in Fig. 18; for instance, careful examination of 3a, 3b, and 3c shows that the discrepancies between the flexible-edge and stiff-edge displacements increases as α increases.

The increase in deformation demands on the resisting planes in the y-direction produced by yielding in the resisting planes in the orthogonal direction may be significant; for the example considered an increase of about 50% over the unidirectional case (Fig. 19: 2a) would be expected for the flexible-edge planes (Fig. 19: 2c). One possible alternative for incorporating this effect into the building design will be proposed in the next chapter; the other possibility would be to bound the actual response of the building by two analysis cases, one assuming full capacity in the orthogonal resisting planes, and the other, ignoring it.

3.4 Conceptual design guidelines

This section summarizes the most relevant observations of the inelastic behavior of asymmetric-plan buildings obtained in the previous section. These observations may be used as conceptual guidelines for improving the design of asymmetric structures:

1. The responses of asymmetric-plan single and multistory buildings of the kind considered, i.e., with regular asymmetry in height (see [6]), show trends that are very similar (Chapter 2). This suggests that, at least conceptually, results obtained by other researchers in single-story systems [e.g., 4,5] may be applicable to this wider class of multistory systems.

2. Stiffness asymmetry in a system influences the story shear and torque combinations inside the SST surface (Fig. 4: 2a, 2b, and 2c) and hence the elastic response of the system. However, changes in the stiffness eccentricity will affect the inelastic response of the system only if these changes lead to changes in the region (or branches) of the SST surface where the inelastic action is developed.

3. Strength asymmetry always produces concentration of deformation demand in resisting planes that are farther from the strongest plane in the plan (Fig. 7: 2c). Furthermore, buildings

with strength asymmetry are prone to develop torsional mechanisms at collapse and, hence, an uneven distribution of displacement demands among resisting planes.

4. The two observations above may be combined into an interesting point. Since stiffness asymmetry controls the behavior inside the SST surface and strength asymmetry the shape of the SST surface, we can, theoretically speaking, adjust both to direct the inelastic behavior in any desired region of the SST surface. In particular, if we have, say positive strength eccentricity, the SST surface will lean toward the first and third quadrants (Fig. 8). Therefore, to get the shear and torque combinations to fall in the constant shear branches we must produce a tendency for them to lie on these quadrants by introducing a negative stiffness eccentricity (CS left of CM). Independently, varying stiffness and strength may seem impractical for conventional steel and R/C buildings, but should be feasible for a system using frictional devices.

5. A reduction in the torsional capacity of stiffness-asymmetric systems may produce, at the expense of larger displacements, more uniform displacement demands among resisting planes (Fig. 11: 3a, 3b, and 3c), implying dominantly translational response.

6. Equivalent three-plane models (Fig. 14: 2a, 2b, 2c) of buildings with multiple resisting planes lead to sufficiently accurate estimations of the building displacements, story shears and story torques. This is the basis for the simplified model developed in the next chapter for preliminary analysis and design of buildings.

7. Increased strength in the resisting planes in the direction orthogonal to the ground motion always reduces the effects of torsion in an asymmetric structure. Their effectiveness of the orthogonal planes must be assessed, however, in conjunction with the intensity of the ground motion along in the orthogonal direction; if substantial yielding is expected in that direction the orthogonal planes should be ignored in the analysis, otherwise their contribution to resist the torsional motions of the system should increase with decreasing yielding.

8. Any design or retrofit solution of an asymmetric building should consider the story shear and response histories together with the SST surfaces for each story. From direct analysis of these data, we have the ability to answer questions like: (1) what mechanism, translational or torsional, is the building likely to develop, (2) if the answer to one is a torsional mechanism, what resisting planes in the plan have larger/smaller displacement demands, (3) how to modify

the SST surfaces to achieve more uniform displacement demands on the resisting planes of each story, (4) what is the effect of yielding in the orthogonal resisting planes, and so forth.

3.5 Retrofit design example

The purpose of this section is to apply the conceptual guidelines developed in the previous section to a hypothetical retrofit solution of a building. Let us assume that we have been asked to provide a retrofit solution for the five-story building shown in Fig. 20. The building has a rectangular plan of dimensions 200 ft by 100 ft for the first story and 100 ft by 50 ft for the second and upper stories; it also has infinitely rigid floor diaphragms, where all the story masses are lumped, and it is subjected to twice the E-W and N-S components of the El Centro earthquake in the x- and y-directions, respectively. The system has three and five resisting planes in the x- and y-directions in the first story, and two and three in these directions, respectively, in upper stories. Further, the stiffnesses of these planes are as shown,' and their yield deformations are all assumed to be equal to $v_y = 0.02$ ft. Consequently, stiffnesses and strengths of different resisting planes are in the same proportion. Note also that the system has asymmetry in both directions as a result of the setback in the second story; besides, the building has resisting planes with lateral stiffness matrices which are not proportional. In that sense, this structure is different to the systems considered earlier in this study. This has been done intentionally to show that the conceptual design guidelines developed earlier for one-way unsymmetric systems with proportional resisting planes can also be applied effectively to more complex structures.

The most important feature of this structure is its irregularity in plan and height due to the setback, which produces an offset equal to $0.25b$ between the centers of mass of the first and upper stories. Also, the building plan in the second and upper stories is asymmetric as a result of the larger stiffness and strength of resisting plane 5 compared to plane 3. Because of the setback and plan asymmetry, the building may develop significant torsional motions that may eventually lead to high demands on some resisting planes, thus, justifying the concern for its seismic safety.

The response results presented next are in a special format (see Fig. 21). Rows (1), (2), and (3) contain the response results for the first, second, and fifth stories of the building, respectively; columns (a), (b), and (c) present the floor displacements, force-deformation relations, and story shear and story torque histories, respectively.

Before proposing different retrofit solutions for this structure it is necessary to understand its

inelastic dynamic behavior. Shown in Fig. 21 is a summary of different response quantities in the building. It is apparent from parts 1a, 2a, and 3a that the floor displacements at the left and right edges of the CM are substantially different. This fact confirms our expectation that the system will undergo significant torsion. Observe that the ratio between peak displacements at the left and right edges ranges between 3 and 5 for different stories. Besides this undesirable discrepancy in edge displacements, the force-deformation histories presented in Figs. 1b, 2b, and 3b demonstrate that the peak deformation ductility demands for the most critical resisting plane in each story are 5, 15, and 1.5, approximately. The large ductility demand in the second story is accompanied by large differences among ductility demands on the different resisting planes; these differences are close to 100% in the first story and 60% on the second story.

All the above observations are verified by looking at the base shear and torque response histories superimposed on the SST surfaces (Fig. 21: 1c, 2c, and 3c). For example, Fig. 1c shows a tendency of developing mechanisms at the upper and lower ends of the constant base shear branches in the first and third quadrants of the SST surface, respectively, associated with significant rotations of the building plan. Similarly, Fig. 21: 2c shows that yielding in the second story is quite extensive and spreads to the large-torque regions of the constant base shear branches where mechanisms become increasingly torsional. Therefore, there is clear evidence that the system is torsionally unbalanced and any proposed retrofit solution should aim to correct this unbalance in order to lead to more uniform deformation demands among resisting planes.

We will now consider two retrofit solutions of the system, which illustrate two important techniques for controlling the torsional behavior of a structure. The first considers the possibility to (1) increase the strength of resisting planes along the orthogonal direction (x-direction); and (2) modify the stiffness and strength of key resisting planes in order to balance the torsional behavior.

First retrofit solution

Recall from point seven in the previous section that the effect of increasing the strength of the orthogonal resisting planes is to lead to more uniform deformation demands of the planes along the y-direction. Although this effect is reduced by the presence of an orthogonal component of ground motion (Fig. 17), increasing the strength of orthogonal planes will always reduce the plan rotations. Therefore, the first retrofit solution considered is to increase the strength and stiffness of these planes (Fig. 20b); the strength of resisting planes A and C in the first story has been increased by 2.5, and by a factor of 2 in upper stories, such that the lateral capacity of each story in the x-direction has been doubled.

Shown in Fig. 22 is the earthquake response of the modified building. It is apparent by comparison with the responses of the original building (Fig. 21) that, as expected, the torsional unbalance in the system has been partially corrected. By this we mean that the displacements of different resisting planes become less different (Fig. 22: 1a, 2a, 3a), their deformation ductility demands also become more similar (Fig. 22: 1b, 2b), and the mechanisms developed at different stories are less torsional (Fig. 22: 1c, 2c). For example, we have reduced the peak deformation ductility demands in the second story to about 10, similar for all resisting planes. The effect of the increased strength in orthogonal planes is most clearly seen in Fig. 1c. The base shear and torque response history for this story clearly shows a larger concentration of shear-torque combinations about the zero torque axis than it did before (see Fig. 21: 1c). Also, the inelastic behavior of this story is now closer to the center of the constant base shear branches of the SST surface, implying that the system at collapse is likely to develop mechanisms that are predominantly translational in the first story.

Although the benefit of increasing the strength in the orthogonal planes is apparent, some aspects of the behavior of the new system are not completely satisfactory. First, given the large increase in strength of the orthogonal planes we would have preferred a better agreement between the left and right edges displacement histories. Second, the force-deformation histories in the second story (Fig. 22: 2b) show that yielding in the resisting planes occurs asymmetrically about the force axis, indicating a residual drift in the structure. Third, the increase in strength in the orthogonal planes is accompanied by an increase in the story torques developed in the system (Fig 22: 2c). Despite these deficiencies, the retrofit solution proposed accomplishes our goal of reducing differences in demands among resisting planes. However, it is possible to achieve a much better performance by adjusting the stiffness and strength in the resisting planes, as shown next.

Second retrofit solution

We first recall from points 2, 3, and 4 in the previous section that by changing the stiffness and strength distribution in the system we may concentrate yielding in specific resisting planes of the structure. Thus, the strategy for this solution is to increase the yielding in those planes that are essentially elastic in the original system and reduce the yielding in planes that deform excessively in that system. More specifically we aim to: (1) increase the yielding of resisting plane 1 and reduce the one of plane 5 in the first story (Fig. 21: 1b); (2) reduce the yielding in plane 3 in the second story (Fig. 21: 2b); and (3) improve the torsional behavior of the second story by inducing mechanisms that are predominantly translational in this story (Fig. 21: 2c).

Improving the torsional performance of a building has little to do with increasing the overall capacity of the system. It is indeed a problem of the planwise distribution of strength (and stiffness to a lesser degree). To emphasize this important concept, the retrofit solution proposed in Fig. 20c is such that it maintains the same lateral capacity as the original system. For this purpose the lateral capacity of resisting planes 1 in the first floor and 5 in the second and upper stories has been slightly reduced. These capacity reductions will not be introduced on the actual retrofit solution but the capacity of other planes will be increased slightly to ensure the relative capacity values presented in this figure. Note that the idea is to increase the first story capacity of plane 5 and simultaneously decrease the one of plane 1 by 25%. This will increase the ductility demand on plane 1 and reduce the demand on plane 5. On the other hand, we have increased the strength of resisting plane 3 in the second floor by 50% and reduced the one of plane 5 by 25%, so as to increase the ductility demand in plane 5 and reduce it in plane 3 (Fig. 21: 2b).

Shown in Fig. 23 is the dynamic response of the system. The results are remarkable in many respects. First, the displacement histories at different locations of the building plan (Fig. 23: 1a, 2a, 3a) are very similar, especially for the second and upper stories. Second, the force-deformation histories (Fig. 23: 1b, 2b, 3b) show essentially identical peak deformation demands on the different resisting planes, as well as symmetric behavior about the force axis. Further, since all resisting planes are used more effectively the peak ductility demands have reduced from 15 in the original system (Fig. 21: 2b) to about 8 in the new system (Fig. 23: 2b). Third, the story shear and torque histories have changed dramatically, especially those of the second and upper stories. Note that the second story shear and torque combinations lie now close to the zero torque axis (Fig. 23: 3b), showing the effectiveness of the retrofit scheme proposed. Although the base shear and torque history in the first story still goes predominantly in the first and third quadrants, the inelastic behavior takes place close to the center of the constant shear branches, implying that the mechanisms developed are mainly translational.

Therefore, as demonstrated by this example, the conceptual guidelines presented in the previous section concerning the inelastic behavior of asymmetric buildings provide a basis to develop practical solutions to improve the torsional behavior of an existing structure, even if that structure is highly asymmetric. Hereafter the retrofit solution can be tested further by inelastic analyses of the system. Such analyses, which seem very costly, can be greatly simplified using the simplified model developed in the next chapter.

3.6 Conclusions

This study of the seismic behavior of asymmetric multistory buildings has led to the following conclusions:

1. The earthquake behavior of asymmetric single and multistory buildings of the class considered in this investigation, show similar trends and is affected by the same building characteristics: the strength of resisting planes and intensity of ground motion in the orthogonal direction, the stiffness and strength asymmetry in the system, and the distribution of strength between the core and edges of the building.

2. Stiffness and strength asymmetry may be effectively used to control the torsional performance of a structure. Stiffness asymmetry influences the story shear and torque combinations in elastic response, inside the SST surface. Thus, by varying the stiffness eccentricity, story shear and torque combinations may be forced to fall into certain quadrants inside the surface. Further, strength asymmetry affects the shape of the SST surface and, hence, it can be used to guide the inelastic behavior into certain desirable regions of the surface, such as the constant shear branches.

3. To create uniform inelastic deformation demands in the resisting planes of a given story, the story shear and torque combinations lying on the SST surface must not deviate significantly from the center of the constant shear branches. On the other hand, the worst behavior is achieved when these combinations lie at all time instants on one of the inclined branches of the surface, implying that the same resisting plane in the plan always remains elastic.

4. Increased strength in the resisting planes orthogonal to the direction of ground motion also leads to more uniform deformation demands among the resisting planes in the direction of ground motion. However, the influence of the orthogonal planes decreases as the intensity of the orthogonal ground motion component increases.

5. The building example considered has shown that it is even possible to correct the torsional unbalance of a very asymmetric system by manipulating the strength (and stiffness). Other retrofit situations may require additional tools, such the use of orthogonal resisting planes, lumping of the strength close to the CM of the structure, or combinations of the above.

6. It has been demonstrated throughout this study that the knowledge of the SST surfaces in conjunction with the story shear and response histories is all that is needed for a conceptual understanding of the earthquake behavior of an asymmetric structure. Therefore, these concepts could be effectively used for preliminary analysis and design of asymmetric structures.

3.7 References

1. Duan, X. and Chandler, A.'Inelastic seismic response of code-designed multistorey buildings with regular asymmetry', Earthquake Engineering and Structural Dynamics 22, 431-445 (1993).

2. Inaudi J.A. and De la Llera J.C., 'Dynamic analysis of nonlinear structures using state-space formulation and partitioned integration schemes', Report No. EERC 92/18, University of California, Berkeley, CA., Nov. 1992.

3. Shakal, A., Huang, M., and Darragh, R. 'CSMIP strong motion records from the Northridge, California earthquake of 17 January 1994', CSMIP report No. OSMS 94-07, California Strong Motion Instrumentation Program, Sacramento, CA, Feb. 1994.

4. Tso, W.K. and Sadek, A.W., 'Inelastic seismic response of simple eccentric structures', Journal of Earthquake Engineering and Structural Dynamics 19, 255-269 (1985).

5. R. K. Goel and A. K. Chopra, 'Inelastic seismic response of one-story, asymmetric plan systems', Report No. EERC 90/14, University of California, Berkeley, CA., Oct. 1990.

6. Hejal, R. and Chopra, A.K.'Response spectrum analysis of class of torsionally-coupled buildings', Journal of Engineering Mechanics ASCE, 115(8).

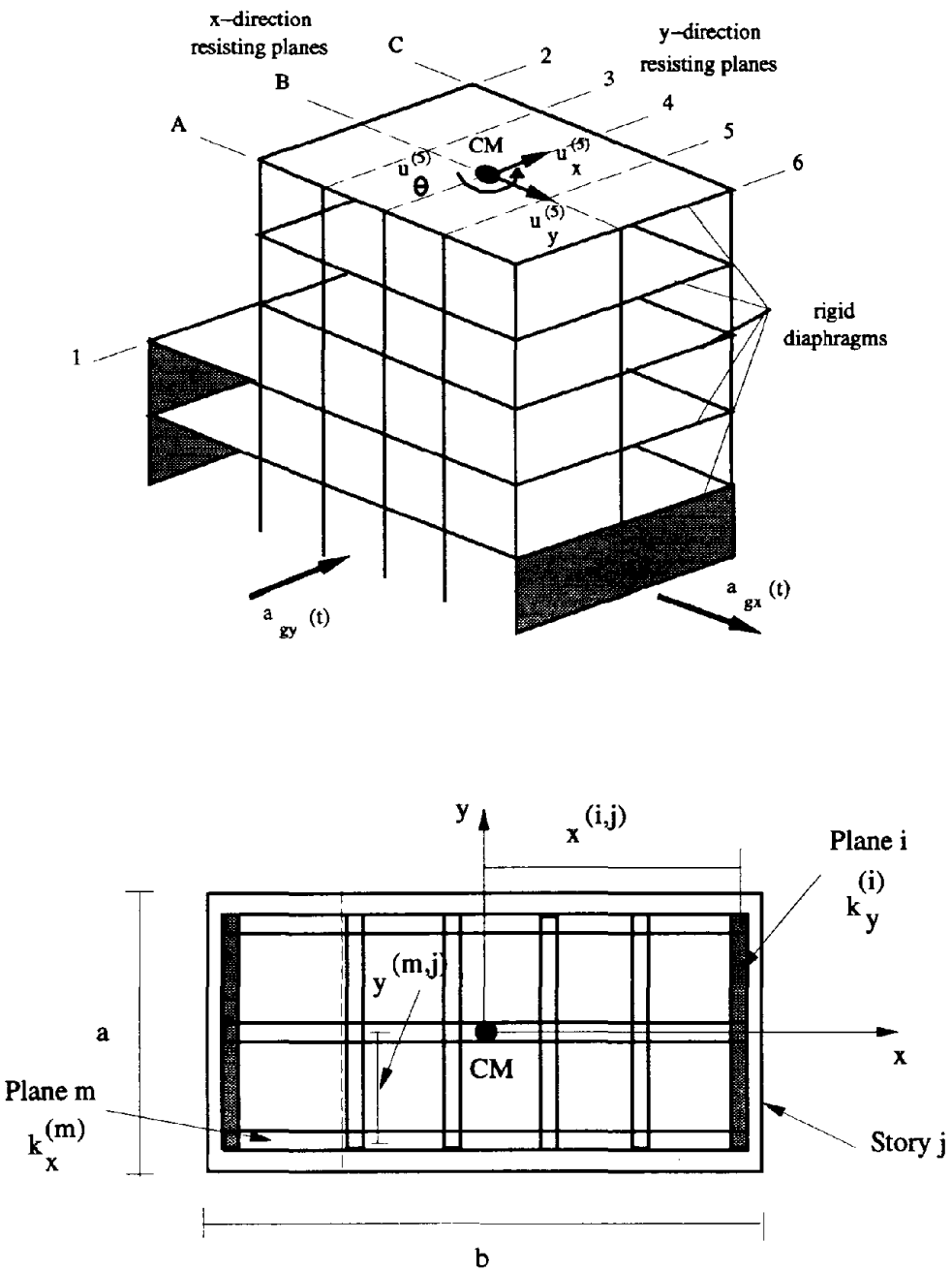

Figure 1 Typical five–story building considered

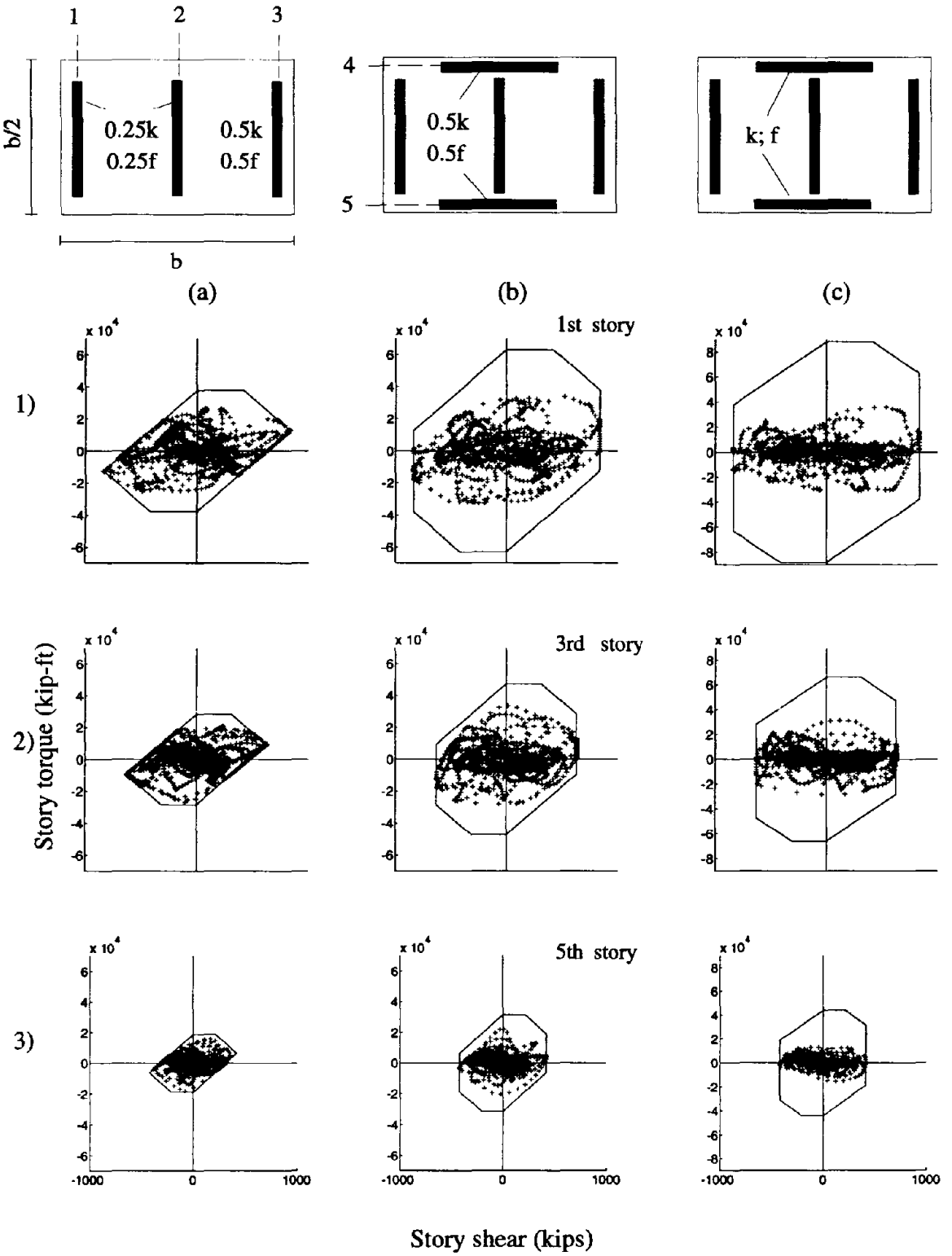

Figure 2 Story shear and torque response histories for buildings with different capacities in the orthogonal resisting planes

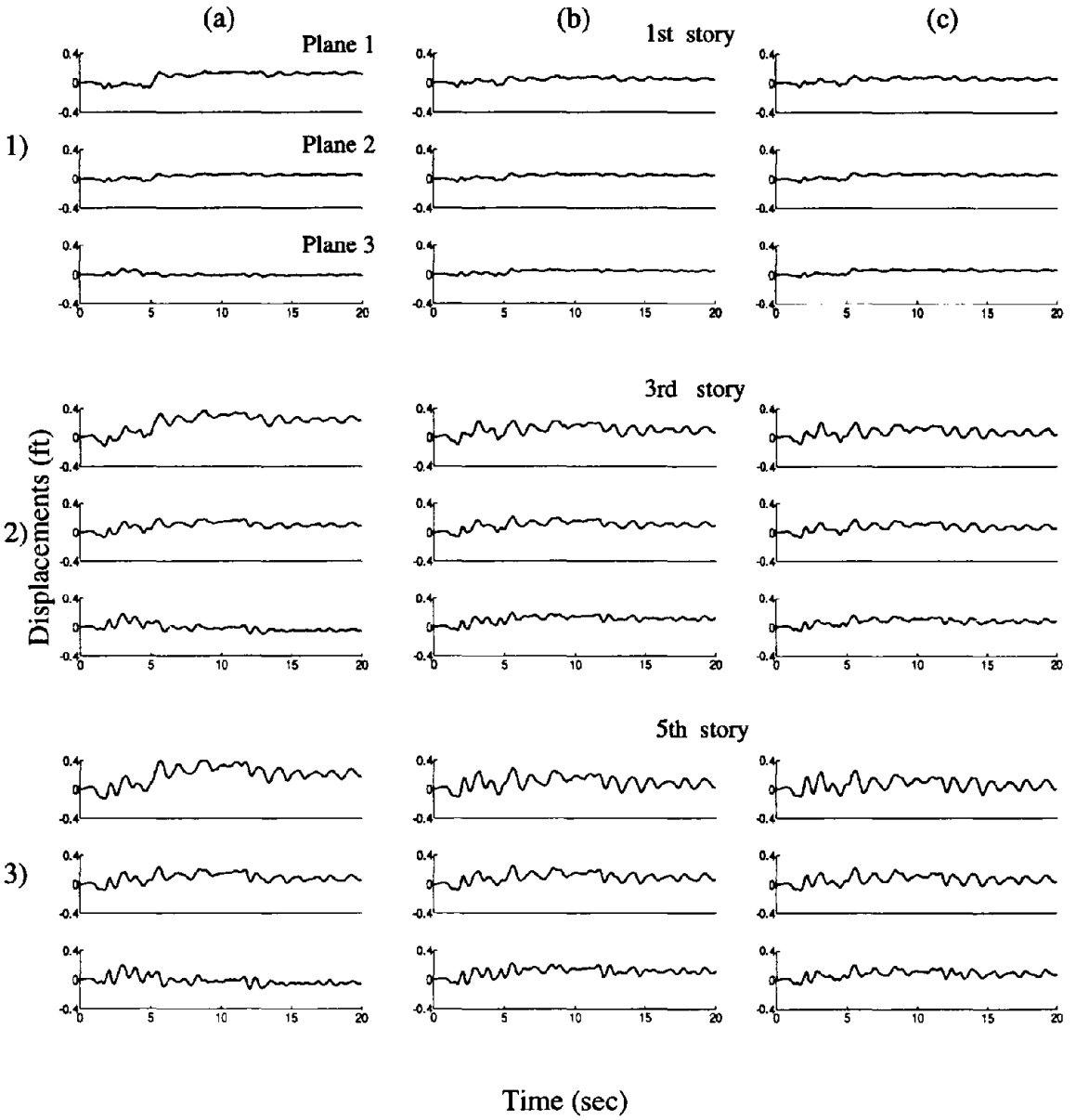

Figure 3 Displacements in edge and central resisting planes for buildings with different capacities in the orthogonal resisting planes

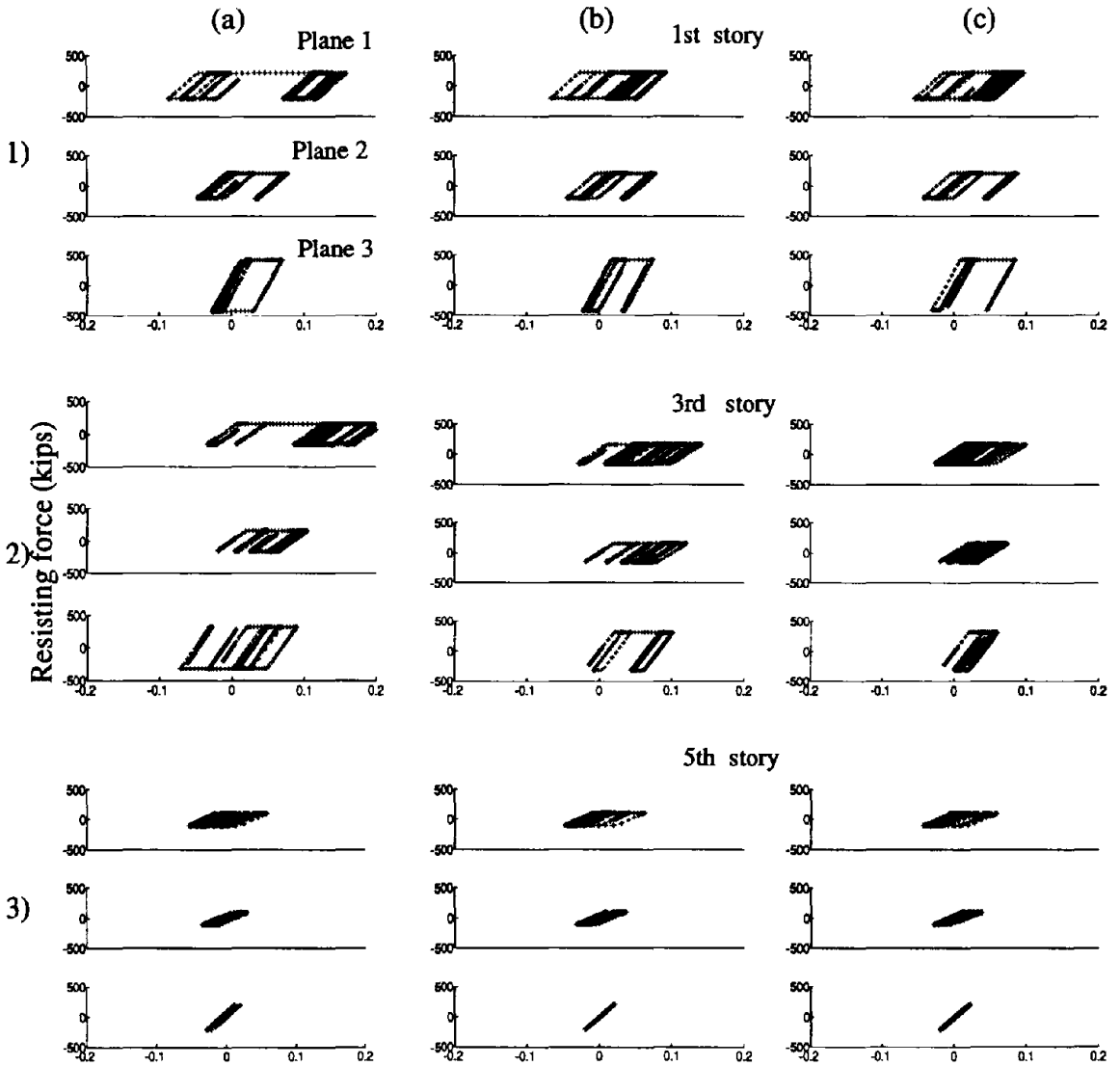

Figure 4 Forces in edge and central resisting planes for buildings with different capacities in the orthogonal resisting planes

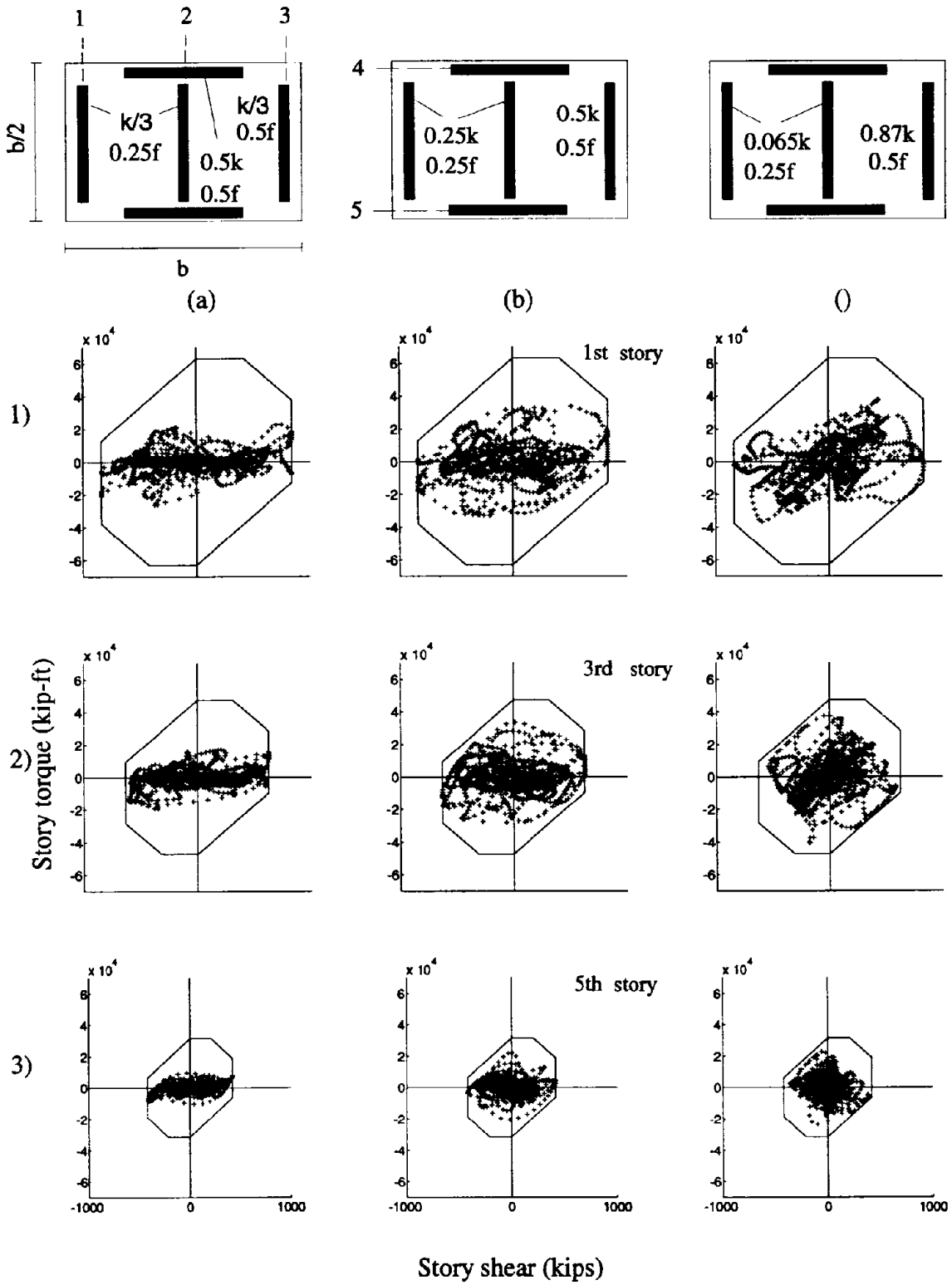

Figure 5 Story shear and torque response histories for buildings with different stiffness eccentricity

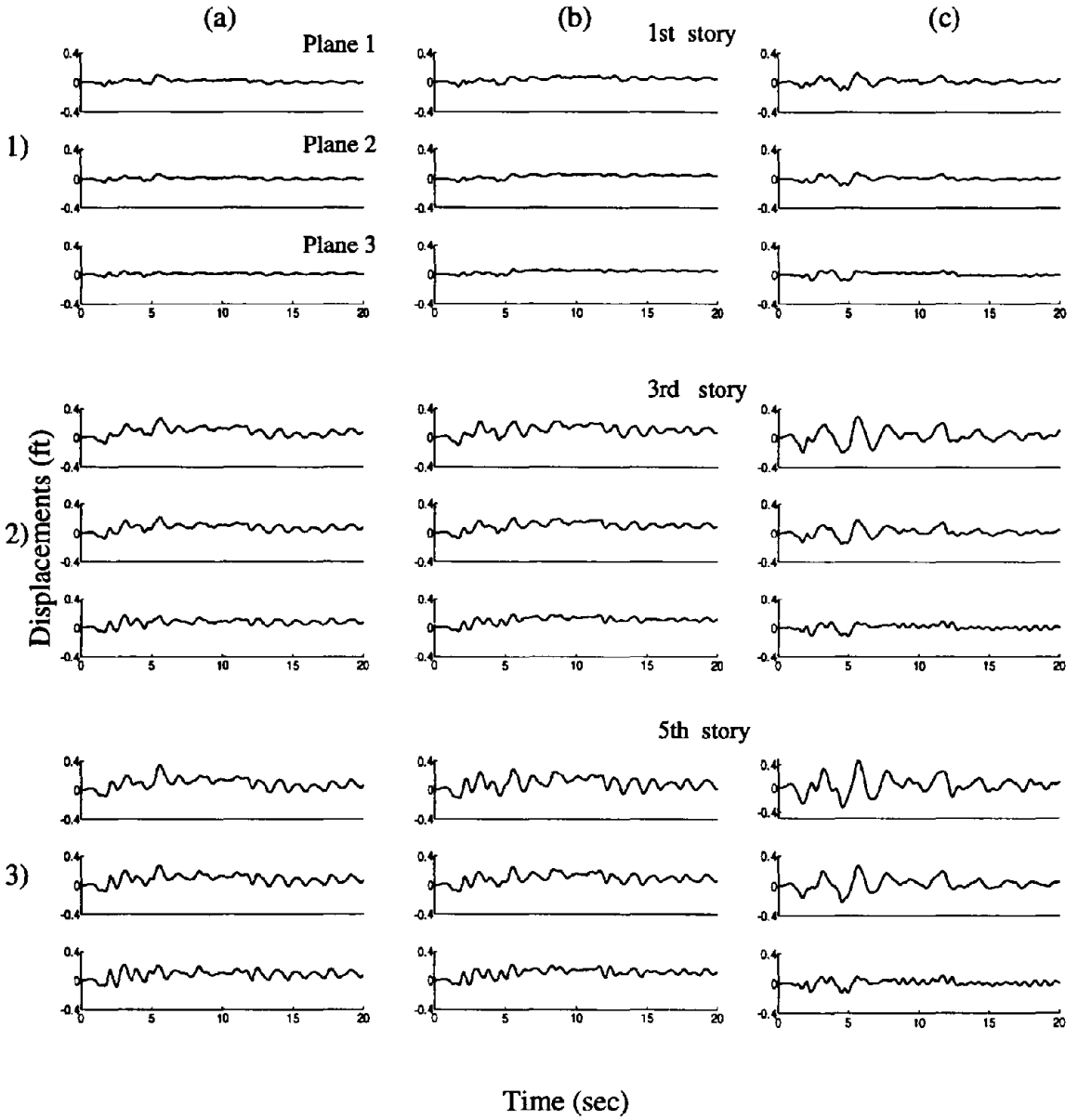

Figure 6 Displacements in edge and central resisting planes for buildings with different stiffness eccentricity

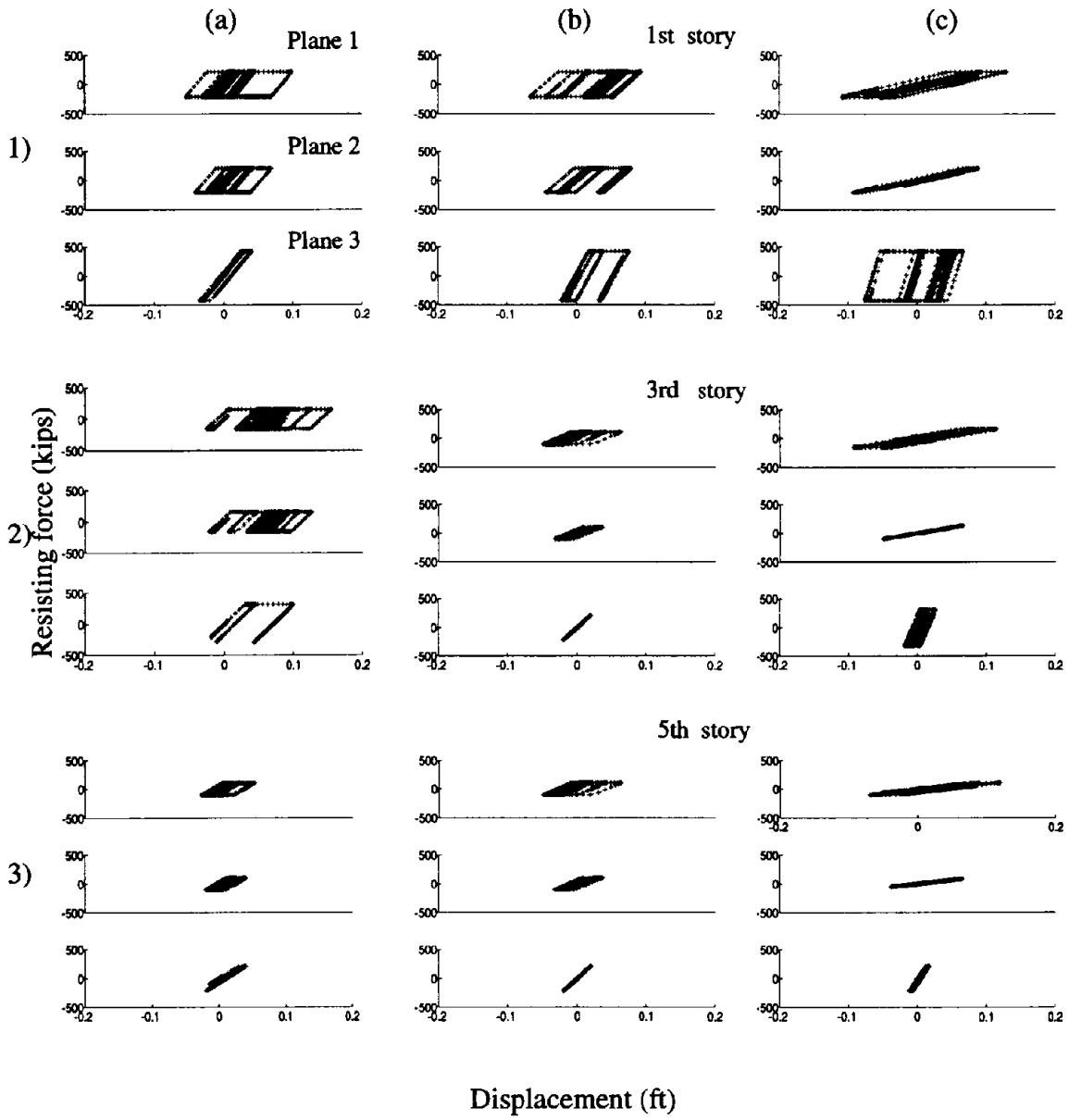

Figure 7 Forces in edge and central resisting planes for buildings with different stiffness eccentricity

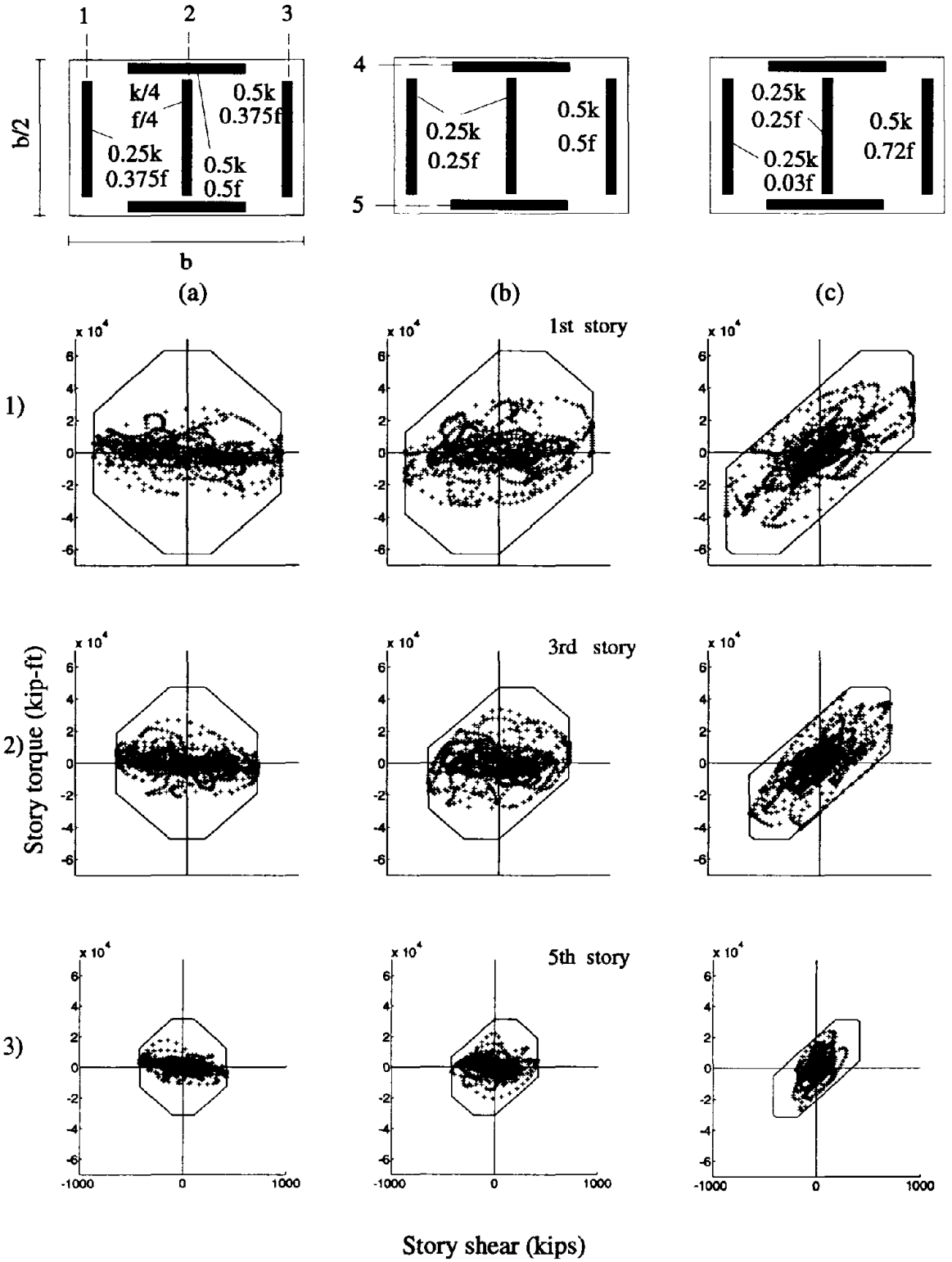

Figure 8 Story shear and torque response histories for buildings with different strength eccentricity

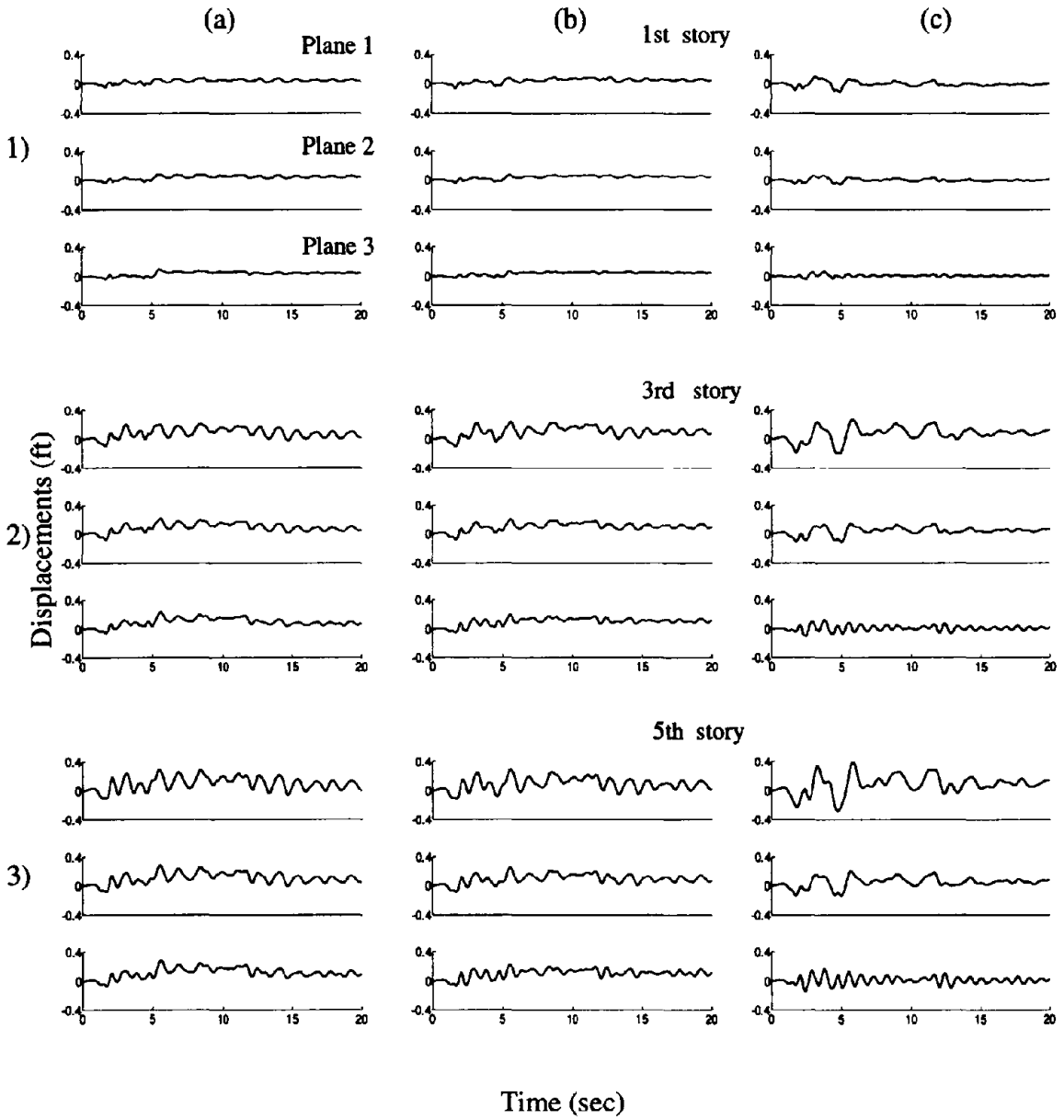

Figure 9 Displacements in edge and central resisting planes for buildings with different strength eccentricity

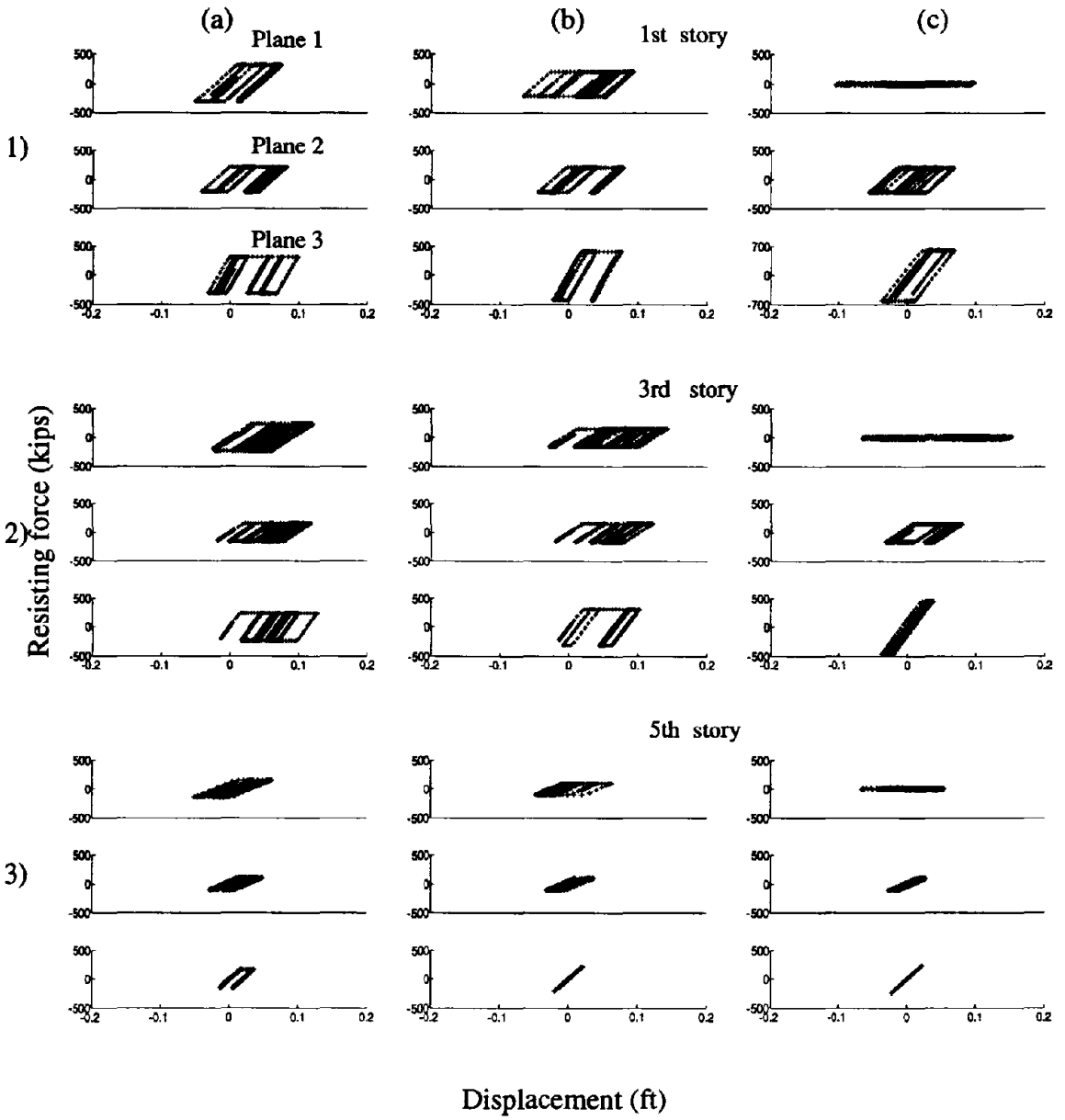

Figure 10 Forces in edge and central resisting planes for buildings with different strength eccentricity

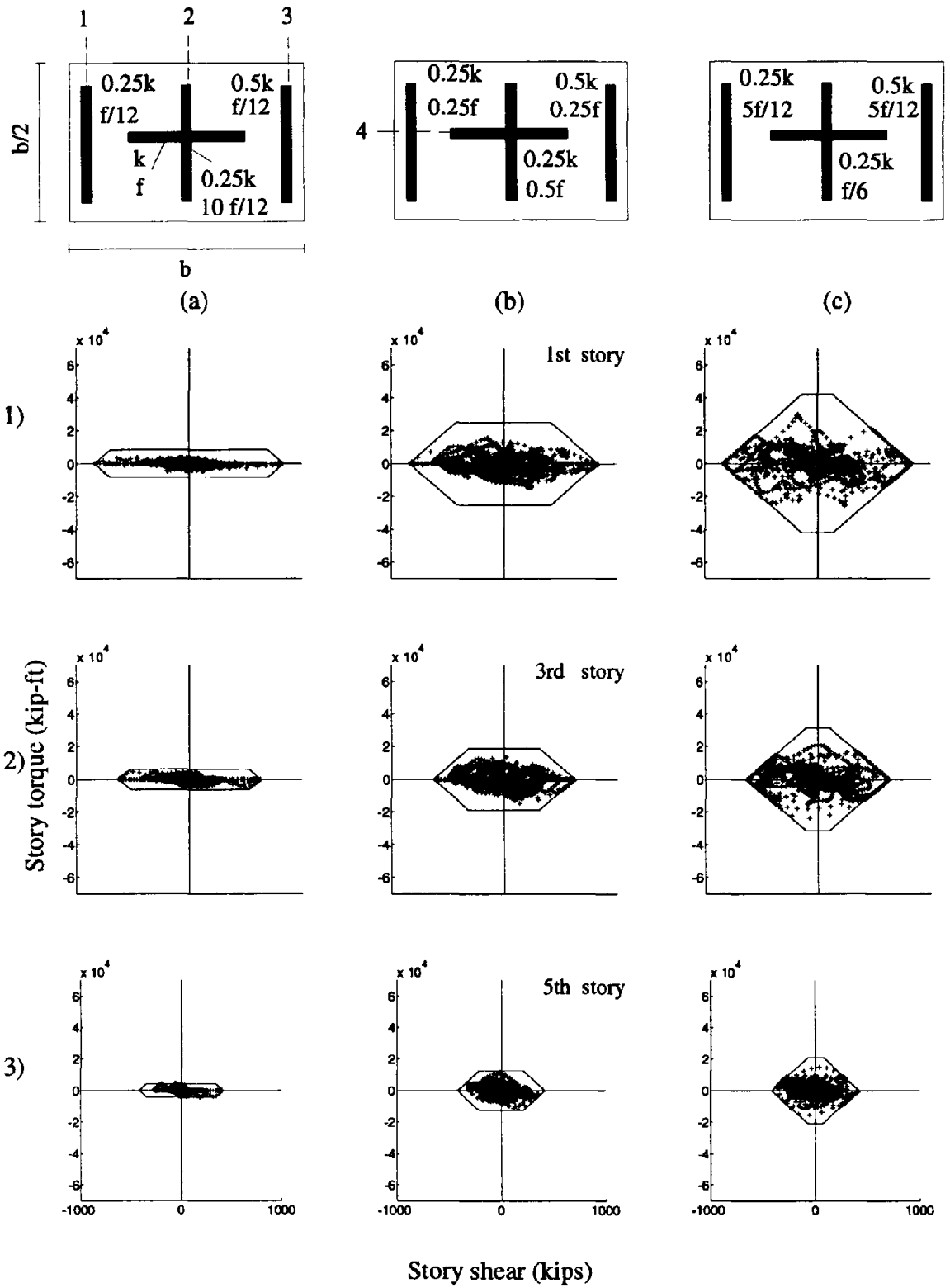

Figure 11 Story shear and torque response histories for buildings with different planwise distribution of strength

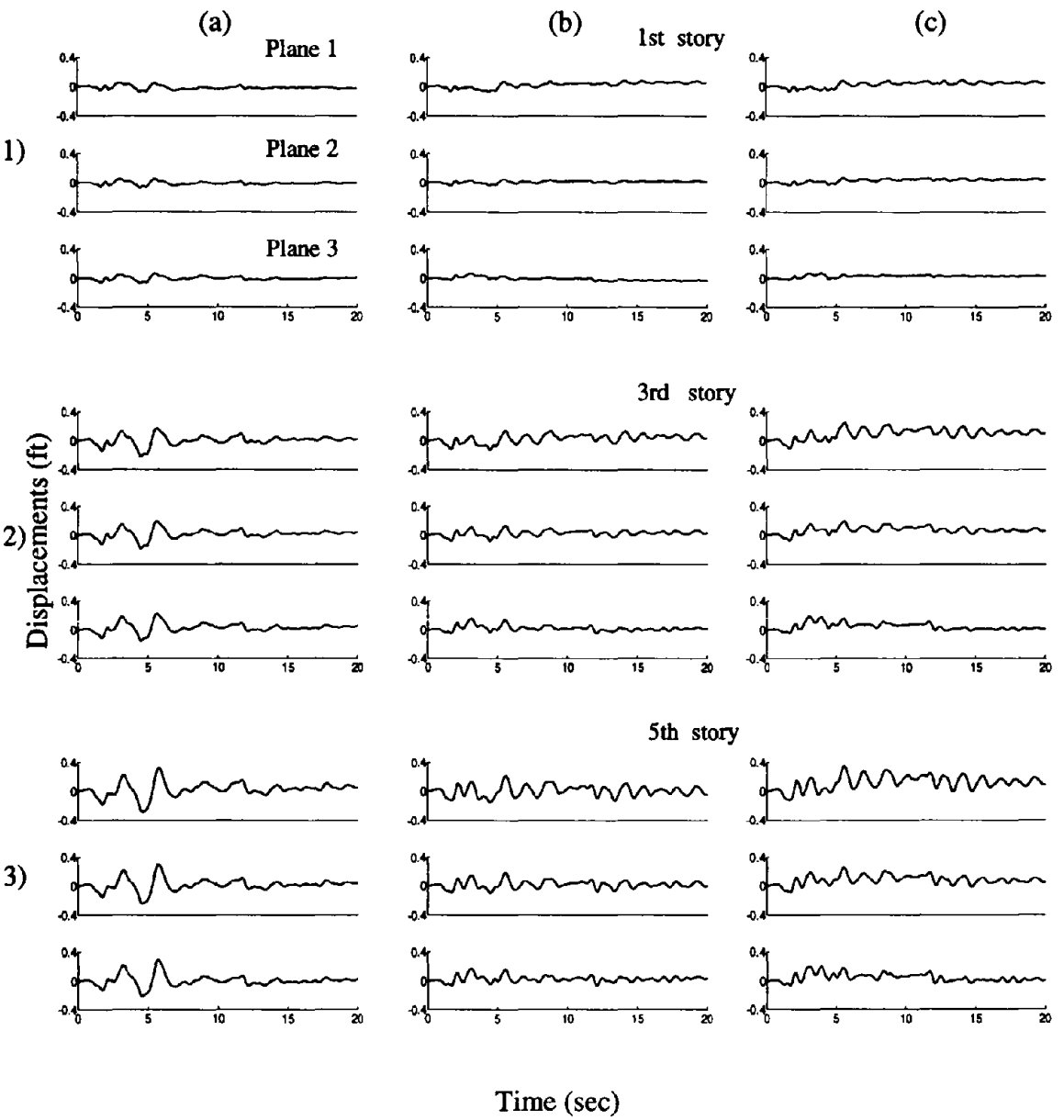

Figure 12 Displacements in edge and central resisting planes for buildings with different planwise distribution of strength

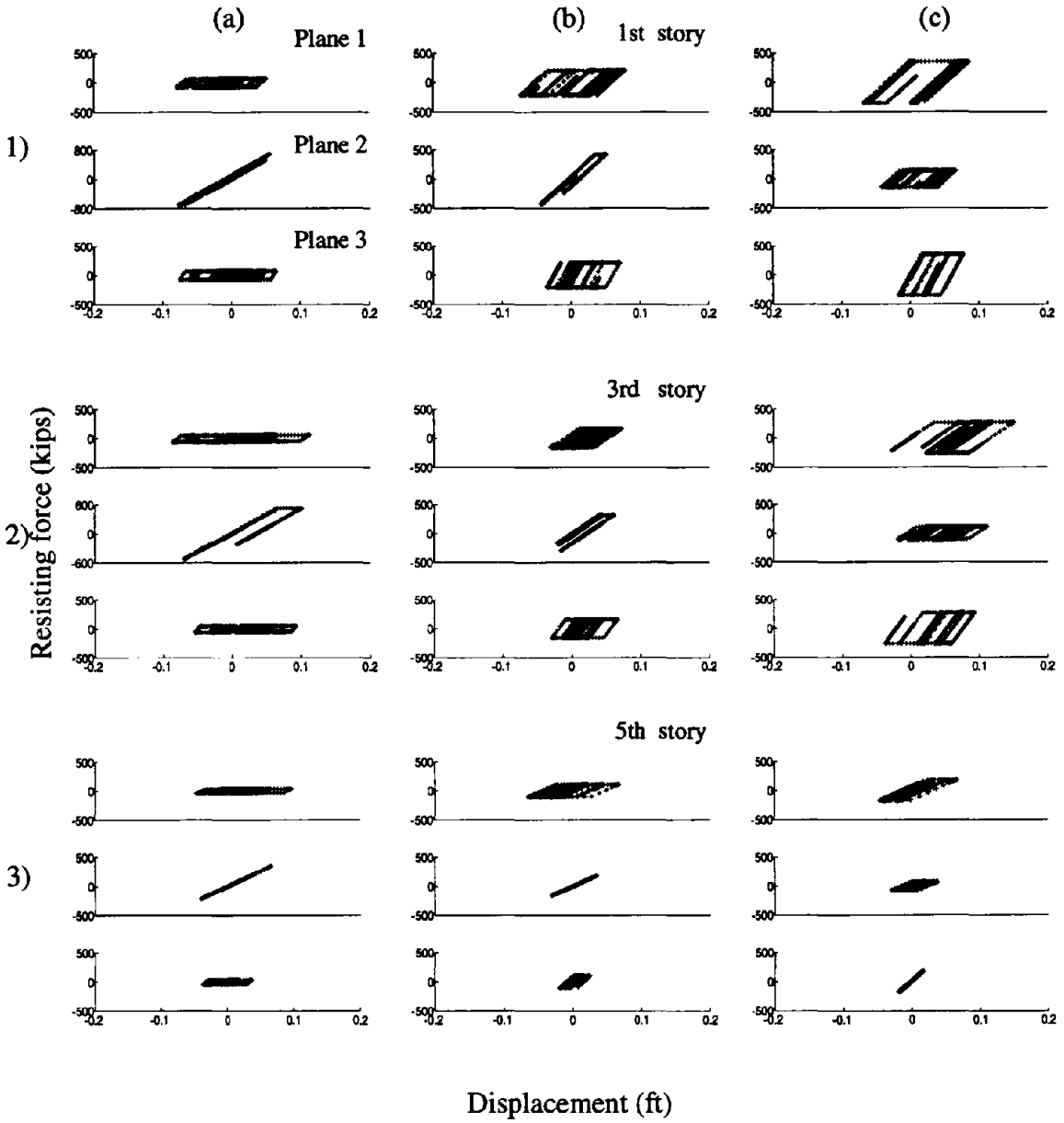

Figure 13 Forces in edge and central resisting planes for buildings with different planwise distribution of strength

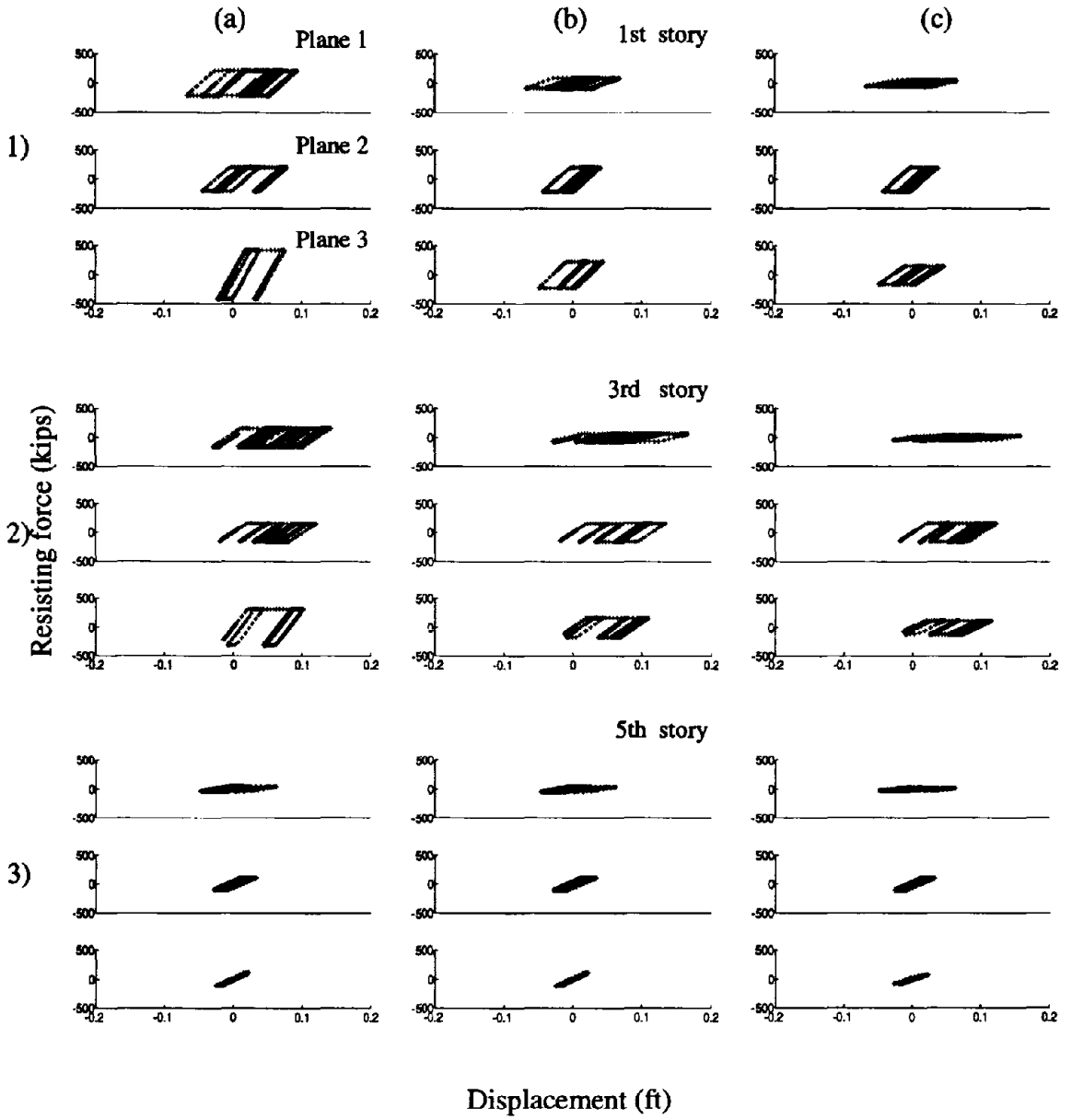

Figure 16 Forces in edge and central resisting planes for buildings with different number of resisting planes

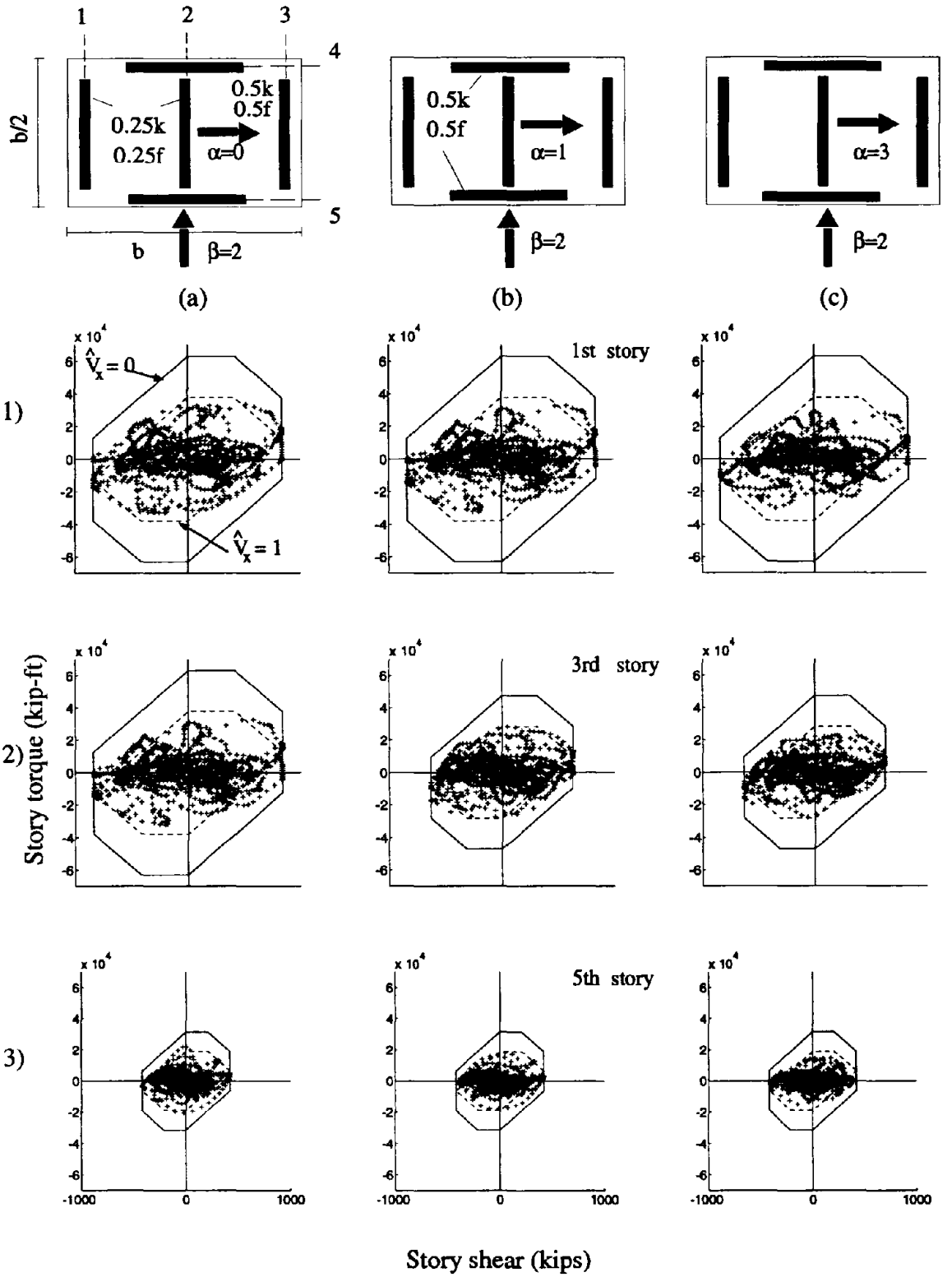

Figure 17 Story shear and torque response histories for buildings subjected to bidirectional ground motion

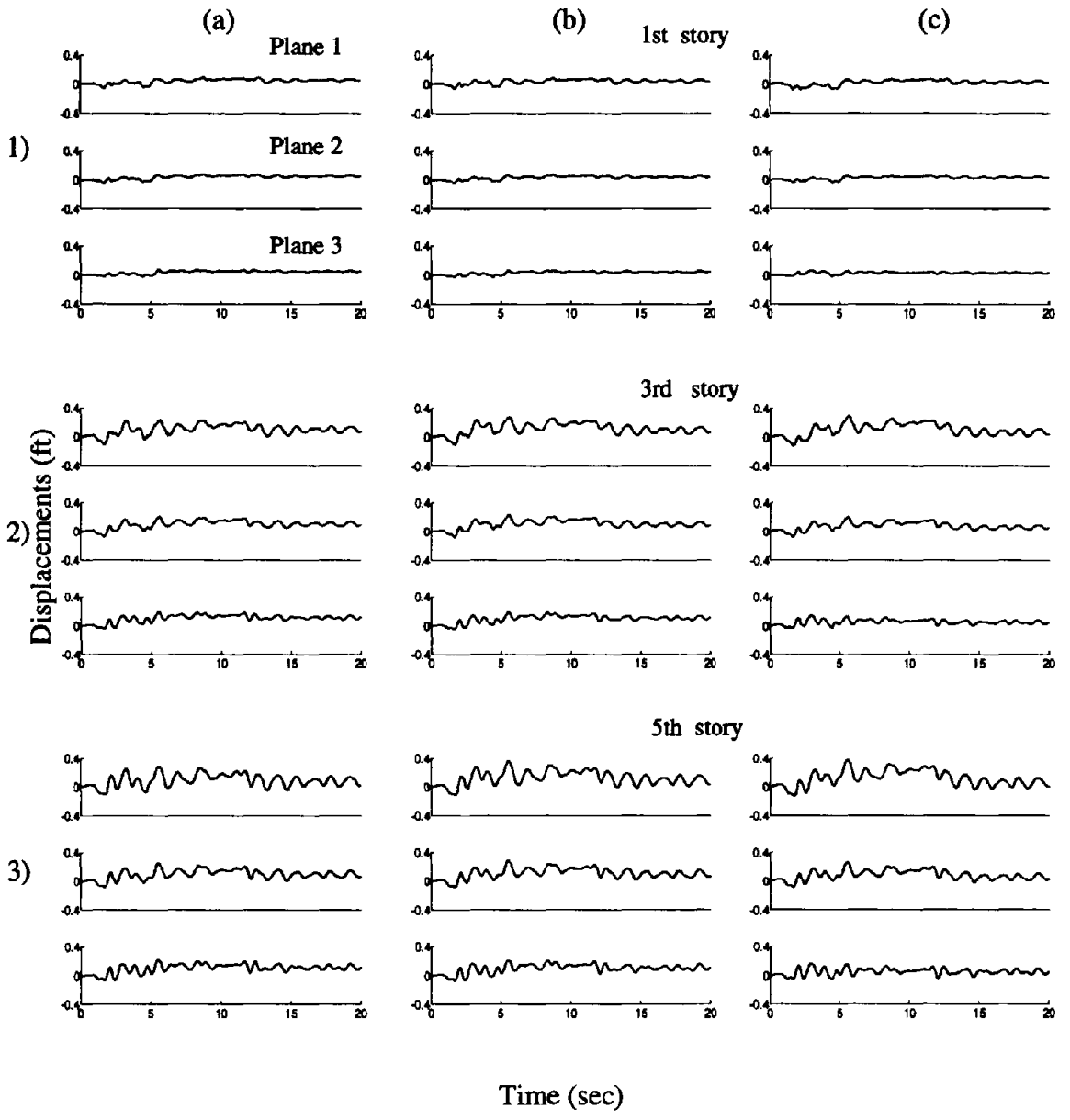

Figure 18 Displacements in edge and central resisting planes for buildings subjected to bidirectional ground motion

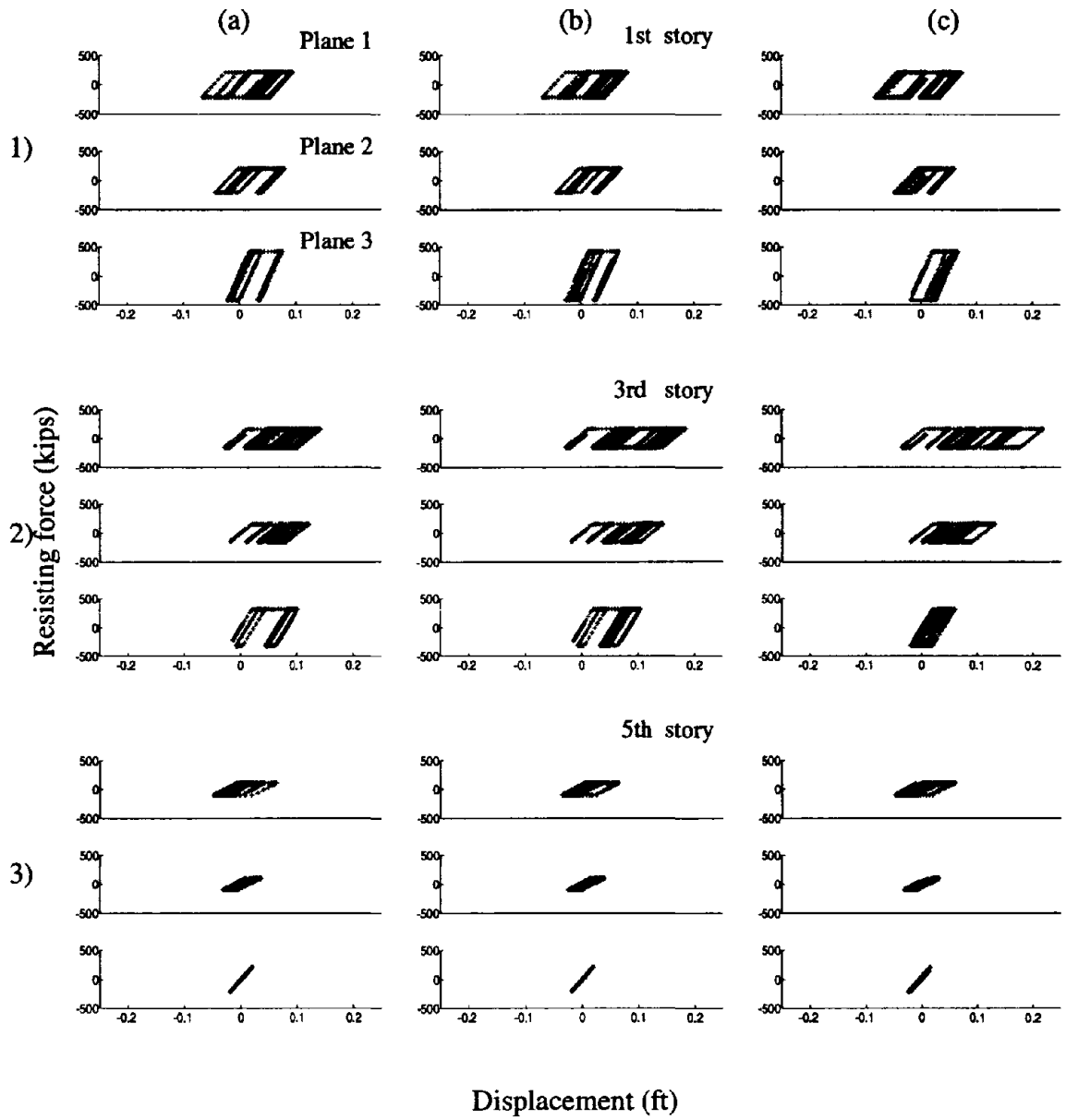

Figure 19 Forces in edge and central resisting planes for buildings subjected to bidirectional ground motion

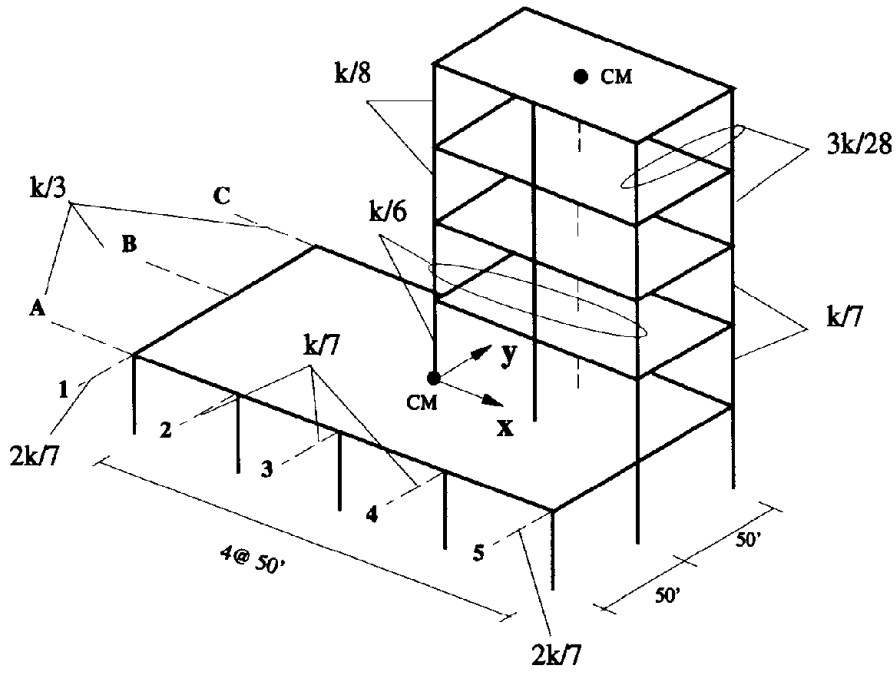

a) Building example considered

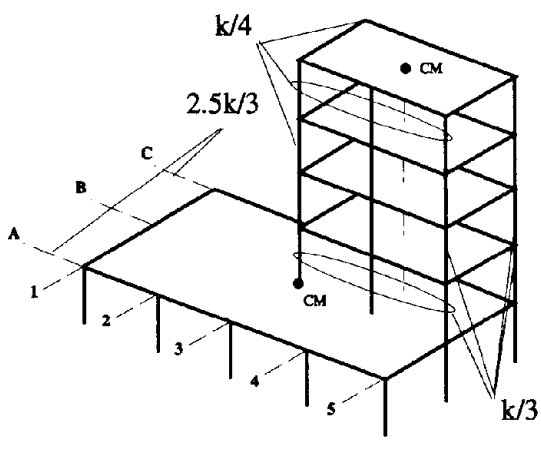

b) retrofit solution 1

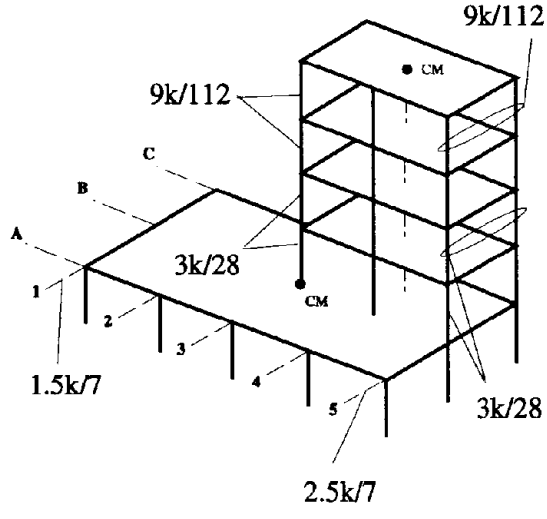

c) retrofit solution 2

Figure 20 Building example considered and two possible retrofit solutions to improve its torsional behavior

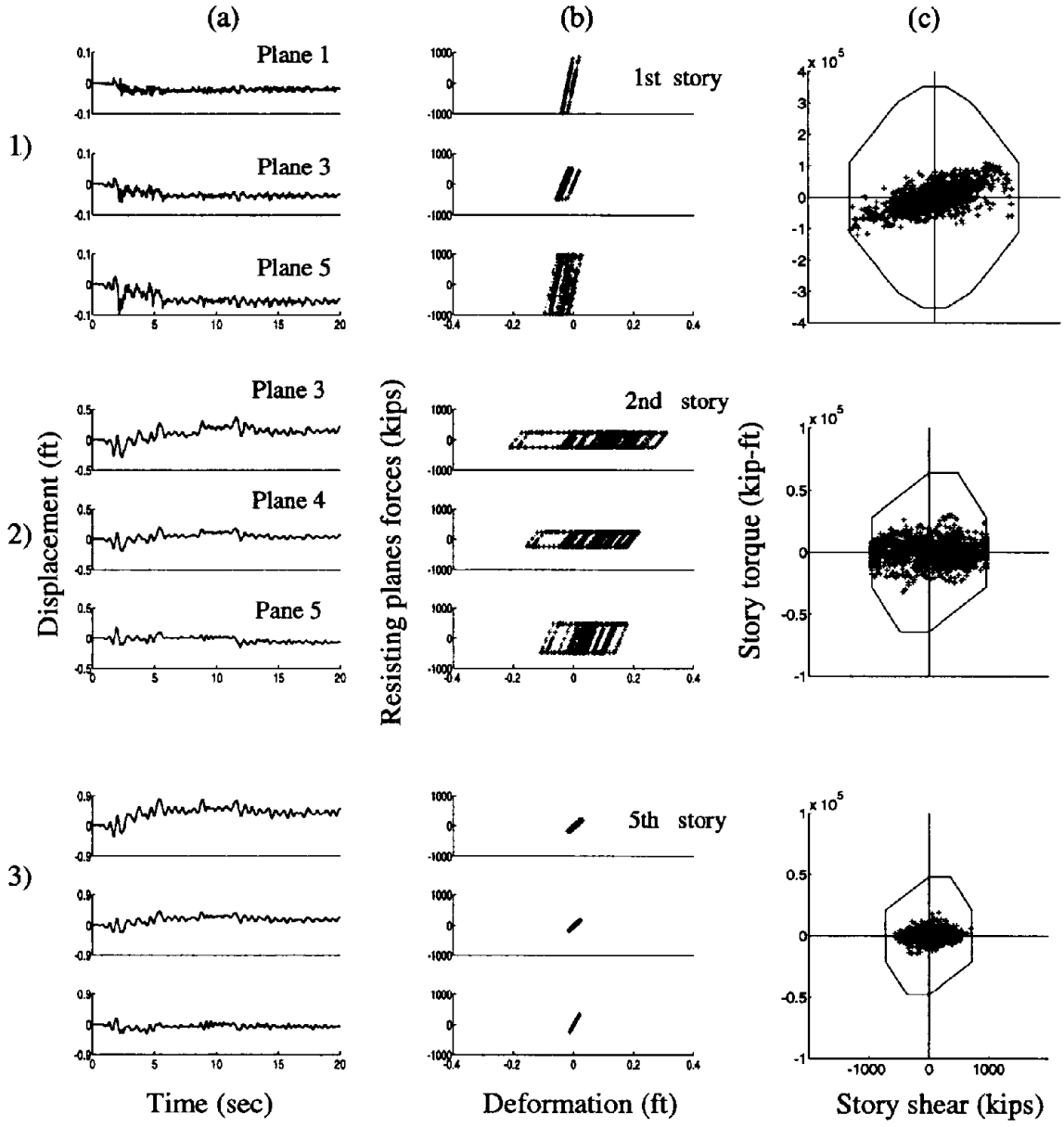

Figure 21 Behavior of building example

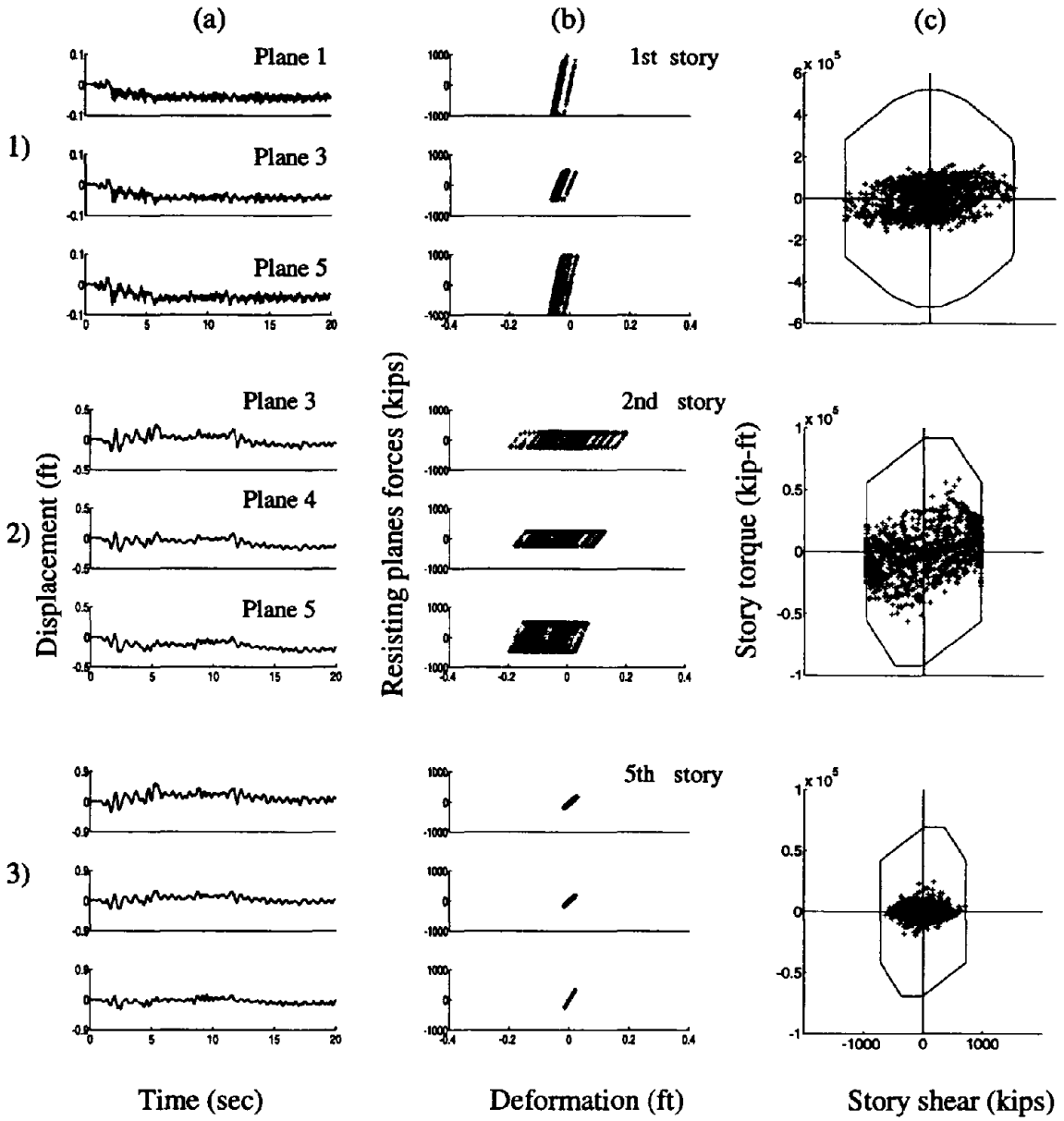

Figure 22 Behavior of building with increased strength in orthogonal resisting planes

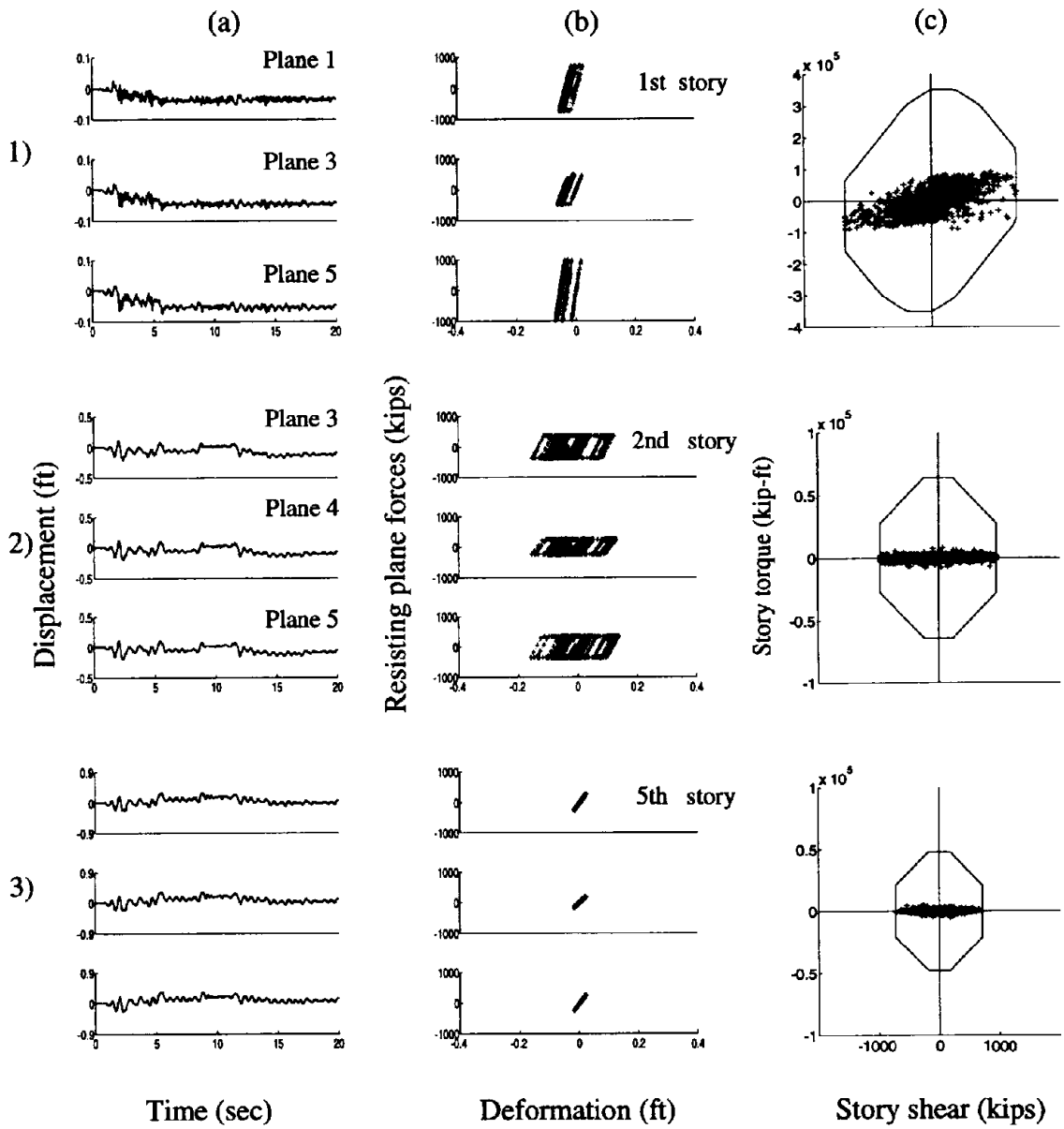

Figure 23 Behavior of building with modified stiffness and strength in edge resisting planes

4. A SIMPLIFIED MODEL FOR ANALYSIS AND DESIGN OF ASYMMETRIC-PLAN BUILDINGS

4.1 Introduction

The objective of this section is to develop a simplified method for analysis of asymmetric-plan multistory buildings. The method considers one structural super-element (SE) per building story, which is capable of representing the elastic and inelastic properties of the story. In the proposed method two important concepts merge: the available knowledge of the seismic response of asymmetric structures developed in Chapters 2 and 3, and some of the analytical tools of more refined inelastic analysis.

This investigation is organized in five sections. After describing the systems considered and their governing equations of motion in Section 4.2, the steps required to construct the SE model for a building story are presented in Section 4.3, where also the accuracy of the SE model is tested. A building example is then developed in Section 4.4 in order to show the steps required for the construction of a SE model for a multistory structure. Finally, some concluding remarks are presented in section 4.5.

4.2 Systems considered and analysis procedure

The multistory buildings considered were already described in Chapter 3 (Section 3.2) and a typical example is presented again in Fig. 1a. The dynamic response of the system to base acceleration $a_{gy}(t)$ in the y-direction is described by the following equations of motion:

$$\boldsymbol{M\ddot{u} + C\dot{u} + R(\delta, \dot{\delta}) = -Mra_g} \tag{1}$$

where $\boldsymbol{u} = \{u_x u_y u_\theta\}^T$; $\boldsymbol{M}$ is the mass matrix given by

$$\boldsymbol{M} = \begin{bmatrix} \boldsymbol{m} & & \\ & \boldsymbol{m} & \\ & & \boldsymbol{I_p} \end{bmatrix} \tag{2}$$

where $\boldsymbol{m}$ and $\boldsymbol{I_p}$ are diagonal matrices containing the masses and polar moments of inertia for each building story; $\boldsymbol{C}$ is the linear viscous damping matrix; $\boldsymbol{R(\delta, \dot{\delta})}$ is the vector of restoring forces in the system; $\boldsymbol{r} = \{\mathbf{o}\ \ \mathbf{1}\ \ \mathbf{o}\}^T$ is the influence vector for the ground acceleration $a_{gy}(t)$; $\mathbf{1}$ and $\mathbf{o}$ are vectors of ones and zeros respectively of dimension equal to the number of stories n.

The resisting force vector $\boldsymbol{R}(\boldsymbol{\delta}, \dot{\boldsymbol{\delta}})$ is , in general, a function of the deformations $\boldsymbol{\delta}$ and deformation rates $\dot{\boldsymbol{\delta}}$ of the resisting planes in the structure. These deformations are computed, within the assumption of small displacements , by a linear transformation $\boldsymbol{\delta} = \boldsymbol{L}\boldsymbol{u}$ of the structural degrees of freedom $\boldsymbol{u}$; similarly, $\dot{\boldsymbol{\delta}} = \boldsymbol{L}\dot{\boldsymbol{u}}$. For example, the lateral deformation of the first-story wall of resisting plane 1 in Fig. 1a is given by

$$\delta = \{\underbrace{0 \ldots 0}_{1xn} \quad \underbrace{1 \ 0 \ldots 0}_{1xn} \quad \underbrace{x^{(1,1)} \ 0 \ldots 0}_{1xn}\} \begin{Bmatrix} u_x \\ u_y \\ u_\theta \end{Bmatrix} \tag{3}$$

Equation (3) constitutes one row of the displacement transformation $\boldsymbol{L}$; subsequent rows will contain the relation between the deformations in other stories and resisting planes and the structural degrees of freedom.

If all resisting planes in the structure remain elastic during the earthquake, the restoring force vector $\boldsymbol{R}(\boldsymbol{\delta}, \dot{\boldsymbol{\delta}})$ is computed by Hooke's law

$$\boldsymbol{R}(\boldsymbol{u}) = \boldsymbol{K}\boldsymbol{u} \tag{4}$$

where $\boldsymbol{K}$ is the stiffness matrix of the system given in block-form by

$$\boldsymbol{K} = \begin{bmatrix} \boldsymbol{K}_x & 0 & 0 \\ 0 & \boldsymbol{K}_y & \boldsymbol{K}_{y\theta} \\ 0 & \boldsymbol{K}_{y\theta} & \boldsymbol{K}_\theta \end{bmatrix} \tag{5}$$

where $\boldsymbol{K}_x = \sum_i \boldsymbol{k}_x^{(i)}$ and $\boldsymbol{K}_y = \sum_i \boldsymbol{k}_y^{(i)}$ are the lateral stiffness matrices in the x- and y-directions, respectively; $\boldsymbol{K}_\theta = \sum_i \boldsymbol{X}^{(i)}\boldsymbol{k}_y^{(i)}\boldsymbol{X}^{(i)} + \boldsymbol{Y}^{(i)}\boldsymbol{k}_x^{(i)}\boldsymbol{Y}^{(i)}$ is the torsional stiffness matrix of the system with respect to the CM; $\boldsymbol{X}^{(i)} = [x^{(i,j)}]$ and $\boldsymbol{Y}^{(i)} = [y^{(i,j)}]$ are diagonal matrices with j^{th} diagonal terms equal to the coordinates of the i^{th} resisting plane at the j^{th} story measured from the CM; and $\boldsymbol{K}_{y\theta} = \sum_i \boldsymbol{k}_y^{(i)}\boldsymbol{X}^{(i)}$ is the matrix representing the elastic lateral-torsional coupling in the system.

On the other hand, if the resisting planes deform beyond their elastic limit, the restoring force vector $\boldsymbol{R}(\boldsymbol{\delta}, \dot{\boldsymbol{\delta}})$ is a general nonlinear function depending on the history of the deformation and deformation rates of the resisting planes. In this case the restoring forces in the structural system are computed by assembling the contribution of the forces resisted by each plane into the vector $\boldsymbol{R}(\boldsymbol{\delta}, \dot{\boldsymbol{\delta}})$. It is the objective of the SE model developed to provide an accurate estimate for the restoring force vector $\boldsymbol{R}(\boldsymbol{\delta}, \dot{\boldsymbol{\delta}})$.

For the numerical examples presented, the equations of motion (Eq. (1)) will be integrated numerically using the partitioned predictor-corrector scheme developed in reference [1]. In this approach the nonlinear restoring force $\boldsymbol{R}(\boldsymbol{\delta}, \dot{\boldsymbol{\delta}})$ is transferred to the right hand side of Eq. (1) and treated as an extra loading term on the system, which is first assumed constant during the integration step and then corrected. This algorithm shows good accuracy and stability properties and is especially efficient when part of the system is known to remain elastic during the complete response history.

The response quantities of interest in this study are: (1) the combinations of story shear and torque at different instants of the response, represented in the three-dimensional space spanned by story shears $V_x^{(j)}$ and $V_y^{(j)}$ in the x and y-directions and the story torque $T^{(j)}$; (2) the displacement histories at the building edges and CM–these displacements are computed from the degrees of freedom $\boldsymbol{u}$ at the CM; and (3) the force-displacement histories in the structural elements.

4.3 Formulation of the SE model

The objective of this section is to develop the theoretical model of the SE. This is done in three phases. First, the parameters required to describe the linear and inelastic properties of the SE are described. Second, the analytical formulation, basically the force-displacement relation, of the model is presented. And finally, the accuracy of the model is tested using several different single-story structural configurations.

4.3.1 Elastic properties

The SE model of a building is composed by a single fictitious structural element per story capable of representing the elastic and inelastic properties of the story and having three degrees of freedom per node (Fig. 1b)—the two horizontal translations and the rotation of the floors connected by the element. The elastic and inelastic properties of the SE are matched to those of the story with multiple resisting planes. This is simple in the elastic case where the SE model is assumed to have the same stiffness matrix as the story considered, i.e.

$$\boldsymbol{K}_{SE} = \begin{bmatrix} \boldsymbol{K} & -\boldsymbol{K} \\ -\boldsymbol{K} & \boldsymbol{K} \end{bmatrix} \tag{6}$$

3. V_{yc} is the capacity of the resisting planes in the y-direction passing through the CM of the system; in practical terms, it will represent the capacity of all resisting planes 'close' to the CM.

4. $T_o = \sum_{i=1}^{N} |f_y^{(i)} x^{(i)}| + \sum_{i=1}^{M} |f_x^{(i)} y^{(i)}|$ is the torsional capacity of the system.

5. $T_\perp = \sum_{i=1}^{M} f_x^{(i)} y^{(i)}$ is the torque provided by the resisting planes in the orthogonal direction.

6. $x_p = \sum_{i=1}^{N} f_y^{(i)} x^{(i)} / V_{yo}$ is the strength eccentricity, or first moment of strength; and

7. $V_{yu} = \sum_{\substack{i=1 \\ i \neq 2}}^{N} f_y^{(i)} \ x^{(i)} / |x^{(i)}|$ is denoted as the 'strength unbalance' in the story.

In order to understand the physical meaning of these parameters, let us consider how do they influence the shape of the SST surface:

1. The normalized story shear $\hat{V}_x$ controls the variation of the SST ultimate surface along the V_x shear axis. Equation (9) shows that this variation is linear; $\hat{V}_x$ varies from 0 at $V_x = 0$ to one at $V_x = V_{xo}$. This variation results from a lesser contribution to the torsional capacity of the system by the resisting planes in the orthogonal direction. In presence of an x-direction component of ground motion, these planes must undergo translation along this direction, and, hence, are limited in their capacity to develop large force-couples to resist the story torque (Chapter 2).

2. The lateral capacity V_{yo} corresponds to the maximum shear that can be developed during a purely translational mechanism of the story (Chapter 2). This value limits the maximum and minimum abscissas of the SST surface.

3. The capacity V_{yc} of resisting planes passing through the CM controls the length of the constant torque branches of the SST surface (Fig. 3). As explained in reference (Chapter 2), these branches are associated to predominantly torsional mechanisms of the story; therefore, an increase in the value of V_{yc} implies a larger number of these mechanisms on the SST surface. In practical structures, this parameter should be used to consider the capacity of resisting planes not only passing exactly through the CM but 'close' to it. Such is the case because resisting planes passing close to the CM determine branches of the SST surface that are essentially flat (Chapter 2). These branches could be modeled, for practical purposes, as part of the same constant torque branch with length V_{yc} equal to the sum of the lateral capacities of all these central planes (see building example later).

4. The torsional capacity T_o corresponds to the torque developed in a purely torsional mechanism of the story. It determines the maximum and minimum ordinates of the SST ultimate surface. Large values of T_o are associated generally with systems with strong resisting planes along the edges; small values of T_o are characteristic of building with strong central cores.

5. The torsional capacity $T_\perp$ provided by the resisting planes in the orthogonal direction controls the length of the constant shear branches of the SST surface. These branches of the surface are associated with story mechanisms that are predominantly translational (Chapter 2), i.e., involving yielding of all resisting planes in the y-direction. Results presented in reference (Chapter 2) showed that this parameter has an important effect on the inelastic behavior of asymmetric buildings, mainly because it controls a critical region of the surface where most inelastic behavior takes place. Larger values of $T_\perp$ lead to constant shear branches (Fig. 3) that are longer, thus, improving the chances for the system to develop mechanisms where the displacement demands and yielding on the resisting planes are more uniform.

6. The strength eccentricity x_p corresponds to the slope of the ray connecting the center of the surface and the middle point of the constant shear branch 1-8 (Fig. 3). Indeed, this middle point is defined by the shear capacity V_{yo} and the torque $T = \sum_{i=1} f_y^{(i)} x^{(i)}$ corresponding to a purely translational mechanism of the story. It is apparent from the figure that the value of x_p determines in part the skewness and width of the SST surface. Large values of strength eccentricity, for instance, lead to very skewed and narrow surfaces as a result of the predominance in strength of one resisting plane. The consequences of this skewness in terms of the building response was studied in Chapter 2.

7. Finally, the 'strength unbalance' V_{yu} controls the abscissa of the central point of the constant torque branch of the SST surface at positive torque (Fig. 3). Physically V_{yu} corresponds to the story shear developed in the system for a purely torsional mechanism about a vertical axis passing through the central resisting plane. As in the case of strength eccentricity, this parameter also controls the skewness of the surface. The strength unbalance is zero only when the lateral capacities of the resisting planes on the two sides of the CM are identical. Otherwise V_{yu} is greater than zero if the sum of the capacities of the resisting planes at the right of the CM is larger than that of the resisting planes at the left of the CM.

At least three important observations can be obtained from the SST surface shown in Fig. 3.

Firstly, as mentioned above, Eq. (10) provides an exact model for the SST surface of systems with three resisting planes along the direction of ground motion. This can be verified in Fig. 4, where the SST surfaces for the exact and the SE models (Eq. (10)) are shown for two three-plane single-story systems; it is apparent from the figure that both SST surfaces are identical. We must also recognize that the potential use of this SE model surface goes much farther than a simple three-plane structure. Three important reasons justify this. First, research results obtained previously [e.g. 2; Chapter 2] have shown that the response of asymmetric structures does not depend significantly on the number of resisting planes. Therefore, it is always possible to construct a three-plane model for a building that captures the essential behavior of the multi-plane structure. This model is the one described by Eq. (10). Second, since the the inelastic behavior of the system usually occurs in small regions of the SST surface, we can always obtain an accurate representation of this region of the surface by the model presented in Eq. (10). Third, because of the convexity property of yield surfaces (Chapter 2), the model proposed is always slightly inside the true SST surface for structures with more than three resisting planes and, hence, leads to conservative results.

Secondly, the constant torque branches 2-3 and 6-7 of the SST surface (Fig. 3) imply that the system has one (or several) central resisting plane(s) passing through (or close to) the CM. We can easily generalize this model and consider the SST surface of a story with an eccentric central resisting plane located at distance x_c relative to the CM. The SST surface for this model is presented using dashed lines in Fig. 3. This surface corresponds to the most general case for a three-plane structure in the direction of ground motion and having orthogonal resisting planes. Comparison between the two SST surfaces shows that the vertices of the new surface have the same abscissas as before, but their ordinates are changed by adding (vertices 1,2,7, and 8) or subtracting (vertices 3,4,5, and 6) the torque $V_{yc}x_c$. Equation (10) will still give the right coordinates of vertices 1,4,5, and 8 provided the strength eccentricity x_p is that of the new system; however, the ordinates of vertices 2,3,6, and 7 need to be adjusted as follows

$$\begin{aligned} y_2 &= T_o + V_{yc}x_c - T_\perp \hat{V}_x \\ y_3 &= T_o - V_{yc}x_c - T_\perp \hat{V}_x \\ y_6 &= -y_2 \quad y_7 = -y_3 \end{aligned} \tag{11}$$

Note that for the model with an eccentric central plane (dashed lines in Fig. 3) V_{yu} and T_o are defined for a torsional mechanism about the central plane. The effect of moving the central plane away from the CM produces, as it should, an inclination of the segment 2-3 (6-7) in a slope equal

to x_c (Chapter 2). More physically, this branch is associated to predominantly torsional story mechanisms that leave the central plane elastic.

Thirdly, from a conceptual standpoint, it is important to note that since we have parameterized the SST surface (of each story) into physically meaningful parameters, they are likely to be those controlling the inelastic response of the system. This resolves, at least in our view, a long standing question among researchers of how many and which parameters controlled the response of asymmetric structures. The necessary parameters are those required to specify the SST surface, and they are described in Eqs. 10 and 11.

4.3.3 Force-deformation relation

The objective of this section is to describe analytically the force-deformation relation of the SE, based on the elastic and inelastic properties of the element stated in the previous sections. The reader is referred to Appendix A for a proof of the equations presented. Further, since all equations refer to the j^{th}-story, the superscript j is omitted next.

In order to simplify the notation, we denote hereafter the forces in the SE element at time $t_n = n\ dt$, where dt is the sampling time, as $\boldsymbol{F}(t_n)$. The force vector $\boldsymbol{F}(t_n)$ contains the story shears and torque at time t_n, i.e., $\boldsymbol{F}(t_n) = \{V_x(t_n)\ \ V_y(t_n)\ \ T(t_n)\}^T$. Associated with this forces, we also define the inter-story deformations $\boldsymbol{v}$ of the element, which are computed from the difference between the displacements $\boldsymbol{u}$ at stories j and $j-1$. Note that the restoring force vector of the building $R(\boldsymbol{\delta}, \dot{\boldsymbol{\delta}})$ is computed at all instants from the assembly of the element force vectors $\boldsymbol{F}$ in each story.

While the SE is in the elastic range, i.e., it remains inside of the SST surface during the integration step $[t_{n-1}\ \ t_n]$, the force vector $\boldsymbol{F}(t_n)$ generated by the imposed element deformations $\boldsymbol{v}(t_n)$ in the element, is given by Hooke's law (Fig. 5a)

$$\boldsymbol{F}(t_n) = \boldsymbol{K}\boldsymbol{v}(t_n) \tag{12}$$

where $\boldsymbol{K}$ is the stiffness matrix of the story.

Now, considering that the SE is governed by an elasto perfectly plastic constitutive relation, it is possible to show that during plastic behavior of the element the forces $\boldsymbol{F}(t_n)$ are given by (Appendix A)

$$\boldsymbol{F}(t_n) = \boldsymbol{F}(t_{n-1}) + \sum_{m=1}^{Nb} \boldsymbol{K}_m^{ep}(\boldsymbol{v}_{m+1} - \boldsymbol{v}_m) \tag{13}$$

where $\boldsymbol{v}_m$ and $\boldsymbol{v}_{m+1}$ are the deformations corresponding to the points where the element reaches and leaves branch m of the SST surface, respectively, as shown schematically in Fig. 5b; N_b is the number of branches visited by the element during the integration step; and $\boldsymbol{K}_m^{ep}$ is the elasto-plastic matrix corresponding to branch m

$$\boldsymbol{K}_m^{ep} = \boldsymbol{K} - \frac{(\partial\Phi/\partial\boldsymbol{F})_m(\partial\Phi/\partial\boldsymbol{F})_m^T\boldsymbol{K}}{(\partial\Phi/\partial\boldsymbol{F})_m^T\boldsymbol{K}(\partial\Phi/\partial\boldsymbol{F})_m} \tag{14}$$

where Φ is the functional form of the SST surface, and $(\partial\Phi/\partial\boldsymbol{F})_m$ represents the gradient of the m^{th} branch of the surface.

4.3.4 Accuracy of the SE model

In order to test the numerical accuracy of the SE, this element was incorporated into the nonlinear dynamic analysis program INADEL [1]. The accuracy of the SE model is tested in single-story systems; however, these results will also carry over to multistory systems as shown by a later example.

It should be apparent that the SE model leads to the exact response in two cases: (1) when the behavior is elastic, and (2) when the system is symmetric (elastic or inelastic). These observations are verified by considering the inelastic response of the single-story system shown in Fig. 6 subjected to two excitations, an initial velocity at $t = 0$ and the N-S component of El Centro earthquake, both along the y-direction. Compared in this figure are the responses computed for the system using the actual distribution of resisting planes (solid line) and the one using the SE model (small circles). Since both responses are identical, the analysis considering the five resisting planes is unnecessary because one SE would predict the same response. This implies that if the system is symmetric, within the assumption of rigid-floor diaphragms, there is no need in practice to perform an inelastic analysis of a multistory symmetric structure considering the actual distribution of resisting planes; a simple stick model with one SE per floor would suffice.

Consequently, the accuracy of the SE model has to be evaluated only in connection with systems having plan asymmetry. Unfortunately this evaluation cannot be done analytically and numerical experimentation on many systems is required. The four systems considered in Fig. 7 represent a sample of the systems considered in reference (Chapter 2). They all have uncoupled lateral frequency $\omega_y = 4\pi$ ($T_y = 0.5$ sec), constant modal damping ratio $\xi = 0.05$, and are designed for displacement ductilities that vary between 2 and 15. These systems have been selected in order to show typical values of the accuracy obtained when using the SE in practical structures.

Shown in Figs. 7a through 7d is a comparison between the displacements at the edges and CM of the different buildings computed using the SE model and the exact multi-plane models. The solution for the exact case is computed assuming that each resisting plane is a one-dimensional element governed by an elasto-plastic constitutive relation. It is apparent from the figure that the accuracy of the response predicted using the SE is satisfactory. Indeed, extensive numerical experimentation has shown that this observation is true in most practical cases (Chapter 2). Also, the observed trends in the actual response, such as the increase in displacements of certain planes versus others, are always captured by the SE. Capturing this trends is all we need to conceptually improve the design of an asymmetric structure.

Based on our experience with the SE model and the results presented in Fig. 7, we note three points. First, the SE model can always be used for conceptual evaluation of structures. It is particularly appropriate for comparing the efficiency of different structural configurations or their preliminary designs. Using this model, it should be possible to foresee the deficiencies of a given plan configuration.

Second, the error of the SE, measured in terms of differences in peak deformations, is less than 20% for most practical systems. However, if the system has stiffness and strength asymmetries in the same direction, the errors in peak response are usually much smaller (less than 10%). On the other hand, numerical experimentation has shown that if the yield deformations of resisting planes differ by orders of magnitude, the SE model could predict results that are in errors larger than 20%. Fortunately, such cases are not common in practice, and the SE model is sufficiently accurate for most buildings for preliminary and perhaps also final design. We should recognize that, despite the possible errors, the SE results are much closer estimates of the actual demands on the resisting planes than predicted by any elastic analysis specified in current seismic codes.

Third, the main source of error in the SE model comes from inaccuracy in the estimation of the plan rotation, as it should, since this model is not able to capture the inelastic behavior of the system in the transition between its elastic and completely plastic states. Gradual yielding of the resisting planes shifts the center of rotation of the plan, which in turn produces different rotations than the ones predicted by an elastic model. It is in this transition phase where most numerical errors are produced; any further improvements in the model should be directed toward the improvement of this phase. The effect can be verified experimentally in the results presented in Fig. 7 by noting that the displacement at the CM is always more accurate than the edge displacements. Similarly, global responses, such as base shear and torque, which somehow average the effects of several

resisting planes in the structure are usually more accurate than the displacements.

4.4 Building example

The example presented next is intended to illustrate the use of the SE model. First, it carries out the different steps required for constructing the SE model of a multistory building as well as describes some of the modeling decisions faced in formulating such a model. Further, it shows how different response quantities for the resisting planes, such as element forces, may be computed once the building displacements are known. Finally, it provides valuable information about the accuracy of the SE model in a realistic multistory structure.

Let us consider the four-story building shown in Fig. 8 having infinitely rigid floor diaphragms, where all the story masses are lumped, plan aspect ratio $a/b = 1/2$, and subjected to an earthquake in the y-direction equal to the N-S component of El Centro amplified by a factor of two. The system has five identical resisting planes in the y-direction, all of them having identical wide-flange columns W 14x30 in all four stories, and two resisting planes with shear walls in the x-direction. The most important feature of this structure is its irregularity in height produced by a setback on the third story. This setback produces an offset equal to $0.125b$ between the centers of mass of the first two and upper two (3rd and 4th) stories. Because of this offset the building has lateral-torsional coupling despite its stiffness and strength symmetry.

The SE model for the building is presented in Fig. 8c together with the floor masses and moments of inertia. The first step is to compute the stiffness matrix $\boldsymbol{K}$ of each story. For the sake of simplicity, let us assume that, because of the relative stiffness of the diaphragms and beams, the columns in each story have fixed-end conditions, i.e., the lateral stiffness of each resisting plane is computed as $\boldsymbol{k}_y^{(i)} = 3\ (12EI/h^3) = 407$ kip/ft, where $i = 1, 2, \ldots, 5$, and E, I, and h are the Young's modulus of steel, the second moment of area of the column section, and the story height, respectively. The stiffness matrix for each story is computed by well established techniques; indeed, in this case this is straight forward since each story has two axes of symmetry and, hence, $K_{y\theta}$ in Eq. (7) is zero. The story stiffness matrices are assembled as in Eq. (5), and the mass matrix is given by Eq. (2). The natural vibration frequencies and modes of the structure are computed; in particular, the fundamental vibration period of this structure is $T_1 = 0.75$ sec.

Just for the sake of simplicity, we assume next that the capacity of a resisting plane at a given story is computed by considering hinge formations at the top and bottom of columns, i.e.,

$f_y^{(i)} = 3\,(2M_p/h)$, where $i = 1, 2, \ldots, 5$, and M_p represents the plastic moment of the section. For the W14x30 section used $M_p = 141.9$ kip-ft [3] and $f_y^{(i)} = 70.95$ kips.

Let us compute now the SST surface of each building story using the results presented in Section 4.3 (Eq. (10)). We start considering the first story surface shown in Fig. 9, which is computed from the story parameters $\hat{V}_x$, V_{yo}, V_{yc}, T_o, $T_\perp$, x_p, and V_{yu} as follows:

1. During severe bidirectional ground motion, yielding is expected to occur in both principal directions of the building. Therefore, according to the results presented in reference (Chapter 2), the building model could assume $\hat{V}_x = 1$; thus, safely ignoring the contribution to the torsional capacity of the system provided by the orthogonal resisting planes. This implies also that $T_\perp = 0$.

2. The coordinates of Point 1 of the surface (Fig. 9) are computed as indicated in Section 4.3.2 (Eq. (10)). The lateral capacity of the first story is $V_{yo}^{(1)} = 5f_y = 354.8$ kips (Fig. 9); thus, $x_1 = 354.8$ kips (Eq. (10)). In computing the ordinate of Point 1, note that the strength asymmetry x_p in the story is zero, and since $\hat{V}_x = 1$ and $T_\perp = 0$, Eq. (10) leads to $y_1 = 0$ kip-ft (Fig. 9).

3. The coordinates of Point 2 require three additional parameters, V_{yu}, V_{yc}, and T_o. According to Eq. (10), the strength unbalance in the story V_{yu} is 0 because the capacities of the y-direction resisting planes are symmetrically arranged with respect to the CM. Further, V_{yc}, the capacity of the resisting planes passing 'close' to the CM, is in this case the capacity of resisting plane 3, i.e., $V_{yc} = f_y = 70.95$ kips. Finally, the torsional capacity of the system T_o is by definition (Eq. (10)) $2f_y(b/2 + b/4) = 12771$ kip-ft. Substitution of these parameters in Eq. (10) leads to $x_2 = 70.95$ kips and $y_2 = 12771$ kip-ft.

4. Similarly, substitution of the parameters computed in items 1 through 3 above in Eq. (10) leads to $x_3 = -70.95$ kips and $y_3 = 12771$ kip-ft for Point 3 (Fig. 9). Furthermore, Point 4 has coordinates $x_4 = -354.8$ kips and $y_4 = 0$ kip-ft (Fig. 9). Note that since the SST surface is point symmetric relative to the origin, the coordinates of Points 5,6,7 and 8 are readily available (Fig. 9).

The SST surfaces for other stories are computed in similar manner. In fact, the first and second-story SST surfaces are identical (Figs. 10a and 10b). The SST surfaces change slightly, however, for the third and fourth stories (Figs. 10c and 10d) because resisting plane 1 is discontinued above

the second story. Consequently, the lateral and torsional capacities V_{yo} and T_o are reduced to 283.8 kips and 8514 kip-ft, respectively, in these stories. Also, the shear capacity of the central plane V_{yc} is increased to $2f_y = 141.9$ kips, i.e., the sum of the capacities of resisting planes 3 and 4. Such is the case because these planes define branches of the SST surface with small slope $b/8$, which are associated, for design purposes, to the branch of constant torque. On the other hand, the strength eccentricity x_p, strength unbalance V_{yu}, and torsional capacity $T_\perp$ in these stories are still zero.

Also shown in Fig. 10 is a comparison between the story shears and torque histories computed from the SE and the exact multi-plane models for each building story. The so-called exact response is computed considering each building story with the actual planwise distribution of resisting planes. As shown in the figure, both responses show remarkable similarity in spite of the rather important lateral-torsional coupling of the structure. For example, both models indicate that stories 1 and 3 reach global yielding mechanisms at few instants during the earthquake, which can be verified by the story shear and torque combinations located on the SST surfaces (Figs. 10a and 10c). Because yielding occurs on branches of the SST surface with negative slope, we conclude that yielding in the first story occurs mainly on the planes at the right of the CM (Chapter 2); the opposite occurs in the third story. Note also that the second and fourth stories remain essentially elastic during the earthquake.

Shown in Fig. 11 is a comparison between the displacements and rotations at the centers of mass computed using the SE model and the exact multi-plane structure. It is apparent that the results of the SE model are quite accurate, especially when predicting, as mentioned earlier in the context of single-story systems, the displacements at the CM. The plan rotations computed from the SE model are always, however, slightly below the exact values.

In order to see the effect of the error in the rotations, we compare in Fig. 12 the exact and estimated edge displacements at floors 1 and 3, i.e., at the location corresponding to planes 1 and 5, and 2 and 5, in these stories, respectively. The results predicted by the SE model are still satisfactory for practical design purposes. However, the effect of the small discrepancy observed before in the plan rotation (Fig. 11), becomes apparent on these results, especially those of planes 1 and 2 in the first and third stories, respectively.

Finally, it is interesting to see how the exact and approximate force displacement relationships of these resisting planes compare in this case. These relations are shown in Fig. 13; they show again that the element forces that would be predicted using the displacements obtained from the SE model are in agreement with the forces computed from the exact multi-plane model. The

biggest discrepancy occurs in plane 1 where the SE model predicts greater inelastic action of the plane. Note that since in the SE model there are no resisting planes (they are implicit in the definition of the SST surface), the forces in the resisting planes must be computed later from the deformation histories resulting from the building displacements predicted by the SE model. The results presented in Fig. 13 show also that most of the nonlinear behavior in the first story occurs in plane 5 to the right of the CM; the opposite occurs in the third story where plane 2 at the left of the CM is more affected. This observation is consistent with the one obtained previously using the story shear and torque histories (Fig. 10). Note also that the peak displacement ductilities for the resisting planes (Fig. 13) are about 2. This small ductility demand is typical of steel-frame buildings where sizing of the elements is usually controlled by service conditions (stiffness); more important, this intermediate ductility case constitutes a tough test for the SE model since we know that the model is, in one hand, exact for elastic behavior and, on the other, becomes more accurate as the intensity of the inelastic behavior increases.

In spite of the simplicity of the SE model used to analyze this structure, we see that this model is accurate enough for use in preliminary design, and even final design of the structure. More important, the base shear and torque histories (Fig. 10) together with the displacement demands on the system (Fig. 12), obtained from analysis of the SE model, are all we need to understand this structure conceptually. We clearly see in this example the physical insight gained by interpreting the building response in terms of the four super-elements instead of the 54 column elements that would be included in the 'exact' analysis.

4.5 Concluding remarks

A new simplified model for inelastic seismic analysis and design of asymmetric structures has been formulated. Some of the advantages of using this model instead of the conventional three-dimensional models of the structure are:

1. The time required in formulating a SE model, analyzing it, and interpreting its results is at least one order of magnitude smaller than for any conventional inelastic 3-D model, making it practical for the engineer to try several structural configurations and search for a design optimum in terms of cost and seismic safety. As a result, engineers will be able to use nonlinear dynamic analysis in practice (at cost similar to elastic analysis), which should result in safer and more cost-effective structures. Finally, unlike conventional models, the complexity of the

SE model does not increase with the complexity of the building plan, or an increase in the number of resisting planes.

2. The SE model is a powerful tool for conceptual design of a building, mainly because it is based on the SST surface for each building story. These surfaces enable us to visualize important features of the inelastic response of the structure even before any dynamic analysis is performed (Chapter 2), and enable us to answer questions like, where is the damage going to be concentrated for a given plan configuration, or how can we make the damage more uniform among resisting planes, or how will the structure eventually collapse, so forth.

3. The SE model is a hybrid analysis-design tool which integrates well accepted procedures of structural analysis based on plasticity theory and the seismic response behavior identified by previous researchers. The latter is done by a careful selection of the parameters that control the shape of the SST surfaces, which simultaneously are those that control the inelastic behavior of asymmetric structures.

4. The accuracy of the SE model is usually satisfactory for most design purposes. Errors in peak responses are less than 20% for most practical structures.

5. As presented, the SE model can also be used for analysis of a structure with bidirectional input. The computational implementation of this case is more cumbersome, however, since the system moves on the three dimensional SST surface. One possibility to eliminate this difficulty (in the context of building design) would be to define the two-dimensional SST surface for a value of $\hat{V}_x$ representative of the values of story shear generated by the motion in the x-direction. In fact, this was done indirectly in the multistory example presented earlier, where the normalized base shear $\hat{V}_x$ was assumed to be one, consistent with an intense ground motion in the x-direction. Although, somewhat speculative at this point, one possibility would be to select $\hat{V}_x$ as the ratio $|\bar{V}_x|/V_{xo}$ between the temporal mean of the absolute value of V_x computed from analysis in the x-direction and the building capacity V_{xo}.

Finally, it is the authors' opinion that research should be conducted in the future for testing the accuracy of the SE model against full three-dimensional inelastic models not based in the assumption of rigid floor diaphragms, or better yet, against recorded earthquake responses in asymmetric structures. Such results would provide valuable data that could be used to calibrate and enhance this simplified model.

4.6 References

1. Inaudi J.A. and De la Llera J.C., 'Dynamic analysis of nonlinear structures using state-space formulation and partitioned integration schemes', Report No. EERC 92/18, University of California, Berkeley, CA., Nov. 1992.

2. R. K. Goel and A. K. Chopra, 'Inelastic seismic response of one-story, asymmetric plan systems', Report No. EERC 90/14, University of California, Berkeley, CA., Oct. 1990.

3. *Manual of steel construction: allowable stress design* , American Institute of Steel Construction, Inc., Chicago, Illinois, 1989.

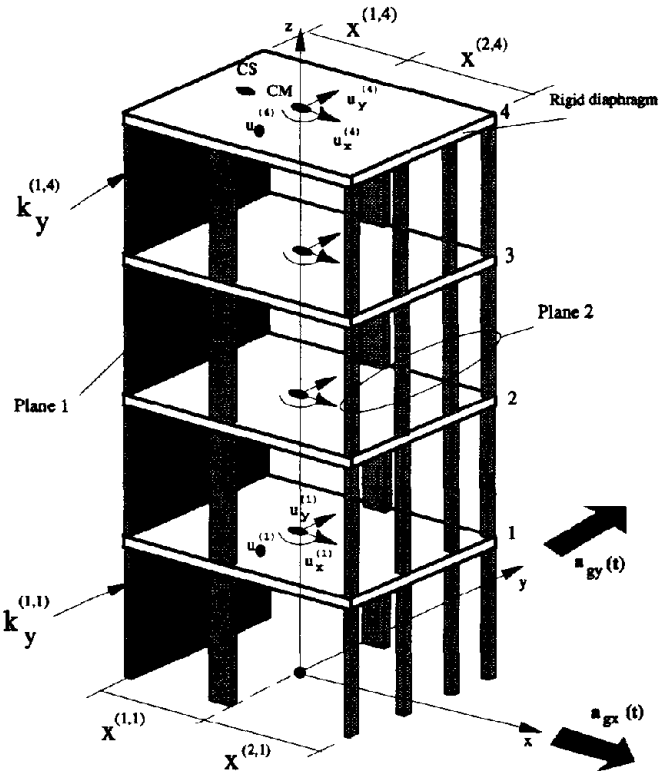

(a) Buildings considered

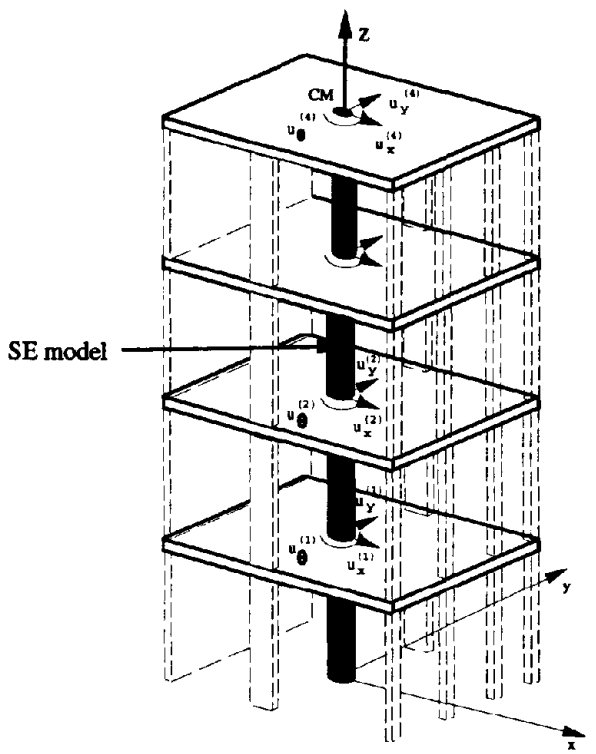

(b) SE model of the buidling

Figure 1 Buildings considered and SE model

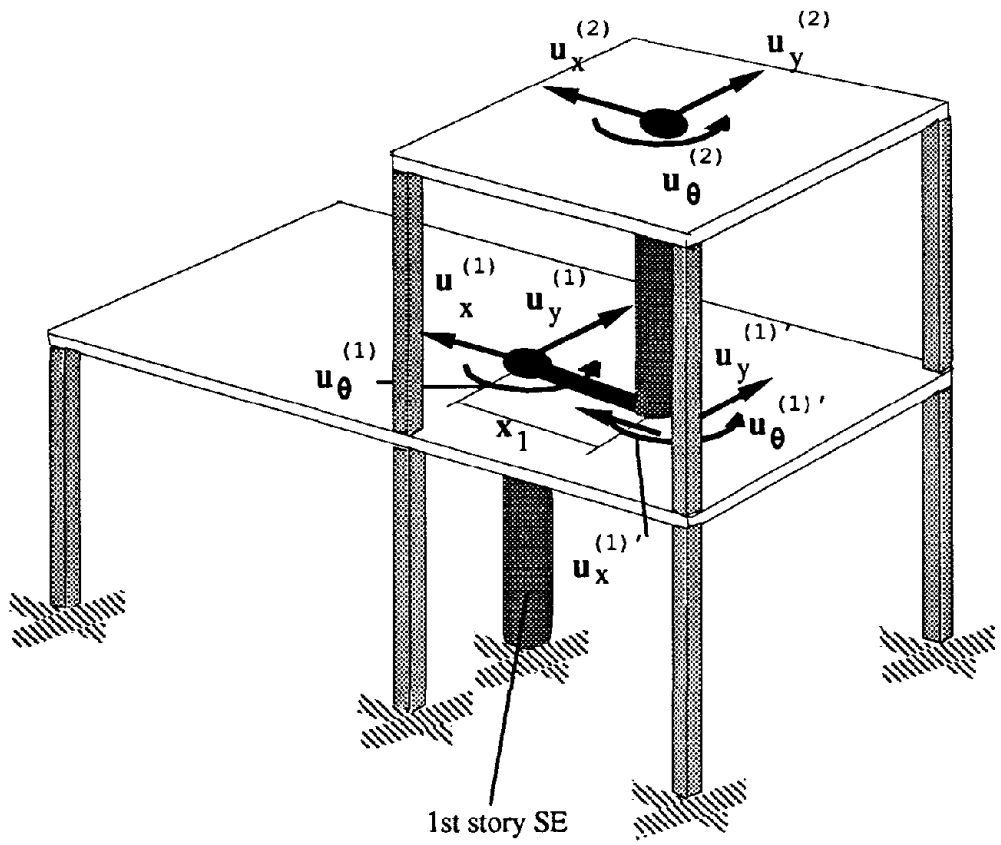

Figure 2 SE model for a building with non–aligned centers of mass

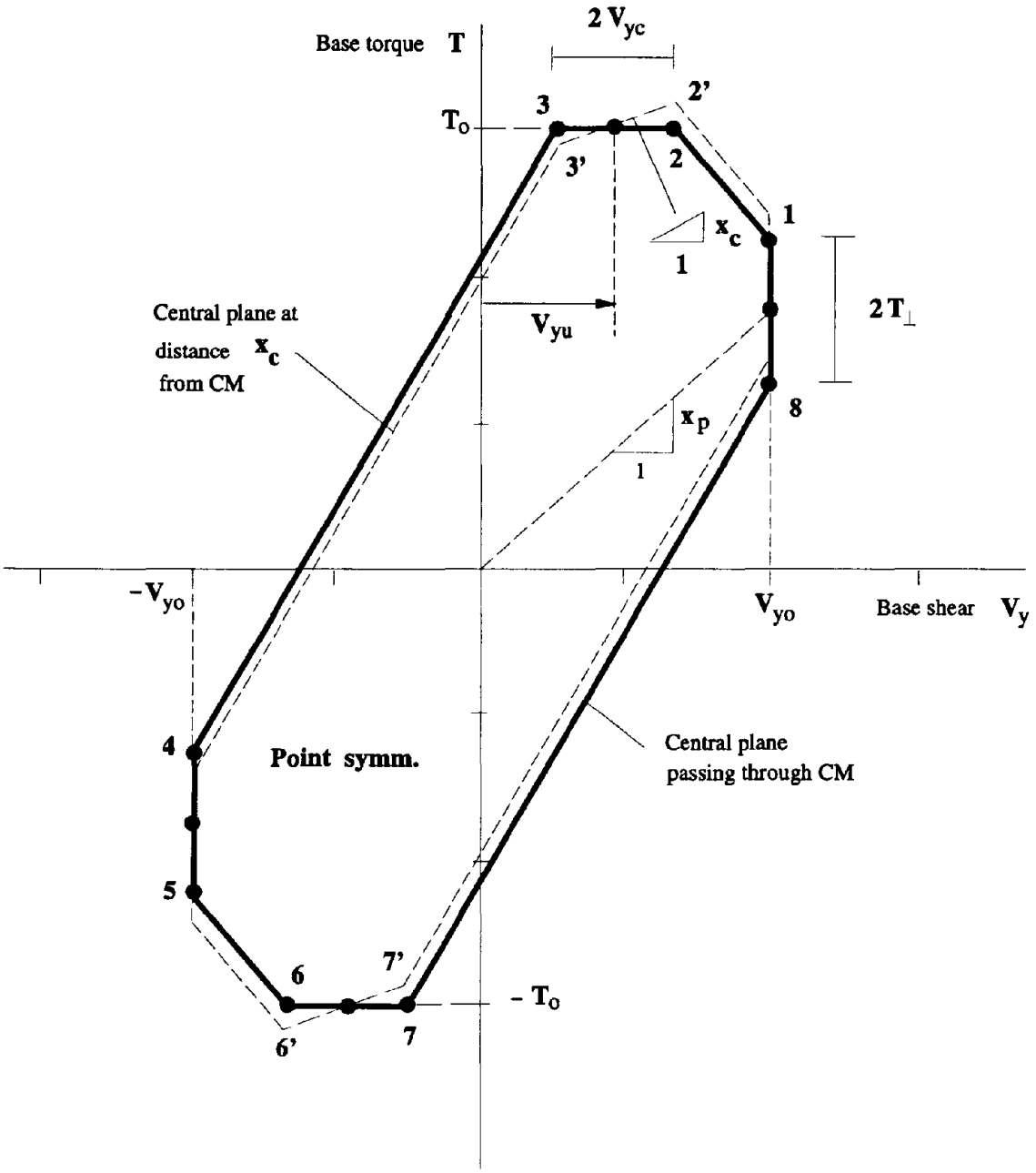

Figure 3 Parametric representation of the BST surface

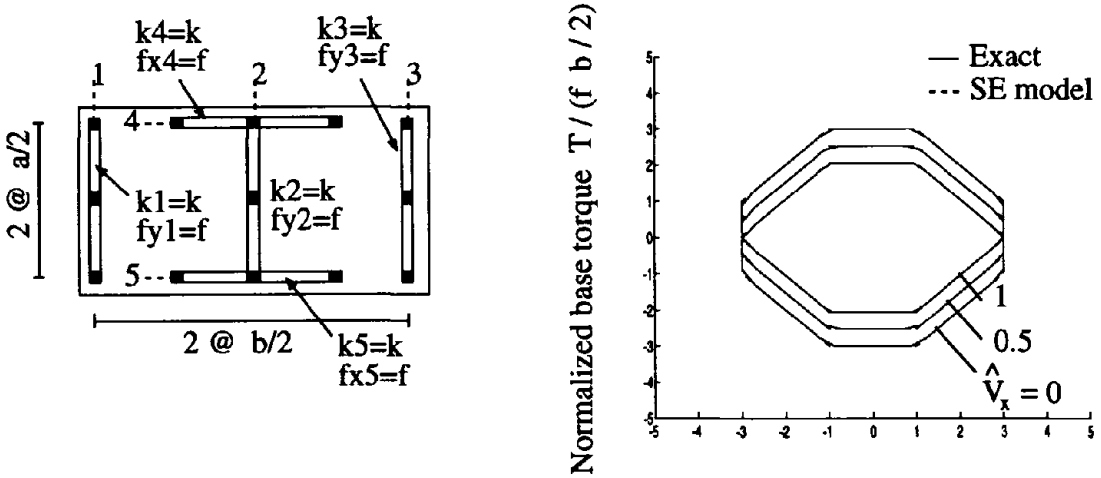

a) Symmetric system

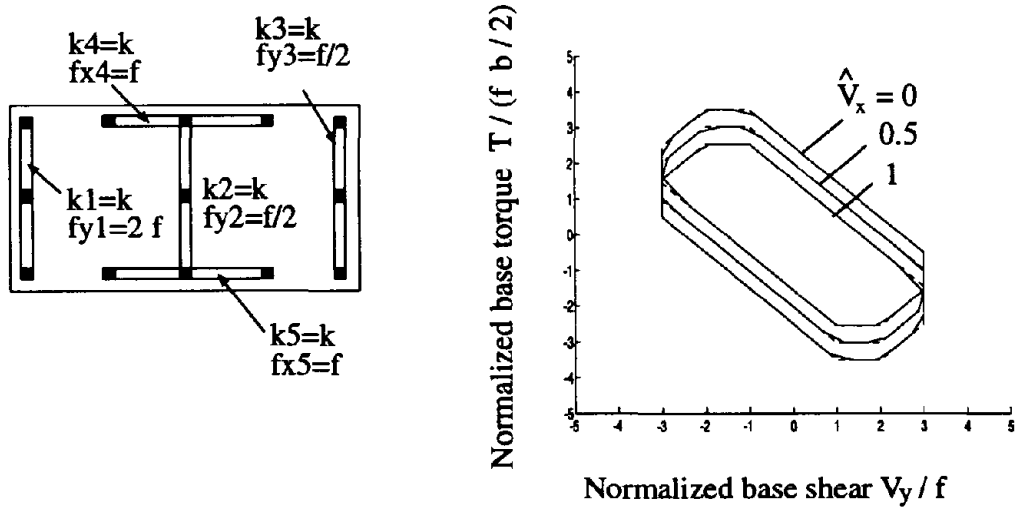

(b) Strength asymmetric system

Figure 4 Comparison between the actual and theoretical BST surfaces in a symmetric and an asymmetric structure

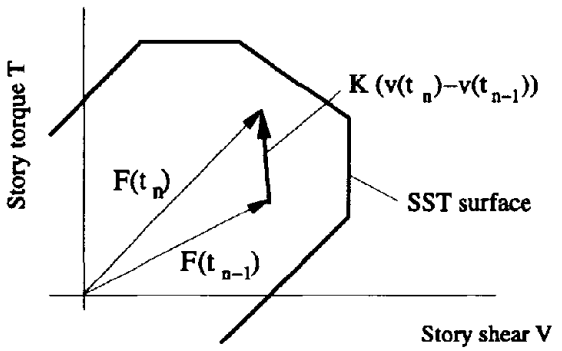

a) Elastic deformation

$$F(t_n)= K v^e (t_n)= F(t_{n-1}) +\sum_{i=1}^{3} K_i^{ep}(v_{i+1}- v_i)$$

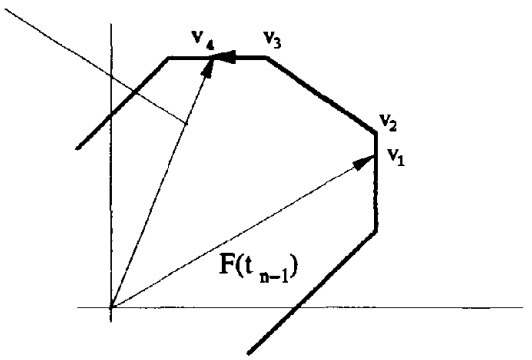

b) Elasto–plastic deformation

$$F(t_n)= K v^e (t_n)= F(t_{n-1})+ K (a\, v(t_n)-v(t_{n-1})) + \sum_{i=1}^{3} K_i^{ep}(v_{i+1}- v_i)$$

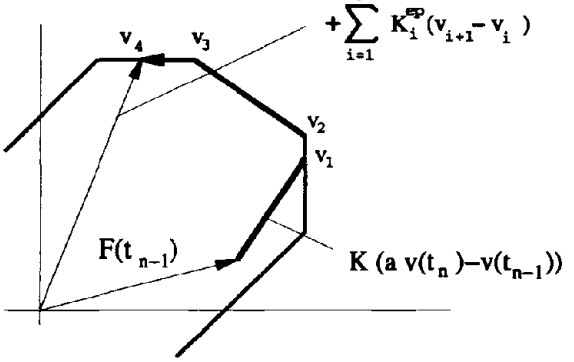

c) Elastic and plastic increments

Figure 5 Integration of constitutive elasto–plastic relation

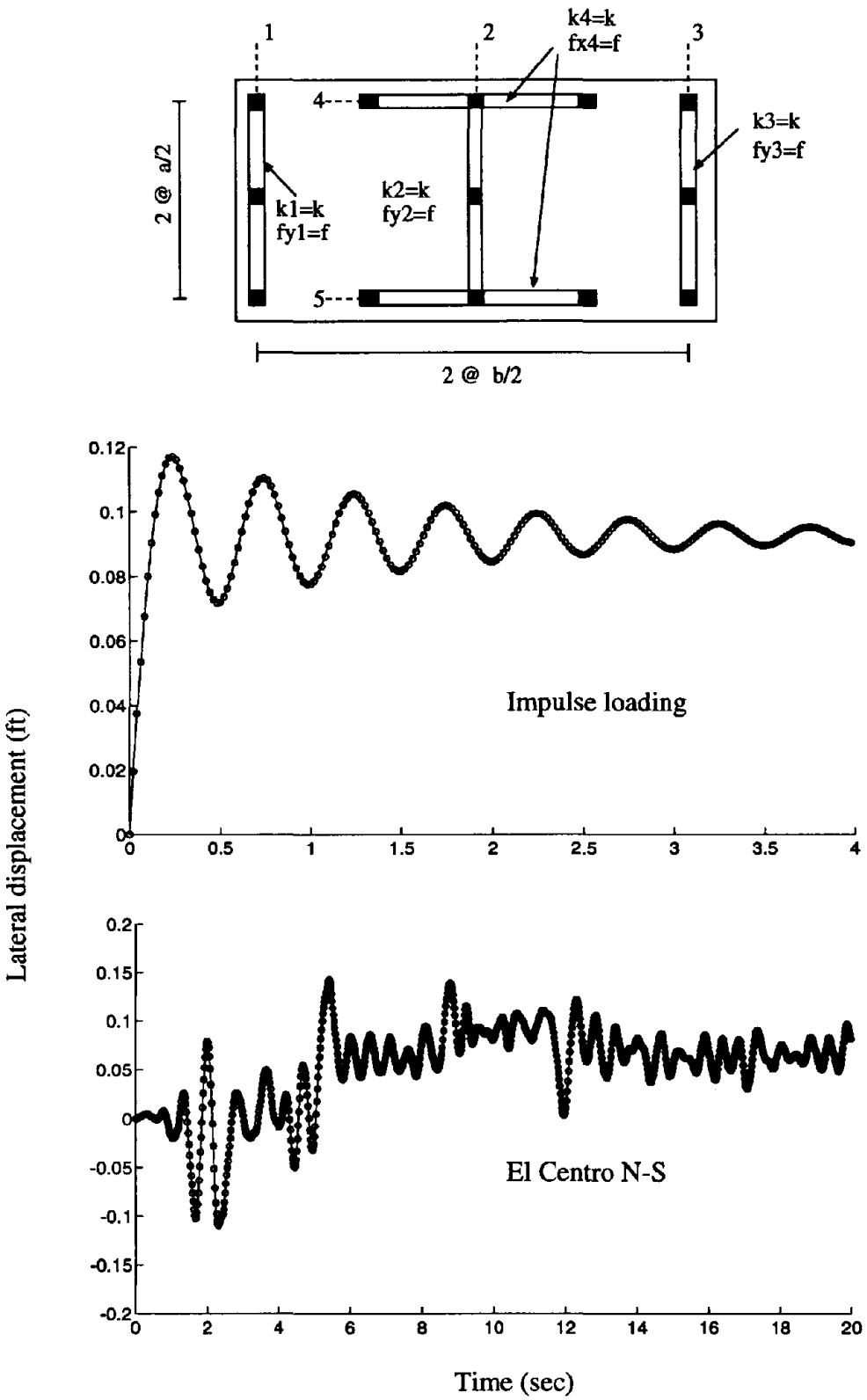

Figure 6 Comparison between the exact and SE-computed responses of symmetric systems

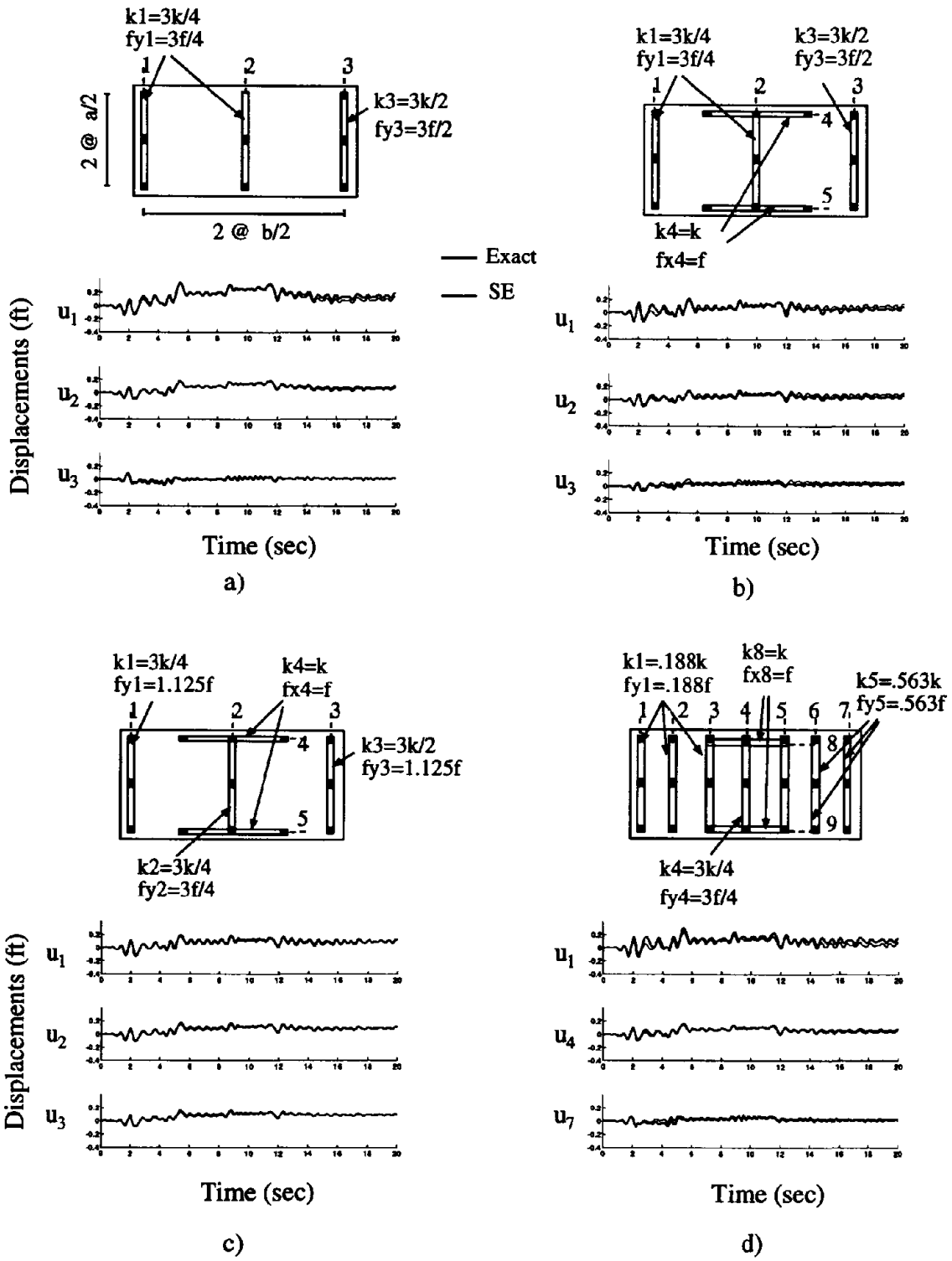

Figure 7: Accuracy of the SE model for different structural configurations

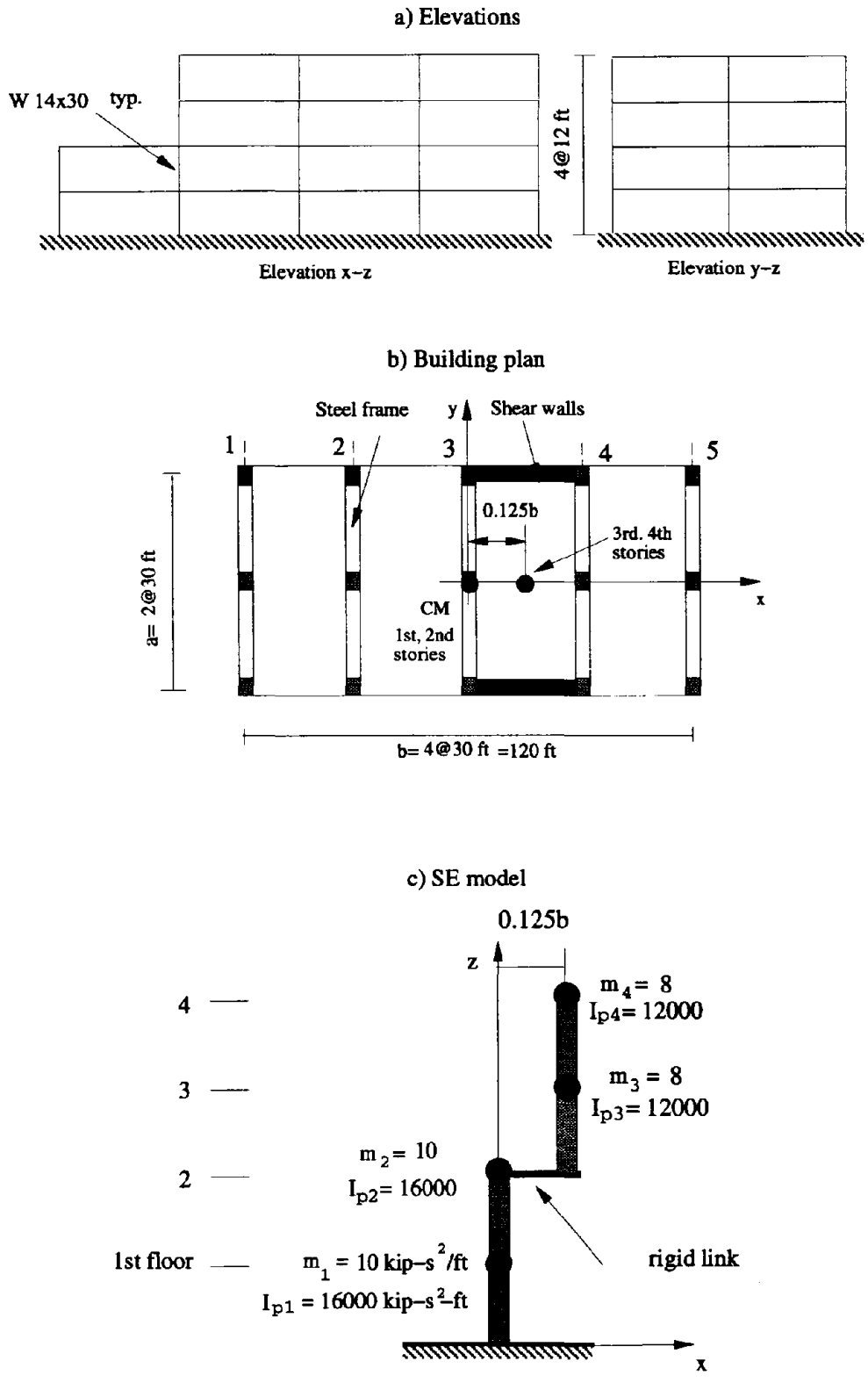

Figure 8 Elevations, plan, and SE model of the building considered in the example

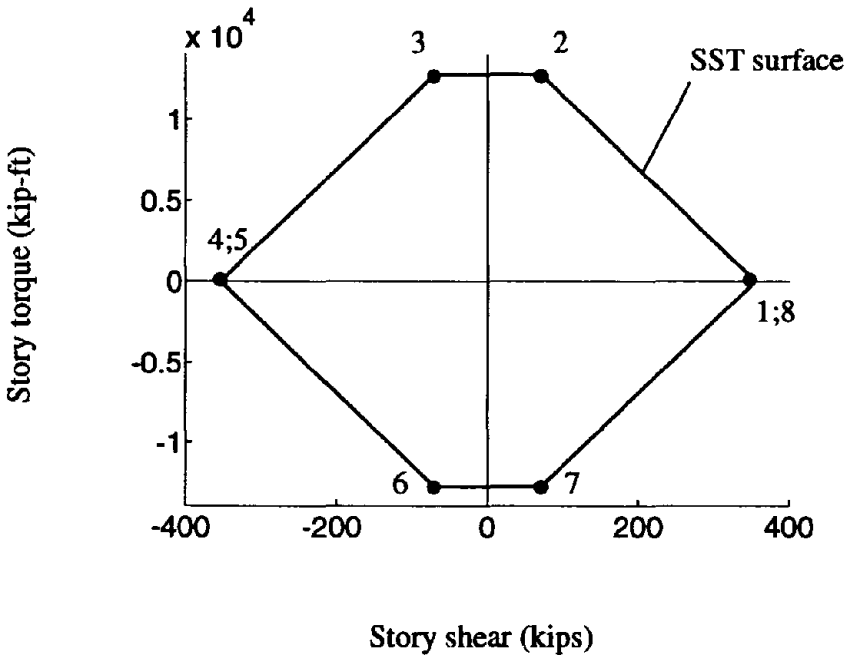

Figure 9 First story SST surface for the building considered

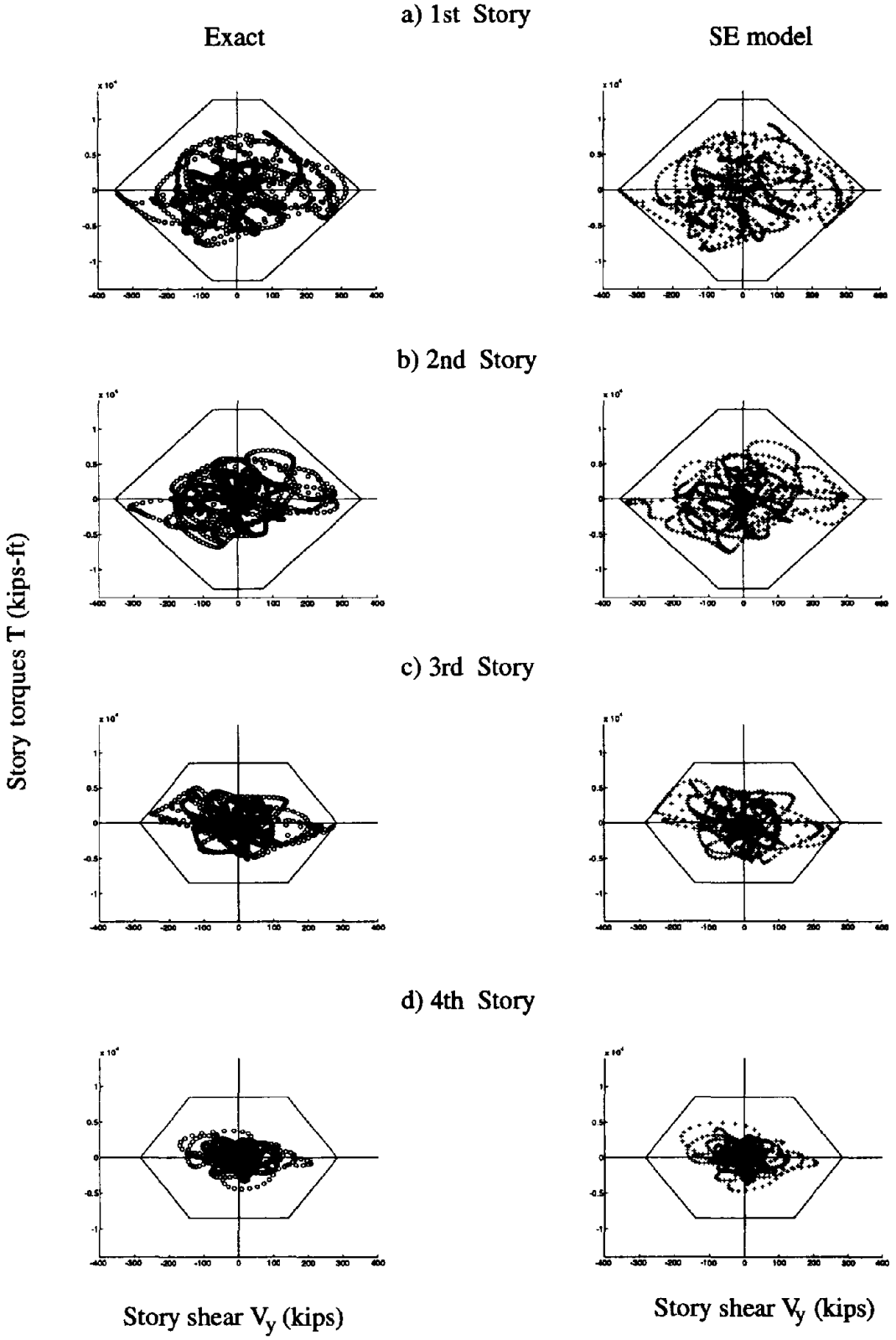

Figure 10 Comparion of base shear and torque diagrams computed from the exact and SE models

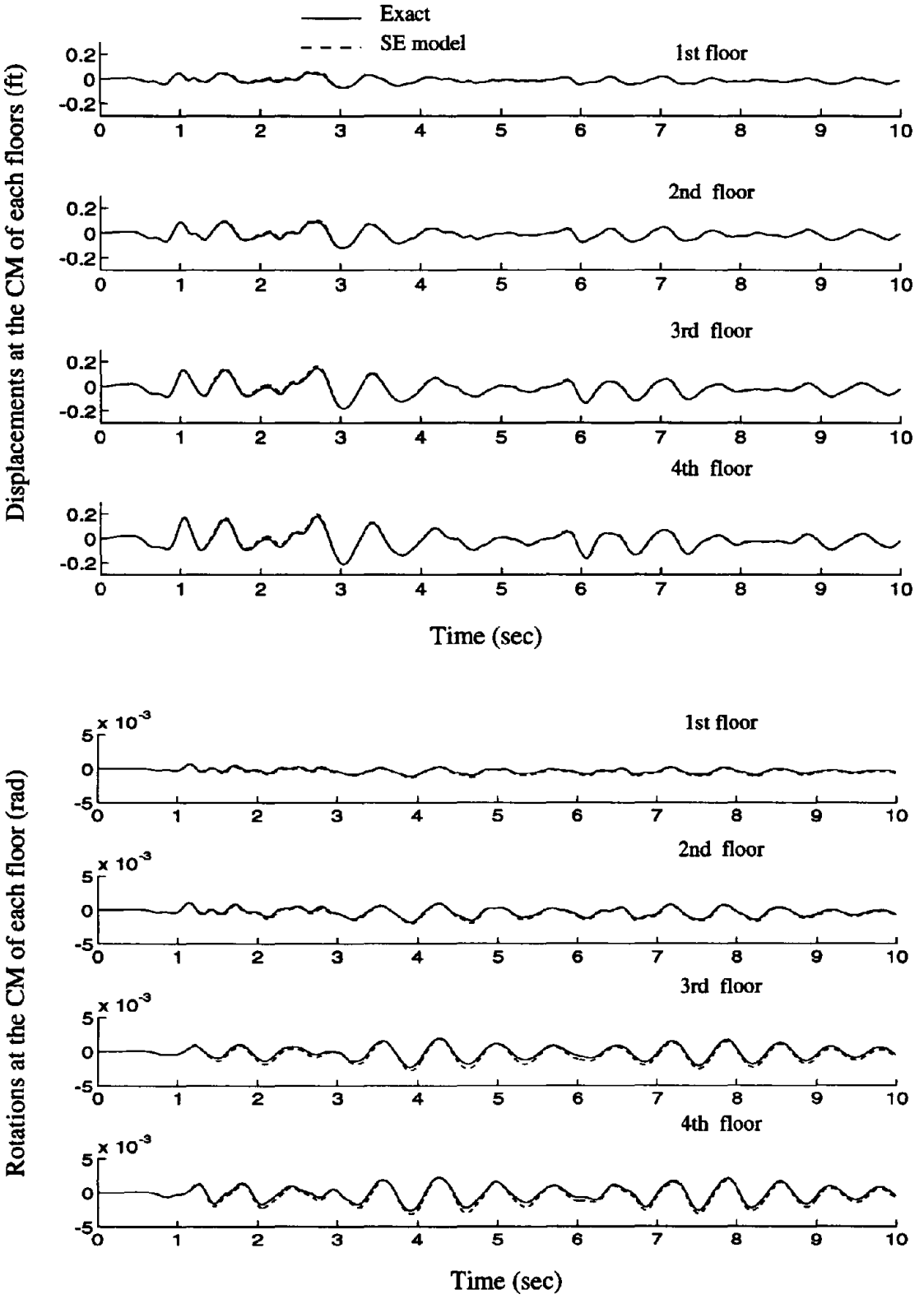

Figure 11 Comparison between building displacments and rotations computed from the exact and SE models

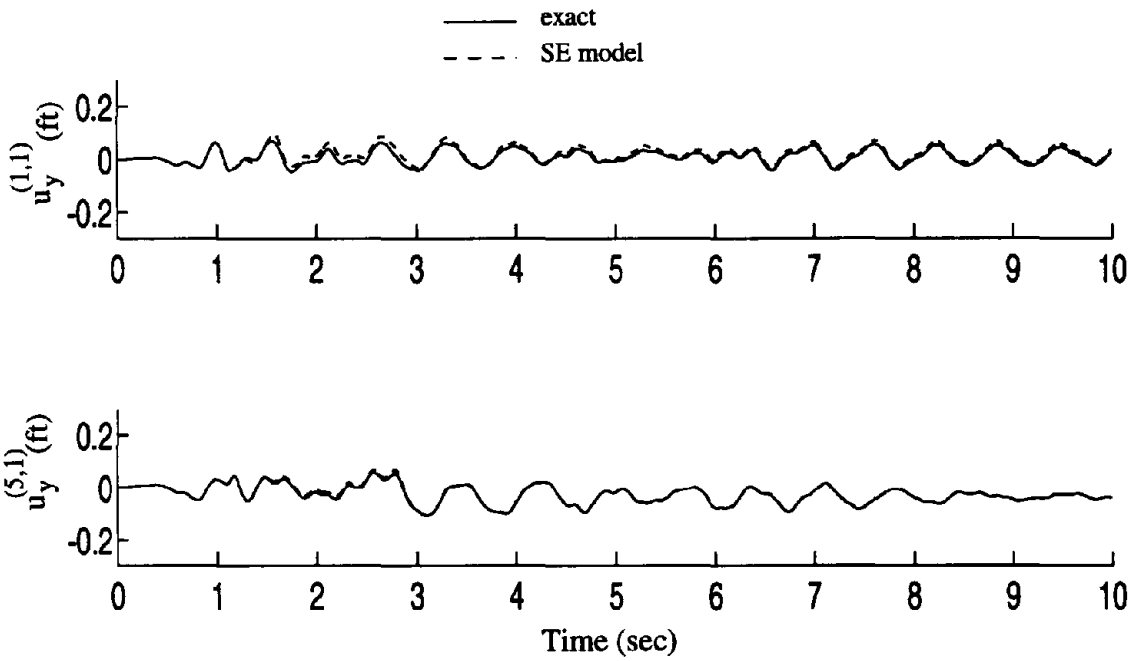

a) Displacements at location of resisting planes 1 and 5 on the first floor

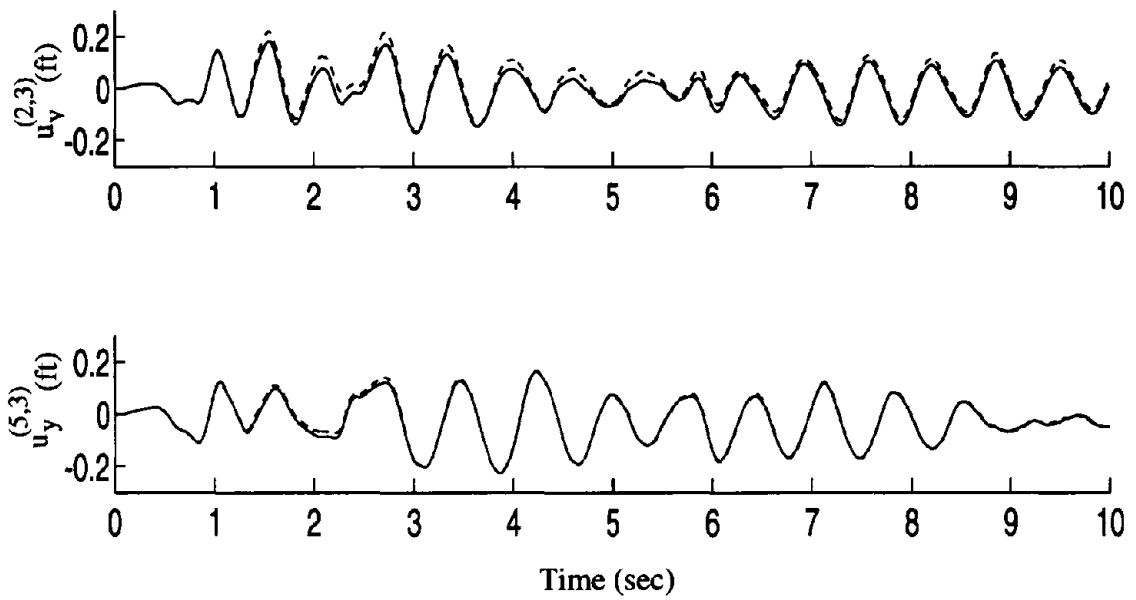

b) Displacements at location of resisting planes 2 and 5 on the third floor

Figure 12 Comparison between the displacements of resisting planes 1 and 5 (first floor) and 2 and 5 (third floor) computed from the exact and SE models

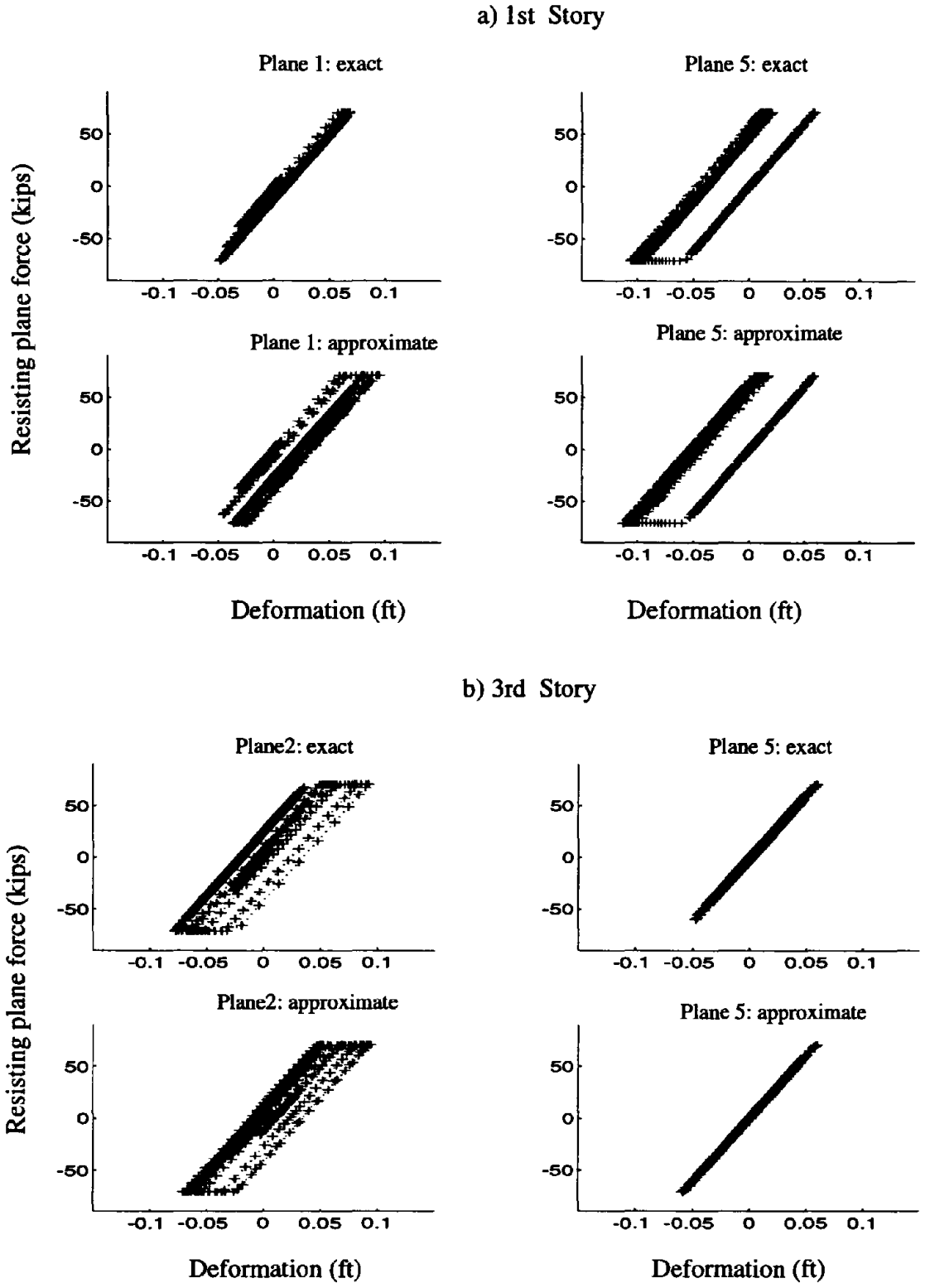

Figure 13 Force-displacement hysteresis loops in resisting planes 1 and 2 (first floor) and 2 and 5 (third floor) computed from the exact and SE models

APPENDIX A: Force-deformation relation of the SE

The objective of this appendix is to describe analytically the force-deformation relation of the SE based on the elastic and inelastic properties of the element stated in section 4.3.1 and 4.3.2. For the derivations next, the SE is considered to have an elasto-perfectly-plastic behavior.

Let us consider the SE connecting stories $j-1$ and j. For the sake of compactness, it will be convenient to work with the interstory deformations $\boldsymbol{v}^{(j)} = \boldsymbol{u}^{(j)} - \boldsymbol{u}^{(j-1)}$ across the element. Associated to these deformations we define the force vector $\boldsymbol{F}^{(j)} = \{V_x^{(j)}\ V_y^{(j)}\ V_\theta^{(j)}\}^T$ containing the shears and torque of the j^{th}-story.(Note that this force vector and the corresponding to other stories are later assembled into the restoring force vector $\boldsymbol{R}(\boldsymbol{\delta}, \dot{\boldsymbol{\delta}})$ used to integrate the equations of motion). Also, the deformations and story forces corresponding to time $t = t_n$ will be denoted as $\boldsymbol{v}^{(j)}(t_n)$ and $\boldsymbol{F}^{(j)}(t_n)$, respectively. Finally, in the understanding that all matrices and terms refer to story j, we will omit hereafter this index.

While the SE is in the elastic range, i.e., it remains inside of the BST surface during the integration step $[t_{n-1}\ \ t_n]$, the force vector $\boldsymbol{F}(t_n)$ generated by the imposed element deformations $\boldsymbol{v}(t_n)$, is given by Hooke's law (Fig. 5a)

$$\boldsymbol{F}(t_n) = \boldsymbol{K}\boldsymbol{v}(t_n) \tag{15}$$

where $\boldsymbol{K}$ is the stiffness matrix of the story.

The inelastic behavior on the SE is assumed to be governed by elasto perfectly plastic behavior and, hence, it can be described by the well known constitutive relations [e.g., 16]

$$\boldsymbol{v} = \boldsymbol{v}^e + \boldsymbol{v}^p \tag{16}$$

$$\boldsymbol{F} = \boldsymbol{K}\boldsymbol{v}^e \tag{17}$$

$$\dot{\boldsymbol{v}}^p = \dot{\lambda}\boldsymbol{\eta} \tag{18}$$

where $\boldsymbol{v}$, $\boldsymbol{v}^e$, $\boldsymbol{v}^p$ represent the total, elastic, and plastic deformations at a given instant; $\dot{\boldsymbol{v}}^p$ is the plastic deformation rate; $\dot{\lambda}$ is a plastic parameter determined by the loading-unloading criterion; and $\boldsymbol{\eta}$ is the plastic flow direction.

Equation (2) denotes the well known additive decomposition of small deformations into elastic and plastic components. Further, Eq. (3) represents Hooke's law relating the elastic deformation and element force through the element stiffness matrix $\boldsymbol{K}$. Finally, Eq. (4) represents the flow rule for the plastic deformation rates.

The plastic parameter λ is computed from the criterion for loading and unloading from the BST surface, which is assumed to satisfy the Kuhn-Tucker conditions, i.e.

$$\dot{\lambda}\Phi(\boldsymbol{F}) = 0, \quad \dot{\lambda} \geq 0, \quad ,\Phi(\boldsymbol{F}) \leq 0 \tag{19}$$

where $\Phi(\boldsymbol{F})$ is the functional form of the BST surface (Fig. 3). The three conditions in Eq. (5) must be satisfied simultaneously during any loading process. If $\Phi(\boldsymbol{F}) < 0$, the first equation implies that $\dot{\lambda} = 0$ and, hence, the behavior is elastic. Contrarily, if $\dot{\lambda} > 0$, then $\Phi(\boldsymbol{F}) = 0$ and the system is on the BST ultimate surface. During plastic deformation, the system cannot go beyond the BST ultimate surface, which defines the so-called plastic consistency condition

$$\dot{\Phi}(\boldsymbol{F}) = \frac{\partial \Phi}{\partial \boldsymbol{F}}^T \dot{\boldsymbol{F}} = 0 \tag{20}$$

where the vector $\partial\Phi/\partial\boldsymbol{F}$ represents the gradient of the BST surface.

A commonly used form adopted for Eq. (4) is the well known associated or normal plasticity rule [16], which assumes the flow direction $\boldsymbol{\eta}$ identical to the direction of the the normal vector $\partial\Phi/\partial\boldsymbol{F}$ of the BST surface. Although this flow rule is used in the computational implementation of the SE element, the formulation presented next does not assume associated plasticity.

In order to compute the forces $\boldsymbol{F}(t_n)$ in the SE corresponding to the element deformations $\boldsymbol{v}(t_n)$, we need to integrate the constitutive relations (Eq. (2)-(4)) during the time step $[t_{n-1} \quad t_n]$, and solve for the elastic and plastic components of the deformation, $\boldsymbol{v}^{(e)}$ and $\boldsymbol{v}^{(p)}$ (Eq. (2)). Integration of Eq. (4) leads to

$$\boldsymbol{v}^p(t_n) = \boldsymbol{v}^p(t_{n-1}) + \int_{\lambda_{t_{n-1}}}^{\lambda_{t_n}} \boldsymbol{\eta}(\boldsymbol{F})\, d\lambda \tag{21}$$

where $d\lambda$ can be obtained from Eqs. (2), (3), and (6) as

$$d\lambda = \frac{(\partial\Phi/\partial\boldsymbol{F})^T \boldsymbol{K}\, d\boldsymbol{v}}{(\partial\Phi/\partial\boldsymbol{F})^T \boldsymbol{K}\boldsymbol{\eta}} \tag{22}$$

Substituting into Eq. (8) the expression given for $\boldsymbol{v}^p$ (Eq. (7)), we obtain an expression for $\boldsymbol{F}(t_n)$

$$\boldsymbol{F}(t_n) = \boldsymbol{F}(t_{n-1}) + \int_{\boldsymbol{v}(t_{n-1})}^{\boldsymbol{v}(t_n)} \boldsymbol{K}^{ep}\, d\boldsymbol{v} \tag{23}$$

where $\boldsymbol{K}^{ep}$ is the elasto-plastic stiffness matrix given by

$$\boldsymbol{K}^{ep} = \boldsymbol{K} - \frac{\boldsymbol{\eta}(\partial\Phi/\partial\boldsymbol{F})\boldsymbol{K}}{(\partial\Phi/\partial\boldsymbol{F})^T \boldsymbol{K}\boldsymbol{\eta}} \tag{24}$$

In the particular case of our polygonal BST surface (Fig. 3), and assuming an associated flow rule, i.e., $\boldsymbol{\eta} = (\partial\Phi/\partial\boldsymbol{F})$, Eq. (9) can be simplified to

$$\boldsymbol{F}(t_n) = \boldsymbol{F}(t_{n-1}) + \sum_{m=1}^{Nb} \boldsymbol{K}_m^{ep}(\boldsymbol{v}_{m+1} - \boldsymbol{v}_m) \tag{25}$$

where $\boldsymbol{v}_m$ and $\boldsymbol{v}_{m+1}$ are the deformations corresponding to the points where the system reaches and leaves branch m, respectively (Fig. 5b); N_b is the number of branches visited by the element during the integration step; and $\boldsymbol{K}_m^{ep}$ is the elasto-plastic matrix for branch m

$$\boldsymbol{K}_m^{ep} = \boldsymbol{K} - \frac{(\partial\Phi/\partial\boldsymbol{F})_m(\partial\Phi/\partial\boldsymbol{F})_m^T\boldsymbol{K}}{(\partial\Phi/\partial\boldsymbol{F})_m^T\boldsymbol{K}(\partial\Phi/\partial\boldsymbol{F})_m} \tag{26}$$

Note that for the polygonal BST surface selected, the forces $\boldsymbol{F}(t_n)$ (Eq. (11)) are exact.

One possible difficulty in using Eq. (11) occurs when the SE is inside the BST surface at time t_{n-1} (elastic) and during step n goes into the plastic range as shown in Fig. 5c. Equations (7) through (12) are still correct in this case; however, they have to be used with the deformation $\boldsymbol{v}^* = (1-a)\boldsymbol{v}$ that results from subtracting from the total deformation $\boldsymbol{v}(t_n)$ the deformation $a\boldsymbol{v}(t_n)$, where a ranges between 0 and 1, that puts the system on the BST surface.

EARTHQUAKE ENGINEERING RESEARCH CENTER REPORT SERIES

EERC reports are available from the National Information Service for Earthquake Engineering (NISEE) and from the National Technical Information Service (NTIS). Numbers in parentheses are Accession Numbers assigned by the National Technical Information Service; these are followed by a price code. Contact NTIS, 5285 Port Royal Road, Springfield Virginia, 22161 for more information. Reports without Accession Numbers were not available from NTIS at the time of printing. For a current complete list of EERC reports (from EERC 67-1) and availablity information, please contact University of California, EERC, NISEE, 1301 South 46th Street, Richmond, California 94804.

UCB/EERC-84/01 "Pseudodynamic Test Method for Seismic Performance Evaluation: Theory and Implementation," by Shing, P.-S.B. and Mahin, S.A., January 1984, (PB84 190 644)A08.

UCB/EERC-84/02 "Dynamic Response Behavior of Kiang Hong Dian Dam," by Clough, R.W., Chang, K.-T., Chen, H.-Q. and Stephen, R.M., April 1984, (PB84 209 402)A08.

UCB/EERC-84/03 "Refined Modelling of Reinforced Concrete Columns for Seismic Analysis," by Kaba, S.A. and Mahin, S.A., April 1984, (PB84 234 384)A06.

UCB/EERC-84/04 "A New Floor Response Spectrum Method for Seismic Analysis of Multiply Supported Secondary Systems," by Asfura, A. and Der Kiureghian, A., June 1984, (PB84 239 417)A06.

UCB/EERC-84/05 "Earthquake Simulation Tests and Associated Studies of a 1/5th-scale Model of a 7-Story R/C Frame-Wall Test Structure," by Bertero, V.V., Aktan, A.E., Charney, F.A. and Sause, R., June 1984, (PB84 239 409)A09.

UCB/EERC-84/06 "Unassigned," by Unassigned, 1984.

UCB/EERC-84/07 "Behavior of Interior and Exterior Flat-Plate Connections Subjected to Inelastic Load Reversals," by Zee, H.L. and Moehle, J.P., August 1984, (PB86 117 629/AS)A07.

UCB/EERC-84/08 "Experimental Study of the Seismic Behavior of a Two-Story Flat-Plate Structure," by Moehle, J.P. and Diebold, J.W., August 1984, (PB86 122 553/AS)A12.

UCB/EERC-84/09 "Phenomenological Modeling of Steel Braces under Cyclic Loading," by Ikeda, K., Mahin, S.A. and Dermitzakis, S.N., May 1984, (PB86 132 198/AS)A08.

UCB/EERC-84/10 "Earthquake Analysis and Response of Concrete Gravity Dams," by Fenves, G.L. and Chopra, A.K., August 1984, (PB85 193 902/AS)A11.

UCB/EERC-84/11 "EAGD-84: A Computer Program for Earthquake Analysis of Concrete Gravity Dams," by Fenves, G.L. and Chopra, A.K., August 1984, (PB85 193 613/AS)A05.

UCB/EERC-84/12 "A Refined Physical Theory Model for Predicting the Seismic Behavior of Braced Steel Frames," by Ikeda, K. and Mahin, S.A., July 1984, (PB85 191 450/AS)A09.

UCB/EERC-84/13 "Earthquake Engineering Research at Berkeley - 1984," by EERC, August 1984, (PB85 197 341/AS)A10.

UCB/EERC-84/14 "Moduli and Damping Factors for Dynamic Analyses of Cohesionless Soils," by Seed, H.B., Wong, R.T., Idriss, I.M. and Tokimatsu, K., September 1984, (PB85 191 468/AS)A04.

UCB/EERC-84/15 "The Influence of SPT Procedures in Soil Liquefaction Resistance Evaluations," by Seed, H.B., Tokimatsu, K., Harder, L.F. and Chung, R.M., October 1984, (PB85 191 732/AS)A04.

UCB/EERC-84/16 "Simplified Procedures for the Evaluation of Settlements in Sands Due to Earthquake Shaking," by Tokimatsu, K. and Seed, H.B., October 1984, (PB85 197 887/AS)A03.

UCB/EERC-84/17 "Evaluation of Energy Absorption Characteristics of Highway Bridges Under Seismic Conditions - Volume I (PB90 262 627)A16 and Volume II (Appendices) (PB90 262 635)A13," by Imbsen, R.A. and Penzien, J., September 1986.

UCB/EERC-84/18 "Structure-Foundation Interactions under Dynamic Loads," by Liu, W.D. and Penzien, J., November 1984, (PB87 124 889/AS)A11.

UCB/EERC-84/19 "Seismic Modelling of Deep Foundations," by Chen, C.-H. and Penzien, J., November 1984, (PB87 124 798/AS)A07.

UCB/EERC-84/20 "Dynamic Response Behavior of Quan Shui Dam," by Clough, R.W., Chang, K.-T., Chen, H.-Q., Stephen, R.M., Ghanaat, Y. and Qi, J.-H., November 1984, (PB86 115177/AS)A07.

UCB/EERC-85/01 "Simplified Methods of Analysis for Earthquake Resistant Design of Buildings," by Cruz, E.F. and Chopra, A.K., February 1985, (PB86 112299/AS)A12.

UCB/EERC-85/02 "Estimation of Seismic Wave Coherency and Rupture Velocity using the SMART 1 Strong-Motion Array Recordings," by Abrahamson, N.A., March 1985, (PB86 214 343)A07.

UCB/EERC-85/03 "Dynamic Properties of a Thirty Story Condominium Tower Building," by Stephen, R.M., Wilson, E.L. and Stander, N., April 1985, (PB86 118965/AS)A06.

UCB/EERC-85/04 "Development of Substructuring Techniques for On-Line Computer Controlled Seismic Performance Testing," by Dermitzakis, S. and Mahin, S., February 1985, (PB86 132941/AS)A08.

UCB/EERC-85/05 "A Simple Model for Reinforcing Bar Anchorages under Cyclic Excitations," by Filippou, F.C., March 1985, (PB86 112 919/AS)A05.

UCB/EERC-85/06 "Racking Behavior of Wood-framed Gypsum Panels under Dynamic Load," by Oliva, M.G., June 1985, (PB90 262 643)A04.

UCB/EERC-85/07 "Earthquake Analysis and Response of Concrete Arch Dams," by Fok, K.-L. and Chopra, A.K., June 1985, (PB86 139672/AS)A10.

UCB/EERC-85/08 "Effect of Inelastic Behavior on the Analysis and Design of Earthquake Resistant Structures," by Lin, J.P. and Mahin, S.A., June 1985, (PB86 135340/AS)A08.

UCB/EERC-85/09 "Earthquake Simulator Testing of a Base-Isolated Bridge Deck," by Kelly, J.M., Buckle, I.G. and Tsai, H.-C., January 1986, (PB87 124 152/AS)A06.

UCB/EERC-85/10 "Simplified Analysis for Earthquake Resistant Design of Concrete Gravity Dams," by Fenves, G.L. and Chopra, A.K., June 1986, (PB87 124 160/AS)A08.

UCB/EERC-85/11 "Dynamic Interaction Effects in Arch Dams," by Clough, R.W., Chang, K.-T., Chen, H.-Q. and Ghanaat, Y., October 1985, (PB86 135027/AS)A05.

UCB/EERC-85/12 "Dynamic Response of Long Valley Dam in the Mammoth Lake Earthquake Series of May 25-27, 1980," by Lai, S. and Seed, H.B., November 1985, (PB86 142304/AS)A05.

UCB/EERC-85/13 "A Methodology for Computer-Aided Design of Earthquake-Resistant Steel Structures," by Austin, M.A., Pister, K.S. and Mahin, S.A., December 1985, (PB86 159480/AS)A10 .

UCB/EERC-85/14 "Response of Tension-Leg Platforms to Vertical Seismic Excitations," by Liou, G.-S., Penzien, J. and Yeung, R.W., December 1985, (PB87 124 871/AS)A08.

UCB/EERC-85/15 "Cyclic Loading Tests of Masonry Single Piers: Volume 4 - Additional Tests with Height to Width Ratio of 1," by Sveinsson, B., McNiven, H.D. and Sucuoglu, H., December 1985, (PB87 165031/AS)A08.

UCB/EERC-85/16 "An Experimental Program for Studying the Dynamic Response of a Steel Frame with a Variety of Infill Partitions," by Yanev, B. and McNiven, H.D., December 1985, (PB90 262 676)A05.

UCB/EERC-86/01 "A Study of Seismically Resistant Eccentrically Braced Steel Frame Systems," by Kasai, K. and Popov, E.P., January 1986, (PB87 124 178/AS)A14.

UCB/EERC-86/02 "Design Problems in Soil Liquefaction," by Seed, H.B., February 1986, (PB87 124 186/AS)A03.

UCB/EERC-86/03 "Implications of Recent Earthquakes and Research on Earthquake-Resistant Design and Construction of Buildings," by Bertero, V.V., March 1986, (PB87 124 194/AS)A05.

UCB/EERC-86/04 "The Use of Load Dependent Vectors for Dynamic and Earthquake Analyses," by Leger, P., Wilson, E.L. and Clough, R.W., March 1986, (PB87 124 202/AS)A12.

UCB/EERC-86/05 "Two Beam-To-Column Web Connections," by Tsai, K.-C. and Popov, E.P., April 1986, (PB87 124 301/AS)A04.

UCB/EERC-86/06 "Determination of Penetration Resistance for Coarse-Grained Soils using the Becker Hammer Drill," by Harder, L.F. and Seed, H.B., May 1986, (PB87 124 210/AS)A07.

UCB/EERC-86/07 "A Mathematical Model for Predicting the Nonlinear Response of Unreinforced Masonry Walls to In-Plane Earthquake Excitations," by Mengi, Y. and McNiven, H.D., May 1986, (PB87 124 780/AS)A06.

UCB/EERC-86/08 "The 19 September 1985 Mexico Earthquake: Building Behavior," by Bertero, V.V., July 1986.

UCB/EERC-86/09 "EACD-3D: A Computer Program for Three-Dimensional Earthquake Analysis of Concrete Dams," by Fok, K.-L., Hall, J.F. and Chopra, A.K., July 1986, (PB87 124 228/AS)A08.

UCB/EERC-86/10 "Earthquake Simulation Tests and Associated Studies of a 0.3-Scale Model of a Six-Story Concentrically Braced Steel Structure," by Uang, C.-M. and Bertero, V.V., December 1986, (PB87 163 564/AS)A17.

UCB/EERC-86/11 "Mechanical Characteristics of Base Isolation Bearings for a Bridge Deck Model Test," by Kelly, J.M., Buckle, I.G. and Koh, C.-G., November 1987, (PB90 262 668)A04.

UCB/EERC-86/12 "Effects of Axial Load on Elastomeric Isolation Bearings," by Koh, C.-G. and Kelly, J.M., November 1987.

UCB/EERC-87/01 "The FPS Earthquake Resisting System: Experimental Report," by Zayas, V.A., Low, S.S. and Mahin, S.A., June 1987, (PB88 170 287)A06.

UCB/EERC-87/02 "Earthquake Simulator Tests and Associated Studies of a 0.3-Scale Model of a Six-Story Eccentrically Braced Steel Structure," by Whittaker, A., Uang, C.-M. and Bertero, V.V., July 1987, (PB88 166 707/AS)A18.

UCB/EERC-87/03 "A Displacement Control and Uplift Restraint Device for Base-Isolated Structures," by Kelly, J.M., Griffith, M.C. and Aiken, I.D., April 1987, (PB88 169 933)A04.

UCB/EERC-87/04 "Earthquake Simulator Testing of a Combined Sliding Bearing and Rubber Bearing Isolation System," by Kelly, J.M. and Chalhoub, M.S., December 1990.

UCB/EERC-87/05 "Three-Dimensional Inelastic Analysis of Reinforced Concrete Frame-Wall Structures," by Moazzami, S. and Bertero, V.V., May 1987, (PB88 169 586/AS)A08.

UCB/EERC-87/06 "Experiments on Eccentrically Braced Frames with Composite Floors," by Ricles, J. and Popov, E., June 1987, (PB88 173 067/AS)A14.

UCB/EERC-87/07 "Dynamic Analysis of Seismically Resistant Eccentrically Braced Frames," by Ricles, J. and Popov, E., June 1987, (PB88 173 075/AS)A16.

UCB/EERC-87/08 "Undrained Cyclic Triaxial Testing of Gravels-The Effect of Membrane Compliance," by Evans, M.D. and Seed, H.B., July 1987, (PB88 173 257)A19.

UCB/EERC-87/09 "Hybrid Solution Techniques for Generalized Pseudo-Dynamic Testing," by Thewalt, C. and Mahin, S.A., July 1987, (PB 88 179 007)A07.

UCB/EERC-87/10 "Ultimate Behavior of Butt Welded Splices in Heavy Rolled Steel Sections," by Bruneau, M., Mahin, S.A. and Popov, E.P., September 1987, (PB90 254 285)A07.

UCB/EERC-87/11 "Residual Strength of Sand from Dam Failures in the Chilean Earthquake of March 3, 1985," by De Alba, P., Seed, H.B., Retamal, E. and Seed, R.B., September 1987, (PB88 174 321/AS)A03.

UCB/EERC-87/12 "Inelastic Seismic Response of Structures with Mass or Stiffness Eccentricities in Plan," by Bruneau, M. and Mahin, S.A., September 1987, (PB90 262 650/AS)A14.

UCB/EERC-87/13 "CSTRUCT: An Interactive Computer Environment for the Design and Analysis of Earthquake Resistant Steel Structures," by Austin, M.A., Mahin, S.A. and Pister, K.S., September 1987, (PB88 173 339/AS)A06.

UCB/EERC-87/14 "Experimental Study of Reinforced Concrete Columns Subjected to Multi-Axial Loading," by Low, S.S. and Moehle, J.P., September 1987, (PB88 174 347/AS)A07.

UCB/EERC-87/15 "Relationships between Soil Conditions and Earthquake Ground Motions in Mexico City in the Earthquake of Sept. 19, 1985," by Seed, H.B., Romo, M.P., Sun, J., Jaime, A. and Lysmer, J., October 1987, (PB88 178 991)A06.

UCB/EERC-87/16 "Experimental Study of Seismic Response of R. C. Setback Buildings," by Shahrooz, B.M. and Moehle, J.P., October 1987, (PB88 176 359)A16.

UCB/EERC-87/17 "The Effect of Slabs on the Flexural Behavior of Beams," by Pantazopoulou, S.J. and Moehle, J.P., October 1987, (PB90 262 700)A07.

UCB/EERC-87/18 "Design Procedure for R-FBI Bearings," by Mostaghel, N. and Kelly, J.M., November 1987, (PB90 262 718)A04.

UCB/EERC-87/19 "Analytical Models for Predicting the Lateral Response of R C Shear Walls: Evaluation of their Reliability," by Vulcano, A. and Bertero, V.V., November 1987, (PB88 178 983)A05.

UCB/EERC-87/20 "Earthquake Response of Torsionally-Coupled Buildings," by Hejal, R. and Chopra, A.K., December 1987.

UCB/EERC-87/21 "Dynamic Reservoir Interaction with Monticello Dam," by Clough, R.W., Ghanaat, Y. and Qiu, X-F., December 1987, (PB88 179 023)A07.

UCB/EERC-87/22 "Strength Evaluation of Coarse-Grained Soils," by Siddiqi, F.H., Seed, R.B., Chan, C.K., Seed, H.B. and Pyke, R.M., December 1987, (PB88 179 031)A04.

UCB/EERC-88/01 "Seismic Behavior of Concentrically Braced Steel Frames," by Khatib, I., Mahin, S.A. and Pister, K.S., January 1988, (PB91 210 898/AS)A11.

UCB/EERC-88/02 "Experimental Evaluation of Seismic Isolation of Medium-Rise Structures Subject to Uplift," by Griffith, M.C., Kelly, J.M., Coveney, V.A. and Koh, C.G., January 1988, (PB91 217 950/AS)A09.

UCB/EERC-88/03 "Cyclic Behavior of Steel Double Angle Connections," by Astaneh-Asl, A. and Nader, M.N., January 1988, (PB91 210 872)A05.

UCB/EERC-88/04 "Re-evaluation of the Slide in the Lower San Fernando Dam in the Earthquake of Feb. 9, 1971," by Seed, H.B., Seed, R.B., Harder, L.F. and Jong, H.-L., April 1988, (PB91 212 456/AS)A07.

UCB/EERC-88/05 "Experimental Evaluation of Seismic Isolation of a Nine-Story Braced Steel Frame Subject to Uplift," by Griffith, M.C., Kelly, J.M. and Aiken, I.D., May 1988, (PB91 217 968/AS)A07.

UCB/EERC-88/06 "DRAIN-2DX User Guide.," by Allahabadi, R. and Powell, G.H., March 1988, (PB91 212 530)A12.

UCB/EERC-88/07 "Theoretical and Experimental Studies of Cylindrical Water Tanks in Base-Isolated Structures," by Chalhoub, M.S. and Kelly, J.M., April 1988, (PB91 217 976/AS)A05.

UCB/EERC-88/08 "Analysis of Near-Source Waves: Separation of Wave Types Using Strong Motion Array Recording," by Darragh, R.B., June 1988, (PB91 212 621)A08.

UCB/EERC-88/09 "Alternatives to Standard Mode Superposition for Analysis of Non-Classically Damped Systems," by Kusainov, A.A. and Clough, R.W., June 1988, (PB91 217 992/AS)A04.

UCB/EERC-88/10 "The Landslide at the Port of Nice on October 16, 1979," by Seed, H.B., Seed, R.B., Schlosser, F., Blondeau, F. and Juran, I., June 1988, (PB91 210 914)A05.

UCB/EERC-88/11 "Liquefaction Potential of Sand Deposits Under Low Levels of Excitation," by Carter, D.P. and Seed, H.B., August 1988, (PB91 210 880)A15.

UCB/EERC-88/12 "Nonlinear Analysis of Reinforced Concrete Frames Under Cyclic Load Reversals," by Filippou, F.C. and Issa, A., September 1988, (PB91 212 589)A07.

UCB/EERC-88/13 "Implications of Recorded Earthquake Ground Motions on Seismic Design of Building Structures," by Uang, C.-M. and Bertero, V.V., November 1988, (PB91 212 548)A06.

UCB/EERC-88/14 "An Experimental Study of the Behavior of Dual Steel Systems," by Whittaker, A.S. , Uang, C.-M. and Bertero, V.V., September 1988, (PB91 212 712)A16.

UCB/EERC-88/15 "Dynamic Moduli and Damping Ratios for Cohesive Soils," by Sun, J.I., Golesorkhi, R. and Seed, H.B., August 1988, (PB91 210 922)A04.

UCB/EERC-88/16 "Reinforced Concrete Flat Plates Under Lateral Load: An Experimental Study Including Biaxial Effects," by Pan, A. and Moehle, J.P., October 1988, (PB91 210 856)A13.

UCB/EERC-88/17 "Earthquake Engineering Research at Berkeley - 1988," by EERC, November 1988, (PB91 210 864)A10.

UCB/EERC-88/18 "Use of Energy as a Design Criterion in Earthquake-Resistant Design," by Uang, C.-M. and Bertero, V.V., November 1988, (PB91 210 906/AS)A04.

UCB/EERC-88/19 "Steel Beam-Column Joints in Seismic Moment Resisting Frames," by Tsai, K.-C. and Popov, E.P., November 1988, (PB91 217 984/AS)A20.

UCB/EERC-88/20 "Base Isolation in Japan, 1988," by Kelly, J.M., December 1988, (PB91 212 449)A05.

UCB/EERC-89/01 "Behavior of Long Links in Eccentrically Braced Frames," by Engelhardt, M.D. and Popov, E.P., January 1989, (PB92 143 056)A18.

UCB/EERC-89/02 "Earthquake Simulator Testing of Steel Plate Added Damping and Stiffness Elements," by Whittaker, A., Bertero, V.V., Alonso, J. and Thompson, C., January 1989, (PB91 229 252/AS)A10.

UCB/EERC-89/03 "Implications of Site Effects in the Mexico City Earthquake of Sept. 19, 1985 for Earthquake-Resistant Design Criteria in the San Francisco Bay Area of California," by Seed, H.B. and Sun, J.I., March 1989, (PB91 229 369/AS)A07.

UCB/EERC-89/04 "Earthquake Analysis and Response of Intake-Outlet Towers," by Goyal, A. and Chopra, A.K., July 1989, (PB91 229 286/AS)A19.

UCB/EERC-89/05 "The 1985 Chile Earthquake: An Evaluation of Structural Requirements for Bearing Wall Buildings," by Wallace, J.W. and Moehle, J.P., July 1989, (PB91 218 008/AS)A13.

UCB/EERC-89/06 "Effects of Spatial Variation of Ground Motions on Large Multiply-Supported Structures," by Hao, H., July 1989, (PB91 229 161/AS)A08.

UCB/EERC-89/07 "EADAP - Enhanced Arch Dam Analysis Program: Users's Manual," by Ghanaat, Y. and Clough, R.W., August 1989, (PB91 212 522)A06.

UCB/EERC-89/08 "Seismic Performance of Steel Moment Frames Plastically Designed by Least Squares Stress Fields," by Ohi, K. and Mahin, S.A., August 1989, (PB91 212 597)A05.

UCB/EERC-89/09 "Feasibility and Performance Studies on Improving the Earthquake Resistance of New and Existing Buildings Using the Friction Pendulum System," by Zayas, V., Low, S., Mahin, S.A. and Bozzo, L., July 1989, (PB92 143 064)A14.

UCB/EERC-89/10 "Measurement and Elimination of Membrane Compliance Effects in Undrained Triaxial Testing," by Nicholson, P.G., Seed, R.B. and Anwar, H., September 1989, (PB92 139 641/AS)A13.

UCB/EERC-89/11 "Static Tilt Behavior of Unanchored Cylindrical Tanks," by Lau, D.T. and Clough, R.W., September 1989, (PB92 143 049)A10.

UCB/EERC-89/12 "ADAP-88: A Computer Program for Nonlinear Earthquake Analysis of Concrete Arch Dams," by Fenves, G.L., Mojtahedi, S. and Reimer, R.B., September 1989. (PB92 139 674/AS)A07.

UCB/EERC-89/13 "Mechanics of Low Shape Factor Elastomeric Seismic Isolation Bearings," by Aiken, I.D., Kelly, J.M. and Tajirian, F.F., November 1989, (PB92 139 732/AS)A09.

UCB/EERC-89/14 "Preliminary Report on the Seismological and Engineering Aspects of the October 17, 1989 Santa Cruz (Loma Prieta) Earthquake," by EERC, October 1989, (PB92 139 682/AS)A04.

UCB/EERC-89/15 "Experimental Studies of a Single Story Steel Structure Tested with Fixed, Semi-Rigid and Flexible Connections," by Nader, M.N. and Astaneh-Asl, A., August 1989, (PB91 229 211/AS)A10.

UCB/EERC-89/16 "Collapse of the Cypress Street Viaduct as a Result of the Loma Prieta Earthquake," by Nims, D.K., Miranda, E., Aiken, I.D., Whittaker, A.S. and Bertero, V.V., November 1989, (PB91 217 935/AS)A05.

UCB/EERC-90/01 "Mechanics of High-Shape Factor Elastomeric Seismic Isolation Bearings," by Kelly, J.M., Aiken, I.D. and Tajirian, F.F., March 1990.

UCB/EERC-90/02 "Javid's Paradox: The Influence of Preform on the Modes of Vibrating Beams," by Kelly, J.M., Sackman, J.L. and Javid, A., May 1990, (PB91 217 943/AS)A03.

UCB/EERC-90/03 "Earthquake Simulator Testing and Analytical Studies of Two Energy-Absorbing Systems for Multistory Structures," by Aiken, I.D. and Kelly, J.M., October 1990, (PB92 192 988)A13.

UCB/EERC-90/04 "Damage to the San Francisco-Oakland Bay Bridge During the October 17, 1989 Earthquake," by Astaneh-Asl, A., June 1990.

UCB/EERC-90/05 "Preliminary Report on the Principal Geotechnical Aspects of the October 17, 1989 Loma Prieta Earthquake," by Seed, R.B., Dickenson, S.E., Riemer, M.F., Bray, J.D., Sitar, N., Mitchell, J.K., Idriss, I.M., Kayen, R.E., Kropp, A., Harder, L.F., Jr. and Power, M.S., April 1990, (PB 192 970)A08.

UCB/EERC-90/06 "Models of Critical Regions in Reinforced Concrete Frames Under Seismic Excitations," by Zulfiqar, N. and Filippou, F.C., May 1990.

UCB/EERC-90/07 "A Unified Earthquake-Resistant Design Method for Steel Frames Using ARMA Models," by Takewaki, I., Conte, J.P., Mahin, S.A. and Pister, K.S., June 1990.

UCB/EERC-90/08 "Soil Conditions and Earthquake Hazard Mitigation in the Marina District of San Francisco," by Mitchell, J.K., Masood, T., Kayen, R.E. and Seed, R.B., May 1990, (PB 193 267/AS)A04.

UCB/EERC-90/09 "Influence of the Earthquake Ground Motion Process and Structural Properties on Response Characteristics of Simple Structures," by Conte, J.P., Pister, K.S. and Mahin, S.A., July 1990, (PB92 143 064)A15.

UCB/EERC-90/10 "Experimental Testing of the Resilient-Friction Base Isolation System," by Clark, P.W. and Kelly, J.M., July 1990, (PB92 143 072)A08.

UCB/EERC-90/11 "Seismic Hazard Analysis: Improved Models, Uncertainties and Sensitivities," by Araya, R. and Der Kiureghian, A., March 1988.

UCB/EERC-90/12 "Effects of Torsion on the Linear and Nonlinear Seismic Response of Structures," by Sedarat, H. and Bertero, V.V., September 1989, (PB92 193 002/AS)A15.

UCB/EERC-90/13 "The Effects of Tectonic Movements on Stresses and Deformations in Earth Embankments," by Bray, J. D., Seed, R. B. and Seed, H. B., September 1989.

UCB/EERC-90/14 "Inelastic Seismic Response of One-Story, Asymmetric-Plan Systems," by Goel, R.K. and Chopra, A.K., October 1990, (PB93 114 767)A11.

UCB/EERC-90/15 "Dynamic Crack Propagation: A Model for Near-Field Ground Motion.," by Seyyedian, H. and Kelly, J.M., 1990.

UCB/EERC-90/16 "Sensitivity of Long-Period Response Spectra to System Initial Conditions," by Blasquez, R., Ventura, C. and Kelly, J.M., 1990.

UCB/EERC-90/17 "Behavior of Peak Values and Spectral Ordinates of Near-Source Strong Ground-Motion over a Dense Array," by Niazi, M., June 1990, (PB93 114 833)A07.

UCB/EERC-90/18 "Material Characterization of Elastomers used in Earthquake Base Isolation," by Papoulia, K.D. and Kelly, J.M., 1990.

UCB/EERC-90/19 "Cyclic Behavior of Steel Top-and-Bottom Plate Moment Connections," by Harriott, J.D. and Astaneh-Asl, A., August 1990, (PB91 229 260/AS)A05.

UCB/EERC-90/20 "Seismic Response Evaluation of an Instrumented Six Story Steel Building," by Shen, J.-H. and Astaneh-Asl, A., December 1990, (PB91 229 294/AS)A04.

UCB/EERC-90/21 "Observations and Implications of Tests on the Cypress Street Viaduct Test Structure," by Bollo, M., Mahin, S.A., Moehle, J.P., Stephen, R.M. and Qi, X., December 1990, (PB93 114 775)A13.

UCB/EERC-91/01 "Experimental Evaluation of Nitinol for Energy Dissipation in Structures," by Nims, D.K., Sasaki, K.K. and Kelly, J.M., 1991.

UCB/EERC-91/02 "Displacement Design Approach for Reinforced Concrete Structures Subjected to Earthquakes," by Qi, X. and Moehle, J.P., January 1991, (PB93 114 569/AS)A09.

UCB/EERC-91/03 "A Long-Period Isolation System Using Low-Modulus High-Damping Isolators for Nuclear Facilities at Soft-Soil Sites," by Kelly, J.M., March 1991, (PB93 114 577/AS)A10.

UCB/EERC-91/04 "Dynamic and Failure Characteristics of Bridgestone Isolation Bearings," by Kelly, J.M., April 1991, (PB93 114 528)A05.

UCB/EERC-91/05 "Base Sliding Response of Concrete Gravity Dams to Earthquakes," by Chopra, A.K. and Zhang, L., May 1991, (PB93 114 544/AS)A05.

UCB/EERC-91/06 "Computation of Spatially Varying Ground Motion and Foundation-Rock Impedance Matrices for Seismic Analysis of Arch Dams," by Zhang, L. and Chopra, A.K., May 1991, (PB93 114 825)A07.

UCB/EERC-91/07 "Estimation of Seismic Source Processes Using Strong Motion Array Data," by Chiou, S.-J., July 1991, (PB93 114 551/AS)A08.

UCB/EERC-91/08 "A Response Spectrum Method for Multiple-Support Seismic Excitations," by Der Kiureghian, A. and Neuenhofer, A., August 1991, (PB93 114 536)A04.

UCB/EERC-91/09 "A Preliminary Study on Energy Dissipating Cladding-to-Frame Connection," by Cohen, J.M. and Powell, G.H., September 1991, (PB93 114 510)A05.

UCB/EERC-91/10 "Evaluation of Seismic Performance of a Ten-Story RC Building During the Whittier Narrows Earthquake," by Miranda, E. and Bertero, V.V., October 1991, (PB93 114 783)A06.

UCB/EERC-91/11 "Seismic Performance of an Instrumented Six-Story Steel Building," by Anderson, J.C. and Bertero, V.V., November 1991, (PB93 114 809)A07.

UCB/EERC-91/12 "Performance of Improved Ground During the Loma Prieta Earthquake," by Mitchell, J.K. and Wentz, Jr., F.J., October 1991, (PB93 114 791)A06.

UCB/EERC-91/13 "Shaking Table - Structure Interaction," by Rinawi, A.M. and Clough, R.W., October 1991, (PB93 114 917)A13.

UCB/EERC-91/14 "Cyclic Response of RC Beam-Column Knee Joints: Test and Retrofit," by Mazzoni, S., Moehle, J.P. and Thewalt, C.R., October 1991, (PB93 120 277)A03.

UCB/EERC-91/15 "Design Guidelines for Ductility and Drift Limits: Review of State-of-the-Practice and State-of-the-Art in Ductility and Drift-Based Earthquake-Resistant Design of Buildings," by Bertero, V.V., Anderson, J.C., Krawinkler, H., Miranda, E. and The CUREe and The Kajima Research Teams, July 1991, (PB93 120 269)A08.

UCB/EERC-91/16 "Evaluation of the Seismic Performance of a Thirty-Story RC Building," by Anderson, J.C., Miranda, E., Bertero, V.V. and The Kajima Project Research Team, July 1991, (PB93 114 841)A12.

UCB/EERC-91/17 "A Fiber Beam-Column Element for Seismic Response Analysis of Reinforced Concrete Structures," by Taucer, F., Spacone, E. and Filippou, F.C., December 1991, (PB94 117 629AS)A07.

UCB/EERC-91/18 "Investigation of the Seismic Response of a Lightly-Damped Torsionally-Coupled Building," by Boroschek, R. and Mahin, S.A., December 1991, (PB93 120 335)A13.

UCB/EERC-92/01 "Studies of a 49-Story Instrumented Steel Structure Shaken During the Loma Prieta Earthquake," by Chen, C.-C., Bonowitz, D. and Astaneh-Asl, A., February 1992, (PB93 221 778)A08.

UCB/EERC-92/02 "Response of the Dumbarton Bridge in the Loma Prieta Earthquake," by Fenves, G.L., Filippou, F.C. and Sze, D.T., January 1992, (PB93 120 319)A09.

UCB/EERC-92/03 "Models for Nonlinear Earthquake Analysis of Brick Masonry Buildings," by Mengi, Y., McNiven, H.D. and Tanrikulu, A.K., March 1992, (PB93 120 293)A08.

UCB/EERC-92/04 "Shear Strength and Deformability of RC Bridge Columns Subjected to Inelastic Cyclic Displacements," by Aschheim, M. and Moehle, J.P., March 1992, (PB93 120 327)A06.

UCB/EERC-92/05 "Parameter Study of Joint Opening Effects on Earthquake Response of Arch Dams," by Fenves, G.L., Mojtahedi, S. and Reimer, R.B., April 1992, (PB93 120 301)A04.

UCB/EERC-92/06 "Seismic Behavior and Design of Semi-Rigid Steel Frames," by Nader, M.N. and Astaneh-Asl, A., May 1992.

UCB/EERC-92/07 "A Beam Element for Seismic Damage Analysis," by Spacone, E., Ciampi, V. and Filippou, F.C., August 1992.

UCB/EERC-92/08 "Nonlinear Static and Dynamic Analysis of Reinforced Concrete Subassemblages," by Filippou, F.C., D'Ambrisi, A. and Issa, A., August 1992.

UCB/EERC-92/09 "Evaluation of Code Accidental-Torsion Provisions Using Earthquake Records from Three Nominally Symmetric-Plan Buildings," by De la Llera, J.C. and Chopra, A.K., September 1992, (PB94 117 611)A08.

UCB/EERC-92/10 "Slotted Bolted Connection Energy Dissipators," by Grigorian, C.E., Yang, T.-S. and Popov, E.P., July 1992, (PB92 120 285)A03.

UCB/EERC-92/11 "Mechanical Characteristics of Neoprene Isolation Bearings," by Kelly, J.M. and Quiroz, E., August 1992, (PB93 221 729)A07.

UCB/EERC-92/12 "Application of a Mass Damping System to Bridge Structures," by Hasegawa, K. and Kelly, J.M., August 1992, (PB93 221 786)A06.

UCB/EERC-92/13 "Earthquake Engineering Research at Berkeley - 1992," by EERC, October 1992.

UCB/EERC-92/14 "Earthquake Risk and Insurance," by Brillinger, D.R., October 1992, (PB93 223 352)A03.

UCB/EERC-92/15 "A Friction Mass Damper for Vibration Control," by Inaudi, J.A. and Kelly, J.M., October 1992, (PB93 221 745)A04.

UCB/EERC-92/16 "Tall Reinforced Concrete Buildings: Conceptual Earthquake-Resistant Design Methology," by Bertero, R.D. and Bertero, V.V., December 1992, (PB93 221 695)A12.

UCB/EERC-92/17 "Performance of Tall Buildings During the 1985 Mexico Earthquakes," by Terán-Gilmore, A. and Bertero, V.V., December 1992, (PB93 221 737)A11.

UCB/EERC-92/18 "Dynamic Analysis of Nonlinear Structures using State-Space Formulation and Partitioned Integration Schemes," by Inaudi, J.A. and De la Llera, J.C., December 1992, (PB94 117 702/AS/A05.

UCB/EERC-93/01 "Seismic Performance of an Instrumented Six-Story Reinforced-Concrete Building," by Anderson, J.C. and Bertero, V.V., 1993.

UCB/EERC-93/02 "Evaluation of an Active Variable-Damping-Structure," by Polak, E., Meeker, G., Yamada, K. and Kurata, N., 1993, (PB93 221 711)A05.

UCB/EERC-93/03 "An Experimental Study of Flat-Plate Structures under Vertical and Lateral Loads," by Hwang, S.-H. and Moehle, J.P., February 1993, (PB94 157 690/AS)A13.

UCB/EERC-93/04 "Seismic Performance of a 30-Story Building Located on Soft Soil and Designed According to UBC 1991," by Terán-Gilmore, A. and Bertero, V.V., 1993, (PB93 221 703)A17.

UCB/EERC-93/05 "Multiple-Support Response Spectrum Analysis of the Golden Gate Bridge," by Nakamura, Y., Der Kiureghian, A. and Liu, D., May 1993, (PB93 221 752)A05.

UCB/EERC-93/06 "On the Analysis of Structures with Viscoelastic Dampers," by Inaudi, J.A., Zambrano, A. and Kelly, J.M., August 1993, PB94-165867.

UCB/EERC-93/07 "Earthquake Analysis and Response of Concrete Gravity Dams Including Base Sliding," by Chávez, J.W. and Fenves, G.L., December 1993, (PB94 157 658/AS)A10.

UCB/EERC-93/08 "Model for Anchored Reinforcing Bars under Seismic Excitations," by Monti, G., Spacone, E. and Filippou, F.C., December 1993.

UCB/EERC-93/09 "A Methodology for Design of Viscoelastic Dampers in Earthquake-Resistant Structures," by Abbas, H. and Kelly, J.M., November 1993.

UCB/EERC-93/10 "Tuned Mass Dampers Using Viscoelastic Dampers," by Inaudi, J.A., Lopez-Almansa, F. and Kelly, J.M., December 1993.

UCB/EERC-93/11 "Nonlinear Homogeneous Dynamical Systems," by Inaudi, J.A. and Kelly, J.M., December 1993.

UCB/EERC-93/12 "Synthesized Strong Ground Motions for the Seismic Condition Assessment of the Eastern Portion of the San Francisco Bay Bridge," by Bolt, B.A. and Gregor, N.J., December 1993, PB94-165842.

UCB/EERC-93/13 "On the Analysis of Structures with Energy Dissipating Restraints," by Inaudi, J.A., Nims, D.K. and Kelly, J.M., December 1993.

UCB/EERC-94/01 "Preliminary Report on the Seismological and Engineering Aspects of the January 17, 1994 Northridge Earthquake," by EERC, January 1994, (PB94 157 666/AS)A05.

UCB/EERC-94/02 "Energy Dissipation with Slotted Bolted Connections," by Grigorian, C.E. and Popov, E.P., February 1994, PB94-164605.

UCB/EERC-94/03 "The Influence of Plate Flexibility on the Buckling Load of Elastomeric Isolators," by Kelly, J.M., March 1994.

UCB/EERC-94/04 "Insitu Test Results from Four Loma Prieta Earthquake Liquefaction Sites: SPT, CPT, DMT and Shear Wave Velocity," by Mitchell, J.K., Lodge, A.L., Coutinho, R.Q., Kayen, R.E., Seed, R.B., Nishio, S. and Stokoe II, K.H., April 1994.

UCB/EERC-94/05 "Seismic Response of Steep Natural Slopes," by Sitar, N. and Ashford, S.A., May 1994.

UCB/EERC-94/06 "Small-Scale Testing of a Self-Centering Friction Energy Dissipator for Structures," by Nims, D.K. and Kelly, J.M., August 1994.

UCB/EERC-94/07 "Accidental and Natural Torsion in Earthquake Response and Design of Buildings," by De la Llera, J.C. and Chopra, A.K., June 1994.

2-101

REPORT DOCUMENTATION PAGE | 1. REPORT NO. NSF/ ENG-94003 | 2.

PB94-203627

4. Title and Subtitle

Accidental and Natural Torsion in Earthquake Response and Design of Buildings"

5. Report Date: June 1994

6.

7. Author(s)

Juan C. de la Llera and Anil K. Chopra

8. Performing Organization Rept. No. UCB/EERC-94/07

9. Performing Organization Name and Address

Earthquake Engineering Research Center
University of California, Berkeley
1301 So. 46th Street
Richmond, Calif. 94804

10. Project/Task/Work Unit No.

11. Contract(C) or Grant(G) No.

(C)

(G) BCS-8921932

12. Sponsoring Organization Name and Address

National Science Foundation
1800 G Street, N.W.
Washington, D.C. 20550

13. Type of Report & Period Covered

14.

15. Supplementary Notes

16. Abstract (Limit: 200 words)

Because of the torsional vibrations of a building during an earthquake, the displacement demands on the different resisting planes of the building may increase relative to those of a similar system with no torsion. It is the overall objective of this work to develop procedures that would enable engineers to predict such an increase in building response resulting from accidental and natural torsion. This report is divided into two parts. In part I, the increase in building response due to accidental torsion is evaluated with the objective of developing an improved procedure to account for these effects in building analysis. In part II, the nonlinear torsional response of single and multistory asymmetric buildings is considered, with the objective of developing a simple conceptual framework in order to understand the earthquake performance of different asymmetric structural configurations, and to develop a simplified method for nonlinear analysis of asymmetric buildings. A new simplified model for inelastic seismic analysis and design of asymmetric structures is also formulated.

17. Document Analysis a. Descriptors

b. Identifiers/Open-Ended Terms

c. COSATI Field/Group

18. Availability Statement: Release Unlimited

19. Security Class (This Report): unclassified

20. Security Class (This Page): unclassified

21. No. of Pages: 311

22. Price